Development of multifunctional polymeric nanoparticles by nano-emulsion templating as advanced nanocarriers targeting the blood-brain barrier

Cristina Fornaguera Puigvert

Universitat de Barcelona
Facultat de Farmàcia
Departament de Físicoquímica
Programa de doctorat:
"Recerca, Desenvolupament i
Control de Medicaments"

Consejo Superior de Investigaciones Científicas
Institut de Química Avançada de Catalunya
Departament de Nanotecnologia Química i
Biomolecular
Grup de Química Col·loidal i Interficial

Development of multifunctional polymeric nanoparticles by nano-emulsion templating as advanced nanocarriers targeting the blood-brain barrier

A dissertation presented by **CRISTINA FORNAGUERA PUIGVERT** in partial fulfillment of the requirements for the degree of Doctor in Research, Development and Control of Medicines of the Universitat de Barcelona.

PhD thesis directed by:

Prof. Conxita Solans Marsà
Institut de Química Avançada
de Catalunya

Dr. Gabriela Calderó Linnhoff
Institut de Química Avançada
de Catalunya

Tutorized by: Prof. MªJosé García-Celma
Departament de Farmàcia i Tecnologia Farmacèutica
Universitat de Barcelona

Cristina Fornaguera Puigvert

Barcelona, 2015

Els meus sincers agraïments:
Mis sinceros agradecimientos:
Mes sincères remerciements:

A les meves directores de tesi, la Dra. Gabriela Calderó i la Prof. Conxita Solans, sense les quals no hauria estat possible aquesta tesi.

A la Gaby, per haver-me introduït en el món de la nanotecnologia, per encomanar-me la seva ilusió, passió i gran estima per la ciència, i sobretot per haver confiat en mi des del principi i haver-me donat ànims per tirar endavant.

I a la Conxita, per haver-me donat l'oportunitat no només de fer la tesi en el seu grup, sinó de sentir-me part d'ell; per haver-me donat tantíssims ensenyaments, des de la química col·loïdal fins a l'escriptura d'aquesta tesi. Gràcies a ella he après els valors de l'esforç, la constància i la feina ben feta, però també la capacitat de ser persona a més de directora, d'entendre els problemes i de trobar-hi sempre solucions. Gràcies Conxita per haver-te implicat completament en aquesta tesi i per haver estat a sobre meu constantment tot i tenir moltes altres preocupacions.

També a la coordinadora d'aquesta tesi, la Prof. Marisa García, per tota l'ajuda administrativa, i a la meva tutora, la Prof. Maria José García-Celma, per ser més que una tutora, per donar-me consell en tots els experiments de caire més biològic i per trobar sempre les persones adequades per poder col·laborar.

Als membres del tribunal, per acceptar formar part del tribunal d'aquesta tesi.

Al Centre de Química Avançada (QCI), a l'Insitut de Química Avançada de Catalunya (IQAC) i al Consell Superior d'Investigacions Científiques (CSIC), al CIBER de Bioenginyeria, Biomaterials i Nanomedicina (CIBER-BBN), i a l'Institute Galien Paris-Sud (UMR CNRS 8612), al Centre Superieur de la Reserche Scientifique (CNRS) i a l'Université Paris Sud, per deixar-me formar part de cadascuna d'aquestes institucions.

A la meva família, que m'ha donat suport en tot durant tota la meva vida, sobretot en els moments més complicats.

Als meus pares, que m'han recolzat sempre i han comprès la importància que per mi tenia aquesta tesi, escoltant-me parlar constantment sobre nanopartícules, un tema que abans no coneixien però del que ara saben una mica més.

A la meva mare, que m'ha ajudat sempre en tot el que he necessitat, des de venir a buscar-me al CSIC, esperant hores perquè jo no acabava, fins a ajudar-me en el format i la presentació de la tesi, escoltant amb atenció les presentacions orals perquè jo practiqués i fins i tot fent-me preguntes!

Al meu pare, que sempre ha confiat en mi, que ha fet tot el que ha estat al seu abast per facilitar-me aquesta etapa, i perquè ha cregut sempre en les meves capacitats i s'ha interessat per la meva tesi.

A la meva germana, per ser com part de mi, per donar-me suport incondicional i per estar sempre al meu costat. Per escoltar-me quan ho he necessitat, per tenir paciència quan m'he fet pesada i per treure'm un somriure quan ho he necessitat.

A l'àvia, per no dubtar mai de mi, per donar-me força per tirar endavant. També per venir-me a buscar tantes vegades al laboratori i per intentar entendre la meva feina i les meves preocupacions.

A la iaia i a l'avi Min, per estar sempre pendents de mi, per fer-me costat sempre i per les seves ganes i confiança en veure'm Doctora. I sobretot pels seus tupers!

Al tiet i la tieta, en Xavier i en Joan, per fer-me passar bons moments i per confiar en mi. També gràcies per ajudar-me en la impressió d'aquesta tesi.

I per sobre de tots ells, moltíssimes gràcies a l'Agus per ser-hi sempre, sempre i sempre. Per fer-me costat, per escoltar-me, per donar-me ànims, per compartir bons i mals moments, per entendre les meves preocupacions, per comprendre les exigències de la meva feina, per tenir paciència, per donar-me bons consells, per ajudar-me... Gràcies Agus per no fallar-me mai!

Moltes gràcies a tots els meus amics per fer-me costat.

A la Laura de Canet, per convertir-se en una de les meves millors amigues, per donar-me sempre ànims, per saber divertir-me i distreure'm i per no oblidar-se mai de mi.

A la Laia i la Cristina Arimany, per totes les divertides sortides al teatre per Barcelona, sobretot a la Cristina, per demostrar també ser una de les meves millors amigues, i per compartir l'etapa de la tesi amb les mateixes preocupacions i interessos.

Als "Friends" de Lloret, en Victor, en Fran, en Pate, l'Erika i en Romà, en especial a l'Anna Pons, per ser la millor cunyada del món, i a l'Alba, per confiar sempre en mi, escoltar-me i tenir paciència durant els dies en què m'he fet més pesada.

Moltes gràcies també a tots els meus companys del Centre QCI, que han estat com una altra família per a mi. Sobretot al "Biolab-CSIC", per donar-me ànims constantment i escoltar tots els meus maldecaps. A l'Aurora (el meu Pepito Grillo personal), perquè des de que va arribar m'ha ajudat en tot, tant en temes professionals com personals, per implicar-se tant en la meva tesi, per oferir-me sempre la seva ajuda, per tots els bons moments viscuts i, sobretot, gràcies per ser una bona amiga. A la Maria Homs, per pensar sempre en tothom, per no oblidar-se mai de cap detall i per oferir la seva sincera ajuda en tot moment. A la Susana, la Silvia, la Neus i la Txell, per la bona acollida quan vaig arribar, pels seus consells, per la seva ajuda i pels seus ànims constants. A l'Alba i a la Natàlia, per tota la feina que m'han ajudat a fer, per la seva constància, el seu interès, el seu bon humor i les seves ganes d'aprendre. A la Camille i la Kelly, per tots els moments bojos que vam compartir. Un record especial a la Núria Azemar, la "mama" del grup, la qual no oblidaré mai. A la MªCarmen, l'Elena, la Marta i la Montse, per les xerrades de suport moral de bon matí. I també a la Laura, el Rodrigo, el Javi, el Ferran, el Jonathan, l'Steffi, la María Martínez, la Maria Valldeperas, la Isabel, l'Àlex, el Jordi Esquena, l'Amalia, la Ella, la Gosha i l'Elwira, la Sarah, el Roland, el Jeremie, l'Allessandro, l'Adaris, la Carolina, la Sheila i el Baltazar.

També volia agrair a totes aquelles persones que han col·laborat en aquesta tesi.

Al grupo de Rafael Gómez, por participar tan activamente en nuestro estudio, por vuestra atención, ayuda y soporte en todo momento. En especial a Marta, por introducirme en la química orgánica y a Elena, por la síntesis de tanto dendrón.

Al grup de la Nanen i el Jordi Vilaplana, en especial a la Itsaso, per tots els experiments i ensenyaments sobre anticossos.

A l'avi Pep.

*"La vertadera grandesa de la ciència
acaba valorant-se per la seva utilitat"*

*Gregorio Marañón
(1887 – 1960)*

TABLE OF CONTENTS

Chapter 1

INTRODUCTION

1.1. Nano-emulsions

1.1.1. General properties

Nano-emulsions are emulsions, dispersions of two immiscible liquids, with very small droplet sizes, typically between 20 and 200 nm (Tadros, 2004; Solans, 2003 and 2005; Pinto Reis, 2006). The liquid dispersed as droplets is the internal, discontinuous or dispersed phase while the other is the external, continuous or dispersant phase (Becher, 1972). Nano-emulsions are designated in the literature with different terminologies. They were first termed as miniemulsions by *Ugelstad et El-Aasser* (Ugelstad, 1973) and this terminology is still being used in the context of polymerization (Miñana-Pérez, 1999; Lansfester, 2000). They have also been termed ultrafine emulsions (Nakajima, 1993) and sub-micrometric emulsions in the pharmaceutical field (Benita, 1993; Sznitzowska, 2001). However, nano-emulsion is the most common term used to define this type of emulsions (Solans, 2005; Mason, 2006; Anton, 2011; McClements, 2012). Nano-emulsions (as conventional emulsions) can be classified as oil-in-water (O/W), when the internal phase is the oil, and water-in-oil (W/O), when the oil is the external phase (Figure 1.1).
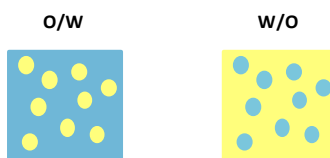
Figure 1.1: Schematic representation of an oil-in-water (O/W) and a water-in-oil (W/O) nano-emulsions.

The <u>visual aspect</u> of nano-emulsions differs from that of conventional emulsions or macroemulsions. While the latter are milky, nano-emulsions are transparent, translucent or slightly turbid due to their small droplet size; with a homogeneous macroscopic appearance (Solans, 2003, 2005 and 2012) (Figure 1.2).

Figure 1.2: Example of the typical aspect of an O/W nano-emulsion.

Nano-emulsions are thermodynamically unstable systems. This is due to the high positive free energy ($\gamma \Delta A$) associated to the creation of the interface at the

contact of the oil and the water phase. The free energy (ΔG) of emulsion formation can be expressed by the Gibbs equation:

$$\Delta G = \gamma \Delta A - T^{\circ} \Delta S \qquad (1.1)$$

where γ is the interfacial tension between two phases; ΔA is the increment of the interfacial area; T° is the temperature and ΔS is the increment of the entropy (Tadros, 1983 and 2004).

Since in nano-emulsions the entropy ΔS is slightly positive, the term $T^{\circ}\Delta S$ cannot compensate $\gamma\Delta A$, which is large due to the high ΔA value produced by the large number of droplets. As a result, the Gibbs free energy is positive; therefore, an energy input is required for nano-emulsion formation (Walstra, 1993). It is worth noting the case of microemulsions, where the γ is low enough to result in a negative value of the Gibbs free energy. For this reason, microemulsions, differently from emulsions, are thermodynamically stable (Tadros, 2004; Solans, 2005).

1.1.2. Surfactant molecules

Surfactants are amphiphilic molecules with a hydrophilic head and a lipophilic tail (Winsor, 1948) (Figure 1.3) having affinity for water and oil phases, respectively. Consequently, surfactants are located preferentially at the interfaces, lowering the interfacial tension between them. For this reason, they are usually used in the emulsification field with the objective to <u>increase the emulsion stability</u>, (Walstra, 1996; Malmsten, 2002).

<div align="center">

Hydrophilic part   **Lipophilic part**

</div>
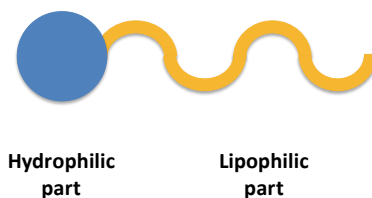
Figure 1.3: Schematic representation of a surfactant molecule. The hydrophilic part is defined as "head" while the lipophilic part is the "tail".

Surfactants are classified depending on their charge in aqueous solution media in ionic, nonionic and zwitterionic. The latter ones are composed of more than one dissociable group that enables them being cationic or anionic depending on the conditions of the solvent or the pH (Rosen, 2004). In this thesis, a nonionic

surfactant was chosen due to their lower toxicity compared with charged surfactants. Although nonionic ethoxylated surfactants are thermosensitive, they are not as much affected as ionic surfactants by electrolyte concentration in the solvent (Karlström, 1990).

A useful parameter to choose the appropriate surfactant is the HLB number (N_{HLB}). HLB stands for hydrophilic – lipophilic balance. The N_{HLB} defines the ratio between surfactant hydrophilic and lipophilic fragments. *Griffin* introduced this parameter as well as the form to calculate the N_{HLB}, an arbitrary value useful for the prediction of the appropriate surfactant for a specific application (Griffin, 1949; Becher, 1965; Shinoda, 1968 and 1973; Kunieda, 1985) (Table 1.1).

Table 1.1: Properties of surfactants as a function of HLB number.

HLB number	Application
4 - 8	Anti-foaming
7 - 11	W/O emulsifier
11 - 14	Wetting agent
12 - 16	O/W emulsifier (detergent)
16 - 20	Solubilizer

N_{HLB} values higher than 10 indicate surfactants with a hydrophilic behavior, thus forming O/W structures; while values lower than 10 indicate a hydrophobic surfactant behavior, forming W/O dispersions. The N_{HLB} for nonionic surfactants with polyoxyethylene groups can be calculated according to the following equation (Equation 1.8) (Griffin, 1949):

$$N_{HLB} = \frac{H}{H+L} * 20 \qquad (1.8)$$

where H and L are the percentages in weight of the hydrophilic and lipophilic groups of the surfactant, respectively; and the number 20 is an arbitrary scale. However, this equation only takes into account the surfactant but not the other emulsion components and parameters such as the effect of the temperature, the pressure, the salinity, the use of a cosurfactant, the interaction among system components and the volume fraction of the dispersed phase.

1.1.3.Nano-emulsion stability

Emulsions, including nano-emulsions, <u>phase separate</u> with time. This process can occur through one or several mechanisms that can take place consecutively or simultaneously. The predominance of one over the others depends on the emulsion type, their components, the emulsion method of preparation and/or the size of the droplets. The main emulsion breakdown processes are the following: sedimentation / creaming, flocculation, coalescence and Ostwald ripening (Figure 1.4).
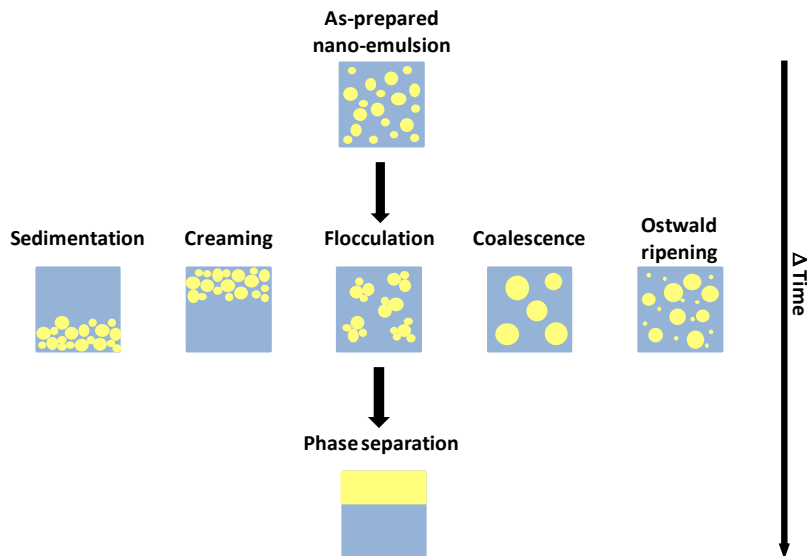
Figure 1.4: Schematic representation of the main emulsion destabilization mechanisms.

Sedimentation or **creaming** are referred respectively to the downward and upward movement of the droplets due to the action of gravity forces on the density differences between the two phases (Tadros, 1983 and 2009; Binks, 1998). They are usually reversible processes with a minimal energy input. The migration velocity ω_{CR} (m/s) of the destabilization process is given by the Stokes law (Equation 1.2):

$$\omega_{CR} = \frac{2(\rho_d - \rho_c)gr^2}{9\eta}$$

(1.2)

where ρ_δ and ρ_c are respectively the densities of the dispersed and continuous phase; g is the gravity force, r is the radius of the droplets and η the viscosity of

the continuous phase. This velocity can be reduced by decreasing the differences between densities, the size of the droplets and/or increasing the viscosity of the continuous phase, thus enabling more stable emulsions. In nano-emulsions, as the droplet size is extremely small, the migration velocity is small. It is overcome by the Brownian motion, which is high for small droplets. Thereby, nano-emulsions are stable against these destabilization processes (Tadros, 2004; Mason, 2006; McClements, 2011).

Flocculation consists in the reversible aggregation of the droplets into clusters (Binks, 1998). It can be described by the DLVO theory, introduced by Derjaguin and Landau (Derjaguin, 1941), and Verwey and Overbeek (Verwey, 1948), which states that the stability of an emulsion is determined by the value of the total energy (E_T) which is made up of the sum of the attractive (E_A) and repulsive (E_R) forces present between two droplets when they approach each other (Equation 1.3, 1.4 and 1.5).

$$E_T = E_A + E_R \tag{1.3}$$

$$E_A = \frac{-A}{12\pi x^2} \tag{1.4}$$

$$E_R = 2\pi\varepsilon r\zeta^2 \exp(-Kx) \tag{1.5}$$

where A is the Hamaker constant and x the distance that separates the two droplets; ε_π is the solvent permeability, r the droplet radius, ζ the zeta potential and κ a function of the ionic composition.

Some authors consider nano-emulsions stable against flocculation (Tadros, 1982 and 2004; Anton, 2008), due to the high curvature that reduces the region of contact of two droplets, thus reducing the probability of two drops to aggregate. Other authors consider that flocculation depends on how often one droplet meets another one; as the Brownian motion is high in nano-emulsion droplets, the probability of these encounters is high, thus enabling destabilization of nano-emulsions by flocculation (Wang, 2008 and 2009). By adding nonionic surfactants, which act as steric barrier, as they have large hydrophilic groups, or co-adsorbed ionic surfactants that increase the emulsion droplet surface charge and act as an electrostatic barrier, flocculation can be decreased (Solans, 2003; Mun, 2005; Binks, 2007; Nambam, 2012).

Coalescence is an irreversible destabilization mechanism through which rupture of the interfacial film between the droplets takes place. Each individual droplet merges with other droplets, forming a bigger drop with less interfacial area. Nano-emulsions can undergo destabilization by this mechanism due to the break of the thin film between the droplets (Walstra, 1993; Mason, 2006). However, some authors consider nano-emulsions stable against coalescence (Taylor, 1994; Rang, 1999; Katsumoto, 2000), if the surfactant chains are long enough and/or the surfactant concentration is high enough to produce a robust interfacial film. Kabal'nov – Wennerström theory (Kabal'nov, 1998) states that prior to coalescence of the droplets, flocculation is required. The coalescence rate, ω_{CO}, can be calculated following the Deminière theory (Equation 1.6) for concentrated emulsions, which describes the spontaneous break of the interface of concentrated emulsions with low polydispersity, considering that the only limiting step is the thinning of the film up to molecular contact (Deminière, 1998 and 1999).

$$\omega_{CO} = \left(\frac{1}{r_0^2} - \frac{1}{r^2} \right) \frac{3}{8\pi t} \tag{1.6}$$

where r is the droplet radius after a time t, r_0 is the radius at t=0.

Surfactants with high molecular weight have been defined in the literature to reduce the coalescence rate, since they have longer chains which enable stronger interactions. For example, the longer the lipophilic part of the molecule, the more stable O/W emulsions.

Ostwald ripening takes place when the dispersed phase diffuses from the smaller droplets to the bigger ones due to the differential solubility as a consequence of the Laplace pressure difference, decreasing the size of small droplets and increasing the size of the big droplets. The Ostwald ripening rate was described by Lifshitz and Slezov (Lifshitz, 1961) and Wagner (Wagner, 1961), the so-called LSW theory. This theory assumes that the droplets are spherical, the distance between the droplets is higher than the droplet size and the mass transfer is only due to diffusion. The rate of Ostwald ripening (ω_{OR}) is given by Equation 1.7; and accordingly, ω_{OR} can be experimentally calculated by the slope of the plot of r^3 as a function of time.

$$\omega_{OR} = \frac{dr^3}{dt} = \frac{8C_\alpha \gamma V_m D}{9RT\rho} \qquad (1.7)$$

where r is the droplet radius, C_α is the solubility of the dispersed in the continuous phase, γ is the interfacial tension between both phases, V_M is the molar volume of the dispersed phase, D is the diffusion coefficient of the dispersed into the continuous phase, R the gas constant, T the temperature and ρ the density.

Ostwald ripening is considered the main destabilization mechanism of nano-emulsions. The Laplace pressure in small droplets is very high while in big droplets is low. Therefore, the more polydisperse a nano-emulsion is, the higher the Laplace pressure differences and diffusion rate (Taylor, 1994; Katsumoto, 2000; Izquierdo, 2002; Tadros, 2004). Thus, the main factors that affect the Ostwald ripening are the polydispersity and the solubility of the dispersed phase in the continuous phase (Taisne, 1996; Kabalnov, 1987; Taylor, 1998). Therefore, to reduce and control Ostwald ripening, two possibilities exist: the reduction of the polidispersity and/or the addition of less soluble molecule in the dispersed phase (Tadros, 2004).

Summarizing the destabilization mechanisms, nano-emulsions tend to be destabilized by Ostwald ripening, due to their small droplet size, while they have stability to sedimentation and creaming (Taylor, 1998; Izquierdo, 2002; Tadros, 2004).

1.1.4. Emulsification by low-energy methods

Nano-emulsions, as all emulsions, are thermodynamically unstable systems, which means that an energy input is required for their formation. This energy can arise from an external or internal source (Walstra, 1993; Anton, 2008). If the energy comes from an external source, the emulsification method is designated as a **high-energy** or dispersion method. By these methods, the small droplets are obtained due to the breaking of bigger drops by the use of mechanical devices, such as colloidal mills, ultrasounds, high-pressure homogenizers and high-shear stirrers (Walstra, 1983 and 1993; Anton, 2008; Delmas, 2011). It is worth noting that only around 0.1% of the energy applied is used for the emulsification, the

rest is lost by viscous dissipation or by heating, therefore, the higher the energy input, the smaller the droplets (Tadros, 2004).

If the energy for the emulsification comes from the internal chemical energy of the components of the system, the emulsification methods are designated as **low-energy** or condensation methods**.** These methods are more cost and energy efficient than the former ones in terms of producing small droplets with low polydispersity and lower energy. Low-energy methods can be classified in two main types: spontaneous emulsification and phase inversion methods (Solans, 2005 and 2012; Anton, 2008).

 Spontaneous emulsification (self-emulsification) is based in the internal chemical energy produced by the system during a dilution process. Generally, it is performed adding the continuous phase, usually at constant temperature. Phase transitions and change in the surfactant curvature are not involved in this process. In the pharmaceutical industry, this process is also called self-nanoemulsifying drug delivery systems (SNEDDS) (Date, 2010; Rahman, 2011; Khan, 2012). This procedure has been carried out sometimes without surfactant; the so-called Pastis or Ouzo effect. It consists in the displacement of molecules from the dispersed to the aqueous phase when adding a huge amount of water to a mixture of a water-miscible solvent and a hydrophobic oil (Ganachaud, 2005; Solans, 2005). One example of self-emulsification making use of surfactants is the formation of O/W nano-emulsions by the dilution of O/W microemulsions. During the dilution, the microemulsion loses its thermodynamic stability due to the fact that the concentration of surfactant is not enough to maintain the required interfacial tension; becoming a nano-emulsion (Taylor, 1994; Solans, 2005). Furthermore, there are examples where nano-emulsions are also formed by the same method (spontaneous emulsification) from other structures, such as direct cubic liquid crystalline phases, as described by *Solè et al.* and *Maestro et al.,* (Solè, 2006 and 2012; Maestro, 2008) in a mixture of nonionic/ionic surfactants. The main disadvantage of this methodology is that the stable nano-emulsions have a low volume fraction of the dispersed phase.

Phase inversion emulsification methods take advantage of the internal energy of the components which is released through phase transitions during the emulsification. A change in the surfactant curvature is produced during the emulsification process. These methods are classified as phase inversion temperature (PIT), when emulsification is triggered by a change in the

temperature, and phase inversion composition (PIC) methods, when the phase inversion is produced by a change in the composition.

The **phase inversion temperature** (PIT) was introduced by Shinoda (Shinoda, 1968). It is based on the physicochemical changes (variation in the surfactant curvature) due to a variation of the temperature during the emulsification process maintaining a constant concentration (Shinoda, 1969; Izquierdo, 2002; Morales, 2003). This method is only useful with termosensitive surfactants, such as polyethoxylated surfactants. At low temperatures, the surfactant has a positive curvature, thus, they form O/W structures due to the solubility of the ethylene oxide groups in water. At high temperatures, the spontaneous surfactant curvature is negative, therefore, W/O structures are formed, due to the dehydration of the ethoxylated chains of the surfactant that increase its hydrophobicity. At intermediate temperatures, the phase inversion temperature (PIT) or HLB temperature (T_{HLB}), the surfactant has a spontaneous curvature around zero, it is no longer soluble in water or in oil, resulting in bicontinuous microemulsions or lamellar liquid crystals. It should be noted that under these conditions, the interfacial tension between oil and water is extremely low and emulsification is favored, but emulsions quickly destabilize by coalescence. Solubilization is also optimum at the T_{HLB}. The use of the PIT methodology to produce nano-emulsions consists in the preparation of the samples at the T_{HLB}, where interfacial tensions are extremely low, and produce a rapid change in the temperature either cooling, to produce O/W or heating, to produce W/O nano-emulsions. By moving fast from the T_{HLB} or PIT, coalescence is avoided and the energy required is minor (Shinoda, 1968 and 1969; Kunieda, 1985; Tadros, 2004).

The **phase inversion composition** (PIC) method is based on the changes in the spontaneous curvature of the surfactant produced during the emulsification process by changing the composition at constant temperature (Figure 1.5). It generally consists in the stepwise addition of one component (water or oil) in a mixture of the two others (oil/surfactant or water/surfactant respectively). When adding water and using, for example, an ethoxylated surfactant, the initial sample is a W/O microemulsion. While the volume fraction of the water increases, the ethoxylated chains of the surfactant increase their hydration grade, and the curvature of the surfactant spontaneously changes from negative to zero, where the hydrophilic-lipophilic properties are balanced, forming bicontinuous or lamellar structures. Adding more water, the curvature of the surfactant turns to positive values, forming O/W nano-emulsions (Forgiarini, 2001; Usón, 2003;

Sadurní, 2005 and 2006; Solè, 2006; Morral-Ruiz, 2011). This method has some advantages compared to the PIT method: 1) it can be applied with surfactants other than ethoxilated ones; 2) if the method is performed at low temperature, it can preserve the material properties of thermolabile molecules, which is very interesting for medical application; and 3) it can be performed in large-scale productions because the experimental procedure is easy (Anton, 2008). Several studies demonstrated that the formation of a liquid crystal phase during the emulsification process is necessary to achieve nano-emulsions with small droplets and low polidispersity (Sagitani, 1981; Forgiarini, 2001; Usón, 2004). For example, *Forgiarini et al.* reported the presence of lamellar liquid crystal phases in the Water / Brij30^R / Decane system in the emulsification process to prepare nano-emulsions by the PIC method, when adding the aqueous phase (Forgiarini, 2001). The velocity of the stepwise addition is critical, as reported by *Solè et al.* (Solè, 2012). The transition from W/O to O/W structures (or the reverse) through lamellar crystalline phases are the same for the PIT and the PIC methods.

It is worth noting that in most practical cases, nano-emulsion formation is achieved by a combination of low-energy methods (phase-inversion and self-emulsification) (Sadurní, 2005; Wang, 2007(1)) or low- and high-energy methods (Nakajima, 1997; Sadurní, 2005).
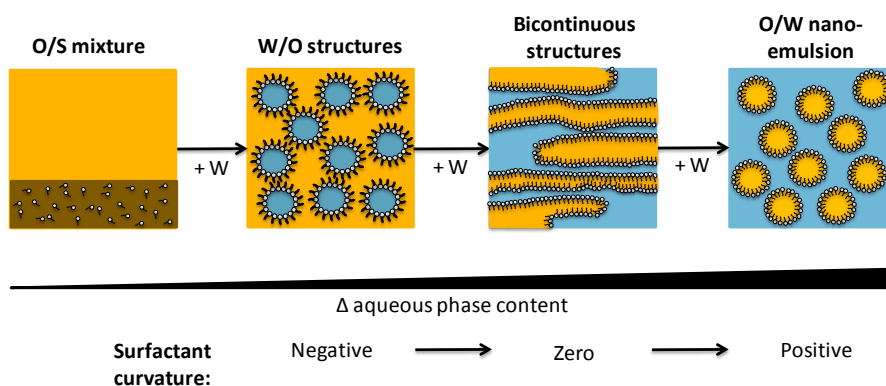
Figure 1.5: Schematic representation of the nano-emulsion formation pathway by the PIC method.

1.1.5.Applications in biomedicine

Nano-emulsions are considered as improved emulsions, due to their smaller droplet sizes, their transparent/translucent appearance and their increased kinetic stability. They have a transparent bluish aspect, which has been interesting for the incorporation of active principles in varied fields, such as food (McClements, 2011; Silva, 2012), perfumery (McClements, 2011; Ziani, 2012) or cosmetics (Sonneville-Auburn, 2004). Nowadays, they are becoming important nanodevices in the **biomedical and pharmaceutical field**, for diverse reasons (Benita, 1993; Buszello, 2000; Solans, 2005; Tamilvanan, 2005; Vyas, 2008; Gref, 2012; Ezhilarasi, 2013):

1) in controlled drug release, they can be useful by active administration by diverse routes
2) in the solubilization of actives inside the droplets, since they can increase the concentration of the poorly water soluble actives, in O/W nano-emulsions
3) for the stabilization/protection of active principles, due to the nano-emulsion increased stability
4) for decreasing the toxicity and the side effects of the encapsulated actives
5) in non-viral gene therapy
6) to achieve more favorable drug release kinetics
7) for the specific targeting of active principles to the specific organs in the body.

The nanometric size of nano-emulsions makes them advantageous for the main administration routes to the body, namely for the intravenous delivery, as they do not obstruct the blood vessels, and for the oral delivery, increasing drug absorption when encapsulated in nano-emulsions (Nicolaos, 2003).

It is noteworthy the use of polymeric nano-emulsions as **polymeric nanoparticle templates** (Asua, 2000; Antonietti, 2002). Among the existing diverse methodologies for the nanoparticle production from nano-emulsions, the most representative are two: polymerization of monomers in the dispersed phase (Ugelstad, 1973) and using preformed polymers as the disperse phase of the nano-emulsion (Desgouilles, 2003; Sahana, 2008; Calderó, 2011).

1.2. Polymeric nanoparticles

The classical definition of nanoparticles for pharmaceutical applications, given by the Encyclopedia of Pharmaceutical Technology and by the Encyclopedia of Nanoscience and Nanotechnology, is the following:

Nanoparticles for pharmaceutical purposes are solid colloidal particles ranging in size from 1 to 1000 nm (1 µm) consisting of macromolecular materials in which the active principle (drug or biologically active material) is dissolved, entrapped, or encapsulated, or to which the active principle is adsorbed or attached.

This definition is in good agreement with the extensive bibliography of nanoparticles (Soppimath, 2001; Tadros, 2004; Pinto-Reis, 2006). Nevertheless, in the nanotechnology field, nanoparticle size usually is defined to range between 1 to 100nm (National Nanotechnology Initiative, 2014). However, in the present thesis, since the formulated nanoparticles are intended for biomedical applications, size ranges of the pharmaceutical field are considered.

Nanoparticles can be divided in two groups: nanocapsules and nanospheres (Vauthier, 2003).

Nanocapsules consist of solid nanoparticles, with a rigid shell that surrounds the core; which could be defined as a reservoir space. The core could be semisolid or liquid, either lipophilic or hydrophilic. **Nanospheres** consist of homogeneous matrices whose entire mass is solid and they are usually spherical (Figure 1.6) (Vauthier, 2009 (1)). Both nanocapsules and nanospheres can be prepared from nano-emulsion templating. For nanospheres, the dispersed liquid phase of the droplet must be removed.

Nanocapsule   **Nanosphere**
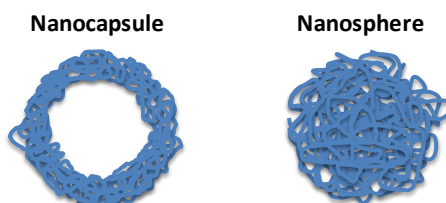
Figure 1.6: Schematic representation of a nanocapsule and a nanosphere.

1.2.1.Nanoparticle preparation

As indicated in section 1.1.5, polymeric nanoparticles can be prepared from O/W **nano-emulsion templating** by two different methods: the polymerization of a monomer or using preformed polymers. The use of preformed polymers is advantageous compared to emulsion polymerization because the polymer properties are well defined, not residual products from the polymerization are produced and cross-reactions between the monomer and the actives are avoided (Soppimath, 2001; Anton, 2008; Vauthier, 2009; Morral-Ruiz, 2011; Solans, 2012).

The preformed polymers dissolved in an organic volatile solvent generally form the dispersed phase of an O/W nano-emulsion. The solvent can be removed from the nano-emulsion, leading to the **precipitation of the polymer** to form the polymeric nanoparticles due to the physico-chemical changes of the medium (Pinto Reis, 2008; Vauthier, 2009 (1)). If the objective is to encapsulate other compounds, such as drugs or fluorescent dyes, they can be also dissolved in the polymer/solvent mixture, prior to the emulsification.

Diverse methodologies have been used to prepare nanoparticles from nano-emulsion templating: solvent evaporation, solvent diffusion, nanoprecipitation, and reverse salting out (Soppimath, 2001; Anton, 2008; Vauthier, 2009 (1); Neha, 2013).

The **solvent evaporation method** (Soppimath, 2001; Pinto-Reis, 2006; Vauthier, 2009; Calderó, 2011) is based in the evaporation of the solvent which diffuses through the continuous phase of the nano-emulsion. The solvent is usually extracted by distillation or under a vacuum, although it can be removed at room temperature and pressure at longer times.

The **solvent diffusion method** (Fessy, 1989) is based in the preparation of nano-emulsions with a solvent saturated with water to achieve the thermodynamic equilibrium of both liquids at the starting moment. Once prepared, the nano-emulsion is diluted with an excess of water, which produces the diffusion of the solvent toward the continuous phase. The disadvantage of this method is the use of high amounts of both, water and solvent and the requirements of using non-volatile water miscible solvents, such as propylene carbonate (Quintanar-Guerrero, 1997; Trimaille, 2003).

The **nanoprecipiation method** (Fessy, 1989; Govender, 1999; Neha, 2013) is based in the spontaneous emulsification of the organic internal phase that contains the polymer. This phase is injected into a stirred water solution containing a surfactant as stabilizer. The diffusion of the solvent leads to an interfacial deposition of the polymer following displacement of a semi-polar solvent miscible with water from a lipophilic solution.

The **reverse salting-out method** (Allémann, 1992; Pinto-Reis, 2006) is based on the extraction of a water-miscible solvent from an aqueous solution taking advantage of the salting-out effect. The polymer is dissolved in a totally water soluble solvent, such as acetone. To induce emulsification, a high concentration of electrolytes (salting-out agents) is added, leading to the emulsification process. The precipitation of the polymer takes place by dilution of the emulsion with water, which enhances solvent diffusion. This method can be considered as a modification of the solvent diffusion method, but in the solvent diffusion, the high amounts of water exist from the preparation and in the salting-out they are added *a posteriori*.

It is worth remarking the existence of the so-called **supercritical fluid technology (SCF)** (Byrappa, 2008; Gulati, 2013), based on the use of environmental friendly solvents (replacing the traditional toxic solvents) to produce nanoparticles with high purity and without any traces of organic solvents (Neha, 2013). In this case, the polymer is dissolved in a supercritical fluid, and the solution is expanded through a nozzle, followed by an evaporation of the solvent due to spray drying. The main advantage of this technology is the use of environmental friendly solvents, however, it requires a high initial inversion (Pinto-Reis, 2006).

1.2.2. Applications of polymeric nanoparticles in biomedicine

Nanoparticles have experienced an increasing interest in the biomedical field (Pinto Reis, 2006; Kreuter, 2014). Focusing on polymeric nanoparticles, the interest in their use for biomedical applications has experienced an exponential increase in the lasts decades, as evidenced by Figure 1.7.
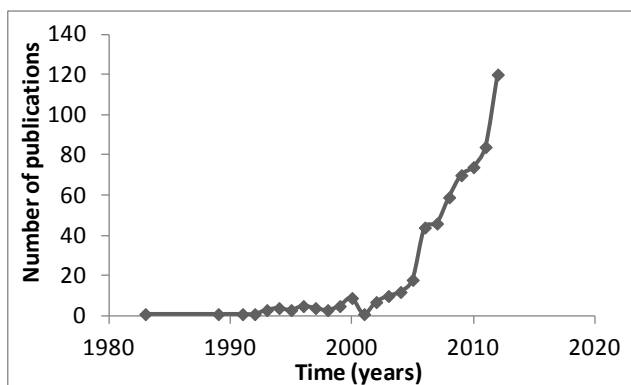
Figure 1.7: Number of publications on "polymeric nanoparticles" and "pharmaceutical uses" in the last 30 years. Source: Scopus.

Several characteristics make nanoparticles particularly interesting for biomedicine:

1) Their nanometric size, which enables their administration to the body (by any route) and the intracellular delivery (Pinto Reis, 2006).

2) They can be functionalized to achieve a targeted delivery at the selected tissue, increasing the effects of the incorporated active principles to the specific site of action and reducing side effects (Klang, 1998; Tamilvanan, 2004; Vauthier, 2009 (1); Date, 2010; Neha, 2013).

3) They can encapsulate, solubilize, trap or adsorb a huge variety of substances to enhance their stability, like drugs, dyes or inorganic materials (Kreuter, 2004; Pinto Reis, 2006; Guterres, 2007; Gref, 2012; Teixera, 2012; Neha, 2013).

4) They can provide controlled principle release, enabling extended duration of action, reduction of dosage frequency, improved management of therapy and compliance, reduction of side effects and cost savings; thus enhancing efficiency and effectiveness (Klang, 1998; Tamilvanan, 2004; Cook, 2005; Brigger, 2012; Gref, 2012; Gupta, 2012; Neha, 2013).

5) Nanoparticles can be prepared easily in large quantities with cost effective methodologies (Neha, 2013).

Pharmaceutically suitable nanoparticles have been developed for many years using different materials.

Nanoparticles can be administered to the human body by a variety of routes, such as the oral or the parenteral routes, among others. Depending on the route of administration, nanoparticles must be developed with the specific appropriate features. In this thesis, nanoparticles intended for the **intravenous route** were prepared. As a parenteral route, the dispersion of injected nanoparticles must be sterile, isotonic, apyrogen, non-toxic, biocompatible, biodegradable, stable and with particle diameters lower than 1 μm (Benita, 1993). It is worth noting the necessity of excipients in parenteral administration preparations. They must be FDA approved to reach clinical trials. The most common used excipients are surfactants, such as lecithins, poloxamers, polysorbate 80 and Cremophor EL, as well as oils such as vegetal oils and triglycerides (Jumaa, 1998; Kan, 1999; Strickley, 2006; Shi, 2009).

Many factors must be taken into account when designing nanoparticles for the intravenous administration (Tosi, 2013). The first factor is the **composition of the nanoparticle**. As indicated above, nanoparticles must be formulated with biocompatible and biodegradable components in order to avoid toxicity problems. Among the synthetic preformed polymers, one of the most used for biomedical applications is poly(lactic-co-glycolic acid) PLGA (Pinto Reis, 2006), which has been widely used due to its biocompatibility and biodegradability (Guzman, 1996; Labhasetwar, 1997; Pinto-Reis, 2006). Therefore, it is accepted by the FDA for *in vivo* applications (Cohen, 2000). PLGA biodegradability enables the slow rate formation of lactic and glycolic acid without affecting the normal cell function, as both are biodegradable monomers (Panyam, 2012).

The second factor is the **size**. To be used as intravenous delivery systems, nanoparticles cannot exceed diameters of 1 μm (Benita, 1993), being more appropriate the dispersions with small sizes (Vauthier, 2009 (1)) and low polidispersity, as the presence of nanoparticles higher than 5 μm could produce embolisms (Wretlind, 1964; Gref, 2012; Kreuter, 2014). It is worth noting the importance of the size of nanoparticles for their biodistribution in the body. The higher the nanoparticle size, the higher their detection by the immune system and the phagocytic rate, which clears rapidly nanoparticles from blood circulation, not enabling them to reach to their targets (Vauthier, 2009; Gref, 2012; Kulkarni, 2013; Neha, 2013; Alyautdin, 2014; Kreuter, 2014). Therefore, the

choice must be small size nanoparticles with low polidispersity. However, not only the size but the surface charge influence in the phagocytic activity: the more charged the nanoparticles, the higher the phagocytic rate (He, 2010).

Another factor is the **activation of the immune system**. Once circulating through the blood, nanoparticles contact with diverse components of the immune system, which is activated when it detects exogenous components. Then, these components will be recognized and eliminated by fagocytosis, not allowing nanoparticles do their action. The activation of the immune system not only depends on the size, but on the surface of the particles. For this reason, nanoparticle surface must be tuned to avoid the recognition of the immune system, enabling longer times of circulation in the blood and increasing the activity of the particles. Different compounds have been used to modify nanoparticle surface, such as polysaccharides and amphyphilic copolymers (Figure 1.8) (Vauthier, 2009 (1)). Among them, the amphyphilic copolymers are specially recommended, as they have a hydrophobic part internalized in the nanoparticles, that allows their attachment to the nanoparticle, and a hydrophilic part that is faced to the surface enabling the desired properties. In this context, one of the most widely used functionalization is the **pegylation**; this is, the functionalization with polyethylene glycol (PEG), that has been reported to decrease the opsonization (Vauthier, 2009 (1)). In the bibliography, there are some articles reporting a decrease of the activity of the immune system due to the use of the PEG at the surface of the nanoparticles. The study of *Chaudhari et al.,* where they pegylated poly (n-butyl cyano acrylate) nanoparticles prepared by emulsion polymerization, adding the PEG coating in a one-step procedure is illustrative. The decrease of the reticuloendothelial system (RES) activity was achieved due to the presence of the PEG coating which reduces the protein aggregation in the nanoparticle surface (Chaudhari, 2012).

The **complement system** is one of the most important processes included in the immune system. It contributes in the acquired and innate immune response, by means of lysis, opsonization and final clearance of exogenous compounds, as well as the protein attachment to these compounds, to amplify the immune response. One of the most important proteins involved in the complement cascade is the C3 protein, since it acts in the three complement activation pathways (classical, alternative and lectin). Therefore, when designing nanoparticles for the intravenous administration, they should be weak or non activators of the complement system, in order to decrease their detection by the immune system

and prolong their blood circulation time, thus enhancing their arrival to the target tissues (Dobrovolskaia, 2013).

The **toxicity requirements** are other factors related with the immune system activation. Toxicology is defined as the study of the adverse effects that substances produce in contact with living organisms (Timbrell, 1998). Nanoparticle toxicity could be produced, for example, by a redox activation (Colvin, 2003), or by the transport of the nanoparticles through cell membranes, especially to reach the mitochondria (Foley, 2002). As the toxicity depends not only on the components of the formulation, but on the features of the resulting materials (such as size or surface charge), nanoparticles must be formulated with non-toxic components, but once formulated, their toxicity must be tested to ensure that they are appropriate to be injected. However, it is worth mentioning that, as Paracelsus quoted, all materials are toxic at doses higher than that of a limit, thus, the toxicity of a component depends mainly of their dose (Timbrell, 1998).

An ultimate factor to be studied is the **vectorization** of the nanoparticles through the target organs. Nanoparticles must be able to release the actives they transport (encapsulated, attached…) to the specific site of action, to achieve a controlled biodistribution that decreases the side effects (Vauthier, 2009(1)). Two different types of vectorization exist. On one hand, there is the **passive diffusion** of the nanoparticles through the biological barriers due to their small size. It must be noted, however, that with a passive vector, only a small fraction of the nanoparticle will arrive at the desired site of action and in most cases, nanoparticles accumulate in the liver and the spleen using the passive targeting (Nobs, 2004). On the other hand, the **active targeting** consists in the specific design of the nanoparticle surface to ensure a delivery in the target cells. To achieve this targeting, nanoparticle surface must be functionalized. **Monoclonal antibodies** have been widely used with this purpose, as they can transport nanoparticles to the recognized antigen, where they will be bound, in the target organs or cells. Antibodies can be attached by a physical adsorption on the nanoparticle surface, but their covalent binding is preferred, as it avoids their displacement once in contact with blood proteins (Illum, 1983; Rolland, 1987; Nobs, 2004). Apart from antibodies, other targeting elements have been reported, such as different types of cell penetrating peptides (CPP), which allow the transport of molecules through the cell membranes (Stewart, 2008), and

dendrons, but the latter are considered as passive targets (Berna, 2006; Ionov, 2012) (Figure 1.8).

a)   b)

PEG   polysaccharide   drug   fluorescent dye   gene   dendron   antibody   CPP
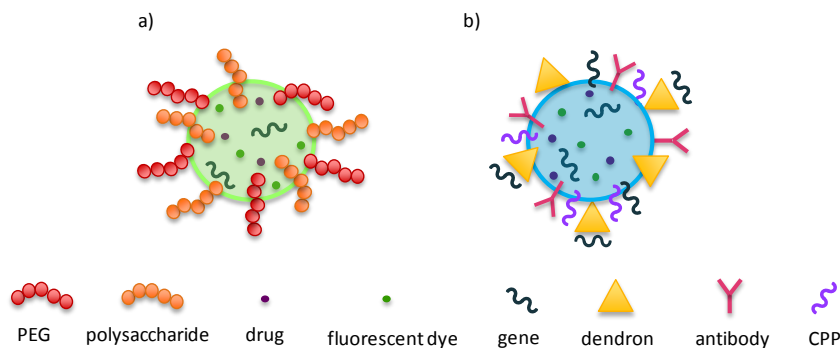
Figure 1.8: Schematic representation of various functionalization molecules: a) elements to bypass the immune system and b) targeting moieties; both including encapsulated compounds.

Apart from a proper design of the nanoparticles taking into account the activation of the immune system, toxicity requirements and functionalization to reach the target tissues, it is important to consider the function of nanoparticles once in the human body. The application of the nanoparticles could be divided in three main groups: diagnosis, therapeutics and theranostics. In the three applications, encapsulated or attached elements are required. In this context, nanoparticles have been defined as *magic* bullets; drugs that can selectively destroy diseased cells but they are not harmful to healthy cells. They could be also defined as **advanced delivery systems** since, after the proper design, they are able to specifically deliver the actives they transport to the specific site of action by a controlled manner. Several examples of the use of PLGA nanoparticles as advanced delivery systems have been reported in previous studies. Different compounds such as hydrophilic / lipophilic drugs (Barichello, 1999; Mundargi, 2008; Vrignaud, 2011), proteins and peptides (Pinto Reis, 2006), magnetic nanoparticles (Lee, 2004; Astete, 2007; Okassa, 2007) and fluorescent dyes (Musyanovych, 2008) have been encapsulated in nanoparticles. However, the encapsulation is not the only way to transport them, since they can be attached to the nanoparticle surface by covalent binding (Michaelis, 2006) or electrostatic adsorption on the surface (Mansouri, 2006). When nanoparticles carry a drug, they are considered **advanced drug delivery systems (DDS)**; not only the conventional drug molecules such as dexamethasone (Fornaguera, 2014(1)) or doxorubicin (Wohlfart, 2011 (1)) but also proteins and peptides are included

(Pinto Reis, 2006). If they transport genetic material, nanoparticles are acting as **non-viral gene delivery systems** (Mansouri, 2006). It is remarkable that diverse strategies have been reported in the literature to achieve an electrostatic binding between nanoparticles and genes. Cationic nanoparticles have been previously used as non-viral gene delivery systems (Panyam, 2002; Mansouri, 2004). They have been previously described to escape from the endosomal pathway, leading to gene escape to the cytosol to enable its expression (Panyam, 2002). The nanoparticle cationic charge was usually obtained by the use of cationic polymers, such as chitosan (Ravi Kumar, 2004) or polyethylenimine (Arora, 2014). In comparison with cationic polymers, the system designed in the present thesis is composed with less toxic components.

When using nanoparticles as advanced drug or gene delivery systems, they are acting as therapeutic agents. If they carry a fluorescent dye, such as coumarin-6 (Chavanpatil, 2006) or radioactive molecules, such as C^{14} ion (Ambruosi, 2006), they are **imaging agents** useful to study the biodistribution of nanoparticles (diagnosis purposes). In addition, there are few studies in which the nanoparticles are designed as **theranostic systems** (Figure 1.8). Most of them have been recently summarized in the review of *Mura and Couvreur* (Mura, 2012), like the use of iron oxide magnetic nanoparticles (MNPs) coated with PLGA carrying the MNPs as the imaging contrast agent and being able to encapsulate hydrophobic drugs such as paclitaxel and rapamycin and/or hydrophilic drugs like carboplatin (Singh, 2011).

1.3. The central nervous system

The central nervous system (CNS) of the human body is composed by the brain and the spinal cord, whose essential building blocks are the neurons. It serves for a variety of functions that can be defined as the comprehension and interpretation of the complete environment of the person. As the CNS is considered one of the most important systems of the body, it is highly protected against the entrance of exogen substances by the blood-brain barrier (Kabanov, 2007). However, the structure, the function or both can be affected for different reasons, thus resulting in a <u>neurological disease</u>. Among all types of neurological diseases, neurodegenerative diseases have an increasing interest in the medical and scientific community due to the increasing prevalence of aged population. They represent huge human and economic costs for the developed societies (Flint Beal, 2005).

1.3.1. Neurolodegenerative diseases

Neurological diseases encompass all disorders affecting the neural system. The World Health Organization (WHO) estimates that about 700 million cases of motor neuron diseases (MND) are newly reported each year, representing the 13% of the global disease burden (Tosi, 2011; WHO, 2011). Among them, **neurodegenerative disorders** are a group of neural diseases linked to aging, environmental cues and/or immunity disorders and genetic predisposition. Their pathogenesis is characterized by the accumulation, aggregation and modification of human proteins, alterations in tissue homeostasis, immunological damages and effects due to viral infections (Kabalnov, 2007). Nowadays, only palliative treatments to manage the symptoms exist. This is due to the fact that most compounds cannot cross the blood-brain barrier; neither reach to the central nervous system. For this reason, better diagnostic and therapeutic tools such as new drug delivery systems are required.

In incidence terms, the most prevalent neurodegenerative disorders are, in this order, Alzheimer's disease (AD), Parkinson's disease (PD), stroke, amyotrophic lateral sclerosis (ALS), HIV-1 associated dementia and lysosomal storage disorders (Kabanov, 2007).

Alzheimer's disease is the most prevalent neurodegenerative disease and the most common dementia present on aged population. It affected 36 million people in 2010 and the rise of affection is expected to achieve 115 million by 2050 (Kaur, 2008). Its clinical manifestation consists in a progressive loss of the cognitive function, which brings to a cortical dementia, characterized by impairments in the memory, cognition and behavior (Clarimón, 2003; Kabalnov, 2007). The neuropathology of the disease consists on both: the presence of senile plaques composed by the neurotoxin $\beta-$amiloid, extracellularly accumulated on blood vessels and in the brain; and neurofibrillary tangles of hyperphosphorilated τ protein intracellularly accumulated (Zlokovic, 2008; Brambilla, 2011). Nowadays, the treatments of the Alzheimer's disease are mainly based in the reduction of the disease manifestations but none of them is extremely effective. The most widely used drugs are the antiapoptotic drugs, such as galanthamine and rivastigmine, which are acetilcholinesterase inhibitors that possibly reduce the formation of the senile plaques due to the increase in the acetylcholine brain levels, enabling a basal synaptic activity. Their reduced effects and their high side effects are produced by the presence of the blood-brain barrier, which limits the crossing of the drugs to the central nervous system, their target tissue, thus new delivery strategies must be developed (Mangialashe, 2010).

1.3.2. Crossing the blood-brain barrier

The **blood-brain barrier (BBB)** was first discovered by Paul Ehrlich in 1885 (Alyautdin, 2014), although it did not receive this name until 1900, by Lewandowsky (Lewandowsky, 1900). It is a highly specific structure composed mainly by endothelial cells that limits the crossing of the substances from the blood vessels to the central nervous system (CNS) due to the presence of the tight junctions between endothelial cells (Figure 1.9) (Duran, 2012). It allows a variety of <u>functions</u> (Kabanov, 2007; Patel, 2012):

1) The maintenance of the homeostasis of the CNS, to enable the correct functions of the neurons, such as the synapsis, the angiogenesis and the neurogenesis.
2) The nutrient supply, as well as the supply of all the required components in the CNS.

3) The protection of the CNS from the exogenous components, which are detected by the immune system as toxic and the BBB does not enable their entrance through the CNS.

4) The elimination of the by-products generated inside the CNS through the bloodstream.
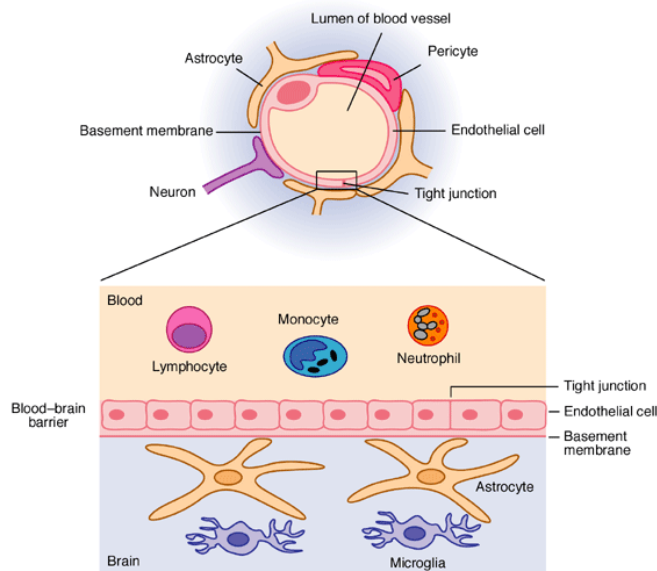
Figure 1.9: Schematic representation of the BBB. Extracted from *Francis et al.* (Francis, 2003).

The proposed mechanisms of delivery of actives across the BBB are the following (Kreuter, 2012; Kreuter, 2014; Neha, 2013):

1. Retention of the nanoparticles in the brain capillaries, together with their adsorption in the capillary walls. This would enable a higher concentration of nanoparticles in the outer side, thus enabling the crossing of nanoparticles due to the concentration gradient.
2. Inhibition of the efflux active system, especially of the P-glycoprotein, which could be produced by some surfactants such as the polysorbate 80.
3. Use of substances with toxic effects on the vasculature of the BBB.
4. Enhanced drug permeability to the BBB due to a fluidization of the cell lipid membranes caused by the presence of a surfactant that could solubilize the cell membrane lipids.
5. Tight junctions opening due to the presence of the nanoparticles.
6. Endocytosis of nanoparticles, followed by the delivery of them in the brain.

24

7. Transcytosis of nanoparticles across the blood-brain barrier.
8. A combination of the different mechanisms.

Nowadays, there is some controversy about the dominant system of BBB crossing. Some studies showed that the main passive diffusion system was the endocytosis (Kreuter, 2013), while other studies indicated that endocytosis was minimal (Kreuter, 2003). The diffusion of the substances through the BBB is only possible when these substances are lipophilic, with molecular weights lower than 400 Da and they are not substrates of the efflux active transport nor metabolized by the endothelial cells (Zlokovic, 2008). However, most of the lipophilic compounds are usually rapid effluxed from the CNS to the blood by the own systems of the BBB, not enabling their action in the brain (Kabanov, 2007), the concentration gradient is not enough to allow the entrance of the drug at therapeutic concentrations (Kreuter, 2012). An advantageous strategy is the design of nanoparticles taking advantage of the specific mechanisms of the **active transport** through the BBB rather than making use of the passive diffusion (Béduneau, 2008). The active transport has been traditionally divided into 3 groups: the carrier-mediated transport, the active efflux transport and the receptor-mediated transport (Neha, 2013). The latter type has been widely used by the conjugation of the specific antibodies to the surface of the delivery system; namely the antibodies that bind the endogenous transferrin receptors, which are overexpressed in the endothelial cells of the BBB; such as the monoclonal antibody OX26, 8D3 or R17-217 (Pardridge, 2002; Garcia-Garcia, 2005; Béduneau, 2008). This approach can be also applied targeting to other receptors such as the insulin receptor (Gabathuler, 2010). Another option is to conjugate the delivery systems with different types of apolipoproteins (mainly A and E), since they specifically interact with the low-density lipoprotein receptors (LDL-r) of the BBB, to profit the LDL-r mediated transcytocis (mechanism 4) through the BBB (Brambilla, 2010). A more limited option is the use of the glucose transporters, like GLUT1 or GLUT3, but the design of the vector must be carefully performed in order to simulate the molecule of glucose, as this is the only nutrient able to enter the CNS due to the glucose receptors, which limits its interactions only with glucose molecules (Béduneau, 2007).

It must be taken into account that the BBB structure is affected in almost all the neurodegenerative disease. However, it is still not known if its alterations appear due to the disease or if they are the source of the disease. Due to these alterations, the BBB is no longer able to develop the above explained functions,

thus worsening the symptoms of the disease (Zlokovic, 2008; Alyautdin, 2014). Although huge efforts have been done, to our best knowledge, not a single study reports the BBB crossing of a nanocarrier with efficiencies higher than 15% (Tosi, 2011). For this reason, more studies are required. In this context, the aim of this thesis was to design novel advanced delivery systems able to cross the BBB with higher efficiencies, enabling the improvement of neurodegenerative diseases' current treatments.

Chapter 2

OBJECTIVES

The increasing prevalence of neurodegenerative diseases, especially Alzheimer's disease, is a serious problem for the developed countries due to human and economical costs. Nowadays, no effective treatment for these diseases has been found yet, mainly due to the presence of the blood-brain barrier (BBB), which limits the entrance of exogenous compounds to the central nervous system (CNS). Due to this drawback, the amount of active principles administered has to be increased to ensure that therapeutic concentrations reach the CNS. However, high amounts of actives in the bloodstream usually produce a variety of side effects without achieving their therapeutic goals (Béduneau, 2007). Therefore, various advanced delivery systems are being developed to achieve a localized and controlled drug release into the brain to increase the drug activity and decrease the side effects (Béduneau, 2007; Kabanov, 2007). One promising strategy that has gained relevancy during the last years is the use of polymeric nanoparticulate systems with their surface functionalized to achieve an active targeting to cross the BBB and reach the CNS, once administered by the intravenous route (Aktas, 2005). In spite of the wide bibliography reporting nanoparticles that cross the BBB, the maximum crossing efficiency values reported are below 15%. Therefore, this strategy still needs to be improved (Tosi, 2011). Nanoparticles for biomedical applications, like all biomedical devices, must be non-toxic; formulated using biodegradable and biocompatible elements, such as the poly(lactic-co-glycolic acid) polymer (PLGA) as well as low-toxicity solvents and surfactants (Trotta, 2003). The use of nano-emulsions as the colloidal template system to prepare nanoparticle dispersions has the advantage among other conventional systems of the presence of small droplets, each one acting as an individual template to form a single nanoparticle. Two different approaches have been proposed for the nanoparticle formation from nano-emulsion templating: *in situ* monomer polymerization and use of preformed polymers. In the former approach, safety concerns arise due to the presence of remaining residual toxic monomers and/or reactive byproducts (Ugelstad, 1973; Antonietti, 2002; Asua, 2002). That is why the second approach, the use of preformed polymers, seems more appropriate, since safety concerns are reduced (Soppimath, 2001; Anton, 2008; Vauthier, 2009; Solans, 2012).

Nano-emulsions are emulsions with nanometric droplet sizes, typically in the range between 20 and 500 nm. Due to this small size, they show enhanced stability against creaming or sedimentation and a transparent to translucent aspect. Nano-emulsion preparation has been traditionally performed with high-

energy methods. However, in the last years, low-energy emulsification methods have gained more attention. These methods represent a better alternative to prepare nano-emulsions, taking advantage of the intrinsic chemical energy of the system components which is released during the emulsification (Solans, 2005 and 2012; Anton, 2008). The most used low-energy methods consist on phase inversion due to a change on the spontaneous curvature of the surfactant either by a change on the composition (Phase Inversion Composition, PIC, method) or a change in the temperature (Phase Inversion Temperature, PIT, method). These methods are advantageous in comparison with high-energy methods because they allow producing nano-emulsions with smaller droplet sizes and lower polydispersity. Moreover, the use of the PIC method, if performed at low temperature, is especially recommended when dealing with thermolabile compounds. Although the literature reporting the production of nanoparticles by nano-emulsion templating is wide, only few articles have described the use of low-energy methods to obtain nano-emulsions (Spernath, 2007).

The **main objectives** of this research was the preparation of polymeric nanoparticles, by nano-emulsion templating, as advanced delivery systems targeting the BBB. This objective includes the partial following objectives:

1. Formulation of Oil-in-Water (O/W) nano-emulsions by low-energy methods with low toxicity components: solvent, polymer and surfactant.
2. Preparation of polymeric nanoparticles by solvent evaporation of the template nano-emulsions and nanoparticle characterization.
3. Encapsulation in the nanoparticles of fluorescent dyes (as imaging agents), drugs (as advanced drug delivery systems) and gene material (as non-viral gene delivery systems).
4. Nanoparticle surface functionalization with targeting purposes, using dendrons and antibodies; and the characterization of the functionalized nanoparticles.
5. *In vitro* and *in vivo* studies of nanoparticles in contact with cells and organisms, such as their toxicity, interaction with blood components, gene transfection and BBB crossing.

To achieve these objectives, the following **working plan** was established:

- Formation of O/W nano-emulsions by the PIC method:
  o Confirmation of phase inversion in the formation of nano-emulsions.
  o Determination of the nano-emulsion formation region in the corresponding phase diagrams of the selected systems.
  o Nano-emulsions characterization, mainly droplet size, by means of Dynamic Light Scattering (DLS) measurements, surface charge, by means of electrophoretic mobility measurements, and stability.

- Formation of polymeric nanoparticles from nano-emulsion templating:
  o Solvent evaporation of selected nano-emulsions under controlled conditions.
  o Characterization of the nanoparticle dispersions, mainly the size by means of DLS, TEM and atomic force microscopy (AFM) measurements as well as the surface charge and the stability.

- Encapsulation of diverse compounds in the core of nanoparticles:
  o Coumarin 6 as a model fluorescent dye. Study of the encapsulation efficiency and *in vitro* drug release.
  o Magnetic nanoparticles to use nanoparticles as diagnostic systems.
  o Loperamide hydrochloride as a model central analgesic drug. Study of the encapsulation efficiency and *in vitro* drug release.
  o Galanthamine as a model antiapoptotic drug. Study of the encapsulation efficiency; *in vitro* drug release and drug activity.

- Surface functionalization of nanoparticles with:
  o Cationic dendrons to achieve a positive surface charge to electrostatically bind oligonucleotides. Study of the appropriate nanoparticle / dendron ratio.
  o Oligonucleotides to use nanoparticles as advanced non-viral gene delivery vectors. Study of the complexation ratio and characterization of the complexes formulated.
  o The monoclonal anti-transferrin receptor antibody to specifically target the BBB. Study of the efficacy of the conjugation reaction and conjugated nanoparticle characterization.

- *In vitro* testing of nanoparticles in cell cultures:
  o Assessment of the cytotoxicity of the nanoparticles by means of the MTT test.
  o Nanoparticle transfection into culture cells by means of the luciferase test.
  o Study of the reaction of nanoparticles with blood components by means of the haemolytic activity generated, the interaction with blood proteins and the activation of the complement activity.

- *In vivo* study of the nanoparticles BBB crossing by means of intravenous administration of the particles followed by the study of the central analgesic effect generated.

Chapter 3

EXPERIMENTAL

In this thesis, the water and oil and surfactant components are abbreviated as W, O, S, respectively. All the percentages are expressed as weight percentages, unless otherwise stated.

3.1. Materials

3.1.1. Polymers

3.1.1.1. Poly(lactic-co-glycolic) acid

D,L-poly(lactic-co-glycolic) acid (PLGA), with a ratio of lactic/glycolic of 75/25 was used. This is a copolymer of lactide and glycolide (Figure 3.1) with a molecular weight between 10,000 and 15,000 g/mol (Boehringer Ingelheim, Evonik). It appears as a white powder at room temperature (25ºC).

PLGA is a bioadsorbable, biocompatible and biodegradable aliphatic polyester, which has been clinically used in intravenous administrations (Rowe, 2006; Italia, 2009; Tosi, 2010) due to its approval by the FDA for parenteral administration (Kreuter, 2014).
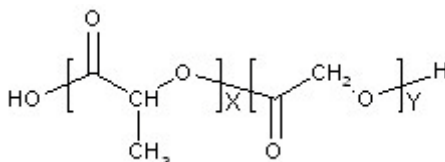
Figure 3.1: Chemical structure of PLGA. "x" represents the number of units of lactic acid and "y" represents the number of units of glycolic acid.

3.1.1.2. Poly(ethylene glycol)

Poly(ethylene glycol) (PEG) is a FDA approved hydrophilic polymer (Alexis, 2008), composed of a variable number of ethylene glycol units (Figure 3.2). In the present thesis, diverse PEGs (Sigma Aldrich) were tested, varying their molecular weight (from 400 Da to 6000 Da). Its appearance at room temperature (25ºC) depends on its molecular weight: PEGs with molecular weights below 1000 Da are viscous colorless liquids, while higher molecular weight PEGs are waxy white solids. Their physicochemical characteristics also depend on their molecular weights (e.g. the melting point increases by increasing the molecular weight) (Harris, 1992).

It has been widely used in pharmaceutical formulations, to produce the so-called "stealth effect"; it decreases the protein and cell membrane interaction with the coated nanostructures, thus reducing immunogenicity and antigenicity of the nanosystems (Harris, 1992).
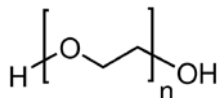
Figure 3.2: Chemical structure of PEG. "n" is the number of ethylene oxides units.

3.1.2. Surfactant

A polysorbate surfactant (Polysorbate 80 from Croda, commercial name: Tween® 80) based on a natural fatty acid commonly used to stabilize emulsions in the biomedical and pharmaceutical field has been used (Gelperina, 2002; Kreuter, 2003; Rowe, 2006). This nonionic ethoxylated surfactant is a yellow translucent liquid, with a hydrophilic-lipophilic balance (HLB value) of 15 that enables the formation of O/W nano-emulsions (Croda International Plc, 2014) at room temperature (25ºC). It is a generally accepted as safe (GRAS) surfactant, accepted for mucosal, oral, ocular, parenteral and topical delivery (Date, 2010). It has a critical micellar concentration (CMC) of 0.012 mM (0.0016 w/v %; 13-15mg/L) at 25ºC (Sigma-Aldrich, 2014).

Polysorbate 80 (Figure 3.3) is a surfactant widely used for biomedical applications, specifically for the intravenous administration of nanoparticles targeting the BBB, since it has been reported that polysorbate 80 enhances the BBB crossing (Chen, 2011; Wohlfart, 2012; Kreuter, 2013(2)).
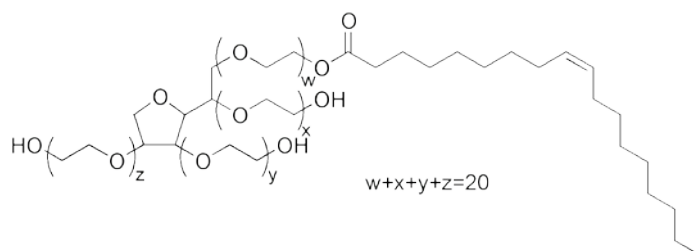
Figure 3.3: Chemical structure of polysorbate 80. "w,x,y,z" represent the number of units of ethylene oxides.

3.1.3. Oil components

3.1.3.1. Ethyl acetate

This is an organic solvent (Merck) that belongs to class 3 of solvent classification of the ICH Guidelines (Figure 3.4) (Pinto-Reis, 2006). It was chosen due to its low toxic potential and suitable properties for dissolving the polymer and for its evaporation at mild temperature. It is a transparent liquid with a density of 0.902g/mL at 20ºC, partially water soluble at 25ºC, being more soluble in water at lower temperatures. It is miscible with acetone¸ chloroform, dichloromethane, ethanol 95%, ether and most other organic liquids. Its high volatility makes it particularly suitable for the solvent evaporation method (Rowe, 2006). Some of its chemical properties are the following: autoignition temperature of 486.1ºC, boiling point of 77ºC, freezing point of -83.6ºC, and refractive index of 1.3719.
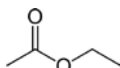
Figure 3.4: Chemical structure of ethyl acetate.

3.1.3.2. Ethanol

This is an organic solvent (Merck) that belongs to class 3 of solvent classification of the ICH guidelines (Figure 3.5) (Hu, 2011). It is a transparent liquid with a density of 0.789g/mL at 20ºC, and a molecular weight of 46.07g/mol. It is completely soluble in water at 20ºC, miscible with chloroform, ether, glycerin and water (Rowe, 2006). Some of its chemical properties are the following: autoignition temperature of 363ºC, boiling point of 78.1ºC; melting point of -114ºC, and a refractive index of 1.361.
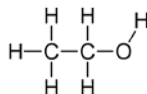
Figure 3.5: Chemical structure of ethanol.

3.1.3.3. Aliphatic hydrocarbons

n-Hexadecane is a linear alkane (Sigma-Aldrich, purity ≥ 99wt %) with a molecular weight of 226.44 g/mol, a melting point of 18ºC and a refractive index of 1.434. It is a colorless liquid, insoluble in water (Figure 3.6).
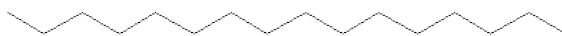
Figure 3.6: Chemical structure of n-Hexadecane ($C_{16}H_{34}$).

Squalane is a natural branched hydrocarbon (Sigma-Aldrich, purity = 99wt %) with a molecular weight of 422.81 g/mol, a melting point of -38ºC, a refractive index of 1.452 and a density of 810mg/mL. It is a colorless transparent liquid, insoluble in water (Figure 3.7).
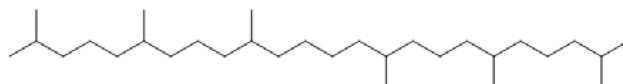
Figure 3.7: Chemical structure of squalane ($C_{30}H_{62}$).

3.1.3.4. Magnetic nanoparticles (MNPs)

Iron oxide nanoparticles (IONPs) used supplied from the Nanocrystals and Chemistry Group from the Institute of Materials Sciences from Madrid (ICMM-CSIC) in the context of MULTIFUN Project.

3.1.4. Aqueous components

3.1.4.1. MilliQ water

Deionized water, designatedas MilliQ water, was used as aqueous phase. It is worth noting that for all _in vitro_ and _in vivo_ experimentation, 10wt% of diethylpyrocarbonate (DEPC) was added to MilliQ followed by the autoclave procedure, to assure nuclease-free water.

3.1.4.2. Phosphate buffered saline (PBS)

Phosphate buffered saline (PBS), which consists in a mixture of sodium chloride (NaCl), sodium phosphate monobasic ($NaH_2PO_4·H_2O$) and disodium phosphate dibasic ($Na_2HPO_4·2H_2O$). The concentration of the salts varies depending on the application. In the present thesis, the concentrations of salts were the following: 136.89 mM of NaCl, 0.93mM of $NaH_2PO_4·H_2O$ and 16.76mM of $Na_2HPO_4·2H_2O$; adjusting the pH at 7.4 with orthophosphoric acid (2.28M). With this buffer, a pH

of 7.4 and an osmolality of 300 mOsm/kg are achieved, thus simulating the physiological blood conditions. The salts used to adjust the pH are a key issue, since some salts could affect the nature of the system components (e.g. Coumarin 6 fluorescence varies in the presence of triethylamine).

3.1.4.3. Hepes buffer

Hepes (4-(2-hydroxyethyl)-1-piperazineethanesulfonic acid) buffer (Figure 3.8) is a zwitterionic organic chemical buffering agent used mostly in cell cultures, as it maintains better the pH at a constant value than other buffers. This buffer was used at 20mM, mainly when nanoparticles were intended for their study *in vitro*, since this medium is appropriate for cell cultures but not for *in vivo* administration because it has a lower osmolality as compared with physiological values.
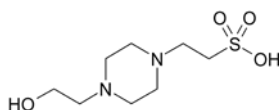
Figure 3.8: Chemical structure of Hepes.

3.1.4.4. TBE buffer

Tris/Borate/EDTA buffer, commonly known as TBE buffer, consist on a mixture of the Tris base, boric acid and ethylenediaminetetracetic acid (EDTA). This buffer was used in the present thesis for the electrophoretic experiments involving oligonucleotides such as the electrophoretic mobility shift assay.

3.1.4.5. Veronal-buffered saline (VBS^{2+})

The veronal buffered saline (VBS^{2+}) consist on a mixture of 0.15mM Ca^{2+} with 0.5mM Mg^{2+}ions, containing EDTA 40mM. This buffer was used for the determination of the activation of the complement system by means of measuring the cleavage of the C3 complement protein in a 2D-immunoelectrophoresis.

3.1.5. Probes and dyes

3.1.5.1. Coumarin 6

Coumarin 6 is a lipophilic fluorescent dye (Figure 3.9) (Sigma-Aldrich, purity = 98 wt %) that has an amino donor group and a carbonyl acceptor group which enables the emission of green light due to the FRET phenomenon (Abdel-Mottaleb, 1989). It has an excitation peak around 444 nm and an emission peak around 505 nm dissolved in ethanol.
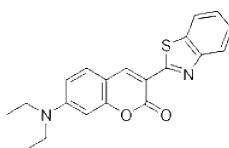
Figure 3.9: Chemical structure of coumarin-6.

3.1.5.2. Fluorescein isothiocyanate (FITC)

This is a hydrophilic fluorescent dye (Figure 3.10) (Sigma-Aldrich, purity > 90 wt %) derivative of fluorescein, functionalized with the isothiocyanate reactive group (SCN). It is reactive towards nucleophile groups. It has an excitation peak around 495 nm and an emission peak around 519 nm when dissolved in water.
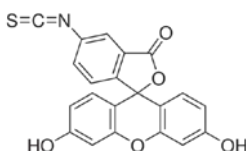
Figure 3.10: Chemical structure of FITC.

3.1.5.3. AlexaFluor 555

AlexaFluor 555 is a fluorescent dye with enhanced photostability and reduced self-quenching (Figure 3.11). It has an excitation peak around 555 nm and an emission peak around 565 nm when dissolved in water.

In the present thesis, this dye was used attached to a secondary goat anti-mouse IgG$_{2a}$ antibody against the 8D3 primary antibody (Life Technologies), with the aim to detect the presence of the 8D3 antibody by fluorescence microscopy, as widely reported in previous studies (Manich, 2013).
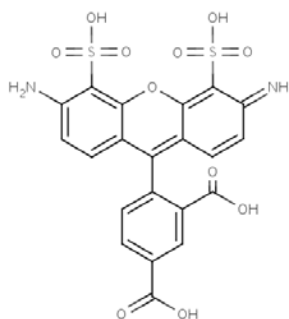
Figure 3.11: Chemical structure of AlexaFluor 555.

3.1.5.4. Rodhamine B

This is a hydrophilic pink – violet fluorescent dye (Sigma-Aldrich, purity = 95 wt %) (Figure 3.12). It has an excitation peak around 554nm and an emission peak of around 627nm in acidic medium.
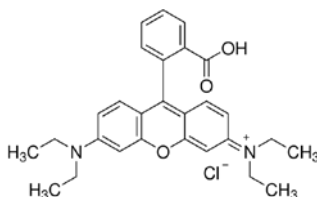
Figure 3.12: Chemical structure of Rhodamine B.

3.1.5.5. Sudan black

This is a lypophilic dye (Scharlau) that has been widely used to stain lipidic cell components (Figure 3.13). It has a maximum absorption of around 596–605nm.
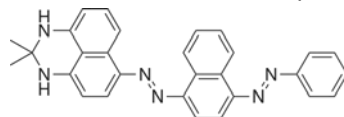
Figure 3.13: Chemical structure of Sudan Black.

3.1.6. Active molecules

3.1.6.1. Loperamide hydrochloride

Loperamide hydrochloride (LOP, Sigma Aldrich) is a lipophilic drug that, apart from its antidyarreic activity, is active in the central nervous system with antinociceptive effects, but it cannot cross the BBB by itself (Kreuter, 2007). Its presentation is like a white crystalline powder and its chemical structure is presented in Figure 3.14. It is freely soluble in methanol, isoprophil alcohol and chloroform, soluble in DMSO, and slightly soluble in water (NCBI, 2014 and SantaCruz Biotechnology, 2014). It has a molecular weight of 513.51 g/mol and a maximum of absorption around 220 – 300 nm, depending on the solvent (USP Pharmacopoeia, 2014; Hewala, 1995). It has been used in this thesis as a model drug to study the pass of the nanoparticles through the blood-brain-barrier (Kreuter, 2007; Gabathuler, 2010; Tosi, 2010).
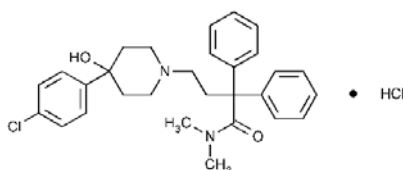
Figure 3.14: Chemical structure of Loperamide hydrochloride.

3.1.6.2. Galanthamine hydrobromide

Galanthamine is a natural compound extracted from the bulbs of different species of *Amaryllidaceae* family (Figure 3.15). It is an active molecule that acts as a selective, reversible and competitive inhibitor of the acetylcholinesterase (AChE), thus increasing the acetylcholine levels triggering to an improved neurotransmission. For this reason, it produces an antiapoptotic action that makes it to be considered as a neuroprotector. As a drug, it was approved by the FDA for the symptomatic treatment of mild to moderate Alzheimer's disease (Villaroya, 2007). Galanthamine is soluble in water (20 mg/ml) and in DMSO (10 mg/ml), each yielding a clear, colorless solution. It has a molecular weight of 368.27 g/mol and a maximum absorption around 310 nm.
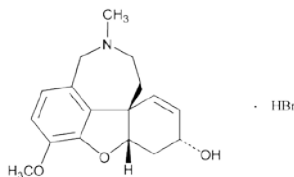
Figure 3.15: Chemical structure of Galanthamine hydrobromide.

3.1.7. Functionalization agents

3.1.7.1. Carbosilane cationic dendrons

Carbosilane dendrons were kindly provided by the Group of Dendrimers for Biomedical Applications of the University of Alcalá de Henares. These dendrons have an amine focal point; the ramification units are composed by a carbosilane (C-Si) structure and the functional end groups are quartenized amines (ammonium groups). The carbosilane structure confers to the dendron major water stability, as compared with other structures such as Si-O, and water solubility, higher with lower dendron generations (Bermejo, 2007; Gonzalo, 2010). They were synthetized as described by *Fuentes-Paniagua* using the thiol-ene click chemistry (Fuentes-Paniagua, 2013). Second generation dendron (G2SN) and third generation dendron (G3SN) were selected for the nanoparticle functionalization. G2SN (MW = 1510.31g/mol) has two ramification points in its backbone, thus resulting in a structure with four ramifications, each one with a positive charge (Figure 3.16). However, since in G3SN (MW = 2947.85g/mol) there is another ramification point, it has eight ramifications with eight positive charges per molecule (Figure 3.17).
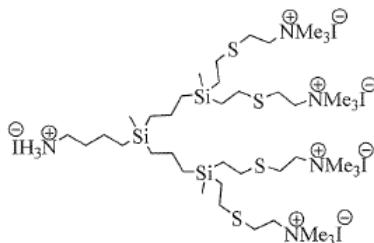
Figure 3.16: Structure of the G2SN dendron.
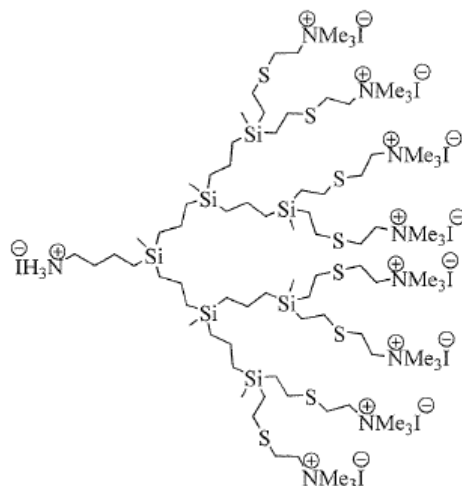
Figure 3.17: Structure of the G3SN dendron.

3.1.7.2. Anti-transferrin receptor monoclonal antibody (8D3)

The transferring receptor (TfR) is a membrane receptor of the transferring molecule, oberexpressed in many tumors and in the blood-brain barrier (BBB) (Ulbrich, 2009). 8D3 is the monoclonal anti-TfR antibody selected (IgG2a monoclonal antibody from AbD Serotec), since it is specific of mouse and mice models will be used for the *in vivo* experimentation (Nicolas, 2003; Pardridge, 2008). It has an estimate molecular weight of around 160,000 Da.

3.1.7.3. Antisense oligonucleotides (ASO)

An antisense phosphorothioate oligonucleotide (sequence 5'-CGT TTC CTT TGT TCT GGA-3') complementary to the mRNA of the *Renilla* luciferase gene (Grijalvo, 2014) targeted to a predominant accessible site between 20 and 40 nucleotides was purchased from Proligo (Sigma-Aldrich). It was prepared by the Group of Nucleic Acids from IQAC-CSIC (IP: Dr. R. Ertija). The ASO was used in the phosphorotioate form due to its enhanced stability in front of nucleases attack, their relative ease of synthesis, their highly water solubility and their enhanced antisense activity (Dias, 2002; Grijalvo, 2014).

3.1.7.4. Small interference RNA (siRNA)

Small interference RNAs (siRNA) are short double-stranded segments of RNA that, once in the cytoplasma, bind their complementary mRNA thus producing its degradation. There are usually rapidly degraded by RNAses, therefore, their protection is a must when working with them, namely when using the intravenous route of administration (Weber, 2008). A phosphorotioate *Renilla* siRNA (Guide: 5'-AUCUGAAGAAGGAGAAAAA-3'; Passenger: 5'-UUUUUCUCCUUCUUCAGAU-3') was used, since its stability is higher than non phosphorotioate siRNAs (Grijalvo, 2014). It was kindly provided by the Group of Nucleic Acids from IQAC-CSIC (IP: Dr. R. Ertija).

3.1.7.5. Lentiviral plasmid vectors

The lentiviral plasmid vector: hrl-mRFP-ttK was used in the resent thesis. This vector was kindly provided by the group of Gene Therpay (IP: Dr. J Blanco) of the IQAC-CSIC. It has a molecular weight of around 100KDa. This plasmid encodes for three chimeric genes: the synthetic *Renilla* luciferase reporter gene (hrl), the monomeric red fluorescence protein (mRFP1) and a truncated but functional version of the timidine kinase coding sequences (ttK) (Ray, 2004).

3.1.8. Other chemical compounds

The following compounds, in alphabetical order, were used:

- Acetonitrile HPLC grade (from Panreac), as eluent for HPLC measurements.
- Agarose > 90% (from Sigma-Aldrich).
- Acrylamide > 99%, HPLC grade (from Sigma-Aldrich).
- Decahydronaphthalene (Decalin) (from Merck).
- Dimethyl sulfoxide (DMSO) (from Sigma-Aldrich).
- Disodium monohydrogenphosphate dihydrate: $Na_2HPO_4 \cdot H_2O$ (from Merck).
- Dulbecco's Modified Eagle's Medium (DMEM), with 10 wt % heat-inactivated fetal bovine serum (FBS) (Gibco).
- Ethanol absolute for UV, IR, HPLC (from Panreac).
- Fetal bovine serum (FBS) (Sigma-Aldrich).
- Goat anti human-C3 monoclonal antibody (Sigma-Aldrich).

- Hepes salt (from Sigma-Aldrich).
- Hydrochloric acid 37%: HCl (from Merck).
- Lipofectamine 2000 (from Invitrogen).
- Luciferase assays kits (Promega)
- *N*-(3-Dimethylaminopropyl)-*N*-ethylcarbodiimide hydrochloride(EDC) (Fluka).
- *N*-hydroxisuccinimide sodium salt (NHS) (from Sigma-Aldrich).
- Ninhydrin (from Sigma-Aldrich).
- Opti-MEM® Reduced Serum Medium (from Gibco, Life Technologies).
- Ortophosphoric acid 85%: H_3PO_4 (from Merck).
- Phenol p.a. ACS, Reag. Ph Eur (from Merck).
- Phosphotungstic acid hydrate: $12WO_3 \cdot H_3PO_4 \cdot xH_2O$ (PTA) (Fluka), for TEM.
- Potassium bromide (KBr) (Merck).
- Potassium cyanide: KCN (Fluka), for the IR measurements and Kaiser test.
- Pyridine anhydrous, 99.8% (from Sigma-Aldrich).
- Sodium chloride: NaCl (purity ≥ 99.9% from Carlo Ebra).
- Sodium hydroxide: NaOH (purity ≥ 99.0% from Carlo Ebra).
- Sodium dihydrogenphosphate monohydrate: $NaH_2PO_4 \cdot H_2O$ (from Merck).
- Tetrahydrofurane HPLC grade (Merck), as eluent for GPC measurements.
- Water: double distilled (milliQ Water).

3.1.9. Cell cultures

3.1.9.1. HEK 293 cells

HEK 293 cells correspond to a human embryonic kidney cells grown in tissue culture. They were cultured at 37ºC, 5% CO_2 in DMEM partially supplemented with 10% FBS, 100mg/mL of penicillin and 100μg/mL of streptomycin. Cells were regularly passaged in order to maintain exponential growth. Twenty-four hours before their experimental use, at 40 – 80% confluence, they were trypsinized and diluted 1:5 with a fresh medium without antibiotics (about 1-3 x 10^5 cells/mL) and transferred to a 24-well or 96-well plate (500μL or 100μL respectively).

3.1.9.2. HeLa cells

HeLa cells were firstly obtained from Henrietta Lacks. They correspond to immortalized cell line from a human cervix carcinoma. In the present thesis, they were cultured at 37ºC, 5% CO_2 in DMEM partially supplemented with 10% FBS,

100mg/mL of penicillin and 100μg/mL of streptomycin. Cells were regularly passaged in order to maintain exponential growth. Twenty-four hours before their experimental use, at 40 – 80% confluence, they were trypsinized and diluted 1:5 with a fresh medium without antibiotics (about 1-3 x 10^5 cells/mL) and transferred to a 24-well or 96-well plate (500μL or 100μL respectively).

3.1.9.3. U87 cells

U87 cell line corresponds to a human glioblastoma / astrocytoma immortalized cell line. The cells were cultured at 37ºC, 5% CO_2 in DMEM/ Nutrient Mixture F-12 (DMEM/F12) partially supplemented with 10% FBS, 100mg/mL of penicillin and 100μg/mL of streptomycin. Cells were regularly passaged in order to maintain exponential growth. Twenty-four hours before their experimental use, at 40 – 80% confluence, they were trypsinized and diluted 1:5 with a fresh medium without antibiotics (about 1-3 x 10^5 cells/mL) and transferred to a 24-well or 96-well plate (500μL or 100μL respectively).

3.1.10. Animal models

The *in vivo* experimental part of this thesis was performed in collaboration with expert groups. Every effort was made to minimize the number of animals used and any animal suffering.

CD1 mice models were used for the animal experimentation (Harlan) with a mass of around 30 – 35 grams, which corresponds to 8 weeks life.

3.2. Methods

3.2.1. Determination of PLGA molecular weight

The molecular weight of the PLGA was determined with the gel permeation technique (GPC). A Shimadzu liquid chromatography instrument composed of two pumps LC-10AT, an automatic system of sample injection SIL-10AD and a UV detector LC-10ATVP was used. The column used was a MZ-Gel SD plus 10^3 Å filled with 5μm particles of cross-linked styrene/divinylbenzene high-performance copolymer. Each sample, including polymer in different preservation states, was analyzed in triplicate. Samples of 1 mL of PLGA dissolved in tetrahydrofurane (THF) at a concentration 0.4wt % were prepared together with the polystyrene standards for the calibration (EasyVial PS-M 2mL, GPC/SEC Calibration Standards, Agilent). PLGA produces an absorption peak around 230 nm wavelength (Laquintana, 2009). GPC conditions were fixed at a flow rate of 1 mL/min, injecting 50 μL volume of each sample, and studying the chromatogram at a wavelength of 230 nm and 254 nm simultaneously (absorption of PLGA and standards respectively), during 15 min; as PLGA retention time is about 8 – 9 min. The mobile phase used was THF. Measurements were analyzed with the Shimadzu Class-VP software. In addition, theoretical calculations of the PLGA molecular weight were also performed from the intrinsic viscosity data given by the supplier. The molecular weight of a polymer is related with the intrinsic viscosity by the Mark-Houwink equation (MHE):

$$MW = ([\eta] / K)^{1/\alpha} \tag{3.1}$$

where MW is the polymer molecular weight, $[\eta]$ is the intrinsic viscosity, K and a are constants of the MHE (K = 5.45x10-4 ; α=0.73).

3.2.2. Determination of the glass transition and melting temperatures

Glass transition temperature experiments were performed in powder state. Therefore, dispersions were lyophilized prior to their use. Lyophilization was performed with the Christ Alpha 2-4 LD Plus Lyophilizer. Samples were placed in a glass container resistant to lyophilization conditions. Then, to freeze the samples, they were submerged in a mixture of dry ice with acetone, achieving temperatures as low as -78ºC. Then, they were placed in the lyophilizer for, at least, 24 hours at the following starting conditions: -89ºC and 0.1 mbar. Around

15 mg of sample were placed in the containers to perform the assay. Differential scanning calorimetry (DSC) measurements were carried out using a DSC model DSC 821 from Mettler Toledo equipped with a Pt temperature captor. Measurements were performed in a range temperature between -10ºC to 100ºC, at intervals of 10ºC; performing a first heating cycle, followed by a cooling cycle and a second heating cycle. The sample measurement is carried out with an inert reference.

3.2.3. Solubility determinations

3.2.3.1. Nano-emulsion phases

The partial solubility between the aqueous and the oil phase was assessed by macroscopic visual observation of the prepared samples. A sample of 8 grams of the aqueous (or oil) component was placed in a transparent glass tube. Droplets of the oil (or aqueous) component were stepwise added to the first component. After a few seconds of stirring, the visual appearance of the sample was assessed. The limit of solubility was reached when the solution turned to a turbid appearance, thus indicating that the oil (or aqueous) component was not any longer soluble in the aqueous (or oil) component.

3.2.3.2. Drugs in the solvents

The solubility of loperamide and galanthamine was determined using two techniques. A first approximation of the solubility consisted on the macroscopic optical observation of the samples after the addition of increasing amounts of the drug on a fixed solvent volume of around 5 grams. When the addition produced a change in the visual appearance (e.g. increase on the turbidity or appearance of powder suspend in the sample), this concentration was taken as the maximum drug solubility.

After these screening tests, drug solubility was calculated more precisely by the measurement of the added drug concentration with an appropriate technique: HPLC determination for loperamide and fluorescent determination for galanthamine (Date, 2007). A **HPLC** Breeze^{TM} 2 (Waters Corporation, Milford, MA, USA) equipped with a 5 mm x 15 cm x 0.46 cm Spherisorb1 ODS column, and a

UV detector was used. Loperamide hydrochloride (LOP) produced the maximum absorption at 220 nm wavelength. HPLC conditions were fixed at a flow rate of 1 mL/min, injecting 50 µL volume of sample, and detecting the variation of the signal during 50 min, (as LOP showed a retention time of about 42 min). The mobile phase used was 1.824 mM ortophosphoric acidacetonitrile (50/50% v/v), at a pH = 3.5 and a temperature of 30ºC (based on Pharmacopeia Standard Specifications provided from Sigma-Aldrich). A Cary Eclipse **Fluorescence Spectrophotometer** (Varian) was used for galanthamine quantification. It uses a Xenon flash lamp as emitting laser, to increase the sensitivity. The excitation wavelength of galanthamine was set at 280nm, and the emission at 280–400nm (emission peak≈310 nm) (Maláková, 2007). Calibration curves were plotted to correlate each fluorescent signal to a concentration of the compound. At least three measurements per sample were performed.

3.2.4. Nano-emulsion preparation by the phase inversion composition method

O/W nano-emulsions were obtained at 25ºC by the PIC method, with the aqueous phase / polysorbate surfactant / [4 wt. % in ethyl acetate] system. The aqueous phase was water or PBS (different concentrations of electrolytes). The oil component, consisting in PLGA polymer dissolved in ethyl acetate was mixed overnight. A mixture of oil component and surfactant was prepared at defined oil/surfactant (O/S) ratio and was homogenized. Afterwards, the required amount of water was stepwise added (at a flow rate around 0.90 mL/min), with a syringe, to the O/S mixture at room temperature under continuous stirring (Vortex Genie2 Model G560E, maximum shaking speed) to obtain O/W nano-emulsions (Calderó, 1997).

For the preparation of fluorescent nano-emulsions, the fluorescent label Coumarin-6 was incorporated in ethyl acetate at a concentration of 0.1wt% together with the polymer. The same procedure was followed by the encapsulation of loperamide and galanthamine at 0.1wt% in the oil phase. To establish the nano-emulsion formation domain region in the corresponding phase diagrams, the exact percentages of the components of each sample were calculated based on the total composition of the nano-emulsion. Nano-emulsions were observed accurately under a spotlight to determine the region of formation. Those samples with a transparent or translucent appearance, showing bluish or

reddish shine were considered nano-emulsions. In order to distinguish nano-emulsions from microemulsions, the same systems were prepared mixing all the components at once. Furthermore, each individual composition was prepared at least three times, to test the reproducibility of the system.

3.2.4.1. Determination of the phase inversion

Since nano-emulsions were prepared by the PIC method, an inversion of the phases, from W/O to O/W structures, was expected when gradually adding the aqueous component to the mixture of O/S. to study the inversion of the phases, two methodologies were carried on. For the systems without electrolytes in the aqueous phase, the inversion of the phases was studied by means of **conductivity measurements**, as previously reported (Calderó, 2011), at 25ºC, by means of a Crison-GLP31 conductimeter, equipped with a Pt/platinised electrode, model 52-92 (cell constant=1cm^{-1}) and a temperature sensor, model 55-31. 4 grams of the sample were prepared, at a fixed O/S ratio, and increasing percentages of water in steps of 10wt%, were added. Conductivity was measured after each water addition. For the systems with electrolytes in the aqueous phase, conductivity measurements could not be performed, since the high amount of salts in the aqueous phase produced an increase in the conductivity, not allowing to evidence phase inversion. For this reason, **two colorants** were used. An hydrophilic dye, rhodamine B (red colour) and sudan black as the lipophylic dye (black coloration) were chosen. About 2 grams of each sample were added to a small amount of each dye, previously placed in a glass tube, and after 5 minutes, their visual appearance was assessed. A diffusion of the hydrophilic colorant (rodhmine B) was only expected in O/W type structures while the lipophylic dye (sudan black) would diffuse in W/O type structures. For bicontinuous structures, both dyes would diffuse but in a lesser extent.

3.2.5. Nanoparticle preparation by solvent evaporation

Nanoparticles were prepared from nano-emulsions by evaporating the solvent, ethyl acetate (or the mixture of ethyl acetate with ethanol), under reduced pressure (43 mbar, 25ºC, 150 rpm) for 45 minutes (Desgouilles, 2003). The Rotavapor® R-210/215 (Buchi Labortechnik AG) was used for the nano-emulsion

solvent evaporation in a controlled and safe manner. After the evaporation, in order to maintain the pH and osmolality, the required amount of water was added to achieve the same weight than the initial weight of the nano-emulsion. The nano-emulsion weight had been reduced due to the evaporation of the solvent and eventually, small amounts of water of the aqueous phase.

3.2.5.1. Batch reproducibility

Industrial production of nanoparticles for biomedical applications, like in other areas, requires that all batches of prepared nanoparticles have the same characteristics. In order to assess the batch reproducibility, nanoparticle droplet size and surface charge of different batches of 4 and 15 grams of nanoparticles were evaluated as explained above. The Student T test was performed to assess the statistical significance of the repeated measures of a same sample.

3.2.6. Nanoparticle purification

The nanoparticle purification was carried out by means of a dialysis step, in order to withdraw all the surfactant excess. The sample to purify was placed inside the dialysis bag, which was placed inside a receptor solution of a volume of at least 100 times the volume of the sample to purify. The receptor solution was changed three times during a total time of 24 hours. The dialysis bags were hydrophilic, made of Biotech Grade Cellulose Ester with a MWCO = 3,500 – 5,000 Da, since the MWCO should be at least three times the molecular weight of the substance to eliminate (Spectrumlabs, 2014). Dialysis bags were prepared manually, from dialysis tubing cellulose, or Float-a-Lyzer or Micro Float-a-Lyzer devices were used (Spectrumlabs). The nature of the receptor solution depended on the desired application of the nanoparticles. For most of the applications, a receptor solution of PBS was used, to obtain the nanoparticles dispersed in a solution simulating physiological conditions. For the *in vitro* cell culture experiment, the receptor solution was Hepes buffer, due to the preference of cell cultures for this buffer.

3.2.7. Nanoparticle concentration

3.2.7.1. Concentration by inverse dialysis

A receptor solution of PEG 400 KDa (50g/L) was used to increase the osmotic pressure, thus enhancing the exit of the dispersant of nanoparticles. To test the influence of the receptor solution volume on the concentration, 3 grams of the sample were dialyzed for 24 hours at room temperature, in triplicates, against a variable volume of the receptor solution (10, 25 and 50mL). Their size and surface charge were characterized prior and after the dialysis, as well as the mass of the nanoparticle dispersion. Results are expressed as a concentration factor, calculated dividing the final mass for the initial mass of the nanoparticle dispersion.

3.2.7.2. Concentration using commercial devices

The Centriprep® YM-3, 3kDa, centrifugal filter units (Millipore) were used, following the manufacturer's instructions. Among the concentration by an inverse dialysis, these filters have the advantage of being faster.

3.2.8. Droplet and nanoparticle size characterization

The hydrodynamic radius of the droplets of the nano-emulsions as well as the hydrodynamic radius of the nanoparticles was determined by **Dynamic Light Scattering** (DLS), with a 3D DLS Spectrometer (LS Instruments, 3D Cross-correlation Correcting Multiple-scattering) equipped with a He-Ne laser (632.8 nm). The scattered light can be detected at different angles ranging from 20 to 134º. At the end of the scattered light pathway, a correlator is placed to analyze the light. The basis of this technique assumes that all particles smaller than 1 μm suspended in a solvent are constantly moving following the Brownian movement, which is produced by the thermal energy generated due to the interaction of the elements with the solvent (Pecora, 2000). They scatter the light if they are under a monochromatic spotlight from a laser. The fluctuation of the intensity of the scattered light depends on some parameters, such as the particle size or shape and the refractive indexes (measured with an Abbe Refractometer Type 3T from ATARGO®). These fluctuations in the intensity of the scattered light are related with the Brownian movement by means of the diffusion coefficient of the

particles with the solvent. The Stokes-Einstein equation relates the diffusion coefficient (D) with the hydrodynamic radius (R_h) of the particles (Equation 3.2).

$$D = \frac{k_B T}{6\pi\eta R_h}$$
(3.2)

where k_B is the Boltzmann's constant; T, the temperature and η the viscosity of the continuous phase. The diffusion coefficient is not only dependent on the size of the particles, but also on the structure of the surface as well as on the type and concentration of ions dissolved in the solvent. Thus, the size that measures the equipment is the hydrodynamic radius or diameter and it is usually larger than those sizes obtained by other techniques such as microscopy. About 100 µL of each sample were measured at 25ºC. The measurements were carried out in triplicate at 90º, during 50-100 seconds. Nano-emulsions were not diluted prior to measurements. For this reason, turbid samples could not be measured due to the detection limit of the equipment. However, nanoparticles were diluted when required in order to avoid the multiple scattering (Dobrovolskaia, 2013) as their size is independent on sample concentration. At least three measurements were carried out for each sample, all of them suspended in a aqueous solution (viscosity (25ºC)=0.9 mPa·s; refractive index = 1.33). Samples are defined as monodisperse if they have a polydispersity index (PDI) below 0.2 (Dobrovolskaia, 2013). The PDI is a dimensionless measure of the broadness of the size distribution that is calculated dividing the mean droplet size by the width of the hydrodynamic radii distributions (Tantra, 2010). It is worth remarking that the nanoparticle hydrodynamic sizes reported in the *In vitro* results section were measured with the ZetaSizer Nano Z. These measurements were performed at an angle of 173º, bigger than the usually used angle (90º).

Moreover, **static light scattering** (SLS) measurements were carried out, at detection angles from 30 to 130º at intervals of 10º. These measurements were performed for the determination of the shape of the nanoparticles. The measurement of the light intensity as a function of the angle of light dispersion enables the calculus of the gyration radius (R_g) according to Equation 3.3.

$$R_g^2 = \int r^2 \, g(r) dr$$
(3.3)

where r is the distance from a reference point; and g(r) is the so-called pair function of the distance. Assuming that the studied samples in this thesis are spherical, the relation with both radii is given by Equation 3.4:

$$R_g^2 = \frac{3}{5}R^2 \qquad\qquad (3.4)$$

Optical microscopy was also used for the nano-emulsion size study, in order to see the presence of big droplets producing high polydispersity. An Olympus BX51 microscope was used. Samples were observed at bright field, as well as at differential interference contrast (DIC) mode depending on the objective of the study. A drop of each sample was placed and dispersions were studied at different magnifications to test the presence of big drops.

Nanoparticle tracking analysis (NTA) was also used in the present work for the size determination of nanoparticles. It was used as an alternative technique, not only to measure the nanoparticles size but also for the measurement of the nanoparticle concentration. For the measurement, the NanoSight NS300 (NanoSight, Amesbury, United Kingdom), equipped with a sample chamber with a 488 nm laser was used. Nanoparticle dispersions were injected in the sample chamber using a Syringe Pump, at a concentration of around 10^8 NP/mL. All measurements were performed at room temperature. The software used for capturing and analyzing the data was the NTA 2.0 Build 127. The samples were measured for 60 seconds, with manual shutter and gain adjustments. Three measurements of the same sample were performed. Results are given as mean standard deviation values for the size and a mean value is given for the nanoparticle concentration.

Nanoparticle size and morphology were also determined by **transmission electron microscopy (TEM)**, with a JEOL 1010TEM (Jeol Korea Ltd., Tokyo, Japan) equipped with an accelerating voltage of 80kV and a Charged Coupled Devide Megaview III (SIS) camera (Münster, Germany) and carbon coated grids (Cooper with Formvar 0.5%, 200 mesh). To visualize the nanoparticles, they must be cleaned from the surfactant and concentrated. Nanoparticle dispersions were centrifuged (25ºC, 4,000 rpm, 1h) or ultracentrifuged (25ºC, 19,000 rpm, 1h) four times, collecting the pellet and dissolving it in MilliQ water each time. Once cleaned and concentrated, one drop of the nanoparticle dispersion was placed in a parafilm strip. A Formvar® carbon coated grid (200 mesh) was placed Formvar side-down on top of the drop for 1 minute to enhance nanoparticle adsorption. The grid was removed, blotted with filter paper and placed onto a drop of phosphotungstic acid (PTA) solution (2wt% in MilliQ water) to achieve a negative contrast (Harris, 1999). Excess solution was removed after 1 minute to obtain a convenient negative staining. The grid was then placed in a Petri dish covered

with Parafilm (Parafilm® M Barrier Film, Structure Probe Inc., West Chester PA, USA) and let dry at room temperature overnight before micrographs analysis. Nanoparticle average size and size distribution were determined with the Image J software measuring at least 1,000 nanoparticles for each sample from several micrographs taken at different magnifications, by means of an image analysis software package (ImageJ). A statistical analysis of the results was then carried out with Origin Pro8 software.

SEM microscopy was also used for the nanoparticle size and surface morphology determination. Nanoparticles were cleaned by repeated centrifugation to eliminate surfactant excess. A drop of the nanoparticle dispersion was placed on the grid, previously covered by an ultrathin conductive layer and let it dry. This procedure was repeated a total of five times, in order to achieve a higher density of nanoparticles. A Carl Zeiss Digital Scanning Electron Microscope DSM 940 A SEM was used.

AFM was also used to measure the nanoparticle size and morphology (topography of the sample) by means of the dynamic (peak force tapping) topographic AFM mode. Determinations were performed with the dispersion of the nanoparticles (liquid conditions), without the liophylization step because it enables the study of the interaction between the nanoparticles and the surfaces. A Multimode 8 AFM equipment in peak force tapping mode, with ScanAsyst as feedback optimization technology (Bruker AXS Corporation, Santa Barnara, CA) was used. For imaging, SNL AFM probes (Bruker), with silicon nitride cantilevers and silicon tips, with a spring constant of 0.35 N/m (nominal), and a resonance frequency 65 kHz were used.

3.2.9. Nano-emulsion and nanoparticle surface charge determination

For the surface charge analysis, the ζ potential of the nanoparticles / droplets, which determines the interaction of the particles with other elements of the samples, was measured by means of electrophoretic mobility. A Zetasizer Nano-Z from Malvern was used. This apparatus consists on the application of an electric field to the sample, which must contain some electrolytes to be moved in a velocity that depends on its electrophoretic mobility (Obiols-Rabasa, 2008). The mobility measurements are based on the particle velocity, which is measured from the frequency shift of the scattered light. This velocity or electrophoretic

mobility can be converted to the zeta potential (ζ) with different equations. The most used one is the Smoluchowski approximation (Dobrovolskaia, 2013) (Equation 3.5):

$$\mu = \frac{\zeta \cdot \varepsilon_r \cdot \varepsilon_0}{\eta}$$
(3.5)

where μ is the electrophoretic mobility, given by the equipment; ζ is the zeta potential; ε_r the dielectric constant of the medium (relative permittivity); ε_0 the vacuum permittivity and η is the viscosity of the sample. From the Smoluchowski equation, the equipment gives a distribution of the ζ potential, from which an average and standard deviation are taken (Figure 3.18).
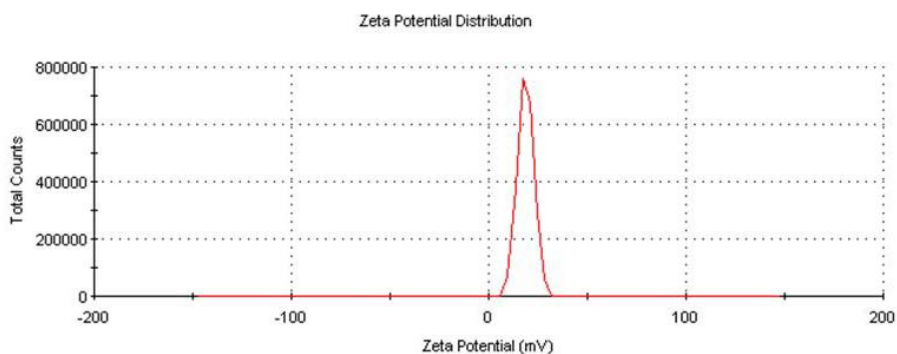
Figure 3.18: Example of the ζ potential distribution of a polymeric nanoparticle dispersion.

The Smoluchowski equation can only be used when the Debye-Hückel parameter (K) multiplied for the radius of the colloid (r) is higher than 100 (Kr > 100); which happens when the colloids are relatively big (considering the size of the ions layer negligible as compared with the colloid size) and have ζ potential values lower than 50mV in absolute value (O'Brien, 1978; Oshima, 1983). The Debye-Hückel parameter is calculated as follows (Equation 3.6):

$$K^2 = \frac{F^2 \sum_i \, C_i z_i^2}{\varepsilon R T^{\circ}}$$
(3.6)

where F is the Faraday's constant (96485.34 C/mol); C_i is the ion concentration; z_i the ion valence; ε the absolute permittivity ($\varepsilon_r \cdot \varepsilon_0$); R the gases constant (8.31J/mol·K) and T° the temperature.

In the case of the present thesis, the Kr value was about 0.2. For this reason, instead of the Smoluchowski equation, the Hückel-Onsager equation was used

(Delgado, 2007) because it is appropriate when the Kr < 1. In fact, it is a modification from the Smoluchowski equation (Equation 3.7):

$$\mu = \frac{2}{3} \frac{\zeta \cdot \varepsilon_r \cdot \varepsilon_0}{\eta} \qquad (3.7)$$

Disposable capillary cells (DTS1061, from Malvern Instruments) were filled with the samples, diluted at the required concentration with water, in order to achieve lower conductivity values, in the range of the appropriate conductivities for the zeta potential determination (<5 mS/cm) (Malvern Instruments Ltd, 2014). Cells were placed in the Zetasizer. The measure setting were fixed for water as the dispersant, since dilutions were made with water (RI = 1.33, η = 0.8872 cP, ε = 78.5, 25ºC), performing 20 runs for each measurement. At least three measurements were taken for each sample.

3.2.10. Nano-emulsion and nanoparticle dispersion stability

3.2.10.1. Visual observation

For the **macroscopic assessment**, samples were kept in a thermostated water bath at 25 or 37ºC, sealed flame closed to avoid sample evaporation and observed at different intervals of time.

3.2.10.2. Optical analysis by light transmission and backscattering

A Turbiscan^{TM} Lab (Formulaction, Toulouse, France) equipment, which measures the **transmitted and backscattered light** of the sample as a function of sample height and time was used. About 15 grams of the samples were introduced in a cylindrical tube. A pulse near infrared LED at a wavelength of 880 nm is directed to the desired measurement position of the sample. Two different synchronous optical sensors received the transmitted light (0º from the light source) and the backscattered light (135º from the light source). Measurements were performed along the sample height (about 50nm), hourly, during 24 hours at 25 or 37ºC depending on the sample. Data were collected at different intervals of time during 24 hours (Lemarchand, 2003). Measurements are expressed as the transmitted or backscattered light as a function of time and sample height. Backscattered is used in the case of opaque or turbid samples; while transmitted

light is analyzed in the case of translucent to transparent samples. The data analysis was performed by the LabExpert software.

3.2.10.3. Variation of droplet size with time

The changes in the sizes were determined measuring the nano-emulsion **droplet size** and nanoparticle **size** as a function of time, at 25ºC, by means of a DLS. The size measurements were performed as previously described in Section 3.2.10.2. Samples were measured without previous agitation, with the aim to study their migration destabilization processes.

3.2.10.4. Variation of the pH with time

The pH of the nanoparticle dispersions was measured with the Mettler Toledo Seven Easy pH meter. About 4 grams of nanoparticles were prepared and the pH measurement was carried out at different time intervals. The pH was plotted as a function of time.

3.2.10.5. Variation of the osmolality with time

The osmolality was measured using the Micro-Osmometer Type 15 from Löser Messtechnik. This apparatus measures the osmotic strength of a solution by means of the freezing point depression (Peltier effect, Figure 3.19). This equipment can measure osmolalities in the range between 0 to 2500 mOsm/kg, with a reproducibility of 0.5% (Löser, 2014).
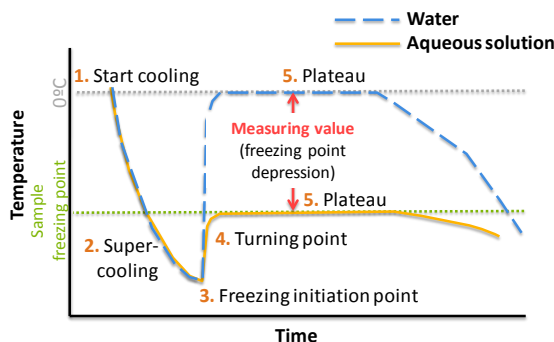
Figure 3.19: Scheme of the typical curves of water and aqueous solutions. The temperature is plotted as a function of time, showing the sample thermodynamics.

To perform the measurements, 100 μL of sample were placed in an eppendorf tube and the eppendorf was placed in the equipment. The measure requires around 1.5 minutes. Results are given in miliOsmols of solute per kilogram of solvent (mOsm/kg). Usually, the physiological osmolality is around 300mOsm/kg. Therefore, nanoparticles dispersion osmolality must be adjusted to this value.

3.2.10.6. Variation of viscosity with time

The viscosity was measured using the CANNON-FENSKE capillary viscometer, model 33, serie 25. About 15 grams of nanoparticle dispersions were prepared. The viscometer was maintained in vertical inverted position and the N branch was introduced to the sample solution. The sample was introduced by suction through the L edge just until the downer limit (F). Then, the viscometer is replaced in vertical position at the water bath with the required temperature (25ºC or 37ºC), maintaining the D part completely submerged (Figure 3.20). The time that takes to the sample to go down from the E to the F marks is measured and cinematic viscosity is calculated by the following equation (Equation 3.8):

$$\text{Cinematic viscosity (cSt)} = C \times t \qquad (3.8)$$

where t is the measured time and C is an arbitrary constant that depends on the capillary viscometer used and the temperature of the experiment.
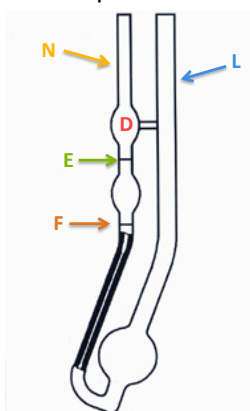
Figure 3.20: Schematic representation of the capillary viscometer.

3.2.11. Active encapsulation

3.2.11.1. Changing the MNPs dispersant

Magnetic nanoparticles (MNPs) were suspended in a heptane solution. For this reason, prior to their use, the change of the dispersant was required. A direct change was not possible, since the polarity of the MNPs surface should change gradually to adapt to the required solvent, ethyl acetate in the present thesis. The dispersion of MNPs was sonicated for 30 minutes in an ultrasound bath, at room temperature (25ºC), in order to decrease nanoparticles aggregation (Jiang, 2013(2)). About 0.2 g of the MNPs dispersed in heptane were weighted in a glass tube to start with the cleaning sequence, which consisted in 4 cleanings with acetone followed by three more cleanings with ethyl acetate. Each acetone cleaning step consisted on the addition of around 6 grams of the solvent, vortexing for 5 minutes, to achieve a mixture as homogeneous as possible and centrifugating 3 minutes at 1,500 rpm. Each ethyl acetate cleaning step consisted on the addition of around 6 grams of the solvent, vortexing for 2 minutes, to achieve a mixture as homogeneous as possible and centrifugating 10 minutes at 5,000 rpm. After the centrifugation, the supernatant (solvent without MNPs) was discarded, and the following cleaning step was performed, starting with the addition of the solvent to the pellet of MNPs. After the cleaning steps, the pellet of the MNPs, with the remaining ethyl acetate is kept for 24 hours at 4ºC, to achieve a dry powder of the MNPs. Once MNPs were encapsulated into polymeric NPs, the encapsulation was studied by means of **enhanced optical microscopy with spectral imaging**. An Olympus optical microscope, with Cytoviva® light source system coupled, together with the fluorescence module was used. The optical images were processed using the Exponent 7 software, while the ENVI 4.8 software was used for the spectral image analysis. The fluorescent module consists on three independent filters, each one appropriate for a certain wavelength. The DAPI filter (AT350/50X single Band DAPI Exciter-25mm), which produce an excitation at wavelengths from 300 to 400 nm; the FITC filter (S492/18X Single Band FITC exciter-25mm), at wavelengths from 480 to 510 nm; and the TexasRed filter, at wavelengths from 560 to 580 nm. In addition, a triple excitation filter exist (61002x 25mm DAPI/FITC/TexasRed Excitation) enabling the excitation at wavelengths between $390 - 440$ nm, $480 - 510$ nm and $560 - 580$ nm, which works together with an emission triple filter (61002m 25mm DAPI/FITC/Texas Red Emission) enabling the detection of light emitted only between $450 - 475$ nm, $520 - 550$ nm and $600 - 650$ nm (Chroma, 2014).

3.2.11.2. Determination of encapsulation efficiency

The encapsulation or entrapment efficiency (EE) was measured by an indirect filtration / centrifugation method to test the EE of loperamide and galanthamine. About 3 grams of the nanoparticle dispersion (or the sample to test) were placed in the Amicon® Ultra-4 Centrifugal Filter Units (Millipore), which consist on a falcon with a Ultracell regenerated cellulose membrane with a MWCO = 3 kDa. They were centrifuged 60 minutes at 5,000 rpm. The liquid that passed through the filter, which contained the non-encapsulated drug, was quantified by means of the HPLC, for loperamide and by means of the fluorimeter, for galanthamine.

The results were expressed as the encapsulation efficiency (in percentage), as well as the drug loading (mg drug / g PLGA) and drug concentration (mg drug / mg NP).

3.2.11.3. Release experiments

This type of experiments was carried out to study the release of Coumarin 6, loperamide hydrochloride and galanthamine hydrobromide. In the release experiments of the drugs, a micellar and aqueous solutions were also studied for comparison purposes. Since the drug solubility in water was below the concentration that it has in the nanoparticle dispersions, experiments in aqueous solution were performed with a lower drug concentration.

It is worth noting that release experiments with the dialysis bag method usually take a sample of the receptor solution for their further analysis. However, in the present thesis, since the amounts of Coumarin 6 and galanthamine were very small, aliquots from the sample inside the bags were withdrawn.

For the experimental procedure, thermojacketted glasses were used to maintain the desired temperature (25ºC). They were filled with the receptor solution, which consisted in 50mL of milliQ water. Spectra/Por® Float-A-Lyzer® G2 (Spectrum®Labs) devices with a membrane composed of Biotech Grade Cellulose Ester with a MWCO of 3.5 – 5 KDA were pre-wetted with 10wt % ethanol for 10 minutes followed by a second wetting step of distilled water. Then, they were filled with 2 mL of the sample and soaked into the receptor solution.

Aliquots of 1mL of the receptor solution were withdrawn for loperamide, while aliquots of 125μL of the sample were withdrawn for Coumarin 6 and galanthamine tests, at controlled intervals of time. Those aliquots were analyzed with proper techniques: loperamide was quantified with HPLC while galanthamine and Coumarin 6 were quantified by fluorescence emission. The experimental results were fitted (experimental points corresponding to the whole diffusion or the first values of diffusion when the entire diffusion was no properly fitted) to the theoretical Fick's second law of diffusion, when possible, to calculate an apparent diffusion coefficient (Higuchi, 1962; Calderó, 2010; Llinàs, 2010; Fornaguera, 2014(1)).

3.2.11.4. Determination of the acetylcholinesterase activity

The protocol followed for the acetylcholinesterase (AChE) activity measurement is a modification of the *Ellman's protocol,* which is a very sensitive method, applicable to small amounts of samples at low concentrations (Ellman, 1961). First, AChE was prepared at 20mM (5U/mL) in the indicated phosphate buffer: 8mM K_2HPO_4, 2.3mM NaH_2PO_4, 0.15M NaCl, 0.05% Tween20, at pH 7.6. Samples to test were diluted in the same buffer at the required concentrations. 50μL of the as-prepared AChE and 50μL of the as-prepared samples were added at a well of a 96-well plate and incubated for 30 minutes at room temperature (25ºC). Then, 100μL of the substrate were added to each well and incubated for 3 minutes. The substrate consist on 0.1M Na_2HPO_4, 0.5mM 5,5'-dithiobis[2-nitrobenzoic acid] (DTNB), 0.6mM acetylcholine iodide (ATCI), in milliQ water, at pH 7.5. Finally, absorbances were read at 405 nm (López, 2002). Each sample was studied, at least, three times. Results are given as a mean normalized value +/- the standard deviation.

3.2.12. Nanoparticle functionalization

3.2.12.1. Functionalization with FITC

The PLGA functionalization with the fluorescent dye FITC was performed directly to the PLGA polymer, prior to the nano-emulsion and nanoparticle preparation. FITC was covalently coupled to the PLGA by the carbodiimide reaction (Yin, 2007; Betancourt, 2009; Li, 2009). First, the carboxylic groups of the PLGA were

activated by mixing 5mL of a solution of NHS 1.6 w/v %, 5mL of a solution of EDC 2.04 w/v % and PLGA 20 w/v% in dicloromethane. The mixture was left to react for 2 hours, at room temperature (25ºC) under continuous agitation. A solution with 38.8 grams of FITC in 500 μL of pyridine plus 500 μL of dicloromethane was added to the PLGA solution. This mixture was incubated overnight, in the dark, at 4ºC. A purification step of the PLGA was included by repeated washings with 5mM HCl to remove the free FITC followed by a precipitation of the PLGA-FITC with methanol for 2 hours at 4ºC. Finally, PLGA-FITC was lyophilized and stored in the dark at 4ºC (Yin, 2007).

3.2.12.2. Functionalization with dendrons

Nanoparticles were dendron functionalized with the second and third generation dendrons (described in Section 3.1.7.1), by means of a peptidic amino bound formation between the amino focal group of the dendrimers and the carboxylic free groups of the PLGA polymer (Figure 3.21). In contrast to the FITC functionalization, the nanoparticles were first prepared and then functionalized.

PLGA NP + **EDC**   + **NHS**   **Activated-NP**

+ **Dendron**   **Dendron-functionalized nanoparticles**
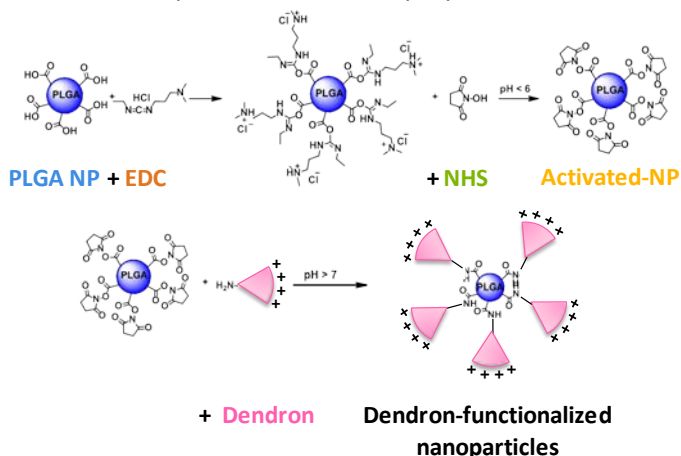
Figure 3.21: Scheme of the PLGA nanoparticles dendronization procedure.

The reaction started with the acidification of around 4 grams of the nanoparticle dispersion (4 < pH < 6) using ortophosphoric acid 2.28M. An excess of the EDC and NHS (10 charge equivalents of each reactant for 1 charge equivalent of PLGA) were added to the acidified solution, in the above-indicated order. This mixture was incubated for at least 2 hours, at 25ºC, under continuous stirring. Following, the activated nanoparticle dispersion was basified using sodium hydroxide 0.1M. The appropriate amount of dendrons (depending on the tested N/P charge ratio

with the nanoparticles), which were kept in aqueous solution, were also basified with sodium hydroxide 0.1M and this solution was incubated around 30 minutes at 25ºC. The dendron solutions were added to the basified activated nanoparticles and the mixture was incubated overnight (at least 18 hours) at room temperature (25ºC). After the reaction step, a purification step was required to eliminate all the reaction products (e.g. EDC) and eventual non-reacted dendrons. The purification step consisted on a dialysis, performed exactly equal than that explained in Sections 3.2.5 and 3.3.6. It is worth remarking that the dendron functionalization was intended to covalently bind the dendrons with the PLGA polymer. However, since the polysorbate 80 surfactant has hydroxyl groups, some could interact with the dendrons, resulting in nanoparticles partially functionalized by the surfactant. To assess the cationization of the nanoparticles, as well as the complete elimination of the components in excess, diverse methodologies were assayed: the Kaiser test, FTIR experiments and thermogravimetric assays.

To perform the **Kaiser test**, the original procedure from *Kaiser et al.,* (Kaiser, 1970) was followed. Around 500 μL of sample were placed in a glass tube, followed by the addition of 3 – 4 droplets (around 20 μL) of the Kaiser's solutions and the steps of incubation. Following this addition, samples were shacked for 10 minutes and heated to 80ºC to ensure the correct formation of the colorant. Positive results give rise to with a bluish – purplish color, while negative results produce in a whitish – yellowish coloration. This test was performed at least 3 times for each sample.

FTIR spectra were obtained with a Fourier Transform Infra-Red (FTIR) spectrometer Nicolet model 510 that measures the transmission of the samples as a function of the wave number from 390 to 3900 cm^{-1} (Pretsch, 2003). Samples were transformed to solid pellets mixing the sample with potassium bromide (KBr) and applying a force of about 10 tons. Spectra from transmittance/absorbance data were recorder and processed.

For the **thermogravimetric assays (TGA),** samples were liophylized to have them in solid state. Then, around 5 mg of sample were placed in the sealed aluminum pans. Samples must be in a solid state. Therefore, before performing TGA tests, samples were lyophilized, as described in Section 3.2.11. The TGA/SDTA 851e model was used. It was set between 20 and 550ºC, increasing the temperature

10ºC/min. Plots of the weight loss as a function of the temperature were represented, as well as their derivatives.

3.2.12.3. Functionalization with oligonucleotides

The oligoucleotide concentration was fixed and the nanoparticle concentration was added according to the desired N/P charge ratio (molar ratio for plasmids). The N/P ratio is defined as the number of positively charged groups (N) divided by the number of negatively charged groups (P). The complexation protocol consisted on the mixing of both, the nanoparticle dispersion and the oligonucleotide at the corresponding proportion, using Hepes buffer as the dispersant. Then, the mixtures were sonicated for 5 minutes, at 25ºC, to facilitate the formation of the complexes, and a final incubation step at 37ºC, for at least 30 minutes was performed to achieve the complexation.

3.2.12.4. Coating with PEG

PEGs with different lengths were tested to obtain the complexes (oligonucleotide/NP) with the appropriate features. Complexes were incubated 30 more minutes at 37ºC with the PEG solution at a PLGA/PEG molar ratio 1/1.

3.2.12.5. Functionalization with antibodies

The 8D3 monoclonal antibody against the transferring receptor, overexpressed in the BBB was covalently attached to the nanoparticles by means of the carbodiimide reaction, as described in Section 3.3.12. The step of the activation of the nanoparticles was performed exactly as explained. The second step, the coupling of the antibody was performed without basifying the pH of the antibody. In this case, various N/P (NP/antibody) molar ratios were tested, following the same experimental protocol than in the case of the dendrons. Once the complexes were obtained, their hydrodynamic size as well as their surface charge were characterized.

To test the 8D3-nanoparticle functionalization, **confocal microscopy** experiments were carried out. A Confocal Laser Scanning Microscope TCS-NT (Leica) was used.

Coumarin 6 loaded nanoparticles were used and a secondary antibody against the 8D3 antibody, dyed with the red fluorescent Alexa Fluor 555 was further incubated. Since these experiments need a solid support to be performed, they were directly performed on mice brain slices. The FITC filter from the confocal microscope was used for the visualization of Coumarin 6 (488nm), while TRIC filter was used for the visualization of Alexa Flour 555 (55nm). Images were taken from both filters and overlaid to interpret the results with the appropriate software (Kupzig, 2010).

To confirm the 8D3-nanoparticle functionalization, **SEC experiments** were also performed with the raw materials (nanoparticles and 8D3 antibody), functionalized samples and physical mixtures of the components without reaction. 100 µL of each sample were placed in the equipment at the as-prepared concentration (depending on the NP/8D3 ratio tested). An Alliance 2695 HPLC Waters system equipped with a UV detector Waters 2996 DAD was used. The column used was an Ultrahydrogel, 250, 6 µm, 7.8 mm x 300 mm, 1K - 80K, Water; and an Ultrahydrogel Column, 500, 10 µm, 7.8 mm X 300 mm, 10K - 400K, Water. Samples of 300 µL of PLGA nanoparticles (without or with the antibody, without or with covalent attachment) dispersed in PBS 0.16M were prepared together with a protein molecular weight standard (alcohol dehydrogenase, MW = 141 kDa). PLGA produces an absorption peak around 230nm wavelength (Laquintana, 2009) while proteins produce the maximum absorption at 280nm (Edelhoch, 1967); for this reason, the absorbance was studied in a wide wavelength range, from 212 to 300 nm. SEC conditions were fixed at a flow rate of 0.35mL/min, injecting 50µL volume of each sample, and studying the chromatogram during 80min (as peaks of the different components appeared until about 65min). Temperature was set at 30ºC to avoid temperature oscillations of ambient temperature. Measurements were analyzed with the Empower 3 Chromatography Data Software. Chromatograms were analyzed at different wavelengths, since the different compounds absorb at different wavelength. The contour plots were analyzed too.

3.2.13. Electrophoretic mobility shift assay (EMSA)

Antisense oligonucleotides (ASOs) or siRNAs were mixed at a concentration of 0.5µM of oligonucleotides with increasing concentrations of the G2SN or G3SN-functionalized nanoparticles (dendron/NP ratio of 1/20 and 1/5 respectively);

from oligonucleotides/NP ratios 0/1 until complexation was achieved. They were sonicated for 5 minutes, at 25ºC, to facilitate the formation of the complexes. Then, complexes were incubated for 30 minutes at 37ºC. When the samples to test included the PEG coating, the appropriate amount of PEG was added after this incubation to achieve a molar PLGA/PEG ratio of 1/1 and complexes were reincubated for 30 minutes more. Electrophoresis was performed with a gel of 20wt% of polyacrylamide, at 150V, for around 8 hours, in TBE buffer 1X. Pictures of the results were taken with Fujifilm LAS-1000 Intelligent Dark Box II with LAS-1000 Lite v1.2, following a previous gel staining with the fluorescent dye SYBR® Green (20μL in TBE 1x 200mL) for 20 minutes under continuous smooth shaking.

3.2.14. *In vitro* cell viability analysis

The cell viability was assessed with the 3-(4,5-dimethylthiazol-2-yl)-2,5-diphenyltetrazolium bromide **(MTT) colorimetric assay**, as previously indicated in many reports (Putnam, 2001; Grijalvo, 2014; Fornaguera, 2014(1) and 2014(2)). For each assay, cells were seeded (about 6 x 10^3 cells per well) on a 96-well plate in 200 μL of DMEM, and cultured for 24 hours at 37ºC. Then, the culture medium was replaced with samples at the required concentrations. Cells were incubated for 4 or 24 hours, depending on the experiment, at 37ºC under 5% CO_2 atmosphere. In the case of 4 hours of incubation, after this time, the media was withdrawn and cells were seeded with 200 μL of fresh DMEM. The MTT reagent was added at a final concentration of 0.5mg/mL (25μL) in PBS and incubated for two more hours at 37ºC. Then, the medium was withdrawn and 200μL of DMSO were added to dissolve the formazan crystals. The plate was stirred for 15 minutes at room temperature. Finally, absorbance was measured at λ = 570 nm with the SpectraMax M5 spectrophotometer (Putnam, 2001).

Another cytotoxicity test, the **lactate dehydrogenase assay** (LDH), was performed. It measures the rupture of the cell membrane by means of the LDH release (Fotakis, 2006; Weber, 2008; Posadas, 2009). The incubation of the cells was performed as for the MTT assay. After the incubation time, 50μL of the supernatant of each well was collected in another plate. 150 mL of PBS were added, followed by the rapid addition of 25 μL of NADH 1.3mM and 25μL of pyruvate 31mM in PBS. The addition of these products produces the following reaction, only in the presence of LDH (Koh, 1987; Fotakis, 2006):

$$\text{Pyruvate + NADH} \rightarrow \text{Lactate + NAD}^+ \qquad\qquad (3.9)$$
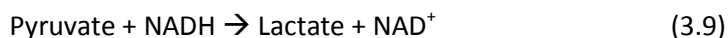
As NADH absorbs at a wavelength of 340 nm, absorbance measurements were carried out at this wavelenght. Only in the presence of LDH, the absorbance should decrease due to the oxidation of NADH with the SpectraMax M5 spectrophotometer (Koh, 1987). Results are presented as viability percentages in both assays.

3.2.15. Cell transfection

ASOs and siRNAs were designed to knockdown the expression of a *Renilla* Luciferase gene. For this reason, their transfection was studied by means of the Dual-Luciferase Reporter Assay System from Promega.

Two luciferase plasmids were used, *Renilla* luciferase (pRL-TK) as the reporter and Firefly luciferase (pGL3) as the control. These vectors were transfected into cells with Lipofectamine 2000 at 0.1μg/well and 1.0μg/well, respectively, since HeLa cells do no express these plasmids themselves. Cells were incubated with the plasmids for 5 hours. After this time, the medium was withdrawn and the cells were washed twice with 500μL of PBS. Then, 500mL of fresh DMEM were added to each well. Depending on the experiment, the DMEM contained 0% or 10% FBS. Complexes between NPs and oligonucleotides were prepared at the desired concentrations, following the same procedure than that described for the EMSA experiments. 100mL of each sample were added to each well. For each sample, a minimum of a triplicate was studied. After 24 hours of complexes incubation, cell lysates were prepared and analyzed following the manufacturer's protocol (Dual-Luciferase Reporter Assay System from Promega). Luminescence was measured with SpectraMax M5 spectrophotometer.

The lentiviral plasmid codifies for the *Renilla* luciferase gene. For this reason, its transfection was studied by means of the produced fluorescence. In this case, a direct observation of the wells was possible after the incubation time, adding 5mL of the substrate to enable the reaction that produces fluorescence. Images were taken using the ORCA-2BT imaging system (Hamama-tsu Photonics, Hamamatsu City, Japan) provided with a C4742–98-LWG-MOD camera and a 512x512 pixel, charge-coupled device (CCD). The fluorescent signals were quantified.

3.2.16. Interaction of blood proteins with nanoparticle surface

3.2.16.1. Study of the proteins adsorbed onto nanoparticle surface

Nanoparticles interaction with blood proteins was studied incubating 1 mL of nanoparticles, at 3mg/mL with 0.185mL of fetal bovine serum (FBS), which includes all blood proteins, at 50mg/mL, for 18 hours, at 37ºC. Then, incubated nanoparticles were cleaned by repeated centrifugation, at 15,000g, for 45 minutes, at 25ºC. Nanoparticles remained in the pellet, with the adsorbed proteins, while the supernatant contained the non-adsorbed proteins. Both fractions were analyzed by SDS-PAGE electrophoresis. Vertical gels were composed of a stacking upper part, with the objective to stack all proteins before separating (Composition: 3.78mL water, 2.42mL Tris/HCl-SDS, 487.5μL acrylamide (30%), 37.5μL ammonium persulphate (10%) and 7.5μL TEMED) and a running gel, at 12.5wt% of acrylamide (Composition: 2.28mL water, 975μL Tris/HCl-SDS , 4.5mL acrylamide (30%), 75μL ammonium persulphate (10%) and 7.5μL TEMED). Some microliters of isopropanol were deposited on the gels to enhance their correct solidification. Once gels were solidified, they were placed in the appropriated BioRad cuvettes. 10 μL of each sample, together with 5 μL of Sample loading buffer (10mL Tris/HCl 1M pH 6.8, 20mL glycerol, 4g SDS, 0.2g bromophenol blue and adjusted with water up to 40mL) were placed in each well. Gels were let to diffuse in a quiet place for around 30 min, at a voltage of 60V, followed by 90 min, at a voltage of around 120V. To visualize the results, gels were stained with Comassie blue; the excess colorant was eliminated with a distaining solution (50mL methanol, 75mL acetic acid and 875mL H$_2$O), followed by a fixation step (454mL methanol, 92mL acetic acid and 875mL H$_2$O). The distance that each protein run depends on its molecular weight: the smaller the protein, the longer the distance.

3.2.16.2. Study of the BSA interaction

3.2.16.2.1.   Surface charge variation

Nanoparticles at a specific surface area of 1000 cm^2 were mixed with increasing BSA concentrations, from 0 to 40 mg/mL of BSA at the final sample. The mixtures were incubated for 10 minutes, at 37ºC. The ζ potential of the samples with the different BSA concentration was determined.

3.2.16.2.2. Immunomethods

Rocket immunoelectrophoresis and radial immunodiffusion were used for the determination of the BSA adsorption onto nanoparticle surface. Rocket immunoelectrophoresis was used for the study of low BSA concentrations (<500 mg/mL) while radial immunodiffusion was used for the study of high concentrations (>300 mg/mL).

First, the specific nanoparticle surface was calculated (see Appendix Section 10.4.2), since these experiments were performed at a same specific nanoparticle surface of 1000 cm^3. For the gel preparation, agarose powder was weighted and mixed with Tricine buffer (lactate calcium 1mM, Tris 63mM, Tricine 27mM, pH 8.6) at 1wt % of agarose for rocket immunoelectrophoresis and agarose was mixed with PBS (10mM; NaCl 140mM KCl 25mM, pH 7.5) at 0.8wt % for radial immunodiffusion. The mixture was weighted above 60 ºC to dissolve the agarose in the buffer, adding 0.3mL of the bovine serum albumina antisera (Sigma-Aldrich). Then, agarose gel plates (8.5 cm x 12 cm) were prepared on Gelbond® films for agarose gel (Amersham BioScience, Uppsala, Sweden). Wells holding 3 or 5µL of each sample (3 for radial immunodiffusion and 5 for rocket immunoelectrophoresis) were formed with a 2mm diameter punch on the gel plates (Labarre, 2005; Bertholon, 2006; Vauthier, 2009(2)). Once the gels were solidified, 3-5µL of each sample were placed in each well, including samples of BSA standard solutions. Gels were placed in a humid chamber and let to diffuse in a quiet place for around 18 and 48 hours for rocket immunoelectrophoresis and radial immunodiffusion respectively (Vauthier, 2011). The electrophoretic conditions for the rocket immunoelectrophoresis were set at 230 V, 12mA (Electrophoresis power supply EPS 600, Amersham, Pharmacia Biotech, Orsay, France). The radial immunodiffusion diffused alone, without any source of energy. At the end of both types of electrophoresis, gels were dried with Watmann® filter papers for around 45 minutes, followed by a wetting with a sodium chloride solution for 15 minutes, another drying during 30 minutes, another wetting with water for 15 more minutes and a final drying until the dry is complete. To visualize the experiment results, a staining step was required. Gels were placed in a plastic cuvette filled with Comassie blue and let there for the staining for around 10 minutes, under continuous agitation. Then, gels were distained, to eliminate the excess of colorant. Finally, the stain was fixed with water and dried with Watmann® papers.

In the case of rocket immunodiffusion, the calibration curve is a linear relationship between the height of the immunoprecipitation peak and the know concentration of the BSA standards. For radial immunodiffusion, the calibration curve is a linear relationship between the diameter of the immunoprecipitation ring and the know concentration of the BSA standards.

3.2.16.3. Study of the fibrinogen interaction

Nanoparticles at a specific surface area of 1000 cm^2 were mixed with fibrinogen, dissolved in phosphate buffer 100mM (pH 7.4) at different concentrations of fibrinogen in the final sample (0 – 2 mg/mL). Results were studied by means of macroscopic optical observation of the samples, for eventual aggregation / precipitation and microscopic optic observation using the phase contrast mode (Olympus BH2) to test the presence of non-macroscopic aggregates.

3.2.16.4. Nanoparticle stability in VBS^{2+} buffer

Nanoparticle stability was studied both, in VBS^{2+} buffer and in VBS^{2+} buffer with serum (FBS). 100 μL of each sample, at the required specific surface area (1000 cm^2), were mixed with 50 μL of VBS^{2+}, or with 50μL of VBS^{2+} and 50μL of FBS. Just after the mixing, samples were regarded macroscopically, to detect the formation of aggregates. In addition, size and ζ potential were studied. Samples were incubated for 1 hour, at 37ºC and, after this time, they were restudied by means of visual macroscopic observation, size and ζ potential.

3.2.16.5. Activation of the complement system

2D immunoelectrophoresis was used for the study of the complement activation (Vauthier, 2011). First, the specific nanoparticle surface was calculated (see Appendix Section 10.4.2), since these experiments were performed at a same specific nanoparticle surface of 1000 cm^3. In addition, before starting these experiments, as they are performed in veronal bovine serum (VBS^{2+}) with FBS, the stability of the samples in this buffer was studied by means of their incubation in VBS^{2+} + FBS for 1 hour, at 37ºC, followed by the macroscopic and

microscopic observation of the formation of aggregates, as explained in the previous section.

For the gel preparation, agarose powder was weighted and mixed with Tricine buffer (lactate calcium 1mM, Tris 63mM, Tricine 27mM, pH 8.6) at 1wt % of agarose. The mixture was weighted above 60 ºC to dissolve the agarose in the tricine buffer. Then, agarose gel plates (5 cm x 7 cm) were prepared on Gelbond® films for agarose gel (Amersham BioScience, Uppsala, Sweden). Wells holding 7μL of each sample were formed with a 2mm diameter punch on the gel plates (Labarre, 2005; Bertholon, 2006; Vauthier, 2009(2)). 100μL of each sample, at a specific surface area of 1000 cm^2 were incubated with 50 μL of VBS^{2+} and 50μL of FBS, at 37ºC, for 1 hour. After their incubation, once the gels solidified, 7μL of each sample were placed in each well. Gels were placed in a humid chamber and let to diffuse in a quiet place for around one hour, the time that takes for the running of the first dimension electrophoresis, with Tricine buffer as the running buffer. The electrophoretic conditions were set at 600V, 9W (Electrophoresis power supply EPS 600, Amersham, Pharmacia Biotech, Orsay, France). Then, each gel was cut into pieces, each one corresponding to each sample. With each piece, another gel was formed, as explained above, to run the second dimension electrophoresis. In contrast to the first dimension, in this second gel, the polyclonal anti-C3 human antibody was dissolved (concentration = 18.5mg/mL). This second running took around 18-19 hours. The electrophoretic conditions were set at 250V, 3W. Next, the gels were dried with Watmann® filter papers for around 45 minutes, followed by a wetting with a sodium chloride solution for 15 minutes, another drying during 30 minutes, another wetting with water for 15 more minutes and a final drying until the dry is complete. To visualize the experiment results, a staining step was required. Gels were placed in a plastic cuvette filled with Comassie blue and let there for the staining for around 10 minutes, under continuous agitation. Then, gels were distained, to eliminate the excess of colorant. Finally, the stain was fixed with water and dried with Watmann® papers. To quantify the percentage of C3 activation, the areas of each peak (C3, C3b and C3c, as shown in Figure 3.22) were measured with the ImageJ® software and relative peak percentages were calculated for each sample.
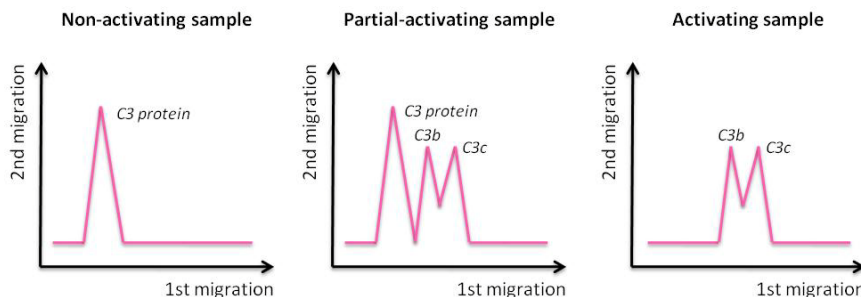
Figure 3.22: Schematic representation of the expected 2D-immunoelectrophoresis gels when studying different types of samples.

Serum diluted in VBS^{2+} was used as negative control, while Sephadex® G 25 superfine (Pharmacia, Orsay, France) was used as positive control. Each sample was studied at least, three times.

3.2.17. Coagulation assay

This study was performed *in vitro*, using blood from healthy donors. Blood was collected in BD Vacutainer tubes (BD Diagnostics Franklin Lakes, New Jersey) containing sodium citrate as anticoagulant. First, the serum was isolated by recollecting the supernatant of the centrifuged blood at 3,000 rpm, 10 min at 25ºC. Then, serum was subjected to clotting tests, specifically the measurement of the activated partial thromboplastin time (APTT) and the prothrombin time (PT). Both measurements were carried out with a Coagulometer KC1, following the protocol by *Dobrovolskaia et al.,* (Dobrovolskaia, 2009) with some modifications. For the assessment of both coagulation times, 10 μL of each sample were added to 100μL of serum and incubated for 30 minutes, under continuous shaking, at 37ºC. Each sample was tested trice.

The **PT test** measures the activation of coagulation by the extrinsic or tissue factor. For the assessment of the coagulation time, once a sample was placed into the coagulometer, 200 μL of the phospholipid calcium thromboplastin were added and the coagulation time was automatically assessed. Normal values for healthy humans are in the range between 12 and 15 seconds.

The **APTT test** consists on the measure of the activation of the contact or intrinsic coagulation pathway. For this reason, 100 μL of cephalin, a negatively charged

phospholipid acting as contact activator, were added to the sample previously placed in the coagulometer. The mixture was incubated for 2 minutes, followed by the addition of 100 μL of calcium chloride to activate the clot formation; and measurement of the coagulation time. For this experiment, the normal values for healthy humans are between 25 -35 seconds (Dobrovolskaia, 2013).

3.2.18. *In vitro* hemolysis assay

Human blood was kindly provided by healthy donors (Barcelona, Spain). Red blood cells (RBCs) were obtained as previously reported (Italia, 2009): the blood was washed three times by centrifuging 10 minutes at 3,000 rpm, at 25ºC. The pellet consisting on erythrocytes was collected and resuspended in an isotonic phosphate buffered saline solution (PBS) containing 136.99 mM NaCl, 1.59 mM $NaH_2PO_4 \cdot H_2O$ and 16.76 mM $Na_2HPO_4 \cdot 2H_2O$ in distilled water (pH = 7.4). The approximate density of the RBC was $8 \cdot 10^9$ cells/mL.

To perform the assay, 1 mL of each sample studied was placed in an eppendorf, where 100 μL of RBC were added. Samples were incubated at 37ºC for 10 minutes and then centrifuged for 15 minutes, at 3,000 rpm, at 25ºC. The percentage of hemolysis was spectroscopically calculated by comparing the absorbance (λ = 540 nm) of the samples with the positive control (distilled water). The results are expressed, in some cases, as a dose-response curve, where the concentration that induces the 50% of hemolysis is extrapolated (IC_{50}) (Figure 3.23).
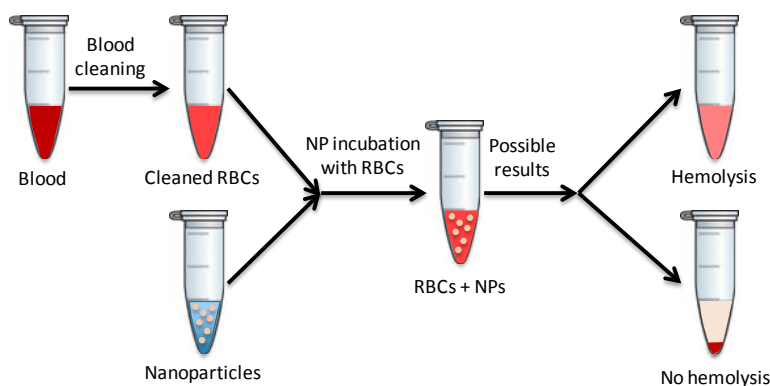
Figure 3.23: Schematic representation of the hemolysis assay performed.

3.2.19. Intravenous administration of nanoparticles

A total volume of 150 µL was injected by one of the lateral tail veins of mice of 8 weeks old (weight around 35 g), at the required sample concentration to achieve the desired dose.

3.2.20. Study of the *in vivo* analgesic effect

To study the *in vivo* analgesic effect, the **hot plate test** was selected. Prior to experimentation, the Ethical Committee of Animal Experimentation from the University of Barcelona approved the Experimental Procedure proposed (see Appendix).

All aqueous solutions were prepared by a direct dilution of the salts – drug – surfactant in milliQ water. The nanoparticle samples were concentrated to achieve therapeutic concentration of loperamide in mice. Nanoparticle dispersions were concentrated using Centriprep® Centrifugal Filter Devices from Millipore for ten times. Then water was added to achieve specifically the required loperamide concentration (or the equivalent non-loaded nanoparticle concentration).

After this step, a dialysis was required to return to the pH and osmolality physiological conditions (pH = 7.4 and osmolality = 300 mOsm/kg). 2 grams of each sample were place inside the Float-A-Lyzer® devices, after their prewetting, and were soaked inside 200mL of the electrolyte solution (0.16M). The electrolyte solution was replaced for a new one after 2 and 5 hours to accelerate the diffusion of ions. The dialysis was performed during a total time of 24 hours. Then, all samples were filtrated with polytetrafluoroethylene (PTFE) filters with pore diameters of 0.22 µm, in order to sterilize them.

The mice manipulation was performed in accordance with the protocol approved by the ethical commission, at the Animal Facilities of the Pharmacy Faculty of the University of Barcelona. All the procedure is schematically explained in Figure 10.2 from Appendix Section. A total of 80 CD1 mice of around 35 grams (around 8 weeks) were used to have at least 8 animals per experimental group. They were weighted prior to be used, in order to know exactly the dose required. Then, the pre-treatment latency time on the hot plate was measured. To prevent animal injuries, the test was truncated after 25 s (cut-off time) (Ulbrich, 2009).

Mice were intravenously administered by one of the lateral tail veins with the required amount of sample (prepared to administer between 150 – 200 µl). A response time of 15 minutes was waited to achieve that samples arrived to the BBB. During this time, animal behavior was observed to test any behavioral change produced by the samples administered. After this time, the post-treatment latency time on the hot plate was measured. Results were statistically analyzed with the software SPSS Statistics 17.0. A Paired – Sample T Test was performed to compare means for each group between the pre-treatment latency times and post-treatment latency times. Moreover, the maximal possible effect (% MPE) was calculated with the Equation 3.10 (Tosi, 2007; Ulbrich, 2009; Gelperina, 2010; Tosi, 2011; Kirby, 2013):

$$\% \text{ MPE} = \frac{\text{Post-treatment latency} - \text{Pre-treatment latency}}{\text{Cut-off time} - \text{Pretreatment latency}} \times 100\% \tag{3.10}$$

Chapter 4

RESULTS AND DISCUSSION

4.1. Selection of system components

This study has the objective to produce polymeric nanoparticles from nano-emulsion templating intended for biomedical applications, specifically for the intravenous administration. Therefore, the system must have some specific features: a water phase, the continuous phase of the template nano-emulsion, with physiological pH and osmolality, an oil dispersed phase composed of a biocompatible and biodegradable polymer dissolved in a volatile organic solvent classified as class 3 by the ICH guidelines, and a FDA approved surfactant as stabilizer. Also, the process conditions should be safe. Therefore a low-energy emulsification methodology, specifically the PIC method was chosen for the preparation of nano-emulsions. Prior to nano-emulsion formation, selection of system components and a study of their suitability were carried out.

4.1.1. Aqueous components

The requirements for the aqueous component are the physiologic blood pH, around 7.4 and the osmolality, around 300mOsm/kg.

The solvent assayed was <u>water</u>, and different concentrations of salts were tested to prepare a buffer. The most common buffer used for biomedical applications is the phosphate buffered saline (<u>PBS</u>), which consists of a mixture of salts such as sodium chloride, sodium phosphate dibasic and disodium phosphate monobasic. In order to achieve blood characteristics, variation of pH and osmolality as a function of electrolyte concentration were determined. As Figure 4.1 shows, the evolution of pH and osmolality with the electrolyte concentration is different. While the pH is low at low electrolyte concentration and keeps constant at concentrations above 0.016M, the osmolality is directly proportional to the concentration of the salts. The PBS solution has the capacity of maintaining the pH at a specific range, between 7 - 8. Therefore, it is a buffer at concentrations approximately higher than 0.016M (if the concentration of ions dissolved is high, a higher electrolyte concentration would be required). However, at low electrolyte concentration, the salts are not enough to act as a buffer. The osmolality of a solution depends on the salt concentration. For this reason, the higher the electrolyte concentration, the higher the osmolality. Therefore, PBS with a concentration of 0.16 M was chosen for further studies,

since it has the physiological blood requirements (Figure 4.1). However, nano-emulsions and nanoparticles formed with water or intermediate concentrations of electrolytes in the aqueous phase were also studied for comparative and characterization purposes.
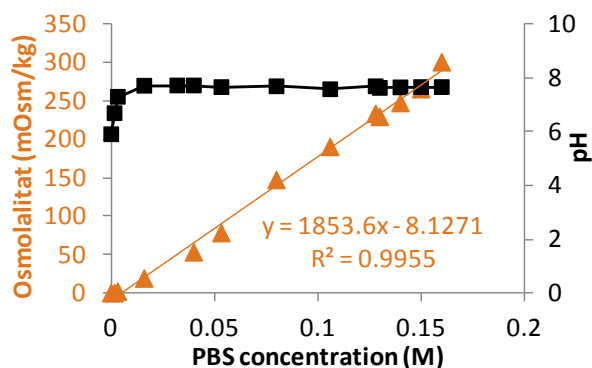
Figure 4.1: pH and osmolality (in mOsm/kg) of the PBS buffer as a function of electrolyte concentration (in M).

In the present thesis, PBS is also referred as electrolyte solution. In all cases, the composition of the buffer consists of the mixture of the same salts with the same concentration.

4.1.2. Surfactants

A surfactant is needed to facilitate emulsification and to enhance nano-emulsion kinetic stability. The surfactant has to be hydrophilic (HLB >10) to prepare O/W nano-emulsions. Nonionic ethoxylated surfactants, water soluble at low temperatures, tend to form O/W structures (Griffin, 1949; Becher, 1965; Shinoda, 1968 and 1973; Kunieda, 1985; Morales, 2006). Among them, polysorbate 80, with an HLB value of 15, which has been widely used for biomedical applications for a long time, was chosen. Moreover, it is used in many FDA approved formulations both for food and drugs (FDA, 2014) and the Toxicology Data Network (TOXNET) has defined it to be nontoxic and nonirritant in parenteral formulations (TOXNET, 2014). From the safety point of view, although polysorbate 80 is a FDA approved surfactant, a low concentration is recommended for pharmaceutical formulations, since it is usually the toxic component in preparations.

Another important factor for the selection of this surfactant is the extensive bibliography relating polysorbate 80 with the BBB crossing. Most studies on polysorbate 80 coated nanocarriers indicate an enhancement in the BBB crossing due to the presence of this surfactant (Calvo, 2001(1); Zensi, 2009; Chen, 2011; Patel, 2012; Wohlfart, 2012; Kreuter, 2014; Neha, 2013). However, in these studies, the surfactant is added *a posteriori*, mainly with the objective of directing nanoparticles through the BBB (Kreuter, 2014). In the present thesis, the main advantage of the nanoparticle preparation method (nano-emulsion templating approach followed by solvent evaporation) is that the polysorbate 80 surfactant is a component of the nanosystem itself; it is added at the initial step of template nano-emulsion formation, thus enabling to produce nanoparticles in a single-step procedure, easy to scale-up.

4.1.3. Oil components

4.1.3.1. Polymer

The polymer is the key component in a polymeric nano-emulsion intended for the preparation of polymeric nanoparticles. In the present thesis, poly-(lactic-co-glycolic acid) (PLGA) with 75wt% of lactic acid and 25wt % of glycolic acid was chosen due to its biocompatibility and biodegradability. Moreover, it is a FDA approved compound that has been recommended for intravenous administration with the aim to reach the BBB due to its rapid biodegradability because of its low molecular weight (Kreuter, 2014). PLGA degradation is mainly by hydrolysis (Catiker, 2000), although there are some studies which found that it occurs by enzymatic cleavage produced by a lipase (Landry, 1996). The rapid biodegradation is a special key issue when working with chronic diseases, such as Alzheimer's disease, in which a repeated chronic administration is required. If the polymer is not biodegradable, problems related with accumulation in the body could arise (Catiker, 2000; Kreuter, 2014). Compared with polylactic acid (PLA) and polyglycolic acid (PGA) homopolymers, PLGA usually is degraded more rapidly, thus avoiding toxicity problems due to polymer accumulation (Catiker, 2000). The more proportion of PGA in PLGA, the more hydrophilic the polymer, thus increasing the biodegradability rate (Catiker, 2000; Grayson, 2012).

Among all types of existing PLGA, in the present thesis, a PLGA with a low molecular weight was chosen. Previous bibliography demonstrated that the use of low molecular weight PLGA resulted in a reduced ruggedness in the particle surface, due to a reduced viscosity; enabling the formation of spherical particles with a smooth surface without porous (Graves, 2004). Solubility determinations of PLGA in various solvents (Table 4.1) showed that this PLGA is soluble in ethyl acetate, at least, up to 40 wt % (Table 4.1). However, in this work, 4wt% of PLGA was chosen since the use of this percentage allowed the formation of droplets of the desired size. PLGA solubility in the other solvents was also determined, since they were also used to prepare nano-emulsions. PLGA solubility in acetone was also above 40wt%, while it decreases below 1wt% with ethanol, which could be attributed to the higher polarity of ethanol as compared with acetone or ethyl acetate. In addition, PLGA solubility was also tested for a mixture of 20/80 wt/wt ethanol/ ethyl acetate, since this mixture was used for loperamide encapsulation. Although PLGA solubility is markedly reduced in presence of ethanol, in this mixture, the PLGA solubility is maintained above 40wt%.

Table 4.1: PLGA solubility (in wt %) at 25ºC, in different solvents.

Solvent	Solubility (wt %)
Acetone	> 40%
Ethyl acetate	> 40%
Ethanol	≤ 1%
ethanol/ ethyl acetate (20/80 v/v)	> 40%

The refraction index of PLGA was also assessed, as it is required in some techniques. As shown in Table 4.2, the refraction index increases when adding salts to water or aqueous solutions.

Table 4.2: Refractive index of the solvents used as the aqueous phase as determined by differential refractometry at 25ºC.

Solvent	Refractive index (RI)
Water	1.3330
Electrolyte solution	1.3351
Ethyl acetate saturated water	1.3373
Ethyl acetate saturated electrolyte solution	1.3394

4.1.3.1.1. Determination of PLGA molecular weight

The specifications of the commercial polymer (Resomer RG 752H, 2014) given by the supplier, Evonik, namely <u>molecular weight</u> (MW), was only an approximation: from 10,000 g/mol to 15,000 g/mol. These values were confirmed by viscosimetry, which allows calculating a theoretical molecular weight (as described in the experimental Section 3.3.1). In order to know more precisely the molecular weight of the polymer, gel permeation chromatography (GPC) was carried out. Since two batches were used in this thesis, both molecular weights were determined. One of them (Batch A) was tested from the provided powder sample and from a PLGA that had been dissolved in ethyl acetate for 20 days, in order to detect if the polymer experienced degradation due to its dissolution in the oil phase. The other batch (Batch B) was tested only as a powder. The results are specified in Table 4.3.

Table 4.3: Main characteristics of the different batches of PLGA used at different preservation states. Theoretical MW (in Da) calculated from viscosities. Experimental MW (in Da) assessed by GPC measurements.

PLGA sample	Ranges of MW	Viscosity (dl/g)	Theoretical MW	Experimental MW
Batch A	10,000 – 15,000	0.18	10,013	10,638
Batch B	10,000 – 15,000	0.16	8,376	12,950
Batch A (dissolved 20 days in ethyl acetate)	10,000 – 15,000	0.18	10,013	9,305

The experimental molecular weight for the initial Batch A is almost the same than the theoretical (Table 4.3). However, for Batch B, the experimental molecular weight differs from the theoretical and it also differs from the Batch A. This could indicate that the materials formed with this second batch could be different than those produced with the first. Nano-emulsions formed with polymer from both batches were compared, and no differences in droplet size, surface charge and stability between them were found. After 20 days of dissolution in ethyl acetate, the experimental molecular weight of the polymer decreased, but only about 10wt% of the initial molecular weight. Characterization of nano-emulsions formed using both, the ready dissolved polymer and that dissolved for longer times in ethyl acetate was also performed, finding no differences. This indicates that the polymer is quite stable once dissolved in ethyl acetate for at least 20 days.

4.1.3.1.2. Determination of PLGA glass transition temperature

Considering that PLGA should be a crystalline polymer in dry state, a study of the polymer sensitivity to temperature was considered appropriate. Differential scanning calorimetry (DSC), which provides information about the physical properties of products, such as their crystalline or amorphous state, was applied to the polymer (powder) to better characterize it. The results are shown in Figure 4.2. The DSC profile of PLGA powder after a first heating followed by a cooling and a second heating run shows that during the first scan, a single relaxation endothermic peak appears due to PLGA polymer loss of tension. T_g is the temperature interval in which the studied material loses its crystalline structure and turns to a mobile chain state. The polymer was maintained below the T_g for a long period (during storage), in which it is rigid and immobile. During this time, the polymer chains accumulate tension that is released when increasing the temperature. This happens in the first heating cycle, in which it is not possible to establish the T_g due to the presence of the relaxation peak. It is in the cooling and in the second heating runs where the T_g can be assessed. For the PLGA polymer, the T_g range is between 41.63ºC and 45.88ºC (midpoint = 43.56ºC and inflection point = 45.24ºC). The results of T_g reported in the literature for PLGA, showed T_g values around 44ºC (Jain, 2000). Moreover, the DSC curve shows a large relaxation endotherm, thus indicating

that the original form of the PLGA is in fact amorphous and with tension (Jain, 2000; Dillen, 2004). This temperature is above the physiological temperature (37ºC), which enables PLGA to be used in biomedical applications (Jain, 2000). At the temperatures studied, there is no a single peak indicating PLGA melting.

The same experiment was carried out with PLGA in presence of fetal bovine serum (FBS), in order to test the stability of the polymer in physiological blood conditions. The T_g range is between 43.21ºC and 47.40ºC (midpoint = 44.66ºC and inflection point = 46.60ºC) (see Figure Ap.1, appendix). These results are similar to the values obtained without FBS, thus, it could be concluded that the presence of FBS does not influence the glass transition temperature of PLGA.
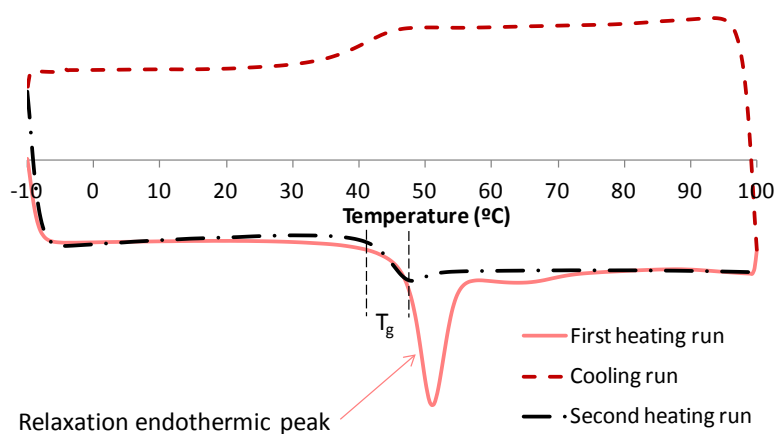
Figure 4.2: DSC profile of PLGA polymer: first heating, cooling and second heating runs, from -10ºC to 100ºC in steps of 10ºC/min.

4.1.3.2. Solvent

Since the formulated nanoparticles are intended for biomedical use, the solvent must have as less toxicity as possible. In this context, the solvent used should belong to the class 3 of the solvent classification of the ICH guidelines (Pinto Reis, 2006). Ethyl acetate was chosen not only for its classification in the class 3 of solvents, but also for its ability to dissolve the polymer and for its easy elimination by evaporation. Ethanol and acetone were chosen as alternative solvents when using loperamide hydrochloride (LOP) due to its higher solubility in these solvents. Ethanol and acetone show similar properties than those mentioned for ethyl acetate.

It is worth noting that ethyl acetate is a partially water soluble solvent, as well as the mixtures ethanol/ethyl acetate and acetone/ethyl acetate (ethanol and acetone are water soluble). The partial solubility between the aqueous and the oil phases of the nano-emulsions formulated were experimentally assessed by visual observation of the aspect of the mixtures, as described in Section 3.3.2. These results are shown in Table 4.4. The solubility of ethyl acetate in the aqueous phases is higher than the partial solubility of the aqueous phases in ethyl acetate. Differences between solubility of water and the electrolyte solution (0.16M) in ethyl acetate are not pronounced, although, the solubility of water in ethyl acetate is higher.

Table 4.4: Solubility (in wt%) of the aqueous phase in the oil phase and of the oil phase in the aqueous phase assessed by visual observation at 25ºC. Results are expressed as means ± standard deviations of 10 replicates.

Samples tested	Solubility (wt%)
Water in ethyl acetate	3.0437 ± 0.0997
Electrolyte solution (0.16M) in ethyl acetate	2.4373 ± 0.1902
Ethyl acetate in water	7.2897 ± 0.1794
Ethyl acetate in electrolyte solution (0.16M)	6.7261 ± 0.0686

4.1.3.3. Encapsulated compounds

Other components have been dissolved in the oil phase, with the objective to encapsulate them during the emulsification process. These components were the drugs loperamide hydrochloride and galanthamine hydrobromide and the fluorescent dye Coumarin 6. Solubility of these compounds was studied in different solvents in order to know the maximum concentration of the encapsulated drug/dye by means of determining the change in the macroscopic visual appearance of the samples when adding these compounds. Results are shown in Table 4.5.

Table 4.5: Solubility (in wt%) of the encapsulated components in different solvents at 25ºC. Grey cells indicate non-tested samples. Water has a pH 5.5 while the electrolyte solution has a pH of 7.4.

Solvent	Solubility (mg/mL)		
	Coumarin 6	Loperamide hydrochloride	Galanthamine hydrobromide
Water	< detection limit	0.099 ± 0.109	0.056 ± 0.005
Electrolyte solution (0.16M)	< detection limit	0.015 ± 0.008	0.082 ± 0.003
Ethyl acetate	3.979 ± 0.284	< detection limit	0.185 ± 0.017
Acetone	3.059 ± 0.346	3.257 ± 0.008	386.746 ± 3.786
Ethanol	0.135 ± 0.018	2.646 ± 0.010	0.006 ± 0.000
Ethanol / ethyl acetate (20/80)		1.366 ± 0.009	

Their solubility in ethyl acetate (or the oil phase chosen) should be sufficient for the drugs to achieve therapeutic concentrations and for Coumarin 6, for imaging purposes. The solubility of Coumarin 6 is much higher in organic solvents than in aqueous solvents, specifically in ethyl acetate and acetone. For this reason, its encapsulation in the nano-emulsion droplets is feasible. For loperamide hydrochloride, in aqueous medium, the solubility is very low, and decreases in the presence of electrolytes. This may be attributed to a salting out effect. Although loperamide hydrochloride has a higher solubility in organic solvents than in aqueous solutions, its solubility in ethyl acetate was very low. For this reason, a mixture between different solvents was tested, achieving solubilities higher than 1 mg/mL when ethyl acetate with a 20 wt% of ethanol was used. For galanthamine hydrobromide, its solubility is lower than that of the other drug in most of the solvents used, with the exception of acetone. However, ethyl acetate was maintained as solvent of the disperse phase because encapsulation of therapeutic concentrations of the drug can be achieved.

It is worth noting that, since both drugs have a pKa value (8.6 for loperamide and 7.97 for galanthamine) (NCBI, 2014), their solubility depends on the pH of the aqueous media. Therefore, at basic pHs, higher than their pKa, their solubility in aqueous phases would be reduced due to the presence of less ionic species, thus enhancing their solubility in oil phases (change in the partition

coefficient). However, basic pHs cannot be used because PLGA polymer, containing ester bonds (Resomer RG 752H, 2014), would undergo hydrolysis.

The solubility of loperamide in water was further studied as a function of pH and temperature (Figure 4.3). At low pH, the solubility of the drug is high, decreasing as the pH increases, reaching low and practically constant values at high pH. This behavior is the expected one, as the pKa of loperamide is 8.6. At low pH values loperamide is ionized, which enhances its solubility in water. However, when increasing the pH value of the medium, the degree of ionization of loperamide decreases, thus decreasing its solubility in water. Regarding the effect of the temperature, the solubility at 25ºC is higher than at 37ºC at low pH values, but it is not temperature dependent at basic pH (Figure 4.2a). This may be attributed to a desolvation at higher temperatures. The solubility of loperamide was also studied in ethanol/water mixtures. It increases exponentially with the increase in the ethanol / water ratio, as expected (Figure 4.2b).
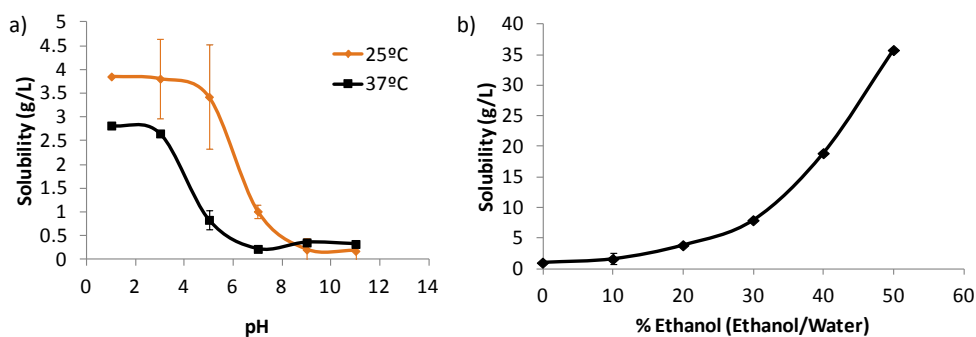
Figure 4.3: Solubility (in wt%) of loperamide hydrochloride in: a) water as a function of pH at 25ºC and 37ºC and b) as a function of the ethanol / water mixing ratio at 25ºC.

Summary

Components of nano-emulsions intended as nanoparticle templates apt for biomedical applications, namely by intravenous delivery, have been selected. A PBS buffer at a concentration of 0.16M was selected since it fulfills the pH and osmolality requirements. The polysorbate 80 was selected as the nonionic ethoxylated surfactant, not only for safety requirement, but also for the potential in BBB passive targeting. The oil phase selected is composed of the FDA approved PLGA polymer, with a low molecular weight and a glass transition temperature above the body temperature, and, ethyl acetate, an organic volatile solvent classified as class 3 for the ICH guidelines. In addition, some drugs (loperamide and galanthamine) and a fluorescent dye (Coumarin 6), with enough solubility in the selected solvents, were chosen for their further encapsulation.

4.2. Nano-emulsion formation by the phase inversion composition (PIC) method and characterization

In this section, the study of the influence of the components on the physico-chemical properties of nano-emulsions is reported for nano-emulsions produced using the following system: aqueous phase (W) / polysorbate 80 surfactant (S) / oil phase (O). The aqueous phase was used at different electrolyte concentration, varying from water to PBS at 0.16M, studying also PBS 0.08M and 0.03M. The oil phase consists on poly-(lactic-co-glycolic acid) (PLGA) polymer dissolved in a solvent. Unless otherwise stated, the PLGA concentration in the oil phase is 4wt% and the solvent used is ethyl acetate. The terms electrolyte solution and PBS are used indistinctly for the aqueous solutions with different concentrations of the following salts: sodium chloride, sodium phosphate dibasic dihydrate and sodium phosphate monobasic hydrate.

4.2.1. Determination of nano-emulsion domains in aqueous / surfactant / oil systems

Nano-emulsions were prepared, as mentioned above, using the phase inversion composition (PIC) method, by stepwise addition of the aqueous phase to mixtures with different oil/surfactant (O/S) ratios, at 25ºC. The influence of electrolyte and polymer concentrations and the solvent type on nano-emulsion formation and properties were studied for the system: *PBS (W) / polysorbate 80 (S) / [4wt % PLGA in ethyl acetate] (O).*

4.2.1.1.   Effect of electrolyte concentration

The electrolyte concentrations were chosen considering the blood pH and osmolality (Dobrovolskaia, 2013). PBS 0.16M was the highest electrolyte concentration tested, considering the results of Section 4.1. The nano-emulsion domains are shown in the pseudoternary phase diagram of Figure 4.4.
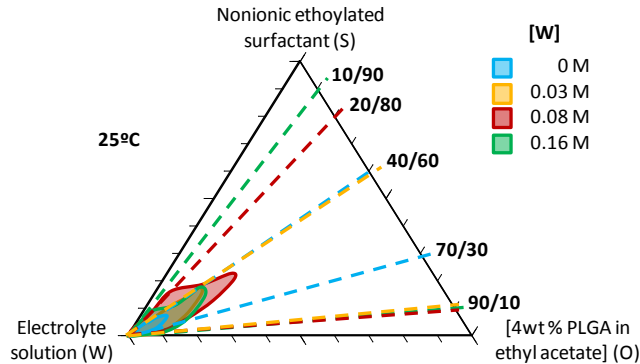
Figure 4.4: Region of nano-emulsion formation in the systems: Aqueous solution (W) / Polysorbate 80 (S) / [4wt % PLGA in ethyl acetate] (O).

Table 4.6 shows the minimum aqueous solution content and the range of O/S ratios in which nano-emulsions form for each aqueous phase (electrolyte concentration).

Table 4.6: Region of nano-emulsion formation for the system *aqueous solution (W) / polysorbate 80 surfactant (S) / [4wt % PLGA in ethyl acetate] (O), at 25ºC,* as a function of the electrolyte concentrations.

Aqueous phase	Nano-emulsion domain	
	W (wt %)	O/S
0.00 M	> 85wt%	40/60 – 70/30
0.03 M	> 70wt%	40/60 – 90/10
0.08 M	> 60wt%	20/80 – 90/10
0.16 M	> 70wt%	10/90 – 90/10

As evidenced in Figure 4.4 and Table 4.6, the extent of nano-emulsion formation is dependent on the composition of the aqueous phase. The presence of <u>electrolytes</u> enables the formation of nano-emulsions in a broader range of O/S ratios and lower aqueous phase contents. Moreover, the higher the electrolyte concentration, the wider the O/S ratios of nano-emulsion formation domain. However, no direct dependency of electrolyte concentration with the water content was found. The <u>nano-emulsion visual appearance</u> (in terms of transparency and shining) was also dependent on the aqueous phase composition. As Figure 4.5 shows, by increasing the electrolyte concentration, the transparency of the nano-emulsions increases. However, decreasing the PBS concentration of the aqueous component, the

transparency of nano-emulsions decreased independently of the electrolyte concentration, becoming more opaque/milky. Regarding nano-emulsion shining, nano-emulsions formed with water as aqueous phase show a reddish translucent aspect, while in the presence of electrolytes, the nano-emulsions become transparent with a bluish shine. The mentioned visual characteristics could be attributed to differences in the droplet sizes (Spernath, 2009, Calderó, 2011) or differences between the refractive indexes between the aqueous and the oil phase (Schalbart, 2010; Heunemann, 2011).
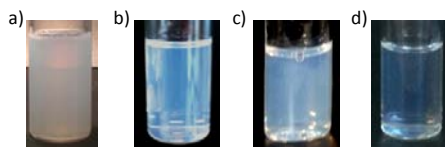
Figure 4.5: Examples of nano-emulsions with 90wt% of aqueous component and an O/S ratio of 70/30. PBS concentration: a) 0M; b) 0.03M; c) 0.08M and d) 0.16M.

4.2.1.2. Effect of solvent

The formation of nano-emulsions was also studied as a function of the <u>nature of the solvent</u> that constitutes the oil phase. A combination of ethanol / ethyl acetate in weight percentage of 20/80 was used, since it was found appropriate for loperamide encapsulation due to drug solubility requirements (shown in Section 4.1.3.3). The nano-emulsion formation region was determined with and without loperamide, with 0.16M electrolyte concentration and 4wt% PLGA in the oil phase (Figure 4.6 and Table 4.7). Nano-emulsions for the system without the drug are formed at O/S ratios between 35/65 and 95/5 and water contents above 40wt%. Nano-emulsions with loperamide (0.1wt% in the oil phase) are formed at O/S ratios between 40/60 to 95/5 and water contents above 45wt%.When adding the drug in the oil component, the nano-emulsion domain is similar at high water contents while it is narrower at low water contents. The decrease in the nano-emulsion domain due to the effect of the addition of the drug has been reported for certain drugs (Date, 2007 and 2010).
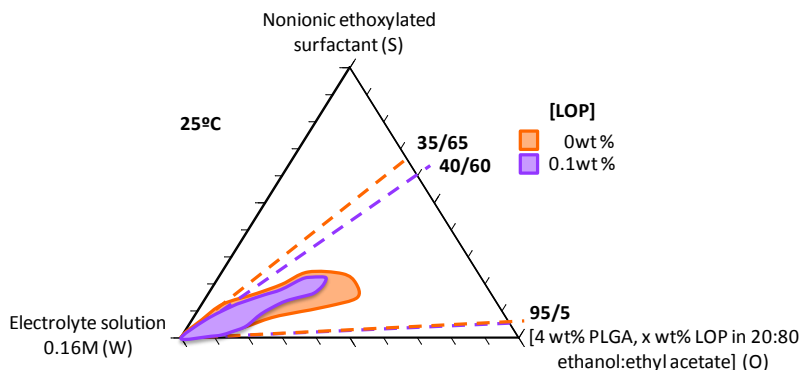
Figure 4.6: Region of nano-emulsion formation, at 25ºC, in the system: 0.16M electrolyte solution (W) / Polysorbate 80 surfactant (S) / [4 wt % PLGA + x wt% loperamide hydrochloride in 20:80 ethanol:ethyl acetate] (O).

Table 4.7: Region of nano-emulsion formation for the system *PBS 0.16M (W) / polysorbate 80 surfactant (S) / [4 wt % PLGA + x wt% loperamide in 20/80 ethanol / ethyl acetate] (O)*.

[loperamide] in the oil phase	Nano-emulsion domain	
	W (wt %)	**O/S**
0wt %	> 40wt%	35/65 – 95/05
0.1wt %	> 45wt%	40/60 – 95/05

4.2.1.3. Effect of polymer concentration

The increase on the polymer concentration in the oil phase could enhance nano-emulsion stability due to a reduction of the Ostwald ripening (Kabal'nov, 1987). For this reason, the effect of increasing the polymer concentration was studied. Formation of nano-emulsions was determined for a polymer concentration of 20wt% (Figure 4.7). The results for 4wt% of polymer concentration in the oil phase (given in Figure 4.4) are also shown in Figure 4.7 for comparative purposes.
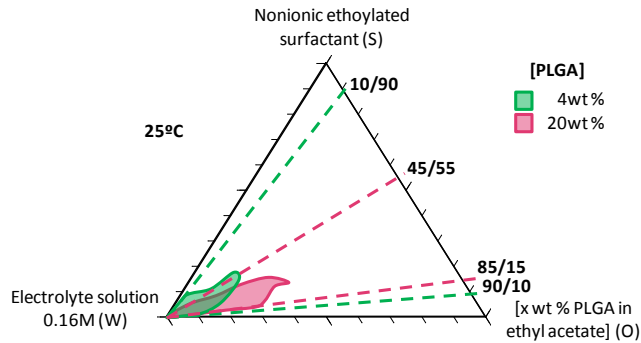
Figure 4.7: Region of nano-emulsion formation with the system: 0.16M electrolyte solution (W) / Polysorbate 80 surfactant (S) / [x wt % PLGA in ethyl acetate] (O).

Figure 4.7 shows that nano-emulsion domain for the system with 20wt% of PLGA comprises O/S ratios between 45/55 and 85/15, and water contents above 55wt%. Comparing with the system with 4wt% of polymer, the nano-emulsion domain is narrower, shifted to higher oil contents (higher O/S ratios). In addition, increasing the polymer content, nano-emulsions can be formed with lower water contents (Figure 4.7 and Table 4.8).

Table 4.8: Region of nano-emulsion formation for the system *PBS 0.16M (W) / polysorbate 80 surfactant (S) / [x wt % PLGA in ethyl acetate] (O)*.

[PLGA] in the oil phase	Nano-emulsion domain	
	W (wt %)	**O/S**
4wt %	> 70wt%	10/90 – 90/10
20wt %	> 55wt%	45/55 – 85/15

The nano-emulsion formation domain increases by increasing the polymer content (Figure 4.7), as well as when using the mixture of 20/80 ethanol/ethyl acetate as the oil phase (Figure 4.6). This could be explained by a change in the partition coefficient of the surfactant between the oil and the water phases, thus producing a synergistic effect between the components and favoring the nano-emulsion formation (Morales, 2003; Sadurní, 2006; Anton, 2008). At high concentrations of the aqueous component, nano-emulsion formation forms for a wider of O/S ratios at 4wt% PLGA concentration. Nevertheless, the selection of the PLGA concentration in the oil phase was carried out according to droplet size and stability results (shown in Sections 4.2.2 and 4.2.4).

4.2.1.4. Assessment of the phase inversion mechanism in nano-emulsion formation

Conductivity of samples with different O/S ratios was measured, at 25ºC as a function of the water content to confirm whether the formation of nano-emulsion was produced by phase inversion (Forgiarini, 2001; Calderó, 2011). Figure 4.8a shows the results of conductivity for samples with O/S ratios of 50/50, 60/40 and 70/30, and 4wt% of PLGA in the oil phase, as a function of water content (without electrolytes). At null or very low water content, the conductivity of the system is low, as expected. Since the system consists of a mixture of commercial oil and surfactant, conductive species coming from their impurities exist, showing a small conductivity. The addition of more water tends to form W/O structures. At these concentrations, isotropic liquid phases could be formed. When increasing the water concentration, the conductivity increases, which could be due first to percolation, producing enhanced mobility of the conducting species of the system. With more water content, the conductivity keeps increasing, reaching a maximum after which the conductivity decreases. After the percolation stage, bicontinuous or lamellar liquid crystalline structures may form and the highest values of conductivity indicate that aqueous continuous (O/W) structures are formed. The decrease in the conductivity at high water concentration is due to a dilution effect (Meziani, 1997 and 2000). Therefore, phase inversion from W/O to O/W structures is produced during the emulsification process..
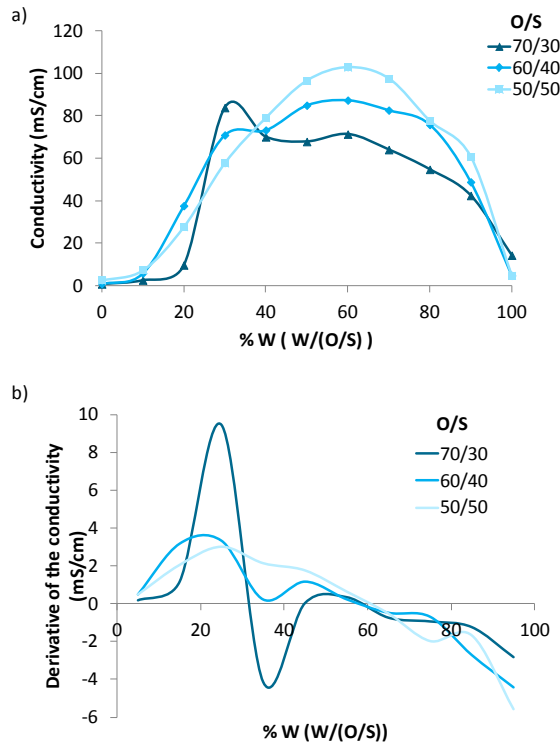
Figure 4.8: Conductivity of the dilution path of a nano-emulsion without electrolytes in the aqueous phase (0M), 4wt % of PLGA in the oil phase and varying the O/S ratio, as a function of aqueous phase percentage. a) Absolute values and b) Derivative of the conductivity.

Concerning the influence of the O/S ratio, it was observed that the higher the oil fraction, the more abrupt the slope of the conductivity curves at the inversion range (Figure 4.8a), and that of its derivatives (Figure 4.8b), which is in good agreement with previous studies using other polymers (Calderó, 2011). This could be due to the less ionic species present in the components, namely the polymer, at lower O/S ratios during the transition. Nevertheless, an inversion of the phases takes places independently of the O/S ratio, thus confirming that these nano-emulsions form by a phase inversion method.

The system with PBS 0.16M (W) / polysorbate 80 (S) / [4wt% PLGA in ethyl acetate] was studied, with an O/S ratio of 70/30. Figure 4.9 shows the results of conductivity as a function of aqueous solution (PBS 0.16M) content. The conductivity is low at low water concentrations (up to 10%). The further addition of water produced a continuous increase in the conductivity. These results were expected, as when adding electrolytes in the aqueous phase, conductivity cannot be used for the assessment of phase inversion due to the continuous increase in conductivity

produced by the increase in electrolyte concentration. For this reason, only the system with water as the aqueous component was studied by means of conductivity to detect phase inversion.

Determination of phase inversion was also attempted by measuring the mobility. Figure 4.9 also shows the derivative of the mobility (mobility results are presented in Figure Ap.2, appendix). A phase inversion could be inferred from 15wt% to 45wt% aqueous contents.
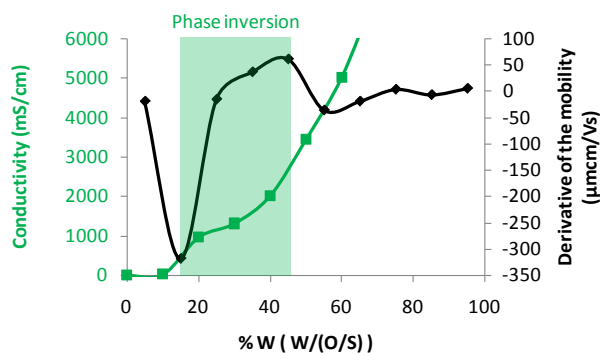
Figure 4.9: Conductivity and derivative of the mobility measurements for a sample with an O/S ratio of 70/30 as a function of aqueous phase content (0.16M).

To confirm that phase inversion was produced in the systems with electrolytes in the aqueous phase, a water soluble (Rhodamine B) and an oil soluble (Sudan Black) dyes were used. The system with PBS 0.16M with an O/S ratio of 70/30 was studied as a model. Figure 4.10 shows the results. Firstly, the phase behavior was explored. At time 0, at low aqueous percentages, samples with a transparent and viscous appearance are formed (Figure 4.10a). Adding more water, the turbidity of the samples increases up to around 70wt% of water content. Further water addition increased the transparency of samples, together with an increase of the bluish shining. Therefore, as studied above (Figure 4.4), nano-emulsions are formed from water contents of around 70wt%. After 60 days (Figure 4.10b), all samples changed their visual appearance, due to destabilization. At low water contents, samples are more transparent. Only the samples with intermediate water contents (30 – 70 wt%) suffered phase separation. At higher water contents, samples are also transparent, without phase separation.

Regarding the diffusion of dyes, the lipophilic dye (Figure 4.10c), diffuses quickly through the sample at low water contents, up to 10wt%, indicating the presence of oil-continuous dispersions (W/O-type structures). In contrast, the hydrophilic dye diffuses through the samples above water contents of around 40 – 45 wt% (Figure 4.10d), thus indicating that these samples have a hydrophilic nature, they are O/W-

96

type structures. At intermediate water contents, between water contents of 15 – 50wt%, a phase separation rapidly takes place (Figure 4.10c and d). After its destabilization, a lipophilic upper part appears, which corresponds to the oil fraction and a hydrophilic lower part, which corresponds to the aqueous phase. The lower part can be assessed to be water due to its higher density as compared with the oil (ethyl acetate). This lower phase increases in volume when increasing the water content, thus confirming its aqueous nature.
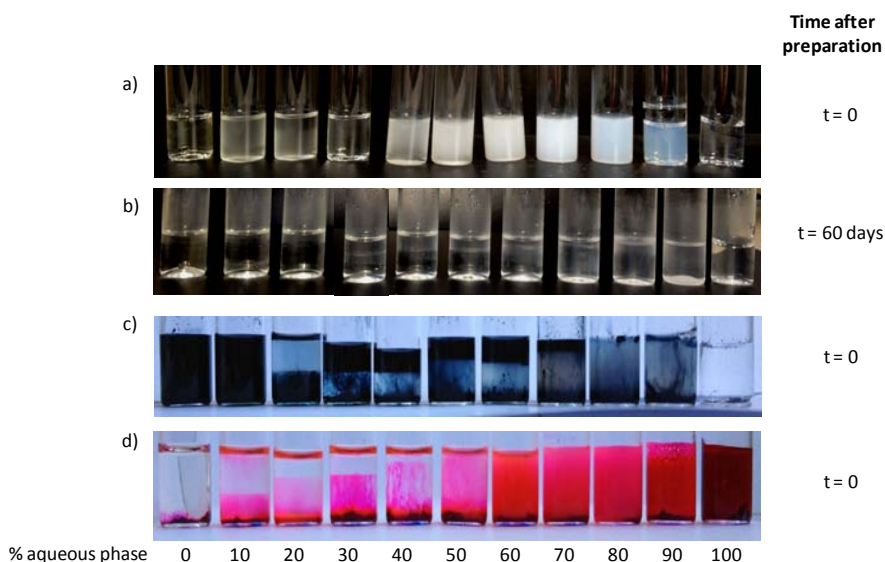
Figure 4.10: Samples prepared with an O/S ratio of 70/30, at different percentages of aqueous phase (PBS 0.16M). a) t=0; b) t= 60 days at 25ºC; c) Samples in the presence of Rhodamine B (t=0); and d) Samples in the presence of Sudan Black (t=0).

Therefore, the formation of the nano-emulsions due to a phase inversion is confirmed for systems with electrolytes.

Summarizing, the study of the nano-emulsion formation as a function of the system components and concentration (Section 4.2.1) reveals that changes in the oil component or other components produce variations in the region of formation of nano-emulsions, as previously reported for other systems (Meziani, 2000; Forgiarini, 2001; Maestro, 2008; Solans, 2012). The increase in the polymer content and the incorporation of ethanol increased the nano-emulsion formation domain which could be explained by a change in the surfactant partition coefficient between the modified oil and the water producing a synergic effect between the components that favor the nano-emulsion region of formation (Morales, 2003; Sadurní, 2006).

In the following sections, nano-emulsions with 90wt% of water content, otherwise stated, will be considered. The selection was based on qualitative observations of their visual aspect and stability.

4.2.2. Nano-emulsion droplet size

Nano-emulsion droplet size of samples with 4wt% PLGA in ethyl acetate, without and with electrolytes was measured by DLS, for different O/S ratios. An example of the size distribution plots of nano-emulsions with an O/S ratio of 60/40 and different concentrations of electrolytes is shown in Figure 4.11.
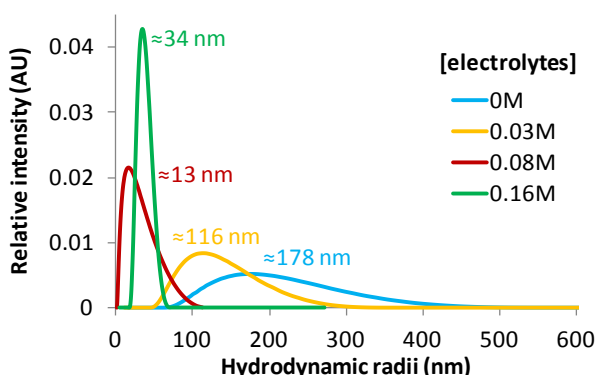
Figure 4.11: Examples of the size distribution of the nano-emulsions with 90wt % of aqueous phase and 60/40 O/S ratio, as a function of the electrolyte concentration.

To study whether the formulated nano-emulsions were a single homogeneous population or not, the DLS results were analyzed using the contin method. The results of the size distributions reveal that all samples are monomodal (Figure 4.11) although the polydispersity indexes (PDI) seem to be bigger than expected (from 0.2 to 0.47) (see Table Ap.1, appendix).

The hydrodynamic droplet radii, as a function of the O/S ratio and different electrolyte concentrations, are plotted in Figure 4.12. An increase in the droplet size when increasing the dispersed phase content (increase in O/S ratio) was expected, as previously reported for other systems and methodologies, due to the reduction of the surfactant concentration (Izquierdo, 2004; Sadurní, 2005). However, the results obtained were not as expected. For the nano-emulsions with water as aqueous component (0 M), the hydrodynamic radius decreases with the increase in the O/S ratios up to an O/S ratio of 50/50 and above this ratio, it keeps constant. The difference in size between the highest (225 nm) and the lowest (180

nm) values is about 45 nm. The variation of the hydrodynamic size with the O/S ratio could be due to a combination of two opposite effects. On the one hand, an increase of the radius with the increase of the O/S ratio (surfactant effect). On the other hand, the diffusion of the solvent, ethyl acetate, to the continuous phase, due to its partial water solubility which produces a decrease in droplet size. . At low O/S ratios, the solvent diffusion seems to be predominant, as nano-emulsion droplets decrease in size, while at high O/S ratios both effects seem to be compensated.

For the nano-emulsions with electrolytes, the behavior strongly depends on the electrolyte concentration. At 0.03 M, the droplet size experiences a pronounced decrease (from 250 nm to 20 nm) with the increase in the O/S ratio (Figure 4.12). At low O/S ratios, up to 50/50, droplet sizes are similar to those without electrolyte. However, at O/S ratios higher than 50/50, a marked reduction of the droplet size is observed: the solvent diffusion effects predominate, since at increasing O/S ratios, droplet sizes decrease dramatically. It can be expected that the addition of electrolytes in the aqueous phases enhances the salting out effect, favoring the solvent diffusion, as discussed below.

For the nano-emulsions with electrolytes at 0.08 M, droplet sizes are mainly low (around 18 nm) and keep constant in a wide range of O/S ratios, experiencing a slight increase at O/S ratios higher than 80/20 (Figure 4.12). Therefore, both effects, surfactant effect and solvent diffusion, are compensated in a wide range of concentrations. The increase in the droplet size at the highest O/S ratio of the nano-emulsion formation domain could be related with the formation of less stable nano-emulsions.

For nano-emulsions with the highest electrolyte concentration (0.16 M), the droplet sizes were high (around 150 nm) at the lowest O/S ratios (20/80 and 30/70), and a pronounced decrease is produced at an O/S ratio of 40/60, remaining low with a slight increase up to an O/S ratio of 80/20. At higher O/S ratios, the size decreases and then increases, which could be due to instability of the samples. It had been observed that nano-emulsions at the edges of the formation region showed lower stability as compared with the nano-emulsions in the central part of the domain. Considering the nano-emulsions with O/S ratios between 40/60 and 80/20, the behavior is similar to that of nano-emulsions with electrolyte concentration of 0.08M.

These sizes obtained in nano-emulsions in the central part of the nano-emulsion domain with 0.08 and 0.16M are lower (30 – 40 nm) as compared with previous studies reported in the bibliography, which is advantageous for their use as templates for the production of nanoparticles with small nanometric sizes, required

for the intravenous route of administration (Kreuter, 1996; Hans, 2002; Couvreur, 2006; Vauthier, 2009(1)). It is worth noting that the use of a low-energy emulsification methodology has allowed the formation of small droplet size, attributed to the change in the spontaneous curvature of the surfactant during the emulsification process (Forgiarini, 2001).
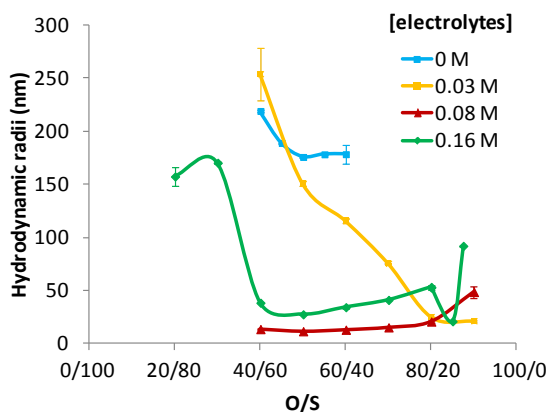
Figure 4.12: Hydrodynamic droplet radius (Rh) of nano-emulsions with 90wt % of water as a function of O/S ratio and electrolyte concentration.

The PDI of the nano-emulsions (see Ap.1, appendix) were slightly higher than 0.2, which is considered the upper limit to define a sample as monodisperse (Schärtl, 2006). At low O/S ratios (below 55/45), PDI increases at increasing the electrolyte concentration, but above this ratio the behavior seems to be the inverse. Due to the polydispersity in these samples, nano-emulsions were observed under the optical microscope in order to detect the presence of big droplets. However, not a single droplet was observed, thus confirming the nanometric droplet sizes (Figure Ap.3, appendix).

The underline influence of electrolytes on nano-emulsion droplet size was studied more systematically using intermediate concentrations to those previously studied. The results, plotted as a function of electrolyte concentration (Figure 4.13) clearly indicate that, independently of the O/S ratio, the abrupt reduction in droplet size from 150 – 200 nm to around 25 nm is produced at an electrolyte concentration of 0.04M. Droplet sizes were high at low electrolyte concentrations (0M). The addition of electrolytes enables the formation of smaller droplets: the nano-emulsion droplet radius is around 175 nm in absence of electrolyte, and it experiences an abrupt reduction at an electrolyte concentration of 0.04M to values of around 20 nm. This happens for all O/S ratios studied except for the 40/60 O/S

ratio, where nano-emulsion droplet size experiences an increase when increasing the electrolyte concentration (up to 0.032M) and then the droplet size decreases, as it occurs for other O/S ratios. The cause of this size reduction could be the combination of two effects, already described. On one hand, the salting out effect, that is, the dehydratation of the polar heads of the surfactant (Kunieda, 1989; Allémann, 1992; Klaus, 2012). The electrolytes have more affinity for water and the polar heads of the surfactant are more dehydrated due to the displacement of the water molecules thus increasing the strength of the surfactant interactions and reducing the size of the droplets (Kunieda, 1989; Klaus, 2012). On the other hand, the solvent diffusion, which has already been related with droplet size variations of nanometric colloids (micelles and microemulsions) (Fessy, 1989; López-Montilla, 2002). The osmotic pressure is always higher in the continuous phase than in the internal oil phase, enabling the solvent diffusion from the inner oil droplets to the continuous phase, thus reducing the droplet size. The solvent diffusion is enhanced when there are electrolytes in the aqueous phase, as electrolytes increase the osmotic pressure and therefore the osmotic gradient between the internal and the external phases. Both effects act in the same direction: the higher the electrolyte concentration, the smaller the droplet size. However, the reduction of the droplet size at increasing electrolyte concentration takes place only up to limit of about 0.04 M (Figure 4.13), above which the aqueous phase is already saturated of ethyl acetate and the addition of more electrolytes does not produce changes in the size.
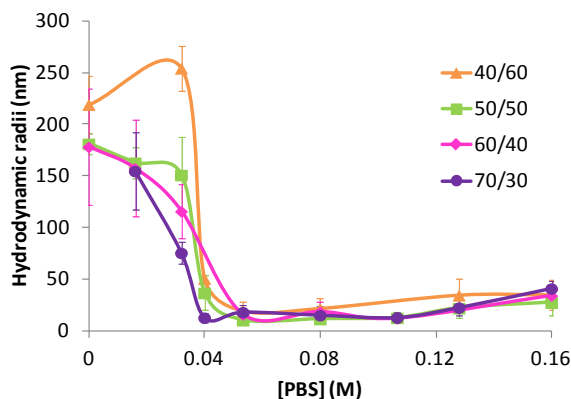
Figure 4.13: Hydrodynamic droplet radius of nano-emulsions with 4wt % of PLGA, as a function of O/S ratio and electrolyte concentration.

Summarizing the results of droplet sizes as a function of the O/S ratios for all the studied systems, in all systems (0M, 0.03M, 0.08M and 0.16M), a combination between the diffusion of the solvent, that reduces the droplet size at increasing the O/S ratio with the effect of the dispersed phase, that increases the droplet size at increasing the O/S ratio, was found. The presence of electrolytes in the aqueous phase enhanced the diffusion effect.

Comparing the droplet size of nano-emulsions with and without electrolytes, with water is nearby one order of magnitude higher than that of nano-emulsions prepared with electrolyte solution. The huge difference is already evident visually (Figure 4.5). The smaller sizes, which would be preferred for the intravenous administration in terms of colloidal issues (Gref, 2012; Dobrovolskaia, 2013) were obtained with PBS 0.08M. However, due to the low osmolality values, they cannot be used for the intravenous administration. It is remarkable that only three studies have been found in the literature (Forgiarini, 2001; Sadurní, 2005; Sonneville-Aubrun, 2009) reporting nano-emulsions with small sizes, comparable with those nano-emulsions with electrolytes presented in this thesis.

It was considered of interest to calculate the number of droplets as a function of O/S ratio, in the presence and absence of electrolytes. The number of droplets was calculated according to Equation 7.7. (See appendix section) (Némati, 1994) for nano-emulsions without and with 0.16M electrolyte, with 4wt% of PLGA and different O/S ratios. As shown in Table 4.9, for both nano-emulsions, the higher the O/S ratio, the higher the number of droplets. These results could explain the size dependency on the O/S ratio. As justified above, increasing the O/S ratio, the nano-emulsion droplet size was expected to increase, but in the system studied in the present thesis, there is also a solvent diffusion effect. When both effects are balanced, the droplet size keeps constant. For this reason, if the oil content increases (at increasing O/S ratio) and the droplet size does not increase, the number of droplets increases. Comparing the results between the nano-emulsions without and with electrolytes, since the droplet size is nearby one order of magnitude smaller with electrolytes, the number of droplets is two orders of magnitude higher. There are more droplets than expected when the droplet radius is smaller, at a same oil content.

Table 4.9: Number of droplets per milliliter as a function of aqueous component (without and with 0.16M electrolyte concentration) and O/S ratio.

Electrolyte concentration	O/S ratio	Number of droplets / mL
0M	50/50	$2.05 \cdot 10^{12}$
	60/40	$2.46 \cdot 10^{12}$
	70/30	$2.88 \cdot 10^{12}$
0.16M	70/30	$2.60 \cdot 10^{14}$
	75/25	$2.80 \cdot 10^{14}$
	80/20	$2.99 \cdot 10^{14}$

The influence of <u>polymer concentration </u>on droplet size was also studied in nano-emulsions with different O/S ratios and 0.16M electrolyte concentration. The results are shown in Figure 4.14. Independently on the polymer concentration (4wt% and 20wt%), the same tendency was observed: at low O/S ratios, the droplet size is high (100 – 150 nm) and at a certain O/S ratio it decreases abruptly to values around 25 nm (Figure 4.14). Comparing the results from both percentages of PLGA, the size tendency is shifted to higher O/S ratios for the nano-emulsions with 20wt% of PLGA in the oil phase. These results are in good agreement with previous bibliography, where bigger droplets were reported when the polymer concentration was increased (Trimaille, 2003). This could be explained because the range of the O/S ratios where nano-emulsions are formed is narrower for the 20wt% of PLGA (Figure 4.7 and Table 4.8). No differences in the PDI values were found in nano-emulsions with both polymer concentrations (Table Ap.2, appendix section).
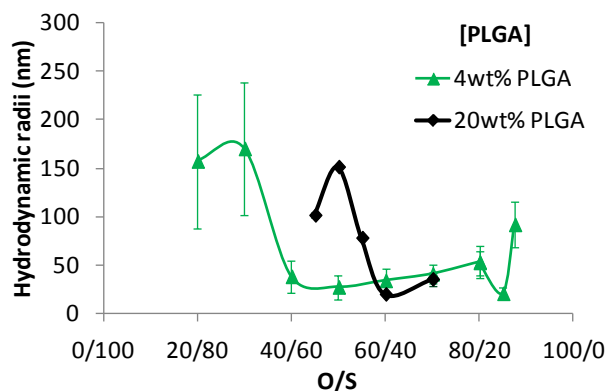
Figure 4.14: Hydrodynamic droplet radius (Rh) of nano-emulsions with PBS 0.16M as the aqueous phase, as a function of O/S ratio, at 25ºC.

Another factor studied was the underline influence of the oil type on nano-emulsion droplet size. As previously discussed, ethanol was added to the oil phase (constituted by ethyl acetate and polymer) to facilitate the incorporation of a drug (loperamide). Moreover, the influence of acetone added to the oil phase was also studied for comparative purposes. The droplet sizes of nano-emulsions with PBS 0.16M and an O/S ratio of 70/30 were determined as a function of the solvent/ ethyl acetate ratio.
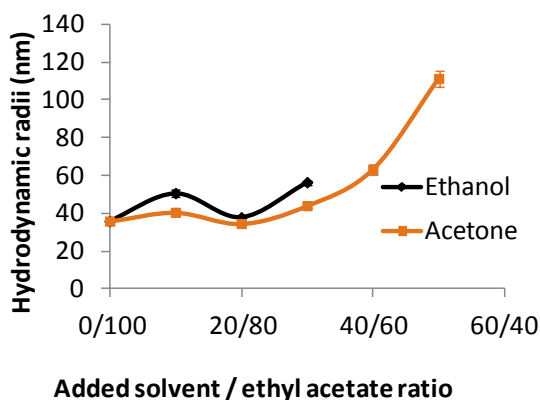
Figure 4.15: Hydrodynamic droplet radius of nano-emulsions prepared with 90wt% PBS at 0.16M and an O/S ratio of 70/30, as a function of added solvent / ethyl acetate ratio, at 25ºC.

The nano-emulsion droplet radii (Figure 4.15) are almost constant up to the 20wt% of added solvent. At higher added solvent / ethyl acetate ratio ratios, the hydrodynamic droplet sizes increase, independently of the solvent added, ethanol or acetone. These results were compared with previous bibliography studies on the effect of the oil phase on nano-emulsion droplet size (Bouchemal, 2004). In that study, it was reported that the higher the oil viscosity, the smaller the droplet size (3cP vs 0.5cP). In the present work, the droplet size cannot be related with the oil phase viscosity, since ethanol and acetone have different viscosities (ethanol = 1.04 cP; acetone = 0.335 cP) (Pal, 1998) and produce the same effect, although high viscosities as those ones reported in the work of *Bouchemal et al.,* (Bouchemal, 2004) are not studied. Another explanation for the size change when incorporating acetone / ethanol could be related with their water solubility. The same study of *Bouchemal et al.,* (Bouchemal, 2004) reported a decrease in the droplet size when the miscibility of the oil phase with the water phase increases. In the present study, the added solvent, acetone and ethanol, are water miscible, while ethyl acetate is only partially miscible in water. When incorporating water miscible solvents, a

decrease in the droplet size was expected. However, the opposite effect was found: increasing the oil phase miscibility, the droplet size increased (Figure 4.15). This could be explained by the nano-emulsion formation method. In the study by *Bouchemal et al.,* (Bouchemal, 2004), they prepared nano-emulsions by spontaneous emulsification triggered by solvent diffusion. Therefore, the more miscible the oil phase, the faster the solvent diffusion and the smaller the droplets. In the present work, in contrast, it is not expected the spontaneous nanoparticle formation during the emulsification process. Another factor could be the diffusion of the surfactant to the water phase. Since both acetone and ethanol are more soluble in water than in ethyl acetate, the diffusion of the surfactant might be facilitated. Therefore, the droplet size may increase due to destabilization of the droplets with less surfactant. Another explanation could be an enhancement of the Ostwald ripening produced by the presence of more soluble oils (ethanol and acetone) in the dispersed phase, thus resulting in an increase on the droplet size. As a results of the different factors, the combination of these two solvents as the oil phase (ethanol or acetone + ethyl acetate) increases the droplet sizes of nano-emulsions for certain ratios.

4.2.3. Nano-emulsion zeta (ζ) potential

Nano-emulsion ζ potential was assessed by means of electrophoretic mobility measurements and applying the Hückel-Onsager equation, as described in Section 3.2.6. Since the PLGA polymer is composed of acidic groups, nano-emulsions with negative charges were expected. Figure 4.16 shows the results of nano-emulsions with different O/S ratios and electrolyte concentrations. The ζ potential did not have a clear tendency as a function of electrolyte concentration neither as a function of the O/S ratio. Comparing different electrolyte concentrations, an increase in the absolute value of the electrophoretic mobility, thus increasing the ζ potential, with the increase on the electrolyte concentration was expected due to the increase on the ionic species. However, the results were not as expected: the ζ potential does not seem to be dependent on the electrolyte concentration.

Comparing different O/S ratios, only at high and low O/S ratios (edges of the nano-emulsion formation domain), a decrease on the ζ potential was produced, which was attributed due to the formation of less stable nano-emulsions.
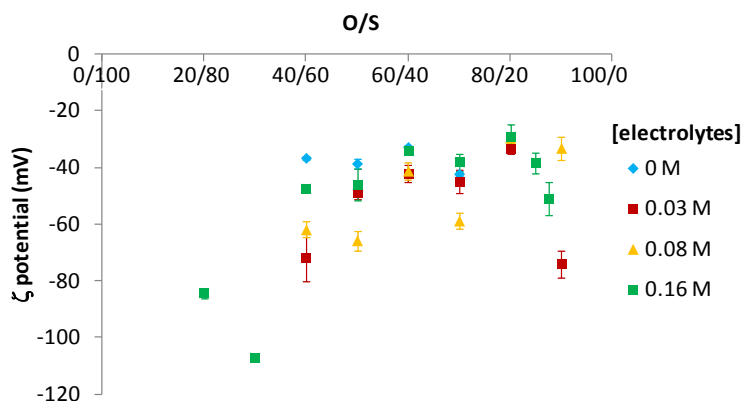
Figure 4.16: ζ potential of nano-emulsions with 90wt % of aqueous phase as a function of O/S ratio and electrolyte concentration in the aqueous phase.

Hydrodynamic droplet radii were compared with the surface charge as a function of the electrolyte concentration for nano-emulsions with 4wt% PLGA and 70/30 O/S ratio (Figure 4.17). The surface charge of the nano-emulsions decreases at low electrolyte concentration, then it increases and it keeps constant at high electrolyte concentrations. As described in Section 4.2.2, by increasing the electrolyte concentration, the droplet size decreases up to a value and keeps constant. The size decrease should end in more stable droplets against gravitational forces, while reduced absolute values of the ζ potential should produce less stable nano-emulsions. In the present thesis, as stated in previous studies (Moreira de Morais, 2005), the steric mechanisms could be predominant, since only the size effect on stability of nano-emulsions is observed.

A surface charge decrease when increasing the electrolyte concentration was found in previous studies on the influence of electrolyte concentration in O/W emulsions (Trimaille, 2003; Moreira de Morais, 2005). This effect was attributed to the interaction of the charges of the electrolytes with the charges of the components of the droplets; this means that the ions forming the salts of the electrolyte solution could compensate the total positive / negative charges, including the negative charges of the polymer, thus decreasing the charge absolute value, but, at the same time, decreasing the sample electrostatic stability. It is remarkable that, as previously discussed, although the ζ potential of the nano-emulsions with electrolytes decreases in absolute value, the obtained nano-emulsions are more stable. This can be explained due to the contribution of different parameters to nano-emulsion stability. Although they are not electrostatically stable, they are colloidally stable.
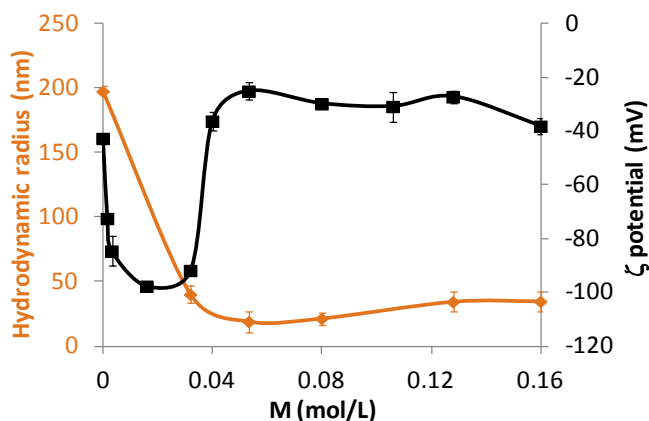
Figure 4.17: Zeta potential and hydrodynamic radii of the nano-emulsion with 90wt % of water content and 70/30 O/S ratio, as a function of the electrolyte concentration in the aqueous phase, at 25ºC.

4.2.4. Nano-emulsion stability

Nano-emulsion stability was studied by means of visual macroscopic observations, light transmission / backscattering and changes of droplet size as a function of time and temperature. Nano-emulsions with 4wt% of PLGA in ethyl acetate, different electrolyte concentration and different O/S ratios were studied. Since the oil component used in this work, ethyl acetate, has a finite solubility in the aqueous phase, these nano-emulsions could be destabilized by Ostwald ripening

4.2.4.1. Visual assessment

Nano-emulsions with O/S ratios from 10/90 to 90/10, with different electrolyte concentrations were observed visually for a period of 60 days. No phase separation was observed within this period of time in any of the nano-emulsions. The macroscopic aspect of samples was not changed, but a sediment (a white powder) appeared with time. The results presented in Table 4.10 show that the time taken to observe a sediment depended on the O/S ratio as well as on the electrolyte concentration. Nano-emulsions with electrolytes tend to sediment more rapidly at the limits of the formation region; the most stable were those nano-emulsions corresponding to the central part of this region. However, in the absence of electrolytes, the higher the surfactant content, the higher the nano-emulsion

stability, which could be attributed to the colloidal stabilization of the surfactant. The solvent of the oil component, ethyl acetate, a solvent that is less dense than water and partially soluble in it, diffuses to water just after the nano-emulsion formation, thus leading the nanoparticle formation. The polymer is more dense than water, but its percentage in the oil component is rather low (only 4wt%). As ethyl acetate migrates to the aqueous continuous phase, droplet size decreases; and, at the same time, its density increases. The size as well as the solvent present in the droplets after ethyl acetate diffusion to the aqueous continuous phase may be the main factors determining the tendency to settle and speed of sedimentation of the dispersed entities (either drops or already formed particles). These early-formed nanoparticles may be the precipitating part due to their higher density as compared with the aqueous phase. This phenomenon of an early nanoparticle formation was already described in previous bibliography (Bouchemal, 2004) for other systems with different materials and methodologies. Therefore, the white powder observed with time, could probably be due to sedimentation of the early-formed nanoparticles.

Comparing the nano-emulsions with different electrolyte concentration, it can be concluded that the presence of electrolytes in the aqueous phase increases the stability to sedimentation, since the less stable samples correspond to the system without electrolytes (Table 4.10). However, the relationship between the concentration of electrolytes and the macroscopic stability is not linear. Nano-emulsions formulated with the intermediate electrolyte concentrations (0.08 and 0.03M) are more stable than those prepared with the highest electrolyte concentration. Some examples in the literature have already reported an increase in the stability of emulsions when adding salts in the aqueous phase. *Kunieda et al.,* (Kunieda, 1989) postulated that the increase of the stability of W/O emulsions was due to a high salting-out effect in the presence of salts, thus increasing the dehydratation of the polar heads of the surfactant (which produces a reduction of the cloud point) which in turns produces an increase in the polar heads lateral interactions. Another example is the work of *Jiang et al.,* (Jiang, 2013 (1)), who reported the increase of W/O nano-emulsion stability due to the presence of electrolytes, using the PIT emulsification method. The stabilization effect of the addition of electrolytes was attributed to an interaction of electrolytes with the surfactant, thus increasing the interfacial tensions and enhancing droplets stability. Furthermore, other studies compared the stability of nano-emulsions formulated with different types of salts and concluded that the most stable nano-emulsions were produced using monovalent salts with weak ionic strength (Mei, 2011). The

fact that nano-emulsions with O/S ratios between 40/60 and 70/30, with an intermediate electrolyte concentration, remained stable for at least two months, (Table 4.10) could be explained by colloid aggregation at higher electrolyte concentrations, as previously reported (Rao, 2011) in other systems in which this effect was attributed to the electrostatic repulsion of the negative charges of the nano-emulsions at high salt concentrations, enhancing flocculation or aggregation. In the present thesis, however, no flocculation neither aggregation was observed prior to sedimentation.

Table 4.10: Time taken to observe sediment in nano-emulsions with 90wt% of aqueous phase, as a function of O/S ratio without / with different electrolyte concentrations at 25ºC.

		Time taken to observe a sediment (days)		
	Water	**Electrolyte solution**		
O/S		**0.032M**	**0.08M**	**0.16M**
10/90	--	--	--	0.5
20/80	--	--	1	0.5
30/70	--	--	31.5	0.5
40/60	--	2	>60	16.5
50/50	4	31.5	>60	16.5
55/45	1.5	42	>60	16.5
60/40	0.5	>60	>60	16.5
65/35	0.5	>60	>60	16.5
70/30	0.5	>60	>60	16.5
80/20	--	>60	11	32
85/15	--	31.5	11	22.5
90/10	--	2	11	11.5

The nano-emulsion instability is not due to one of the usually reported destabilization mechanisms (coagulation, flocculation and / or Ostwald ripening) (Taylor, 1998; Izquierdo, 2002; Tadros, 2004). These nano-emulsions are destabilized due to the diffusion of the solvent from the dispersed phase to the continuous phase, thus forming early nanoparticles. Therefore, sedimentation is produced by the early formed nanoparticles. Nevertheless, the stability of the nano-emulsions, even without electrolytes, is sufficient for the purpose of this thesis (to be used as nanoparticle templates), since the solvent evaporation process takes place in less than one hour.

4.2.4.2. Light transmission/ backscattering

The stability of nano-emulsions was also assessed by light transmission and backscattering measurements. Nano-emulsions without and with increasing electrolyte concentrations (0.03M, 0.08M and 0.16M), with an O/S ratios of 50/50 and 70/30 were selected. Light backscattering data was used for nano-emulsions formulated without electrolytes, since they have a translucent to opaque appearance (Lemarchand, 2003), while transmission data were used for nano-emulsions with electrolytes, due to their transparent to translucent appearance. The results shown in Figures 4.18 to 4.21 are presented as the percentage of the transmitted / backscattered light as a function of time and sample height. The left part of the plot corresponds to the bottom of the sample (low values), while the right part corresponds to the sample surface (abrupt decrease to low values). It is worth noting that when adding electrolytes in nano-emulsions, the transmitted light of the sample along the time oscillates.

Regarding <u>the nano-emulsions without electrolytes</u>, light backscattering (Figure 4.18) was constant in most of the sample height as a function of time for nano-emulsions with 50/50 O/S ratio (Figure 4.18a), but a slight increase appeared for the 70/30 O/S ratio (Figure 4.18b). This increase is related with an increase on the sample turbidity which can be attributed to an increase in the droplet size. Moreover, around about 3 – 5 mm from the bottom of the sample a peak appears (circled in blue color) at both O/S ratios, which has been attributed to sample sedimentation, previously observed by visual observations. Although sedimentation is not observed visually at an early time (below 1 day), the peak attributed to sedimentation appears from the beginning. It should be noted that this technique enables accelerated study of the stability.
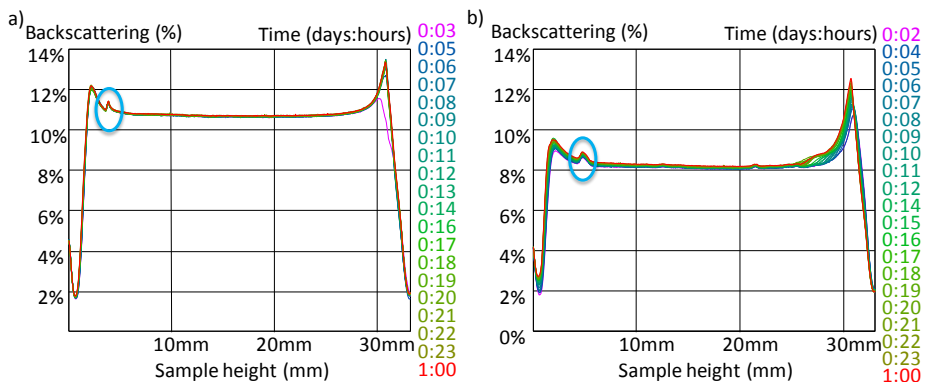
Figure 4.18: Light backscattering of nano-emulsions as a function of sample height and time, at 25ºC. O/S ratio: a) 50/50 and b) 70/30. The circle marks the sedimentation of the samples.

110

Regarding the nano-emulsions with an intermediate electrolyte concentration (0.03M and 0.08M), light transmission was constant along sample height and time (Figure 4.19 and Figure 4.20, respectively), thus indicating that these samples are stable against creaming or sedimentation. Comparing both O/S ratios studied, for the electrolyte solution 0.03M, a slight increase on the nano-emulsion transmission was observed for the 50/50 O/S ratio (Figure 4.19a), while for the 70/30 O/S ratio (Figure 4.19b), transmission did not increase along the time. However, for the electrolyte solution 0.08M, neither O/S ratio experienced variation on the light transmission along the time (Figure 4.20). These results are in good agreement with visual observations, since only nano-emulsions formulated with 0.03M electrolyte solution at an O/S ratio of 50/50 (out of the four samples studied) were destabilized below 2 months (Table 4.10).
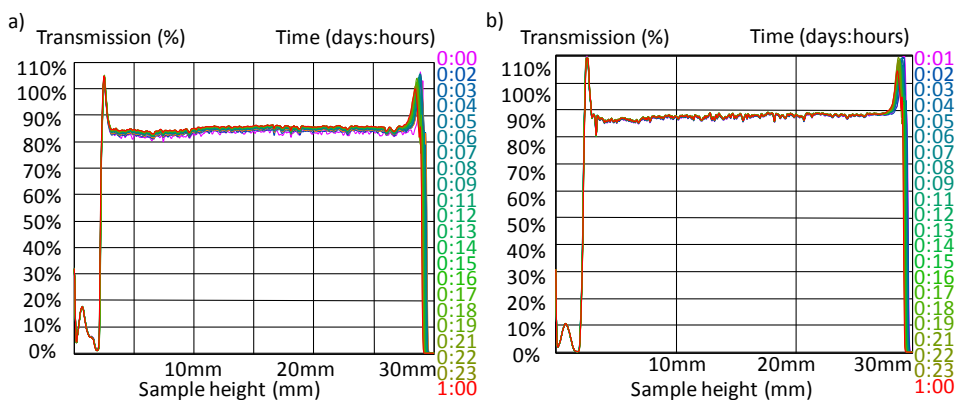
Figure 4.19: Light transmission of nano-emulsions with 90wt % of electrolyte solution (0.03M) as a function of sample height and time, at 25ºC. O/S ratio: a) 50/50 and b) 70/30.
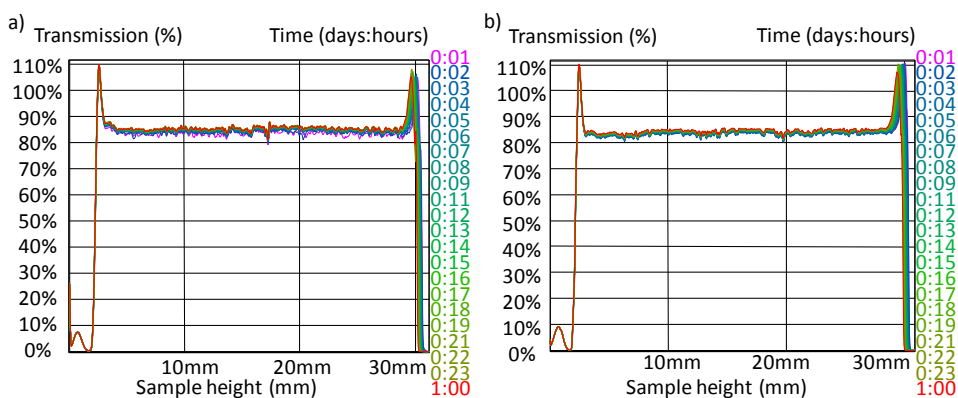
Figure 4.20: Light transmission of nano-emulsions with 90wt % of electrolyte solution (0.08M) as a function of sample height and time, at 25ºC. O/S ratio: a) 50/50 and b) 70/30.

Regarding nano-emulsions with <u>higher electrolyte concentration</u> (0.16M), the transmitted light did not show variation along the sample height (Figure 4.21). However, there were differences with the O/S ratios: while nano-emulsions with an O/S ratio of 50/50 showed no variation of the transmitted light along the time, the transmitted light of the nano-emulsion with 70/30 O/S decreased around 10% along 24 hours (Figure 4.21b). The slight decrease in the transmitted light indicates an increase in sample turbidity which was also detected by visual observations. This could be due to an increase in the number of droplets, due to destabilization processes or an increase in the droplet size, which was ruled out on the basis of light scattering measurements.
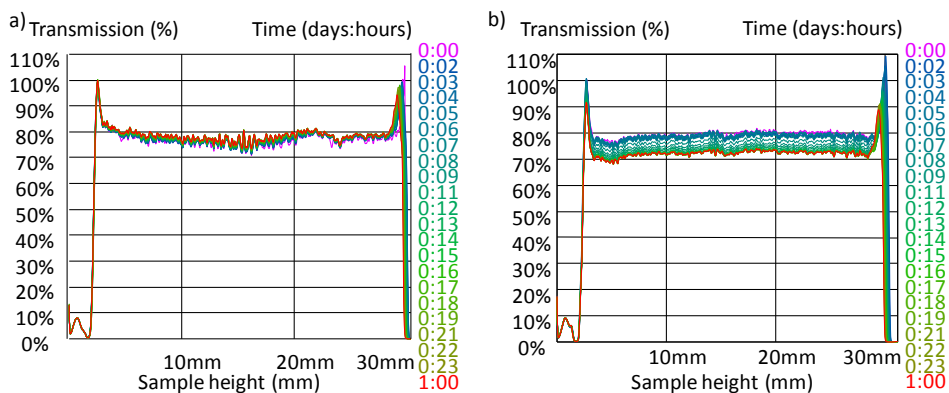
Figure 4.21: Light transmission of nano-emulsions with 90wt % of electrolyte solution (0.16M) as a function of sample height and time, at 25ºC. O/S ratio: a) 50/50 and b) 70/30.

4.2.4.3. Variation of size

This study was carried out with nano-emulsions with an O/S ratio of 50/50 and 70/30, 4wt% of PLGA, and the different electrolyte concentrations (0M, 0.03M, 0.08M and 0.16M). Initially, at short times, droplet sizes suffer oscillations for all tested samples (Figures 4.22 to 4.25), which could be attributed to a combination of different destabilization mechanisms: coalescence or flocculation of the droplets, which increases the droplet size at early times, followed by Ostwald ripening, or even sedimentation (not visually observed after 60 days for 0.03M and 0.08M PBS), which tends to reduce droplet size.

The results of the hydrodynamic radii as a function of time, with the <u>nano-emulsions without electrolytes</u>, are shown in Figure 4.22. In these nano-emulsions,

the initial oscillations in size were found for a period of around 4 days, after which the size started to decrease. As described above, these nano-emulsions are macroscopically stable for only 4 days and then a sediment appears. This is in good agreement with the measurement of the droplet sizes. The decrease in the droplet size is due to the sedimentation of the bigger droplets of the nano-emulsion, since size measurements were performed with sedimented samples, without mixing. Therefore, these results are also in agreement with the measurement of the backscattered light, where a sedimentation was detected (Figure 4.18).
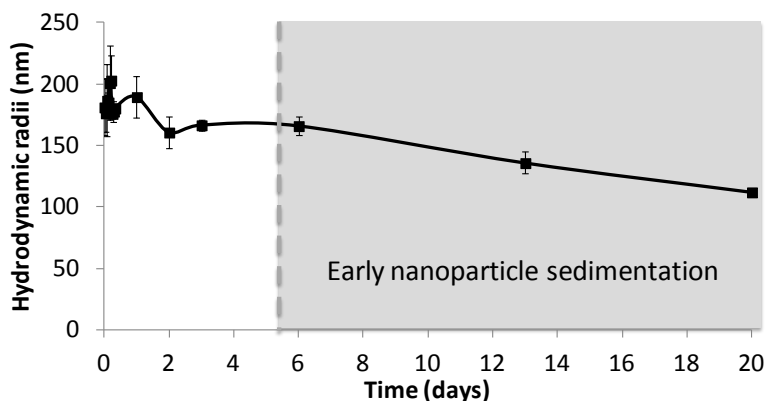
Figure 4.22: Hydrodynamic radii of nano-emulsions with 90wt % of water content and an O/S ratio of 50/50 as a function of time, at 25ºC. Discontinuous line marks the starting of the sedimentation.

Droplet size of <u>nano-emulsions with 0.03M and 0.08M PBS</u> and with O/S ratios of 50/50 and 70/30 experienced some variations up to about 10 days. For the nano-emulsions with 0.03M PBS, the droplet sizes of the O/S ratio of 50/50 are markedly bigger than those from the 70/30 O/S ratio (Figure 4.23), while it does not depend on the O/S ratio for those with PBS 0.08M (Figure 4.24), as described above. After the oscillations at short times, droplet sizes suffer a slight increase for 0.03M PBS (Figure 4.23) but they keep constant for 0.08M PBS (Figure 4.24). The slight increase in droplet size for nano-emulsions with 0.03M PBS is in good agreement with light transmission results, where a slight decrease in transmitted light was observed (Figure 4.19). The slight decrease in the transmitted light is produced by an increase on the sample turbidity, which could be due to the increase in the droplet size. Nano-emulsion visual appearance did not vary for 60 days. For nano-emulsions with 0.08M PBS, the size variations are smaller, although the light transmission decreased slightly (Figure 4.20).
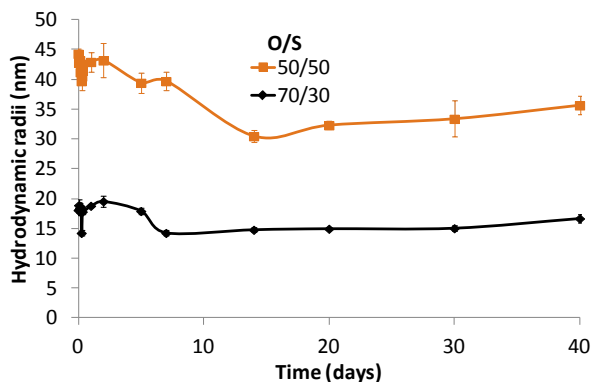
Figure 4.23: Hydrodynamic radii of nano-emulsions with 90wt % of aqueous solution (0.03M) content and an O/S ratio of 50/50 and 70/30 as a function of time, at 25ºC.
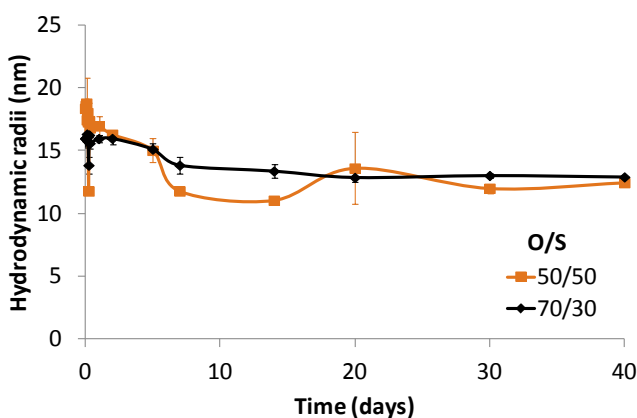
Figure 4.24: Hydrodynamic radii of nano-emulsions with 90wt % of aqueous solution (0.08M) content and an O/S ratio of 50/50 and 70/30 as a function of time, at 25ºC.

Droplet size of nano-emulsions with 0.16M PBS and O/S ratios of 50/50, 70/30 and 80/20 (Figure 4.25) experienced some initial variations within the first day, followed by constant hydrodynamic radii (which increases with the increase in the O/S ratio). At higher O/S ratios, the enhanced increase in the droplet size observed during the first hours could be due to both: coalescence, since the less relative amount of surfactant in the nano-emulsion is not able to stabilize the droplets and solvent evaporation due to the higher amount of oil present in the samples. However, coalescence seems to predominate. Comparing with nano-emulsions without electrolytes, the droplet size variations are smaller in the presence of the salts, which could be attributed to the formation of a more tight interfacial film.
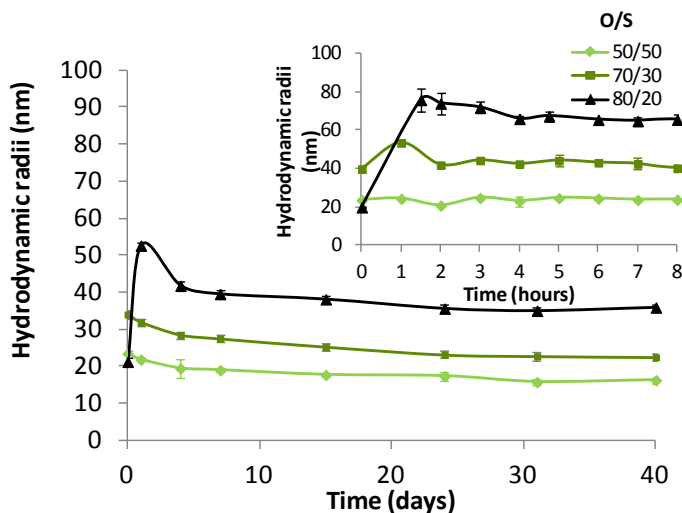
Figure 4.25: Hydrodynamic radii of nano-emulsions with 90wt % of electrolyte solution (0.16M) content, at different O/S ratios, at 25ºC.

The initial size increase observed for all nano-emulsions, has been related to Ostwald ripening and/or coalescence, the main nano-emulsion destabilization mechanism. Through Ostwald ripening, the size of big droplets becomes bigger and that of small droplets becomes smaller resulting in an increased mean droplet size of the whole nano-emulsion (Lifshitz, 1961; Wagner, 1961; Solans, 2005; Solans, 2012; Solè, 2012). However, in nano-emulsions with partially water soluble oil phases, Ostwald ripening could be compensated by a reduction of the droplet size due to the solvent diffusion.

It is well known that Ostwald ripening can be reduced by using an oil less soluble in the aqueous phase, such as long-chain lipids or polymers. Therefore, the effect of increasing the PLGA concentration in the oil phase was one of the strategies proposed. The droplet size of nano-emulsions with PBS 0.16M and O/S ratio of 70/30 and 20wt % of PLGA was measured during 10 days. Droplet sizes of these nano-emulsions experience slight initial variations, followed by a slight increase and further slight droplet size decrease (Figure 4.26). Therefore, it was concluded that in the system studied, the increase of the polymer concentration did not reduced Ostwald ripening. The higher number of polymer molecules present in the droplet may increase the osmotic pressure inside the drop preventing ethyl acetate from diffusing to the continuous phase and hence slowing down droplet size decrease by this effect.
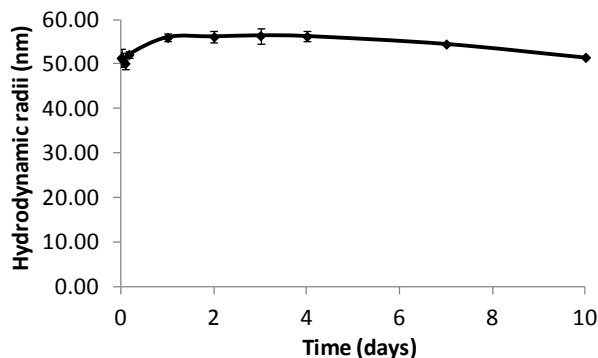
Figure 4.26: Hydrodynamic radii of nano-emulsions with 90wt % of water content (0.16M) and an O/S ratio of 70/30, as a function of time, with 20wt % of PLGA in the oil phase.

Long chain lipids (squalane and hexadecane) were also added to nano-emulsions with PBS 0.16M and O/S ratio of 70/30. Figure 4.27 shows the hydrodynamic radii as a function of time and lipid concentration in the oil phase. Nano-emulsion droplet size was measured for 10 days. For both compounds, the droplet size slightly decreases during the first hours, while it remained quite constant afterwards. Increasing the percentage of long chain lipids, the initial size variations are more marked. Therefore, none of both lipids was able to reduce the initial droplet size variations. These results suggest that in the nano-emulsions studied, solvent diffusion from the droplets to the continuous phase is the main parameter determining droplet size.
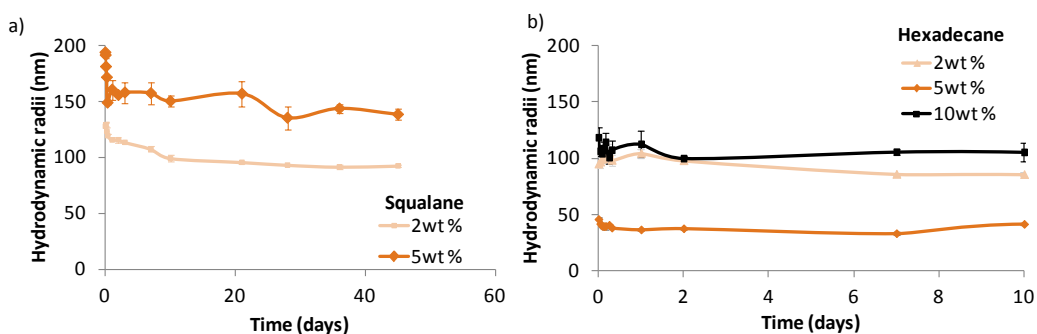
Figure 4.27: Hydrodynamic radii of nano-emulsions (90wt% of PBS 0.16M, 70/30 O/S), as a function of time and a) squalane and b) hexadecane concentration in the oil phase at 25ºC.

4.2.4.4. Influence of temperature on droplet size

In the presence work, nano-emulsions were formulated with a nonionic ethoxylated surfactant (polysorbate 80). Like all ethoxylated surfactants, polysorbate 80 is sensitive to temperature changes (Shinoda, 1968; Tadros, 2005). The droplet size of nano-emulsions formulated with 90wt % of electrolyte solution (0.16M) and 70/30 O/S ratio was studied as a function of time and temperature. The temperature was set at 25ºC and 37ºC since they represent the room and the body temperatures, respectively.
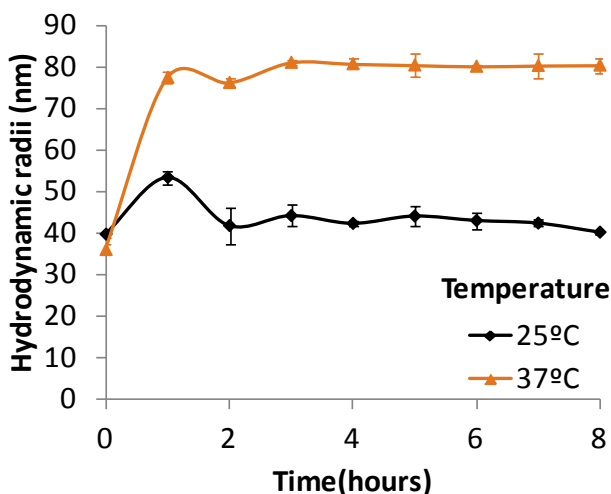
Figure 4.28: Hydrodynamic radii of nano-emulsions with 90wt % of electrolyte solution (0.16M) and an O/S ratio of 70/30, at 25ºC and 37ºC, as a function of time.

The results (Figure 4.28) show that nano-emulsion droplet size increases during the first hour of study, after which it remains constant as a function of time. At 37ºC, the nano-emulsion droplet size increase is more pronounced, being double than at 25ºC during the first hour of preparation. This huge increase in the droplet size with the increase of the temperature could be due to the use of an ethoxylated surfactant, which are thermosensitive, as previously discussed (Shinoda, 1968; Tadros, 2005). The higher the temperature, the more dehydrated the polar heads of the polysorbate 80. At higher temperatures, the closer the temperature to the T_{HLB} of the polysorbate 80, the higher the nano-emulsion destabilization (Yang, 2013). In addition, the increase of the temperature enhances the solvent diffusion. Concerning the polydispersity index, at 25ºC is around 0.2, while at 37ºC is above 0.3 (see Table Ap.3, appendix). Therefore, it can be concluded that the increase of

the temperature produces an increase in the droplet size and in the polydispersity, without affecting stability of the nano-emulsions.

After the systematic study of nano-emulsion stability, it can be concluded that nano-emulsions are stable to phase separation. Ostwald ripening and coalescence cannot be ruled out but they are not the main destabilization mechanisms. They can occur at short times, but theoretical calculations of the cube of the hydrodynamic radii as a function of time to confirm Ostwald ripening enabled to rule out this mechanism, since no lineal dependency was found (Figure Ap.4, appendix). The only destabilization observed is sedimentation, but not of the nano-emulsion droplets but of early formed nanoparticles. As indicated above, these nanoparticles are formed due to the solvent diffusion to the aqueous phase.

Comparing the stability of nano-emulsions at both O/S ratios studied, at the lowest O/S ratio (50/50), the higher proportion of surfactant enables higher stability to sedimentation for all the electrolyte concentrations studied; except for 0.03M electrolyte concentration (visual assessment).

Comparing the nano-emulsions with different electrolyte concentrations, the presence of electrolytes enhances the stabilization of nano-emulsions up to an electrolyte concentration from which electrostatic stability decreases.

The size of nano-emulsions 0M and 0.16M PBS was compared with the results of macroscopic stability (Figure 4.29). For nano-emulsions without electrolytes (0M), the stability decreases with the increase in O/S ratios. However, for nano-emulsions with 0.16M electrolyte concentration, the stability is higher at the central part of the nano-emulsion domain, where the hydrodynamic droplet radius is smaller. Therefore, the stability enhancement of nano-emulsions prepared with PBS 0.16M could be due to a combination of two factors: the increase in the surfactant concentration, and the reduction in the droplet size, thus reducing the gravitational destabilization mechanisms. For nano-emulsions without electrolytes, the surfactant effect predominates, thus increasing the stability at low O/S ratios; but for nano-emulsions with 0.16M electrolyte concentration, the droplet size effect predominates, since droplet sizes are practically constant in a wide range of O/S ratios.
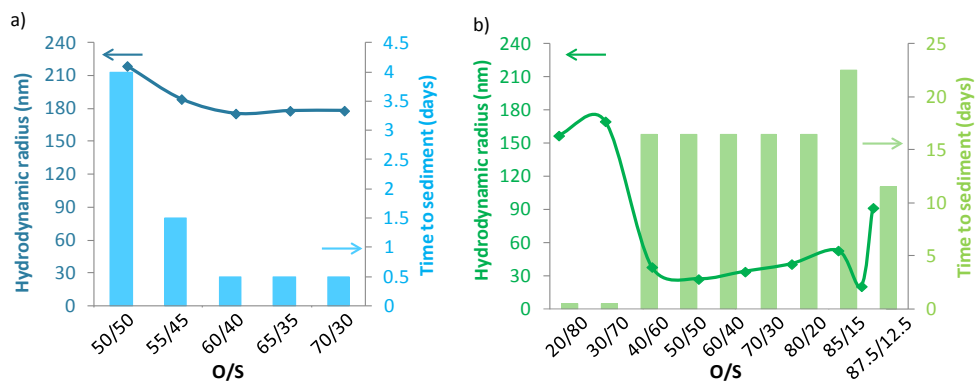
Figure 4.29: Macroscopic stability (time taken to observe sedimentation) and hydrodynamic radius of nano-emulsions as a function of the O/S ratio, at a) 0M PBS and b) 0.16M PBS, at 25ºC.

Summary

The <u>domain</u> of nano-emulsion formation has been studied for the aqueous solution (W) / polysorbate 80 (S) / [x wt% PLGA in ethyl acetate] (O) systems, as a function of electrolyte concentration (0M, 0.03M, 0.08M and 0.16M), nature of the solvent (adding increasing percentages of ethanol / acetone), percentage of polymer (4wt % or 20wt % in the oil phase) and added model drug (loperamide). The domain of nano-emulsion formation is broader for intermediate electrolyte concentrations, as compared with samples without electrolytes. Furthermore, the addition of a more polar solvent in the oil phase, as well as the increase in the polymer concentration increased the nano-emulsion domain; while the incorporation of the drug shrinks the domain. Nano-emulsions with 90wt % of aqueous phase were selected for further studies.

Conductivity measurements, as well as the use of hydrophilic / lipophilic colorants were used to confirm phase inversion (from W/O structures) to O/W nano-emulsions during emulsification.

The nano-emulsion mean <u>droplet sizes</u>, as measured by DLS, was about 200 nm for nano-emulsions with 4wt % of PLGA, without electrolytes. The incorporation of electrolytes produced a marked decrease in the droplet size to sizes to around 25 nm due to the salting out effect, as well as the solvent diffusion to the continuous phase. The size was also influenced by the increase of the polymer concentration; and by the addition of water soluble solvents, which increased droplet sizes.

The <u>surface charge</u> of nano-emulsions showed negative values due to the carboxylic groups of the polymer, without a clear dependency with the O/S ratio neither to the electrolyte concentration.

Nano-emulsion <u>stability</u>, by means of visual observations, confirmed that they were destabilized by sedimentation. This sedimentation is produced by the early formed nanoparticles due to the diffusion of the solvent from the droplets to the aqueous phase. The addition of electrolytes enhanced nano-emulsion stability, being optimal the intermediate electrolyte concentrations (stabilities higher than 2 months). Measurements of the stability by light backscattering / transmission as well as by the variation of the hydrodynamic droplet size as a function of time confirmed the results observed visually.

After studying the visual macroscopic appearance, the size, the surface charge and the stability of the nano-emulsions, it can be stated that nano-emulsions suitable for biomedical applications have been <u>successfully prepared</u>. Taking into account these results, all the following work was carried out with nano-emulsions prepared with PBS 0.16M because of pH (7.4) and osmolality (around 300 mOsm/kg) requirerements for biomedical applications (Dobrovolskaia, 2013). However, results regarding other systems/compositions will be presented for comparison purposes.

4.3. Nanoparticle preparation by nano-emulsion templating and characterization

Polymeric nanoparticles were prepared from the template nano-emulsions by solvent evaporation under controlled conditions.

A complete physic-chemical characterization of nanoparticles, intended for biomedical applications, includes size, surface charge, hydrophobicity and targeting moieties (Dobrovolskaia, 2013). Except for their hydrophobicity, which was previously known for each of the materials used, all other parameters were determined in this thesis.

Nano-emulsions with 90wt% of aqueous solution were used for the nanoparticle preparation. Nanoparticle size and morphology were exhaustively characterized by means of different techniques: DLS, SEM, TEM and AFM. The surface charge and stability of the as-prepared nanoparticles were also characterized.

4.3.1. Formation of nanoparticles

Nanoparticles were formed by <u>solvent evaporation</u> (Figure 4.30), using nano-emulsions as templates. Due to the use of the nano-emulsion templating methodology, nanoparticles are expected to have spherical morphology, with slightly smaller sizes than the droplets of the nano-emulsion template. In addition, the ζ potential of the formulated nanoparticles is expected to have negative values due to the anionic charges of the carboxylic groups of the PLGA polymer.
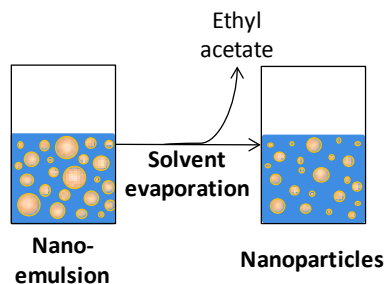
Figure 4.30: Schematic representation of the nanoparticle formation from nano-emulsions by solvent evaporation.

In the present section, nanoparticles prepared from nano-emulsions (with 90wt % of aqueous phase) will be described. To facilitate the reading, an identification code has been assigned to each nanoparticle type. For nanoparticles prepared from nano-emulsions with water as the aqueous phase, NP-W identification has been given. For nanoparticles prepared from nano-emulsions with electrolyte solution as the aqueous component, the identification is NP-XE, where X = electrolyte molar concentration (e.g. NP-0.16E corresponds to nanoparticles prepared from nano-

emulsions with 0.16M PBS as the aqueous component). In addition, for all nanoparticle types, the O/S ratio from the template nano-emulsion is also specified as NP-W-Y or NP-XEY, where Y corresponds to the oil percentage in the O/S mixture (e.g. NP-W70 corresponds to nanoparticles prepared from nano-emulsions with water as the aqueous phase and with an O/S ratio of 70/30). A schematic summary of the identification code is given in Table 4.9.

Table 4.9: Nanoparticle identification codes.

Identification	Aqueous phase
NP-W	Water
NP-WY	
NP-XE	Electrolyte solution
NP-XEY	

X = *Molar electrolyte concentration*
Y = *Percentage of oil in the O/S mixture of the template NE*

After solvent evaporation of template nano-emulsions with different O/S ratios, the macroscopic appearance of nanoparticle dispersions was first observed. The visual appearance of nanoparticles prepared from nano-emulsions with water (NP-W) and electrolytes at 0.16M (NP-0.16E) is shown in Figure 4.31. While NP-W nanoparticles are opaque and milky, NP-0.16E nanoparticles have a transparent to translucent appearance. These results were already expected, since they agree with the template nano-emulsions visual appearance (Figure 4.5).

a)   b)

O/S: 50/50 55/45 60/40 65/35 70/30   O/S: 70/30 75/25 80/20 85/15
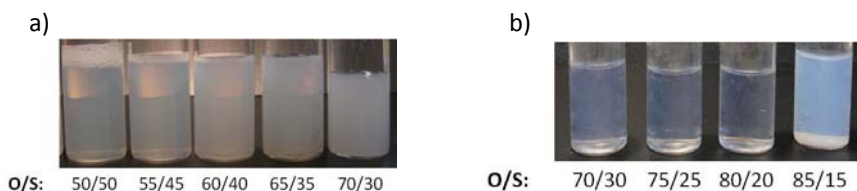
Figure 4.31: Visual appearance of a) NP-W and b) NP-0.16E nanoparticle dispersions, as a function of O/S ratio of the template nano-emulsions.

4.3.2. Nanoparticle size characterization

The size of the NP-W and NP-0.16E nanoparticles was characterized by dynamic light scattering (DLS). The results are presented in Figure 4.32 - 4.34. CONTIN analyses showed that the dispersions are monomodal, although the size distribution is narrower for the NP-0.16E nanoparticles. As an example, Figure 4.32 shows the size distribution for NP-W70 and NP-0.16E70.
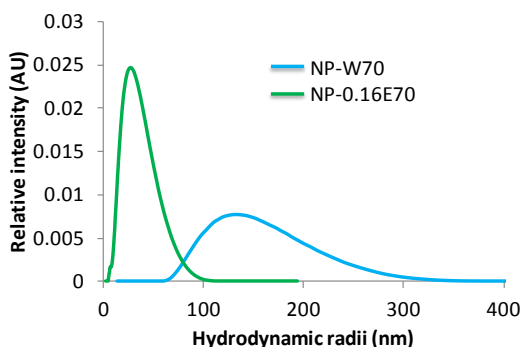
Figure 4.32: Examples of the CONTIN plot of nanoparticles NP-W70 and NP-0.16E70.

As expected, the hydrodynamic radii of the nanoparticles (Figure 4.33a) depend mainly on the nature of the aqueous phase: the nanoparticle radius decreases from around 150 nm when prepared with water (NP-W) to around 20 – 30 nm when prepared with electrolyte solution (NP-0.16E). The huge decrease in nanoparticle size is directly related to the huge decrease in nano-emulsion droplet radii of the template nano-emulsions. In contrast, the size dependency on O/S ratio found for nano-emulsions (Figure 4.12) was not observed for nanoparticle dispersions.

The polydispersity indexes (PDI) are slightly higher than 0.2, (considered the threshold of polydispersity) (Figure 4.33b). Therefore, NP-W and NP-0.16E nanoparticles can be considered as low polydisperse systems (Schärtl, 2006; Dobrovolskaia, 2013). NP-0.16E nanoparticles, in most dispersions show higher PDI values than NP-W nanoparticles (Figure 4.33b). Nevertheless, it is worth noting that nanoparticle sizes are maintained within the range of nanosystems appropriate for the intravenous administration (Gref, 2012; Dobrovolskaia, 2013), which is one of the aims of this study.
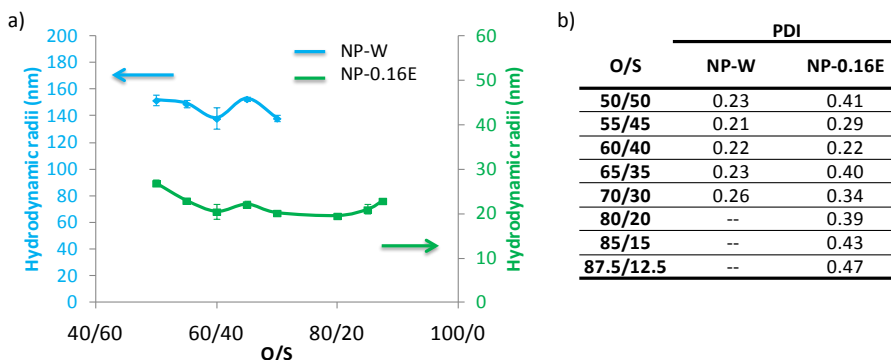
Figure 4.33: a) Nanoparticle radii as a function of the O/S ratio of the template nano-emulsions; b) Polydispersity indexes of the NP-W and NP-0.16E nanoparticles.

As described in Section 4.2.3.2, the reason for the decrease in nano-emulsion droplet size when electrolytes are incorporated in the aqueous phase is a combination of salting out and osmotic gradient effects. It was considered of interest to study more systematically the effect of electrolyte concentration (in the template nano-emulsions) on nanoparticle size. The results (Figure 4.34) show that the variation of nanoparticle size (determined by DLS) follows the same trend as that of nano-emulsions (Figure 4.13). Independently of the O/S ratio of the template nano-emulsion, no further decrease in nanoparticle size is produced beyond 0.04M. These results suggest that there exists a critical electrolyte concentration above which nanoparticle size cannot be further reduced and keeps roughly constant.
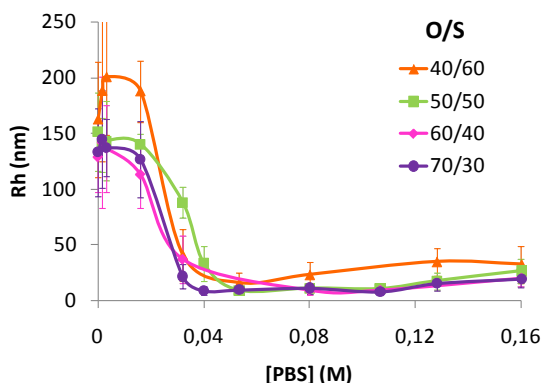
Figure 4.34: Hydrodynamic nanoparticle radii of nanoparticles, as a function of O/S ratio and electrolyte concentration.

Moreover, the <u>effect on nanoparticle size varying the electrolyte concentration of the aqueous medium containing the nanoparticles</u> after their preparation with electrolytes was also studied. The as-prepared nanoparticles were dialyzed against a receptor solution of PBS 0.16M and their hydrodynamic radii were determined before and after the dialysis. As Table 4.10 shows, the hydrodynamic radii of nanoparticles did not change significantly after the dialysis step, thus allowing to conclude that once nanoparticles have been formed, they maintain their size regardless the ionic strength of the medium. Therefore, the nanoparticle size is determined by the conditions of the template nano-emulsification process rather than the conditions of the resulting nanoparticles (Pinto-Reis, 2006). However, it is worth noting that the dispersion of the values is considerably reduced after the dialysis step (Table 4.10).

Table 4.10: Hydrodynamic radii of nanoparticles before and after a dialysis step using PBS 0.16M as a receptor solution, as a function of the initial electrolyte concentration.

	Hydrodynamic radius (nm)	
Initial dispersant	**Before dialysis**	**After dialysis**
Water	139.11 ± 4.17	134.03 ± 0.41
PBS 0.03M	20.22 ± 0.15	16.71 ± 0.12
PBS 0.08M	12.12 ± 4.59	11.34 ± 0.48
PBS 0.16M	19.81 ± 3.05	23.77 ± 0.73

To further confirm that the physico-chemical properties of the nanoparticles are kept after their formation, their surface charge was also assessed before and after the dialysis. The absolute value of the surface charge increased, as expected, due to the higher concentration of electrolytes after the dialysis, which could be a confirmation that dialysis occurred (Table 4.11).

Table 4.11: Surface charge of nanoparticles before and after a dialysis step using PBS 0.16M as a receptor solution, as a function of the initial electrolyte concentration.

	ζ potential (mV)	
Initial dispersant	**Before dialysis**	**After dialysis**
Water	-61.70 ± 2.90	-68.75 ± 1.56
PBS 0.03M	-25.75 ± 0.62	-33.70 ± 3.24
PBS 0.08M	-24.30 ± 0.94	-31.45 ± 2.48
PBS 0.16M	-18.90 ± 0.75	-18.90 ± 1.19

The hydrodynamic radii of NP-0.16E70 nanoparticles was further studied <u>as a function of the scattering angle</u>, by means of DLS measurements. Figure 4.35 shows the results. The dependency of the size on the angle of measurement may be an indication of the polydispersity of the sample or an indication of a morphology different from an sphere.
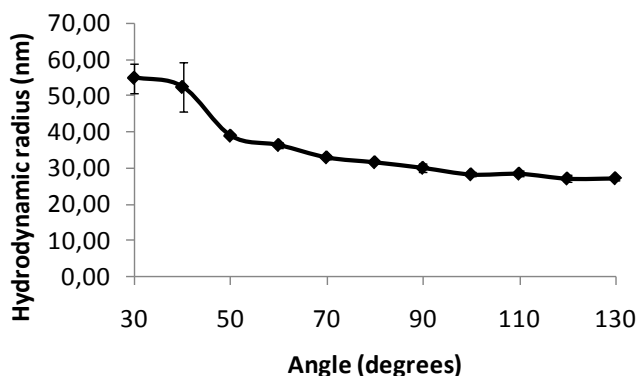
Figure 4.35: Hydrodynamic radii of a NP-0.16E70 nanoparticles as a function of the measurement angle (by DLS).

In addition, <u>nanoparticle tracking analysis</u> (NTA) technique was used for the determination of hydrodynamic nanoparticle sizes. As described in Section 3.3.2.15, this technique is advantageous among DLS techniques because it also enables the determination of the nanoparticle concentration and the visualization of nanoparticles (Filipe, 2010). NP-0.16E70 nanoparticles were used for these measurements. As Figure 4.36a shows, nanoparticles can be visualized using the microscope of the NTA equipment. These nanoparticles, which are quite monodisperse in microscopic appearance, were at a concentration of around $2 \cdot 10^8$ NPs/mL. Taking into account that the measurements were performed under a dilution of 10^6 from the original nanoparticle dispersions, the as-prepared nanoparticles are at an experimental concentration of around $2 \cdot 10^{14}$ NPs/mL.

A mean hydrodynamic radius of 27.35 ± 0.75 nm was obtained. The size distribution is plotted in Figure 4.36b and, for comparison purpose, DLS size distribution is also plotted. As this figure shows, DLS gave a monomodal size distribution, with a mean hydrodynamic radius of 20.24 ± 2.05 nm. In contrast, NTA measurements gave a multimodal nanoparticle population, having the main population sizes similar to those of DLS. Previous bibliography stated the more accuracy of NTA in differentiating two populations with similar sizes (Filipe, 2010), as observed for our results (Figure 4.36).
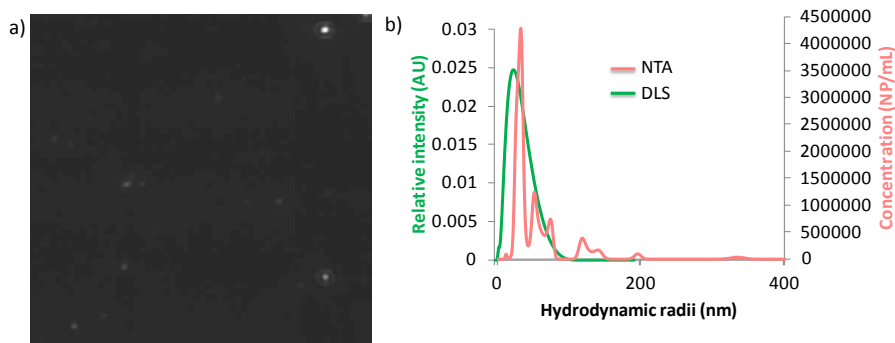
Figure 4.36: a) Micrographs of NP-0.16E70 nanoparticles obtained from the NanoSight; b) Size distribution from NTA and DLS measurements (DLS data provided for comparison).

Static light scattering (SLS) measurements were also carried out for the NP-0.16E70 nanoparticles to find out the nanoparticle shape. This technique allows for the measurement of gyration radius (Schärtl, 2006), which resulted in values of around 18 nm for these nanoparticles. The gyration radius of nanoparticles is lower than the hydrodynamic radius because it measures the hard sphere radii, while hydrodynamic radius includes the solvation layer (Schärtl, 2006; Weiner, 2010). Previous studies indicated that the relation between the gyration radius and the hydrodynamic radius should be around 0.77 to define the particles as spheres (Weiner, 2010; Malvern, 2014). In the present thesis, this value is around 0.76, thus the shape of the nanoparticles can be considered spherical.

To identify and confirm morphology and size of nanoparticles, SEM and TEM experiments were carried out. SEM studies were performed to identify surface texture, shape and size of nanoparticles. Some representative micrographs corresponding to NP-0.16E70 nanoparticles are presented in Figure 4.37.
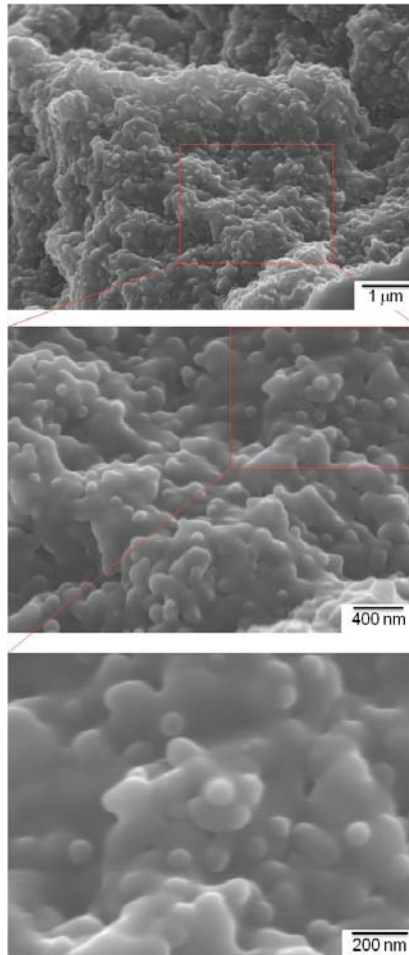
Figure 4.37: Micrographs of the as-prepared NP-0.16E70 nanoparticles, at different magnifications.

Nanoparticles are sticky; once the nanoparticle dispersion has been dried, nanoparticles seem to be part of a layer, as previously reported for nanoparticles in this and larger size range (Nizri, 2005; Fonte, 2012; Whitby, 2012). This could be due to different reasons. On the one hand, the surfactant of the nanoparticles could produce nanoparticle aggregation during the preparation of the SEM grids, but this could be ruled out, since nanoparticles were prepared following the same procedure as for the TEM measurements, in which case there was no evidence that surfactant influences nanoparticle stickiness. On the other hand, for the SEM determination, a metallic coating of the nanoparticles was performed; maybe this was the cause of the layers between particles and the high nanoparticle sizes (up to around 75 nm), which resulted in values more than double of those expected. Also, for the visualization of the samples, an electronic beam impacts on nanoparticle

128

coating, producing a charge on the sample, bigger if the conductive species of the technical grade surfactant are present; which could produce the deformation of the samples. For these reasons, the sizes of nanoparticles were not assessed by SEM observations.

Although nanoparticles seem to be spheres (Figure 4.37), the resolution of the SEM instrument is not enough to unambiguously define their size and shape (Gaumet, 2008). Therefore, TEM studies were carried out. Two nanoparticle dispersions without electrolytes (NP-W50, NP-W70), and two nanoparticle dispersions with electrolytes (NP-0.16E50 and NP-0.16E70) were selected. As an example, micrographs of NP-W70 and NP-0.16E70 nanoparticles are showed in Figure 4.12. Both samples appear as a population of nanospheres with low polydispersity. No core shell structures corresponding to nanocapsules were observed. The same results were obtained for NP-W50 and NP-0.16E50 nanoparticles. These results are in good agreement with previous studies on nanospheres formed by the solvent evaporation method from nano-emulsion templating using a preformed polymer (Soppimath, 2001; Anton, 2008; Calderó, 2011; Fornaguera, 2014(1) and 2014(2)). The spherical shape of nanoparticles was attributed to the method of formation, using template nano-emulsions. The sphere morphology found by this technique, confirms that the change in the size of the nanoparticles as a function of the scattering angle (Figure 4.37) was caused by the slight polydispersity of the sample and not by non-spherical shape.

As shown in Figure 4.38a, NP-W70 nanoparticle surface is cracked, while not a single crack was observed for NP-0.16E70 (Figure 4.38b). Only two references have been found in the literature reporting the presence of similar crashes in polymeric nanoparticle surface (Whitby, 2012; Calderó, 2014). However, in the study by *Whitby et al.,* some kind of fractures onto the nano-emulsion droplet surface was found when using PLGA nanoparticles for the stabilization of nano-emulsions. And in the study of *Calderó et al.,* nanoparticles were prepared using ethyl cellulose instead of PLGA. The formation of these cracks is believed not to be caused by chemical degradation of the polymer, but by the brittleness and low elasticity of this polymeric material. However, when nanoparticles are prepared with electrolytes, these cracks are no longer observed. Although bibliographic references reporting a relationship between nanoparticle cracked surface and presence/absence of electrolytes was not found, two different explanations could be hypothesized. On the one hand, when electrolytes are incorporated in the dispersion media, nanoparticle sizes are nearby one order of magnitude lower than those prepared without electrolytes (Figure 4.33). Therefore, the surfactant curvature should be higher, thus increasing the tensions between the polymer

chains and producing the cracks. However, the inverse was observed, which could be attributed to the formation of porous onto nanoparticle surface, only in the presence of electrolytes, to reduce the surface tension, thus avoiding the formation of the cracks. On the other hand, the presence of electrolytes could affect the Tg of the polymer. In the present work, the Tg of the PLGA powder was found around 45ºC (Section 4.1.3.1.2), while the Tg for PLGA nanoparticles dispersed in PBS 0.16M was found around 44ºC (results showed below). Therefore, the Tg slight decrease could produce a slight increase on the polymer chains mobility, thus decreasing the surface tension of the nanoparticles and avoiding the formation of the cracks.
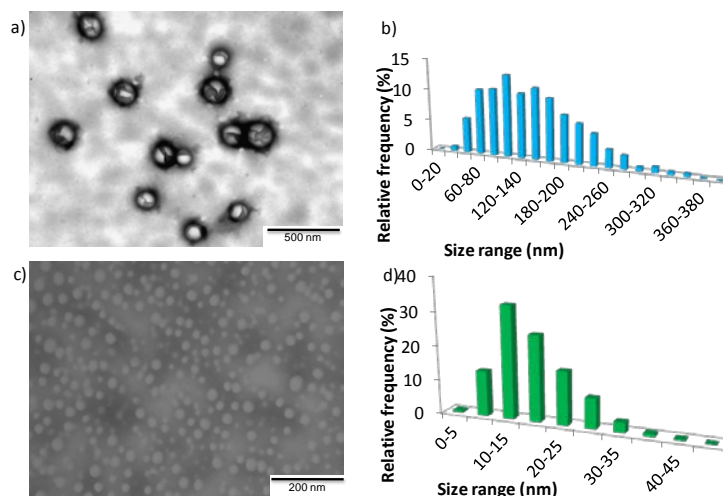
Figure 4.38: Micrographs of the nanoparticles: a) NP-W70 and c) NP-0.16E70; and nanoparticle size distributions of: b) NP-W70 and d) NP-0.16E70.

TEM micrographs were also used to assess nanoparticles mean diameter using the SPSS software. The results are presented in Table 4.12. Nanoparticles prepared with nano-emulsion with water as the aqueous phase have sizes of around 100 nm, while the addition of electrolytes (0.16M) produced a decrease down to around 20 nm. Moreover, the nanoparticle size distribution is narrower with the addition of electrolytes (Figure 4.38b and d). In agreement with DLS measurements, nanoparticle size depends mainly on the aqueous phase composition. This was already expected, since nanoparticle characteristics depend on their template nano-emulsions. For the same electrolyte concentration, no significant differences were found as a function of the O/S ratio of the template nano-emulsion.

Table 4.12: Nanoparticle diameter assessed from TEM micrographs.

Sample	Nanoparticle diameter (nm)
NP-W50	92.92 ± 35.57
NP-W70	100.95 ± 69.75
NP-0.16E50	21.57 ± 6.29
NP-0.16E70	16.74 ± 6.61

Comparing the results from both techniques (DLS and TEM), it was expected a reduced size in the TEM measurements as compared to the DLS measurements. These differences were expected considering that the TEM measures the hard sphere while the DLS measures the nanoparticle hydrodynamic size (hard sphere + solvation shell). The hard sphere sizes of NP-W are of around one third of their hydrodynamic sizes, while NP-0.16E hard sphere sizes are around a half of their hydrodynamic sizes. Comparing with previous studies (Jeon, 2008; Holzer, 2009(2); Zhou, 2009), *Holzer et al.* (Holzer, 2009(2)), for example, also found a size reduction when measuring PLGA nanoparticles with TEM, as compared with DLS measurements. However, in that case, differences of only 30 nm were found (130 nm vs 160nm). In addition, *Jeong et al.,* (Jeong, 2008) also found a size reduction of around 30 or 50 nm (100 nm vs 130 nm and 300 nm vs 350 nm) when they measured PLGA nanoparticle diameters by TEM, as compared with DLS measurements. In the present study, the differences between the measurements of both techniques are much higher. These higher differences could be due to the presence of surfactant molecules, which could enhance the solvation layers of the nanoparticles, thus resulting in higher hydrodynamic sizes.

The effect of different post-treatments (dialysis, ultracentrifugation and rotaevaporation) in the nanoparticle size was assessed by TEM using NP-0.16E70 nanoparticles. The **dialysis** is the usual procedure for nanoparticle purification from remaining reactants / raw products. It was performed at 25ºC, using the dialysis bag method with a PBS 0.16M receptor solution. **Ultracentrifugation** and **excess rotaevaporation** are generally used for nanoparticle concentration. In the present work, **ultracentrifugation** was performed at 25ºC, for 1h, at 19,000rpm; while excess rotaevaporation was performed at 25ºC, 43mbar, for 30 min. The resulting nanoparticle sizes are presented in Figure 4.39 and Table 4.13. Independently of

the treatment, nanoparticles remained spherical, without showing a core shell structure; therefore, in the experimental conditions used, the post-treatments did not influence nanoparticle morphology (Figure 4.39).
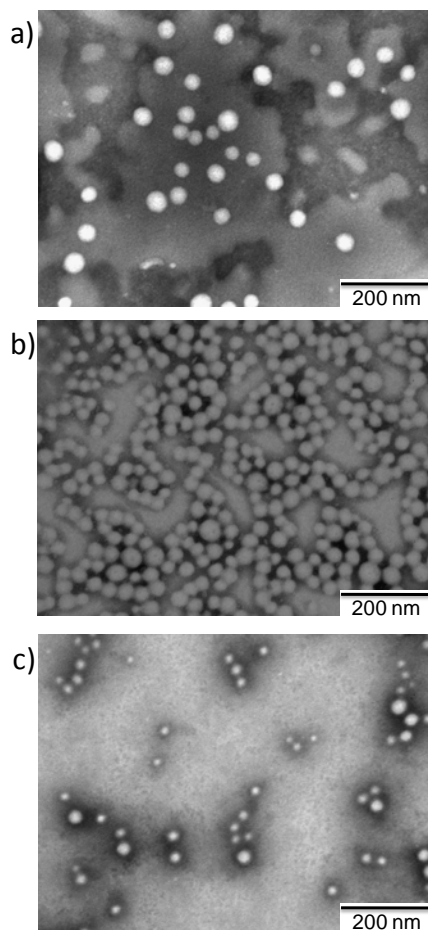
Figure 4.39: TEM micrographs of the NP-0.16E70 nanoparticles as a function of the post-treatment: a) Dialysis; b) Ultracentrifugation and c) Rotaevaporation.

However, nanoparticle post-treatment produces an increase in nanoparticle size (Table 4.13). The dialysis, a mild methodology produces the increase of only a few nanometers, the ultracentrifugation produced an increase of around a decade and the rotaevaporation, performed under a high vacuum, doubled the nanoparticle size. Therefore, the nanoparticle size increase is higher when the treatment is more drastic.

Table 4.13: NP0.16E70 nanoparticle diameter as a function of the post-treatment, as assessed by TEM image analysis.

Sample	Nanoparticle post-treatment	Nanoparticle diameter (nm)
NP-0.16E70	-	16.74 ± 6.61
	Dialysis	22.67 ± 5.71
	Ultracentrifugation	27.32 ± 8.41
	Rotaevaporation	32.75 ± 8.72

Nanoparticle size distribution was also determined for the different post-treatments applied (Figure 4.40). Nanoparticle size distributions show monomodal Gaussian distributions, thus indicating a monomodal sample, with nanoparticles with sizes around the mean size. It seems that a slight tendency to widen the nanoparticle size distribution to the bigger sizes is observed when the treatment is more drastic. The widening of nanoparticle dispersions could not be attributed to the formation of aggregates, since they were not observed by TEM (Figure 4.39). A plausible explanation not only for the widen size distributions but also for the higher nanoparticle sizes could be related with the time taken between the nanoparticle preparation and the TEM measurements. The as-prepared nanoparticles, without any post-treatment, should have a compact morphology, but, after some time, the water molecules could penetrate between the polymer chains, thus producing a nanoparticle swelling. This swelling is usually favored by the presence of surfactant molecules. The amount of surfactant is higher after the rotaevaporation and even higher after the ultracentrifugation, while it is lower after the dialysis. This explanation is in good agreement with the experimental results, where a lower increase in size is produced for the dialysis post-treatment (Table 4.13).
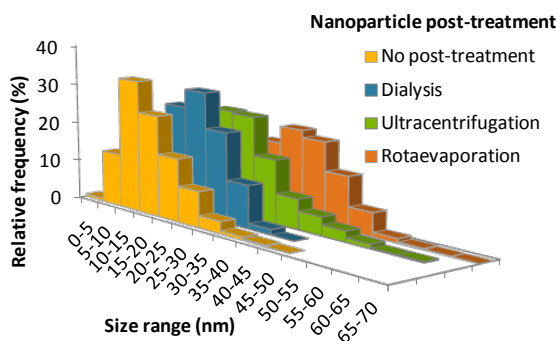
Figure 4.40: Nanoparticle size distributions of NP0.16E70 nanoparticles for different post-treatments.

Since after the post-treatments to concentrate nanoparticles, their sizes were not appropriate for further application in the present work, an alternative methodology was tested to concentrate nanoparticles. The concentration step consisted on an <u>inverse dialysis</u>, which was performed using NP-W70 nanoparticles. The nanoparticle dispersion (initial osmotic pressure of 63mOsm/kg) was dialyzed against a receptor solution of higher osmotic pressure (around 310mOsm/kg), thus forcing the diffusion of water molecules from the nanoparticle dispersion to the receptor solution to equilibrate osmotic pressures (final osmotic pressure of inner and outer solutions of around 300mOsm/kg), and producing a concentration of the nanoparticles. The influence of the volume of the receptor solution was tested. Table 4.14 shows the results. The concentration of the nanoparticles was achieved using all the tested volumes. As expected, the higher the volume of the receptor solution, the higher the concentration (lower concentration factor – Fv). The nanoparticle size as well as PDI was not significantly modified after the concentration step. Therefore, it was concluded that concentration of nanoparticles by an inverse dialysis is feasible. Nevertheless, it is worth noting that in further studies (to achieve loperamide therapeutic concentrations) commercial devices were used.

Table 4.14: Characterization of NP-W70 nanoparticle dispersion before and after the inverse dialysis concentration step using different volumes in the receptor solution. Fv: concentration factor. Fv = final mass / initial mass of the nanoparticle dispersion.

Receptor solution volume (mL)	Fv (m_f/m_i)	Hydrodynamic radius (initial, nm)	Hydrodynamic radius (final, nm)	PDI
10	0.87		135.89 ± 2.20	0.23
25	0.80	131.71 ± 2.09 (PDI = 0.28)	130.27 ± 1.70	0.28
50	0.76		136.33 ± 3.21	0.22

AFM measurements were carried out to further analyze the size and morphology of the nanoparticles. The results corresponding to the NP-0.16E70 (Figure 4.41) show that nanoparticles are spherical and uniform, as it was observed by TEM. With this technique, a mean particle size around 30 nm was obtained by nanoparticle height measurement (Figure 4.41). In addition, nanoparticle aggregation was ruled out. These results are in good agreement with previous studies, in which PLGA nanoparticles with similar sizes were measured by AFM, finding non-aggregated spherical nanoparticles (Ravi Kumar, 2004; Dobrovolskaia, 2009).
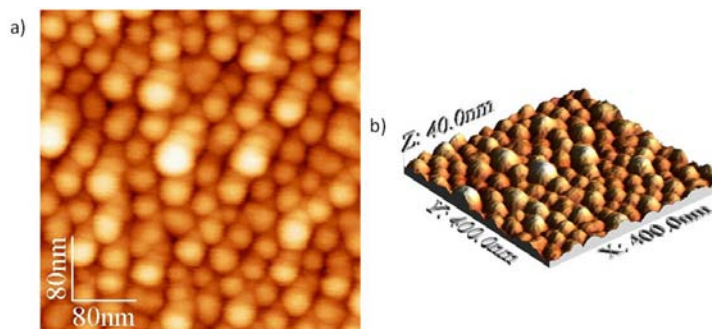
Figure 4.41: AFM images of NP0.16E70 nanoparticles. Figure a) represents the 2D image, while Figure b) corresponds to the 3D representation of the same image.

Comparing the nanoparticle sizes obtained with all the techniques used, at first some contradictory results seem to appear. However, they can be interpreted considering the characteristics of each technique. First of all, as discussed above, the results from the SEM determinations cannot be taken into account when defining nanoparticle size, since the method is not appropriate due to the low nanometric sizes of the nanoparticles. The nanoparticle sizes are bigger when determined by DLS and NTA than those determined with the other techniques (TEM, AFM), but this was previously expected, since the size by DLS and NTA includes not only the hard sphere sizes but also the solvation layer around the nanoparticles. The AFM resulted in sizes of around 30 nm. Since the measurement is performed by a tip, it cannot exactly limit the rounded edges of the nanoparticles when scanning the sample surface. Therefore, the real size of the nanoparticles is expected to be slightly smaller than the value given by AFM. This is in good agreement with TEM results, which gave nanoparticle sizes of around 20 nm, 10 nm less than by AFM. In addition, comparing the nanoparticle sizes obtained in this study with previous studies, although sizes similar to NP-W nanoparticles are reported (Stolnik, 1995; Trimaille, 2003; Pinto-Reis, 2006; Harush-Frenkel, 2007, Chen, 2011; Danhier, 2012), not a single study was found reporting PLGA nanoparticles as small as the NP-0.16E nanoparticles. This reduction in the size could be explained by the use of the low-energy emulsification PIC method for the formation of the template nano-emulsions, together with a solvent diffusion effect (Solans, 2012).

The nanoparticle size can also be theoretically predicted considering the nano-emulsion droplet size and taking into account the evaporated solvent of the disperse phase. NP-W60, NP-0.03E60, NP-0.08E60 and NP-0.16E60 nanoparticles (from template nano-emulsions with an O/S ratio of 60/40) were selected for these

calculations (see calculus in appendix section 8.2.1). A marked reduction on nanoparticle sizes from nano-emulsion droplet sizes due to the solvent evaporation was expected. Nanoparticle sizes assessed by means of DLS measurements showed correlation with the theoretical expected sizes for most nanoparticle dispersions, with the exception of the NP-W nanoparticles (Table 4.15). In addition, these calculations are important to assess if the size measured for nano-emulsions, especially for those with electrolytes, corresponds really to droplets, or due to solvent evaporation, they consist on nanoparticles. For NP-0.08E60 and NP-0.16E60 nanoparticles, theoretical predicted sizes are slightly lower than those obtained experimentally. Therefore, it could be stated that these nano-emulsions are formed by oil droplets although the presence of early formed nanoparticles cannot be ruled out. In addition, higher experimental nanoparticle sizes than those theoretically predicted, especially for NP-W60 nanoparticles, could be due to the above-mentioned effect of nanoparticle swelling. The theoretical sizes could correspond to those of compact nanoparticles, while experimental sizes found could correspond to the swelled nanoparticles with water molecules within the polymeric matrix.

Table 4.15: Experimental hydrodynamic droplet radii of nano-emulsions and nanoparticles and theoretical radii predicted for NP-W60, NP0.03E60, NP0.08E60 and NP-0.16E60 nanoparticles.

Sample	Hydrodynamic radii (nm)		
	Precursor NE (experimental)	NP (experimental)	NP (theoretical)
NP-W60	178.31	138.24	53.76
NP-0.03E60	115.73	37.59	34.89
NP-0.08E60	12.83	9.87	3.87
NP-0.16E60	34.06	20.54	10.27

Knowing the nanoparticle size, other theoretical parameters (Némati, 1994) such as the number of nanoparticles per volume unit or the density of PLGA molecules in a nanoparticle were calculated for NP-W70 and NP-0.16E70 nanoparticles. This information will be useful for the calculation of the nanoparticle surface, for example, in the experiments concerning nanoparticle interaction with blood components. The results are presented in Table 4.16. Considering that each droplet of the template nano-emulsion forms a nanoparticle, the number of nanoparticles in the nanoparticle dispersions is equivalent to the number of the nano-droplets. Therefore, nano-emulsion droplet sizes as well as nanoparticle sizes are one order

of magnitude lower for NP-0.16E70 than for NP-W70. The number of polymer molecules for a single nanoparticle and its density in a specific volume is higher when the nanoparticles are bigger. For this reason, the number of PLGA molecules for a nanoparticle is higher in NP-W70. However, the characteristics of a single PLGA molecule (surface and volume) are independent on the nanoparticle size.

It is work noting that theoretical calculations resulted in $2.60 \cdot 10^{14}$ NPs/mL, for NP-0.16E70 nanoparticles, which is in close agreement with the experimental nanoparticle concentration given by the NTA technique (result discussed above in this section). Therefore, theoretical calculations approximate quite well the experimental (real) values.

Table 4.16: Theoretical calculations of different parameters of NP-W70 and NP-0.16E70.

	NP-W70	NP-E70
Number of template NE droplets /mL (Nº/mL)	$2.88 \cdot 10^{12}$	$2.60 \cdot 10^{14}$
Number of NPs/mL (Nº/mL)	$2.88 \cdot 10^{12}$	$2.60 \cdot 10^{14}$
Number of PLGA molecules/NP (Nº/NP)	$1.87 \cdot 10^{4}$	$1.84 \cdot 10^{2}$
Density of PLGA molecules/NP (Nº/mL)	$6.09 \cdot 10^{12}$	$9.15 \cdot 10^{11}$
Volume of 1 PLGA molecule in NPs (m³)	$1.33 \cdot 10^{-18}$	$1.46 \cdot 10^{-18}$
Surface of 1 PLGA molecule in NPs (m²)	$1.64 \cdot 10^{-13}$	$1.09 \cdot 10^{-12}$

4.3.3. Nanoparticle surface charge

Nanoparticle surface charge was assessed by determining the electrophoretic mobility and using the Hückel-Onsager equation, as for nano-emulsions. The surface charge of nanoparticles was determined as a function of the O/S ratio of the template nano-emulsion. The results for NP-W, NP-0.03E, NP-0.08E and NP-0.16E nanoparticles are shown in Figure 4.42. Negative values of the surface charge were already expected as nanoparticles are formed by the PLGA polymer, which has carboxylic terminal groups that possess negative charges. Indeed, the results of ζ potential were negative for all nanoparticles. These results agreed with other studies reporting the production of PLGA nanoparticles, in which negative ζ potentials were also found (Stolnik, 1995; Harush-Frenkel, 2007; Singh, 2013).

Nanoparticles prepared without electrolytes have lower surface charges; they are more negatively charged. Comparing the different electrolyte concentrations, a decrease in the surface charge when the electrolytes were incorporated was expected, due to the presence of ionic species. This could be due to the

compensation between negative and positive charges of the salts, whose contribution is counteracted not only by the charges of the solution but also by the PLGA charges. This behavior was observed for all the nanoparticles prepared, independently on the electrolyte concentration. Moreover, some authors have reported that the ζ potential is dependent on the pH of the solvent: the lower pH, the higher the ζ potential value (Dobrovolskaia, 2013). This is in good agreement with the results obtained in this thesis, since the more acidic the nanoparticle dispersions (those prepared with water without electrolytes), the more negative the ζ potentials.

Comparing the ζ potential values of nanoparticles as a function of their template nano-emulsions O/S ratios, when increasing the oil fraction, the amount of the PLGA increases, thus increasing the total amount of negative charges. For this reason, a decrease in the ζ potential was expected when increasing the O/S ratio. This behavior was found for the system without electrolytes. However, with electrolytes, the behavior was contrary to that expected. Increasing the O/S ratio, the ζ potential approached to null values. The explanation of this phenomenon could be the compensation of the PLGA negative charges by the charges of the electrolytes of the solvent.
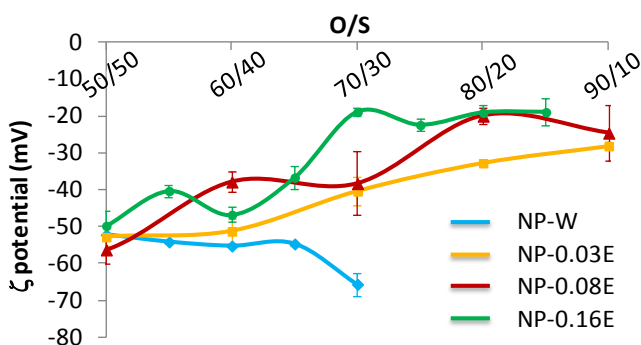
Figure 4.42: Zeta potential of NP-W, NP-0.03E, NP-0.08E and NP-0.16E nanoparticle dispersions as a function of O/S ratio of the template nano-emulsion.

For biomedical applications, namely for the intravenous administration, nanoparticle surface charge is an important parameter that determines the biodistribution (Dobrovolskaia, 2013). Slight negative charged nanoparticles are advantageous because they cannot interact with proteins and cells (because these also have negative charges) thus reducing the activation of the immune system and enabling longer circulation times to reach the target organs (Toti, 2010).

The ζ potential of nanoparticles prepared from nano-emulsions with an O/S ratio of 70/30 was further studied as a function of the electrolyte concentration. The

results are shown in Figure 4.43. For comparative purposes, the hydrodynamic radii (given in Figure 4.33) are also plotted. As it was previously discussed, the hydrodynamic radius decreases when increasing the electrolyte concentration up to a concentration (0.04M) after which it keeps almost constant, due to the combination of the salting out and surfactant effects (Section 4.2). Regarding the ζ potential results (Figure 4.43), at low electrolyte concentrations, it decreases with the increase in the electrolyte concentration, up to a concentration of 0.03M. Then, it increases abruptly up to a concentration of 0.04M, after which it remains almost constant. Therefore, the evolution of the ζ potential as a function of the electrolyte concentration is opposite to that of the hydrodynamic radius. This behavior is exactly the same than that obtained for nano-emulsions; therefore, the same explanation could be given for nanoparticles. The small sizes are usually associated with more stable systems, while the ζ potential values around null values are related with less stable dispersions. In these nanoparticles, a non-electrostatic contribution to the stabilization must exist; the steric stabilization seems to predominate, since the smaller nanoparticles seem to be more stable although they have lower surface charges (Stolnik, 1995).
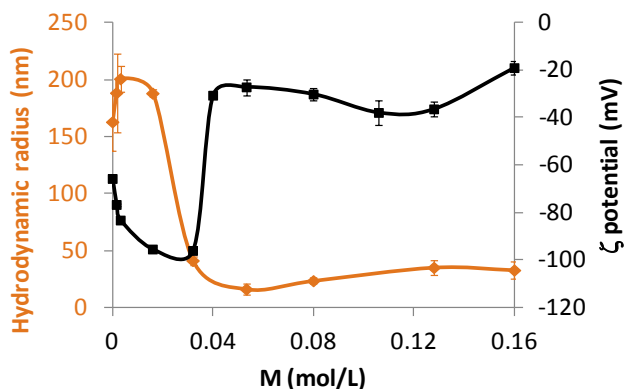
Figure 4.43: Hydrodynamic radii and ζ potential of the nanoparticle dispersions formed from template nano-emulsions with an O/S ratio of 70/30 as a function of the electrolyte concentration in the aqueous phase.

4.3.4. Nanoparticle dispersion osmolality

Blood properties should be maintained when administering nanoparticles by intravenous route. One of these properties is the osmolality, which is around 275 – 300 mOsm/kg in the blood (Dobrovolskaia, 2013). At slightly higher osmolality values, inflammation is produced; even cell death by apoptosis was reported at

higher osmolalities (Singh, 2013). For this reason, to maintain the osmotic balance, nanoparticle dispersions should have an osmolality around 275 - 300 mOsm/kg.

The osmolality of NP-E70 nanoparticles (prepared from nano-emulsions with 70/30 O/S ratio) was studied as a function of the electrolyte concentration. As Figure 4.44 shows, the osmolality of the nanoparticles is directly proportional to the electrolyte concentration of the solvent, reaching the blood range osmolality values at the highest electrolyte concentration (0.16M). Therefore, NP-0.16E70 nanoparticles can be considered appropriate for the intravenous delivery regarding osmolality requirements.
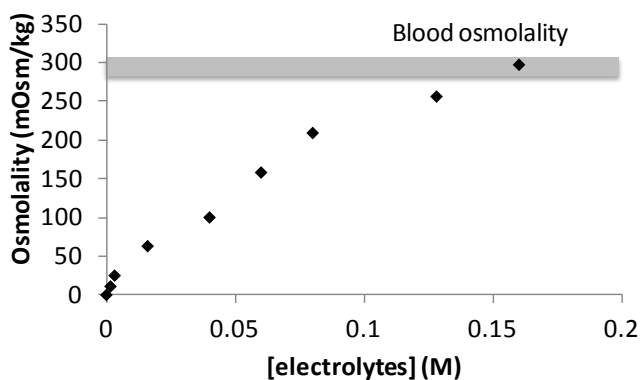
Figure 4.44: Osmolality (in mOsm/kg) of nanoparticles prepared from a nano-emulsion with 90wt % of aqueous phase and 70/30 O/S ratio, as a function of the electrolyte concentration in the aqueous phase. Grey zone represents the range of blood osmolality.

4.3.5. Nanoparticle stability

Nanoparticle stability is another important property to study, since it will determine if the nanoparticles are appropriate for use and storage. Nanoparticle dispersion stability was studied from two points of view: the colloidal stability and the chemical stability of the polymer in nanoparticles. The degradation of a polymer is a chemical process that, in the case of PLGA polymer happens naturally in the human body. For this reason it is a biodegradable polymer (Pillai, 2001; Danhier, 2012). The biodegradation of the polymers is dependent on various factors: the chemical structure and characteristics of the nanoparticles, physical and physico-chemical factors, morphology of the nanoparticles, the polymer type (which determines the mechanism of degradation), its molecular weight distribution and also the route of administration (Pillai, 2001).

4.3.5.1.   Colloidal stability

4.3.5.1.1.   Visual assessment

First, nanoparticle stability was assessed by visual macroscopic observations. Stability of the NP-W and NP-0.16E nanoparticles as a function of the template nano-emulsion O/S ratio was studied. The results are shown in Table 4.17. NP-W nanoparticles tend to sediment quickly, before 10 days while NP-0.16E nanoparticles are stable for longer times (Table 4.17). The higher the surfactant concentration in the template nano-emulsion (lower O/S ratios), the higher the stability. This could be attributed to a nanoparticle dispersion stabilization effect of the surfactant. In addition, theoretical values of the sedimentation velocity were calculated, using the Stokes equation (Tadros, 1983 and 2009; Binks, 1998). Results are also shown in Table 4.17. The fastest velocity of sedimentation was found for NP-W nanoparticles, with sedimentation velocities one order of magnitude higher than those of NP-0.16E nanoparticles. The Stokes equation relates the sedimentation velocity with the nanoparticle sizes. Therefore, since NP-W nanoparticles are bigger, a faster sedimentation was expected. Theoretical calculations are in close agreement with experimental results observed: the NP-W nanoparticles are bigger (Figure 4.33), therefore, they sediment fatser (Table 4.17).

Table 4.17: Stability (experimental time to observe sedimentation and theoretical velocity of sedimentation calculated from the Stokes equation) of NP-W and NP-0.16E nanoparticles, as a function of O/S ratio of the template nano-emulsion.

O/S ratio	NP-W		NP-0.16E	
	Time to sediment (days)	Velocity of sedimentation (nm/s)	Time to sediment (days)	Velocity of sedimentation (nm/s)
50/50	9	5707	>90	180
70/30	1.5	4435	>90	108
75/25	--	--	82	99
80/20	--	--	82	99
85/15	--	--	82	99

4.3.5.1.2. Stability by light transmission/ backscattering

NP-W, NP-0.03E, NP-0.08E and NP-0.16E nanoparticles were studied from template nano-emulsion with O/S ratios of 50/50 and 70/30. Light backscattering was measured for NP-W nanoparticles since the samples had a translucent to opaque appearance while in NP-E nanoparticles, light transmission was measured. The results, obtained with a TurbiscanLab^{TM} equipment, are shown in Figures 4.45 and 4.46. All results are presented as the percentage of the transmitted / backscattered light as a function of time and sample height. The left part of the plots corresponds to the bottom of the sample, while the right part corresponds to the sample surface. For this reason, at the limits of the plots the light percentage varies from the rest of the sample and has no physical meaning.

The results for NP-W nanoparticles at 25ºC and 37ºC (Figure 4.45) showed that the backscattering percentage is around 6% in NP-W50 nanoparticles and around 8% in NP-W70 nanoparticles, thus NP-W70 nanoparticles are more turbid, indicating a bigger size. Light backscattering was constant along the sample height for both samples, with the exception of the peak observed at the bottom of the samples, which could be attributed to nanoparticle sedimentation (Lemarchand, 2003). In addition, light backscattering was constant as a function of time for NP-W50 nanoparticles, but it slightly increased for NP-W70 nanoparticles. The increase in the backscattered light along the time can be related with an increase on the sample turbidity, which enables less light to pass through. The increase on the sample turbidity could be related with an increase in the nanoparticle size, which could be due to coalescence-like destabilization mechanism (Lemarchand, 2003). The only difference between both temperatures studied, for the same nanoparticle dispersion, is that at 37ºC the sedimentation peak is more pronounced (Figure 4.44c and d). These results are in good agreement with macroscopic observation, where bigger nanoparticles tended to rapidly sediment (Table 4.17) and also with those of template nano-emulsion stability results (Figure 4.17). It is worth mentioning that sedimentation is not macroscopically observed within 24 hours. However, as mentioned, the optical analysis method used is an accelerated methodology that gives information on the main destabilization mechanisms.

Summarizing, NP-W nanoparticles are not stable against sedimentation. Increasing the O/S ratio of the template nano-emulsion and the temperature, their stability decreases.
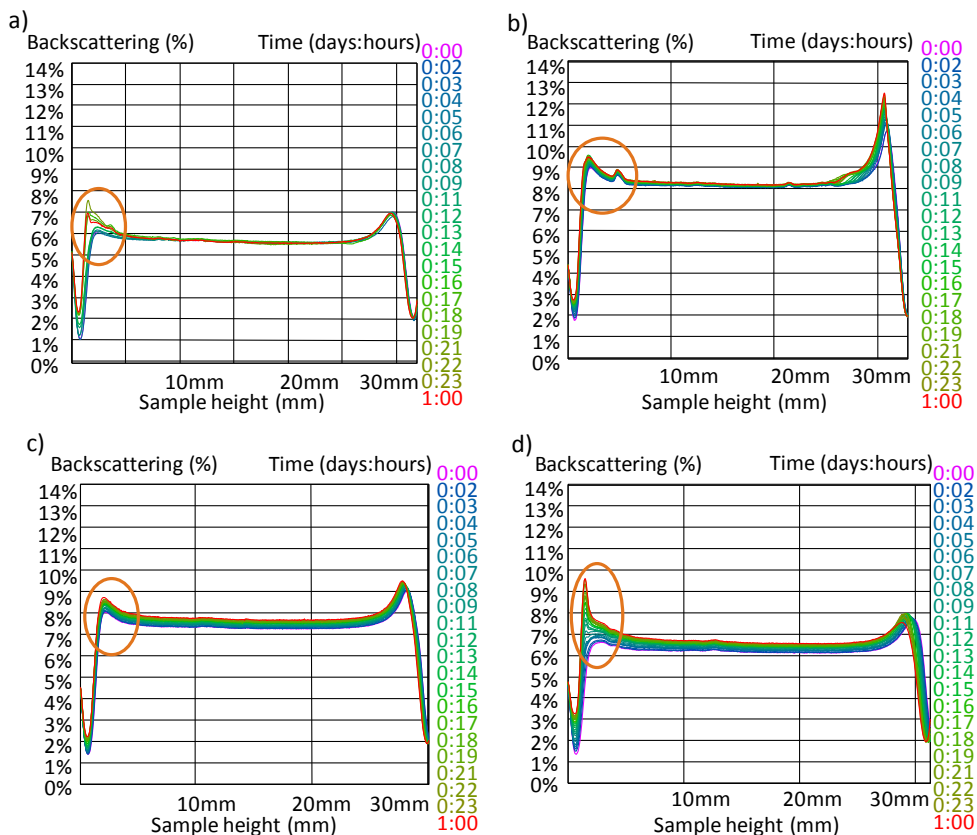
Figure 4.45: Light backscattering of: a) and c) NP-W50 and b) and d) NP-W70 nanoparticles at: a) and b) 25ºC and c) and d) 37ºC. The circle marks the sedimentation of the samples.

The results of NP-0.16E50 and NP-0.16E70 nanoparticles at 25ºC and 37ºC are shown Figure 4.46. All dispersions showed that light transmission was constant as a function of time and sample height, thus indicating that nanoparticles are stable at both studied temperatures. The slight fluctuations in the sample transmission along the sample height are due to the presence of PBS electrolytes. Light transmission results are in good agreement with visual observations, in which no macroscopic changes were observed for at least 80 days, as well as with their template nano-emulsion stability results. Nevertheless, a very small increase in the light transmission was observed for all NP-0.16E nanoparticles, independently on the temperature. This increase was previously attributed in the literature to an increase in the sample turbidity, which could be related to a clarification of the sample. This clarification could be produced by sedimentation of the nanoparticles (Lemarchand, 2003), which was previously assessed macroscopically in the visual observations at longer times (also for the NP-0.16E nanoparticles).
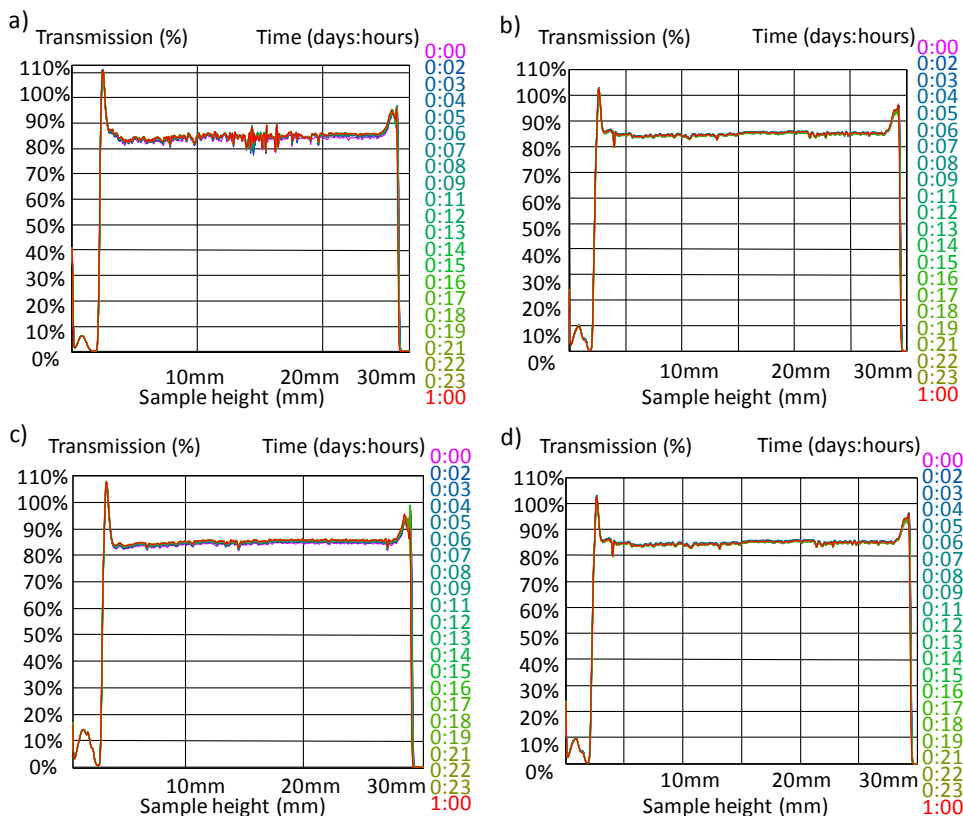
Figure 4.46: Light transmission of: a) and c) NP-0.16E50 and b) and d) NP-0.16E70 nanoparticles at: a) and b) 25ºC and c) and d) 37ºC.

4.3.5.1.3. Variation of size with time

The nanoparticle hydrodynamic radii were followed as a function of time by DLS to better study the colloidal stability of the nanoparticle dispersions. NP-W50, NP-0.03E50, NP-0.03E70, NP-0.08E50, NP-0.08E70, NP-0.16E50 and NP-0.16E70 nanoparticles were studied. Figure 4.47 shows the results for NP-W50 nanoparticles. The radii are around 150 nm just after their preparation. Nanoparticle size is quite constant up to ten days, when the size tends to decrease; although during the first day, a slight size increase was detected. As observed visually, nanoparticles tend to sediment after approximately 9 days, which would explain the decrease in size found by DLS (it should be noted that dispersions were not shakes before DLS measurements). These results are also in good agreement with those of the template nano-emulsion (Figure 4.19). The slight increase observed during the first day could be related with nanoparticle swelling, although

nanoparticle sedimentation probably predominates. However, backscattering results seemed to indicate an increase on the nanoparticle size, due to the increase on the backscattered light. The nanoparticle size tendency obtained by DLS seem to differ from backscattering results, but, as mentioned above, nanoparticle size measurements were performed without agitating the samples, thus, bigger nanoparticles precipitated during the study.
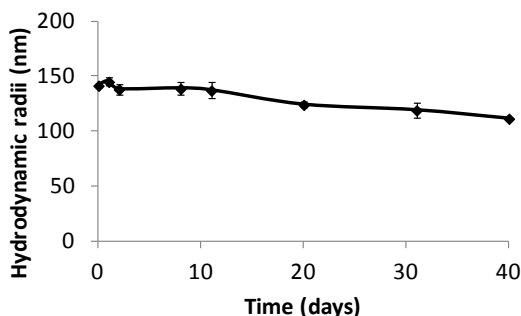
Figure 4.47: Hydrodynamic radii (nm) of NP-W50 as a function of time, without agitation of the dispersion.

The results for nanoparticles with intermediate electrolyte concentration (NP-0.03E50, NP-0.03E70, NP-0.08E50 and NP-0.08E70) are shown in Figure 4.48. At early times, oscillations in nanoparticle sizes were observed, tending to a slight decrease with time which could be attributed to slight destabilization mechanisms. After around 10 – 15 days, nanoparticle size keeps practically constant for at least 40 days. Regarding NP-0.03E nanoparticles (Figure 4.48a), NP-0.03E50 nanoparticle sizes are approximately double than those of NP-0.03E70. However, for NP-0.08E nanoparticles (Figure 4.48b), although NP-0.08E50 nanoparticles are bigger at the beginning, they suffered a more marked decrease than NP-0.08E70 nanoparticles, and after around 15 days they show similar sizes. The results are equivalent to those obtained for their template nano-emulsions (Figure 4.20 and Figure 4.23).
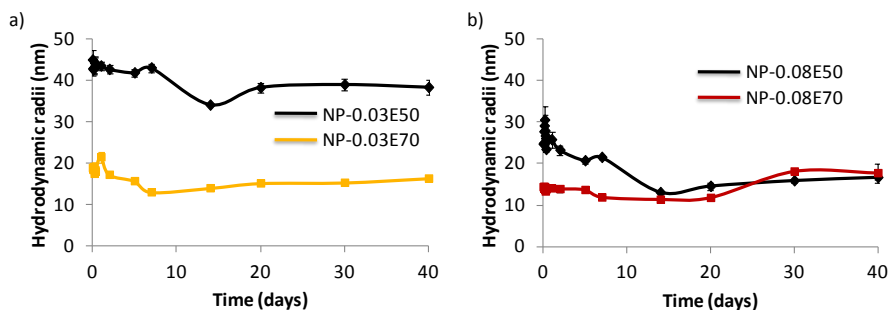
Figure 4.48: Hydrodynamic radii (nm) of a) NP-0.03E50 and NP-0.03E70 and b) NP-0.08E50 and NP-0.08E70 nanoparticles. Dispersions were not shaken before measurements.

145

The results for NP-0.16E50 and NP-0.16E70 nanoparticles (Figure 4.49) showed that nanoparticle sizes keep constant along the time, thus, they are stable for at least 40 days, confirming the macroscopic observation. It is worth noting that NP-0.16E50 nanoparticles are bigger than NP-0.16E70 nanoparticles, as it was observed for NP-0.03E nanoparticles. This could be attributed to the above mentioned diffusion of the solvent of the template nano-emulsions, thus producing a higher nano-emulsion droplet size decrease at the higher oil contents. This was already evidenced in Figure 4.32, where nanoparticle sizes were assessed as a function of the template nano-emulsion O/S ratio. In addition, the above-mentioned nanoparticle swelling produced at early times could be the cause of the higher sizes of the NP-0.16E50 nanoparticles, since the surfactant content in the corresponding template nano-emulsions was higher.
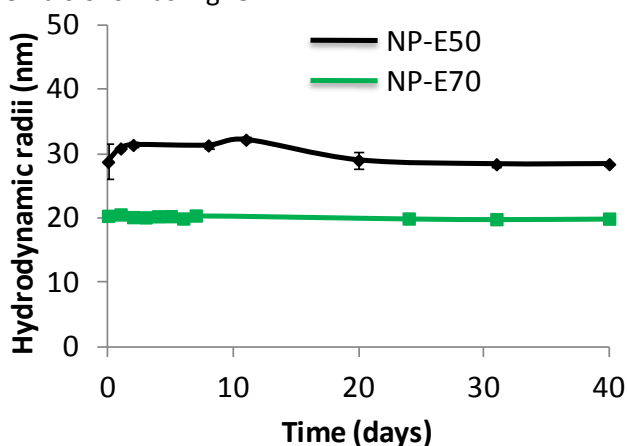
Figure 4.49: Hydrodynamic radii (nm) of NP-0.16E50 and NP-0.16E70 nanoparticles. Samples were not shaken before the measurements.

It is worth remarking that the slight size increase at early times, found in most of nanoparticle dispersions (Figure 4.46 – 4.49) is in good agreement with the initial swelling hypothesized to explain the slight higher sizes found after nanoparticle post-treatment in TEM measurements (Table 4.13).

146

4.3.5.2. Chemical stability of the polymer in the nanoparticles

The chemical polymer stability in the nanoparticles (chemical groups, thermal behavior, variations in temperature, pH, osmolality and viscosity) was studied as a function of time for NP-W70 and NP-0.16E70 nanoparticles. It is worth mentioning the importance of the polymer biodegradation in order to avoid polymer accumulation and toxicity related problems (Catiker, 2000). Once PLGA is degraded into lactic and glycolic acid polymers, lactic acid is eliminated through respiration as carbon dioxide and glycolic acid enters to the tricarboxylic acid cycle and is eliminated as carbon dioxide and water or it is excreted directly by the kidney (Wu, 1995; Catiker, 2000; Jain, 2000).

FTIR and TGA experiments were performed to confirm the presence and integrity of the PLGA polymer once nanoparticles have been prepared. FTIR results are presented in Figure 4.50, for NP-W70 and NP-0.16E70 nanoparticles. In both nanoparticle dispersions, the FTIR peaks corresponding to the chemical groups of the PLGA polymer (ether group (COC) at 1091 cm^{-1}; C-O bond corresponding to an ester or an acid group (CO) at 1756 cm^{-1}; and methyl and methylen groups (CH_3 and CH_2 respectively) at 2993 cm^{-1}) remain intact (Pretsch, 2003). Therefore, the chemical nature of the PLGA does not vary due to the formation of nanoparticles. These results are in good agreement with previous bibliography (Catiker, 2000; Parveen, 2011; Galán-Herranz, 2014).
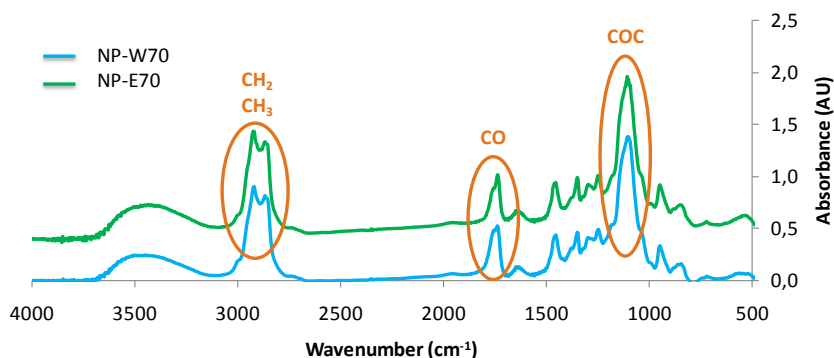
Figure 4.50: FTIR spectra of NP-W70 and NP-0.16E70 nanoparticles.

TGA results (Figure 4.51) indicate that nanoparticle decomposition due to thermal heating is produced at similar temperature intervals without and with electrolytes, having a midpoint of 331.65ºC and 322.74ºC respectively, which is consistent with previous studies for PLGA polymers with 75wt % of lactic acid and 25wt % of glycolic acid (D'Antone, 2001; Galán-Herranz, 2014).

147
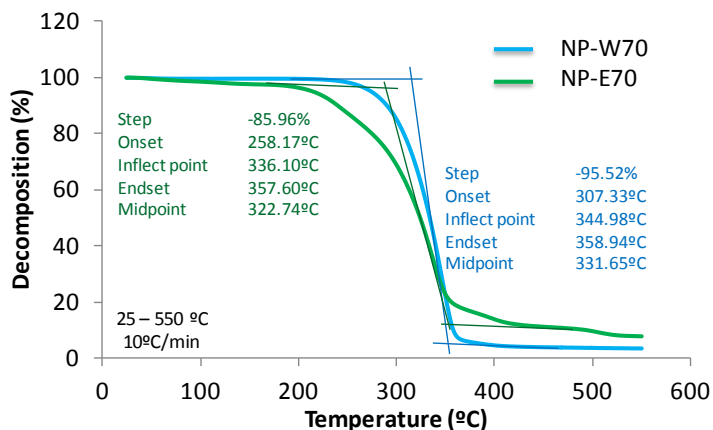
Figure 4.51: TGA plot from NP-W70 and NP-0.16E70 nanoparticles.

4.3.5.2.1.   Influence of the temperature on nanoparticle size

The effect of temperature was studied by determining nanoparticle size as a function of time at 25ºC and 37ºC. The results for NP-0.16E70 nanoparticles are shown in Figure 4.51. The hydrodynamic radius is about 20 nm (Figure 4.52), and keeps constant as a function of time at both temperatures. Although there is a difference of few nanometers between the nanoparticles at 25ºC and 37ºC, the polydispersity index at 37ºC is higher than at 25ºC, as was also observed for the template nano-emulsions. This could be explained as due to the closer proximity of 37ºC to the PLGA T_g (around 40ºC). Since T_g is not a fixed temperature, but a range of temperatures, at 37ºC some PLGA chains could start to change its amorphous state, thus contributing to an increase in the sample polydispersity of the template nano-emulsion (Loo, 2005; Bouissou, 2006). The stability of the nanoparticles size was expected to be independent on the temperature, as once nanoparticles have been formed, they maintain their characteristics below the polymer T_g (around 40ºC for PLGA). The constant sizes as a function of time are an indication of the PLGA integrity.
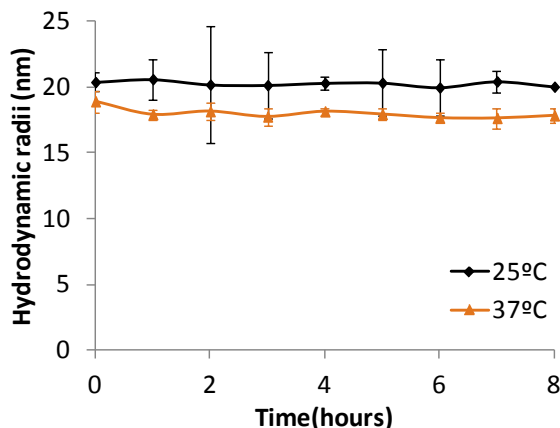
Figure 4.52: Hydrodynamic radii of NP-0.16E70 nanoparticles, at 25ºC and 37ºC, as a function of time, without shaking the dispersions.

4.3.5.2.2. Variation of the pH with time

An increase in the carboxylic end groups of the PLGA polymer during its biodegradation may occur with the consequent decrease in the pH values, since individual monomer chains of lactic and glycolic acid appear as a consequence of the hydrolysis of the ester bonds. Indeed, a pH decrease with time was previously reported for PLGA nanoparticles (Jain, 2000; Singh, 2013). The biodegradation rate of PLGA polymers depends on the lactic to glycolic molar ratio, the molecular weight of the polymer, the degree of crystallinity and the T_g of the polymer (Catiker, 2000; Jain, 2000). Moreover, the biodegradation rate is slightly faster *in vivo* than in *in vitro* studies (Grayson, 2012).

In this work, the effect of the pH was studied at 25ºC and 80ºC. The results are presented in Figure 4.53. A pH of around 7 was expected for the NP-0.16E nanoparticles (dispersed in PBS) and of around 5.5 for the NP-W nanoparticles (dispersed in water). The results were as expected (Figure 4.53). It was also expected that the pH of both nanoparticle dispersions would decrease with time, being the decrease more accelerated at 80ºC. This decrease can be related with the degradation of the polymer in the nanoparticles, releasing the lactic and glycolic acids, which acidify the dispersion further enhancing hydrolysis (Zweers, 2004).

Comparing the two nanoparticle dispersions studied, since the electrolyte solution (PBS) is a buffer, the decrease of pH is not as fast as that of the aqueous

dispersions. Considering the results at room temperature (25ºC) (Figure 4.53a), the pH decreases slightly the firsts days, until approximately 15 days, and then, the degradation is slightly accelerated up to 60 days, after which the pH keeps practically constant. After 60 days, no more degradation of the PLGA chains is evidenced. Although it could be thought that due to the polymer degradation nanoparticles are eroded, taking into account the results of the size measurement with time, it is clear that nanoparticle dispersions are stable for at least 90 days, thus confirming the presence of PLGA in the as-prepared nanoparticles. Only some polymer chains are degraded, thus decreasing the pH of the dispersions. The degradation rate observed is in good agreement with previous bibliography, in which PLGA degradation was found after 10 weeks (Zweers, 2004).
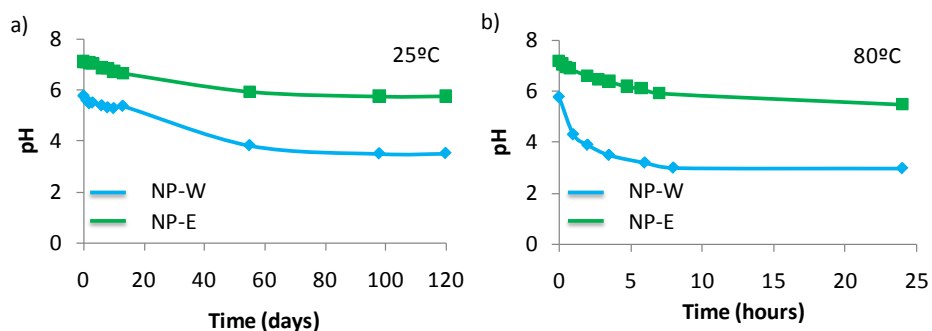
Figure 4.53: pH of NP-W70 and NP-0.16E70 nanoparticle dispersion as a function of time at a) 25ºC and b) 80ºC.

4.3.5.2.3. Variation of the osmolality with time

Osmolality was determined as a function of time, since previous studies demonstrated that PLGA degradation increases osmolality, due to the formation of lactic and glycolic acid molecules (Codewener, 2000; Singh, 2013). For a determined concentration of PLGA, the number of lactic and acid lactic molecules (after PLGA degradation) is higher than that of the PLGA molecules (initially). Therefore, the osmolality is higher after PLGA degradation. The osmolality was studied first with NP-W70 nanoparticles at 25ºC and 37ºC. They were studied for comparative purposes knowing that their osmolality was not appropriate for intravenous administration, due to the lack of electrolytes in the aqueous phase. As it was expected, the osmolality of these nanoparticles increases with time (Figure

4.54), indicating that the PLGA degradation takes place. At both temperatures, the increase of the osmolality at early times is not pronounced, but it suffers a marked increase after 15 days (Figure 4.54). This late increase is more pronounced at 37ºC, indicating that the temperature influences the PLGA degradation rate. This higher degradation at higher temperature was already expected, since as mentioned in previous studies, the nearer the temperature to the polymer T_g, the faster the degradation rate (Zweers, 2004). This was justified due to the higher mobility of the PLGA chains nearer to the T_g, thus enabling higher water penetration into the polymer matrix, which enhances the PLGA degradation.
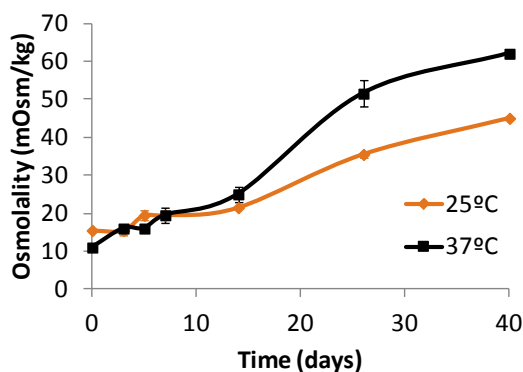
Figure 4.54: Osmolality (in mOsm/kg) of NP-W70 nanoparticles, as a function of time, at 25ºC and 37ºC.

With this first study, the possibility to follow PLGA degradation by means of osmolality determinations was confirmed. However, since NP-W70 nanoparticles did not have the appropriate osmolalities to be intravenously injected, further studies with NP-0.16E nanoparticles were needed. With this purpose, NP-0.16E70 nanoparticles were studied. The temperature was set at 37ºC, since it is the body temperature, and the study was performed without and with fetal bovine serum (FBS), to simulate physiological conditions (Dobrovolskaia, 2013). The results are given in Figure 4.55. Without FBS, nanoparticle initial osmolality is around 275 mOsm/kg, appropriate for the intravenous administration. With FBS, the initial osmolality was already higher than the blood osmolality, which was previously expected due to the presence of salts and proteins in the FBS. During the first days, the osmolality increases more when FBS is present, thus indicating less stability of PLGA against serum. However, after around 7 days, the osmolality values increase with the same rate for both samples.

These results confirm the degradation of PLGA along the time, which is more marked with the presence of FBS. This degradation is progressive but slow, thus enabling the intravenous administration of nanoparticles.
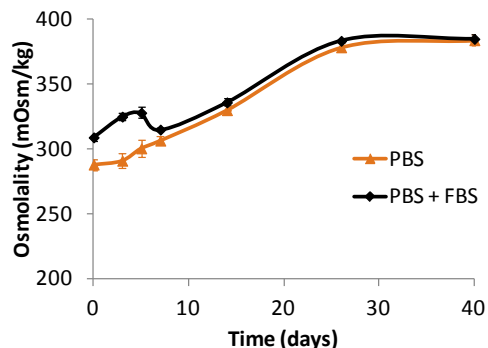
Figure 4.55: Osmolality (in mOsm/kg) of NP-0.16E70 nanoparticles, as a function of time, without and with FBS, at 37ºC.

4.3.5.2.4. Variation of viscosity with time

The chemical stability of PLGA was also studied measuring the viscosity of the nanoparticle dispersions, since previous bibliography reported the use of this methodology for this purpose (Catiker, 2000).

The viscosity was determined at 25ºC and 37ºC to study the effect of temperature on PLGA degradation for NP-0.16E70 nanoparticles, with and without FBS. As Figure 4.56 shows, independently of the temperature, without FBS, nanoparticles are stable in terms of viscosity, at least for 10 hours. However, when adding FBS to the nanoparticle dispersions, after approximately half an hour, the viscosity of the samples starts to increase at both temperatures, thus indicating a degradation of the PLGA, and it keeps constant after 6 hours. These results are in good agreement with previous chemical stability studies, in which an increased PLGA degradation in the presence of FBS was found. It was described as an advantage of this polymer as accumulation problems can be avoided (Catiker, 2000).
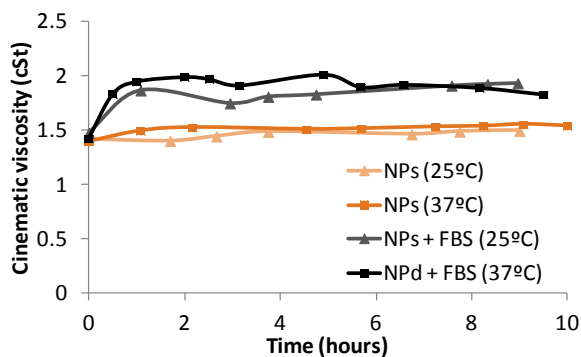
Figure 4.56: Viscosity (in cSt) of NP-0.16E70 nanoparticles, as a function of time, at 25ºC and 37ºC, without and with FBS.

Taking together all the polymer chemical stability studies, it can be postulated that PLGA polymer in the nanoparticles is stable for at least 20 days. Afterwards, the PLGA chains start to degrade into lactic and glycolic acids, thus decreasing the pH of the nanoparticle dispersion as well as increasing its osmolality. However, by measuring the cinematic viscosity, although a slight tendency to an increase was observed, the variations of this value are minimal as a function of time (except when nanoparticles are in the presence of FBS).

The degradation of PLGA reported in the present thesis seems to be faster than in previous bibliography (Zweers, 2004; Wolhfart, 2011(2)), in which nanoparticles were prepared with other methods. However, this could be an advantage in terms of polymer accumulation, as described above.

4.3.6. Reproducibility of nanoparticle batches

The final aim of this thesis is to achieve a novel delivery system by means of nanoparticles. All the studies described in this section have been performed at a laboratory scale, but to reach clinical stages, their production will have to be at a large scale. In all the scalable procedures it is very important to work with reproducible techniques. For this reason, the reproducibility of the as-prepared NP-0.16E70 nanoparticles was assessed by means of size and surface charge (Tosi, 2011). The results are displayed in Table 4.18. Since both values have a standard deviation of around 2 (nm and mV, respectively) (Table 4.18), it could be stated that the technology of nanoparticle production by means of solvent evaporation by nano-emulsion templating is reproducible.

Table 4.18: Example of the nanoparticle size (nm) and surface charge (mV) of ten batches of NP-0.16E70 nanoparticles.

Nanoparticle batch	Hydrodynamic radii (nm)	Surface charge (mV)
1	20.24	-18.99
2	24.57	-20.00
3	26.00	-24.60
4	26.92	-23.04
5	23.55	-20.05
6	23.26	-21.40
7	21.49	-24.23
8	24.12	-25.23
9	20.10	-20.07
10	19.81	-20.40
Mean ± Standard deviation	23.01 ± 2.52	-21.80 ± 2.27

Summary

The systematic study on the formation and characterization of polymeric nanoparticles described in this section allowed to predict that they could be promising systems for the intravenous administration of active substances in the body. It has been shown that nanoparticles have been produced with a reproducible, green, cost effective and versatile technology, apt for biomedical applications (Couvreur, 2006; Pinto-Reis, 2006; Solans, 2012). In addition, the components used, including a small fraction of surfactant (3wt %), are biocompatible and biodegradable; as compared with other previous studies (Date, 2010). The NP-0.16E70 nanoparticle physicochemical characteristics (pH, osmolality, sizes, surface charges and stabilities) are appropriate for their intravenous administration (NP-W did not possess the required osmolality and stability). Therefore, NP-0.16E70 nanoparticles were chosen for performing the encapsulation and functionalization studies, since they represent a compromise between the reduced size (radius around 20nm), the negative surface charge (around -40mV), the enhanced stability (>90 days) and the reduced surfactant content (3wt %), having the appropriate pH and osmolality for the intravenous delivery (Tosi, 2010; Dobrovolskaia, 2013).

Comparing with other PLGA nanoparticle studies (Stolnik, 1995; Trimaille, 2003; Pinto-Reis, 2006; Harush-Frenkel, 2007, Chen, 2011; Danhier, 2012), the nanoparticle sizes reported previously are bigger than those of NP-0.16E nanoparticles, obtained in this thesis. The small sizes are advantageous to avoid sedimentation as well as embolization and/or detection and further elimination by the immune system once in the blood (Stolnik, 1995; Vauthier, 2009(1); Gref, 2012; Kulkarni, 2013; Neha, 2013; Alyautdin, 2014; Kreuter, 2014).

However, to apply these nanoparticles as advanced delivery systems, more studies, such as the encapsulation of active compounds (Part 4 of the Results Section) and their surface functionalization (Part 5 of the Results Section) were required.

4.4. Encapsulation of active molecules in nanoparticles

Active molecules can be dissolved, attached or encapsulated in nanoparticles (Neha, 2013). Among these alternatives, encapsulation was selected for the actives studied in this thesis. This strategy is considered advantageous since it enables incorporation of an enhanced amount of lipophilic compounds (such as loperamide and galanthamine drugs), a prolonged blood circulation time, the increase of the drug bioavailability, a reduction of the compound toxicity (e.g. MNPs), protection of the compounds from their degradation, control of the release profile and reduction of the side effects (Kumari, 2010; Panyam, 2012; Kulkarni, 2013; Nicolas, 2013).

In this section, the encapsulation of Coumarin 6, magnetic nanoparticles, loperamide hydrochloride and galanthamine hydrobromide in polymeric nanoparticles will be described. They were dissolved / dispersed in the oil component of the nano-emulsions, prior to nano-emulsion formation, to achieve high encapsulation efficiencies. A complete characterization of the loaded nanoparticles was performed. The encapsulation efficiencies as well as the release profiles were also investigated.

4.4.1.Coumarin 6

Coumarin 6 was chosen as a fluorescent dye since it was reported in previous bibliography (Panyam, 2003; Singh, 2013) that it is appropriate for biomedical applications. Although previous studies have already described the encapsulation of Coumarin 6 in PLGA nanoparticles, nanoparticle size was high, thus increasing the immune response, as discussed in previous studies (Vauthier, 2009; Gref, 2012; Kulkarni, 2013; Neha, 2013; Alyautdin, 2014; Kreuter, 2014). Moreover, the reported nanoparticles could be toxic due to the presence of polyvinyl alcohol (PVA) residues (Panyam, 2003). Coumarin 6 solubility was tested in diverse solvents (Table 4.18). It is soluble in ethyl acetate, as well as in other organic solvents, while the solubility is very low in water and PBS 0.16M. Therefore, Coumarin 6 is appropriate for encapsulation in O/W nano-emulsions. In this work, a concentration of 0.1 wt % of coumarin 6 in the nano-emulsion oil phase was used.

Table 4.18: Solubility (in mg/mL) of Coumarin 6 in different solvents, as determined by visual observations at 25ºC.

Solvent	Solubility (mg/mL)
Water	< detection limit
Electrolyte solution (0.16M)	< detection limit
Ethyl acetate	3.979 ± 0.284
Acetone	3.059 ± 0.346
Ethanol	0.135 ± 0.018

Another important factor to select a component to be encapsulated is its easy detection. Coumarin 6, as a fluorescent dye, can be easily detected by fluorescence emission. Moreover, in this work, Coumarin 6 was also detected by enhanced optical microscopy with the fluorescent filter FITC (fluorescein isothiocyanate). As Figure 4.57 shows, Coumarin 6 is detected both, in its solid and liquid states with white light or the FITC filter.
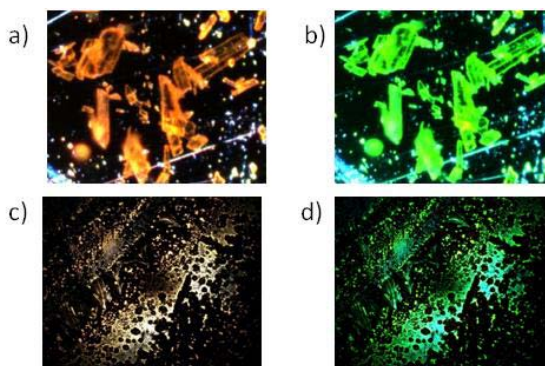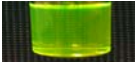
Figure 4.57: Visual appearance of coumarin 6: a) white field, coumarin 6 powder; b) FITC filter, coumarin 6 powder; c) white field, coumarin 6 in ethyl acetate, after drying; and d) FITC filter, coumarin 6 in ethyl acetate, after drying.

Using this microscope, not only images but also the spectral profiles, characteristics of each material, can be obtained (as previously described in the Methods Section). The spectrum of Coumarin 6 has a maximum at 555 nm .

4.4.1.1. Characterization of Coumarin 6 loaded nanoparticles

Following the studies for non-loaded nanoparticles, C6-loaded NP-0.16E70 nanoparticles and their template nano-emulsions were characterized. As expected, nano-emulsions and nanoparticles showed a transparent to translucent yellowish appearance (Table 4.19). Nano-emulsion droplet hydrodynamic radii were around 35 nm, while those of nanoparticles were around 23 nm (Table 4.19). Both sizes are similar to those obtained for non-loaded nano-emulsions (Figure 4.12) and nanoparticles (Figure 4.33a). Surface charge of C6-loaded nano-emulsions and nanoparticle dispersions was also assessed (Table 4.19). Negative surface charges were found for both systems, as expected, due to the carboxylic groups of the PLGA. Nanoparticles showed ζ potential around -15 mV, while for their template nano-emulsions the values are around -47 mV. These results are in good agreement with non-loaded nanoparticles and their template nano-emulsions, confirming the hypothesis that physico-chemical characteristics of nanoparticles and their template nano-emulsions are not necessarily influenced by an encapsulated compound.

Table 4.19: Characterization of a C6-loaded nano-emulsions with 90wt% electrolyte solution (0.16M) and 70/30 O/S and the corresponding nanoparticles by means of DLS (hydrodynamic radius, nm) and electrophoretic mobility (surface charge, mV).

Sample	Visual appearance	Hydrodynamic radius(nm)	ζ potential (mV)
NE		34.28 ± 0.97	-47.05 ± 1.42
NPd		23.71 ± 0.82	-14.83 ± 3.77

The size of Coumarin 6-loaded nano-emulsion droplets and nanoparticles were determined as a function of O/S ratio of the template nano-emulsions and compared with those of the corresponding non-loaded dispersions. As Figure 4.58 shows, both non-loaded and C6-loaded dispersions show similar sizes and similar size tendency as a function of the O/S ratio. As described for non-loaded dispersions, at low O/S ratios, nano-emulsion droplet sizes are big, around 150 nm. Increasing the O/S ratio, nano-emulsion droplet size increase up to around 250 nm, but a further O/S ratio increase produces an abrupt decrease of the droplet size to values below 50 nm. These sizes are maintained at higher O/S ratios, except for the

highest O/S ones, where sizes suffer a slight increase (Figure 4.58a). For nanoparticles, sizes are maintained around 20 – 30 nm for both non-loaded and C6-loaded nanoparticles except at the lowest O/S ratio, where C6-loaded nanoparticles have higher sizes (Figure 4.58b). These could be related to the fact that the lowest O/S ratio is in the limit of the nano-emulsion formation domain, where dispersions are quite unstable.

The similar results for non-loaded and C6-loaded dispersions mean that the encapsulation of this dye at the concentration chosen (0.1wt% in the oil nano-emulsion phase) does not influence nano-emulsion and nanoparticle formation. These results are in good agreement with some previous bibliography reporting the production of PLGA nanoparticles without and with coumarin 6; in which the hydrodynamic diameter remained unchanged, but around 270 nm (Panyam, 2003). However, in other studies, the incorporation of this fluorescent dye in PLGA nanoparticles produced an increase in nanoparticle diameter from 95 to 120 nm (Hu, 2011). The controversy between different studies could be due to the nanoparticle preparation methodology. While *Panyam et al.,* (Panyam, 2003) used exactly the same methodology to prepare non-loaded and loaded nanoparticles, *Hu et al.,* (Hu, 2011) added a purification step by column chromatography only to the coumarin 6 loaded nanoparticles. In this study, the same protocol was followed for the preparation of non-loaded and loaded nanoparticles. Therefore, it can be concluded that nanoparticle size is not affected by the presence of encapsulated Coumarin 6.

It is worth noting that nanoparticle sizes achieved in this study are smaller than those reported in previous literature for non-loaded and C6-loaded PLGA nanoparticles (Panyam, 2003; Hu, 2011). The smaller size could be an advantage, for example, for the intravenous administration in terms of reduced immune system activation (Vauthier, 2009; Kulkarni, 2013; Neha, 2013; Alyautdin, 2014).
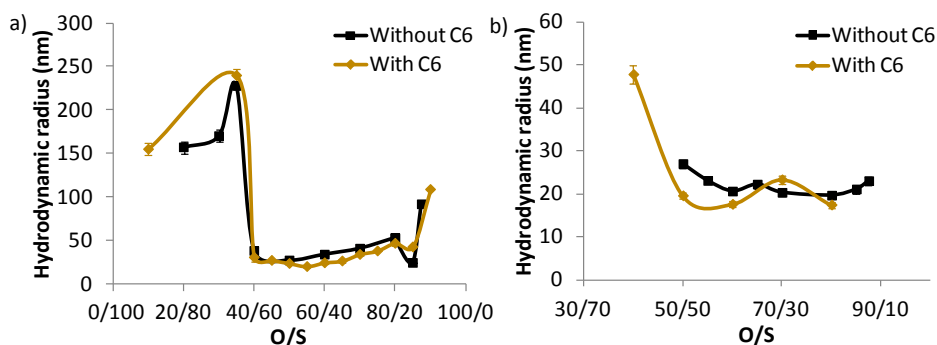
Figure 4.58: Hydrodynamic radius (nm) of a) nano-emulsions (90wt% PBS 0.16M, 70/30 O/S ratio) and b) NP-0.16E70 nanoparticles, without and with encapsulated C6, as a function of the O/S ratio of the template nano-emulsion.

The <u>stability of C6-loaded nanoparticles</u> was studied by means of visual observations (Table 4.20) and changes in the droplet size as a function of time (Figure 4.59).

Macroscopic optical observations were performed at 25ºC and 37ºC, to study the effect of temperature. Samples were defined as stable until a sediment was observed. The results (Table 4.20) showed that the higher the temperature, the less stable the samples. The results of stability of C6-loaded and non-loaded nanoparticles (Section 4.3.5.1.1) as well as that of their template nano-emulsions (Section 4.2.4.1) were compared. While nano-emulsions have similar sedimentation times (around 20 days, at 25ºC), a huge difference between the destabilization of non-loaded and C6-loaded nanoparticles is observed. Non-loaded nanoparticles are stable for more than 3 months and C6-loaded nanoparticles are stable for only 24 days, at 25ºC. Although the presence of coumarin 6 was found not to influence the physico-chemical properties of nanoparticles (size and surface charge), the results of Table 4.20 clearly show that nanoparticle stability is negatively affected by the presence of the dye, as sedimentation is faster.

Table 4.20: Macroscopic visual stability (time to observe sedimentation) of C6-loaded nano-emulsions and nanoparticles at 25ºC and 37ºC.

Temperature (ºC)	C6-loaded NE	C6-loaded NPd
25ºC	19 days	24 days
37ºC	4.5 days	7 days

The stability was also studied by measuring the size of C6-loaded dispersions as a function of time. The results are presented in Figure 4.59. Nanoparticles sizes experience some slight variations for the first ten days, after which, their sizes remain constant (around 25 nm) for, at least, 40 days. However, nano-emulsion droplet sizes decrease from around 35 nm to 28 nm for the firsts 5 days, and afterwards droplet sizes are stabilized, for at least 40 days. The reduction for nano-emulsion droplet size could be attributed to the early nanoparticle formation, previously mentioned, which produces nanoparticle sedimentation due to its higher density, thus decreasing the mean nano-emulsion droplet sizes. These results are in good agreement with macroscopic observations, in which nanoparticles are more stable than nano-emulsions.

Moreover, comparing with non-loaded systems, non-loaded nano-emulsions also suffered the slight droplet size decrease at initial times (Figure 4.25) and non-loaded nanoparticles showed constant sizes along the time (Figure 4.49).
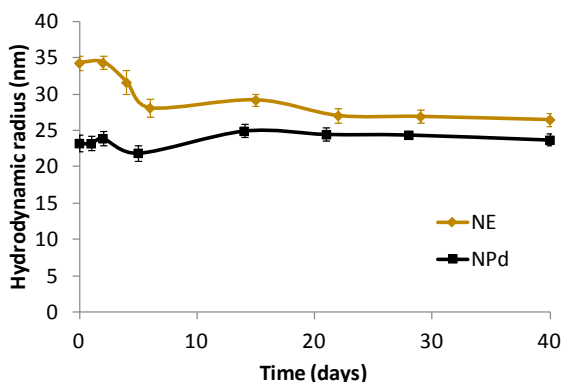
Figure 4.59: Hydrodynamic radius (nm) of C6-loaded nano-emulsions and nanoparticles as a function of time, at 25ºC.

4.4.1.2. Efficiency of encapsulation

Prior to quantitatively study the efficiency of coumarin 6 encapsulation, observations of the nanoparticles by enhanced optical microscopy were performed with the aim to study the colocalization of the signal of the nanoparticles with the signal of the fluorescent dye.
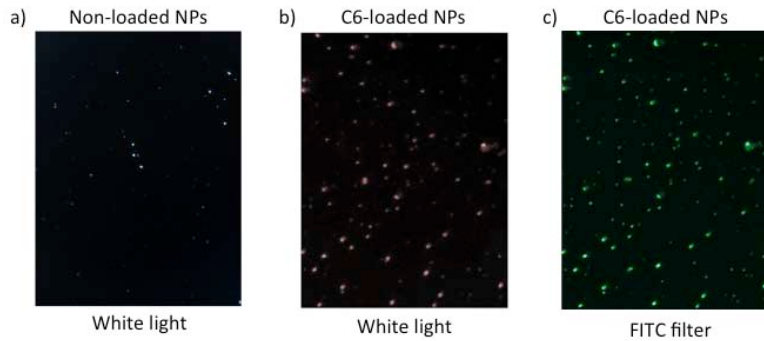
Figure 4.60: Enhanced optical micrographs of NP-0.16E70 nanoparticles: a) non-loaded, without fluorescent filter; b) C6-loaded, without fluorescent filter; and c) C6-loaded, with the FITC filter.

Nanoparticles without any loading (NP(NL)) were viewed under white light and C6-loaded nanoparticles were viewed also under white light and also with the FITC filter (Figure 4.60). It should be noted that the number of nanoparticles observed at each micrograph is not significant of the concentration of the sample, since it depends not only on the concentration of the nanoparticle dispersion but also in the zones observed. Observing different regions of the samples, different coverage of nanoparticles was found (see Figure Ap.5, appendix). The spectral analysis resulted in a peak around 550 nm for non-loaded nanoparticles and around 625 nm for C6-loaded nanoparticles (Figure 4.61). Therefore, since spectra are characteristic of material types, C6 encapsulation can be assumed due to the displacement of the maximum intensity to higher wavelength values.
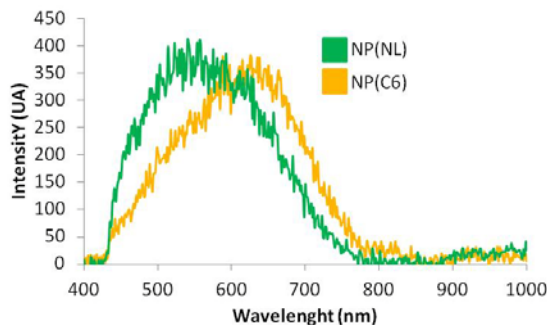
Figure 4.61: Example of the spectral plot of NP-0.16E70 nanoparticles without and with C6.

The efficiency of Coumarin 6 encapsulation was assessed by means of the indirect filtration – centrifugation method. The filtrate was transparent, thus indicating the absence of the dye (Figure 4.62a). No fluorescent signal was found in the filtrate, confirming the visual observation and thus indicating that Coumarin 6 encapsulation was 100wt%. Nevertheless, these results could be due to a concentration of Coumarin 6 under the limit of detection. FTIR determinations were also performed with these samples. As Figure 4.62b shows, the FTIR spectrum for the filtrate of the nanoparticle dispersions clearly differs from those for nanoparticle dispersion and for a Coumarin 6 aqueous solution (Figure 4.62b). As expected, the C6 aqueous solution showed peaks at around 1000, 1600 and 2750 cm^{-1}, which corresponds, respectively, to the COC, CO and CH$_2$ and CH$_3$ groups. These peaks also appeared in the C6-loaded nanoparticles, thus confirming the presence of C6 in the nanoparticles. In the filtrate, although the peaks corresponding to CO and COC groups appeared, they were attributed to the surfactant excess, since the spectrum was different from other two.
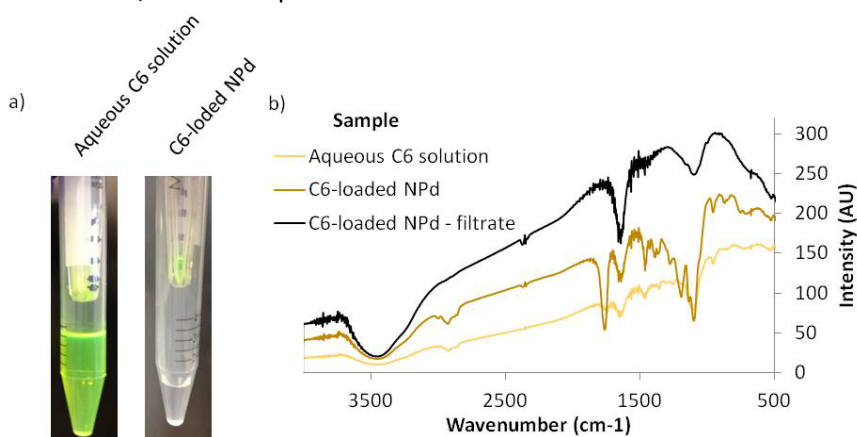
Figure 4.62: a) Visual appearance of the C6-loaded NP-0.16E70 nanoparticles after their filtration and b) FTIR (in transmittance) of the same samples.

The high encapsulation values achieved in the present work are attributed to the method of nanoparticle formation. Since Coumarin 6 is dissolved in the oil phase, prior to nano-emulsion formation (it is a component of the oil of the nano-emulsion), when the solvent is evaporated, Coumarin 6 remains entrapped among the polymeric chains of the nanoparticles, that is within the matrix of the nanoparticle, being this entrapment favored by the low water solubility of the dye. This could also explain the high encapsulation efficiencies obtained by *Zhang et al.,* (Zhang, 2010) from 60 – 90 wt %, using W/O/W emulsions for the preparation of

nanoparticles. However, in another study by *Trapani et al.*, (Trapani, 2009), encapsulation efficiencies of nanoparticles where nanoparticles produced by ionic gelation with sizes around 340 nm, only reached values up to 30wt %.

4.4.1.3. *In vitro* release kinetics

Coumarin 6 release was studied by means of the dialysis bag method and fluorescence detection, as described in Section 3.2.11.3. The release kinetics were studied using NP-0.16E70 nanoparticles with PBS as the receptor solution, at neutral (pH = 7.4) and acid (pH = 4) conditions because the cellular pH depends on the cell compartments (Panyam, 2012). The nanoparticle mechanism of cell penetration was not studied in this work. However, there seems to be agreement that nanoparticles usually penetrate cells by different kinds of endocytosis (Panyam, 2012). By the endocytic pathway, nanoparticles would be engulfed by the endosomes, initially at a neutral pH. Then, during the endocytic pathway to become lysozomes, the pH gradually decreases, reaching acidic pH values around 4.5 (Panyam, 2012).

Figure 4.63 shows that the percentage of Coumarin 6 (C6) released as a function of time is very similar at both pH values. During the first hour, around 60wt% of Coumarin 6 has already been released. However, after this period of time, the release is more sustained, achieving 80wt% of Coumarin 6 release after 6 hours, where a plateau is reached, and no more Coumarin is released up to 24 hours. The pH of the environment does not influence Coumarin 6 release. Moreover, since Coumarin 6 can be detected after 24 hours of being in contact with an acidic pH, it can be concluded that it remains intact. It is worth noting that polysorbate 80 could interfere C6 fluorescence, therefore, the apparent C6 released could be, in fact, higher than the real C6 released.

Different theoretical models were used and compared with the experimental results obtained. However, none of them fitted the experimental points (Higuchi, 1962; Calderó, 2010; Fornaguera, 2014(1)).
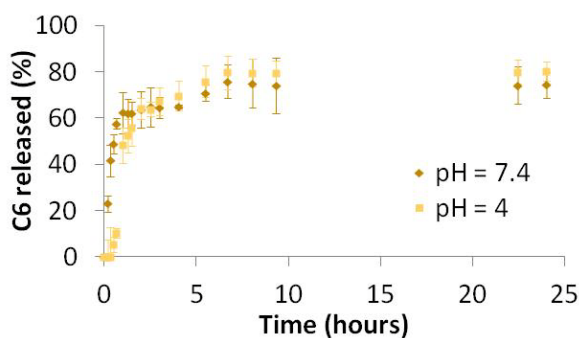
Figure 4.63: Coumarin 6 release from NP-0.16E70 C6-loaded nanoparticle dispersions as a function of time and pH of the receptor solution, at 25ºC.

Although the release profile obtained in the present work is quite similar to those reported in the bibliography (a rapid initial release followed by a slow release), most studies found a release of around 1wt% after 8 hours from polymeric nanoparticles (Singh, 2013), namely PLGA nanoparticles (Trapani, 2009; Zhang, 2010). The differences between the low release from previous studies and high release from our study could be attributed to the nanoparticle size. Since previous bibliography reported nanoparticles with sizes of around half and one order of magnitude higher than those obtained in this thesis, more amount of Coumarin 6 should be encapsulated per a single particle. Therefore, if fewer molecules are encapsulated in a higher number of nanoparticles, their release will be facilitated.

Since C6-loaded nanoparticles were designed with imaging purposes, the fluorescent dye should remain in the nanoparticles for sufficient time to detect the nanoparticles reaching the target tissues. After the first hour, nearby 60wt% of Coumarin 6 was released. However, it takes around 10 minutes after intravenous administration in mice for a blood cell to return to the starting point after travelling around the whole blood stream (Riches, 1973). Thus, the time to reach the brain, the target of the present thesis, is lower than the hour required to start noticing a remarkable Coumarin 6 release. Therefore, it can be predicted that most of Coumarin 6 would be released in the target organs.

4.4.2.Magnetic nanoparticles (MNPs)

Magnetic nanoparticles (MNPs) have been widely used in biomedical applications, mainly for imaging purposes, since they are active as contrast agents for magnetic resonance imaging (MRI) as well as for the cancer treatment, since they are potential heating mediators (hyperthermia treatment) (Salas, 2012; Jiang, 2013(2)). Among all types of magnetic nanoparticles, iron oxide nanoparticles (IONPs), specifically, their magnetite (Fe_3O_4) and maghemite (γ-Fe_2O_3) forms were chosen.

MNPs were encapsulated in PLGA nanoparticles with imaging purpose, as an alternative to fluorescence detection. It is worth noting that the encapsulation of IONPs into polymeric nanoparticles is advantageous for the intravenous administration to hydrophilize their hydrophobic surface to enable longer blood circulation times (Salas, 2012); moreover, their encapsulation in a polymeric matrix facilitates their administration due not only to biodegradability and biocompatibility of the polymer (Sun, 2012) but also for the reduction of the immune system recognition (Liu, 2007). It is worth noting that previous studies reporting the use of PLGA nanoparticles for encapsulation of magnetite (Liu, 2007; Okassa, 2007; Nkansah, 2011; Sun, 2012) confirm their possible use as contrast agents for MRI and as nanosystems able to generate hyperthermia.

4.4.2.1. Characterization of the MNPs-loaded nanoparticles

Iron oxide nanoparticles (IONPs) with hydrodynamic radius of around 43 nm, negative surface charge of around -36mV and stability lower than 5 minutes after their sonication for 30 minutes were used. They were initially suspended in heptane, therefore the first step consisted in dispersing them in ethyl acetate. However, direct transfer to ethyl acetate resulted in nanoparticles sedimentation but not redispersion. Thus, a progressive transfer first to acetone and then to ethyl acetate was necessary, as described in Section 3.3.11.1. The transfer from one solvent to another through different solvents has been described in the bibliography, in order to increase the IONPs content in the final polymeric nanoparticles (Liu, 2007; Okassa, 2007; Salas, 2012). Once MNPs were apt to be suspended in ethyl acetate, nano-emulsions were formed in the system: electrolyte solution (0.16M) / polysorbate 80 surfactant / [4wt % PLGA + x wt % MNPs] in ethyl acetate. The concentration of MNPs in the oil phase was selected considering nano-emulsion stability. As Figure 4.64 shows, at high MNPs concentrations,

unstable nano-emulsions were obtained. At a concentration of 0.3wt% of MNPs in the oil phase of the template nano-emulsion, a transparent sample was obtained, but, it was completely separated after 1 hour. For this reason, MNPs concentration was further decreased to 0.06wt %, where nano-emulsions with a transparent appearance, and stability over one hour were obtained. Therefore, this concentration was chosen for further studies.
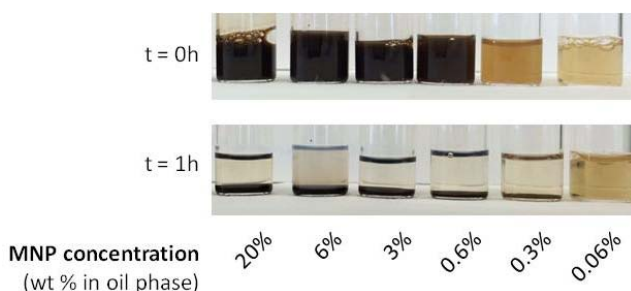
Figure 4.64: Visual appearance of nano-emulsions of the PBS (0.16M) / polysorbate 80 / [4wt % PLGA in ethyl acetate] system, with 90wt% PBS and 70/30 O/S ratio as a function of MNPs concentration in the oil phase after their preparation (t=0) and after 1 hour (t=1h).

Characterization of MNP-loaded nano-emulsions (NE@MNP) and nanoparticles (NPs@MNP) with 0.06wt% MNPs showed that the sizes (Table 4.21) increased as compared to those without any loading (Figures 4.26 and 4.38a). Comparing the nano-emulsion droplet sizes and nanoparticles sizes without and with MNPs encapsulated, it is worth noting the double droplet size when MNPs are encapsulated; as compared with the encapsulation of other materials. Nano-emulsion droplet sizes increase from around 32 nm to 62 nm, while nanoparticles increased from around 23 nm to 48 nm. The increase in the droplet sizes cannot be attributed to the encapsulation, since when Coumarin 6 was encapsulated, no changes in the droplet sizes were observed (Table 4.19). Nevertheless, MNPs have bigger sizes than the molecule of Coumarin 6. Therefore, the bigger sizes of MNPs could be the cause of polymeric nanoparticles size increase. Their surface charges were negative, as expected, since all components forming the nanoparticles have negative charges, which is in good agreement with previous studies reporting the encapsulation of iron oxide nanoparticles in PLGA nanoparticles (Liu, 2007; Okassa, 2007). The small changes in the absolute values of the surface charge, as well as the increase in the sizes, were taken as an indication of MNPs encapsulation (Liu, 2007).

It is worth noting that encapsulation of MNPs in polymeric nanoparticles have been reported using the emulsification approach and high-energy emulsification methods (Pascolo, 2014). Our approximation, by low-energy emulsification methods, is advantageous over this previous study as production of nanoparticles with smaller sizes (48 nm in front of 105 nm of hydrodynamic radius) is achieved.

Table 4.21: Characterization of NPs@MNPs (NP-0.16E70 polymeric nanoparticles) and their template nano-emulsion. The concentration of MNP in the oil phase of the nano-emulsions was 0.06wt%.

Sample	Visual appearance (t=0)	Hydrodynamic radii (nm)	Surface charge (mV)	Visual stability (time to observe a sediment)
NE@MNPs		62.39 ± 3.17	-32.25 ± 1.85	> 1 hour
NPs@MNPs		48.39 ± 0.79	-27.15 ± 1.58	1 day

The stability of MNPs-loaded PLGA nanoparticles and their template nano-emulsions was determined by means of visual observations and measuring the droplet sizes along the time. By visual examination (Table 4.21), it was observed that nano-emulsion stability was slightly higher than 1 hour. Therefore, although the incorporation of MNPs reduced nano-emulsion stability, they were stable enough to be used as nanoparticle templates. In addition, nanoparticle stability also decreased, as compared with nanoparticles without any loading. Regarding hydrodynamic radii along the time (Figure 4.65), during the first five days, droplet sizes of MNPs-loaded nano-emulsions, as well as nanoparticles, decreased, which was attributed to the sedimentation of nanoparticles. After around 5 days, droplet sizes were constant along the time.
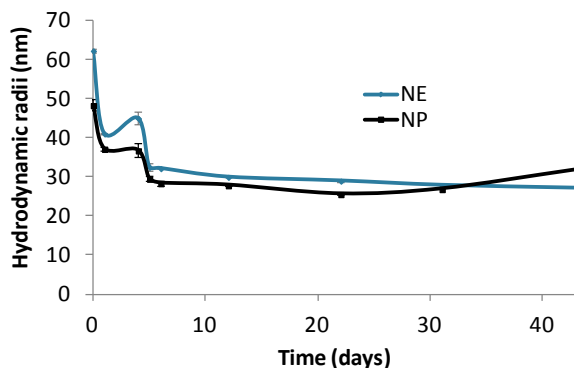
Figure 4.65: Hydrodynamic radii (nm) of NPs@MNPs (NP-0.16E70 polymeric nanoparticles) and their template nano-emulsion as a function of time, at 25ºC. The concentration of MNP in the oil phase of the nano-emulsions was 0.06wt%.

4.4.2.2.   Isolation of polymeric nanoparticles

The magnetic properties of MNPs-loaded nanoparticles enable their purification by the use of magnets. For this reason, a magnetic separator was used to test the possibility to separate the nanoparticles. As Figure 4.66 shows, when a dispersion of polymeric nanoparticles with encapsulated MNPs (NPs@MNPs) is placed inside the separator, after one day, some aggregates are formed at the edges of the tube, just next to the magnets. Therefore, it was confirmed that MNPs maintained their magnetic properties.
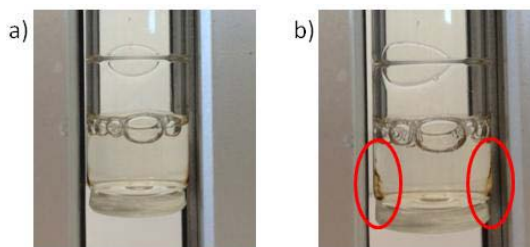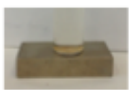
Figure 4.66: Examples of the nanoparticle dispersions with the MNPs encapsulated as a function of time remaining in the magnetic separator: a) t = 0h; and b) t = 24h.

To confirm the encapsulation of MNPs, and to further study both separated fractions, the hydrodynamic radii of the pellets (aggregates) and the supernatant (dispersion media) were studied (Tables 4.21 and 4.22). In addition, spectral image analyses were performed (Figure 4.67). It was expected that polymeric

nanoparticles, with the MNPs encapsulated, would migrate to the walls of the magnet separator and the supernatant would be free from nanoparticles. However, when droplet sizes were measured, while in the pellets of the separated fraction, a huge increase in droplet size was observed due to aggregation of MNPs because of the strong magnetic field, objects with sizes equivalent to nanoparticles with loading were found in the supernatant. Several hypotheses could be formulated to explain these results. One was that MNPs might not be encapsulated in the polymeric nanoparticles, and they would migrate to the magnets without the polymeric nanoparticles. However, this hypothesis is not very plausible as the droplet size of template nano-emulsion increases when MNPs are incorporated. Another hypothesis was that MNPs do encapsulate inside polymeric nanoparticles but they are able to exit due to the strong magnetic forces of the magnet. A combination of both phenomena could take place, resulting in a mixture of encapsulated and not encapsulated MNPs producing a migration only of the MNPs-loaded polymeric nanoparticles.

Table 4.22: Characterization of the separated fractions of NPs@MNPs (NP-0.16E70 polymeric nanoparticles). The concentration of MNP in the oil phase of the nano-emulsions was 0.06wt%. SN = supernatant.

Separation type	Sample	Visual appearance	Hydrodynamic radii (nm)	Surface charge (mV)
Magnet separator	NPs@MNPs SN		28.90 ± 0.39	-37.65 ± 3.27
	NPs@MNPs pellet		96.35 ± 12.77	-39.05 ± 3.26
Usign a magnet for MNPs sedimentation	NPs@MNPs SN		23.71 ± 0.85	-42.35 ± 2.21
	NPs@MNPs pellet		73.75 ± 3.38	-39.45 ± 2.90

In order to find out which one of the above hypothesized phenomena was taking place, the same experiment, using a magnet located under the sample rather than the magnet separator, was performed with the aim to reduce the strength of the magnetic field. The results (Table 4.22) were similar to those in the previous step. However, droplet size of the pellets was smaller. Since neither study was conclusive, separated fractions from the magnetic separator were analyzed by means of spectra profiles generated through enhanced optical microscopy. The results are presented in Figure 4.67. The shape of the spectra profile of polymeric

nanoparticles, NPs@MNPs and the supernatant fraction is similar. In contrast, MNPs and the pellet fraction show also the same spectral profile, different from the other samples (NPs, NPs@MNPs and NPs@MNPs SN). In addition, the maximum absorbance wavelength of polymeric nanoparticles, NPs@MNPs and the supernatant also coincide (around 560 nm) and are different from those for MNPs and the pellet fraction (around 606 nm). Similarities between different spectra indicate that the materials are similar. Therefore, the pellet is richer in MNPs, while in the supernatant both polymeric and MNPs may be present.
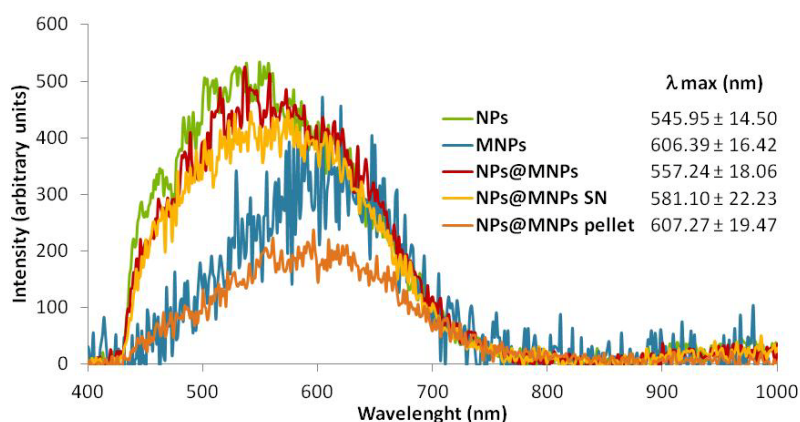
Figure 4.67: Spectra profiles of the different samples tested, took at 100x of magnification.

Encapsulation of the MNPs was not completely confirmed by spectral analyses. For this reason, TEM studies were performed with polymeric nanoparticles encapsulating MNPs as well as the pellet and supernatant fractions, obtained by the use of the magnetic separator. TEM micrographs (Figure 4.68) showed that NPs@MNPs have 0 or 1 or 2 MNPs encapsulated for each polymeric nanoparticle (Figure 4.68a). Although not all nanoparticles are loaded, observing the pellets (Figure 4.68b), both MNPs and polymeric nanoparticles are present, but in this case, MNPs do not seem to be encapsulated inside nanoparticles. In contrast, in the micrographs of the supernatants (Figure 4.68c), only polymeric nanoparticles were observed. Therefore, TEM micrographs confirmed the encapsulation of MNPs inside polymeric nanoparticles, as well as the diffusion of MNPs from polymeric nanoparticles to the dispersant when a magnetic field is applied.
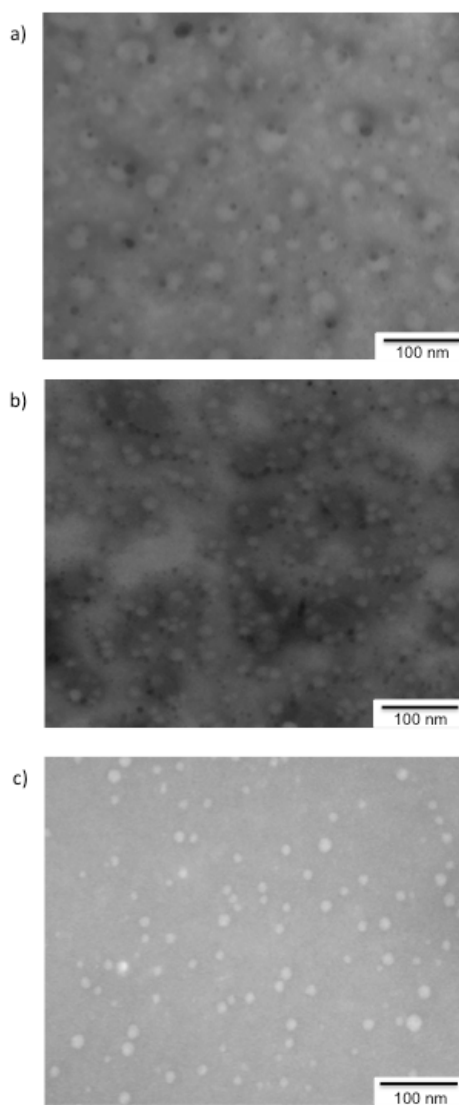
Figure 4.68: TEM micrographs of: a) NPs@MNPs; b) pellet and c) supernatant.

MNPs and polymeric nanoparticles were characterized by TEM (Figure 4.68). The mean diameters are shown in Table 4.23. MNP-loaded polymeric nanoparticles showed sizes of around 22 nm, higher than those of non-loaded nanoparticles (Figure 4.33). However, the sizes of loaded nanoparticles were reduced in both fractions after the magnetic separation. This could be an additional evidence of the diffusion of the previously encapsulated MNPs. In addition, the presence of polymeric nanoparticles in both fractions after the separation, confirmed that not all polymeric nanoparticles encapsulated MNPs. These results are in good

171

agreement with previous studies, which indicated heterogenicity in the number of MNPs encapsulated into polymeric nanoparticles (Liu, 2007). MNPs, however, are only present in the non-separated dispersion and in the pellet, thus confirming the magnetic separation. Their sizes did not vary after the separation.

Table 4.23: Summary table of the mean sizes and morphological study of NPs@MNPs by means of TEM.

Fraction	Type of NPs	Size (nm)
MNPs@NPs	Polymeric NPs	22.11 ± 6.42
	MNPs	7.97 ± 2.59
Pellet	Polymeric NPs	16.20 ± 4.27
	MNPs	7.09 ± 2.09
SN	Polymeric NPs	16.90 ± 6.13
	MNPs	Not observed

Nanoparticle size distribution was plotted for polymeric and magnetic nanoparticles (Figure 4.69). The original polymeric nanoparticles showed a wide size distribution, which is narrowed after the magnetic separation in both fractions. This is another indication of the MNPs encapsulation and of their diffusion. In contrast, MNPs size distributions are similar between the encapsulated and the pellet fraction, although in the pellet it is slightly shifted to lower sizes.

172
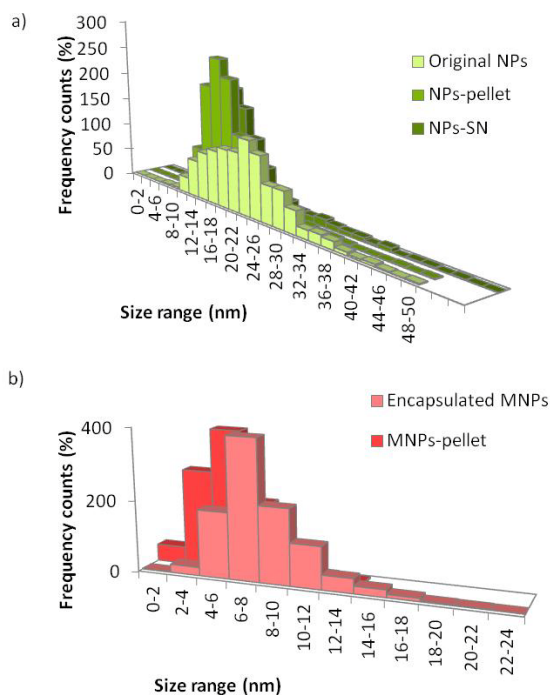
Figure 4.69: Nanoparticle size distribution of a) polymeric nanoparticles prepared from nano-emulsions with 90wt % of electrolyte solution (0.16M) and an O/S ratio of 70/30, with MNPs encapsulated and b) MNPs encapsulated in polymeric nanoparticles, as a function of the fraction (pellet or SN=supernatant) studied.

Comparing with previous bibliography (Liu, 2007; Okassa, 2007; Nkansah, 2011; Sun, 2012), the present work has advantages among them in terms of IONPs-loaded nanoparticle sizes, since their reduced size could reduce the macrophage NP elimination in the bloodstream, thus increasing the blood half life (Vauthier, 2009; Kulkarni, 2013; Neha, 2013; Alyautdin, 2014). Nevertheless, the percentage of IONPs encapsulation is low (around 0.06wt% in the present thesis) as compared with bibliography results, higher than 15wt% (Liu, 2007; Okassa, 2007; Nkansah, 2011), being a drawback for the MRI detection (Sun, 2012). However, it could become an advantage in terms of nanoparticle shape, since previous bibliography demonstrates a deformation of the spherical shapes when the iron content was high (Liu, 2007). Moreover, when considering theranostic applications of nanoparticles, the need to incorporate a drug in the MNPs-loaded nanoparticles requires reduced sizes (Liu, 2007). Therefore, the MNPs-loaded nanoparticles designed in this thesis could be useful as theranostic nanosystems.

4.4.3.Loperamide hydrochloride

Loperamide hydrochloride (LOP) is a drug widely used nowadays for the management of diarrhea since it reduces the gut's motility (Holzer, 2009(1)). However, loperamide has also a central analgesic effect, but it is not explored by the pharmaceutical industry because it cannot cross the BBB by itself (Kreuter, 2002; Tosi, 2010; Danhier, 2012). In this research, loperamide was encapsulated in polymeric nanoparticles to study the BBB crossing mediated by nanoparticles. If an analgesic effect would be observed after the administration of loperamide-loaded nanoparticles, it would mean that nanoparticles can cross the BBB and deliver the drug in the central nervous system (Kreuter, 2002; Tosi, 2010; Danhier, 2012). Loperamide was first used by Michaelis et al. (Michaelis, 2006) to study the transport of different types of nanoparticles with different functionalizations to the brain, since, as explained above, the free drug is not able to cross the BBB by itself, thus not enabling the antinociceptive effect (Michaelis, 2006; Kreuter, 2014). Since then, several studies have reported the central analgesic effect of loperamide hydrochloride (Chen, 2011; Tosi, 2011; Danhier, 2012; Kreuter, 2014). For this reason, this drug was selected in the present study. Moreover, its chemical structure, consisting in three aromatic rings, confers a hydrophobic character to the drug; which is advantageous for the encapsulation strategy used in this work.

4.4.3.1. Adjustment of nano-emulsion components, composition and formation of loperamide-loaded nanoparticles

As described previously, the low solubility of loperamide hydrochloride in ethyl acetate (Table 4.5) did not allow its encapsulation at therapeutic concentrations. For this reason, the oil phase was modified adding 20wt % of ethanol (Section 4.2.1.2). The incorporation of ethanol in the oil phase of the nano-emulsions enhanced nano-emulsion formation domain broadening the O/S ratios and lowering aqueous phase contents. However, when loperamide was incorporated in the oil phase, the O/S ratios limiting the region of nano-emulsion formation were narrower (Figure 4.6). The size of NP-0.16E70 nanoparticles and their template nano-emulsions (Table 4.24) were maintained around 40 nm and 30 nm respectively when ethanol was incorporated in the oil phase (without the drug). ζ potentials were also similar to those without the ethanol (Table 4.24).

Table 4.24: Characterization of non-loaded NE and NPs prepared with the system: PBS 0.16M / polysorbate 80 / [4wt % PLGA in 20/80 ethanol/ethyl acetate].

Sample	Hydrodynamic radii (nm)	Surface charge (mV)
NE	37.59 ± 7.14	- 38.70 ± 1.36
NPs	30.26 ± 2.14	- 26.79 ± 7.19

The drug was incorporated in nano-emulsions of the system: Electrolyte solution (0.16M) / polysorbate 80 / [4wt% PLGA in 20:80 ethanol: ethyl acetate], at a concentration of 0.15wt% in the oil phase. This concentration is lower than the maximum loperamide solubility in the oil phase, but maximum values were ruled out to avoid solubility problems. In addition, nano-emulsions were not formed at high loperamide concentrations (higher than 0.20wt% in the oil phase). As at 0.15wt% loperamide concentration, the nano-emulsion droplet radius was increased up to 170 nm, the drug concentration was reduced to 0.1wt %. Hydrodynamic droplet radii of around 120 nm were achieved (Table 4.25). The dependency of the droplet sizes on the drug concentration was already reported in the bibliography and is in good agreement with the results found in this work: the higher the drug concentration, the bigger the droplets (Date, 2007 and 2010). Using this formulation, nanoparticles with hydrodynamic radii of around 100 nm were achieved (Table 4.25). It is worth noting that loperamide therapeutic effect would not be enough in the as-prepared nanoparticles due to the low concentration used. However, as described below, the concentration can be increased with a concentration step.

Table 4.25: Characterization of the loperamide-loaded (0.1wt %) NP0.16E70 nano-emulsions and nanoparticles.

Sample	Visual appearance	Hydrodynamic radii (nm)	Surface charge (mV)	Visual stability (time to sediment)
NE		119.73 ± 2.11	-51.30 ± 2.91	15 days
NPs		99.98 ± 2.81	-16.28 ± 0.34	> 90 days

Table 4.25 also shows that the surface charge of the nano-emulsion is around -50 mV, while nanoparticles surface charge is around -15 mV. A reduction in the absolute values of the surface charges was already observed for non-loaded nanoparticles (Figure 4.42), whit similar values than loperamide-loaded nanoparticles (Table 4.25). Thus, it could be concluded that the presence of loperamide does not influence the surface charge of the formulated systems.

4.4.3.2. Efficiency of encapsulation

Loperamide encapsulation efficiency was studied by the indirect filtration – centrifugation method, with HPLC drug quantification, as described in Section 3.2.11.2. The parameters of encapsulation obtained are shown in Table 4.26. Loperamide encapsulation efficiency is high, achieving values higher than 99.9wt%. As described for Coumarin 6, the high encapsulation efficiencies achieved in this thesis are due to the nanoparticles preparation method. The drug is incorporated prior to nano-emulsion formation, in the oil phase, being entrapped by the polymer/solvent droplets when nano-emulsions are formed, and remaining inside the polymeric matrix after the solvent evaporation due to its low water solubility. For this reason, the majority of the drug is encapsulated into nanoparticles. In previous bibliography, loperamide encapsulation efficiencies inside PLGA nanoparticles were lower (Dalwadi, 2009; Chen, 2011).

Another parameter reported is the drug loading (the amount of drug per amount of polymer). In the present work, loadings (around 87wt%) were also higher than those reported in previous bibliography (Ulbrich, 2009).

Table 4.26: Parameters of Loperamide encapsulation in NP-0.16E70 nanoparticles.

Encapsulation efficiency (EE) (%)	99.92 ± 0.01
Drug loading (mg LOP/g PLGA)	86.73 ± 1.84
Drug concentration (mg LOP / g NPd)	$9.08 \pm 7 \cdot 10^{-4}$

However, drug concentration in the as-prepared nanoparticle dispersions is around 9 mg/g, lower than previous reports (Vergoni, 2009; Tosi, 2011), thus not achieving therapeutic concentrations, as previously indicated. Since nanoparticle dispersions can be concentrated, the low drug concentrations did not represent a problem.

Therefore, by the filtration-centrifugation technique (Section 3.2.11.2), nanoparticles dispersions were concentrated to achieve therapeutic concentrations. It was necessary a concentration of ten times that of the dispersions to achieve loperamide doses of around 3mg/kg, which is in the range of therapeutic doses (Shannon, 2002; Tosi, 2007).

After nanoparticle concentration, the electrolytes present in the dispersion media were also concentrated, thus the physiological conditions (pH and osmolality) of the blood might be lost. For this reason, a dialysis against a buffered electrolyte solution (0.16M, pH = 7.4 and 300mOsm/kg) was performed following the pH and the osmolality of the nanoparticle dispersion and the receptor solution along the time. As Figure 4.70a shows, the pH of nanoparticles was not varied due to the buffer characteristics of PBS initially (0.16M) and higher electrolyte concentrations. Although, eventually, it was slightly higher than 7.4, pH was adjusted with a few droplets of acidic solution after dialysis. In contrast, osmolality markedly increased up to around 3000 mOsmol/kg (Figure 4.70b) after the concentration step. It took around 7 hours of dialysis to recover the physiological osmolality.
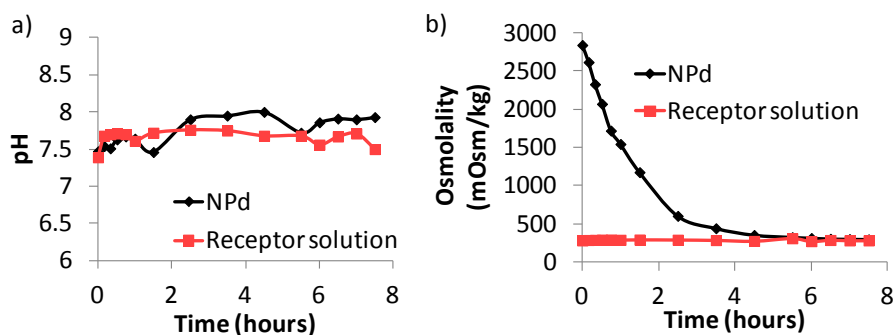
Figure 4.70: a) pH and b) Osmolality (mOsm/kg) of the concentrated NP-0.16E70 LOP-loaded nanoparticles and the correspondent receptor solution as a function of the dialysis time.

Nevertheless, it is worth noting that, since the formulated nanoparticles are intended to target specifically the site of action, less amount of drug, but localized, could produce the same effects due to the local drug release.

4.4.3.3. *In vitro* drug release

In vitro loperamide release was studied from a nanoparticle dispersion and for comparison purposes from an aqueous and a micellar solutions loaded with the same drug concentration. As expected, the drug release from nanoparticles is slower than that of a micellar solution, which, in turns, is slower than that of the aqueous solution (Figure 4.71). These results are in close agreement with reports on drug release from PLGA nanoparticles produced by the same methodology encapsulating other type of drugs (Fornaguera, 2014(1)).

Figure 4.71: Loperamide release to water as a function of time and sample type, at 25ºC. Samples: a) Aqueous loperamide solution; b) Micellar loperamide solution with polysorbate 80; and c) NP-0.16E70 LOP-loaded nanoparticles.

For the aqueous solution, complete loperamide release is achieved after 80 – 100 hours (8 days). However, for the micellar solution and the nanoparticle dispersions, the total drug concentration was not released. In the case of the micellar solution, it was expected a sustained release, as Figure 4.71 shows, but reaching complete release. For the nanoparticle dispersions, a more sustained release took place, as expected, but the drug was neither completely released.

Although there are only few studies on loperamide release from nanoparticles, most of them reported practically the complete loperamide release (Dalwadi, 2009; Vergoni, 2009). However, one of these authors, *Dalwadi et al.,* (Dalwadi, 2009) using dalargin instead of loperamide, found similar results than those presented in this work. In that case, since dalargin is a cationic molecule, it interacted with the anions of the carboxylic groups of the PLGA, thus remaining entrapped in the

nanoparticles after the dialysis. In the present study, ionic attractions cannot take place, but the retention of loperamide could be explained by the formation of hydrogen bonds between the drug, PLGA and polysorbate 80. Although these types of interactions are not strong, it may be the cause of the retention of loperamide in micelles and nanoparticles. Comparing both samples, since nanoparticles are bigger than micelles, the path for loperamide molecules to be released is longer than that from micelles, thus increasing the retention of the drug. This phenomenon could be also favored by the low solubility of loperamide in aqueous solutions.

Experimental data were fitted to the theoretical Fick's second law of diffusion (Higuchi, 1962; Calderó, 2010; Fornaguera, 2014(1)), although the fitting was not very good, probably due to the incomplete loperamide release. The diffusion coefficients obtained are shown in Table 4.27. Loperamide release is sustained in the micellar solution, as compared with the aqueous solution, since the diffusion coefficient is reduced to the half value. In addition, for the nanoparticle dispersions, this reduction is about two orders of magnitude, thus indicating that loperamide release was more sustained.

Table 4.27: Diffusion coefficients of loperamide release from different samples, calculated by the Fick's second law of diffusion. Samples: a) Aqueous loperamide solution; b) Micellar loperamide solution with polysorbate 80; and c) NP-0.16E70 LOP-loaded nanoparticles.

	Diffusion coefficient (m²/s)
Aqueous solution	$2.22 \cdot 10^{-9}$
Micellar solution	$1.05 \cdot 10^{-9}$
Nanoparticle dispersion	$3.01 \cdot 10^{-11}$

In most previous bibliography, an initial burst release is experienced when studying drug release, followed by a sustained release (Ueda, 1997; Vergoni, 2009; Kirby, 2013). However, some studies, as that of the present work, do not find this typical initial burst release (Dalwadi, 2009). Contrarily, a latency time was found for the first three hours (Figure 4.71). This absence of an initial burst could be the confirmation of loperamide encapsulation, since previous studies attributed the initial burst to the drug attached to nanoparticle surface (Ueda, 1997).

Comparing the results of loperamide encapsulation into nanoparticles with other studies formulating LOP-loaded nanoparticles; nanoparticle with sizes in the same nanometric range (around 100 nm) were achieved, as well as with similar surface

charges and drug concentration in nanoparticle dispersions (Tosi, 2007; Vergoni, 2009; Kirby, 2013). Although it should be better to increase the loperamide concentration in the oil phase instead of concentrating in a final step, previous bibliography pointed out the importance of the small sizes to avoid nanoparticle detection by the immune system in the bloodstream. These authors (Kreuter, 2014) already indicated a compromise between the reduced size and the loperamide concentration. In the present work, due to the low initial concentrations followed by nanoparticle concentration, both requirements are achieved, so these nanoparticles are promising advanced drug delivery systems for the sustained loperamide release by the intravenous route of administration, considering physicochemical and dose requirements. Comparing with previous studies with loperamide incorporated in nanoparticles, our approach is advantageous in terms of reduced preparation time and costs, since in previous studies loperamide was added *a posteriori*, thus having an additional step in the preparation (Ulbrich, 2009).

4.4.4. Galanthamine hydrobromide

Galanthamine hydrobromide is an antiapoptotic drug which main action consists in an inhibition of the acethylcholinesterase activity (Villaroya, 2007). This drug was chosen as a "gold standard" for the symptomatic treatment of neurodegenerative diseases, namely Alzheimer's disease (Villaroya, 2007).

NP-0.16E70 nanoparticles were chosen. For comparison purposes with loperamide, 0.1wt % of galanthamine was incorporated in the oil phase. Since this drug at this concentration is soluble in ethyl acetate, no other solvents had to be added in the oil phase.

4.4.4.1. Characterization of the galanthamine-loaded nanoparticles

Galanthamine-loaded nanoparticle dispersions, as well as the template nano-emulsions were characterized by means of droplet size and surface charge (Table 4.28). Nano-emulsions droplets showed radii of around 33 nm, while in nanoparticles, hydrodynamic radii were reduced to 22 nm. Comparing with the respective non-loaded dispersions, hydrodynamic sizes did not vary, like for

Coumarin 6, thus confirming that the encapsulation of a small molecular weight compound does not affect nano-emulsion and nanoparticle formation and properties. In addition, from these results, it could be also inferred that the increase in droplet sizes observed for loperamide-loaded nano-emulsions and nanoparticles is due to the presence of the second solvent. The study of the surface charge also reported similar results than non-loaded nano-emulsions and nanoparticles (Table 4.28).

Table 4.28: Characterization of the galanthamine-loaded (0.1wt %) NP-0.16E70 nano-emulsions and nanoparticles.

Sample	Visual appearance	Hydrodynamic radius(nm)	ζ potential (mV)
NE		32.73 ± 0.39	-24.15 ± 6.74
NPd		21.50 ± 0.25	-11.18 ± 0.89

4.4.4.2. Efficiency of encapsulation

Galanthamine encapsulation efficiency into nanoparticles was also studied and the results are shown in Table 4.29. As for other encapsulation examples presented in this work, the encapsulation efficiency of galanthamine is high, achieving nearby the total amount of the drug added to the initial formulation. The explanation for these high encapsulation efficiencies, higher than those reported in previous bibliography, is attributed, as for loperamide (Section 4.4.3.2), to the method used. However, as found for loperamide, therapeutic concentrations of galanthamine were not obtained in the as-prepared nanoparticle dispersions, being necessary a further concentration step (Farlow, 2001; Lanctôt, 2003; Cummings, 2004; Suh, 2004).

It is worth noting that there is not a single study reporting the encapsulation of galanthamine into nanoparticles. Although some studies reported the encapsulation of galanthamine into nanoliposomes, encapsulation efficiencies were not as high as those reported in the present work (Mufamadi, 2013; Alyautdin, 2014).

181

Table 4.29: Related parameters with the Galanthamine encapsulation in nanoparticles.

Encapsulation efficiency (EE) (%)	98.47 ± 0.43
Drug loading (mg GAL/g PLGA)	56.87 ± 34.79
Drug concentration (mg GAL / g NPd)	6.01 ± 0.01

4.4.4.3.   *In vitro* drug release

In vitro galanthamine release was studied from nanoparticles and, with the sake of comparison, from micellar and aqueous solutions. The release from the aqueous solution is the fastest, followed by the micellar solution and then the nanoparticle dispersion (Figure 4.72). These results are in good agreement with those concerning loperamide release and also with other own studies (Fornaguera, 2014(1)). In contrast to loperamide, the three samples achieved the total release of the drug. This could be due to the absence of interaction between the drug and the components of the nanoparticles and/or due to the higher solubility of galanthamine as compared with loperamide in aqueous solutions (DrugBank, 2014). After 24 hours, 96wt % of galanthamine has been released from the aqueous solution, while only 77wt % from the micellar solution and 50wt % of the nanoparticle dispersion. Thus, to achieve the total release of galanthamine, it took 24 hours for the aqueous solution, 72 hours for the micellar solution and 120 hours for the nanoparticle dispersion. Another difference from the loperamide release is the presence of the initial burst release, previously described in other studies. The initial burst usually indicates the release of the drug which is attached to the nanoparticle surface instead of encapsulated (Ueda, 1997). Following this early release, a slower release took place, which corresponds to the encapsulated galanthamine.

It is worth noting that in some cases, at late times, another accelerated release is observed, which is usually attributed to the polymer degradation, facilitating the release of the drug (Ueda, 1997). Nevertheless, shrinkage of the polymer particles cannot be ruled out. Since in the present study accelerated release was not observed in any case, Coumarin 6, loperamide and galanthamine, (Figures 4.63, 4.71 and 4.72), chemical stability of PLGA, for at least 120 hours, can be assumed.
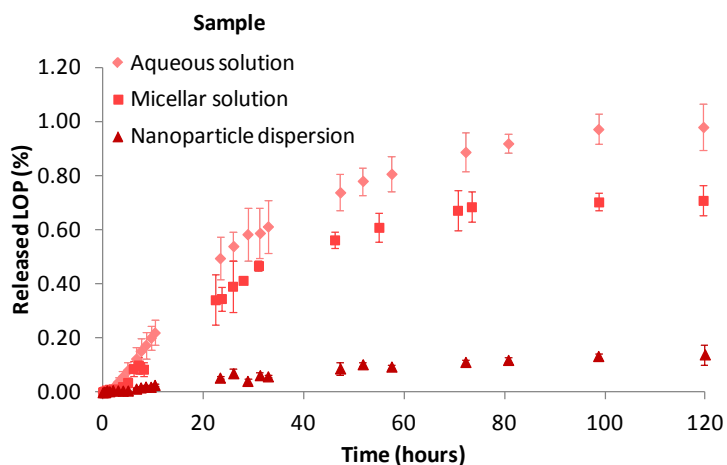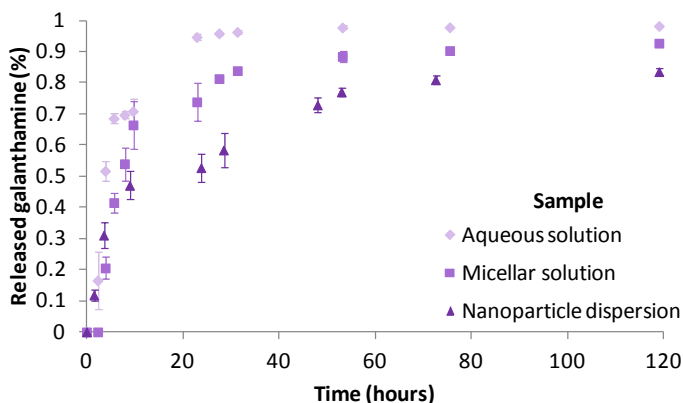
Figure 4.72: Galanthamine release to water as a function of time and sample type, at 25ºC. Samples: a) Aqueous galanthamine solution; b) Micellar galanthamine solution with polysorbate 80; and c) NP-0.16E70 GAL-loaded nanoparticles.

The experimental values were fitted to the theoretical Fick's second law of diffusion, and the diffusion coefficients were calculated (Table 4.30). The release from the aqueous solution is about one order of magnitude faster than that from the micellar solution and the nanoparticle dispersion, thus indicating a sustained release, namely by nanoparticles. In contrast to loperamide, galanthamine release from the micellar solution is closer to that of the nanoparticle dispersion than that of the aqueous solution, thus indicating a sustained release. It could be thought that, since galanthamine release from nanoparticles achieves values higher than loperamide release, some kind of degradation and / or shrinkage takes place on the polymer. However, stability of the PLGA was widely studied in this work, and it was shown that the polymer is stable for more than 120 hours, the time of the studied release.

Table 4.30: Mean diffusion coefficients of galanthamine release from different samples, calculated by the Fick's second law of diffusion. Samples: a) Aqueous galanthamine solution; b) Micellar galanthamine solution with polysorbate 80; and c) NP-0.16E70 GAL-loaded nanoparticles.

	Diffusion coefficient (m²/s)
Aqueous solution	$1.05 \cdot 10^{-8}$
Micellar solution	$4.22 \cdot 10^{-9}$
Nanoparticle dispersion	$1.92 \cdot 10^{-9}$

The sustained controlled release of galanthamine from nanoparticles suggest that they are promising as advanced drug delivery systems. Not only to control the pharmacokinetics of this drug, but also to decrease the number of drug administrations required for the patients, since the effects of the drug would last for a prolonged period of time, thus increasing patients compliance (Morris, 1992).

Comparing the release from the three compounds studied: Coumarin 6, loperamide and galanthamine (Figure 4.63, 4.71 and 4.72 respectively), it is quite clear that loperamide release differs from the other two. These results can be attributed to the large size of loperamide-loaded nanoparticles as compared to that of the other two. In fact, they could be expected, since previous bibliography described a reduction of the initial burst release on larger nanoparticles (Nicolas, 2013); which is in good agreement with the results presented in this thesis.

4.4.4.4. Acetylcholinesterase activity

Galanthamine, as previously described, is an anticholinergic drug, acting mainly by the inhibition of the acetylcholinesterase activity, which is increased in patients with neurodegenerations (Lilienfeld, 2006).

In the present work, galanthamine activity was studied by means of measuring the acetylchholinesterase activity once the drug has been encapsulated into the nanoparticles for the as-prepared nanoparticles, but also for the galanthamine aqueous and micellar solutions, taking them as positive controls. Results are presented in Figure 4.73. The inhibition of the acetylcholinesterase is plotted as a normalized percentage between the maximum and the minimum inhibition. Galanthamine-loaded nanoparticles achieved an inhibition of around 80wt % of acetylcholinesterase, thus indicating that after its encapsulation into the nanoparticles, galanthamine maintains its activity.

The loss of a 20wt % of activity could be due to the polymeric nanoparticle matrix, which is an obstacle for the drug to be in close contact with the enzyme. However, taking into account that these nanoparticles are intended for the localized drug delivery in their targets, it is feasible that an enhancement of the drug activity is produced after the administration of an equivalent drug dose to those of current treatments. In addition, it is worth noting that the inhibition of the acetylcholinesterase activity is the main effect of galanthamine, but not the only one, since the neuroprotection achieved in clinical trials when galanthamine was

used might not only come from the acetylcholinesterase inhibition (Villaroya, 2007).
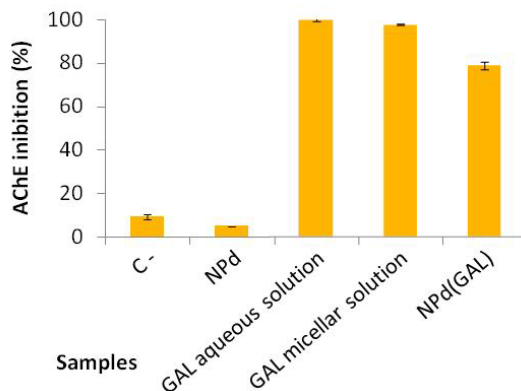
Figure 4.73: Acetylcholinesterase (AChE) inhibition (in %) for the tested samples with the same galanthamine concentration for all them.

The importance of this part of the work arise from the current absence of studies intended on the encapsulation of galanthamine in polymeric nanoparticles for the BBB crossing (Wohlfart, 2012; Kreuter, 2014). It is worth noting the novelty of the methodology approach reported in this work, since no previous studies have described the encapsulation of galanthamine neither in PLGA nor in other polymer nanoparticles.

Summary

High encapsulation efficiencies were obtained for both drugs and Coumarin 6, due to the methodology of nanoparticle production from nano-emulsions obtained by the PIC method with the drugs added prior to nano-emulsion formation. In previous bibliography, the difficulty of working with a single solvent in the oil component in terms of nano-emulsification and enough drug encapsulation on it has been pointed put (Date, 2010). In the present work, with the exception of loperamide, this has been achieved with only ethyl acetate as the oil component of the former nano-emulsions. In addition, the prepared nanoparticles have nanometric sizes, appropriate for the intravenous administration, which was previously reported to be difficult when high encapsulation efficiencies are achieved (Ishihara, 2009; Singh, 2013). Drug release is sustained when drugs are encapsulated into nanoparticles,

thus enabling prolonged periods of drug activity after the administration. In addition, the encapsulation of the drug did not modify its activity. MNPs were also successfully encapsulated in polymeric nanoparticles, representing a promising approach for imaging and theranostic purposes.

4.5. Nanoparticle functionalization

Polymeric nanoparticle surface modification represents a feasible and efficient strategy to achieve one of the objectives of the present thesis: the crossing of the BBB for the delivery of drugs / genes to the central nervous system.

NP-0.16E70 nanoparticles, in which different kinds of compounds were successfully encapsulated, were selected. This section deals with the use of diverse molecules with small sizes for nanoparticle surface functionalization, since a reduced size may enhance the specific targeting (Alexis, 2008). Among all the possible functionalization agents, the following were chosen: fluorescein isothiocyanate (FITC) as a fluorescent marker, carbosilane cationic dendrons to provide a positive surface charge, diverse gene materials to use nanoparticles as non-viral gene delivery vectors, poly(ethylene glycol) (PEG) to protect the genes and a monoclonal antibody against the transferrin receptor to actively vectorize nanoparticles to the blood-brain barrier. In addition, encapsulation of some compounds followed by nanoparticle functionalization was also tested with different purposes, as described below.

4.5.1. Functionalization with fluorescein isothiocyanate (FITC)

Fluorescein isothiocyanate (FITC) was used as an imaging agent to detect nanoparticles. It was bound to PLGA by a covalent attachment, using the carbodiimide reaction to form a peptidic bond, prior to nano-emulsion formation. The covalent binding of a fluorescent instead of its encapsulation inside nanoparticles, has the advantage of enabling the encapsulation of other compounds since the inner space of the nanoparticle remains available (Yin, 2007). Although some carboxylic groups of the PLGA would be bound to FITC, there would still remain some unbound groups, allowing further functionalizations.

The functionalization of nanoparticles is usually performed after nanoparticle formation, since it avoids the interaction of the functionalizing element with the components of the nano-emulsion templates, and for proteins, the loss of the secondary structure due to sensitivity to organic solvents (Nicolas, 2013; Tosi, 2013). However, for FITC, early PLGA functionalization is not problematic because FITC is a stable molecule in organic solvents (Sigma-Aldrich, 2014) and its hydrophilicity favors orientation to the dispersion media during nanoparticle formation (Tosi, 2013).

Once PLGA was functionalized, nano-emulsions and nanoparticles were prepared and characterized in order to study the influence of FITC. Both, nano-emulsion droplets and nanoparticles sizes are considerably bigger (Table 4.31) than those obtained without FITC (Figures 4.12 and 4.33a). Moreover, surface charges are more negative with FITC. Since the carboxylic groups of the polymer, which gave the negative surface charge, have been converted to amides, negative charges come from the non-functionalized carboxylic groups as well as the deprotonated alcohol terminal groups of the FITC. Therefore, FITC has a strong influence on nano-emulsion formation and properties, as previously described for most of colloidal nanocarriers (Nicolas, 2013). Although the more appropriate systems for the intravenous administration are recommended to have neutral charges (less protein interaction), negative charges are not a real drawback. The erythrocyte membranes have negative charges, therefore, these systems would not interact either disrupt them (Dobrovolskaia, 2013). For these reasons, FITC-NPs could be appropriate systems for their intravenous administration as imaging agents.

Table 4.31: Characterization FITC-loaded nano-emulsions (90wt% PBS 0.16M, 70/30 =/S ratio) and NP-0.16E70 nanoparticle dispersions.

	Nano-emulsions	Nanoparticles
Visual appearance		
Hydrodynamic radius (nm)	≈ 140 nm	≈ 120 nm
Surface charge (mV)	≈ -60 mV	≈ -75 mV

4.5.2. Functionalization with cationic dendrons

Carbosilane cationic dendrons of the second (G2SN) and third (G3SN) generation were used for nanoparticle functionalization to achieve cationic nanoparticles for further electrostatic binding of different types of oligonucleotides, as schematically indicated in Figure 4.74. In the following, nanoparticles functionalized with the second-generation dendron will be referred to as G2SN-NPs and with the third-generation dendron will be designated as G3SN-NPs.

Both G2SN and G3SN dendrons showed hydrodynamic radii of around 20 nm (PDI = 0.45), although in the bibliography they are described to have diameter sizes between 1 – 10 nm (Dhanikula, 2009; Pisani, 2009; Galán-Herranz, 2014). The unexpected hydrodynamic size increase could be due to dendron aggregation, or

due to the high polydispersity (Li, 2012). They possess positive surface charges, of around 70 (G2SN) and 55 (G3SN) mV.

It is worth noting that previous publications indicated that specifically this type of dendrons was appropriate for the BBB crossing (Jiménez, 2010). Although successful *in vitro* results were reported, dendronized nanoparticles could be advantageous due to the higher versatility. For this reason, the use of these dendrons as cationization agents has an extra advantage as compared with other types of cationization.

PLGA nanoparticles were functionalized with these dendrons by means of the carbodiimide reaction, where a peptidic bond between the carboxilic groups of the polymer and the focal amino group of the dendrons was formed. After the reaction, a purification step consisting of a dialysis was carried out to eliminate the reaction products. The carbodiimide reaction usually has the drawback of its low specificity regarding the reaction groups, thus producing heterogeneity between the orientations of the attached molecules. However, dendrons have a unique focal point, therefore, a single orientation is possible (Sapsford, 2011; Nicolas, 2013).
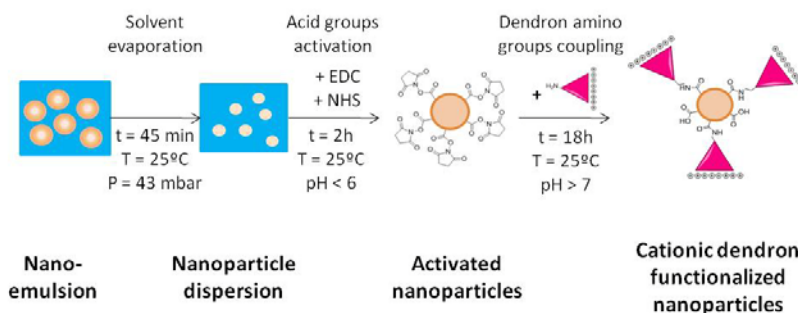
Figure 4.74: Schematic representation of the preparation of dendron-functionalized nanoparticles.

4.5.2.1. Characterization of the functionalized nanoparticles

Different N/P (NP/dendron) molar ratios were tested in order to achieve functionalized nanoparticles with cationic charges. The resulting ζ potential values of the complexes showed that the higher the dendron fraction, the higher the ζ potential, as expected (e.g. G2SN-NP surface charge on Figure 4.75). It is worth noting that at low N/P ratios, the ζ potential is lower than that of the non-functionalized nanoparticles (N/P=0/1), which could be caused by a reorganization of the polymeric matrix resulting in a differential distribution of the charges. Tables

4.32 and 4.33 show ζ potential values and hydrodynamic radii for G2SN-NP and G3SN-NP nanoparticles, respectively. The hydrodynamic radii suffered an increase when the dendron ratio was increased, which could be due to aggregation caused by the non-equilibrated N/P ratio; followed by a decrease at the highest dendron fractions tested, which could be attributed to the stabilization of the complexes at the appropriate ratio.
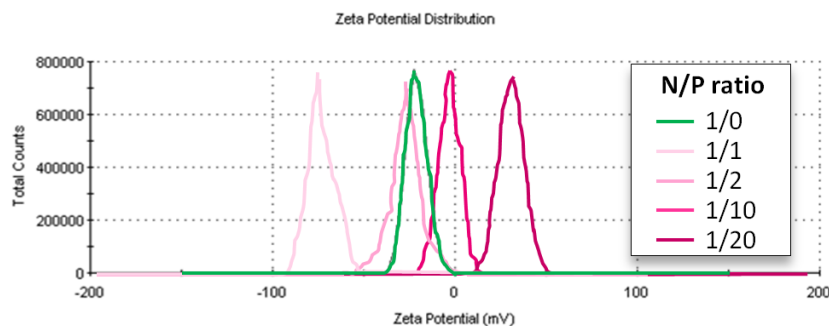
Figure 4.75: Examples of the ζ potential distribution of G2SN-functionalized NP-0.16E70 nanoparticles as a function of the N/P ratio.

A N/P molar ratio of 1/20 for the G2SN dendron, and a N/P ratio of 1/5 for the G3SN dendron was required to achieve cationized nanoparticles. Since the G2SN dendron has half positive charges than the G3SN dendron (four positive charges per molecule in front of eight positive charges), it was already expected that higher amount of the G2SN dendron would be needed to achieve nanoparticles with a cationic surface. These N/P ratios were chosen for further studies. In the following, G2SN-NP or G3SN-NP refer to functionalized nanoparticles with N/P ratios of 1/20 and 1/5, respectively.

Table 4.32: Characterization of the G2SN-NPs (hydrodynamic radius and surface charge), as a function of the NP/G2SN ratio, at 25ºC.

	NP/G2SN ratio				
	1/0	1/1	1/2	1/10	1/20
Hydrodynamic radius (nm)	20.24 ± 6.98	25.56 ± 7.65	25.28 ± 9.69	40.56 ± 7.64	25.84 ± 9.23
PDI (from DLS)	≈ 0.34	≈ 0.59	≈ 0.55	≈ 0.50	≈ 0.36
Surface charge (mV)	$-22,5 \pm 2.21$	-75.71 ± 0.87	-30.60 ± 1.08	-3.15 ± 0.40	32.00 ± 0.74

Table 4.33: Characterization of the G2SN-NPs (hydrodynamic radius and surface charge), as a function of the NP/G3SN ratio, at 25ºC.

	NP/G3SN ratio		
	1/0	1/1	1/5
Hydrodynamic radius (nm)	20.24 ± 6.98	50.26 ± 3,08	22.95 ± 8.13
PDI (from DLS)	≈ 0.34	≈ 0.41	≈ 0.36
Surface charge (mV)	-22,5 ± 2.21	-7.50 ± 0.09	32.60 ± 3.37

The variations of the ζ potential to positive values, together with the slight increase on the nanoparticle size can be taken as indications of nanoparticle functionalization (Cho, 2011; Li, 2014).

Dendronized-nanoparticle sizes were also assessed by means of AFM. G2SN-NPs showed nanoparticle sizes (measurement of the height) of around 23 nm, while G3SN-NPs showed heights of around 32 nm (Figure 4.76). Although sizes for both samples were similar by DLS measurements, it should be noted that both techniques give different measurements. As described above, DLS measures the hydrodynamic size and AFM measures the hard sphere size. For this reason, different results from both techniques were expected due to the formation of solvation layers of different thickness, which would end up with similar hydrodynamic radii. It is worth mentioning that previous bibliography reported the difficulty, even the impossibility of size measurement of dendronized polystyrene nanoparticles (Sakthivel, 2003), which was achieved in the present work using two different techniques.
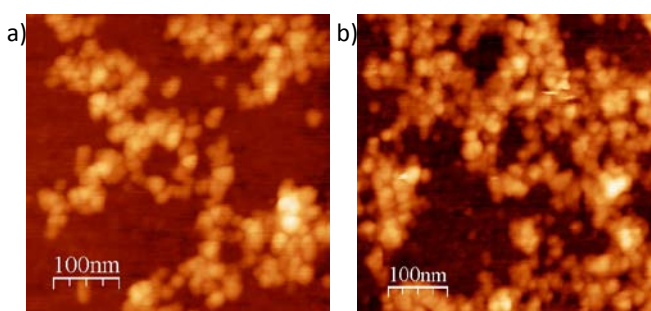
Figure 4.76: AFM micrographs of a) G2SN-NPs and b) G3SN-NPs.

Dendronized-nanoparticles stability was assessed by visual observation. Both samples were stable, no macroscopic changes appeared, for at least, three months.

Once the N/P complexation ratio was assessed, C6-loaded nanoparticles were functionalized with the G3SN dendron, following the same protocol, to study the influence of an encapsulated compound. C6-loaded G3SN-functionalized nanoparticles showed hydrodynamic radii around 20 nm and surface charges around 30 mV. Both results are in good agreement with the results for the non-loaded (Coumarin 6-free) dendronized nanoparticles, thus confirming that the encapsulation of Coumarin 6 does not influence their functionalization.

4.5.2.2. Efficiency of the reaction

The efficiency of the carbodiimide reaction was tested by different techniques: FTIR, Kaiser test and TGA.

FTIR spectra were studied to determine the formation of the amide bound, detected by the appearance of a peak corresponding to the carbonyl group, which differs from the acid and ester group bands. Figure 4.77 shows the results. In non-functionalized nanoparticles, the main peaks correspond to the $-CH_2$, $-CH_3$ ($\approx$2900 cm^{-1}), $-CO$ ($\approx$1750 cm^{-1}) and $-COC$ ($\approx$1200 − 1100 cm^{-1}), chemical groups (Pretsch, 2003); which can be adscribed mainly to the PLGA polymer (Catiker, 2000; Galán, 2014). In dendrons, the main peaks correspond to the $-NH$ ($\approx$3460 − 1635 cm^{-1}), $-CH_2$, $-CH_3$ ($\approx$2900 cm^{-1}) and $-SO_3$ ($\approx$1200 − 1050 cm^{-1}). In the dendronized nanoparticles, the bands corresponding exclusively to the dendron (sulfate and carbosilane groups) are not observed due to the superposition with the bands from the PLGA polymer corresponding to the ester. However, the formation of the amide group was observed by the appearance of its characteristic bands (groups $-NH$) around 3500 − 1600 cm^{-1}. For both dendrons, the spectra of functionalized nanoparticles are almost the same than those of nanoparticles, while the spectra of dendrons are clearly different. Therefore, it was confirmed by FTIR the presence of the amide bond in the dendronized samples, thus indicating the correct nanoparticle functionalization by covalent attachment of dendrons.
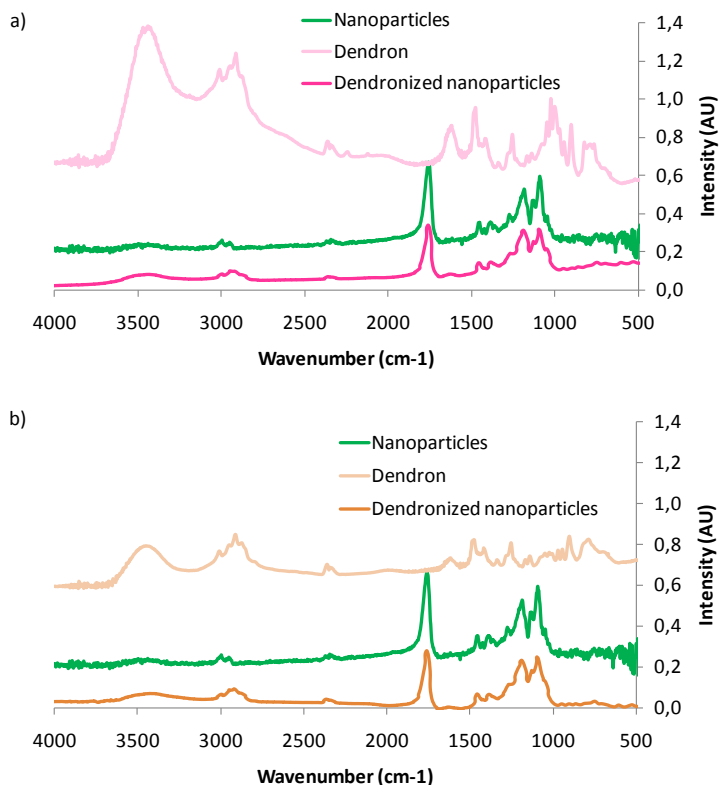
Figure 4.77: FTIR spectra from nanoparticles, dendrons and dendronized nanoparticles (dialyzed to eliminate the reactants) with a) second generation dendron and b) third generation dendron.

The <u>Kaiser test</u> is a colorimetric method to qualitatively detect the primary free amines, widely used due to its high sensibility, detecting percentages as small as 1wt % of amine groups in the sample (Kaiser, 1970; Polizzi, 2007). In the present work, this method was also used to qualitatively confirm the formation of the peptide bond between the PLGA and the dendrons. Figure 4.78 shows the results. As expected, dendrons gave a positive result (purple-bluish opaque coloration, Figure 4.78b and e), since they have a primary free amine. Nanoparticles do not have primary amines, therefore, they gave a negative result to this test (white-yellowish translucent to transparent coloration, Figure 4.78a). Dendron-functionalized nanoparticles (at the appropriate N/P ratios and after a cleaning dialysis) resulted in a negative coloration of the Kaiser test, thus confirming the absence of primary free amines, corresponding to the complete nanoparticle functionalization (Figure 4.78c and f). In addition, positive controls, consisting of a physical mixture of the nanoparticles with the dendrons were also tested, resulting

in a positive coloration of the Kaiser test, thus indicating the presence of the primary free amines of the dendrons (Figure 4.78d and g).

It is worth noting that Kaiser test is an efficient methodology not only to prove the reaction, but also to prove the absence of free dendrons. Therefore, this test also confirmed that the dialysis method is efficient for the funtionalized-nanoparticle purification.
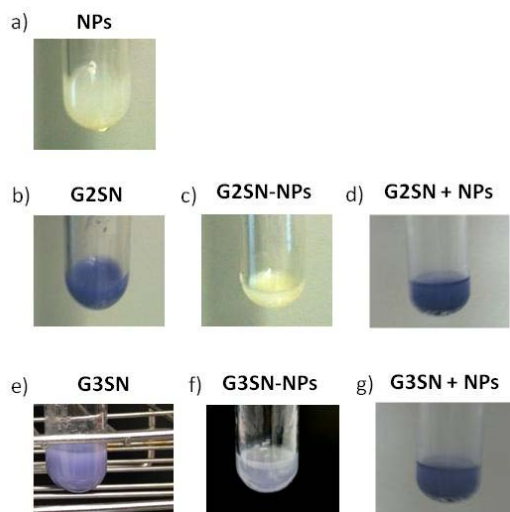
Figure 4.78: Examples of the visual appearance after performing the Kaiser test on: a) NP-0.16E70 nanoparticles; b) G2SN dendron; c) G2SN-NPs; d) a physical mixture of G2SN dendron and nanoparticles; e) G3SN dendron; f) G3SN-NPs and g) a physical mixture of G3SN dendron and nanoparticles.

Thermogravimetric analyses (TGA) were performed to study the thermal stability of the raw materials (nanoparticles and dendrons), dendronized nanoparticles and a physical mixture between the components without reaction (nanoparticles + dendron), to further confirm nanoparticle functionalization. Results are shown in Figure 4.79 where the first derivative is plotted as a function of the temperature (the TGA thermograms obtained are shown in Figure Ap.8, appendix). Figure 4.79 shows peaks that correspond to the inflection points for each mass loss.
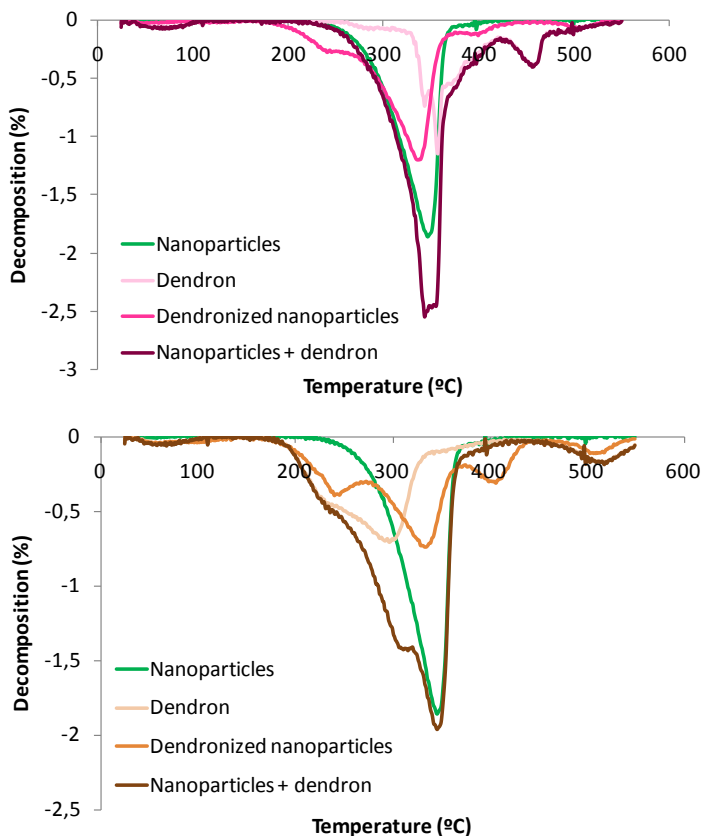
Figure 4.79: First derivative of the TGA spectra from nanoparticles, dendrons, their physical mixture and dendronized nanoparticles with a) second generation Dendron and b) third generation dendron.

At temperatures below 100ºC a small peak is observed for all samples, which corresponds to a small mass loss related with water evaporation. Although the samples were previously lyophilized, a slight amount of water appears due to the hygroscopic properties of the components, namely dendrons; which is in good agreement with the smaller loss observed for the non-functionalized nanoparticles (Figure 4.79) (Godipas, 2003; Galán, 2014). At temperature higher than 200ºC the main decomposition of the samples took place. For <u>nanoparticles</u>, only a single peak around 325ºC appears, which corresponds to the decomposition of the polymer. This is in close agreement with previous bibliography reporting the decomposition of PLGA with 75wt% of lactic and 25wt % of glycolic acids (D'Antone, 2001). For the <u>dendrons</u>, an early peak around 275ºC appears for the G2SN dendron and around 225ºC for the G3SN dendron. A second main peak around 350ºC appears for the G2SN dendron, while for the G3SN it appears at

300ºC. A smaller peak around 450ºC also appears for the G2SN and around 525ºC for the G3SN dendron. Each of these peaks corresponds to a mass loss of a different structure. The first peak (around 100ºC) could be attributed to the water evaporation, as previously discussed. The second degradation (around 300 – 350ºC) could be attributed to the sulphonate groups, while the degradation peak around 450 – 525ºC could be attributed to the carbosilane backbone. This is consistent with previous studies, which reported the early degradation of the organic structures, followed by the late degradation of the inorganic structures due to their higher thermal resistance (Godipas, 2003; Wang, 2007(2); Galán, 2014).

When <u>nanoparticles are dendronized</u>, the decomposition as a function of the temperature show different peak patterns than those of the components (Figure 4.79). The thermograms show three peaks (apart from the water degradation), the first around 250ºC, the second and more pronounced around 330ºC and the third and less pronounced around 400ºC. The first peak was attributed to the mass loss associated to the sulfonate groups of the dendrimer, as well as to the start of the decomposition of the polymeric backbone; while the last peak was attributed to the carbosilane backbone of the dendrons (Galán, 2014). The change in the dendronized nanoparticle thermogram from the raw materials is an indication of the variation of the material properties, thus also confirming the formation of the ester bonds and the dendronization of the nanoparticles. <u>Physical mixtures</u> of NP and dendrons were also studied as negative controls. In Figure 4.79 clear differences were observed between the decomposition of these mixtures and that of the dendronized nanoparticles. This indicates that the physical mixture is different than dendronized nanoparticles in terms of thermal resistance, thus confirming the functionalization of the nanoparticles.

In spite of the difficulties on characterizing the efficiency of the functionalization reaction, in the present work, the combination of different techniques enable confirmation of the amide bond formation between the nanoparticles and the dendrons. It is worth mentioning that previous studies reported dendron functionalization of PLGA nanoparticles (Costantino, 2006; Ribeiro, 2007). *Costantino et al.,* (Costantino, 2006 and 2009), for example, the covalent attachment of the zero and first generation Lin's amine dendron (dendron with a carbon – oxygen structure) to PLGA polymer prior to the formation of nanoparticles (size around 150nm). *Ribeiro et al.,* (Ribeiro, 2007), reported PLGA-dendriplex particles with sizes of around 500 nm. In both cases, dendronized nanoparticle sizes are bigger than those reported in the present study. Dendronized

nanoparticles were intended as vehicles for cellular uptake, consequently, smaller sizes are advantageous (Costantino, 2006).

4.5.3.Functionalization with oligonucleotides

Gene therapy has been widely studied with both viral and non-viral vectors. In the present work, the aim was to use nanoparticles as non-viral gene delivery vectors. Non-viral vectors are advantageous as compared with viral vectors in terms of less activation of the immune system (Mansouri, 2004). Antisense oligonucleotides (ASO) and siRNAs were selected with a phosphorotioate structure, since it enhances the gene stability. Both codify to knockdown the expression of a *Renilla* Luciferase gene (Grijalvo, 2014). Moreover, a plasmid construction, codifying for a fluorescent protein was also used. All of the genes used were electrostatically bound to cationic dendronized nanoparticles, as schematically shown in Figure 4.80. The conjugation of the oligonucleotide in the nanoparticle surface has the advantage of its simplicity and time-efficiency in comparison with other methodologies, and it allows obtaining stable conjugates with improved biological properties (Tosi, 2013; Grijalvo, 2014).
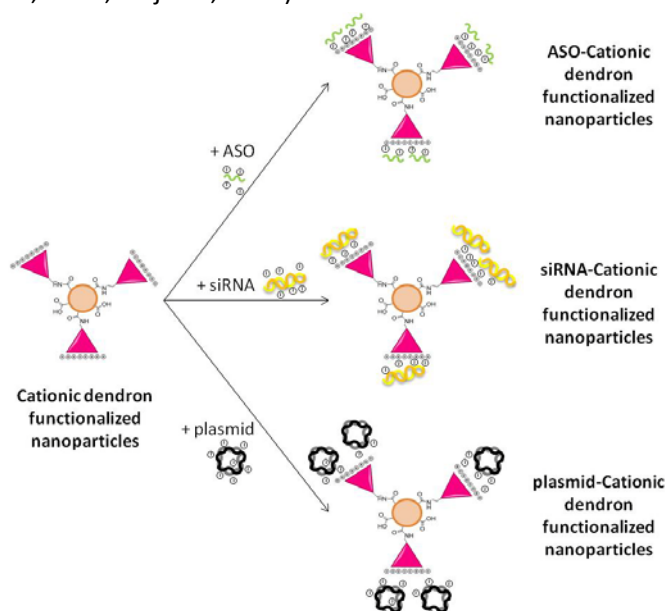
Figure 4.80: Schematic representation of the electrostatic gene attachment to dendron-functionalized nanoparticles.

4.5.3.1. Antisense oligonucleotides (ASO)

Previous studies demonstrated the ability of carbosilane cationic dendrons to electrostatically bind antisense oligonucleotides (ASOs) and to enhance the transport of the gene material inside the cells due to the reduction of their interaction with serum proteins (Bermejo, 2007; Ionov, 2012). For this reason, G2SN and also G3SN carbosilane cationic dendrons were chosen for the cationization of nanoparticle surface.

Different N/P (dendronized-nanoparticles / ASO) charge ratios were tested to achieve complexation (neutral surface charge) (Dobrovolskaia, 2013). As Figure 4.81 shows, for both dendrons, increasing the N/P ratio (i.e. increasing dendronized nanoparticles proportion), the surface charge increases, as expected, followed by a plateau at high N/P ratios due to saturation. For G2SN-NPs, the complexation ratio is between 0.75/1 and 0.875/1 and for the G3SN-NPs, the complexation ratio is slightly below 0.5/1. Since surface charges of dendronized nanoparticles are nearly equal for both dendrons (Tables 4.32 and 4.33), similar complexation ratios were obtained, as expected.
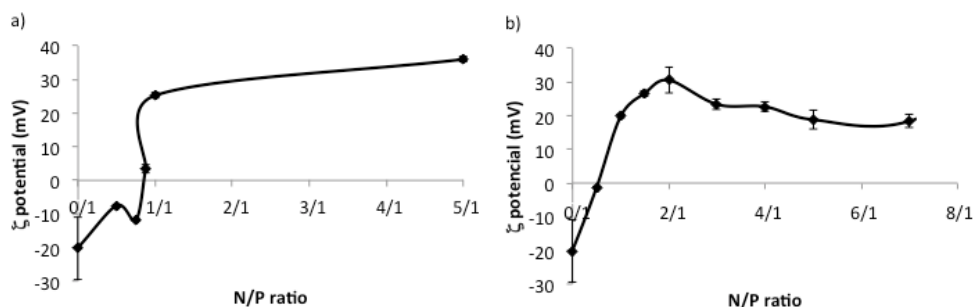
Figure 4.81: ζ potential of the complexes formed with the a) G2SN-NP and b) G3SN-NP and the ASO, as a function of the N/P charge ratio.

Moreover, the same experiments were carried out in the presence of 10wt % of fetal bovine serum (FBS), to simulate physiological conditions. As Figure 4.82 shows, the surface charge is negative for all complexes tested. In the presence of FBS, the surface charge does not depend on the N/P charge ratio due to the negative charges of serum proteins, which predominate over the charges of the complexes (Dobrovolskaia, 2009).
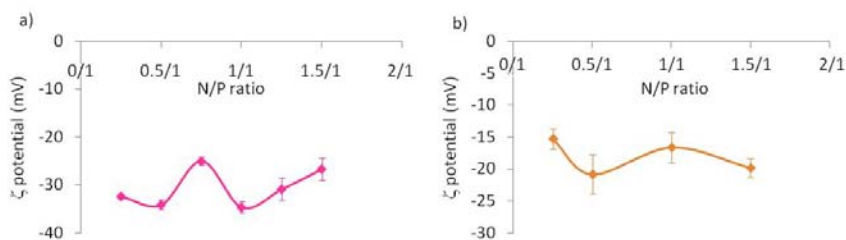
Figure 4.82: ζ potential of the complexes formed with the: a) G2SN-NP with the ASO and b) G3SN-NP with the ASO, as a function of the N/P ratio, in the presence of 10wt % of FBS.

In order to obtain with more accuracy the N/P complexation ratio, electrophoretic mobility shift assays (EMSA) were carried out for both dendronized nanoparticles. In this type of electrophoresis, molecules migrate with a speed depending on their charge. Figure 4.83 shows the results. When samples have a negative charge, they run easily, resulting in a single band. When the complexation takes place, the null charges of complexes result in a diffused pathway instead of a band. For the G2SN-NPs, the retardation starts at N/P ratios of 0.25/1, but the complete complexation takes place at N/P ratios of 0.5/1. For the G3SN-NPs, sample retardation starts at 0.5/1 N/P ratios, but the optimal complexation takes place at 1/1 N/P ratios. Both results are in good agreement with surface charge measurements.
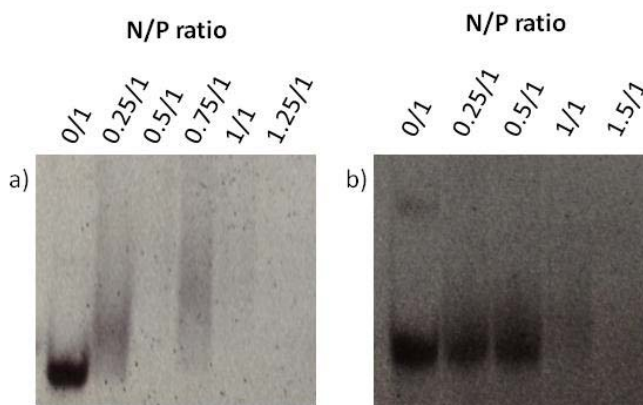
Figure 4.83: EMSA of the complexes formed with the: a) G2SN-NP with the ASO and b) G3SN-NP with the ASO, as a function of the N/P ratio.

The complexes formed using G2SN-dendronized nanoparticles were further tested by determining the spectra profiles obtained using enhanced optical microscopy with spectral analysis. They were compared with the spectra corresponding to nanoparticles and also G2SN dendronized nanoparticles. As Figure 4.84 shows, the spectra of non-functionalized nanoparticles have a maximum around 550 nm, while G2SN dendron-functionalized nanoparticles have a maximum around 600 nm and

after their complexation with ASOs around 650 nm. The wavelength of the maximum peak of a spectrum is a characteristic that defines a material; thus, the variation of the peak of the spectra when functionalizing and further complexing nanoparticles is another indication that nanoparticles have been successfully functionalized and complexed with ASOs.
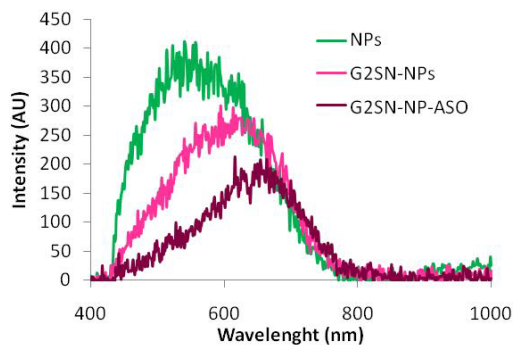
Figure 4.84: Example of the spectral profiles of nanoparticles, G2SN-functionalized NPs (N/P = 0.75/1) and G2SN-NPs functionalized with ASOs.

The stability of the complexes was studied by means of DLS as a function of time. As Figure 4.85 shows, the hydrodynamic radii of the complexes initially fluctuates, and afterwards it remains constant with time, for the experimental time of three months, thus indicating that these complexes for, at least, are stable. Similar stability results were found in the bibliography for complexes between ASOs and dendritic structures (Jiménez, 2010). The hydrodynamic sizes of the complexes (Figure 4.85) are around 90 nm for G2SN-complexes, while they are around 45 nm for G3SN-complexes. Therefore, comparing with the sizes of dendronized nanoparticles, by using G2SN dendron, complex sizes quadruplicates while using G3SN dendron, it only duplicates. The increase in the hydrodynamic radii was already expected, as found in previous studies (Arora, 2014). However, the differences between both dendrons were not expected. They could be attributed to the technique used. Since ASOs could remain within different grades of compactation, the solvation layer could be different for both dendrons, thus resulting in different sizes. Another explanation could be the use of higher concentration of G2SN dendron, in terms of mass, for surface cationization, as compared with that of G3SN dendron.
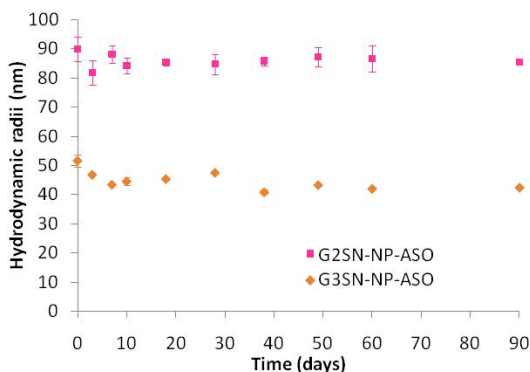
Figure 4.85: Hydrodynamic radius (nm) as a function of time, for the complexes prepared with the G2SN-NPs at an N/P ratio of 0.75/1 and with the G3SN-NPs at an N/P ratio of 1/1, conjugated at an ASO concentration of 60nM.

4.5.3.2.   Small interference ribonucleic acid (siRNA)

siRNAs have increasing interest as a method to specifically, selectively and accurately knockdown proteins (Posadas, 2009). In the present work, G2SN-NPs were used for electrostatic bind of a siRNA.

As for ASOs, the first study consisted in the determination of the complexation N/P charge ratio (G2SN-NP/siRNA ratio). The complexes surface charge increased when the N/P charge ratio increased (Figure 4.86), from negative to positives values, achieving neutral values around an N/P ratio of 0.5/1; which is in close agreement with the results with ASO complexes.
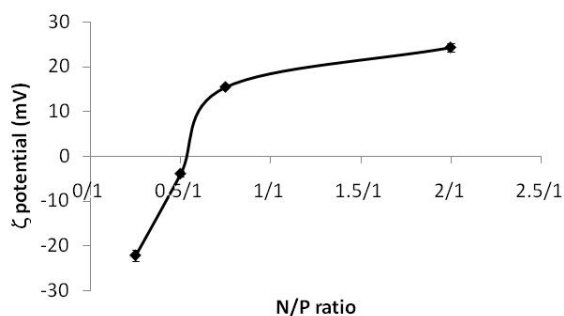
Figure 4.86: ζ potential of the complexes formed with the G2SN-NP and the siRNA, as a function of the N/P charge ratio.

Moreover, to better define the N/P ratio, EMSA experiments were carried out. The results are shown in Figure 4.87. It should be noted that the presence of a second band in the lower part of the gel corresponds to some single siRNA chains produced as impurities during its synthesis. Figure 4.87 clearly shows that the complexation starts at a N/P of 0.25/1, but the optimal complexation took place at an N/P ratio of 0.5/1. These results are in good agreement with ζ potential measurements as well as with the ASOs results, thus confirming the 0.5/1 N/P ratio as the complexation ratio.
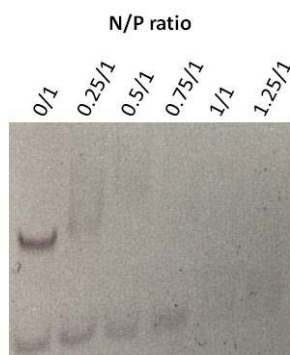
Figure 4.87: EMSA of the complexes formed with the G2SN-NP with the siRNA, as a function of the N/P ratio.

The characterization of the size of the complexes by DLS resulted in <u>hydrodynamic radii</u> of around 100 nm. As expected, the attachment of the siRNA increased nanoparticles sizes, as for ASOs, which is another evidence of complexes formation. As for ASOs, the <u>stability</u> of the complexes was studied by means of size measurements along the time. Figure 4.88 shows the results. The hydrodynamic radius of these complexes increased as a function of time (Figure 4.88a), from initial sizes around 100 nm to final sizes of around 600 nm. The size increase could be an indication of instability of these complexes along the time, since siRNA molecules are more sensitive than ASOs to the nucleases attack. In addition, polydispersity indexes (Figure 4.88b) also increased as a function of time, which is an indication of the appearance of complexes with different sizes. It is worth noting that instability of these complexes could produce problems regarding their intravenous administration, since the final sizes are bigger than those recommended for a safe intravenous administration due embolization of thinner blood vessels (Gref, 2012; Dobrovolskaia, 2013).
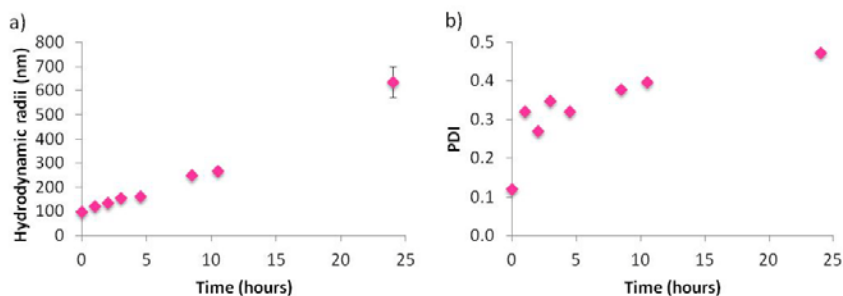
Figure 4.88: a) Hydrodynamic radii and b) PDI, as a function of time, for G2SN-NPs-siRNA.

Previous studies reporting the use of a cationic dendron to electrostatically bind a siRNA were not found. For this reason, the results presented in this section were compared with previous bibliography reporting the electrostatic complex formation between a siRNA and the same carbosilane cationic dendrimers (Ionov, 2012). In that case, by increasing the N/P ratios (dendrimer/siRNA), the surface charges also increased from negative to positives values. However, their N/P complexation charge ratio was around 4/1 and 6/1, they needed more amount of dendrimer to compensate an equivalent amount of siRNA charge. This could be due to the higher charges of a dendrimer as compared with a dendron of a same generation. In addition, they obtained bigger complexes (Ionov, 2012). Therefore, the complexes of the present work are advantageous in terms of reducing toxicity due to the less amount of dendron used and the expected reduced immune detection due to smaller sizes (Dobrovolskaia, 2008; Zolnik, 2010).

4.5.3.3. Lentiviral plasmid vectors

Lentiviral plasmid vectors were also electrostatically attached to G2SN-nanoparticles. Characterization of the plasmids prior to use showed that they have negative surface charge, as expected, and a hydrodynamic radius of around 250 nm (Table 4.34), bigger than expected. After sonication, the hydrodynamic radius was around 38 nm, which was attributed to changes in their conformational structure or a possible aggregation in the original sample.

It is worth noting that the plasmid selected is markedly bigger than other gene material used. Nevertheless, its complexation with dendronized nanoparticles was tested since previous studies demonstrated the ability of carbosilane dendrimers to complex with big gene structures (Bermejo, 2007).

Table 4.34: Characterization of the lentiviral plasmid (size and surface charge).

Hydrodynamic radius (nm)	249.26 ± 8.00
Hydrodynamic radius, after 5 min ultrasonification (nm)	37.88 ± 3.12
ζ **Potential** (mV)	-39.00 ± 1.72

The complexation N/P ratio (NP/plasmid) was assessed by means of surface charge measurements. However, in this case, complexation ratios are given in molar, instead of in charge as in previous studies (due to the circular plasmidic structure, without free charges). As Figure 4.89a shows, increasing the nanoparticle concentration, the surface charge of the complexes increases, starting with negative values and ending with positive surface charges. Complexation takes place at N/P molar ratios around 200/1. Regarding the complex hydrodynamic sizes (Figure 4.89b), in absence of nanoparticles, hydrodynamic radii are high, corresponding to the radii of the plasmids without any treatment (Table 4.34). As nanoparticle concentration increases, the hydrodynamic radius decreases, approaching radii of the nanoparticles without the complexation. Since these complexes are intended for the intravenous delivery, their sizes should keep in the range of appropriate sizes (below 1 μm) (Gref, 2012; Dobrovolskaia, 2013). At the complexation ratio (200/1), the hydrodynamic radii of the complexes are around 60 nm, thus, they are appropriate for the intravenous delivery.
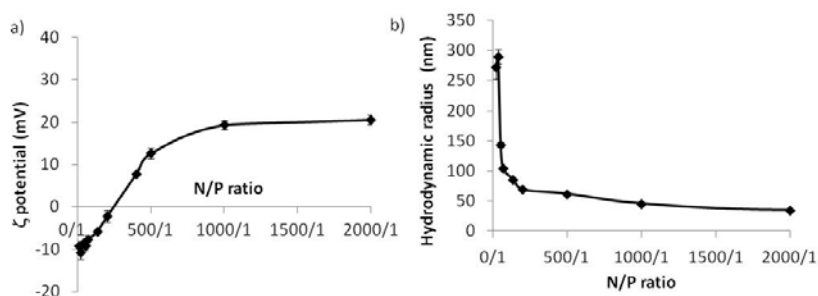
Figure 4.89: a) ζ potential and; b) hydrodynamic radius of the complexes formed with NP-G2SN (0.75/1) and the lentiviral plasmids as a function of the N/P molar ratio.

It is worth noting the novelty of the methodology to produce non-viral gene delivery vectors using nanoparticles as the hard core. Similar approximations are reported. For example, the work by *Ribeiro et al.* (Ribeiro, 2007), in which PLGA nanoparticles were formulated for the encapsulation of DNA and a dendrimer, to form a dendriplex. However, as an O/W nano-emulsion was used as a template for

the DNA encapsulation, solubility issues could arise, since DNA is hydrophilic. Other studies reported the adsorption of dendrons to nanoparticle surface (Sakthivel, 2003), but, since no covalent interaction took place, the nanoparticle-dendron binding was weak and it could be easily reversed before gene attachment. One more set of studies (Zhou, 2013) reported the formation of dendriplexes formed by a dendron with gene material. However, in these studies, low transfection efficiencies are reported due to the low stability of the complexes. In other previous studies, the electrostatic binding between a dendritic structure and an ASO was reported (Bermejo, 2007). However, a stable complexation was neither achieved. Not a single paper reporting the same functionalization strategy to carry genes was found in previous bibliography. Our strategy is advantageous among these previous reports, since the use of nanoparticles enables higher versatility as compared with the systems composed of dendron – gene material. In addition, it is advantageous in terms of vectorization to target organs, since nanoparticle surface can be actively functionalized.

4.5.3.4. Coating with PEG

Polyethyleneglycol (PEG) is a hydrophilic polymer, with flexible chains, electrically neutral, without functional groups. These features enable the so-called "stealth" effect: PEG-coated nanoparticles do not react with biological compounds in the blood, namely blood proteins, thus decreasing the activity of the reticuloendothelial system (RES) (Gref, 2012; Neha, 2013). The reduction of the protein binding onto nanoparticle surface is due to the hydrophilic character of PEG chains; it acts as a steric barrier that prevents the interaction of the proteins (e.g. opsonines and immune system proteins), which are mainly lipophilic, with the non-PEGylated hydrophobic nanoparticles (Ishihara, 2009). Therefore, PEG has been widely used to enhance nanoparticle half-life in the bloodstream (Jain, 2000; Parveen, 2011; Chen, 2012; Gref, 2012; Neha, 2013).

PEGs with different lengths were tested for the nanoparticle coating, using G2SN-NP-ASO. Figure 4.90 shows the sizes as a function of the PEG molecular weight. The longer the PEG chains, the bigger the coated nanoparticles. These results are in close agreement with previous studies, which stated that the longer the PEG chain, the more decreased the RES activity, but the complexes sizes increased (Jain, 2000; Parveen, 2011). The nanoparticle coating with PEG 400Da produced only a slight increase in their hydrodynamic radii. For this reason, it was chosen, since

complexes maintain appropriate sizes for the intravenous administration (Gref, 2012; Dobrovolskaia, 2013). In the following, PEG with 400 Da is always termed as PEG.
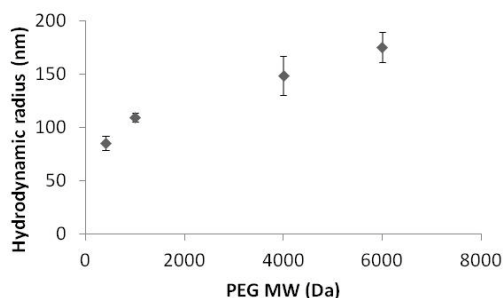
Figure 4.90: Hydrodynamic radii of the complexes (G2SN-NP-ASO) coated with PEGs of different MW. The incubation for the PEG coating was performed during 1 hour, at 37ºC.

Different strategies have been reported for the PEG coating, such as covalent binding or conjugation (Chen, 2012). Although the covalent linkage could represent a strong attachment of PEG to the nanoparticles (Shimoda, 2012), it usually enlarges nanoparticle sizes (Rebolj, 2012), which could produce blood vessels opsonization and embolization (Gref, 2012).

In the present work, PEG coating was performed by means of surface adsorption of PEG molecules onto G2SN-NP-ASO nanoparticles, with the aim to protect these ASO from degradation. It is important to protect not only ASOs but also all kinds of genes to enhance their arrival to their specific targets, thus reducing gene administered doses and decreasing toxicity problems related with accumulation (Chonco, 2007). Different incubation times were tested to achieve the optimal coating conditions, at 37ºC. As Figure 4.91 shows, the hydrodynamic radius of the coated complexes remains constant up to around 1 hour of incubation, but further incubation produced size increase up to 120 nm. Since PEG is a hydrophilic polymer, the solvation layers of the nanoparticles are expected to increase when PEG is added (Kirby, 2013). The ζ potential suffers a slight decrease up to 30 minutes and after that, it remains almost constant around -6mV. Therefore, 30 minutes incubation was selected as the optimal time, since hydrodynamic radii are maintained around 85 nm and ζ potential has already reached slightly negative values, which were reported in previous bibliography as an indication of PEG coating (Dobrovolskaia, 2013). In addition, slight negative charges are desired for the intravenous delivery, since plasma protein adsorption is decreased and the rates of non-specific cellular uptake are lowered (Alexis, 2008).

206
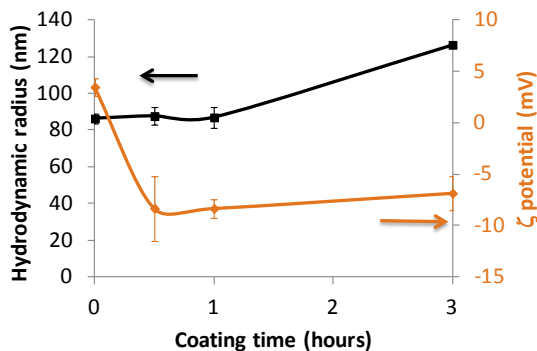
Figure 4.91: Hydrodynamic radius (nm) and ζ potential (mV) of the NP-G2SN-ASO coated with PEG as a function of incubation time (hours) with PEG, at 37ºC.

To further confirm the nanoparticle PEGylation, spectral analyses were performed. Since the spectra are a specific characteristic of a material, they should vary after PEGylation of G2SN-NPs-ASO nanoparticles. In addition, since PEG is the outer component, PEG-coated nanoparticles spectra should coincide with PEG spectra. Figure 4.92 shows a superimposition of an image of PEG-coated nanoparticles with the spectra of PEG polymer. Nanoparticles are represented in yellow/light green, due to the filter used for a better observation. The colored pixels of the picture are the points were the spectrum of PEG was recorded in the nanoparticles image. The colored pixels colocalize with nanoparticles. Therefore, it could be concluded that PEG coating was achieved for G2SN-ASO functionalized nanoparticles, although it seems that there are some parts of nanoparticles without PEG coating.
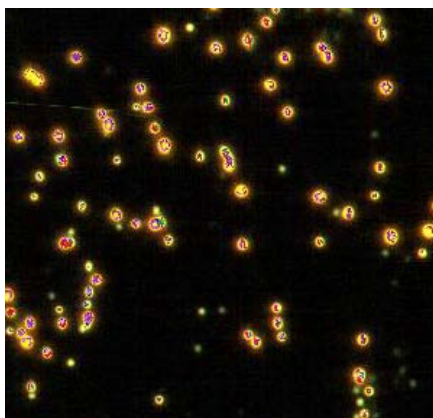
Figure 4.92: Micrograph showing the colocalization of the spectrum of PEG on an image of the PEG-coated G2SN-NPs-ASO. PEG-coated G2SN-NPs-ASO are the yellow spots. PEG spectra are represented as spots of other colors.

G2SN-NP-siRNA were also PEGylated for their use in *in vitro* experiments. However, their characterization was limited to the measurement of their hydrodynamic sizes

and stability. They showed radii of around 150 nm, slightly higher than before PEGylation, confirming PEGylation. The stability of the PEGylated complexes was studied by means of size measurement along the time, as for the non-PEGylated complexes (Figure 4.88). The results for the PEGylted complexes are shown in Figure 4.93 and, for comparison purposes, the results of the non-PEGylated complexes are also presented in the same plots. As discussed for non-PEG coated complexes, PEGylated nanoparticle sizes increase from 150 nm to around 1200 nm (Figure 4.93a), as well as the PDI values (Figure 4.93b). This size increase is more pronounced after the addition of the PEG coating, which could be due to an enhanced aggregation of the complexes. Therefore, PEGylated complexes carrying siRNA could also be problematic for the intravenous administration due to their size increase (Gref, 2012; Dobrovolskaia, 2013), which could be hypothesized to be due to aggregation.
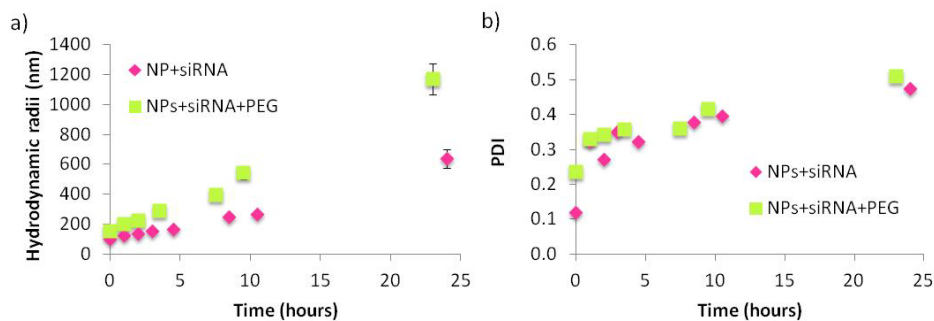
Figure 4.93: a) Hydrodynamic radii and b) PDI, as a function of time, for complexes formulated with siRNA, without and with the PEG coating.

It is worth noting that some previous studies found the so-called accelerated blood clearance (ABC) phenomenon in the presence of PEG (Joshi, 2008; Ishihara, 2009; Lila, 2013). This phenomenon consists of a reduction in the blood circulation time of the PEG-coated nanostructures (polymeric nanoparticles in the case of *Ishihara et al.)* due to the development of an immunogenic response that enhances nanoparticle elimination after repeated administration. This could constitute a great drawback for the clinical application. However, in the present thesis, the polymeric nanoparticle PEGylation is proposed only in the event of using nanoparticles as non-viral gene delivery vectors. Since genes need less nanoparticle concentration than encapsulated drugs to produce a therapeutic effect, the amount of the PEG administered is markedly small. Furthermore, in the above mentioned studies it was stated a dependency between the ABC phenomenon and the PEG length: the longer the PEG, the higher the ABC phenomena. The PEG used in the present study is short; therefore, the ABC phenomena should be small.

4.5.4. Functionalization with antibodies

To use the active transport to overcome the BBB and reach the CNS, nanoparticle surface must be functionalized with the specific targets to the BBB. Among the active targeting elements, the <u>anti-transferrin receptor (TfR) monoclonal antibody</u> was chosen due to the overexpression of TfR in the blood-brain barrier (BBB) (Gabathuler, 2010; Nicolas, 2013), enabling therapeutic effects at central nervous system level due to the BBB crossing via receptor-mediated transcytosis (Gabathuler, 2010; Alyautdin, 2014). Many specific monoclonal antibodies species, targeting the TfR exist. The 8D3 monoclonal anti-TfR antibody, chosen in the present work, is specific of mice (Nicolas, 2003; Pardridge, 2008).

4.5.4.1.   Characterization of the functionalized nanoparticles

Nanoparticles were functionalized with 8D3 antibody by means of the carbodiimide reaction, at a NP/8D3 molar ratio of 50/1. This ratio was chosen taking into account the required antibody concentration to achieve a significant BBB crossing, as reported in previous studies (Manich, 2013) and considering all PLGA carboxylic groups appropriate for the antibody binding. The differences in the molar ratio between both components are due to the high molecular weight of 8D3 antibody (150KDa) as compared with PLGA molecular weight (10KDa). Comparing with previous studies, the NP/antibody ratio is quite high (Ramon, 2013). Nevertheless, since nanoparticles prepared in the present thesis are non-toxic at this concentration (1.5mg/g), the higher amount required does not represent a drawback.

Non-loaded, coumarin 6-loaded and loperamide-loaded nanoparticles were functionalized with the antibody. The resulting complexes were characterized by means of hydrodynamic radius, surface charge and macroscopic visual stability (Table 4.35). Nanoparticles showed sizes of around 20 nm, 25 nm, and 100 nm, respectively, similar to those without antibody functionalization. The surface charge of the complexes is slightly decreased in absolute value as compared to the bare nanoparticle surface charge. They show stability higher than one month. Therefore, the antibody functionalization only affected the nanoparticle surface charge, as expected, which is a first indication of the complex formation.

Table 4.35: Characterization of the 8D3-functionalized nanoparticles as a function of the encapsulated compound.

	Non-loaded NPs	Coumarin 6-loaded NPs	Loperamide-loaded NPs
Hydrodynamic radius (nm)	20 nm	25 nm	100 nm
Surface charge (mV)	-15 mV	-10 mV	-10 mV
Visual stability (time to sediment)	> 3 months	> 1 month	> 3 month

In addition, <u>FITC-functionalized nanoparticles</u> were also functionalized with the 8D3 antibody. In these samples, and in contrast to the bare PLGA nanoparticles, the hydrodynamic radii of the complexes after the antibody functionalization markedly increased from 120 nm to 680 nm. This huge increase is an indication of nanoparticle aggregation. For this reason, the complexes were sonicated for 5 minutes, thus reducing their hydrodynamic radii slightly. Their surface charge and stability remained constant before and after antibody functionalization. Therefore, functionalization of PLGA polymer before nanoparticle and template nano-emulsion fabrication seems to modify the final physico-chemical properties of antibody-functionalized nanoparticles. In contrast, encapsulated compounds seems not to influence nanoparticle properties.

4.5.4.2. Efficiency of the reaction

To confirm that the 8D3 antibody was attached by covalent binding, diverse techniques were performed: confocal microscopy, spectral image analysis coupled to enhanced optical microscopy and size exclusion chromatography.

4.5.4.2.1. Confocal microscopy

In order to evidence that the 8D3-nanoparticle functionalization, mice brain slices were used to perform an ELISA-like experiment, as described in Section 3.2.12.5, visualizing the results with confocal microscopy. Coumarin 6 –loaded nanoparticles were used. Since 8D3 targets the anti-transferrin receptor, overexpressed in the endothelial cells of the BBB (Pardridge, 2008), a colocalization of Coumarin 6 signal (green) with the signal of a secondary antibody against 8D3 (red) was expected. Figure 4.94 represents an example of the micrographs obtained. A blood vessel is

stained with the red dye, corresponding to the dye of the secondary antibody against the primary antibody (8D3). However, the green dye, corresponding to the coumarin 6 encapsulated in the nanoparticles could not be detected in any sample (the green coloration of the brain tissue corresponds to the autofluorescence or the inespecific signal of the slice). Therefore, using this technique, the covalent binding between NPs and 8D3 could not be confirmed. The problems on the detection of fluorescent dyes were previously reported by *Kreuter et al.,* (Kreuter, 2014), who stated that fluorescent signals are usually not strong enough to be detected. As a solution, they suggested that immune techniques would improve these results.
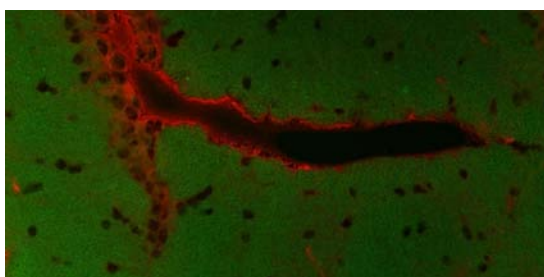
Figure 4.94: Confocal micrograph of a brain slice incubated with C6-loaded 8D3-functionalzied nanoparticles.

4.5.4.2.2. Spectral image analysis

Enhanced optical microscopy with spectral image analysis was used to confirm nanoparticle functionalization with the 8D3 antibody. Like in confocal studies, brain slices were used to perform an ELISA-like experiment with coumarin 6 loaded nanoparticles.

As described in Section 4.4, the spectral profile of the nanoparticles is different than that of C6-loaded nanoparticles (Figure 4.60). When C6-loaded nanoparticles were further functionalized with the 8D3 antibody, the peak of the spectrum was around 575 nm, also different than those without the functionalization (Figure Ap.6, appendix). This was a first indication that antibody-nanoparticle functionalization was achieved. Results of the above-mentioned ELISA-like experiment are presented in Figure 4.95. The brain slices were observed under white light and using the appropriate filters for each dye. In all cases, the signals from both filters colocalized (Figure 4.95a), both, inside the brain slices and without any tissue. Moreover, regarding the spectral profiles, there is a peak around 530

nm together with a peak around 630 nm (Figure 4.95c), which correspond respectively to green and red light (see Figure Ap.6 and Ap.7, appendix). These spectra profiles were not found in the regions where nanoparticles were not localized, thus confirming that the signals came from nanoparticles. Therefore, using this technique, the 8D3-nanoparticle functionalization by covalent binding was evidenced.
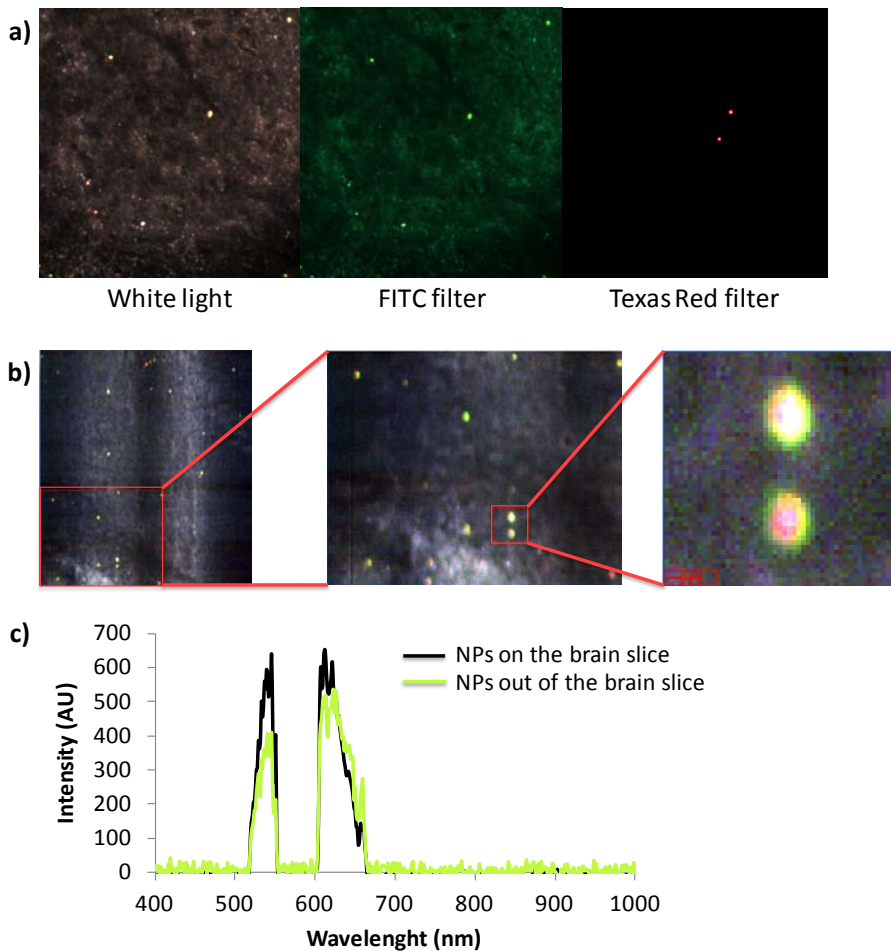
Figure 4.95: Study of the C6-loaded 8D3-functionalzied nanoparticles in brain slices, by means of optical microscopy with the Cytoviva technology coupled. a) Optical image visualized under different filters; b) Spectral image under white light and c) Spectral profiles of the nanoparticles.

4.5.4.2.3. Size exclusion chromatography studies

Size exclusion chromatography (SEC) was also used to further confirm nanoparticle – 8D3 antibody covalent binding. This technique enables the determination of the molar mass of the tested compounds (Rebolj, 2012). In principle, with this technique, samples appear like peaks, each peak representing a compound of the sample, with a longer retention time if they have smaller molecular weight. The SEC columns are filled with inert polymers, in order to avoid their interaction with the samples. However, in most cases, the molecular weight separation is difficult, since some interactions with the stationary phase usually occur (in the case of the present thesis with the residual carboxyl functionality of the stationary phase of the column filling) and the compound separation does not only depend on the molecular weight but also on the solvation layer (the hydrodynamic size), which is related with the 3D conformational shape of the compound (Rebolj, 2012). For example, filamentous compounds tend to have shorter retention times than spheres, because their solvation layer is bigger and they behave like bigger compounds (Rebolj, 2012). Therefore, some authors stated that SEC separates compounds by their hydrodynamic sizes instead of molecular weights (Rebolj, 2012). For this reason, in the present thesis, SEC results were not studied regarding the retention time; other parameters were taken into account.

The absorption spectra of each sample were regarded to determine the maximum wavelength of each compound (Figures Ap.9 and Ap.10, appendix). Since the analyzed compounds showed a maximum of absorption at different wavelengths, the chromatograms were studied at different wavelengths. Moreover, the contour plots (the plots indicating the intensity of the absorption of each compound as a function of wavelength and time) were also taken into account to select the chromatograms to be studied. Their differential shape between samples is an indication of the different nature of the samples.

Non-functionalized nanoparticles, commercial 8D3 antibody and 8D3-functionalized nanoparticles were studied at 50/1 NP/8D3 molar ratio. Figure 4.96 shows the corresponding contour plots. The contour plots of each sample show a different shape, thus indicating a differential absorption profile. This is a first indication of the different nature of each sample, which is, in turn, an indication of nanoparticle functionalization, since 8D3-functionalized nanoparticles show a contour plot that differs from those of both raw materials.

213
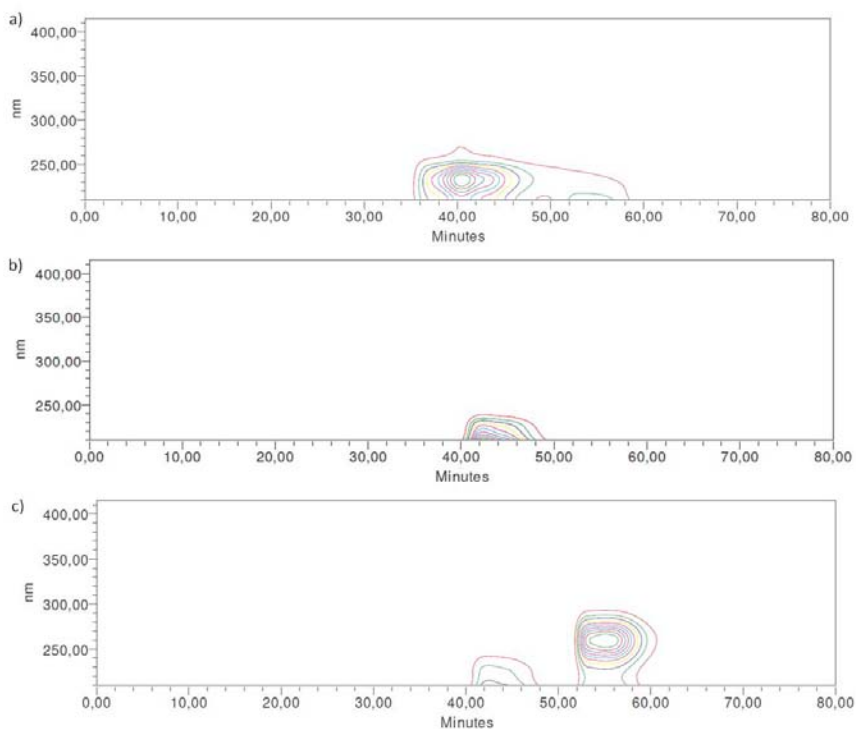
Figure 4.96: Contour plots of: a) NP; b) 8D3 antibody; c) 8D3-functionalized NP.

Figure 4.97 shows the chromatograms of each compound at their maximum absorption wavelength. Nanoparticles present a peak around 40 min, with their maximum absorption at 234nm (Figure 4.97a), as expected, due to the presence of ester groups (Catiker, 2000). This peak is wide, with surrounding background, which was attributed to the presence of more than one component in nanoparticles (e.g. PLGA and surfactant). 8D3 antibody gave a peak around 42 min, having the maximum absorption around 278nm (Figure 4.97b). 8D3-functionalized nanoparticles present a marked retardation of the peak, around 55 min, with the maximum absorption around 260nm (Figure 4.97c). The 8D3-functionalized nanoparticles absorb at a different wavelength and they have a different retention time than both components separately, thus indicating the functionalization of the nanoparticles. Since the antibody has a bigger molecular weight, a shorter retention time was expected, therefore, interactions of the complexes with the column cannot be ruled out, as previously discussed.
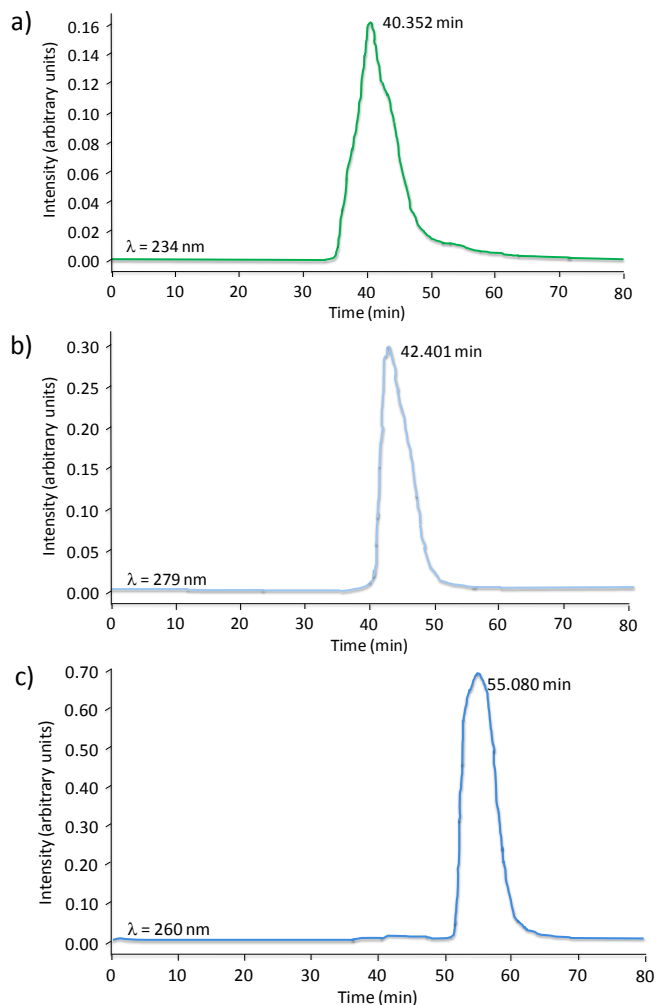
Figure 4.97: SEC chromatogram of the: a) Nanoparticles at 234 nm; b) 8D3 antibody at 279 nm; c) 8D3-functionalized nanoparticles at 260 nm.

Additional studies were performed at different NP/8D3 ratios (50/1, 25/1 and 12.5/1) to identify if the NP/8D3 ratio was appropriate. The shape of the contour plots is independent on the NP/8D3 ratio (Figure 4.96c and Figure Ap.11, appendix), thus indicating the same nature of the sample; which could be attributed to a nanoparticle functionalization in all the ratios studied. Chromatograms were studied at the three wavelengths where each compound showed a maximum (Figure 4.98 260nm; Figure Ap.12 234nm and Figure Ap.13 279nm, appendix). A peak at around 50 – 55 min appears independently of the wavelength, which corresponds to the peak of the 8D3-functionalized nanoparticles. At 234 nm, however, another peak appears at around 40 – 42 min

for the three molar ratios studied (Figure Ap.12, appendix), which was firstly attributed to an excess of non-functionalized nanoparticles. However, when reducing the NP/8D3 ratio (reduction of the nanoparticles amount), this peak does not seem to be reduced, thus not enabling confirmation of the nanoparticle excess (Figure Ap.12, appendix). At 279 nm, it also appears a slight peak at around 40 – 42 nm (Figure Ap.13, appendix). This peak could be also attributed to an excess of nanoparticles, since nanoparticles also absorb at this wavelength. From the above results, it can be concluded that, although there is an excess of nanoparticles remaining non-functionalized, 8D3-nanoparticle functionalization has been successfully achieved.
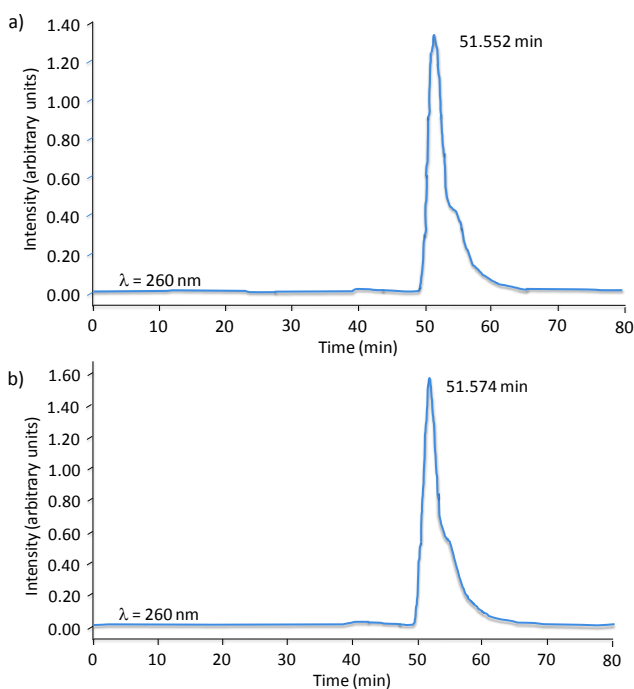
Figure 4.98: SEC chromatogram of the NP/8D3 complexes at 260 nm with a NP/8D3 ratio of: a) 25/1 and b) 12.5/1.

To further study the 8D3 covalent attachment to nanoparticles, samples with fluorescent dyes were studied. For <u>Coumarin 6-loaded nanoparticles</u>, the elution chromatogram was recorded at 234 nm. A peak at around 35 – 40 min was observed (Figure 4.99a), as for non-loaded nanoparticles. These nanoparticles, functionalized with the 8D3 antibody were also studied. A peak at around 50 – 55 min, with its maximum absorption at 260 nm was observed (Figure 4.99b). In addition, a slight peak was observed at around 40 min, at 234 nm (Figure Ap.14,

appendix), as for non-loaded nanoparticles, attributed to an excess of nanoparticles. Therefore, the encapsulated fluorescent did not vary nanoparticle elution chromatograms, confirming the covalent binding of the 8D3 antibody even with the presence of an encapsulated compound.

To further clarify the results, a physical mixture between C6-loaded nanoparticles and 8D3 antibody was studied. In this case, a double peak at around 40 min appeared at the three wavelengths studied (Figure 4.99c shows the chromatogram at 260nm and Figure Ap.15, appendix, shows the chromatogram at 234 and 278 nm), which could be attributed to the presence of nanoparticles and 8D3 separately. It clearly differs from the chromatogram of functionalized nanoparticles (Figure 4.99b).

It is worth noting that a peak around 65 min appeared in some chromatograms (e.g. 4.99b), which was attributed to the salts of the PBS dispersion media, that have a slight adsorption around 260 nm.
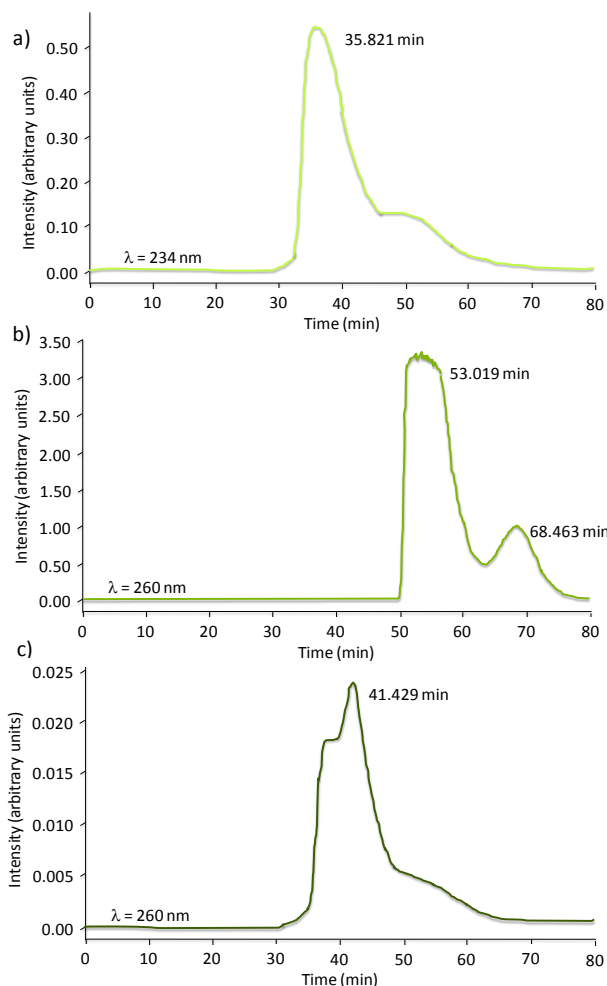
Figure 4.99: SEC chromatogram of the: a) C6-encapsulated NPs at 234 nm; b) C6-encapsulated NP/8D3 complexes at 260 nm with a NP/8D3 ratio of 12.5/1 and b) a physical mixture of C6-encapsulated NPs and the 8D3 at 260 nm at a NP/8D3 ratio of 12.5/1.

FITC-functionalized nanoparticles (FITC-NP), further functionalized with 8D3 antibody, were also studied. The FITC-NPs without the antibody resulted in a peak at around 38 – 40 min, with its maximum absorption at 234nm (Figure 4.100a), similar to that observed for nanoparticles without any fluorescent dye. When FITC-NPs were further functionalized with the 8D3 antibody, the peak was observed at around 55 min, with a maximum absorbance at 260 nm (Figure 4.100b). This result is also in good agreement with nanoparticles without any fluorescent dye. The physical mixture of FITC-NPs and the 8D3 antibody resulted in three peaks, at 40, 55 and 65 min, at 260nm (Figure 4.100c). The peak at 40 min was first attributed to the mixture of both components, since it is broader than previous peaks. However,

since the peak at 55min appeared also at 278nm but not at 234nm (Figure Ap.16, appendix), it was ascribed to the antibody. The delay in the antibody elution could be attributed to a change in its conformation. This chromatogram is clearly different than that that from 8D3-functionalized FITC-NPs (Figure 4.100b). Therefore, covalent 8D3 binding was confirmed. In addition, it was evidenced that prior FITC functionalization of the PLGA polymer did not prevent 8D3-nanoparticle functionalization. It is worth noting that the peak around 40 min, previously attributed to an excess of nanoparticles, was not found for FITC-NPs functionalized with 8D3 antibody at any wavelength (Figure 4.100b and Figure Ap.16, appendix) Since FITC was covalently bound to the carboxylic groups of the PLGA prior to nanoparticle formation, less carboxylic groups remain free for the further 8D3-functionalization of nanoparticles. Therefore, the selected NP/8D3 ratio (12.5/1) seems to be appropriate for the entire functionalization of the remaining PLGA carboxylic groups.
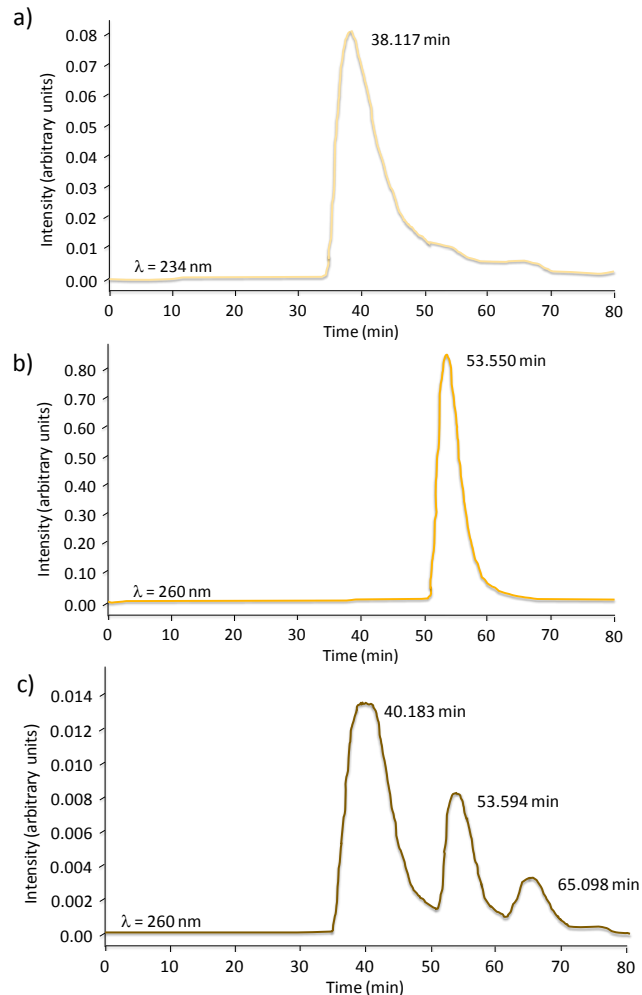
Figure 4.100: SEC chromatogram of the: a) FITC-NPs at 234 nm; b) FITC-NP/8D3 complexes at 260 nm with a NP/8D3 ratio of 12.5/1 and b) a physical mixture of the FITC-NPs and the 8D3 antibody at 260 nm at a NP/8D3 ratio of 12.5/1.

The elution fractions from FITC-8D3-functionalized nanoparticles were further studied by means of fluorescence spectra determinations. Figure 4.101 shows the fluorescent intensity as a function of the wavelength for each elution fraction. All samples showed some fluorescence with a peak around 510 nm, corresponding to the FITC emission wavelength. The maximum fluorescence intensity was observed from sample 27, which corresponds to the elution minute 54, where the peak of the functionalized nanoparticles was found. This is an indication not only of the 8D3-functionalization of nanoparticles, but also of the FITC-functionalization of the PLGA polymer.
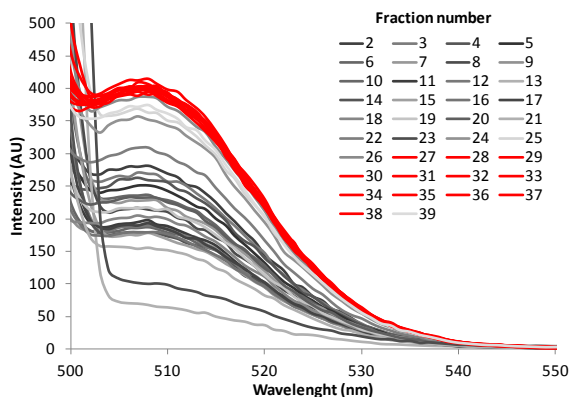
Figure 4.101: Fluorescence spectrum of each fraction obtained after the SEC experiment, for the sample of the FITC-8D3-functionalized nanoparticles at a NP/8D3 ratio of 12.5/1. Each sample represents the recollection of two minutes of the eluted mobile phase. Red lines correspond to the samples with the maximum fluorescence detected.

<u>Summarizing all the SEC study</u>, it is worth noting that the peaks (mainly those corresponding to nanoparticles) have surrounding background, which could be due to the presence of more than one substance for each peak; for example, PLGA and the surfactant. In addition, in most chromatograms, a late slight peak appears at around 65 min, which was attribute to the salts present in the mobile phase (electrolyte solution at 0.16M), which have a slight absorbance at these wavelengths.

<u>Summarizing the whole study of the 8D3-functionalization</u>, its covalent binding was confirmed, since both dyes (red from antibody and green from nanoparticles) colocalized in spectral optical microscopy analyses and the elution pattern clearly changed after the functionalization (retention time and wavelength of the elution peak). Comparing the covalent binding between the antibody and the nanoparticles with other types of attachments, it is not only advantageous due to the enhanced stability (Ulbrich, 2009), but also because it is performed without spacers or other intermediate elements. In addition, it is advantageous in terms of procedure simplicity and reduction of the use of chemical components (Byrne, 2008). The antibody conjugation after the nanoparticle formation is also advantageous as compared with prior covalent binding, as the antibody stability and conformation are maintained due to the avoidance of its contact with organic solvents (Tosi, 2013).

Summary

Nanoparticles have been successfully functionalized with a fluorescent dye, FITC, enabling their use as imaging agents. In addition, nanoparticles surface cationization has been achieved by covalent binding of cationic dendrons. The aim of the functionalization was to achieve nanoparticles suitable as non-viral gene delivery vectors. Therefore, their further functionalization with different kinds of gene material was performed and has also been achieved. The appropriate N/P ratios between NP/dendrons and dendronized-NP/oligonucleotides were determined.

Non-loaded, Coumarin 6-loaded and FITC-functionalized nanoparticles have been successfully functionalized by the covalent binding of 8D3 monoclonal antibody, with the aim to actively target the BBB. Therefore, 8D3-functionalized nanoparticles could be promising delivery systems crossing the BBB.

4.6. *In vitro* studies

In this section, in vitro studies of the designed nanoparticles to assess their possible use as therapeutic nanodevices is described. First, a complete study of nanoparticle toxicity will be described, including cytotoxicity and hemolytic studies. It will be followed by the results on gene transfection, which has been studied for all the gene material (referred in the previous section: ASOs, siRNA and plasmids) attached to nanoparticle surface. Finally, a wide characterization of nanoparticle interaction with blood components will be described, including a coagulation study, interaction of nanoparticles with two model proteins and the activation of the complement system.

4.6.1.Cytotoxicity assays

To test the cytotoxicity of nanoparticles is of utmost interest to assess their application in the biomedical field. In current bibliography, there is a lack of systematic cytotoxicity studies of polymeric nanoparticles, not enabling their use for industrial applications yet (Voigt, 2014(1)).

In the vast majority of studies, the cytotoxicity is performed *in vitro* (Hansen, 1989; Putnam, 2001; Lewinsky, 2007), knowing that it represents a first approximation. Generally, it is retested (performing experiments with animals) to test, for example, the cumulative effect of the complexes produced by repeated administrations (Kreuter, 2014).

It is worth mentioning that the cytotoxicity has been performed in the present study with the as-prepared nanoparticles in most cases (NPs non-loaded, C6-loaded, LOP-loaded or GAL-loaded; non-functionalized, G2SN-functionalized, G3SN-functionalized, without or with the ASO or 8D3-functionalized), without a previous cleaning step of the surfactant. Previous bibliography reported the need of nanoparticle cleaning to achieve non-cytotoxic systems (Gulyaev, 1999). The possibility to avoid this step is advantageous in terms of preparation time and cost efficiency.

Among the different tests to assess the cytotoxicity, the most widely used (not only for the assays with nanomaterials), is the <u>colorimetric MTT assay</u>, which measures the cell viability by the determination of its mitochondrial activity (Hansen, 1989; Lewinski, 2007). For this reason, it was used in this study. It is worth noting the importance of performing different cytotoxicity assays, since they measure different metabolic functions that could be affected by nanoparticles in a different

way. Therefore, although the MTT assay is more sensitive than the LDH assay (which measure the integrity of the cell membrane), measurement of LDH is also important (Fotakis, 2006; Gonzalo, 2010).Most of the cytotoxicity tests were performed in HeLa cells, although some test were also performed in U87 cells.

The cytotoxicity of the complexes formulated with nanoparticles, the dendrons and oligonucleotides was first studied in HeLa cells at different concentrations (equivalent concentrations of ASO), since the toxicity was described to depend on the concentration (Müller, 1996; Singh, 2013). The N/P (NP/ASO) charge ratio tested was 0.75/1 and 1/1 for G2SN and G3SN-dendronized nanoparticles respectively. The results (Figure 4.102) showed high viabilities (>80%) for almost all the samples tested, without a clear dependency on the complex concentration or the components of the complex tested. However, for the G3SN dendron, a slight tendency to a viability decrease was observed when the complex concentration is increased. At the highest concentration tested (300nM), the viability values are slightly below 80%, suggesting a slight toxicity for the complexes with the G3SN dendron at high concentrations. This result is an indication that this complex is not as appropriate as the G2SN complex regarding toxicity issues.
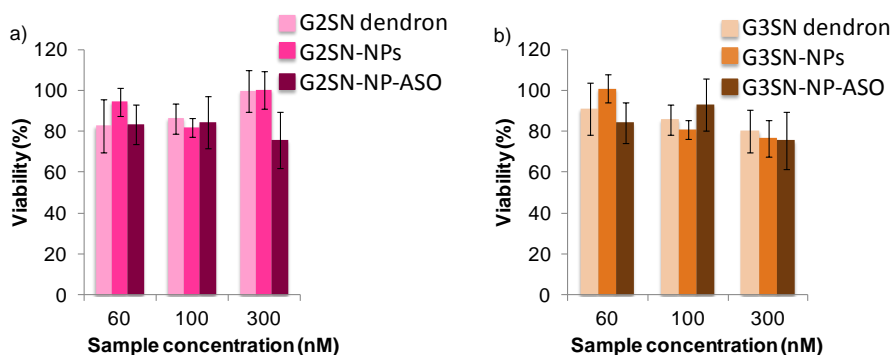
Figure 4.102: Viability (%) of the HeLa cell line, by means of the MTT test, as a function of sample equivalent oligonucleotide concentration (nM) after cell incubation with different samples for the studies with: a) G2SN dendron and b) G3SN dendron.

These results agree with previous bibliography, in which it was pointed out that the higher the dendron generation, the higher the cytotoxicity (Bermejo, 2007; Svenson, 2009; Karolckzak, 2012; Li, 2014). Previous studies by *Jiménez et al.* (Jiménez, 2010) showed that these carbosilane dendrons were non-toxic up to a concentration of 24 μg/mL in an astrocytoma cell culture (Jiménez, 2010). In the present work, the maximum concentration of dendrons tested was around 40μg/mL. This higher concentration than those reported in the study by *Jiménez et*

al. could be the cause of the slight cytotoxicity values found for the G3SN dendronized complexes.

To further confirm the non-cytotoxicity of these complexes, <u>LDH assays</u> were performed to measure the integrity of the cell membrane. As Figure 4.103 shows, most of the samples also showed non-cytotoxic effects on HeLa cells. However, the third generation dendron produced a marked cytotoxicity at the highest tested concentration, thus confirming that the higher the dendron generation, the higher the cytotoxicity (Bermejo, 2007; Svenson, 2009; Karolckzak, 2012; Li, 2014). Moreover, this result is in good agreement with previous bibliography using dendrons with the same structural composition, in which the cytotoxicity of dendritic structures was decreased when they were complexed with other components due to the reduction of the cationic charges of the dendron (Weber, 2009).
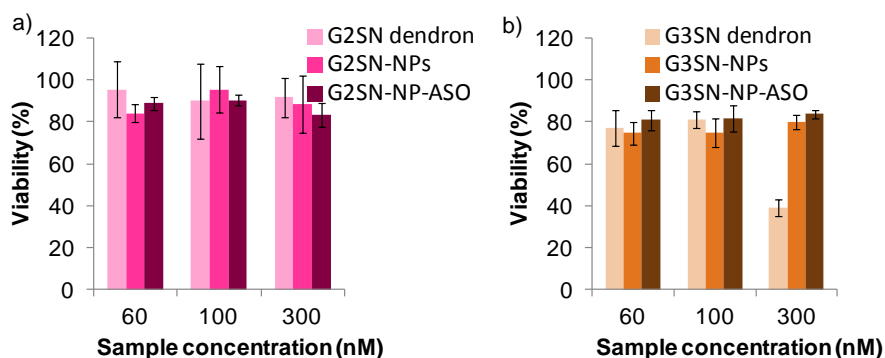
Figure 4.103: Viability (%) of the HeLa cell line, by means of the LDH test, as a function of sample equivalent oligonucleotide concentration (nM) after cell incubation with different samples for the studies with: a) G2SN dendron and b) G3SN dendron.

MTT and LDH assays were performed in <u>U87 cells</u> ([ASO] = 300nM) to further assess the complexes non-cytotoxicity. As Figure 4.104 shows, all viabilities were higher than 80%, therefore, nanoparticles were non toxic for U87 cell line. Although previous bibliography indicated that toxicity is dependent on the cell line (Fotakis, 2006), the results of U87 cells are in close agreement with HeLa cells.
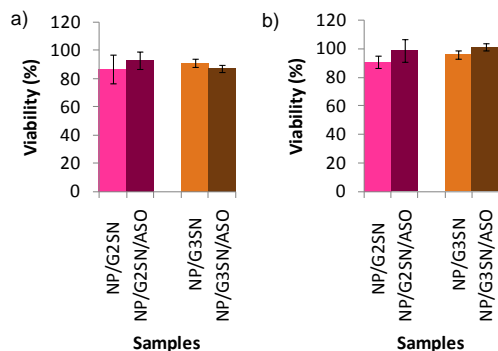
Figure 4.104: Viability of U87 cells after the incubation (300nM ASO) with multifunctionalized nanoparticles by means of the: a) MTT test and b) LDH test.

The cytotoxicity of the as-prepared nanoparticles, loaded with loperamide, galanthamine and coumarin 6, as well as of antibody-functionalized nanoparticles was also tested in HeLa cells to study the influence of the encapsulated / functionalizing compounds. The results of the MTT assay are shown in Figure 4.105. At the concentration of use, all tested samples showed high cell viabilities (>80%), thus indicating that neither the encapsulated compounds, nor the functionalization elements affected cell viability. It is worth noting that nanoparticle concentrations for these experiments are markedly higher than those used when working with oligonucleotides, because oligonucleotides produce therapeutic effects at lower equivalent doses. Since nanoparticle concentration was increased, cytotoxicity issues could appear. However, none of the formulated samples produced toxicity to HeLa cell cultures, therefore, they could be used for biomedical applications at the tested concentrations.
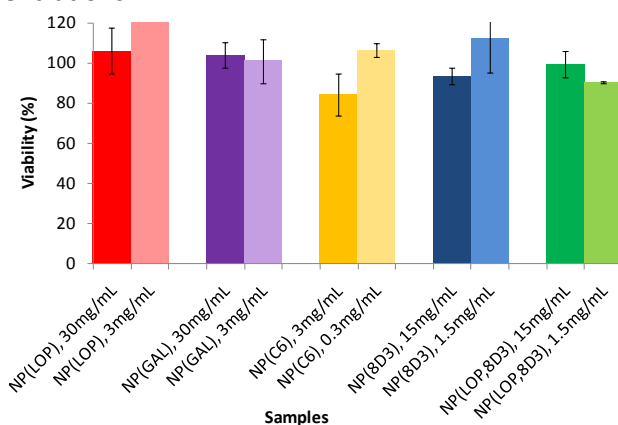
Figure 4.105: Viability (%) of nanoparticles with different encapsulations / functionalizations, at the PLGA concentration of use, assessed by the MTT test.

The transfection efficiency of a lentiviral plasmid was studied in HEK and U87 cell lines. Since the cytotoxicity has been described to depend on the cell line, as indicated above, (Singh, 2013; Geys, 2008; Ryman-Ramsmussen, 2007), the cytotoxicity of the complexes formulated with the plasmid was studied in these cell lines, by means of the MTT test. Since G2SN dendrons showed better biocompatibilities than G3SN dendrons (Figures 4.102 – 4.104), only the complexes with the G2SN dendron, with two N/P (NP/plasmid) molar ratios were studied, at an equivalent plasmid concentration of 0.31nM (1.67mg/mL), without and with a PEG coating. It is worth noting that the equivalent plasmid molar concentration, as compared with ASO and siRNA concentrations (60 – 300nM), is about two orders of magnitude lower, which is due to the higher molecular weight of this construction as compared with ASO and siRNA. The results (Figure 4.106) showed high viabilities (>80%) for most of the tested samples in both cell lines, which is in good agreement with previous experiments. Moreover, the PEGylation of these complexes does not vary their cytotoxicity. Thus, the complexes formed with plasmids are non-toxic for these cell lines up to the concentrations studied.
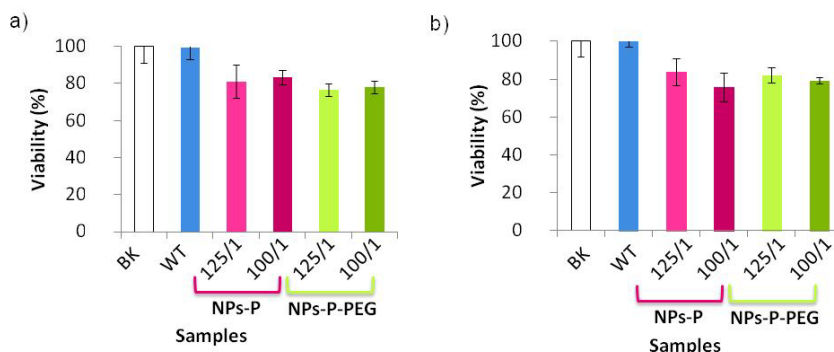
Figure 4.106: Viability of the a) HEK cell line and b) U87 cell line, by menas of the MTT test, as a function of N/P ratio after cell incubation with different samples formulated with the NPs-G2SN conjugated with the lentiviral vector, at a concentration of 0.31nM (1.67mg/L).

The cytotoxicity results obtained with different tests are in good agreement with previous studies, which described G2SN dendrons to be non-toxic up to a concentration of 50μM, clearly higher than the concentrations used in this study (dendron concentration = 25 μM), with an increasing toxicity when increasing the dendron generation; (Bermejo, 2007; Chonco, 2007). Moreover, gene constructions have been widely defined to be non-toxic, therefore, the addition of genes to the complexes was expected not to modify the toxicity, as obtained (Bermejo, 2007). Indeed, the results confirmed the expectations. Concerning PLGA concentration, in the present work, the maximum PLGA concentration is around 13 μg/mL. Since

previous studies reported experiments in cell cultures at higher PLGA concentrations, without any cytotoxicity, the biocompatibility of this component was already expected (Alshamsan, 2010). Therefore, these results confirmed that the as-prepared polymeric nanoparticles are safe, ensuring its feasibility for further application as CNS-targeting novel advanced delivery systems.

4.6.2. Nanoparticle transfection into cells

Nanoparticle transfection into cells was studied by means of the Dual Luciferase Assay, as reported in Section 3.2.15, in HeLa cells, with the complexes formulated with both dendrons and binding ASO or siRNA as the gene silenciators. The results are presented as normalized luciferase activity of each sample. Since a silencing of this gene was expected if the complexes work properly, the expected results for the samples transfecting cells will be those with the lower luciferase activities.

4.6.2.1. Antisense oligonucleotides (ASO)

First, transfection efficiency was studied with a culture medium <u>without Fetal Bovine Serum</u> (FBS), to test the optimum N/P <u>(NP/ASO) charge ratio</u>, at an ASO concentration of 30nM. As Figure 4.107 shows, transfection efficiencies achieved values up to 20%. For the G2SN dendron, the worst results were obtained with a N/P ratio of 0.5/1, while for the G3SN dendron, the worst results were obtained with a N/P ratio of 5/1. For this reason, both N/P ratios were ruled out.
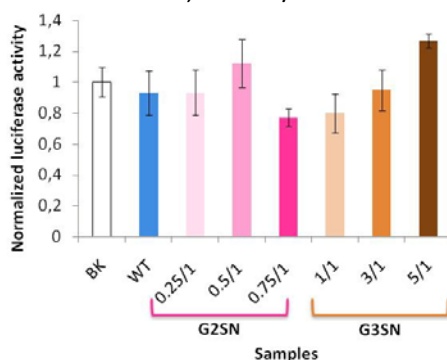
Figure 4.107: Normalized luciferase activity as a function of sample composition, at a concentration of ASO of 30nM; without the presence of FBS in the culture medium, for a HeLa cell culture. Transfection experiments were performed in triplicate and at least two independent experiments were carried out.

Once N/P appropriate ratios were selected, the transfection efficiency was tested at <u>higher concentration</u> (60nM of ASO) without FBS. Figure 4.108 shows that higher transfection efficiencies were achieved, up to 60%, for the complex formed with the G2SN dendron at a N/P ratio of 0.75/1. G3SN dendron was ruled out for further transfection studies due to its cytotoxicity. Therefore, G2SN complex was selected for further studies. It is worth noting that the enhanced transfection efficiencies using the G2SN dendron could be due to the formation of complexes with appropriate sizes to transfect cells (around 90 nm, Figure 4.84 from Section 4.5), as indicated in previous literature (where the best sizes for transfection were reported to be around 100nm) (Jiang, 2013(2)).
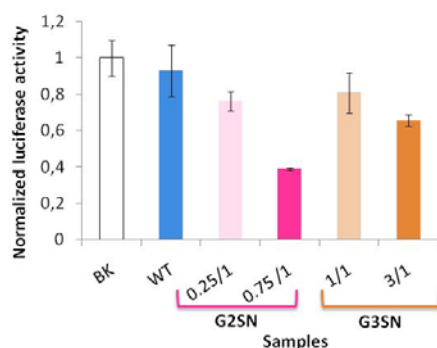
Figure 4.108: Normalized luciferase activity as a function of sample composition, at an ASO concentration of 60nM; without the presence of FBS in the culture medium, for a HeLa cell culture. Transfection experiments were performed in triplicate and at least two independent experiments were carried out.

Transfection studies were then performed <u>with 10wt% of FBS</u> in the culture medium, to simulate physiological conditions, although it difficults the transfection due to the adsorption of serum proteins onto nanoparticles surface (Lee, 2002). The results were not as promising as expected, since, independently of the complex concentration, transfection efficiencies up to 20% were achieved (Figure 4.109, pink bars). The decreased transfection efficiencies could be due to a disruption of the complexes caused by the displacement of the ASO by the negatively charged serum proteins, as previously reported for complexes with lipids (Mansouri, 2004). When the complexes were **coated with PEG**, a protection of the ASO occurred, as well as a stealth effect to avoid their opsonization, thus resulting in better transfection efficiencies, from 40 – 90% (Figure 4.109, green bars), as previously reported in other studies (Owens III, 2006; Chen, 2011). Increasing the ASO concentration, the transfection efficiency for the PEGylated complexes increased, achieving transfection efficiencies up to nearly 90% (ASO = 200-300nM), which

indicates that the formulated complexes are promising candidates as non-viral gene delivery vectors.
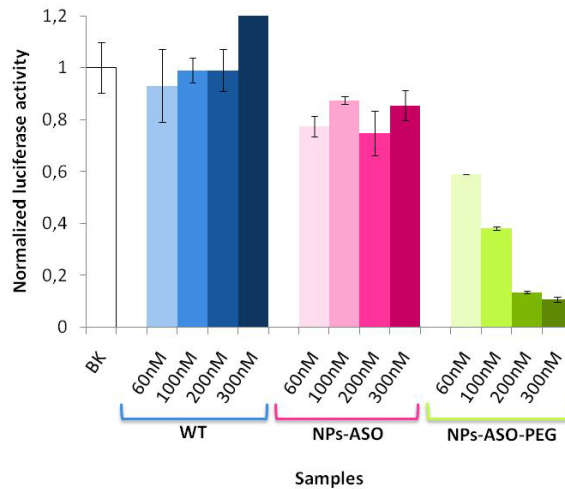
Figure 4.109: Normalized luciferase activity as a function of sample composition and ASO concentration, at a NP/ASO ratio of 0.75/1 for the samples prepared with the G2SN dendron; with the presence of 10wt % FBS in the culture medium, for a HeLa cell culture. Transfection experiments were performed in triplicate and at least two independent experiments were carried out.

It is worth remarking that commercially available transfection vectors, such as Lipofectamine 2000®, as well as the use of viral vectors, such as adenoassociated virus, allow for high transfection efficiencies (Fisher, 1997; Dalby, 2004). The strategy proposed in the present work is advantageous, since it enables transfection efficiencies as high as those of the commercially available transfection vectors, without the toxicity problems related with commercial lipid vectors (e.g. inflammatory lung reactions or cell membrane disruption) and the immune responses related with the viral vectors (Bermejo, 2007). Moreover, as compared with previous studies, the transfection efficiencies achieved in the present work are markedly higher (Bielinska, 1996; Bermejo, 2007). The study of *Bielinska et al.,* (Bielinska, 1996), for example, used PAMAM dendrimers as non-viral vectors, achieving transfection efficiencies of around 25 – 50%. In addition, in their study, an increase on the oligonucleotide concentration was required due to the inability of the vector to enhance the cell transfection. In our work, with reduced oligonucleotide concentrations (200nM), higher transfection efficiencies were achieved.

4.6.2.2. Small interference ribonucleic acid (siRNA)

Transfection efficiency was also studied for the complexes formulated with siRNA – G2SN dendron – NPs, directly with HeLa cells containing 10wt% FBS, at a N/P ratio of 0.75/1. The transfection efficiency was studied as a function of siRNA concentration. These experiments were carried out only for PEGylated complexes, since siRNA are molecules very sensitive to the nuclease attack; therefore, the PEGylation was required for their protection, as previously reported (Weber, 2008). The transfection efficiency (Figure 4.110) improved by increasing the siRNA concentration, from efficiencies around 50% at 60nM to around 70% at 200nM. However, further increase of siRNA concentration (300nM) resulted in nearly null transfection efficiencies. Therefore, the siRNA results were not as good as those for ASO transfection. The lower siRNA transfection efficiencies as compared with ASO results (Figure 4.109) could be related to the lower stability of the complexes. As described in Section 4.5.3.2 (Figure 4.88 and 4.93), the stability of siRNA PEGylated complexes is less than 24 hours and they are bigger (size increase from 150 nm to 1200 nm). Therefore, the lower transfection efficiencies could be caused by sizes higher than those appropriate to cell penetration or due to instability. Since the transfection efficiency was studied for 24 hours, during the last hours, complexes would have changed their size. One consequence of the instability could be the siRNAs detachment from nanoparticles, not enabling the enhancement of the transfection efficiency found for nanoparticles in the case of ASOs. This effect is especially present at high siRNA concentrations (300nM). Further studies on siRNA complexes should include an increase on the PEG concentration with the aim to enhance siRNA protection. Nevertheless, it is worth noting that transfection efficiency found at 200 nM is higher than those reported previously for siRNA-dendron complexes (Jimenez, 2010). Therefore, nanoparticle complexes formulated in the present work could also be promising non-viral vectors for the siRNA delivery into cells.
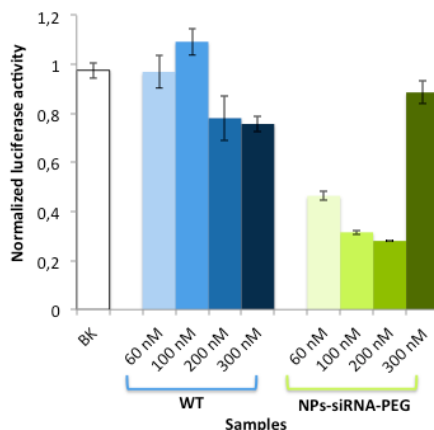
Figure 4.110: Normalized luciferase activity as a function of siRNA concentration, at a NP/siRNA ratio of 0.75/1 for the samples prepared with the G2SN dendron; with the presence of 10wt % FBS in the culture medium, in HeLa cells. Transfection experiments were performed in triplicate and at least two independent experiments were carried out.

4.6.2.3. Lentiviral plasmid vectors

The transfection efficiency of the complexes formulated with the <u>lentiviral plasmid</u> (NP/G2SN ratio = 0.75/1) was also studied as a function of the NP/P molar ratio without and with PEGylation. HEK cell line was used and the transfection efficiency was studied by means of fluorescence enhancement produced by the lentiviral plasmid vector. Therefore, the higher the normalized fluorescence, the higher the transfection efficiency (Figure 4.111 is an example).
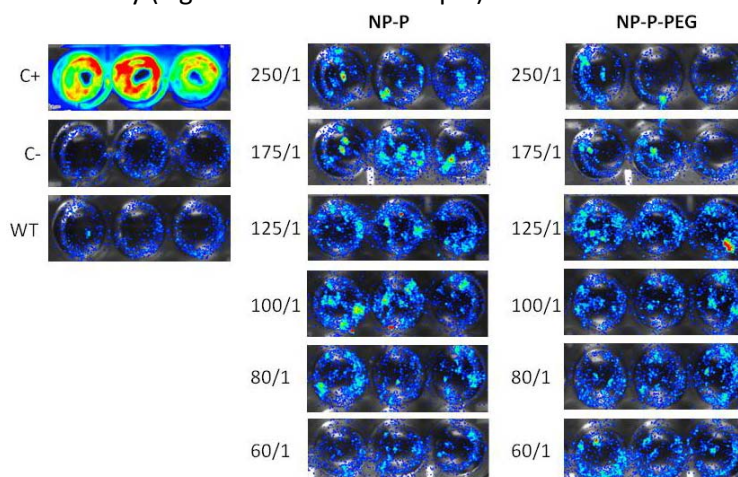
Figure 4.111: Example of the fluorescence of the plasmid incubated in the HEK cell line, as a function of the NP/Plasmid molar ratio.

Figure 4.112 shows a transfection efficiency dependence on the NP/P ratio as well as on the presence of the PEG coating. The best transfection efficiencies were achieved for the 125/1 and 100/1 NP/P ratios for the non-coated complexes and 125/1 NP/P ratio for the PEGylated complexes. Therefore, the 125/1 NP/P ratio was chosen as the best ratio, achieving transfection efficiencies around 75% without the coating and nearly 90% for the PEGylated complexes. These results confirm that the PEG coating enhances transfection efficiencies, maybe due to the protection of genes and that cationized nanoparticles could be appropriate non-viral gene delivery systems also for the transfection of lentiviral plasmids.

Comparing these results with previous bibliography using the same plasmid with other vectors (e.g. lentivirus), lower transfection efficiencies were reported (60-70%) (Ray, 2004). Therefore, the system proposed in the present thesis is advantageous.
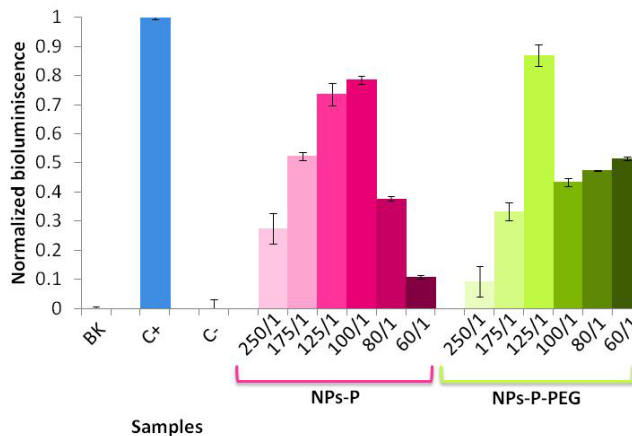
Figure 4.112: Normalized bioluminescence activity as a function of the N/P ratio for the samples functionalized with the G2SN dendron, at a lentiviral plasmid concentration of 1ug of plasmid with the HEK cell line.

High transfection efficiencies achieved using nanoparticles as non-viral gene delivery systems could be attributed to the nanometric size of the complexes (around or below 100nm), in accordance with previous studies that reported an enhancement of the transfection efficiency for the smallest nanoparticles (Costantino, 2006; Tosi, 2013).

However, in the present work, although the PEG-coated nanoparticles have a negative surface, as previously described, they have relatively high transfection efficiency. This could be explained by different mechanisms. The PEG coating could act as a DNA protection from the nuclease hydrolysis, thus enabling an enhanced stability of the gene material due to a reduction of its interaction with biological

components (Wattiaux, 2000; Chonco, 2007). The enhanced transfection could be also due to the use of another pathway to penetrate the cells. Since these nanoparticles have smaller sizes than those reported in the above mentioned studies, they could penetrate cells due to caveole-mediated endocytosis. The cell penetration of nanoparticles depends, among others, on the nanoparticle size (Verma, 2009).

4.6.3. Interaction of NPs with blood constituents

The intravenous route of administration was selected in this work as a compromise between its reduced invasiveness (as compared with the intracranial route) and the easier pathway that nanoparticles have to follow to reach the BBB (as compared for example with the oral route) (Kreuter, 1991). After intravenous injection, once nanoparticles are in the bloodstream, they interact with blood plasma proteins (depending on their nature), a process known as opsonization (Vauthier, 2009(2)). It is worth noting the importance of studying the protein interaction with nanoparticles, since it will determine the nanoparticle biodistribution (Gelperina, 2010). If an interaction with the machophage membranes is produced, nanoparticles would be cleared up by the reticuloendothelial system (RES) and they would reach only to the liver and spleen (Neha, 2013). Low binding protein capacity nanoparticles activate less the complement system, thus increasing their circulation time in the bloodstream (Vauthier, 2009(2)). The protein binding onto nanoparticles depends mainly on the surface composition (Tosi, 2013). For this reason, it is very important to study the interaction of formulated nanoparticles with blood components. *Dobrovolskaia et al.,* according to remarked the International Recognized Standard ISO-10993, remarked specifically the importance of studying: 1) the activation of the complement system, 2) the influence of nanoparticles on the coagulation cascade and 3) the hemolysis produced (Dobrovolskaia, 2008 and 2013). These aspects were studied in the present work.

4.6.3.1. Influence of serum on nanoparticles

The influence of fetal bovine serum (FBS) on nanoparticles physico-chemical properties was studied by means of differential scanning calorimetry (DSC), since previous reports demonstrated that the adsorption of FBS proteins onto nanoparticle surface modifies nanoparticles characteristics detectable by DSC (Dobrovolskaia, 2013). Using this technique, the transition glass temperature (T_g) of NP-0.16E70 nanoparticles (prepared from nano-emulsions with 90wt% PBS 0.16M and 70/30 O/S ratio) and that of these nanoparticles incubated with 10wt% of FBS was studied. For NP-0.16E70 nanoparticles, without serum, the T_g is around 44ºC both, measured during the first heating and the second heating runs (Figure 4.113a). This value is in close agreement with the T_g found for PLGA powder (Figure 4.2), thus confirming the PLGA nature of nanoparticles. In contrast, after the incubation of NP-0.16E70 nanoparticles with 10wt % of serum, the T_g values shift from the first heating run (around 44ºC) to the second heating run (around 41ºC) (Figure 4.113b). Therefore, an effect of the heating to the FBS incubated nanoparticles was evidenced. Since PLGA is not stable at high temperatures, during the first heating run, the polymeric nanoparticles powder melts and the results from the second heating round could not be attributed to the nanoparticles but to the materials present in the sample. For this reason, when serum is not present, the nanoparticle T_g does not depend on their physical state. But when they are incubated with 10wt% FBS, their T_g changes due to the presence of a mixture of proteins, that interacts different than before the PLGA melting. In addition, the temperature decrease could be an indication of the less stability of nanoparticles in serum conditions, which is in good agreement with previous results regarding the chemical stability of PLGA in different conditions (see Section 4.3). It is worth remarkable that the same experiment was carried out with PLGA powder, in absence or presence of 10wt % FBS. As described above (see Section 4.1), no changes were observed with the addition of serum (Figures 4.2 and Ap.1, appendix). These results confirmed that the shift of the T_g when nanoparticles were incubated with 10wt% FBS was due to a differential interaction depending on the physical PLGA state caused by the presence of proteins.
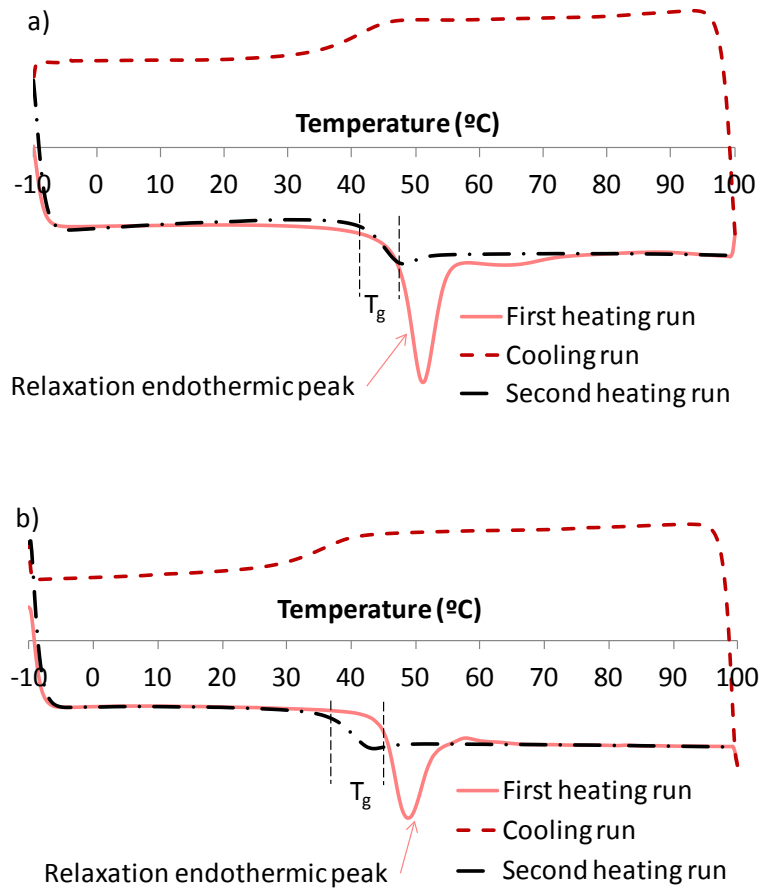
Figure 4.113: DSC profile of a) PLGA NPs, and b) PLGA NPs in presence of 10wt% of FBS: first heating, cooling and second heating runs, from -10ºC to 100ºC in steps of 10ºC/min.

4.6.3.2.   Interaction of nanoparticles with blood proteins

The adsorption of blood proteins onto nanoparticles surface (e.g. opsonization) is one of the first events that occurs *in vivo* when nanoparticles enter to the blood (Dobrovolskaia, 2013). Nanoparticles with low protein binding capacities are desired, since they would be weak activators of the complement system, thus enabling longer blood circulation times (Vauthier, 2009(2)). Moreover, the interaction protein pattern of a specific type of nanoparticles would influence its fate in the body (Bertholon, 2006; Dobrovolskaia, 2007; Kulkarni, 2013).

Prior to individual characterization of selected serum proteins, NP-0.16E70 nanoparticles interaction with the whole protein fraction of the blood (serum) was studied by means of a SDS-PAGE electrophoresis tests, as described in Section 3.2.16.1. After 24 hours of incubation with FBS, nanoparticles were cleaned to rule out the non-bound proteins and only adsorbed proteins were separated with the electrophoresis. Proteins are separated depending on their molecular weight (MW). Figure 4.114 shows the results concerning cleaned nanoparticles (pellet), the supernatant (SN) resulting from the cleaning step and the original serum used, at different concentrations. Only the first SN of the cleanings was studied since furthers cleanings did not contained proteins (see Figure Ap.17, appendix). The intensity of the bands for nanoparticles incubated with serum using 10 μg of sample is similar to that of the serum using 1 μg. Therefore, it could be hypothesized that the tenth part of the proteins are adsorbed onto nanoparticle surface. Therefore, most of proteins remain free, without attaching to nanoparticle surface. Regarding the bands individually, most of them were found in the three samples studied. The major band found for all samples is located at an equivalent molecular weight of around 65 kDa, which corresponds to the molecular weight of the albumin (around 64 kDa). Therefore, it indicates that the most abundant protein in the serum, both, free and attached, is the albumin, as expected (Vauthier, 2011).
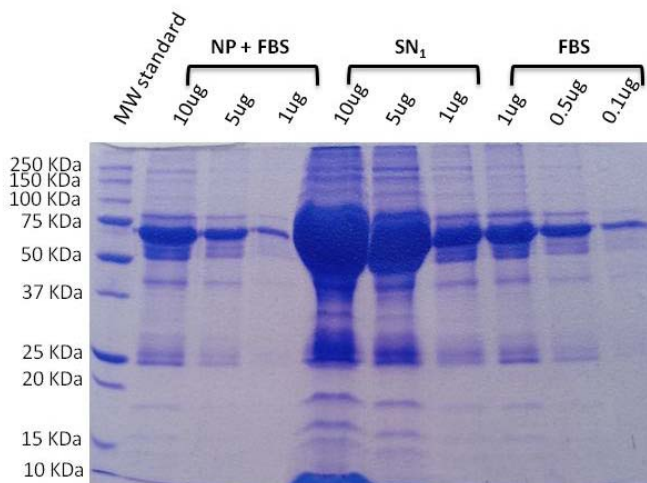
Figure 4.114: SDS-PAGE electrophoresis of the NP incubated with fetal bovine serum. NPs + FBS = cleaned nanoparticles, pellet. SN_1 = first supernatant. FBS = Fetal bovine serum.

However, some bands of the serum fractions were not found (or slightly present) in the cleaned nanoparticles (Figure 4.114). These bands have a molecular weight of around 150 kDa, 100 kDa and 15 kDa. Therefore, some proteins of the serum were

not adsorbed (or more slightly attached as compared with the other proteins) onto nanoparticles surface. Absent proteins could be predicted from their MW extrapolation from MW standards. Different proteins have similar molecular weights, thus, each absent band could be attributed to various proteins (Table 4.36). The non-attached proteins with a molecular weight around 150 kDa are probably Immunoglobulins G, since they are one of the most abundant proteins in the blood (Dobrovolskaia, 2013). However, absent spots at MW around 100 kDa and 15 kDa cannot be attributed to a single protein. Although immunoglobulins G adsorption onto nanoparticle surface was expected due to their high concentration, the lack of their adsorption was stricking. If they would not be adsorbed onto nanoparticle surface, nanoparticles would not be detected by the immune system; therefore, their blood circulation time would be enhanced, thus favoring nanoparticle arrival to their target organs (Dobrovolskaia, 2013).

Table 4.36: Hypothesized blood proteins for each absent band (corresponding to a molecular weight) in the electrophoresis of nanoparticles. Adapted from Sigma-Aldrich.

	Protein	MW (kDa)	Concentration in normal plasma (mg/100mL)
Around 150 kDa	Immunoglobulin G	150	800 - 1800
	Inter-α-tripsin inhibitor (α-globulin)	160	20 - 70
	C8 complement component	160	8
Around 100 kDa	C1 sterase inhibitor	104	15 - 35
	C6 complement component	105	7
	C2 complement component	102	2 - 3
	C-reactive protein (β-globulin)	105	< 1
Around 15 kDa	Lyzozim	14	0.5 – 1.5
	γ2-globulin	14	0.1

As indicated above, one of the most prevalent blood proteins is the human serum albumin (HSA); or bovine serum albumin (BSA) in the case of bovine animals ($\in$ 4 wt%). For this reason, it is expected to be one of the firsts proteins to attach to nanoparticle surface, as shown in Figure 4.114. Then, other proteins can be either attached throug the BSA on nanoparticles surface or attached directly to the

nanoparticles, displacing the BSA if they have more affinity for nanoparticles (Ehrenberg, 2009; Vauthier, 2009(2), Vauthier, 2011).

Previous studies reported that the protein corona formed by the adsorbed proteins depends on the physical characteristics of the nanoparticles (Gulati, 2013). In the present work, all nanoparticles were formulated using polysorbate 80 surfactant, advantageous due to its passive targeting to the BBB. Ethoxylated surfactants were reported to partially solve the problem of the rapid nanoparticle uptake by the RES, since they allow for a preferred adsorption of proteins with receptors overexpressed in the BBB, such as apolipoproteins; thus prolonging the nanoparticles blood half-life and directing nanoparticles to the BBB (Vauthier, 2009(2); Chen, 2011; Kreuter, 2013). Therefore, in this work, BSA adsorption onto nanoparticle surface was further studied with different techniques for NP-0.16E70 nanoparticles with different loadings / functionalizations.

First, **immunoelectrophoretic techniques** (rocket immunoelectrophore-sis and radial immunodiffusion) were assayed, since they have been widely used for the study of BSA interactions with nanoparticles (Mancini, 1965; Laurell, 1966; Vauthier, 2009(2) and 2011). However, they could not be used for the BSA – nanoparticle interaction determination of the present study (Fornaguera, 2014(3)). In the following, a brief description of the factors which prevent the use out of these methodologies is given. Figure 4.115 shown an example of a rocket immunoelectrophoresis (Figure 4.115a) and a radial immunodiffusion (Figure 4.115b), where the following samples were studied: 1) aqueous BSA standard solutions (C); 2) aqueous BSA standard solution with 3wt% of polysorbate 80 (the surfactant concentration contained in the template nano-emulsions for the preparation of NP-0.16E70 nanoparticles); 3) aqueous BSA standard solutions with 0.3wt% of polysorbate 80 (diluted 1/10 to represent the decrease of the surfactant content in the nanoparticles after the purification step); and 4) NP-0.16E70 purified with the aim to eliminate the maximum surfactant excess. Rocket immunoelectrophoretic (Figure 4.115a) consist in a migration of the proteins, in this case the BSA protein, through the opposite pole due to the presence of an electric field. Therefore, the higher the BSA concentration, the longer the height of the migration. Radial immunodiffusion, in contrast (Figure 4.115b) is based on the BSA diffusion through the agarose gel, forming circles around the charged well. Therefore, in this case, the bigger the ring diameter, the higher the BSA concentration. For the standard BSA solutions, BSA concentrations of 200, 100, 50 and 20 µg/mL were studied for rocket immunoelectrophoresis, while 200, 100 and 50 µg/mL were used for radial immunodiffusion. As expected, the height / ring

diameter of the migration increases as the concentration increases. Same BSA concentrations were studied for both aqueous solutions of polysorbate 80. In both cases and using both techniques, the direct relationship between the height / diameter of the migration and the BSA concentration were also found. However, comparing the migrations between the polysorbate solutions and the standard BSA solution, at a same BSA concentration, the migration peaks / rings are longer / bigger when the polysorbate is incorporated (Figure 4.115). It should be noted that nanoparticles were studied at BSA concentrations comparable to those of the standard solutions. In this case, only the non-adsorbed BSA onto nanoparticle surface migrates. The same phenomenon as that of polysorbate 80 aqueous solutions, even increased, was found for PLGA nanoparticles (which contain polysorbate 80). Therefore, the presence of polysorbate 80 in the samples influences the migration of the BSA protein. Since the migration / diffusion is proportional to the BSA concentration, it is impossible that for the same BSA concentration, a longer migration / bigger ring appears. For this reason, it was hypothesized that polysorbate 80 produces artifacts in the gels interfering with the BSA quantification as a higher BSA concentration is obtained. For this reason, when nanoparticles contain polysorbate 80, immunoelectrophoretic methods cannot be used.
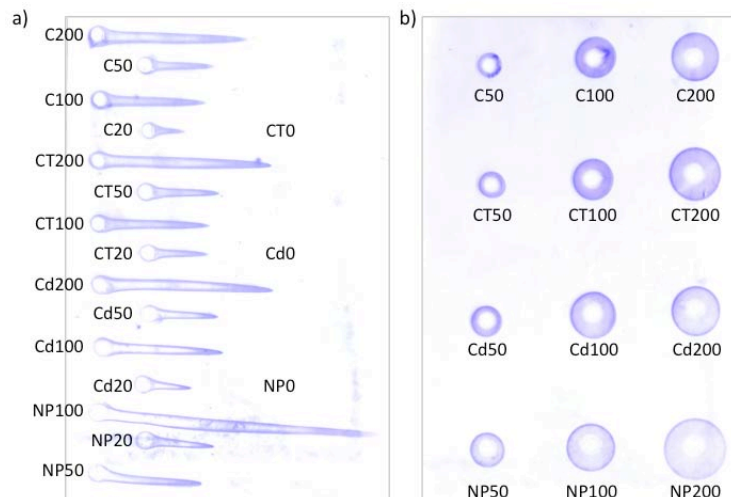
Figure 4.115: a) Rocket immunoelectrophoresis and b) Radial immunodiffusion gels obtained for the determination of the adsorption isotherm of BSA on the nanoparticles. The concentrations of BSA in reference BSA solutions (C), reference BSA solutions + polysorbate 80 at 3wt% (CT), reference BSA solutions + polysorbate 80 at 0.3wt% (Cd) and the nanoparticle dispersions (NP) are indicated in µg/mL.

Diverse alternatives for the study of BSA adsorption onto nanoparticle surface exist. Many are based in the spectroscopic determination of BSA concentration (Patil, 2007; Lynch, 2008). However, since polysorbate 80 also interferes on these measurements (e.g. it adsorbs in a wide range of UV/visible spectra) (Wuelfing, 2006), spectroscopic techniques cannot either be used for the studies of BSA adsorption. For this reason, another alternative found in the literature for other purposes using BSA proteins (Brewer, 2005) was tested: the measurement of the changes on the **surface charge** of the nanoparticles before and after its incubation with increasing concentrations of BSA. The concentrations of BSA was varied from 0 up to 40mg/mL, the blood BSA concentration (Vauthier, 2009(2)). Nanoparticle concentration was adjusted considering the same specific surface area, 1000 cm^2, for all samples. Since the protein adsorption takes place at the surface level, the same surface must be studied for comparative purposes (Vittaz, 1996). BSA is a negative-charged molecule, thus, when it is adsorbed onto nanoparticle surface, in most cases, the total surface charge decreases. Adsorption isotherms were plotted (e.g. Figure 4.116, see other examples of other nanoparticles in Figures Ap.18 to Ap.21, appendix) to define the concentration of BSA saturation onto nanoparticle surface. For non-functionalized nanoparticles, non-loaded or loaded with Coumarin 6, no changes in the surface charge were found after their incubation with BSA (see Figure Ap.18, appendix). To explain the absence of surface charge variation, two different argumentations could be hypothesized: a) ζ potential is not a good technique to measure the BSA adsorption onto the surface of these types of nanoparticles; or b) negligible amount of BSA molecules were adsorbed onto their surface. For other sets of nanoparticles studied (non-loaded and C6-loaded, but functionalized with 8D3 or G2SN or G3SN or LOP-loaded, either non-functionalized or functionalized with G2SN or G3SN) changes were found (Figure 4.116 and Figures Ap.19 to Ap.20, appendix). Therefore, surface charge measurement was a good alternative technique to study BSA adsorption for most of nanoparticles. As expected, BSA adsorption produced a decrease in the ζ potential of all dendron-functionalized nanoparticles (Figure 4.116 and Figures Ap.19 and Ap.20, appendix), from positive values at null and low BSA concentrations to slightly negative values at higher BSA concentrations. However, for non-functionalized and 8D3-functionalized nanoparticles, at null and low BSA concentrations, the ζ potential was highly negative, thus, by increasing the BSA concentration, the ζ potential increased, and, at high BSA concentrations, slightly negative values were obtained (Figures Ap.20 and Ap.21, appendix).
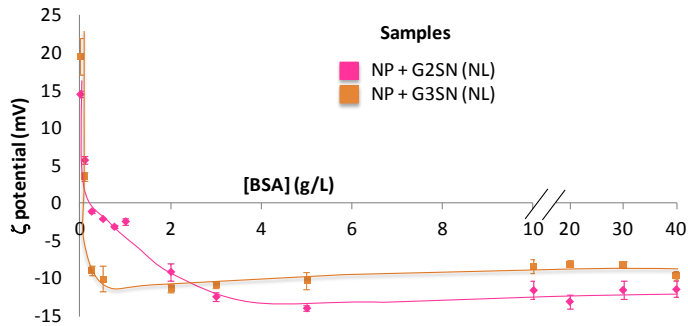
Figure 4.116: Example of the adsorption isotherms for samples composed of non-loaded nanoparticles functionalized with the second and third generation dendrons.

Using this technique, the concentration of BSA saturation for all studied samples is below 300μg/cm^2 (10g/L), in most of them below 100μg/cm^2 (around 3.3g/L), which indicates that low amounts of BSA are attached to nanoparticle surface (Table 4.37). This can be considered a positive result in terms of nanoparticle specific vectorization, sine nanoparticles would not be completely covered by unspecific proteins, such as BSA. Comparing different types of nanoparticles studied, non-functionalized and dendron-functionalized nanoparticles showed BSA concentrations of saturation between 100 − 250 μg/cm^2, independently of the nanoparticle loading. In contrast, 8D3-functionaliized nanoparticles showed lower BSA concentrations of saturation (below 50 μg/cm^2), which indicates that, as expected, the BSA adsorption depends on nanoparticle surface. It is worth noting that the change in the adsorption pattern of 8D3-functionalized nanoparticles represents another confirmation of nanoparticle functionalization.

242

Table 4.37: Nanoparticle hydrodynamic size, [BSA]$_{saturation}$ ($\mu g/cm^2$), and number of BSA molecules adsorbed onto the surface of a single nanoparticle (N$_{BSA}$), for different sets of NP-0.16E70 nanoparticles considering a nanoparticle surface of 1000 cm^2. Parameters for non-functionalized nanoparticles, non-loaded or C6-loaded could not be calculated, since a change in the ζ potential was not observed. NF = Non-functionalized, NL=Non-loaded, C6 = Coumarin 6, LOP = loperamide.

Nanoparticle set	Hydrodynamic radii (nm)		[BSA]$_{saturation}$ ($\mu g/cm^2$)	N$_{BSA}$ (BSA/NP)		
				Theoretical		Experimental
	Initial	After BSA incubation		$S_{BSA} = 64nm^2$	$S_{BSA} = 32nm^2$	
NPs (NF,NL)	20	---	---	78.5	157	---
NPs + G2SN (NL)	25	125	150	78.5	157	179
NPs + G3SN (NL)	23	35	100	78.5	157	118
NPs(C6,NF)	23	---	---	78.5	157	---
NPs(C6) + G2SN	20	75	100	78.5	157	118
NPs(C6) + G3SN	20	25	100	78.5	157	118
NPs(LOP,NF)	100	45	250	1962.5	3925	21960
NPs(LOP) + G2SN	100	115	100	1962.5	3925	8784
NPs(LOP) + G3SN	100	65	100	1962.5	3925	8784
NPs + 8D3 (NL)	20	150	37.5	78.5	157	44
NPs(C6) + 8D3	25	150	50	78.5	157	59
NPs(LOP) + 8D3	100	160	12.5	1962.5	3925	1098

In this study, the <u>size of nanoparticles</u> was also studied before (data previously discussed in the corresponding sections) and after BSA incubation at the highest concentration (40mg/mL). Regarding the size of the nanoparticles after their incubation at the BSA concentration of saturation (Table 4.37), in most cases, it increased, which could be due to the molecules of BSA adsorbed onto their surfaces, which increase the nanoparticle sizes. Therefore, it could be hypothesized an external location of the BSA molecules when adsorbed onto nanoparticle surface, without penetrating the polymeric matrix, as previously described (Vauthier, 2009).

It is worth remarking the <u>orientation that BSA molecules adopt</u> when adsorbed onto nanoparticle surface. BSA molecules have the following dimensions: 8x8x4 nm (Figure 4.117c), approximately; therefore, two size surfaces can be in contact with nanoparticle surfaces (32 nm^2 or 64 nm^2), thus forming a dense and flat layer, when the big surface is in contact with the nanoparticle (Figure 4.117a) or a thick and not dense layer, when the small surface enters in contact with the nanoparticles

243

(Figure 4.117b) (Vauthier, 2009(2) and 2011). For this reason, two theoretical numbers of maximum BSA molecules adsorbed for a single nanoparticle can be calculated (Table 4.37). The number of BSA molecules attached onto each individual nanoparticle was also calculated using the BSA saturation concentrations experimentally found. This value depends not only on the BSA concentration of saturation but also on the number of nanoparticles, which, in turns, depends on nanoparticle size. Experimentally, it was found around a hundred BSA molecules were attached to each nanoparticle in most of the samples, except in those with encapsulated loperamide (Table 4.37). Since loperamide-loaded nanoparticles are bigger, the number of nanoparticles for the same specific surface is lower; therefore, at an equivalent BSA concentration, more molecules of BSA can be attached to a single nanoparticle. Comparing experimental results of the BSA molecules / nanoparticle with theoretical calculations (Table 4.37), in most nanoparticle sets, they are closer when the BSA surface in contact with nanoparticles is around 32 nm^2. Therefore, a BSA contact by its small surface, forming a thick layer with a low density seems feasible, as shown in Figure 4.117b. In contrast, 8D3-functionalized nanoparticles, independently of their loading, show BSA adsorption values closer to those of a BSA theoretical surface contact of around 64 nm^2. Thus, for 8D3-functionalized nanoparticles, the most probable configuration of the BSA molecules is as that represented in Figure 4.117a: the BSA contacts with nanoparticles by its bigger surface, forming a dense and flat layer. It is worth noting that all the above BSA conformational discussion was performed assuming a BSA monolayer around each nanoparticle. Nevertheless, for loperamide-loaded nanoparticles, markedly higher experimental numbers of BSA molecules / nanoparticle were found than those of theoretical calculation (Table 4.37). In this case, the BSA adsorption could take place in a multilayer conformation (Olivier, 1995), perhaps due to an enhanced BSA affinity for these kinds of nanoparticles, preferentially by loperamide molecules. In addition, diverse theoretical models were tested to fit adsorption isotherms (e.g. Langmuir). Since none of them fitted the experimental values, it is possible to envisage absorption of the BSA in a multilayer form, not only for 8D3-functionalized nanoparticles, but also for other nanoparticle sets (Chavany, 1992).
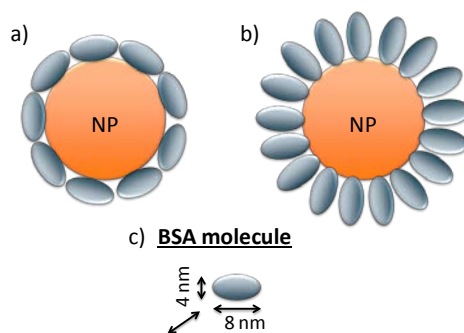
Figure 4.117: Schematic representation of the two possible orientations of BSA molecules onto nanoparticle surface. a) Surface in contact = 64 nm^2; b) Surface in contact = 32 nm^2; and c) Dimensions of a BSA molecule.

Comparing BSA adsorption results onto nanoparticles surface with previous bibliography, similar results were found. *Vauthier et al.,* (Vauthier, 2011), for example, studying poly(butyl-cyanoacrylate) nanoparticles, found concentrations of BSA saturation between 1 – 3 mg/m^2 (in the present study 1.25 – 3.5 mg/m^2) and size increments due to the presence of aggregates. In terms of the number of BSA molecules adsorbed for each individual nanoparticle, these authors reported values of around 64 molecules of BSA per nanoparticles (Vauthier, 2009(2)), quite similar to those found in the present thesis.

Since BSA is the most abundant protein in the serum, the BSA isotherms give an indication of the protein maximum aggregation onto nanoparticle surface. However, protein adsorption depends on the protein type; therefore, adsorption tests performed with different proteins could give different results. It is worth noting the importance of studying different types of proteins in terms of size (e.g. fibrinogen is much bigger than BSA) and shape (e.g. BSA is spherical, and fibrinogen is elongated), since both parameters influence in the protein adsorption onto nanoparticle surface (Vauthier, 2011). For this reason, another blood prevalent protein was studied: the fibrinogen, a critical component of the blood coagulation cascade (Dobrovolskaia, 2009), which activates this cascade and plays an important role in the opsonization, for the activation of the immune system (Salvador-Morales, 2009). Adsorption studies with fibrinogen were considered of interest, not only due to its abundance in the blood but also due to its bigger size (MW = 340kDa), and a rod-like 3D conformation (Vauthier, 2011). The study of fibrinogen adsorption consisted on the visual and microscopic observation, as well as on the determination of size and surface charge of nanoparticle dispersions with different loadings / functionalizations incubated with fibrinogen at the plasma concentration

(2mg/mL) (Vauthier, 2011). Macroscopic appearances and micrographs are shown in Figure 4.118. Fibrinogen aggregation is produced in most of the dispersions tested. It is worth noting that all nanoparticles that did not aggregate fibrinogen were negatively charged. Among the samples that did aggregate fibrinogen, most of them are cationic. This is in good agreement with previous results found by *Vauthier et al.,* (Unpublished results), who tested different types of polymeric nanoparticles and found that fibrinogen aggregation onto nanoparticle surface was produced when nanoparticle surfaces were cationic. Thus, the study of the fibrinogen aggregation onto nanoparticle surface is not representative of the adsorption of other proteins, as demonstrated in the present work, since BSA adsorption results did not correlate with those of fibrinogen. It is noteworthy that, apart from the cationic nanoparticles, those with the 8D3 antibody functionalization also produced fibrinogen aggregation. This phenomenon was previously described by *Nicolas et al.,* (Nicolas, 2003), who stated that nanoparticles functionalized with an antibody have an enhanced protein adsorption.
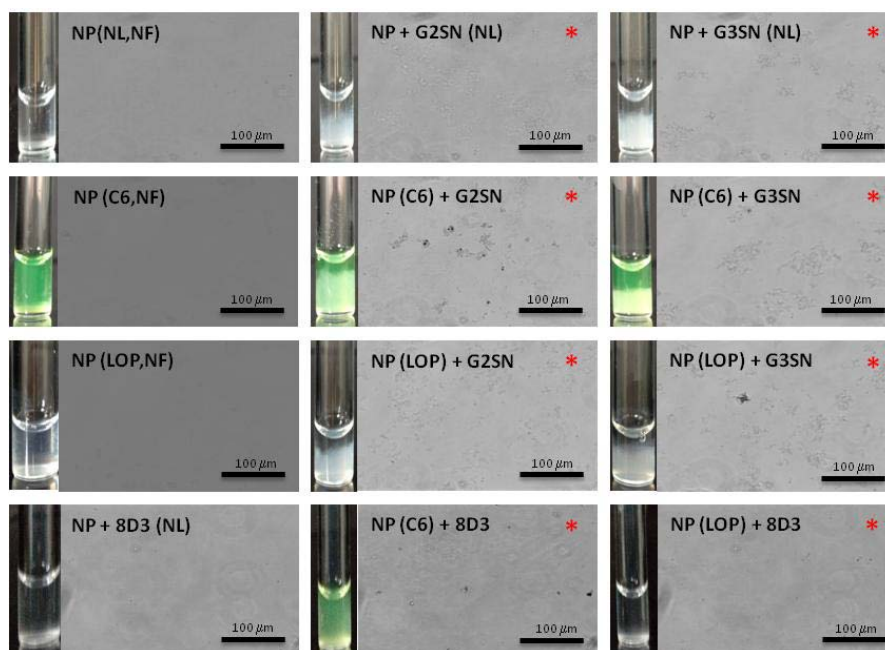
Figure 4.118: Macroscopic appearance and micrographs of the non-loaded or loaded nanoparticles and/or non-functionalized / functionalized, after fibrinogen incubation. Red stars indicate the presence of aggregates in the micrographs.

Changes in the sizes as well as in the surface charge were also studied for the fibrinogen adsorption. However, results were obtained only for those nanoparticle

246

dispersions that did not aggregate. They are shown in Table 4.38. **Hydrodynamic radii** were slightly higher for all nanoparticle sets except those nanoparticles containing loperamide, where a size reduction was observed. The increase on the droplet size was expected, thus indicating the fibrinogen adsorption preferentially onto nanoparticle surface, as happened for BSA protein. However, the size decrease found for loperamide-loaded nanoparticles was not expected. An interaction of the fibrinogen with the drug could be hypothesized, thus producing shrinkage of the polymeric matrix, resulting in smaller sizes. **Surface charges** of nanoparticles remained negative after fibrinogen incubation (Table 4.38), as expected, since fibrinogen is an anionic molecule.

Table 4.38: Hydrodynamic radii (nm) and ζ potential (mV) of non-aggregated nanoparticle dispersion sets before and after fibrinogen incubation.

Sample	Hydrodynamic radii (nm)		ζ potential (mV)	
	Before fibrinogen incubation	*After fibrinogen incubation*	*Before fibrinogen incubation*	*After fibrinogen incubation*
NP(NL,NF)	20.24 ± 2.51	29.53 ± 4.51	-21.90 ± 1.19	-9.98 ± 1.06
NP(C6,NF)	23.26 ± 1.09	29.48 ± 2.24	-14.83 ± 3.77	-12.56 ± 0.48
NP(LOP,NF)	99.98 ± 5.45	77.32 ± 5.49	-36.60 ± 1.82	-17.60 ± 1.71
NP+8D3 (NL)	20.85 ± 0.34	31.66 ± 4.21	-15.05 ± 3.05	-14.55 ± 1.61

4.6.3.3. Interaction of nanoparticles with the complement cascade

The protein adsorption onto nanoparticle surface is a known phenomenon that occurs when nanoparticles enter in the bloodstream, as previously discussed. Most times, it produces an activation of the complement system (Dobrovolskaia, 2013). This activation, mainly through the protein C3, is strongly involved in the opsonization (Bertholon, 2006). Once C3 protein binds to nanoparticle surface, it changes its conformation, thus inducing a protein cascade that triggers to the activation of the complement system (Vauthier, 2011). This signaling cascade led to the elimination of the attached nanoparticles, therefore, C3 binding to nanoparticles surface must be studied. For this reason, after the study of protein adsorption onto nanoparticle surface, the **activation of the complement system** by different types of nanoparticles was studied by means of 2D immunoelectrophoresis. The concentration of nanoparticles was adjusted to have

equivalent nanoparticle surface areas (NP surface = 1000 cm^2). To perform these experiments, the Veronal buffered saline (VBS^{2+}) was used. First, a study on the assessment of the <u>stability of nanoparticles in this buffer</u> by means of the visual appearance, size and surface charge was carried out. The stability in VBS^{2+} was studied without and with the presence of human serum (HS), since samples are incubated with serum when performing the experiments to study the activation of the complement system.

The <u>macroscopic visual appearance</u> of the nanoparticles, before and after the incubation in VBS^{2+} buffer remained invariable without serum (see Figure Ap.22a and b, appendix) while some dispersion experienced an increase of their turbidity with the presence of serum (see Figure Ap.22c and d, appendix). This turbidity increase was independent on nanoparticles loading or functionalization and was attributed to the formation of aggregates. Micrographs of these nanoparticles were observed, in order to assess the formation of the suspected aggregates. Figure 4.119 shows the micrographs of aggregated samples together with the macroscopic appearance after their incubation with fibrinogen. Although the presence of some aggregates was observed, specifically in nanoparticles functionalized with the G3SN dendron, these aggregates are small, as compared with previous studies (Vauthier, 2011). Therefore, these samples were not ruled out for the study of the complement activation.
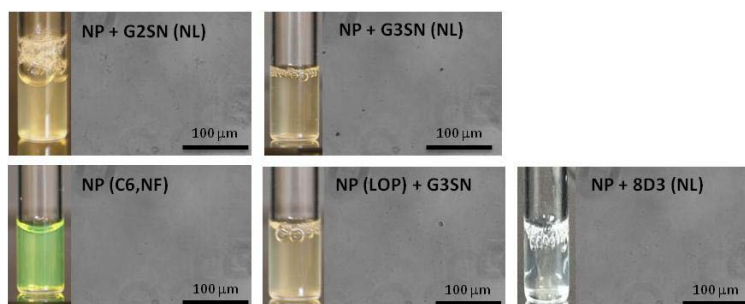
Figure 4.119: Visual appearance and micrographs of the nanoparticles with increased turbidity after their incubation (1h) with the VBS^{2+} buffer and human serum, where aggregation was suspected.

The <u>ζ potential and hydrodynamic sizes</u> of the nanoparticles were studied for the same experimental conditions, initially and after 1h incubation with VBS^{2+} buffer in absence or presence of 10wt% HS (data of nanoparticles that aggregated in the presence of HS, after 1 hour of incubation,are not given). Regarding the <u>ζ potential</u> (Figure 4.120), in the absence of HS, nanoparticles show initial surface charges of

around +/- 20 mV, negative except those functionalized with dendrons, as described in Sections 4.3, 4.4 and 4.5. Their incubation with VBS^{2+} did not change their surface charge. Nevertheless, independently of their initial surface charge, after nanoparticle incubation with serum, their surface charge shifted to slight negative values for most nanoparticles, except those functionalized with G3SN dendron, whose surface charge decreased but did not reach negative values. These results are independent on the incubation time, thus indicating that the effect of HS is nearly immediate. The surface charge shift indicates a modification of the nanoparticle surface, which could be an indication of protein aggregation. The surface charge reduction in absolute value was previously reported for other types of nanoparticles incubated with serum (Dobrovolskaia, 2009).
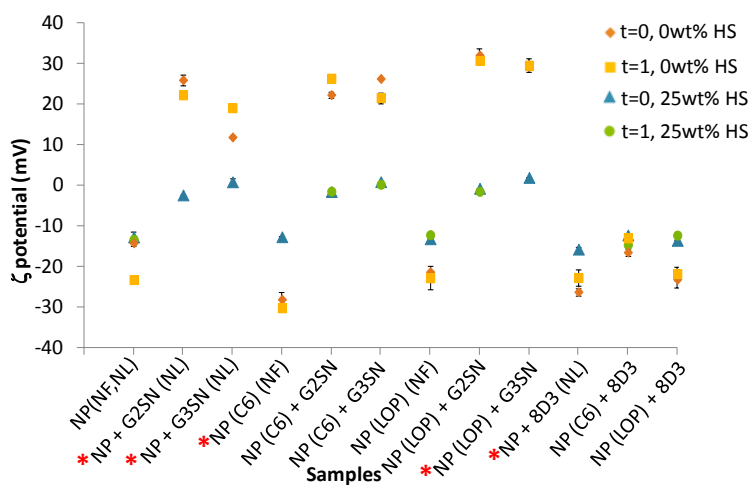
Figure 4.120: ζ potential of the studied nanoparticles dispersed in VBS^{2+} buffer containing 0 or 25wt% of serum, in the moment of sample preparation (0h) and after 1 hour of incubation. Red stars indicate sedimentated samples with HS, where measurements after HS incubation could not be performed.

The influence of VBS^{2+} and HS on the <u>size</u> of nanoparticles was also studied. Nanoparticle sizes remained constant after their incubation with the buffer (Figure 4.121 and Figure Ap.23, appendix, in logarithmic scale to better study the low size values), therefore, they are not influenced by VBS^{2+}. However, the incubation of nanoparticles with serum produced a remarkable increase in their sizes, of more than one order of magnitude (Figure 4.121), independently of the incubation time. This behavior, as found for surface charge measurements, is independent on the nanoparticle composition. The nanoparticle size increases as well as the changes in surface charge in the presence of HS were previously reported by other types of polymeric nanoparticles, independently of the nanoparticle initial surface charges

(Ehrenberg, 2009). It is worth noting that the observed nanoparticle size increase is due to the formation of aggregates between the particles and the serum proteins, which are detected as a single unit by DLS, and not due to the change of nanoparticles hard sphere size (Dobrovolskaia, 2013).
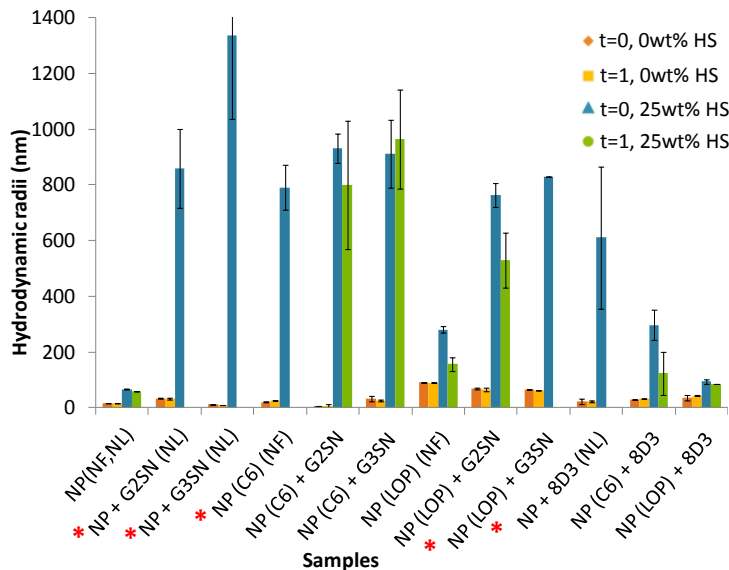
Figure 4.121: Hydrodynamic radii of nanoparticles dispersed in VBS^{2+} buffer containing 0 or 25wt% of serum, in the moment of sample preparation (0h) and after 1 hour of incubation. Red stars indicate sedimentated samples with HS, where measurements after FBS incubation could not be performed.

The <u>activation of the C3 complement protein</u> was studied by 2-D immunoelectrophoresis, for the same set of samples than those reported in the protein aggregation section. Figure 4.122 shows example profiles of the 2D-electrophoresis of the studied dispersions. The left peak corresponds to the C3 whole protein, while the right peak corresponds to the C3b and C3c fragments, in some cases, showing a double peak, with both fragments separated, but in other cases both fragments (C3b and C3c) resulted in a single peak (schematic representation in Figure 3.22, section 3.2.16.5). However, in some samples, an extra peak wass observed at the left limit of the gel, just above the sample loading well. In those samples, the proteins did not run properly in the first dimension electrophoresis. A strong protein attachment to nanoparticles, only (partially) broken in the second electrophoresis is hypothesized. This effect was previously reported when surfactants or other type of coating were included in the samples and was attributed to a strong protein adsorption onto nanoparticle surface (Sahu, 2001; Labarre, 2005). The nanoparticles tested in the present work were prepared

with Tween 80 surfactant, but, after their preparation, the excess surfactant was cleaned. Since bad migration is not observed for all the samples (Figure 4.122), this effect cannot be attributed to the surfactant. Mainly nanoparticles containing the third generation dendron (G3SN) are those showing bad migrations. For this reason, the bad migration can only be attributed to the G3SN dendron.
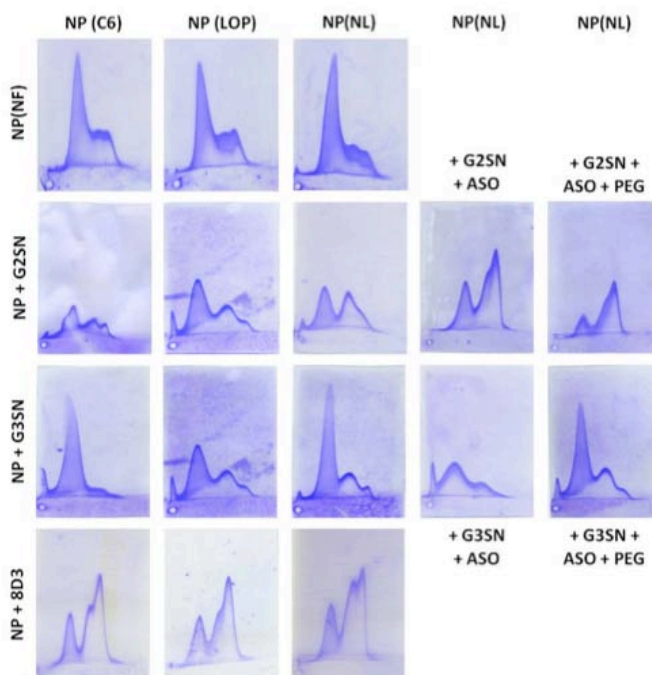
Figure 4.122: Example profiles of the complement activation for nanoparticles with different functionalizations and loadings (S_{NP} = 1000cm^2).

The results of complement activation are given as a percentage of C3 activation (Table 4.39). Non-loaded and non-functionalized nanoparticles (**NP(NL,NF)**) show an activation of around 24%, similar to activations of negative controls (see Figure Ap.24, appendix). Therefore, they could be defined as non-activators of the complement system. The **encapsulation of a compound** in non-functionalized nanoparticles as well as the **nanoparticle functionalization** produced an increase on the complement activation, being this increase higher for functionalized nanoparticles (Table 4.39). Thus, nanoparticle surface properties have a more marked influence on the complement activation than the nanoparticle loadings, as expected (Labarre, 2005; Bertholon, 2006). In addition, this increase was independent on the nature of the encapsulated compound (Coumarin 6 or loperamide), reaching values of around 35 – 40%; but dependent on the functionalization compound. The dendron nanoparticle functionalization produced

an increase of the complement activation only for the G2SN dendron (around 50%), independently of the encapsulated compound. In contrast, for the G3SN dendron, complement activation percentage did not increase. However, it is worth noting that, as indicated above, some proteins did not run properly for these samples (Figure 4.122). Therefore, higher complement activation could be hypothesized, taking into account that proteins that did not run properly in the first electrophoresis could correspond to the activated C3 (false negative results).

The further functionalization of **G2SN-NPs with ASOs** also resulted in higher complement activation (up to around 66%), which was even increased when these nanoparticles were coated with **PEG** (up to around 82%) (Table 4.39). In contrast, G3SN-NPs functionalization with ASOs and further PEGylation did not produce an increase in the complement activation, which could be due to the perturbed migration explained above (Figure 4.122). Usually, PEG coatings are added to nanoparticles to hydrophilize their surface, forming the so called "stealth" nanoparticles, less detected by the whole immune system (Pinto-Reis, 2006; Alexis, 2008; Dobrovolskaia, 2013). For this reason, after the PEG coating, a decrease in the complement activation was expected, but the results were the inverse. However, previous studies stated that PEG coating sometimes does not protect nanomaterials from complement activation (Alexis, 2008; Moghimi, 2011; Dobrovolskaia, 2013). A possible explanation could be related to the PEG length. Previous studies reported the need of a PEG molecular weight of about 10,000 Da to decrease the C3 activation (Bertholon, 2006; Alexis, 2008; Dobrovolskaia, 2013). In this work, the PEG used have a lower molecular weight ($\approx$ 400Da), required to keep nanoparticle size appropriate (Figure 4.90). Another explanation could be related with PEG density on nanoparticle surface (Alexis, 2008; Moghimi, 2011; Dobrovolskaia, 2013). The amount of PEG added in the present work was selected aiming to gene material protection, but it could be insufficient to decrease complement activation. A third explanation could be related with the coating method. PEG is adsorbed onto nanoparticle surface, without strong interactions. C3 protein could have higher affinity for nanoparticles, thus displacing PEG (Moghimi, 2011; Dobrovolskaia, 2013). The enhanced protein affinity of nanoparticles as compared with PEG was previously reported by *Kreuter et al.* (Kreuter, 2012), namely for nanoparticles with polysorbate 80, since apolipoproteins of the serum have a high affinity for this surfactant. In the present work, polysorbate 80 is a component of nanoparticles, thus, the affinity explanation could be the most plausible, not only for PEGylated nanoparticles but also for the weak to higher activation produced for all other nanoparticles. It is also possible a combination of

the different factors to explain the lack of reduction of the complement activation when coating nanoparticles with PEG.

The nanoparticle functionalization with the **8D3 antibody** also produced an increase on the complement activation up to around 70%, independently on the nanoparticle loading (Table 4.39). The increased complement activation in the presence of antibodies is an effect widely described in previous bibliography (Byrne, 2008; Moghimi, 2011; Pham, 2011). *Pham et al.,* (Pham, 2011) stated that the classical pathway of the complement system, where C3 protein is also involved, is usually activated due to the presence of antibodies. *Moghimi et al.,* (Moghimi, 2011), in addition, found an increase in the complement activation when nanoparticles of sizes around 250 nm were antibody-functionalized, while this increase was not found for nanoparticles with sizes around 600 nm. Since our nanoparticles are smaller (around 20nm), the increase in the complement activation may be hypothesized.

Table 4.39: Percentage of C3 complement protein activation for nanoparticles with different functionalizations and loadings (S_{NP} = 1000cm^2).

	NP (C6)	NP(LOP)	NP(NL)	NP(NL)	NP(NL)
NP(NF)	40 ± 1	35 ± 2	24 ± 1		
NP + G2SN	48 ± 1	33 ± 1	51 ± 2	+ G2SN + ASO 66 ± 1	+ G2SN + ASO + PEG 82 ± 1
NP + G3SN	8 ± 2	34 ± 2	22 ± 3	+ G3SN + ASO 21 ± 5	+ G3SN + ASO + PEG 34 ± 4
NP + 8D3	71 ± 2	68 ± 3	69 ± 1		

Aiming to reach the target tissue, the less immune system detection was desired. Therefore, in terms of immune detection, the lower the activation of the complement system, the more appropriate the nanoparticles for the intravenous administration (Bertholon, 2008). Accordingly, nanoparticles producing the highest complement activation (NPs + G2SN + ASO + PEG) (Table 4.39) could not be used for the intravenous delivery at the tested concentrations (S = 1000 cm^2). The required concentrations of these nanoparticles for gene therapy purposes are one order and a half of magnitude lower than those assayed in the present study. The activation of the complement system was previously reported to directly depend on the concentration of the nanoparticles (Moghimi, 2003; Vonarbourg, 2006).

Therefore, since these nanoparticles would be used at lower concentrations, their activation of the complement system would be reduced. In contrast, for drug-loaded nanoparticles, higher concentrations are required to produce a therapeutic effect. Nevertheless, their percentages of complement activation was lower at an equivalent concentration.

Comparing with previous studies, *Bertholon et al.,* (Bertholon, 2006) found similar activation percentages (>25%) for dextran nanoparticles. Usually, nanoparticles with negative surface charges and hydrophobic surfaces promote protein absorption and activate the complement system, while nanoparticles with sizes below 100 nm are less uptaken by macrophages and less recognized by opsonins (Kulkarni, 2013; Neha, 2013). These relationships were not found in our study. *Bertholon et al.,* (Bertholon, 2006) found, as in our studied, no relation between the nanoparticle size and the activation of the complement system. *Vauthier et al.,* (Vauthier, 2011) also found, with poly(isobutylcyano-acrylate) (PIBCA) nanoparticles an activation of the complement cascade higher than 30%, reaching even up to 90% of complement activation when they used PIBCA – dextran nanoparticles. Therefore, the results obtained in the present work are in the same range than previous publications. Some of the activation percentages are even lower (Table 4.39), therefore, the nanoparticles developed in this thesis could be appropriate for the intravenous delivery.

Summarizing the activation of the complement cascade, previous studies reported a marked dependency of the complement activation on the adsorbed proteins, which in turn depends on the nanoparticle surface nature, thus influencing the nanoparticle biodistribution in the body (Labarre, 2005; Bertholon, 2006; Dobrovolskaia, 2913). The results obtained in the present work are in good agreement with this statement (Table 4.39). Nevertheless, some authors (Sahu, 2001, Bertholon, 2006) reported a marked tendency of the C3b fragment to adsorb onto the hydroxyl groups, without discriminating the origin of the groups. Therefore, a weak activation of the complement system was expected for all the formulated nanoparticles, since they are composed of PLGA and polysorbate 80 surfactant, both containing hydroxyl groups.

Summarizing the protein aggregation onto nanoparticle surface, results were studied as a function of some nanoparticle characteristics. The smaller the nanoparticle size, the smaller the opsonization reported (Alyautdin, 2014). In the present work, a relationship between the increment of the size and the enhanced

protein aggregation was only found for BSA adsorption (Table 4.37). Other studies reported a dependency between the nanoparticle surface charge and the opsonization (Dobrovolskaia, 2007 and 2009; Michin, 2008). Although there is controversy between the surface charges that produce the lesser opsonization, this controversy was attributed to the difficulty of changing a single parameter when studying opsonization (Dobrovolskaia, 2007). In the present work, only in the case of fibrinogen aggregation, an increased protein adsorption was found when the surface charge was positive. There are also some studies reporting the influence of nanoparticle surface functionalization on the opsonization (Dobrovolskaia, 2007). In the present study, the fibrinogen adsorption as well as the complement activation increased when nanoparticles were functionalized with dendrons and antibodies, which is in close agreement with previous bibliography. Therefore, no direct relationship between the three proteins tested was found: although an increase of the complement activation was expected when BSA and fibrinogen adsorption increased, the results were not as expected. Earlier studies reported a lack of relationship between protein adsorption and complement activation (Bertholon, 2006). The lack of correlation could be attributed to the influence of other proteins present in the serum. In addition, BSA protein has a molecular weight of around 64,000 Da, the fibrinogen of around 340,000 Da, and the C3 complement protein has a molecular weight of around 185,000 Da (Vauthier, 2011). BSA molecules can be adsorbed onto nanoparticle surface, on the small holes produced by the polymeric entangled net. However, since C3 protein is markedly bigger, its adsorption on the smaller holes would not be possible. Therefore, the different molecular weight of both proteins could be a plausible explanation of the divergences between both results, which could be also reinforced by the divergent 3D conformation of the three proteins (e.g. fibrinogen has an elongated shape) (Vauthier, 2011). Another explanation of the lack ofcorrelation could be related to the enhanced activation of the complement system in the presence of hydroxyl groups (Sahu, 2001; Bertholon, 2006), while fibrinogen adsorption does not depend on the presence of hydroxyl groups. A final and very plausible explanation could be related with The "Vroman effect" (Vroman and Adams, 1986) which states that the adsorption of proteins is transient. The more abundant smaller proteins from blood plasma (e.g. BSA) are firstly adsorbed, but rapidly displaced by the less abundant larger proteins that have higher affinities for the nanoparticle surface. Relating this effect with the present work, BSA was the highly abundant protein studied, whose adsorption onto nanoparticle surface could be displaced by the subsequent adsorption of less abundant proteins such as fibrinogen or the C3 complement protein (Ehrenberg, 2000; Norde, 2000).

4.6.3.4.   Interaction of nanoparticles with the coagulation cascade

The coagulation or clotting time is another important parameter to study before *in vivo* intravenous delivery of nanoparticles (Dobrovolskaia, 2013). In the present work, nanoparticles with different loadings / functionalization compounds were tested (Figure 4.123) as a function of the nanoparticle concentration by means of the activated partial thromboplastin time (APTT) and the prothrombin time (PT). Results are shown in Figure 4.123. At the highest concentration (3mg/mL), most nanoparticles produced a slight increase on the **APTT**, except dendron-functionalized nanoparticles, which produced a high increase. Studying **PT** times, only dendron-functionalized nanoparticles resulted in an increase at 3mg/mL of nanoparticles. At 1mg/mL (recommended concentration to test coagulation) (Dobrovolskaia, 2006) all nanoparticles showed coagulation times in the range of normal values, except the APTT of the G3SN-NPs, which remained high. The differences on both coagulation times studied are due to the fact that the APTT measures the intrinsic coagulation pathway, while the PT measures the extrinsic coagulation pathway. Therefore, G3SN-nanoparticles have a more marked influence on the intrinsic coagulation pathway than on the extrinsic. Further decrease of nanoparticle concentration (up to 0.75mg/mL) achieved normal values for the coagulation times for all samples. Therefore, most nanoparticles did not influence the coagulation cascade at concentrations up to 3mg/mL. Dendron-functionalized nanoparticles, namely those using the G3SN dendron produced an antiocoagulant effect at concentrations higher than 1mg/mL, which is in good agreement with previous studies reporting increased coagulation times for nanoparticles functionalized with other compounds (Dobrovolskaia, 2007). The anticoagulant effect could be a drawback only in case of traumas of injected individuals (Oslakovic, 2012). Previous bibliography related reduced coagulation times with cytotoxicity of the administered compounds (Dobrovolskaia, 2008; Kim, 2008). However, increased coagulation times were not related with toxicity. Therefore, it could be concluded that the formulated nanoparticles, independently of their loading, do not produce changes in the coagulation time. This is another result that confirms that there are apt for intravenous administration.
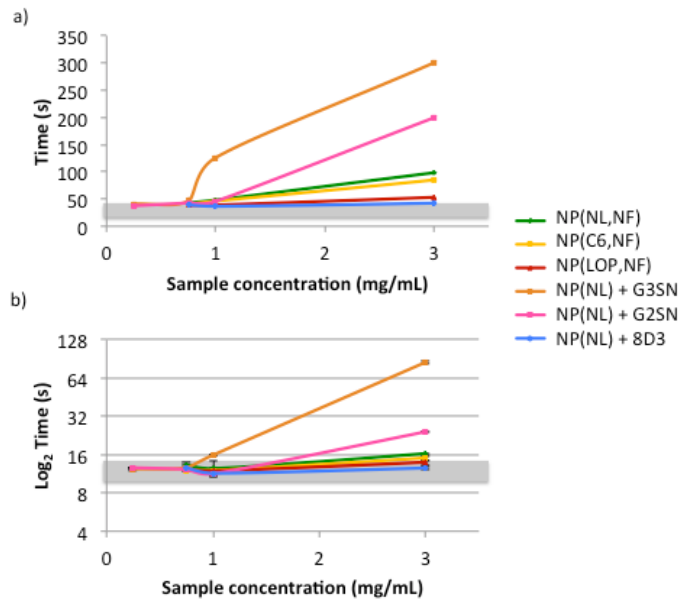
Figure 4.123: Coagulation time as a function of the simple type and concentration. Figure a) represents the APTT results while b) corresponds to the PT results. Grey zones correspond to the expected times for healthy donors.

Since <u>fibrinogen is one of the proteins involved in the coagulation</u> cascade, nanoparticle interaction with fibrinogen will influence the coagulation time (Dobrovolskaia, 2009 and 2013). Therefore, both results should be in agreement, although the coagulation cascade requires Ca^{2+} and Mg^{2+} and they were not included in the fibrinogen aggregation studies. Fibrinogen adsorption onto nanoparticle surface produced nanoparticle aggregation when nanoparticles were functionalized with dendrons (Figure 4.119). Contrarily, the coagulation time was increased for the same sets of nanoparticles; an anticoagulant effect was produced (Figure 4.123). Therefore, both results are not in good agreement, which could be attributed to the lack of the ions required for the formation of the thrombus.

4.6.3.5.   Determination of the hemolysis

Blood hemolysis was assessed *in vitro* using human blood from healthy donors. This test was performed not only for the nanoparticles formulated with PBS as the dispersant medium, but also with nanoparticles formulated with water, for comparative purposes.

Figure 4.124 shows the hemolysis of NP-W70 nanoparticles, <u>dispersed in water</u> as a function of the nanoparticle concentration (nanoparticles were diluted using PBS at physiological conditions). Hemolysis is null at low nanoparticle concentrations. By increasing nanoparticle concentration, hemolysis remained null up to a concentration of around 1.5mg/mL, from which, hemolysis increased exponentially, and achieved hemolysis percentages of around 70% at the concentration of the as-prepared nanoparticles. The hemolysis found at high nanoparticle concentrations cannot be attributed to nanoparticle physico-chemical characteristics, but to the osmotic imbalance. Since the as-prepared nanoparticles are dispersed in water, their osmolality is around 60 mOsm/kg, and pH values around 5.5, both lower than those of the blood (pH = 7.4, 300 mOsm/kg). Therefore, an osmotic balance is required to avoid hemolysis.
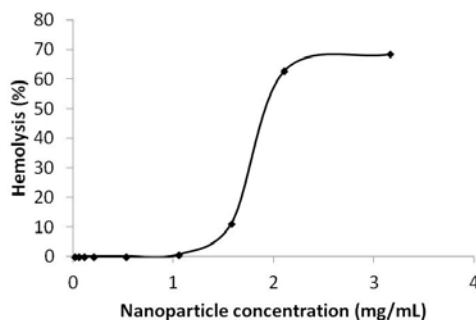
Figure 4.124: Hemolysis percentage as a function of nanoparticle concentration, for NP-W70 nanoparticles. Nanoparticle dilution made with PBS at the physiological conditions.

<u>NP-0.16E70 nanoparticles</u>, dispersed in PBS (pH = 7.4, osmolality = 300 mOsm/kg), with different loading / functionalization agents, were also studied at the required nanoparticle concentration to achieve therapeutic effects. Moreover, carbosilane cationic dendrons were also tested. Nanoparticle hemolysis was nearly null (Table 4.40) both, after 10 min and 24h of incubation for all tested nanoparticles with the exception of the G3SN systems (dendrons and dendronized nanoparticles). Therefore, neither the loading nor the functionalization agents were hemolytic in

most cases. The G3SN dendrons produced slight hemolysis after 10 minutes of incubation, which was markedly increased after 24 h of incubation (Table 4.40 and Figure 4.125). Similar results were found for the G3SN-functionalized nanoparticles. Therefore, G3SN dendrons cannot be used for the intravenous delivery, since they are hemolytic. This result could have been expected, since some cytotoxicity was evidenced using this dendron (Figure 4.103). In addition, since G3SN dendrons and G3SN-NPs have positive surface charges, their interaction with erythrocytes membranes, which have negative charges, would be higher, thus enhancing the hemolysis (Dobrovolskaia, 2013). Comparing these results with bibliography, previous studies stated the increased toxicity of dendrons by increasing the dendron generation (Bermejo, 2007; Svenson, 2009), which is in good agreement with the enhanced hemolysis of G3SN dendron as compared with G2SN dendron.

PLGA nanoparticles hemolysis was studied in previous bibliography (Kim, 2005). In presence of nonionic surfactants, an increased hemolysis up to 80 % was found, which was attributed to the surfactants. However, when coating with PEG, the hemolysis decreased down to 20 % (Kim, 2005). In our work, nanoparticles were also formulated with the polysorbate 80 surfactant. However, this surfactant did not produce any toxicity at the concentrations studied (3wt%). The controversy of the hemolytic character of the surfactants was studied by *Jumaa et al.,* and *Date et al.,* (Jumaa, 2000; Date, 2010), who found that although many surfactants are hemolytic, when used for the template nano-emulsion formulation, their hemolysis is clearly reduced. Our results are in good agreement with those studies.

Table 4.40: Percentage of viability of erythrocytes after their incubation with the tested samples, as a function of incubation time.

Sample	[PLGA] (mg/g)	Hemolysis (%)	
		10 min	24 h
NPd	3	0.00 ± 0.00	0.00 ± 0.00
G2SN	---	0.00 ± 0.00	0.00 ± 0.00
G2SN-NPs	1.5	0.00 ± 0.00	0.00 ± 0.00
NPd-G2SN-ASO	0.00075	0.00 ± 0.00	0.00 ± 0.00
NPd-G2SN-ASO-PEG	0.00075	0.00 ± 0.00	0.00 ± 0.00
G3SN	---	8.52 ± 0.01	88.93 ± 0.020
G3SN-NPs	1.5	35.30 ± 0.07	99.04 ± 0.03
8D3-NPd	1.5	0.00 ± 0.00	0.00 ± 0.00
NPd(C6)	3	0.00 ± 0.00	0.00 ± 0.00
NPd(LOP)	3	2.43 ± 0.08	0.00 ± 0.00

Hemolytic activity was further studied by microscopic observations of the tested nanoparticles. Figure 4.125 shows some examples of the macroscopic and microscopic appearance of some nanoparticles. The micrographs of most samples were similar to the negative control (C-), with a numerous population of healthy erythrocytes. However, the micrographs of the samples which produced hemolysis showed a decreased number of erythrocytes, without their characteristic shape, such as the positive control (C+), thus visually confirming the hemolysis found.
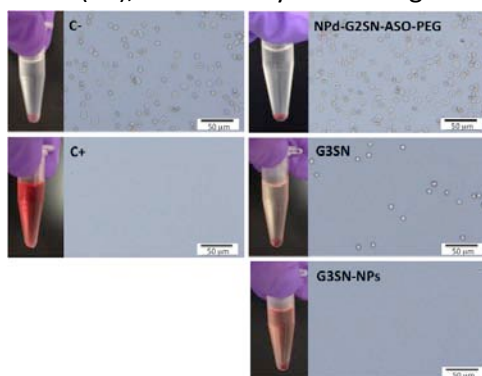
Figure 4.125: Examples of the visual appearance (left) and micrographs (right) of the samples tested by the hemolysis test for an incubation time of 10 minutes, after their centrifugation (pellets correspond to intact erythrocytes).

It is worth noting that the raw materials for the nanoparticle production come from commercial products. Therefore, the impurities contained in each batch could change, thus producing different degrees of hemolysis (Dobrovolskaia, 2013). For this reason, the hemolysis assessment performed in the present work consisted in a study of at least three batches of the raw materials, finding reproducible results. Although a relationship between the hemolysis and the complement activation was expected, it was not found, which was attributed to the hemolysis methodology used. In the present work, the hemolysis was studied to test toxicity of nanoparticles in the blood. Hemolysis experiments were performed with isolated erythrocytes without proteins in the medium. However, complement activation is a phenomenon produced by proteins. Therefore, lack of correlation should have been expected.

Summary

In terms of safety concerns, the nanoparticles formulated in the present study could be used as nanomedicines for the intravenous administration, since they are non-cytotoxic and non-hemolytic at the required therapeutic concentrations, as assessed in vitro studying different assays performed in various cell lines.

The transfection efficiency of nanoparticles intended for gene therapy purposes was shown to be dependent on the cell line as well as on the gene type. It can be confirmed that the as-prepared nanoparticles, cationic dendron functionalized, are able to introduce all kinds of genes tested (ASO, siRNA and plasmids) into cells. The best transfection efficiencies were achieved for antisense oligonucleotides protected with a PEG coating, reaching transfection efficiencies as high as 90%. Therefore, nanoparticles carrying antisense oligonucleotides represent promising non-viral gene delivery vectors, advantageous among the commercial vectors in terms of higher transfection efficiency, less toxicity and less immunogenicity.

The interaction of the designed nanoparticles with blood components is also a key issue, since it will influence the nanoparticle fate in the body (Gelperina, 2010; Dobrovolskaia, 2013). Nanoparticles formulated in the present study did not affect the coagulation at the required therapeutic concentrations. Although some of the formulated nanoparticles adsorbed some proteins of the blood (e.g. dendronized nanoparticles adsorbed both, BSA and fibrinogen), they could be defined as weak activators of the complement system, thus not activating at all the immune

response. In addition, the highest activators could be also used for the intravenous delivery at reduced concentrations (e.g. gene delivery vectors) and/or slow administrations (e.g. drug delivery nanoparticles).

In conclusion, nanoparticle structure and composition have been properly engineered for intravenous administration.

4.7. *In vivo* studies

After the in vitro testing of the designed and functionalized nanoparticles, which confirmed the possibility to use them for biomedical applications, in vivo experimentation was undertaken to study the blood-brain barrier (BBB) crossing of the nanoparticles by means of measuring the central analgesia will be described.

4.7.1. Intravenous administration of nanoparticles

The nanoparticles presented in this work, as previously discussed, are intended for their intravenous administration, with the aim to target and cross the BBB for the treatment of neurodegenerative diseases. The intravenous administration (i.v.) was selected because, although it is a route that cannot be applied by the patients themselves, it represents a low invasive route of administration, specifically compared with the intracranial administration, currently used for the treatments of the central nervous system (CNS) (Alyautdin, 2014). In this context, the intravenous administration of targeted nanoparticles could represent a promising approach for those patients with CNS diseases in terms of administration facility and post-treatment recuperation.

Knowing that the formulated nanoparticles are non-cytotoxic and non-hemolytic at the concentration of use (*in vitro* experimentation), they were intravenously administered to mice for further experimentation. A good tolerability of the nanoparticles was expected, since *in vivo* results (Dobrovolskaia, 2013) usually correlate well with *in vitro* results, and nanoparticles were non-toxic *in vitro*. Tests performed on CD-1 male mice, as described in section 3.3.19, using NP-0.16E70 nanoparticles with different loadings / functionalizations (non-loaded, loperamide-loaded, non-functionalized and 8D3-functionalized) showed that none of the administered animals died neither showed intoxication symptoms (e.g. behavior changes, weight loss…), thus the non-toxic character of the formulated NP-0.16E70 nanoparticles (non-loaded or loaded with loperamide, non-functionalized or 8D3-functionalized) was confirmed *in vivo*.

It is worth noting that, although in this study nanoparticles are intended for the intravenous administration, the drawbacks of this route were taken into account. Being a non-self administering route, patients should require the technicians to receive their treatment, usually at the hospital facilities, which represents a decrease in patients compliance (Lublin, 1996; Good, 1998; Mercadante, 2010).

Future work should consist in the modification of the formulated nanoparticles for their oral administration. Nevertheless, it should be mentioned that the use of nanoparticles as advanced delivery systems would enable a control of the released active (drugs and genes). Therefore, the release could be extended for longer periods of times, thus reducing the doses that a patient receives and enhancing its compliance to the treatment, even if it is by intravenous administration.

4.7.2. Study of the BBB crossing

Once nanoparticles have been intravenously administered, they should reach to the BBB thanks to their targeting moieties, and then they should cross it to reach the CNS. It is noteworthy that to study the BBB crossing, experiments with animals are required, since *in vitro* BBB models do not simulate accurately the BBB (Jiménez, 2010). Different methodologies have been reported in the bibliography to study the BBB crossing. Among them, the study of the analgesic effect produced at a central level by drugs not permeable to the BBB (e.g. loperamide, dalargin) has been widely used by the group of *Kreuter et al.,* (Kreuter, 2002, 2003 and 2007) and other groups (Gabathuler, 2010; Tosi, 2010). In this work, this experiment was chosen for the easy performance, the reduction of animal manipulation and the time efficiency (see Figure Ap.25, appendix as an schematic procedure carried out). Loperamide hydrochloride was chosen as the analgesic drug, since it has an analgesic central effect in the CNS but it cannot cross the BBB itself neither by intravenous administration nor by other routes of administrations (Alyautdin, 1997). All samples were prepared using PBS 0.16M as the solvent / dispersant, since it accomplishes pH (7.4) and osmolality (300mOsm/kg) requirements of blood (Dobrovolskaia, 2013). These experiments were intended for the study of the BBB crossing of <u>two types of nanoparticles</u> loaded with loperamide (Table 4.41): 8D3-functionalized nanoparticles, to test if this monoclonal antibody was able to target the formulated nanoparticles to the transferrin receptor overexpressed in the BBB, as previously described in other studies for other formulations (Lee, 2000; Zhang, 2005; Manich, 2013); and the non-functionalized nanoparticles, to test if the remaining polysorbate 80 surfactant forming the nanoparticles is able to target these nanoparticles to the BBB, since previous studies demonstrated the efficiency of polysorbate 80 to specifically bind to the apolipoprotein B of the blood, which has a receptor in the BBB (Alyautdin, 1997; Michaelis, 2006, Wholfart, 2012).

A wide set of <u>controls</u> was included in the experiment in order to assess the effect of each component of the formulations. As a <u>positive control</u>, the opiate analgesic

drug morphine was used, since previous bibliography defined its ability to cross the BBB (Swinyard, 1990). Moreover, a micellar solution composed of loperamide with Tween 80 (polysorbate 80) was also included, since, as indicated previously, this surfactant was defined in the bibliography to enhance BBB permeability (Michaelis, 2006, Kreuter, 2012; Wholfart, 2012). It was also expected a maximum analgesic effect with this sample, as it was reported previously for even low concentrations of the surfactant (around 1%) (Alyautdin, 1997). As <u>negative controls</u>, first, the buffered electrolyte solution (PBS 0.16M) was used. Moreover, the micellar surfactant solution (without loperamide) was also included, as well as a dispersion of non-loaded non-functionalized nanoparticles, and a dispersion of the non-loaded 8D3-functionalized nanoparticles with the aim to study the effects of the formulation components on the analgesia (Table 4.41).

Table 4.41: Scheme of the samples tested in the *in vivo* analgesic test. Concentrations are referred to the concentrations of the initial samples, before their administration, while drug dose is referred to the dose administered into the animals. All samples are suspended in PBS at the physiological conditions. *NP = nanoparticles; NL = non-loaded; NF = non-functionalized; LOP = loperamide; 8D3 = antibody-functionalized.*

Sample	Used as a:	[PLGA] (mg/mL)	[Tween80] (%)	[Drug] (mg/mL)	Drug dose (mg/kg)
Electrolyte buffer (0.16M)	Negative control	-	-	-	-
Aqueous morphine	Positive control	-	-	0.7 mg/mL	3 mg/kg
NPs (NL,NF)	Negative control	30 mg/mL	< 30 %	-	-
NPs (NL,8D3)	Negative control	30 mg/mL	< 30 %	-	-
NPs (LOP,NF)	Test sample	30 mg/mL	< 30 %	0.7 mg/mL	3 mg/kg
NPs (LOP,8D3)	Test sample	30 mg/mL	< 30 %	0.7 mg/mL	3 mg/kg
Aqueous Tween 80 + LOP	Positive control	-	15 %	0.7 mg/mL	3 mg/kg
Aqueous Tween 80	Negative control	-	15 %	-	-

It should be mentioned that in some animals, changes in the behavior after nanoparticle administration were observed, namely when the injected samples containing loperamide. Specifically, periods of hyperactivity followed by akinesias, even immobility, arched back and the typical erect tail were observed, which was previously reported in the bibliography to be a typical effect of the opiate drugs

acting at a central level (Tosi, 2007; Gelperina, 2010). Therefore, these behavioral changes are an indirect indication of some kind of central action produced by nanoparticles. Although it could be thought that these effects are due to some kind of toxicity produced by the injected nanoparticles, as previous studies stated (Olivier, 1999), many reasons enable to rule out toxicity. First, a wide assessment of the toxicity was performed using different assays and cell lines, resulting in all cases in non-toxic nanoparticles. Second, the degradation products of the components of nanoparticles are usually those producing toxicity and in the present work, the components of the PLGA nanoparticles are biodegradable (Guzman, 1996; Labhasetwar, 1997; Pinto-Reis, 2006). And third, as indicated above, the behavior changes observed in the animals are attributed to the opiate effect generated at a central level (Tosi, 2007; Gelperina, 2010).

It was **statistically studied** if the administration of each sample produced significant differences in the latency time pre and post – treatment, by means of the paired-sample t-test, assessing a confidence level of 95%. Results are presented in Figure 4.126 (see also Table Ap.4, appendix, for the paired-sample T test numerical values and Figure Ap.27, appendix, as an example of the Paired-Samples T-test results). As expected, no significant differences were found for the <u>negative controls</u> before and after the treatment, indicating that analgesia was not produced. 8D3-functionalized, non-loaded nanoparticles (NPs(NL,8D3)) as well as the surfactant aqueous micellar solution did have significant differences before and after the treatment, but these differences are close to the limit of the significant level, therefore, they could be ruled out, concluding that all negative controls behaved as expected, without producing analgesia. <u>Positive controls,</u> as expected, resulted in an increase on the latency post-administration time; significant differences in the reaction time pre and post treatment were found; thus, analgesia was produced in both cases. Considering the <u>nanoparticles encapsulating loperamide</u>, non-functionalized nanoparticles did not show significant differences, although an increase on the reaction time was produced, the analgesic effect was not strong enough to be detected with 95% of confidence. However, for the 8D3-functionalized nanoparticles, a marked increase on the reaction time was observed, resulting in significant differences, thus confirming analgesia. Therefore, it can be concluded that 8D3-functionalized nanoparticles can cross the BBB, therefore, they could be promising systems for the delivery of actives to the CNS using the intravenous route of administration.
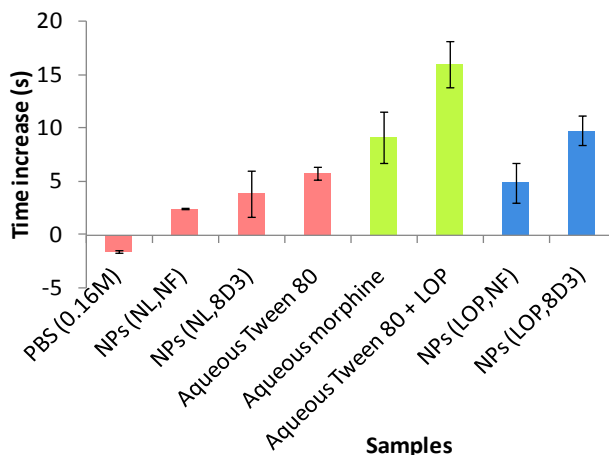
Figure 4.126: Mean and standard deviation of the differences between the pre-treatment and post-treatment time. Pink bars negative controls, green bars represent positive controls and blue bars the tested samples.

Apart from the statistic study, the **maximal possible effect** (MPE) was also calculated to clarify the results (Figure 4.127 and Figure Ap.26, appendix, normalized percentages between 0 – 100%), since it is usually given in the bibliography (Kreuter, 1995; Costantino, 2006; Vergoni, 2009; Gelperina, 2010; Chen, 2011; Tosi, 2011; Wholfart, 2012; Kirby, 2013). Negative controls showed MPE values below 15%, as expected, except for the aqueous solution of the surfactant, which resulted in higher MPE percentage (around 33%). This higher value is in agreement with previous bibliography, where higher MPE values than controls, using an aqueous solution of polysorbate 80 were found (Kreuter, 1995). This could be due to the permeabilization of the BBB produced by polysorbate 80. In the present study, the polysorbate 80 concentration is higher than in previous studies, therefore, a higher permeabilization resulting in a higher MPE value was expected. Positive controls also gave expected results, the highest MPE values due to the high analgesia produced. The studied samples resulted in 25% and 52% of MPE without and with the antibody functionalization, respectively. Although non-functionalized nanoparticles resulted in higher effects than most of negative controls, their differences are not significant enough to confirm that analgesia was produced for this set of nanoparticles. However, since behavioral changes were observed, a fraction of loperamide should have crossed the BBB (Gelperina, 2010). In addition, previous studies reported similar MPE values at an equivalent dose (Kreuter, 1995). Therefore, a slight crossing of non-functionalized nanoparticles could be hypothesized due to the presence of the polysorbate 80. For 8D3-functionalized nanoparticles, the MPE reach values similar to those obtained for

one of the positive controls (around 52%), therefore, it can be stated that 8D3-functionalized nanoparticles are able to cross the BBB. Therefore, MPE calculations confirm the conclusions of the statistical study.
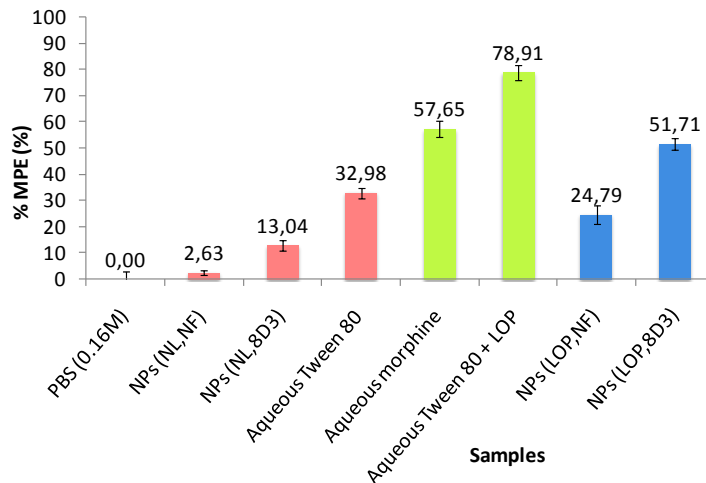
Figure 4.127: % MPE of different groups (normalized to the negative PBS control), performed with the pre and post treatment latency times for each group. Labels indicate the mean % MPE. Green bars represent positive controls, pink bars negative controls and blue bars the tested samples.

Comparing with previous studies with PLGA nanoparticles, similar MPE values (to the 8D3-functionalized nanoparticles) were also found, when nanoparticles were specifically functionalized against receptors in the BBB, such as the peptide g7 (Tosi, 2011), other peptides (Costantino, 2006) or a modified ether PEG coating (Kirby, 2013), which could penetrate the BBB by other mechanisms due to the different targeting elements (Gelperina, 2010; Wholfart, 2012). Furthermore, previous studies reporting the crossing of PLGA nanoparticles through the BBB, did not find an increase in the MPE value without a specific functionalization (Vergoni, 2009), even if those nanoparticles contained polysorbate 80 surfactant (Chen, 2011; Kirby, 2013). These results are in good agreement with those obtained in the present work. Only those studies on the coating of polymeric nanoparticles composed of poly(butyl cyanoacrylate) polymer (PBCA) with proteins with specific receptors in the BBB (e.g. apolipoproteins) achieved higher MPE percentages (Kreuter, 2002) than those reported in the present study. However, PBCA is not a commercial polymer, the corresponding nanoparticles are produced by polymerization, having the drawback of the high toxicity of the monomers used (Huang, 2007). Another drawback of the PBCA nanoparticles is that the effects that they produce usually disappear faster than when using PLGA nanoparticles, where

the analgesic effect is reported to be prolonged (Gelperina, 2010). The prolonged analgesic effect could be related with the slow release of the drug from PLGA nanoparticles. Therefore, in terms of safety issues, PLGA nanoparticles are advantageous although they have not achieved as high MPE percentages as PBCA nanoparticles (Kreuter, 2012). In addition, taking into account the target diseases of the present study, neurodegenerative diseases (e.g. Alzheimer's disease), it is worth noting that patients affected by a neuredegenration present an increase of the BBB permeability (Zlokovic, 2008; Tosi, 2011; Alyautdin, 2014). Therefore, nanoparticles crossing would be enhanced.

Other aspects that could be compared with previous bibliography are the latency time after the injection and the dose of loperamide administered. Concerning latency time, previous bibliography reported antinociceptive effect at long times (Alyautdin, 1997; Tosi, 2007 and 2010; Gelperina, 2010). In the present study, the antinociceptive effect was only studied within 15 minutes post injection, since this time is enough for nanoparticles to reach the CNS of mice. However, taking into account the slow release of loperamide from the designed nanoparticles, it could be possible an enhancement of the analgesic effect after longer times, as previously reported (Kreuter, 1995). Considering loperamide dose, in the present work 3mg/kg of loperamide was chosen, since it is an intermediate dose compared to those reported by previous studies (Alyautdin, 1997; Tosi, 2007; Gelperina, 2010; Chen, 2011). An increase on the drug dose could produce an increase on the analgesic effects observed (Kreuter, 1995).

Although there are studies on loperamide-loaded PLGA nanoparticles, coated with polysorbate 80 surfactant (Gelperina, 2010), the method of preparation used in the present work represents a novelty. First, PLGA nanoparticles were produced from nano-emulsion templating, using the low-energy nano-emulsification method (PIC method) for the nano-emulsion production. This method is advantageous not only for the production of nano-emulsions with small sizes and low polydispersity, but also for being time, cost and energy efficient (Solans, 2005 and 2012; Anton, 2008). In addition, drugs, such as loperamide, are encapsulated prior to nano-emulsion formation, thus obtaining high entrapment efficiencies (Klang, 1998; Tamilvanan, 2004; Cook, 2005; Brigger, 2012; Gref, 2012; Gupta, 2012; Neha, 2013); reaching to therapeutic concentrations after a simple step of concentration. In addition, regarding polysorbate 80, the method presented in this work is also advantageous, since polysorbate 80 was the surfactant chosen for the production and stabilization of the nanoparticles; it was introduced from the beginning of the process (nano-

emulsification), therefore, no addition coating steps are required. For all these reasons, it could be postulated that a promising novel advanced delivery system able to cross the BBB after its administration using the intravenous route has been designed.

Summary

The nanoparticles designed and produced in the present thesis are non-toxic upon intravenous administration in murine animal models; therefore, they could be useful for biomedical applications involving the intravenous delivery.

The BBB crossing of nanoparticles has been partially achieved by non-functionalized nanoparticles and completely successfully achieved by 8D3-functionalized nanoparticles, as assessed by in vivo analgesic tests with loperamide-loaded nanoparticles; thus, the 8D3-functionalized nanoparticles are promising delivery systems to efficiently cross the BBB and treat neurodegenerative diseases after intravenous administration.

It is noteworthy that the passive targeting to the BBB with polysorbate 80 was achieved taking advantage of this novel approximation, the incorporation of this surfactant as a part of the formulation, in a single step procedure. Previous bibliography of the use of polysorbate 80 to passively vectorize nanoparticles through the BBB is numerous (Bambrilla, 2010; Chen, 2011), but none of the studies reported the preparation of nanoparticles using this surfactant as one of the system components.

Chapter 5

CONCLUSIONS

In the present thesis, polymeric PLGA nanoparticles have been designed, widely characterized and their properties tuned with the aim to use them as advanced delivery systems for the treatment of neurodegenerative diseases by the intravenous route of administration. The most important conclusions of this study are the following:

Formation of O/W nano-emulsions by the PIC method and characterization

Nano-emulsification of PLGA dissolved in ethyl acetate has been successfully achieved by the phase inversion composition method (PIC), a low-energy method, using polysorbate 80 as the surfactant and water or electrolyte solutions as the aqueous component. Nano-emulsion formation by phase inversion has been confirmed by conductivity measurements and solubilization of hydrophilic/lipophilic colorants.

The study of the electrolyte solution (W) / polysorbate 80 (S) / [4wt % PLGA in ethyl acetate] (O) system demonstrated that:

- O/W nano-emulsions are formed at high water contents, independently on the electrolyte concentration.
- The presence of electrolytes broadens the nano-emulsion domain towards lower water contents.
- Increasing the PLGA concentration up to 20wt%, the nano-emulsion domain expands to lower water contents and shifts to higher O/S ratios.
- The presence of 20wt% of ethanol combined with ethyl acetate as the oil phase broadens the nano-emulsion domain.
- The presence of loperamide reduces the region of nano-emulsion formation.

Characterization of the designed nano-emulsions showed that:

- Nano-emulsions with hydrodynamic radii as low as 20 nm are achieved at an intermediate electrolyte concentration (0.08M) and O/S ratios from 40/60 to 70/30.
- Nano-emulsion droplet sizes are reduced when:
  o Electrolytes are incorporated in the water phase, due to enhanced slating out effect.

272

- o Compositions of the central part of the nano-emulsion domain are selected, independently on the PLGA concentration in the oil phase, due to their higher stability.
- o The solvent ethyl acetate is used as the unique solvent of the oil phase or combined with a maximum of 20wt% of acetone or ethanol.
- Nano-emulsions of the studied system are stable to phase separation for at least, 60 days. However, due to diffusion of the solvent to the aqueous phase, early formation of nanoparticles takes place, resulting in sedimentation.
- The increased stability of nano-emulsions in the presence of electrolytes has been attributed to the salting out effect.
- The pH and osmolality of nano-emulsions formulated with 0.16M PBS are within the range of physiological values (pH=7.4; osmolality=300mOsm/kg).

Nano-emulsions with an electrolyte concentration of 0.16M, 90wt% of aqueous content and 70/30 O/S ratio were chosen as templates for nanoparticle preparation, because they accomplish physiological conditions, possess appropriate size (hydrodynamic radii of around 40nm) and stability and, in addition, their surfactant content is rather low.

Formation of polymeric nanoparticles from nano-emulsions by solvent evaporation

PLGA nanoparticles were successfully obtained from nano-emulsion templating by solvent evaporation. Their characterization enabled to conclude that:

- Nanoparticle <u>sizes</u> are reduced as compared with their template nano-emulsion droplet sizes, which was attributed to evaporation of the solvent, since nanoparticle sizes are, mainly, those expected by theoretical calculation of solvent evaporation.
- The absence of <u>cracks</u> in the surface of nanoparticles obtained from template nano-emulsions formulated with PBS 0.16M as aqueous phase is attributed to the possible porous formation which produces more flexibility of the structure.

273

- Nanoparticle <u>size was not affected</u> by changes in temperature or in electrolyte concentration after preparation or by a post concentration step. Only changes during the emulsification process produce effects on nanoparticle sizes.
- Nanoparticle <u>colloidal stability</u> was higher in the presence of electrolytes due to smaller nanoparticle sizes. Sedimentation was confirmed as the main destabilization process.
- The <u>chemical stability</u> of PLGA, which is degraded along the time, is enhanced in the presence of electrolytes and in absence of serum.

The method of production of nanoparticles was found to be reproducible. Small sizes, together with their high stability and reproducible physico-chemical characteristics make them apt as delivery systems for the desired biomedical application (intravenous administration).

Encapsulation of actives in nanoparticles

- A fluorescent dye, <u>Coumarin 6</u> has been successfully encapsulated with high encapsulation efficiencies, for imaging purposes. The encapsulation of Coumarin 6 did not vary the studied physico-chemical characteristics of the nanoparticles. Coumarin 6 release was sustained and independent on the pH of the receptor solution.
- Iron oxide <u>magnetic nanoparticles</u> have been encapsulated in PLGA nanoparticles, as evidenced by magnetic separation of the nanoparticles, followed by assessment of the presence of magnetic nanoparticles encapsulated in polymeric nanoparticles, even after the magnetic separation, by means of spectral analysis and TEM image analysis.
- A model analgesic drug, <u>loperamide hydrochloride</u> has been successfully encapsulated, with the aim to study the BBB crossing of nanoparticles. The increase in the droplet / nanoparticle size produced with the incorporation of this active was attributed to the characteristics of the oil phase (ethyl acetate + 20wt% ethanol). High entrapment efficiency was achieved, as well as a sustained and lower drug release. The nanoparticle concentration step, performed with the aim to achieve loperamide therapeutic concentrations, did not change their physico-chemical characteristics.

274

- An antiapoptotic drug, commonly used for the treatment of neurodegenerative diseases, galanthamine hydrobromide, has been successfully encapsulated in PLGA nanoparticles without changing the physico-chemical main characteristics of the nanoparticles. High encapsulation efficiencies as well as sustained control release have been achieved, maintaining the antiapoptotic activity of the drug.

The formulated nanoparticles represent a good alternative for the encapsulation of different kinds of compounds, since they enable high encapsulation efficiencies, with a slow and controlled release, maintaining the functional properties of the encapsulated compounds.

Functionalization of nanoparticle surface

- Nanoparticle surface functionalization with fluorescein isothiocyanate (FITC), with imaging purposes, resulted in an increase of nanoparticles sizes, attributed to the influence of the FITC in the emulsification step. Nevertheless, nanoparticles sizes remain in the nanometric range (<200nm), appropriate for the intravenous administration.
- Nanoparticles have also been successfully functionalized with carbosilane cationic dendrons, covalently bound to the as-prepared nanoparticles (as confirmed by means of surface charge determination, FTIR experiments, the Kaiser test for the detection of primary free amines and thermogravimetric analyses). The dendronized nanoparticles showed increased sizes and positive surface charges.
- Electrostatic binding of a model antisense oligonucleotide (ASO) and siRNAs to cationized nanoparticles was achieved at low NP/gene ratios, as assessed by surface charge measurement and electrophoretic mobility shift assays.
- A model lentiviral plasmid vector has also been electrostatically bound to cationized nanoparticles. However, higher amounts of nanoparticles were required due to the bigger size of the plasmid, as compared with other genes.
- The protection of ASOs and siRNAs, conjugated to nanoparticles surface, was achieved by PEG coating.

- For <u>active targeting to the BBB</u>, the 8D3 monoclonal antibody against the anti-transferrin receptor, overexpressed in the BBB, has been successfully bound to nanoparticles surface by a covalent attachment, as confirmed by spectral analyses, as well as chromatographic studies.

It has been shown that nanoparticle functionalization can be successfully performed using different binding techniques (covalent bound formation, electrostatic attachment, affinity coating) to bind different kinds of compounds (fluorescent dyes, cationization elements, genes and targeting compounds). Therefore, these nanoparticles constitute highly versatile nanosystems that could be useful for imaging purposes, gene therapy and to specifically target the BBB.

In vitro **nanoparticle evaluation**

<u>Toxicity experiments</u> enabled to confirm that:

- Nanoparticles are non-cytotoxic at the required concentrations of use, as assessed by different techniques (MTT and LDH assays) and cell lines (HeLa, HEK and U87). The cytotoxicity of nanoparticles slightly increases in the presence of G3SN dendron, while it was not changed with the other encapsulated / functionalizing compounds used.
- Nanoparticles dispersed in PBS are non-hemolytic at the required concentration of use, except those containing G3SN dendron. Nanoparticles dispersed in water produced hemolysis due to the imbalance of the osmolality.

<u>Transfection assays</u> allow to conclude that:

- Optimal NP/gene charge ratios for transfection are dependent on the dendron as well as on the gene type. The best transfection efficiencies were found:
  - o <u>For ASOs</u>: at NP/gene ratio of 0.75/1 for G2SN-nanoparticles and 1/1 for G3SN-nanoparticles. The PEGylation of the G2SN-ASO-NPs enhances transfection efficiencies to values of around 90%.

- o <u>For siRNAs</u>: at NP/gene charge ratio of 0.75/1 for G2SN-nanoparticles coated with PEG. The transfection efficiencies were as high as 70%, lower than those from ASOs due to the less stability and/or higher sizes of the complexes.
- o <u>For lentiviral plasmids</u>: at NP/gene molar ratios of 125/1, independently of the presence of the PEG coating. The transfection efficiencies were as high as 80%.

<u>Experiments with blood components</u> enabled to conclude that:

- Nanoparticles (independently of the loading / functionalization) do not produce alteration in the coagulation kinetics at therapeutic concentrations.
- Nanoparticles are coated by BSA proteins of the serum when they enter to the bloodstream, but concentrations of BSA saturation are low (at the level found by other studies). BSA molecules orientation onto nanoparticle surface as well as the number of BSA layers around nanoparticles depends on the nanoparticle composition (surface functionalization and loading).
- Fibrinogen was adsorbed onto nanoparticles surface when they possessed cationic charge due to electrostatic interactions.
- PLGA nanoparticles are weak activators of the complement system.

The absence of toxicity in both, adherent cell cultures and in the blood, confirmed that the designed nanoparticles are promising for biomedical applications.

The high transfection efficiencies found using nanoparticles as non-viral gene delivery vectors, makes PLGA nanoparticles an advantageous alternative to viruses and other commercial vectors due to their versatility and reduced toxicity / immunogenicity.

The interaction of nanoparticles with blood components (BSA, fibrinogen and complement system) is weak.

The formulated nanoparticles are good candidates to test *in vivo* their BBB crossing, since they have the required features to be used as delivery systems for the intravenous administration.

In vivo **nanoparticle evaluation**

The use of murine animal models for the *in vivo* testing of the designed systems enabled to confirm that:

- Nanoparticles are non-toxic upon intravenous administration at the required therapeutic doses.
- 8D3-functionalized nanoparticles can cross the BBB after their intravenous administration, showing brain penetration values similar to those reported for positive controls.

The designed 8D3-functionalized PLGA nanoparticles could be apt as delivery systems crossing the BBB and acting at the CNS level after their intravenous administration.

Final remark

The development of PLGA nanoparticles by nano-emulsion templating using the PIC low-energy emulsification method, followed by solvent evaporation enabled to produce promising systems for many biomedical uses. These polymeric nanoparticles, intended for the treatment of neurodegenerative diseases by the intravenous route of administration, represent a novel contribution to this field of study, since their **crossing through the BBB** was demonstrated. They may positively contribute to achieve better treatments for current and future diseases, not only for those affecting the central nervous system but also for a wide range of diseases where pharmacological therapies are still inefficient. These formulated nanoparticles represent a promising approach.

Chapter 6

FUTURE WORK

The main objectives of this thesis were reached in achieving the Blood-Brain Barrier (BBB) crossing of 8D3-functionalized nanoparticles, prepared from nano-emulsion templating, using a low-energy nano-emulsification method (PIC method) followed by solvent evaporation. However, each step of the study could be improved performing more investigations. For this reason, for each section of the present thesis, some suggestions are listed below:

Selection of the system components

-   Study other surfactants, different than polysorbate 80, for the nano-emulsion formation by the PIC method.

Formation of O/W nano-emulsions by the PIC method

-   Perform more complete phase behavior studies for the selected systems in order to understand better the mechanisms of nano-emulsion formation.
-   Carry out deeper stability studies on stability to find out the exact mechanisms of nano-emulsion destabilization.
-   Test other low-energy methods (e.g. spontaneous emulsification) for the production of nanoparticles from nano-emulsion templating.

Formation of polymeric nanoparticles from nano-emulsion solvent evaporation

-   Study of other methods for the nanoparticles formation.

Encapsulation of actives in nanoparticles

-   Test other fluorescent dyes, emitting in another wavelength range, to widen the application of nanoparticles for imaging purposes.
-   Increase the stability of encapsulated magnetic nanoparticles, to enhance the magnetic properties of nanoparticles.
-   Encapsulate several compounds with theranostic purposes or for treatments by a combined gene-drug or two-drug therapy.

Functionalization of nanoparticle surfaces

- Test other active targeting components, such as cell penetrating peptides, to achieve the BBB crossing by different receptors.
- Deepen the study on the PEGylation of nanoparticles, to achieve a better protection of the gene material.
- Multifunctionalization of nanoparticle dispersions with different compounds.

In vitro **nanoparticle evaluation**

- Further studies of toxicity: variation of the cell lines, increase of nanoparticle concentrations and test different toxicity assays.
- Re-evaluation of the transfection efficiency using other tests.
- Deepen the study of the specific blood proteins adsorbed onto nanoparticle surface.

In vivo **nanoparticle evaluation**

- Further studies of the BBB crossing, including variations of the time and dose.
- Studies of the biodistribution of nanoparticles once administered by the intravenous route.
- Tuning nanoparticles to switch to the oral route of administration.

Chapter 7

SUMMARY IN CATALAN

Desenvolupament de nanopartícules polimèriques multifuncionals obtingudes a partir de nano-emulsions per vectorització a la barrera hemato-encefàlica

7.1. Introducció

7.1.1. Nano-emulsions

Les **nano-emulsions** són emulsions, dispersions de dos líquids immiscibles, amb mides de gota nanomètriques, entre 20 i 200 nm (Tadros, 2004; Solans, 2003 and 2005; Pinto Reis, 2006). Estan formades per una fase interna o dispersa (les gotes) i una fase externa o contínua. Depenent de la naturalesa de les fases, les nano-emulsions es classifiquen en oli-en-aigua (O/W), si la fase interna és l'oli; o aigua-en-oli (W/O) si la fase interna és l'aigua.

Com totes les emulsions, les nano-emulsions són termodinàmicament inestables, degut a la elevada energia necessària per crear les interfases (Tadros, 1983 i 2004); però a diferència de les emulsions convencionals, degut a la seva reduïda mida de gota, presenten estabilitat a la sedimentació. Una altra conseqüència de la mida petita és l'aspecte transparent o translúcid (Solans, 2005 i 2012).

Tensioactius

Els **tensioactius** són molècules amb un cap hidròfil i una cua lipòfila (Winsor, 1948), que s'adsorbeixen a les interfases degut al seu caràcter amfifílic. Per això, els tensioactius disminueixen la tensió interficial entre fases, augmentant l'estabilitat de les emulsions (Walstra, 1996; Malmsten, 2002).

Els tensioactius es poden classificar segons la seva càrrega en solució, en iònic, noiònics i zwitteriònics (Rosen, 2004). També es poden classificar segons el número HLB (N_{HLB}), que correspon al balanç hidròfil – lipòfil, és a dir, a la proporció entre la part lipòfila i hidròfila. El paràmetre N_{HLB} permet predir el tensioactiu més apropiat per l'aplicació desitjada, com es mostra a la Taula 7.1 (Griffin, 1949; Becher, 1965; Shinoda, 1968 and 1973; Kunieda, 1985).

Taula 7.1: Propietats dels tensioactius en funció del N_{HLB}.

N_{HLB}	Aplicació
4 - 8	Antiescumant
7 - 11	Emulgent W/O
11 - 14	Humectant
12 - 16	Emulgent O/W (detergent)
16 - 20	Solubilitzant

En aquesta tesi doctoral, es va utilitzar un tensioactiu noiònic etoxilat, el polisorbat 80, que té un N_{HLB} = 15, ja que es volen obtenir nano-emulsions O/W.

Estabilitat d'emulsions

Les emulsions (incloent nano-emulsions), tendeixen a la separació de fases, que es pot produir a través d'un o varis mecanismes. La predominança d'un sobre els altres depèn del tipus d'emulsió, dels components, del mètode de preparació i/o de la mida de gota. Els principals mecanismes, especificats en la Figura 7.1, són: sedimentació / cremat, floculació, coalescència i maduració d'Ostwald.
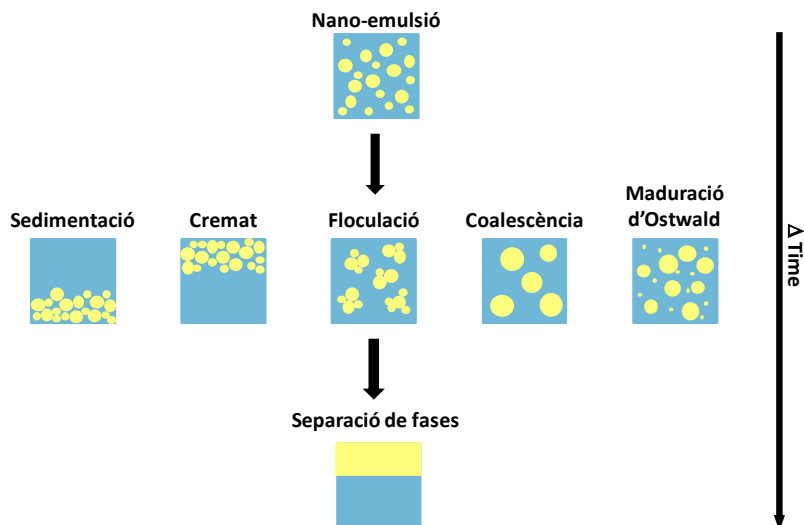
Figura 7.1: Representació esquemàtica dels principals mecanismos de desestabilització de les nano-emulsions.

La sedimentació i el cremat són processos de desestabilització deguts a la força gravitatòria (Tadros, 1983 i 2009). Són processos reversibles i amb una mínima aportació energètica es restableix la dispersió original. Les nano-emulsions, degut a la mida nanomètrica de les gotes, són estables contra aquest procés (Tadros, 2004; McClements, 2011).

La floculació consisteix en l'agregació reversible de les gotes de l'emulsió (Binks, 1998). Hi ha controvèrsia entre autors sobre si les nano-emulsions són estables a la floculació (Tadros, 2004; Anton, 2008) o no (Wang, 2008); però el que està demostrat és que l'addició de tensioactius la disminueix (Solans, 2003; Binks, 2007).

La coalescència consisteix en la ruptura irreversible del film interficial provocant que dues gotes es fusionin (Walstra, 1993; Masson, 2006). Aquest procés sí que es dóna en les nano-emulsions, tot i que també es pot reduir amb la selecció apropiada de tensioactius, sobretot els de cadena llarga, que augmenten el gruix del film interficial.

La maduració d'Ostwald consisteix en un fenomen de difusió de la fase dispersa de les gotes més petites cap a les gotes més grans, degut a les diferències en la pressió de Laplace, de manera que les gotes petites es fan més petites i les grans més grans (Lifshitz, 1961; Wagner, 1961). Aquest és el principal mecanisme pel qual les nano-emulsions tendeixen a separar-se irreversiblement en fases i el seu efecte és afavorit en mostres amb altes polidispersitats (Taylor, 1994; Tadros, 2004).

Mètodes de preparació de nano-emulsions

Les emulsions necessiten una aportació energètica per formar-se, ja que són sistemes termodinàmicament inestables. Tot i que habitualment les nano-emulsions es preparen per mètodes d'alta energia (Walstra, 1983; Anton, 2008), els **mètodes de baixa energia**, que aprofiten l'energia alliberada pels propis components del sistema, poden resultar avantatjosos en termes no només energètics i econòmics, sinó també per la producció de gotes més petites i monodisperses (Anton, 2008; Solans, 2012). Entre els mètodes de baixa energia, dins del subtipus de mètodes d'inversió de fases, basats en el canvi de la curvatura del tensioactiu, destaca el mètode d'inversió per canvi de composició a temperatura constant (mètode PIC), que consisteix en l'addició lenta d'un component (e.g. W) sobre la barreja dels altres dos (e.g. O/S), a temperatura

constant, de manera que es passa d'una estructura W/O a una O/W o viceversa (Figura 7.2). A més de ser un mètode fàcilment escalable, aquest mètode és avantatjós en treballar amb principis actius ja que es pot utilitzar a temperatura ambient, sense danyar els compostos termolàbils (Forgiarini, 2001; Usón, 2003; Sadurní, 2005 and 2006; Solè, 2006).
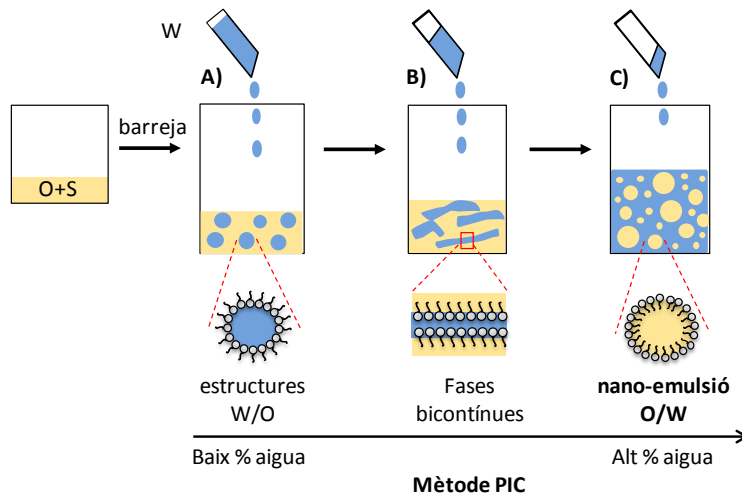
Figura 7.2: Esquema de la formació de nano-emulsions pel mètode de PIC.

Aplicacions de les nano-emulsions

Tot i que tradicionalment s'han aplicat en camps tan variats com l'alimentació, la farmàcia, la cosmètica i altres tecnologies químiques (Benita, 1993; Sonneville-Auburn, 2004; McClements, 2011), també són molt importants les aplicacions farmacèutiques. En la present tesi doctoral s'estudia l'aplicació de les nano-emulsions com a **plantilles per la formació de nanopartícules polimèriques** (Antonietti, 2002) a partir de la utilització de polímers preformats, incorporats en la fase oliosa abans de l'emulsificació (Desgouilles, 2003).

7.1.2. Nanopartícules polimèriques

Les **nanopartícules polimèriques** són partícules col·loïdals nanomètriques, amb mides d'un a mil nanòmetres (1-1000 nm), formades per una matriu polimèrica, que poden contenir principis actius dissolts, atrapats o encapsulats i la superfície de les quals es pot modificar (Soppimath, 2001; Tadros, 2004; Pinto-Reis, 2006).

287

La preparació de les nanopartícules polimèriques es pot fer a partir de nano-emulsions polimèriques (Vauthier, 2009; Solans, 2012). Amb aquest objectiu, és necessari que un polímer preformat formi part de les gotes de la nano-emulsió de partida, de manera que cada gota de la nano-emulsió formarà una nanopartícula degut a la precipitació del polímer (Pinto-Reis, 2008; Vauthier, 2009(1)). S'han utilitzat diferents metodologies per la formació de nanopartícules a partir de nano-emulsions polimèriques (Soppimath, 2001; Anton, 2008; Vauthier, 2009(1)). Entre elles, destaca el mètode d'evaporació del solvent, escollit en aquesta tesi, que consisteix en la utilització d'un solvent volàtil per la formació de les gotes de la nano-emulsió (Soppimath, 2001; Pinto-Reis, 2006; Vauthier, 2009; Calderó, 2011).

Aplicacions de les nanopartícules polimèriques en biomedicina

En els darrers anys, l'interès en les nanopartícules polimèriques per aplicacions biomèdiques ha augmentat exponencialment (Pinto-Reis, 2006; Kreuter, 2014). Són vàries les característiques que les fan apropiades per usos biomèdics, com la mida nanomètrica; la versatilitat tant en l'encapsulació de diferents tipus de compostos, com en la vectorització de la superfície per arribar als òrgans diana; el control de la cinètica d'alliberament de fàrmacs i la possibilitat d'escalat del procés (Pinto Reis, 2006; Vauthier, 2009(1)).

En la present tesi doctoral, la **via intravenosa** es va seleccionar per la **vectorització de les partícules a la barrera hemato-encefàlica** (BBB), amb l'objectiu de tractar malalties neurodegeneratives. Per utilitzar aquesta via, és important que els materials que formen les nanopartícules siguin biocompatibles, biodegradables i no tòxics, preferentment aprovats per la Food and Drug Administration (FDA); que la mida de les nanopartícules sigui inferior a 1000 nm i que es provoqui la mínima activació del sistema immune (Benita, 1993, Vauthier, 2009(1)).

Actualment, les malalties neurodegeneratives són una de les principals causes de mortalitat en la població humana (Tosi, 2011), degut a la dificultat de fer arribar principis actius al sistema nerviós central, ja que la BBB no deixa passar substàncies exògenes. Per aquesta raó, el desenvolupament de noves teràpies, com l'administració de les nanopartícules per via intravenosa, amb capacitat de travessar la BBB, és de vital importància.

7.2. Objectius

Els objectius de la present tesi doctoral són els següents:

1) Formulació de nano-emulsions O/W utilitzant mètodes de baixa energia i components poc tòxics.
2) Preparació de nanopartícules polimèriques mitjançant l'evaporació del solvent a partir de les nano-emulsions, i la seva caracterització.
3) Encapsulació de molècules fluorescents, fàrmacs i unió de material genètic, per utilitzar-les com sistemes d'imatge i/o terapèutics.
4) Funcionalització de la superfície de les nanopartícules amb dendrons o anticossos per aconseguir una vectorització específica.

7.3. Resultats i discussió

7.3.1. Selecció dels components del sistema

Abans de formular les nano-emulsions, és necessari escollir els components adequats per l'aplicació final de les nanopartícules obtingudes.

Com a fase aquosa, es va escollir el tampó fosfat salí (PBS), a una concentració de 0.16M, ja que compleix els requeriments del pH i osmolalitat fisiològics de la sang (pH = 7.4; 300mOsm/kg) (Dobrovolskaia, 2013). Tot i això, també s'han utilitzat concentracions inferiors de PBS i aigua amb fins comparatius.

Com a tensioactiu, es va seleccionar el polisorbat 80, un tensioactiu noiònic etoxilat, adequat per la formació de nano-emulsions O/W utilitzant el mètode de PIC (Shinoda, 1968 and 1973). A més, estudis previs han demostrat que el polisorbat 80 augmenta el pas a través de la BBB, ja que té una adsorció preferencial de les apolipoproteïnes de la sang, que tenen receptors específics a la BBB (Kreuter, 2014).

Com a fase oliosa, s'ha escollit una barreja d'un solvent orgànic volàtil i un polímer, per poder obtenir nanopartícules polimèriques. El polímer escollit va ser l'àcid poli-(làctic-co-glicòlic) (PLGA) amb una proporció de làctic / glicòlic 75/25 (MW = 10,000Da), ja que és un polímer biocompatible, biodegradable, i amb ús parenteral aprovat per la FDA (Kreuter, 2014). Inicialment, com a solvent es va escollir l'acetat d'etil, ja que és un solvent que correspon a la classe 3 de les guies de ICH (Pinto

Reis, 2006), a més, la temperatura d'evaporació és baixa i el PLGA és prou soluble en ell com per formar les nanopartícules. Els següents components es van dissoldre en la fase oliosa prèviament a la formació de nano-emulsions per poder ser posteriorment encapsulats en les nanopartícules: el marcador fluorescent cumarina 6, nanopartícules magnètiques (MNPs) i els fàrmacs loperamida i galantamina. Per a encapsular el fàrmac loperamida, es va haver d'utilitzar com a solvent una barreja d'etanol/acetat d'etil al 20/80, degut a requeriments de solubilitat.

7.3.2. Formació de nano-emulsions pel mètode d'inversió per canvi de la composició i caracterització

Les nano-emulsions es van preparar en el sistema: *fase aquosa (W) / polisorbat 80 (S) / [4wt % PLGA en acetat d'etil] (O)* amb el mètode PIC, a 25ºC, mitjançant l'addició lenta de la fase aquosa a barreges d'O/S*.* Es van canviar diversos paràmetres / condicions per estudiar l'efecte en la zona de formació de la nano-emulsió, la mida de les gotes obtinguda, l'estabilitat i la càrrega superficial.

Efecte de la variació de la concentració d'electròlits

Referent a la **zona de formació** de la nano-emulsió, es va posar de manifest una dependència, tot i que no lineal, amb la concentració d'electròlits (Figura 7.3); a les concentracions de PBS estudiades: 0M, 0.03M, 0.08M i 0.16M. La zona de formació s'eixampla en afegir electròlits, i es formen nano-emulsions a menors continguts d'aigua. Així mateix, les nano-emulsions es tornem més transparents i brillants en presència d'electròlits.
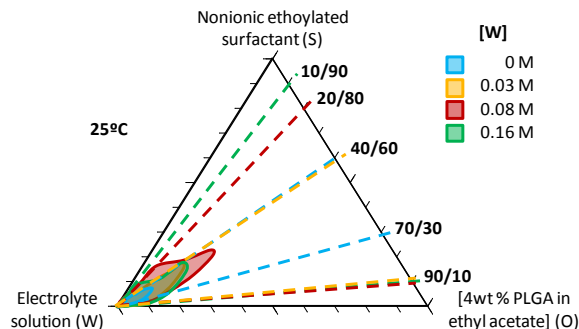
Figura 7.3: Regió de formació de les nano-emulsions en el sistema Solució aquosa(variant la molaritat) / polisorbat 80 / [4wt% PLGA en acetat d'etil].

Es van seleccionar nano-emulsions amb un 90wt% de contingut de fase aquosa en els següents estudis.

Amb els sistemes formulats amb aigua, es va estudiar la **conductivitat** en funció del percentatge de fase aquosa. Es va evidenciar, per diferents proporcions O/S, una conductivitat baixa a baixos continguts d'aigua, que indica la presència d'estructures W/O. La conductivitat augmenta en augmentar el contingut d'aigua, degut a la inversió de fases, tornant a disminuir en afegir més aigua degut a un factor de dilució. D'aquesta manera, es va confirmar que les nano-emulsions es produïen per una inversió de fases. En els sistemes amb PBS, en canvi, degut a la alta concentració d'electròlits, no és possible l'estudi del procés d'inversió per conductivitat. Tot i això, la inversió de fases es va corroborar mitjançant l'addició de colorant lipòfils i hidròfils.

El **radi hidrodinàmic** de les gotes de les nano-emulsions, estudiat per dispersió de llum (DLS), es va posar de manifest que depenia tant de la concentració d'electròlits com de la proporció O/S (Figura 7.4). Les nano-emulsions formulades amb aigua mostren mides al voltant dels 200 nm, amb una lleugera tendència a la disminució en augmentar la relació O/S (O/S baixos). En afegir electròlits a 0.03M, a relacions O/S baixes, les mides són similars a les del sistema amb aigua, que disminueixen progressivament fins als 25 nm en augmentar la relació O/S. Amb el sistema amb PBS 0.08M, en canvi, excepte per altes relacions O/S, els radis es mantenen baixos, al voltant dels 20 nm. En augmentar fins a 0.16M la concentració de PBS, les mides són grans per les relacions O/S extremes, tot i que per relacions O/S intermitges, les mides es mantenen petites (30nm). El canvi de mida es pot atribuir a la combinació de dos fenòmens. Per una banda, la mida disminueix en disminuir la proporció O/S, ja que hi ha més tensioactiu que pot estabilitzar més les gotes; però per altra banda, la mida disminueix en augmentar la proporció O/S ja que hi ha més solvent que pot difondre cap a la fase contínua.

Cal remarcar que en totes les mostres estudiades en la present tesi, els índex de polidispersitat (PDI) estan lleugerament per sobre del rang de monodispersitat (0.2) (Schärtl, 2006).
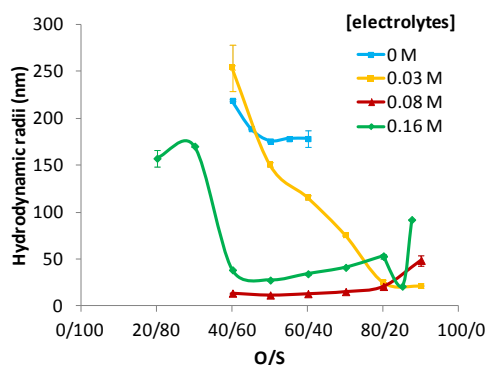
Figura 7.4: Radi de gota hidrodinàmic de les nano-emulsions amb un 90wt% de fase aquosa en funció de la proporció O/S, per diferents concentracions d'electròlits

Tant la càrrega superficial de les nano-emulsions com la seva estabilitat es va estudiar pels sistemes mencionats en l'anterior figura (7.4). Es va posar de manifest que les nano-emulsions obtingudes tenen **potencial zeta** negatiu, degut als grups carboxílics del PLGA, sense una tendència clara ni en funció de la proporció O/S ni en funció de la concentració d'electròlits.

Referent a l'**estabilitat**, les nano-emulsions haurien de se estables en front la sedimentació i el cremat, tal i com s'ha comentat anteriorment (Tadros, 2004). Per *observació visual* es va evidenciar la formació d'un sediment en forma de pols blanca, que es va atribuir a la formació accelerada de nanopartícules degut a la difusió del solvent cap a la fase aquosa. Tot i això, en cap de les mostres estudiades es va veure una separació de fases. En afegir electròlits, l'estabilitat de les nano-emulsions incrementa de 4 a més de 30 dies, sent les nano-emulsions amb concentracions intermèdies de PBS (0.03M i 0.08M) les més estables. La disminució d'estabilitat en les nano-emulsions amb alta concentració de PBS (0.16M) es va atribuir a una coagulació provocada per l'excés de sals, que prèviament s'havia observat en altres estudis (Rao, 2011). A més, les nano-emulsions amb relacions O/S intermèdies són les més estables. Per confirmar aquests resultats, es va fer un estudi amb *llum transmesa i retrodifusa* així com també el *canvi de mida* (per DLS) en funció del temps. Es va confirmar que les nano-emulsions es desestabilitzen per sedimentació, en el sistema amb aigua, i que quan s'afegeixen electròlits, l'estabilitat augmenta, de manera que no es posen de manifest fenòmens de desestabilització per difusió de llum ni canvis en la mida de gota (després de variacions inicials atribuïdes a una combinació de la coalescència amb la difusió del solvent). A més, la incorporació de lípids de cadena llarga (e.g. esqualà) va

permetre descartar la maduració d'Ostwald com el principal mecanisme de desestabilització de les nano-emulsions formulades.

Efecte de la variació del solvent

El solvent escollit inicialment, l'acetat d'etil, es va combinar amb etanol, en una relació etanol/acetat d'etil de 20/80, per aconseguir solubilitzar la loperamida.

Es va posar de manifest que l'addició d'etanol provoca un augment de la zona de formació de nano-emulsions formulades amb PBS 0.16M, que es va atribuir a un canvi del coeficient de partició del tensioactiu. Referent a les mides de gota, no obstant, es va evidenciar que es podia afegir fins a un 20wt % d'etanol (i també d'acetona) en l'oli sense modificació de les mides.

L'addició de loperamida, un principi actiu amb activitat analgèsica central, a la fase oliosa, va produir disminució de la zona de formació de les nano-emulsions, fenomen prèviament observat per altres fàrmacs (Date, 2010).

Efecte de la concentració del polímer

L'increment de la concentració de polímer del 4wt% al 20wt% va produir un desplaçament de la zona de formació cap a continguts majors d'oli, (menys quantitats de PBS). Tot i que les mides de les nano-emulsions amb 20wt% de PLGA varien en funció de la relació O/S igual que ho feien amb el 4wt% de PLGA, aquesta variació està desplaçada degut al desplaçament de la zona de formació.

Efecte de la temperatura

Com que el tensioactiu utilitzat és noiònic etoxilat, i aquests tensioactius són sensibles a la temperatura (Tadros, 2005), es va estudiar l'evolució de la mida de gota a 25 i 37ºC. Es va produir un augment de la mida de gota (de 40 nm a 80 nm) en augmentar la temperatura, atribuït a la desestabilització de les gotes en augmentar la temperatura sobre el tensioactiu etoxilat.

Les nano-emulsions formulades amb el sistema: *PBS 0.16M / polisorbat 80 / [4wt % PLGA en acetat d'etil]* amb 90wt% de fase aquosa s'escullen per posteriors estudis degut a la seva mida reduïda (radi al voltant dels 30nm) i l'osmolalitat adequades per l'administració intravenosa.

7.3.3. Formació de nanopartícules emprant nano-emulsions com a plantilles

Les nanopartícules polimèriques s'han format a partir de les nano-emulsions mitjançant el mètode d'evaporació de solvent. Per tal de facilitar la lectura d'aquesta secció i les següents, s'han assignat uns codis identificatius als diferents tipus de nanopartícules, segons la Taula 7.2.

Taula 7.2: Codis d'identificació de les nanopartícules.

Identificació	Fase aquosa
NP-W o NP-WY	Aigua
NP-XE or NP-XEY	Solució d'electròlits

X = *Concentració molar d'electròlits*
Y = *Percentatge d'oli en funció de la proporció O/S de la NE plantilla*

La **mida de les nanopartícules** (NP) s'ha caracteritzat usant diferents mètodes: DLS, SEM, TEM i AFM, ja que és un paràmetre molt important per l'administració intravenosa (es necessiten mides menors a 1000 nm (Dobrovolskaia, 2013)). Només es descriuran els resultats de DLS i TEM, ja que pels altres dos mètodes no s'han pogut trobar resultats significatius.

S'han estudiat les mides de les nanopartícules NP-W i NP-0.16E amb <u>DLS,</u> en funció de la proporció O/S de la nano-emulsió (NE) plantilla. Les NP-W tenen radis hidrodinàmics molt més grans (al voltant dels 150 nm), que les NP-0.16E (al voltant dels 25 nm), de manera que l'addició d'electròlits té el mateix efecte que per les nano-emulsions; però per les nanopartícules no hi ha diferències en funció de la proporció O/S. Tant en NE com en NPs, tot i que hi ha una lleugera polidispersitat, les mides de les nanopartícules són monomodals. S'han estudiat les nanopartícules NP-W50 i NP-W70 i les NP-0.16E-50 i NP-0.16E70 mitjançant <u>TEM</u>. Com s'esperava, ja que aquesta tècnica mesura l'esfera rígida, sense la capa de solvatació que es mesura amb DLS, les mides de les nanopartícules són menors (NP-W al voltant dels 100 nm de diàmetre i NP-0.16E al voltant dels 20 nm de diàmetre). A més de la mida, per estudis de TEM, també s'ha pogut estudiar la *morfologia* de les nanopartícules. Per totes les NPs estudiades, s'han trobat nanopartícules esfèriques, amb poca polidispersitat (Figure 7.5). En les nanopartícules formulades amb aigua, a més, s'han observat escletxes a la superfícies (Figura 7.5b), que s'han atribuït a la poca elasticitat del polímer, degut al seu baix pes molecular.
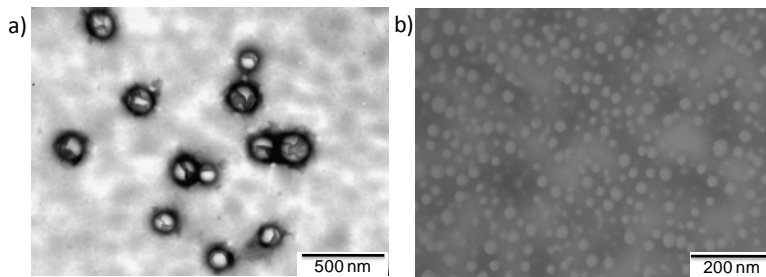
Figura 7.5: Micrografies de TEM de les nanopartícules: a) NP-W70 i b) NP-0.16E70.

A més, la mida s'ha estimat mitjançant càlculs teòrics (veure apèndix 8.2.1) a partir de les mides de les NE. Aquests càlculs es van aplicar per les nanopartícules amb diferents concentracions d'electròlits. Només en les concentracions d'electròlits més altes (NP-0.08E i NP-0.16E) es van obtenir mides menors que les experimentals, fet que es va atribuir a la presència de nanopartícules ja formades en la nano-emulsió degut a la difusió del solvent de les gotes a la fase contínua.

La **càrrega superficial** de les nanopartícules es va caracteritzar mitjançant mesures de la mobilitat electroforètica i transformant aquestes dades a potencial zeta mitjançant l'equació de Hückel-Onsager (Delgado, 2007). Com era d'esperar, i d'acord amb els resultats de les NE, es van obtenir potencials zeta negatius, degut als grups carboxílics del PLGA en solució. Els potencials zeta de les nanopartícules formulades amb aigua són menors que el de les formulades amb electròlits, fet que es va atribuir a un efecte compensatori de les càrregues negatives del PLGA amb les càrregues dels electròlits. Per l'administració intravenosa, són apropiades càrregues neutres o lleugerament negatives, per evitar les interaccions amb proteïnes de la sang o amb cèl·lules. Així doncs, les nanopartícules formulades podrien ser adequades considerant les càrregues.

L'**osmolalitat** també es va estudiar en funció de la concentració d'electròlits per les nanopartícules formulades amb una proporció 70/30 de O/S de la nano-emulsió de partida, i es va evidenciar, com anteriorment s'havia indicat, que una concentració de 0.16M d'electròlits és adequada per l'administració intravenosa (300 mOsm /kg).

L'**estabilitat col·loïdal de les nanopartícules** es va estudiar per observació visual, pels canvis en la llum retrodifusa i transmesa al llarg del temps i per determinació de canvis en la mida de les nanopartícules NP-W i NP-0.16E en el temps. Per observació visual es va detectar que les NP-W sedimenten al cap d'uns dies d'estar

preparades, mentre que les NP-0.16E són molt més estables, ja que, després de 90 dies, només es va observar sedimentació en aquelles nanopartícules on les relacions O/S de la nano-emulsió precursora es trobaven en el límit de la zona de formació. Per estudis de retrodifusió i transmissió de llum es va observar sedimentació de les NP-W50 i NP-W70 al cap de 24h, sent el pic de sedimentació més pronunciat en augmentar la temperatura d'estudi, degut a la major proximitat a la temperatura de transició vítria del polímer. Per les dispersions de nanopartícules NP-0.16E50 i NP-0.16E70, en canvi, no es va observar cap fenomen de desestabilització per aquesta tècnica en el temps experimental de 24h. Per estudis de canvi de mida en el temps (per DLS, fets amb les mateixes nanopartícules que en els estudis anteriors i també amb NP-0.08E i NP-0.03E), després de certes oscil·lacions a temps curts, la mida s'estabilitza per totes les nanopartícules estudiades excepte per les formulades amb aigua, on la mida disminueix amb el temps, degut a la sedimentació. Aquests resultats concorden tant amb les observacions visuals i els estudis de transmissió i retrodifusió de llum com amb els resultats de les nano-emulsions.

També es va estudiar l'**estabilitat química del polímer** en les nanopartícules NP-W70 i NP-0.16E70. En formar les nanopartícules, l'espectre de FTIR del PLGA així com també la seva descomposició termal (TGA) demostren que el polímer es manté inalterat en el procés de formació. Al llarg del temps, en augmentar la temperatura augmenta la mida de les nanopartícules degut a l'apropament a la temperatura de transició vítria del polímer. En relació al pH, s'esperava una disminució en funció del temps, degut a la degradació de les cadenes de PLGA en els àcids làctic i glicòlic. Efectivament, els resultats van ser els esperats, ja que es produeix una disminució, que era més accentuada per les NP-W. No obstant, el pH ja no disminueix més a partir de 50 dies, fet que es pot atribuir a què ja no es degraden més cadenes. Mitjançant mesures d'osmolalitat, es va posar de manifest que aquesta incrementava amb el temps degut a la formació dels dos àcids provinents de la degradació del polímer, confirmant els resultats anteriors. Cal remarcar que l'addició de sèrum, per simular condicions fisiològiques, accelera la degradació del polímer (confirmat tant per mesures de viscositat com d'osmolalitat).

Mitjançant mesures de mida i potencial zeta, es va evidenciar que la metodologia de producció de les nanopartícules és un procés reproduïble.

Resum

Les característiques de les nanopartícules vénen determinades per les característiques de les NE de les quals provenen. Canvis en el medi de dispersió de les nanopartícules no provoquen canvis en les seves característiques físico-químiques (mida, potencial zeta, osmolalitat). Tot i això, post-tractament agressius (e.g. ultracentrifugació) fan que la mida de les nanopartícules augmenti.

De les nanopartícules formulades, les NP-0.16E70 es van escollir com a material més apropiat per la seva utilització en etapes posteriors, ja que suposen un equilibri entre concentracions baixes de tensioactiu (3wt% en la nano-emulsió de partida), mides petites (25 nm de diàmetre), càrrega superficial negativa (uns -40 mV), pH i osmolalitat sanguinis.

7.3.4. Encapsulació de compostos actius en nanopartícules

Les nanopartícules seleccionades a l'etapa anterior s'han utilitzat per encapsular diversos tipus de compostos: cumarina 6 i nanopartícules magnètiques (per usar les nanopartícules com a sistemes d'imatge) així com loperamida i galantamina (per utilitzar les nanopartícules com a sistemes terapèutics avançats). Tots aquests compostos es van incorporar a la fase oliosa de la nano-emulsió, abans del procés d'emulsificació. L'aspecte de les dispersions es mostra a la Figura 7.6.

Figura 7.6: Exemples de l'aspecte visual de dispersions de nanopartícules encapsulant: a) Cumarina 6 al 0.01wt%; b) nanopartícules magnètiques al 0.06wt%; c) Loperamida al 0.1wt% i d) Galantamina al 0.1wt%.

Cumarina 6

La Cumarina 6 (C6) es va escollir com a marcador fluorescent degut a la seva elevada solubilitat en acetat d'etil i la seva fàcil detecció per fluorescència (cap als 555 nm). La seva incorporació en les nanopartícules no va provocar canvis en les característiques físico-químiques de les nano-emulsions ni de les corresponents nanopartícules.

Es va comprovar qualitativament que la C6 havia estat encapsulada dins les nanopartícules, mitjançant estudis microscòpics de col·localització de senyal fluorescent amb senyal òptica de nanopartícules (anàlisis hiperespectrals) així com estudis de FTIR. Així mateix, es va determinar que l'eficiència d'encapsulació és aproximadament del 100wt%.

Encara que l'alliberació del fàrmac cap a una solució receptora es produeix en poques hores, és temps suficient per a poder utilitzar les nanopartícules com a sistemes d'imatge per l'administració intravenosa, ja que en 10 minuts la sang arriba a tots els òrgans d'un ratolí (Rigues, 1973).

Nanopartícules magnètiques (MNPs)

Es van escollir nanopartícules d'òxid de ferro per ser encapsulades en les nanopartícules, ja que previs estudis havien demostrat que podrien ser adequades com a sistemes d'imatge (Salas, 2012). Es va aconseguir encapsular fins a un 0.06wt% de MNPs. Tot i que el potencial zeta i l'estabilitat de les nanopartícules no es van modificar, les mides eren aproximadament el doble que les de les nanopartícules originals.

Estudis de microscopia electrònica (TEM) van permetre confirmar que les MNPs estaven encapsulades dins de les nanopartícules polimèriques, tot i que no totes les nanopartícules polimèriques contenien MNPs, degut a la baixa concentració d'aquestes últimes. Tot i això, la separació magnètica d'aquestes nanopartícules es va aconseguir amb imans de diferents forces. Per tant, aquest podria ser un altre sistema d'imatge després de l'administració intravenosa per estudis, per exemple, de biodistribució.

Loperamida

La loperamida es va seleccionar com a model de fàrmac a encapsular per estudiar el pas de les nanopartícules a través de la BBB. Aquest fàrmac té activitat analgèsica a nivell central, tot i que per si sol no és capaç de travessar la BBB. Degut a la insuficient solubilitat de la loperamida en acetat d'etil per assolir concentracions terapèutiques, es va incorporar un 20wt% d'etanol a la fase oliosa de les nano-emulsions. Aquesta modificació, juntament amb l'addició del fàrmac, va provocar un augment de la mida de les gotes de la nano-emulsió (i de les corresponents nanopartícules) fins a radis hidrodinàmics al voltant dels 120 nm

(100 nm per les nanopartícules), que es mantenen dins del rang de mides apropiades per materials injectables per via intravenosa.

Amb la loperamida, es van aconseguir eficiències d'encapsulació gairebé del 100%. Tot i això, no es va arribar a concentracions terapèutics, i va ser necessari un pas posterior de concentració, mitjançant dispositius de filtració / centrifugació comercials, seguit de diàlisi per recuperar el pH i l'osmolalitat de les nanopartícules.

Estudis d'alliberació del fàrmac a una solució receptora van posar de manifest que després d'una setmana d'estudi, només s'allibera al voltant del 15wt% del fàrmac, cosa que indica que està ben retingut en les nanopartícules; per tant, aquestes es poden utilitzar com a sistemes avançats d'alliberament de la loperamida.

Galantamina

La galatamina es va escollir com a model de fàrmac antiapoptòtic, ja que té activitat inhibidora d'acetilcolinesterasa, molt útil i utilitzada actualment pel tractament de malalties neurodegeneratives (Villaroya, 2007). Es va aconseguir directament encapsular un 0.1wt% de fàrmac en la fase oliosa de les nano-emulsions. D'aquesta manera, en no haver de variar el solvent de la fase aquosa, no es va modificar significativament ni la mida ni el potencial zeta de les nano-emulsions ni de les corresponents nanopartícules. Tot i que es van aconseguir eficiències d'encapsulació de gairebé el 100wt%, no es va arribar a dosis terapèutiques, pel que seria necessari el posterior pas de concentració de nanopartícules per l'administració intravenosa.

A diferència de la loperamida, però, es va aconseguir alliberar fins a un 80wt% de galantamina de les nanopartícules a una solució aquosa. De totes maneres, aquest alliberament va ser molt més lent que el provinent directament d'una solució del fàrmac. A més, cal destacar que es va comprovar que l'activitat inhibidora d'acetilcolinesterasa es mantenia quan el fàrmac estava encapsulat, de manera que les nanopartícules podrien ser útils com a sistemes d'alliberament de galantamina.

Resum

La tecnologia de fabricació de nanopartícules a partir de nano-emulsions polimèriques permet encapsular compostos de diferent naturalesa amb altes

eficiències d'encapsulació (majors del 90wt%) així com també controlar-ne l'alliberament.

7.3.5. Funcionalització de les nanopartícules

Les nanopartícules es van funcionalitzar amb compostos de diferent naturalesa, per aconseguir objectius específics. Es va comprovar la correcta funcionalització en cada cas així com també la caracterització dels complexes formats. A continuació es detallen els principals resultats obtinguts.

Fluoresceïna isotiocianat (FITC)

La fluoresceïna isotiocianat (FITC) es va seleccionar com a marcador fluorescent, alternatiu a la Cumarina 6, amb objectiu d'utilitzar les nanopartícules com a sistema d'imatge. En aquest cas, però, es va fer una unió covalent de FITC al PLGA, prèvia a la formació de la nano-emulsió, ja que FITC és estable en solvents orgànics i s'orientarà cap a la superfície de les nanopartícules gràcies a la seva hidrofilicitat. Després de múltiples etapes de rentat, la pols de polímer es mantenia de color taronja (degut a la presència del fluorescent), indicació de què el FITC s'havia incorporat a les nanopartícules. Com era d'esperar, la mida tant de nano-emulsions com de nanopartícules va augmentar, fins a 140 i 120 nm de radi hidrodinàmic respectivament. El potencial zeta també va variar, essent molt més negatiu (caps als -60 mV per les NE). Tot i aquests canvis, però, les nanopartícules marcades amb FITC es poden considerar un sistema adequat per l'administració intravenosa.

Dendrons catiònics

Es van unir covalentment dendrons catiònics amb estructura de carbosilà per donar càrrega positiva a la superfície de les nanopartícules amb l'objectiu de poder-hi unir electrostàticament material genètic. Es van utilitzar dues generacions del mateix tipus de dendrons, la segona (G2SN) i la tercera (G3SN).

Per **comprovar l'eficàcia de la unió covalent**, (reacció de la carbodiimida per unir el grup carboxílic de les nanopartícules amb el grup focal amina dels dendrons) es va emprar el test de Kaiser, que detecta la presència de grups amina lliures. Aquest test donava negatiu després de la reacció (i posterior rentat per eliminar reactius i

materials de partida); el potencial zeta passava a ser positiu, hi havia un canvi en el patró de bandes de FTIR i també en la descomposició tèrmica (estudis de TGA).

Es van assajar **diferents proporcions** nanopartícula / dendró (NP/G2SN o NP/G3SN). Es va evidenciar que les proporcions molars òptimes (càrrega cap als 30 mV i mida cap als 25 nm de radi hidrodinàmic) eren 1/20 per NP/G2SN i 1/5 per NP/G3SN. Ja era d'esperar que es necessités més dendró de segona generació que de tercera, ja que un mol de G2SN té la meitat de càrregues positives (4) que G3SN (8). Tots dos complexos van resultar estables durant més de 9 dies, per observació visual. Així doncs, es van considerar ambdós adequats pels posteriors estudis d'unió amb els oligonucleòtids.

Oligonucleòtids

Es van unir electrostàticament tres tipus diferents d'oligonucleòtids a les nanopartícules funcionalitzades amb dendrons amb l'objectiu d'utilitzar els complexes formats com a vector no virals de teràpia gènica. Els oligonucleòtids units van ser: oligonucleòtids antisentit (ASO), RNA d'interferència (siRNA) i plasmidis.

ASOs

Fixant una concentració d'ASO, es va variar la proporció en càrrega de NP/ASO per trobar l'òptim de complexació, on la càrrega superficial és gairebé nul·la. La proporció adequada per NP-G2SN va ser al voltant de 0.75/1, mentre que per G3SN-NP es va observar que era al voltant de 0.5/1. Per precisar més la proporció, es van realitzar assajos de mobilitat electroforètica retardada, on es va confirmar que les G2SN-NPs començaven a complexar al voltant de la proporció en càrrega 0.25/1 i les G3SN-NPs al voltant de 0.5/1. A més, caracteritzant ambdós complexes, es va posar de manifest que les G2SN-NPs havien augmentat de radi hidrodinàmic fins a 85 nm, mentre que les G3SN-NPs havien augmentat només fins a 40 nm. En ambdós casos, però, els complexes eren estables almenys 90 dies, per tant, es poden utilitzar com a vectors no virals de teràpia gènica.

siRNA

Es van fer les mateixes proves que en el cas anterior utilitzant un material genètic diferent. Tot i això, aquesta vegada, només es van utilitzar les G2SN-NPs. Per estudis tant de potencial zeta com de mobilitat electroforètica retardada es va evidenciar que la proporció de complexació estava al voltant de 0.5/1 (siRNA/NP).

Plasmidis lentivirals

També es va assajar la unió electrostàtica de plasmidis lentivirals amb les G2SN-NPs. Cal remarcar, però, que com que el material genètic és molt major als anteriors (al voltant de 250 nm de radi hidrodinàmic), podrien existir dificultats en la transfecció cel·lular degut a problemes estèrics.

Els estudis de la proporció de complexació, en aquest cas molar, de NPs / plasmidi van demostrar que la mida del complex format disminuïa en augmentar la proporció de nanopartícules. Es va posar de manifest que la proporció de complexació era al voltant de 200/1, amb càrrega gairebé neutra, però la mida augmentava molt; per això es va escollir la proporció 125/1, amb càrrega també neutra i mides al voltant dels 60 nm de radi hidrodinàmic. Per tant, tot i haver començat amb mides majors, aquests complexes també es van considerar adequats per posteriors estudis de transfecció cel·lular.

Polietilenglicol (PEG)

El polietilenglicol (PEG) es va utilitzar per recobrir els complexes formats amb ASO i siRNA, com a sistema de protecció del material genètic. Tot i això, cal remarcar que també és útil per emmascarar les nanopartícules i evitar la seva detecció pel sistema immunitari a la sang (Ishihara, 2009).

Es van utilitzar els complexes amb G2SN i ASO per escollir el pes molecular adequat del PEG. El PEG de 400Da va resultar ser el més adequat, ja que s'obtenien complexes amb mides al voltant dels 80 nm (si s'augmenta el pes molecular del PEG, augmenta la mida dels complexes). També es van determinar les condicions òptimes de conjugació (30 minuts d'incubació a 37ºC). Es van aconseguir formular complexes recoberts de PEG. Tot i això, en el cas dels siRNAs, l'estabilitat dels complexes no era tan elevada com amb els ASOs.

Anticòs monoclonal contra el receptor de transferrina (anti-TfR mAb)

L'anticòs monoclonal contra el receptor de la transferrina (anti-TfR mAb) es va escollir amb l'objectiu de fer una vectorització específica cap a la BBB, perquè el receptor de transferrina està sobreexpressat a BBB. Es va realitzar la reacció de la carbodiimida, com en el cas dels dendrons, per aconseguir la unió covalent. Aquesta unió covalent es va poder confirmar mitjançant estudis de microscopia òptica amb anàlisi espectral, on es va veure que col·localitzaven el fluorescent d'un anticòs secundari contra el anti-TfR mAb (vermell) i la C6 encapsulada (Verd) (Figure 7.7). Els estudis cromatogràfics també van confirmar la unió ja que es donava un canvi en la longitud màxima d'absorció i en el temps de retenció. En aquest cas, també es van assajar diferents proporcions molars d'anticòs/NPs, es va evidenciar que la proporció molar 12.5/1 (NP/anticòs) era la més adequada.
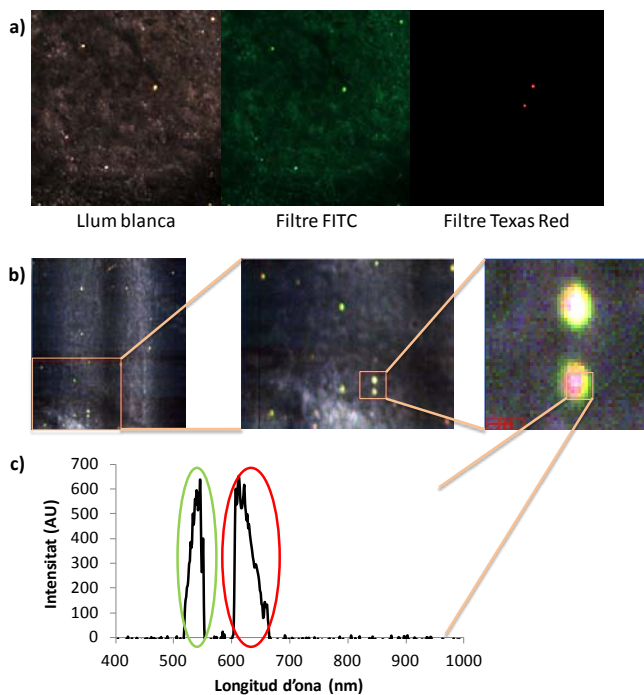
Figura 7.7: Estudi de nanopartícules funcionalitzades amb anti-TfR mAb, encapsulant C6, incubades sobre talls de cervell (per tenir un suport físic), mitjançant microscòpia òptica amb anàlisi espectral de la imatge. a) Imatge òptica utilitzant diferents filtres; b) Anàlisi espectral amb llum blanca i c) Exemple del perfil espectral de les nanopartícules, amb senyal en el verd i en el vermell, marcades amb un cercle del color corresponent.

La formació dels complexes no va modificar la mida, el potencial zeta ni l'estabilitat de les nanopartícules. Cal remarcar que l'estudi es va fer tant amb NPs sense cap encapsulació com amb C6 i loperamida encapsulades i es van obtenir els mateixos resultats.

D'aquesta manera, també es pot afirmar que les nanopartícules han estat funcionalitzades amb l'anticòs anti-TfR mAb i es podrien provar com a sistemes de vectorització cap a la BBB.

7.3.6.   Estudis *in vitro*

Un cop definides les nanopartícules com a apropiades per l'administració intravenosa, considerant característiques físico-químiques, és necessari comprovar la seva toxicitat tant en cultius cel·lulars com amb cèl·lules sanguínies, així com també estudiar la capacitat de transfecció dels gens units i la interacció amb els components sanguinis.

Estudis de citotoxicitat

La citotoxicitat dels complexes formulats amb ASOs s'ha estudiat utilitzant tant cèl·lules HeLa com U87, amb assajos de MTT i de LDH. Excepte pel dendró G3SN sol, no s'ha trobat citotoxicitat en cap mostra a la concentració més alta estudiada (300nM d'ASO), fet que permet afirmar que aquests complexes es podrien utilitzar com a vectors no virals de teràpia gènica, tot i que és millor utilitzar el complex formulat amb el dendró G2SN, ja que per si sol tampoc provoca toxicitat. La toxicitat observada en G3SN podria ser degut a la seva alta càrrega positiva.

Per completar els estudis de citotoxicitat, també es van estudiar les nanopartícules amb loperamide, galantamina i C6 encapsulades, i també les funcionalitzades amb l'anti-TfR mAb; a la concentració d'ús, amb cèl·lules HeLa. Així mateix, la línia cel·lular HEK també es va utilitzar per estudiar la citotoxicitat provocada pels complexes amb el plasmidi. En cap dels casos s'han trobat efectes citotòxics, de manera que aquestes nanopartícules es poden emprar en aplicacions biomèdiques.

Transfecció cel·lular

La transfecció cel·lular s'ha estudiat pels complexes formulats amb ASO i siRNA, mitjançant inhibició de la luminescència generada pel gen luciferasa (introduït artificialment a les cèl·lules) i mitjançant la producció de llum fluorescent produïda pel plasmidi utilitzant els complexes que contenen aquest plasmidi.

La **transfecció dels ASOs** en absència de sèrum es va veure que era molt més alta amb els complexes formulats amb G2SN, per això es van descartar els formulats amb G3SN, i també per possibles problemes citotòxics. En condicions fisiològiques (10wt % sèrum en cultiu), es van assajar diferents proporcions NP/ASO, amb i sense recobriment de PEG, l'òptim de transfecció es va trobar a una proporció NP/ASO de 0.75/1 amb el recobriment de PEG. Amb aquest complex es van aconseguir eficiències de transfecció gairebé del 90% (Figura 7.8), valors equiparables als vectors comercials existents actualment, però sent aquests complexos desenvolupats en aquesta tesi avantatjosos ja que no provoquen citotoxicitat (Fisher, 1997; Dalby, 2004).
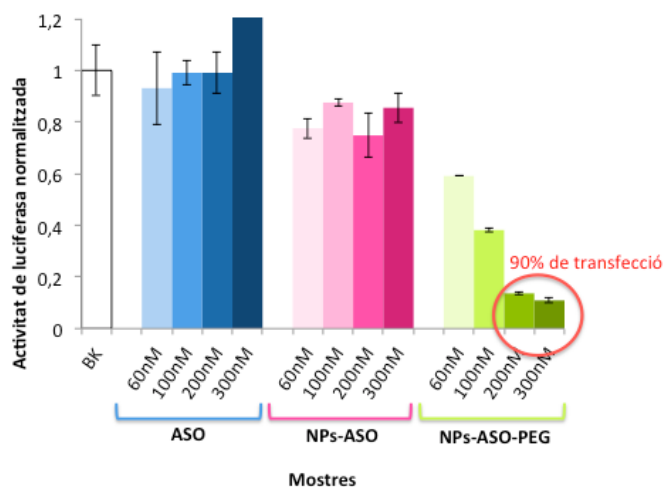
Figura 7.8: Activitat de luciferasa normalitzada en funció de la concentració d'ASO, a una proporció NP/ASO de 0.75/1 per les mostres preparades amb el dendró G2SN, amb un 10wt% de sèrum, en un cultiu de HeLa.

La **transfecció dels siRNA** també es va estudiar, però només pels complexes formats amb G2SN i recoberts amb PEG. Les millors eficiències de transfecció es van aconseguir a 200nM de siRNA, tot i que aquestes eficiències no són tan altes com pels ASOs, fet que es va atribuir a la menor estabilitat d'aquests complexes.

La **transfecció dels plasmidis lentivirals** també es va estudiar pels complexes formats amb G2SN, i també es van aconseguir bones eficiències de transfecció, del voltant del 80-90% amb una proporció de NP/plasmidi 125/1.

Cal remarcar que s'aconsegueixen eficiències de transfecció comparables als vectors comercials i, a més les nanopartícules dissenyades en aquest treball tenen l'avantatge que no són tòxiques.

Estudis d'hemòlisi

És necessari estudiar la toxicitat produïda quan les nanopartícules entren en contacte amb la sang, ja que la via intravenosa és l'escollida per l'administració. L'hemòlisi és el trencament dels eritròcits provocat per productes tòxics.

Es van assajar les mateixes nanopartícules que pels estudis de citotoxicitat, tant als 10 minuts del contacte com a les 24 hores. Només es va obtenir hemòlisi pels complexes formulats amb el dendró G3SN i pel dendró sol.

A mode comparatiu, tot i saber que les nanopartícules disperses en aigua no compleixen requeriments d'osmolalitat, també se'n va estudiar l'hemòlisi i es va observar que, efectivament, quan l'osmolalitat no era l'adequada, es produïa hemòlisi.

Interacció amb components sanguinis

Dels diversos components que té la sang, per poder administrar nanopartícules per via intravenosa, és imprescindible estudiar tres paràmetres com a mínim: l'hemòlisi, ja estudiada anteriorment, la coagulació i l'activació del sistema del complement (Dobrovolskaia, 2013). A més, l'adsorció de certes proteïnes sobre la superfície de nanopartícules també es va estudiar, ja que determina la biodistribució (Bertholon, 2006).

La influència en el temps de **coagulació sanguínia** es va estudiar per les nanopartícules sense cap modificació, ensapsulant C6 o loperamide i amb G2SN, G3SN o anti-TfR mAb funcionalitzat la seva superfície. Per una concentració de 1 mg/mL de nanopartícules, l'aconsellada per fer aquests estudis, no es va evidenciar modificació dels temps de coagulació en cap cas, de manera que les nanopartícules no provoquen efectes adversos en aquest sentit. Tot i això, augmentant la concentració a 3mg/mL, les nanopartícules funcionalitzades amb els dendrons sí

que provoquen retard en la coagulació, de manera que es podrien utilitzar com a anticoagulants.

Referent a l'**adsorció proteica**, primerament es va fer un estudi electroforètic per determinar les proteïnes unides, sense especificar per tipus de proteïna. Es va posar de manifest que, com s'esperava, la proteïna que més es trobava era l'albúmina sèrica, ja que és la majoritària de la sang. Tot i això, no tota quedava unida, cosa que ja interessa per no obstruir possibles unions amb altres. A més, també es van trobar bandes corresponents a altres proteïnes (Figura 7.9).
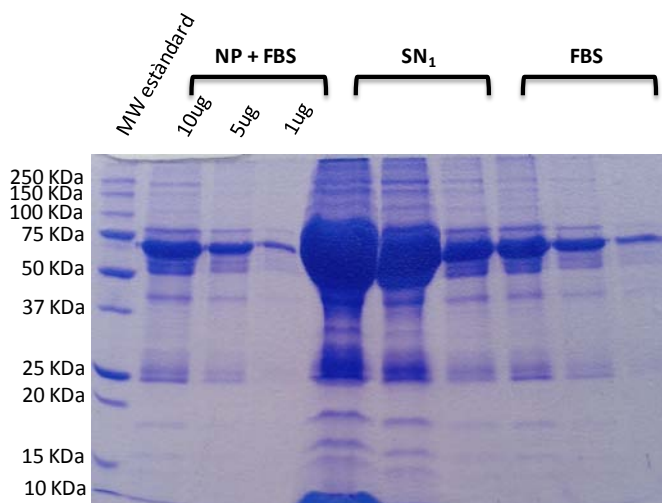
Figura 7.9: Gel electroforètic de les nanopartícules sense encapsular, sense funcionalitzar, incubades amb sèrum (NP+FBS). Amb fins comparatius també es mostren les proteïnes eliminades en un rentat (SN$_1$) i les del sèrum (RBS).

Per conèixer més específicament les interaccions de proteïnes amb les nanopartícules, es van estudiar diverses proteïnes sanguínies individualment. Es va escollir *l'albúmina sèrica* (BSA), ja que és la majoritària de la sang., i es va estudiar la seva adsorció en superfície tot mesurant el canvi de potencial zeta produït per nanopartícules soles i amb BSA fins a una concentració de 40mg/mL, la fisiològica. Es van estudiar les nanopartícules sense encapsulat, amb C6 encapsulada, o amb loperamida encapsulada, amb funcionalització amb el dendró G2SN, G3SN i l'anticòs. En tots els casos, excepte per les nanopartícules amb loperamida i el dendró de tercera generació, es va observar que la superfície quedava saturada amb concentracions de BSA menors a 3 mg/mL, cosa que permet afirmar que la quantitat adsorbida és poca, tal i com es pretenia aconseguir per evitar un reconeixement excessiu del sistema immunitari. El nombre de molècules de BSA

adsorbides per nanopartícula és equivalent a l'obtingut en anteriors publicacions (Vauthier, 2009(2)) excepte per les nanopartícules que encapsulen loperamida, que n'adsorbeixen moltes més perquè tenen mides més grans. Els augments de mida trobats no són massa importants ja que són degut a l'agregació de diferents nanopartícules (s'estudia per DLS), però la mida dels agregats es manté dins el rang de l'injectable.

El *fibrinogen* es va escollir com una altra proteïna model, ja que és un dels components crítics en la cascada de coagulació de la sang. En aquest cas, l'agregació provocada es va estudiar mitjançant visualització macroscòpica i microscòpica de les mostres. Només es va trobar agregació en superfícies positives, com previs estudis havien evidenciat per altres tipus de nanopartícules (Vauthier, En preparació).

Finalment, es va estudiar l'**activació del sistema del complement**, per saber si les nanopartícules activen el sistema immunitari en entrar en contacte amb la sang. Per fer-ho, es va estudiar concretament la *proteïna C3*, ja que és un dels components del sistema del complement; mitjançant electroforesis en dues dimensions. En aquest cas, d'acord amb assajos previs, es van haver de descartar les nanopartícules amb el dendró G3SN a la superfície, ja que provocava una mala difusió pel gel degut a la presència d'impureses que no el deixaven migrar bé.

Per les nanopartícules no funcionalitzades i sense cap element encapsulat, es va evidenciar una dèbil activació (al voltant del 20% similar als controls negatius), que augmentava en funcionalitzar la superfície tant amb G2SN com amb l'anticòs. En canvi, l'addició de loperamida o cumarina a l'interior, només provocava lleugers augments de l'activació del complement, de manera que, com era d'esperar, la superfície influeix més en l'activació del complement que no pas els compostos encapsulats, ja que l'activació es dóna per interacció amb la superfície de les nanopartícules. Estudis complementaris incloent l'activació provocada per les nanopartícules amb G2SN i ASO amb o sense PEG van mostrar augments de l'activació, tot i que el PEG se suposava que la disminuiria. L'explicació es va trobar en el fet que, encara que el PEG torna la superfície hidròfila, com previs estudis ja indicaven, si no té un pes molecular prou gran, o no hi ha prou densitat superficial de PEG, aquest pot no ser útil per disminuir l'activació del sistema del complement (Bertholon, 2006; Dobrovolskaia, 2013).

Cal remarcar que, tot i que a les concentracions estudiades només les nanopartícules no funcionalitzades, sense res encapsulat, provoquen activacions del complement del nivell dels controls negatius, les altres nanopartícules es podrien utilitzar per la via intravenosa si se'n disminueix la concentració, ja que disminuiria l'activació del complement.

Com que s'han obtingut resultats prou favorables dels tres estudis imprescindibles per l'administració intravenosa (hemòlisi, coagulació i osmolalitat), es pot afirmar que les nanopartícules són apropiades per administrar per la via intravenosa.

7.3.7. Estudis *in vivo*

Després de l'estudi *in vitro*, confirmant la idoneïtat de les nanopartícules per ser administrades per la via intravenosa, el següent pas són els estudis *in vivo*. En la present tesi, s'han utilitzat per comprovar l'absència de citotoxicitat provocada per les nanopartícules i per estudiar el creuament de BBB després de l'administració intravenosa.

L'administració intravenosa de diversos tipus de nanopartícules (no funcionalitzades i sense encapsular i encapsulant loperamida i/o l'anticòs i les diverses combinacions) no va provocar canvis de comportament en cap dels animals, i tampoc es va morir cap animal, de manera que es va reafirmar el caràcter no tòxic de les nanopartícules formulades.

Per estudiar **el creuament de BBB** de les nanopartícules formulades, es va escollir el fàrmac loperamida, com anteriorment s'ha raonat, ja que provoca efectes analgèsics a nivell central però per ell sol no és capaç de travessar la BBB. Aquest estudi va incloure un ampli set de controls negatius (tampó fosfat, nanopartícules sense encapsular ni funcionalitzar, nanopartícules sense encapsular amb l'anticòs i solució aquosa de polisorbat 80) i positius (solució de morfina, solució aquosa de polisorbat 80 i loperamida). Com a mostres a estudiar, es van seleccionar les nanopartícules amb loperamida, sense cap funcionalització específica, per estudiar si el polisorbat 80 era suficient com a vectorització inespecífica i amb l'anticòs com a funcionalització, per estudiar-lo com a vectorització activa a BBB.

Dels resultats obtinguts, es va observar que les nanopartícules no funcionalitzades només aconseguien augmentar els efectes analgèsics fins al voltant del 20%,

mentre que amb l'anticòs com a element de vectorització s'aconseguien efectes analgèsics augmentats en un 50%, valors molt similars als controls positius. D'aquesta manera, es pot afirmar que les nanopartícules funcionalitzades amb l'anticòs són capaces d'arribar i travessar la BBB.

7.4. Conclusions

Les conclusions més rellevants que es poden extreure dels resultats obtinguts són les següents:

1) Mitjançant el mètode d'emulsificació de baixa energia d'inversió de fases per canvi de composició a temperatura constant (comprovat per conductimetria i difusió de colorants) s'han obtingut nano-emulsions polimèriques usant el sistema solució d'electròlits (W) / polisorbat 80 (S) / [4wt% PLGA en acetat d'etil] (O). S'ha demostrat que aquestes nano-emulsions O/W:

   - Es formen amb alts continguts d'aigua, independentment de la concentració d'electròlits. La presència d'electròlits eixampla la zona de formació cap a menors continguts d'aigua. La zona de formació es modifica en canviar el percentatge de polímer, i en incorporar un segon solvent o un fàrmac a la fase oliosa.
   - Tenen radis hidrodinàmics al voltant dels 20 nm a concentracions intermèdies d'electròlits (0.08M) i relacions O/S entre 40/60 i 70/30. La mida de gota es veu afectada per la presència d'electròlits, la relació O/S i l'addició d'un segon solvent.
   - Són més estables en presència d'electròlits, almenys durant 60 dies, degut a un efecte més accentuat de "salting out". No obstant, es va observar una formació accelerada de nanopartícules degut a la difusió del solvent cap a la fase aquosa.
   - Tenen pH i osmolalitat dins del rang dels valors fisiològics, en presència d'electròlits a 0.16M. Per això, es van seleccionar aquestes nano-emulsions com a plantilles per la formació de nanopartícules polimèriques, així com també per les mides apropiades per l'administració intravenosa, el baix contingut de tensioactiu i l'elevada estabilitat.

2) Les nanopartícules polimèriques es van formar mitjançant l'evaporació del solvent de les nano-emulsions. La seva caracterització ha permès deduir que:
- Les característiques de les nanopartícules (mida, potencial zeta i estabilitat) depenen de les característiques de les nano-emulsions de les quals provenen.
- La mida de les nanopartícules es redueix de la trobada per les nano-emulsions, degut a l'evaporació del solvent. Les nanopartícules tenen morfologia esfèrica i la població és uniforme.
- El procediment de formació de nanopartícules a partir de nano-emulsions és reproduïble, de manera que seria apropiat per la seva aplicació industrial.

3) S'ha aconseguit encapsular compostos de diferent naturalesa dins les nanopartícules, mitjançant la seva dissolució en la fase oliosa, prèvia a la formació de la nano-emulsió:
- Cumarina 6 com a marcador fluorescent. No modifica les característiques físico-químiques de les nanopartícules, es va aconseguir una alta encapsulació i una difusió independent del pH.
- Nanopartícules magnètiques com a sistema d'imatge, que provoquen solament un lleuger augment de la mida de les nanopartícules.
- El fàrmac loperamida, després de la modificació de la fase oliosa de la nano-emulsió de partida, per problemes de solubilitat. Això va provocar un augment de la mida de les nano-emulsions plantilla així com de les nanopartícules, però es mantenen dins del rang esperant. Les eficiències d'encapsulació són gairebé del 100%, amb una baixa difusió del fàrmac.
- El fàrmac galantamina, com a model d'antiapoptòtic. No ha modificat les característiques físico-químiques de les nanopartícules. S'aconsegueix una alta eficiència d'encapsulació i un alliberament controlat del fàrmac.

4) S'ha aconseguit funcionalitzar la superfície de les nanopartícules amb diferents components i tecnologies:
- FITC, per utilitzar les nanopartícules com a sistemes d'imatge, s'ha unit covalentment.
- Diversos tipus de material genètic per utilitzar les nanopartícules com a vectors no virals de teràpia gènica. Per aconseguir una unió electrostàtica, prèviament s'han unit covalentment dendrons d'estructura carbosilà catiònics.

- L'anticòs monoclonal contra el receptor de la transferrina, per aconseguir una vectorització específica cap a la BBB.

5) Estudis *in vitro* han demostrat la idoneïtat de les nanopartícules per aplicacions biomèdiques mitjançant l'administració intravenosa, ja que:
    - Els sistemes escollits no són citotòxics ni hemolítics.
    - Les eficiències de transfecció dels gens arriben fins a percentatges equivalents als comercials.
    - No es produeix alteració en el temps de coagulació sanguínia.
    - L'adsorció de proteïnes a la superfície de nanopartícules és baixa.
    - L'activació del sistema del complement es pot considerar dèbil i fins i tot es pot reduir disminuint les concentracions.

6) Esudis *in vivo* han confirmat que les nanopartícules no són tòxiques i que, després de la seva funcionalització amb l'anticòs específic contra el receptor de la transferrina, aconsegueixen travessar la BBB amb un alt percentatge.

Així, es pot concloure que s'ha aconseguit formular nanopartícules polimèriques utilitzant mètodes de baixa energia i compostos compatibles amb sistemes biològics, amb un procés escalable. Aquestes nanopartícules són adequades pel tractament de malalties neurodegeneratives, ja que, a través de l'administració intravenosa són capaces de travessar la BBB i produir efectes a nivell de sistema nerviós central.

Chapter 8

BIBLIOGRAPHY

A

Abdel-Mottaleb M.S.A., Loufty R.O., Lapouyade R., (**1989**). Non-radiative deactivation channels of molecular rotors, Journal of Photochemistry and Photobiology, A: Chemistry, 48, 87-93.

Agilent Technologies, (**2014**).

Aktas Y., Yemisci M., Andrieux K., Gürsoy N., Alonso M.J., Fernandez-Megia E., Novoa-Carballal R., Quiñóá E., Riguer R., Sargon M.F., Cüelik H.H., Demir A.S., Hincal A.A., Dalkara T., Cüapan Y., Couvreur P., (**2005**). Development and brain delivery of chitosan-PEG nanoparticles functionalized with the monoclonal antibody OX26, Bioconjugate Chemistry, 16, 1503 – 1511.

Alexis F., Pridgen E., Molnar L.K., Farokhzar O.C., (**2008**). Factors affecting the clearance and biodistribution of polymeric nanoparticles, Molecular Pharmaceutics, 5(4), 505 – 515.

Allémann E., Gurny R., Doelker E., (**1992**). Preparation of aqueous polymeric nanodispersions by a reversible salting-out process: Influence of process parameters on particle size, International Journal of Pharmaceutics, 87(1-3), 247 – 253.

Alshamsan A., Haddadi A., Hamdy S., Samuel J., El-Kadi A.O.S., Uludag H., Lavasanifar A., (**2010**). STAT3 Silencing in Dendritic Cells by siRNA Polyplexes Encapsulated in PLGA Nanoparticles for the Modulation of Anticancer Immune Response, Molecular Pharmaceutics, 7(5), 1643 – 1654.

Alyautdin R., Gothier D., Petrov V., Kharkevih D., Kreuter J., (**1995**). Analgesic activity of the hexapeptide dalargin adsorbed on the surface of polysorbate 80-coated poly(butyl cyanoacrylate) nanoparticles, European Journal of Pharmaceutics and Biopharmaceutics, 41, 44 – 48.

Alyautdin R.N., Petrov V.E., Langer K., Berthold A., Kharkevich D.A., Kreuter J., (**1997**). Delivery of loperamide across the blood-brain barrier with polysorbate 80-coated polybutylcyanocrylate nanoparticles, Pharmaceutical Research, 14(3), 325 – 328.

Alyautdin R., Khalin I., Nafeeza M.I., Haron M.H., Kuznetsov D., (**2014**). Nanoscale drug delivery systems and the blood-brain barrier, International Journal of Nanomedicine, 9, 795 – 811.

Ambruosi A., Khakansky A.S., Yaramoto H., Gelperina S., Begley D.J., Kreuter J., (**2006**). Biodistribution of polysorbate 80-coated doxorubicin-loaded $[^{14}C]$-poly(butyl

cyanoacrylate) nanoparticles after intravenous administration to glioblastoma-bearing rats, Journal of Drug Targeting, 14(2), 97 – 105.

Anton N., Benoit J.-P., Saulnier P., (**2008**). Design and production of nanoparticles formulated from nano-emulsions – A review, Journal of Controlled Release, 128(3), 185 – 199.

Anton N., Vandamme T., (**2011**). Nano-emulsions and micro-emulsions: clarifications of the critical differences, Pharmaceutical Research, Springer Netherlands, 28, 978 – 985.

Antonietti M., Landfester K., (**2002**). Polyreactions in miniemulsions, Progress in Polymer Science, 27(4), 689 – 757.

Arora S., Swaminathan S.K., Kirtane A., Srivastava S.K., Bhardwaj A., Singh S., Panyan J., Singh A.P., (**2014**). Synthesis, characterization, and evaluation of poly (D,L-lactide-co-glycolide)-based nanoformulation of miRNA-150: potential implications for pancreatic cancer therapy, International Journal of Nanomedicine, 9, 2933 – 2942.

Astete C.E., Kumar C.S., Sbliov C.M., (**2007**). Size control of poly(d,l-lactide-co-glycolide) and poly(d,l-lactide-co-glycolide)-magnetite nanoparticles synthetized by emulsion evaporation technique, Colloids and Surfaces A, 299, 209 – 216.

Asua J.M., (**2002**). Miniemulsion polymerization, Progress in Polymer Science, 27(7), 1238 – 1346.

B

Barichello J.M., Morishita M., Takayama K., Nagai T., (**1999**). Encapsulation of hydrophilic and lipophilic drugs in PLGA nanoparticles by the nanoprecipitation method, Drug Development and Industrial Pharmacy, 25, 471 – 476.

Beal M.F., Lang A.E., Ludolph A.C., (**2005**). Neurodegenerative Diseases: Neurobiology, Phatogenesis and Therapeutics, Cambridge University Press.

Becher P., (**1965**). Emulsions: Theory and practice, Second edition, Reynold publishing corp. New York.

Becher P., (**1972**). Emulsiones, Teoría y Práctica, edited by Blumeor.

Béduneau A., Saulnier P., Benoit J.-P., (**2007**). Active targeting of brain tumors using nanocarriers, Biomaterials, 28(33), 4947 – 4967.

Béduneau A., Hindré F., Clavreul A., Leroux J.-C., Saulnier P., Benoit J.-P., (**2008**). Brain targeting using novel lipid nanovectors, Journal of Controlled Release, 126(1), 44 – 49.

Beil R.D., Ehlers M.D., (**2014**). Breaching the Blood-brain barrier for drug delivery, Neuron, 81, 1 – 3.

Benita S., Levy M.Y., (**1993**). Submicron emulsions as colloidal drug carriers for intravenous administration: Comprehensive physicochemical characterization. Journal of Pharmaceutical Sciences, 82, 1069 – 1079.

Bermejo J.F., Ortega P., Chonco L., Eritja R., Samaniego R:, Müllner M., de Jesus E., de la Mata F.J., Flores J.C., Gomez R., Muñoz-Fernandez A., (**2007**). Water-Soluble Carbosilane Dendrimers: Synthesis Biocompatibility and Complexation with Oligonucleotides; Evaluation for Medical Applications, Chemistry, A European Journal, 13, 483 – 495.

Berna M., Dalzoppo D., Pasut G., Manunta M., Izzo L., Jones A.T., Duncan R., Veronese F.M., (**2006**). Novel monodisperse PEG-dendrons as new tools for targeted drug delivery: synthesis, characterization and cellular uptake, Biomacromolecules, 7, 146 – 153.

Bertholon I., Vauthier C., Labarre D., (**2006**). Complement activation by core-shell poly(isobutylcyanoacrylate)-polysaccharide nanoparticles: influences of surface morphology, length and type of polysaccharide, Pharmaceutical Research, 23(6), 1313 – 1323.

Betancourt T., Byrne J.D., Sumaryo N., Crowder S.W., Kadapakkam M., Patel S., Casciato S., Brannon-Peppas L., (**2009**). PEGilation strategies for active targeting of PLA/PLGA nanoparticles. J Biomed Mat Res Part A, 91A(1), 263 – 273.

Bielinska A., Kukowska-Latallo J.F., Johnson J., Tomalia D.A., Baker Jr J.R., (**1996**). Regulation of in vitro Gene Expression Using Antisense Oligonucleotides or Antisense Expression Plasmids Transfected Using Starburst PAMAM Dendrimers, Nucleic Acid Research, 24(11), 2176 – 2182.

Binks B.P., (**1998**). Emulsions: recent advances in understanding, Modern Aspects of Emulsion Science, edited by Binks B.P., The Royal Society of Chemistry, Cambridge, 1 – 48.

Binks B.P., Rodrigues J.A., Frith W.J., (**2007**). Synergistic interaction in emulsions stabilized by a mixture of silica nanoparticles and cationic surfactant, Langmuir, 23(7), 3626 – 3636.

Bouchemal K., Briançon S., Perrier E., Fessi H., (**2004**). Nano-emulsion formulation using spontaneous emulsification: solvent, oil and surfactant optimization, International Journal of Pharmaceutics, 280(1-2), 241 – 251.

Bouissou C., Rouse J.J., Price R., van der Walle C.F., (**2006**). The Influence of Surfactant on PLGA Microsphere Glass Transition and Water Sorption: Remodeling the Surface Morphology to Attenuate the Burst Release, Pharmaceutical Research, 23(6), 1295 – 1305.

Brambilla D., Le Droumaguet B., Nicolas J., Hashemi H., Wu L-P., Moghimi S.M., Couvreur P., Andrieux K., (**2011**). Nanotechnologies for Alzheimer's disease: diagnosis, therapy and safety issues, Biomaterials, 7, 521 – 540.

Bredesen D.E., Rao R.V., Mehlen P., (**2006**). Cell death in nervous system, Nature, 443, 796 – 802.

Brewer S.H., Glomm W.R., Johnson M.C., Knag M.K., Franzen S., (**2005**). Probing BSA Binding to Citrate-Coated Gold Nanoparticles and Surfaces, Langmuir, 21, 9303 – 9307.

Brigger I., Dubernet C., Couvreur P., (**2012**). Nanoparticles in cancer therapy and diagnosis, Advanced drug delivery reviews, 64, 24 – 36.

Brodal P., (**2010**). The Central Nervous System: Structure and function, Oxford University Press, Fourth Edition.

Buzzello K., Müller B.W., (**2000**). Emulsions as drug delivery systems, Pharmaceutical emulsions and suspensions, Drugs and the Pharmaceutical Science, edited by Nielloud F., Marti-Mestres G., Marcel Dekker, New York, 105, 191 – 228.

Byrne J.D., Betancourt T., Brannon-Peppas L., (**2008**). Active targeting schemes for nanoparticle systems in cancer therapeutics, Advanced Drug Delivery Reviews, 60(15), 1615 – 1626.

C

Calderó G., García-Celma M.J., Solans C., Plaza M., Pons R., (**1997**). Influence of composition variables on the molecular diffusion from highly concentrated water-in-oil emulsions (gel-emulsions), Langmuir, 13(3), 385-390.

Calderó G., Llinàs M., García-Celma M.J., Solans C., (**2010**). Studies on controlled release of hydrophilic drugs from W/O high internal phase ratio emulsions. Journal of Pharmaceutical Sciences, 99(2), 701 – 711.

Calderó G., García-Celma M. J., Solans C., (**2011**). Formation of polymeric nano-emulsions by a low energy method and their use for nanoparticle preparation, Journal of Colloid and Interface Science, 353, 406 – 411.

Calderó G., Montes R., Llinàs M., García-Celma M.J., Porras M., Solans C., (**2014**). Studies on the formation of polymeric nano-emulsions obtained via low-energy emulsification and their use as templates of for drug delivery nanoparticle dispersions. *Submitted.*

(1) **Calvo** P., Gouritin B., Chacun H., Desmaële D:, D'Angelo J., Noel J.P., Georgin D., Fattal E., Andreux J. P., Couvreur P., (**2001**). Long-Circulating PEGylated Polycyanoacrylate Nanoparticles as New Drug Carrier for Brain Delivery, Pharmaceutical Research, 18(8), 1157 – 1166.

(2) **Calvo** P., Gouritin P., Brigger I., Lasmezas C., Deslys J.P., Williams A., Andreux J.P., Dormont D., Couvreur P., (**2001**). PEGylated polycyanoacrylate nanoparticles as vector for drug delivery in prion diseases, Journal of Neuroscience Methods, 111, 151 – 155.

Catiker E., Gümüsderelioglu M., Güner A., (**2000**). Degradation of PLA, PLGA homo- and copolymers in the presence of serum albumin: a spectroscopic investigation, Polymer International, 49, 728 – 734.

Chaudari K.R., Ukawala M., Manjappa A.S., Kumar A., Mundada P.K., Mishra A.K., Mathur R., Mönkkönen J., Murthy R.S.R., (**2012**). Opsonization, biodistribution, cellular uptake and apoptosis study of PEGylated PBCA nanoparticle as potential drug delivery carrier, Pharmaceutical Research, 29, 53 – 68.

Chavanpatil M.D., Patil Y., Panyam J., (**2006**). Susceptibility of nanoparticle-encapsulated paclitaxel to P-glycoprotein-mediated drug efflux, International Journal of Pharmaceutics, 320, 150 – 156.

Chavany C., Le Doan T., Couvreur P., Puisieux F., Hélène C., (**1992**). Polyalkylcyanoacrylate nanoparticles as polymeric carriers for antisense oligonucleotides, Pharmaceutical Research, 9(4), 441 – 449.

Chavany C., Saison-Behmoaras T., Le Doan T., Puisieux F., Couvreur P., Hélène C., (**1994**). Adsorption of oligonucleotides onto polyisohexylcyanoacrylate nanoparticles protects them against nucleases and increases their cellular uptake, Pharmaceutical Research, 11(9), 1370 – 1378.

Chen Y-C., Hsieh W-Y., Lee W-F., Zeng D-T., (**2011**). Effects of surface modification of PLGA-PEG-PLGA nanoparticles on loperamide delivery efficiency across the blood-brain barrier, Journal of Biomaterials Applications, 27(7), 909 – 922.

Chen Y., Liu L., (**2012**). Modern methods for delivery of drugs across the blood–brain barrier, Advanced Drug Delivery Reviews, 64(7), 640 – 665.

Cho T.J., Zangmeister R.A., MacCuspie R.I., Patri A.K., Hackley V.A., (**2011**). Newkome-Type Dendron-Stabilized Gold Nanoparticles: Synthesis, Reactivity, and Stability, Chemistry of Materials, 23, 2665 – 2676.

Chonco L., Bermejo-Martín J.F., Ortega P., Shcharbin D., Pedziwiatr E., Klajnert B., de la Mata F.J., Eritja R., Gómez R., Bryszewska M., Muñoz-Fernandez M.A., (**2007**). Water-soluble carbosilane dendrimers protect phosphorothioate oligonucleotides from binding to serum proteins, Organic and Biomolecular Chemistry, 5, 1886 – 1893.

Chroma Technology Corp®, an employee-owned company, (**2014**). Webpage: www.choma.com. Last time consulted: 27/09/2014.

Clarimón J., (**2003**). Doctoral Thesis: Factors genètics de risc en la malaltia d'Alzhèimer.

Cohen H., Levy R.J., Gao J., Fishbein I., Kousaev V., Sosnowski S., Slomkowski S., Golomb G., (**2000**). Sustained delivery and expression of DNA encapsulated in polymeric nanoparticles, Gene Therapy, 7(22), 1896 – 1905.

Colvin V.L., (**2003**). The potential environmental impact of engineered nanoparticles, Nature Biotechnology, 21, 1166 – 1170.

Cook R.O., Pannu R.K., Kellaway I.W., (**2005**). Novel sustained release microspheres for pulmonary drug delivery, Journal of Controlled Release, 104(1), 79 – 90.

Cordewener F.W., van Geffen M.F., Joziasse C.A:P., Schmitz J.P., Bos R.R.M., Rozema F.R., Pennings A.J., (**2000**), Cytotoxicity of poly(96L/4D-lactide): The influence of degradation and sterilization, Biomaterials, 21, 2433 – 2442.

Costantino L., Gandolfi F., Bossy-Nobs L., Tosi G., Gurny G., Rivasi F., Vandelli M.A., Forni F., (**2006**). Nanoparticulate drug carriers based on hybrid poly(D,L-lactide-co-glycolide)-dendron structures, Biomaterials, 27, 4635 – 4645.

Couvreur P., Vauthier C., (**2006**), Nanotechnology: Intelligent design to treat complex diseases, Pharmaceutical Research, 23(7), 1417 – 1450.

Croda International Plc, **2013**. Webpage: http://www.croda.com/home.aspx?s=1&referer=https://www.google.es/

Cummings J.L., Schneider L., Tariot P.N., Kershaw P.R., Yuan W., (**2004**). Reduction of Behavioral Disturbances and Caregiver Distress by Galantamine in Patients With Alzheimer's Disease, The American Journal of Psychiatry, 161, 532 – 538.

Cytoviva ®, Illuminating the future, (**2014**). Webpage: www.cytoviva.com.

D

Dakwar G., Hammad I.A., Popov M., Linder C., Grinberg S., Heldman E., Stepensky D., (**2012**). Delivery of proteins to the brain by bola amphiphilic nano-sized vesicles, Journal of Controlled Release, 160, 315-321.

Dalby B., Cates S., Harris A., Ohki E.C., Tilkins M.L., Price P.J., Ciccarone V.C., (**2004**). Advanced transfection with Lipofectamine 2000 reagent: primary neurons, siRNA, and high-throughput applications, Methods, 33(2), 95 – 103.

Dalwadi G., Sunderland B., (**2009**). An ion pairing approach to increase the loading f hydrophilic and lipophilic drugs into PEGylated PLGA nanoparticles, European Journal of Pharmaceutics and Biopharmaceutics, 71, 231 – 242.

Danhier F., Ansorena E., Silva J.M., Coco R., Le Breton A., Préat V., (**2012**). PLGA-based nanoparticles: An overview of biomedical applications, Journal of Controlled Release, 161, 505 – 522.

D'Antone S., Bignotti F., Sartore L., D'Amore A., Spagnoli G., Penco M., (**2001**). Thermogravimetric investigation of two classes of block copolymers based on poly(lactic-glycolic acid) and poly(e-caprolactone) or poly(ethylene glycol), Polymer Degradation and Stability, 74, 119 – 124.

Date A.A., Nagarsenker M.S., (**2007**). Design and evaluation of self-nanoemulsifying drud deliver systems (SNEDDS) for cefpodoxime poxetil, International Journal of Pharmaceutics, 329, 166 – 172.

Date A.A., Desai N., Dixit R., Nagarsenker M., (**2010**). Self-nanoemulsifying drug delivery systems: formulation insights, applications and advances, Nanomedicine, 5(10), 1595 – 1616.

Davda J., Labhasetwar V., (**2002**). Characterization of nanoparticles uptake by endothelial cells, International Journal of Pharmaceutics, 233, 51-59.

Delgado A.V., González-Caballero F., Hunter R.J., Koopal L.K., (**2007**) Measurement and interpretation of electrokinetic phenomena, Journal of Colloids and Interface Science, 309, 194 – 224.

Delmas T., Piraux H., Couffin A.-C., Teixer I., Vinet F., Poulin P., Cates M.E., Bibette J., (**2011**). How to prepare and stabilize very small nanoemulsions, Langmuir, 27, 1683 – 1692.

Deminière B., Colin A., Calderon F.L., Bibette J., (**1998**). Vieillissement par coalescence et durée de vie d'une emulsion concentere, Comptes Rendus de l'Académie des Sciences – Series IIC – Chemistry, 1, 163 – 165.

Deminière B., Colin A., Leal-Calderon F., Muzy J.F., Bibette J., (**1999**). Cell growth in a 3D cellular system undergoing coalescence, Physical Review Letters, 82, 229 – 232.

Derjaguin B., Landau L., (**1941**). Theory of the stability of strongly charged lyophobic sols and the adhesion of strongly charged particles in solutions of electrolytes, Acta Physico Chemica URSS, 14, 633.

Desgouilles S., Vauthier C., Bazile D., Vacus J., Grossiord J.L., Veillard M., and Couvreur P., (**2003**). The design of nanoparticles obtained by solvent evaporation: A comprehensive study, Langmuir, 19(22), 9504-9510.

Dhanikula R.S., Hammady T., Hildgen, (**2009**). On the Mechanism and Dynamics of Uptake and Permeation of Polyether-Copolyester Dendrimers Across an In Vitro Blood–Brain Barrier Model, Journal of Pharmaceutical Sciences, 98(10), 3748 – 3760.

Dias N., Stein C.A., (**2002**). Antisense Oligonucleotides: Basic Concepts and Mechanisms, Molecular Cancer Therapeutics, 1, 347 – 355.

Díez-Pascual A.M., Naffakh M., (**2012**). Grafting of an aminated poly(phenylene sulphide) derivative to functionalized single-walled carbon nanotubes, Carbon, 50, 857 – 868.

Dillen K., Vandervoort J., Van den Mooter G., Verheyden J., Ludwig A., (**2004**). Factorial design, physicochemical characterisation and activity of ciprofloxacin-PLGA nanoparticles, International Journal of Pharmaceutics, 275 (1-2), 171 – 187.

Dinamarca M.C., Sagal J.P., Quintanilla R.A., Godoy J.A., Arrázola M.S., Inestrosa N.C., (**2010**). Amyloid-β-Acetylcholinesterase complexes potentiate neurodegenerative

changes induced by the Aβ peptide. Implications for the pathogenesis of Alzheimer's disease, Molecular Neurodegeneration, 5(4), 1 – 15.

Dobrovolskaia M.A., Neun B.W., (**2006**). NCL Method ITA-12, Coagulation Assays, Nanotechnology Characterization Laboratory, National Cancer Institute-Frederick, SAIC-Frederick, Frederick, MD 21702, (301) 846-6939.

Dobrovolskaia M.A., McNeil S.E., (**2007**). Immunological properties of engineered nanomaterials, Nature Nanotechnology 2, 469 – 478.

Dobrovolskaia M.A., Aggarwal P., Hall J.B., McNeil S.E., (**2008**). Preclinical Studies To Understand Nanoparticle Interaction with the Immune System and Its Potential Effects on Nanoparticle Biodistribution, Molecular Pharmaceutics, 5(4), 487 – 495.

Dobrovolskaia M.A., Patri A.K., Zheng J., Clogston J.D., Ayub N., Aggarwal P., Neum B.W., Hall J.B., McNeil S., (**2009**). Interaction of colloidal gold nanoparticles with human blood: effects on particle size and analysis of plasma protein binding profiles, Nanomedicine, 5, 106 – 117.

Dobrovolskaia M.A., McNeil S., (**2013**). Handbook of immunological properties of engineered nanomaterials, Frontiers in Nanobiomedical esearch, SAIC-Frederick, Inc., USA.

Dols-Pérez A.,(**2013**). Doctoral Thesis: Nanoscale structural and mechanical properties of lipid bilayers in air environment

Drugbank, (**2014**). Webpage: http://www.drugbank.ca/drugs/DB00836 and http://www.drugbank.ca/drugs/DB00674.

Duran-Vilaregut J., (**2012**). Doctoral Thesis: Estudi de la neurodegeneració i les alteracions de la barrera hematoencefàlica en rates tractades amb acid 3-nitropropiònic.

E

Edelhoch H., (**1967**). Spectroscopic Determination of Tryptophan and Tyrosine in Proteins, Biochemistry, 6(7), 1948 – 1954.

Ehrenberg M.S., Friedman A.E., Finkelstein J.N., Oberdörster G. McGrath J.L., (**2009**). The influence of protein adsorption on nanoparticle association with cultured endothelial cells, Biomaterials, 30, 603 – 610.

Ellman G.L., Courtney K.D., Andres V., Featherstone R.M., (**1961**). A new and rapid colorimetric determination of acetylcholinesterase activity, Biochemical Pharmacology, 7, 88 – 95.

Ezhilarasi P. N., Karthik P., Chhanwal N., Anandharamakrishnan C., (**2013**). Nanoencapsulation Techniques for Food Bioactive Components: A Review, Food Bioprocess Technology, 6, 628 – 647.

F

Faraji A.H., Wipf P., (**2009**). Nanoparticles in cellular drug delivery, Bioorganic and Medicinal Chemistry, 17(8), 2950 – 2962.

Farlow M.R., (**2001**). Pharmacokinetic Profiles of Current Therapies for Alzheimer's Disease: Implications for Switching to Galantamine, Clinical Therapeutics, 23(A), 13 – 25.

Farlow MR., (**2003**). Clinical pharmacokinetics of galantamine, Clinical Pharmacokinetics, 42(15), 1383 – 1392.

Fazil M., Baboota S., Sahni J.K., Ali J., (**2012**). Nanotherapeutics for Alzheimer's disease (AD): Past, present and future, Journal of Drug Targeting, 20(2), 97 – 113.

Food and Drug Administration (FDA) (http://www.accessdata.fda.gov/scripts/cdrh/cfdocs/cfCFR/CFRSearch.cfm?fr=172.840). Last time consulted: February **2014**.

Fessi H., Puisieux F., Devissaguet J.P., Ammoury N., Benita S., (**1989**). Nanocapsule formation by interfacial polymer deposition following solvent displacement, International Journal of Pharmaceutics, 55 , 1 – 4.

Filipe V., Hawe A., Jiskoot W., (**2010**). Critical evaluation of nanoparticle tracking analysis (NTA) by NanoSight for the measurement of nanoparticles and protein aggregates, Phermaceutical Research, 27(5), 796 – 810.

Fisher K.J., Joss K., Alston J., Yang Y., Haecker S.E., High K., Pathak R., Raper S.E., Wilson J.M., (**1997**). Nature Medicine, 3(3), 306 – 312.

Folley S., Crowley C., Smaihi M., Bonfils C., Eflanger B.F., Seta P., Larroque C., (**2002**). Cellular localization of a water-soluble fullerene derivative, Biochemical and Biophysical Research Communications, 294(1), 116 – 119.

Fonte P., Soares S., Costa A., Andrade J.C., Seabra V., Reis S., Sarmento B., (**2012**). Effect of cryoprotectants on the porosity and stability of insulin-loaded PLGA nanoparticles after freeze-drying, Biomatter, 2-4, 329 – 339.

Forgiarini A., Esquena J., González C., Solans C., (**2001**). Formation of nano-emulsions by low-energy emulsification methods at constant temperature, Langmuir, 17, 2076 – 2083.

Formulaction, 2014. Webpage: http://www.formulaction.com/stability-turbiscan-lab.html

(1) **Fornaguera** C., Llinàs M., Solans C., Calderó G., (**2014**). Design and in vitro evaluation of biocompatible dexamethasone-loaded nanoparticle dispersions obtained from nano-emulsions, for inhalatory therapy, Submitted.

(2) **Fornaguera** C., Grijalvo S., Galán M., Fuentes-Paniagua E., de la Mata F.J., Gómez R., Eritja R., Calderó G., Solans C., (**2014**). Novel non-viral gene delivery systems composed of carbosilane dendron functionalized nanoparticles prepared from nano-emulsions as non-viral carriers for antisense oligonucleotides. Submitted.

(3) **Fornaguera** C., Calderó G., Solans C., Vauthier C., (**2014**). Surfactants influence the protein – nanoparticles interaction study in immunoelectrophoretic methods. In preparation.

Fotakis G., Timbrell J.A., (**2006**). In vitro cytotoxicity assays: Comparison of LDH, neutral red, MTT and protein assay in hepatoma cell lines following exposure to calcium chloride, Toxicological Letters, 160, 171 – 177.

Francis K., van Beek J., Canova C., Neal J.W., Gasque P., (**2003**). Innate immunity and brain imflammation: the key role of complement, Expert Reviews in Molecular Medicine, 2003, 5, 1 – 19.

Fuentes-Paniagua E., Peña-González C.E., Galán M., Gómez R., de la Mata F.J., Sánchez-Nieves J., (**2013**). Thiol-Ene Synthesis of Cationic Carbosilane Dendrons: a New Family of Synthons, Organometallics, 32, 1789 – 1796.

G

Gabathuler R., (**2010**). Approaches to transport therapeutic drugs across the blood-brain barrier to treat brain diseases, Neurobiology of Disease, , 37, 48 – 57.

Galán M., (**2014**). Doctoral thesis: Síntesis de sistemas dendríticos aniónicos de naturaleza carbosilano mediante química *click* tiol-eno y su aplicación como agentes antivirales frente a VIH.

Ganachaud F., Katz J.L., (**2005**). Nanoparticles and nanocapsules created using the Ouzo effect: spontaneous emulsification as an alternative to ultrasonic and high-shear devices, Journal of Chemical Physics and Physical Chemistry, 6(2), 209 – 216.

Garcia-Garcia E., Andrieux K., Gil S., Couvreur P., (**2005**). Colloidal carriers and blood-brain barrier (BBB) translocation: A way to deliver drugs to the brain?, International Journal of Pharmaceutics,298(2), 274 – 292.

Gaumet M., Vargas A., Gurny R., Delie F., (**2008**). Nanoparticles for drug delivery: The need for precision in reporting particle size parameters, European Journal of Pharmaceutics and Biopharmaceutics, 69(1), 1 – 9.

Gelperina S.E., Khalansky A.S., Skidan I.N., Smirnova Z.S., Bobrudskin A.I., Severin S.E., Turowski B., Zanella F.E., and Kreuter J., (**2002**). Toxicological studies of doxorubicin bound to polysorbate 80-coated poly(butyl cyanoacrylate) nanoparticles in healthy rats and rats with intracranial glioblastoma, Toxicological Letters, 126, 131-141.

Gelperina S., Maksimenko O., Khalansky A., Vanchugova L., Shipulo E., Abbasova K., Berdiev R., Wohlfart S., Chepurnova N., Kreuter J., (**2010**). Drug delivery to the brain using surfactant-coated poly(lactide-co-glycolide) nanoparticles: Influence of the formulation parameters, European Journal of Pharmaceutics and Biopharmaceutics, 74, 157 – 163.

Geys J., Nemmar A., Verbeken E., Smolders E., Ratoi M., Hoylaerts M.F., Nemery B., Hoet P.H., (**2008**). Acute toxicity and photrombotic effects of quantum dots: Impact of surface charge, Environmental Health perspectives, 116, 1607 – 1613.

Godipas K.R., Whitesell J.K., Fox M.A., Nanoparticle-cored dendrimers: Synthesis and characterization, (**2003**). Journal of the American Chemistry Society, 125(21), 6491 – 6502.

Gonzalo T., Clemente M.I., Chonco L., Weber N., Díaz L., Serramía M.J., Gras R., Ortega P., de la Mata F.J., Gómez R., Lopez-Fernández L.A., Muñoz-Fernández M.A., Jiménez J.L.,

(**2010**). Gene Therapy in HIV-Infected Cells to Decrease Viral Impact by Using an Alternative Delivery Method, ChemMedChem, 5, 921 – 929.

Good J.L., Chehrenama M., Mayer R., Richard F., Koski C.L., (**1998**). Pulse cyclophosphamide therapy in chronic inflammatory demyelinating polyneuropathy, Neurology, 51(6), 1735 – 1738.

Govender T., Stolnik S., Garnett M.C., Illum L., Davis S., (**1999**). PLGA nanoparticles prepared by nanoprecipitation: drug loading and release studies of a water soluble drug, Journal of Controlled Release, 57, 171 – 185.

Graves R.A., Pamujula S., Moiseyev R., Freeman T., Bostanian L.A., Mandal L.K., (**2004**). Effect of different ratios of high and low molecular weight PLGA blend on the characteristics of pentamidine microcapsules, International Journal of Pharmaceutics, 270(1-2), 251 – 262.

Grayson A.C.R., Voskerician G., Lynn A., Anderson J.M., Coma M.J., Langer R., (**2012**). Differential degradation rates in vivo and in vitro of biocompatible poly(lactic acid) and poly(glycolic acid) homo- and co-polymers for a polymeric drug-delivery microchip, Journal of Biomaterials Science, Polymer Edition, 15(10), 1281 – 1304.

Gref R., Domb A., Quellec P., Blunk T., Müller R.H., Verbavatz J.M., Langer R., (**2012**). The controlled intravenous delivery of drugs using PEG-coated sterically stabilized nanospheres, Advanced Drug Delivery Reviews, 64, 316 – 326.

Grijalvo S., Alagia A., Puras G., Zárate J., Pedraz J.L., Eritja R., (**2014**). Cationic vesicles based on non-ionic surfactant and synthetic aminolipids mediate delivery of antisense oligonucleotides into mammalian cells, Colloids and Surfaces B, 119, 30 – 37.

Gulati M., Chopar D.S., Singh S.K., Pathak P., Bansal P., (**2013**). Patents on Brain Permeable Nanoparticles, Recent Patents on CNS Drug Discovery, 8, 220 – 234.

Gulyaev E.A., Gelperina S.E., Skidan I.N., Antropov A.S., Kivman G.Y., Kreuter J., (**1999**). Significant Transport of Doxorubicin into the Brain with Polysorbate 80-Coated Nanoparticles, Pharmaceutical Research, 16(10), 1564 – 1569.

Gupta M.K., Prakash D., Mishra B., (**2012**). Biodegradable microparticulate drug delivery system of diltiazem HCl, Brazilian Journal of Pharmaceutical Sciences, 48(4), 699 – 709.

Guterres S.S., Alves M.P., Pohlmann A.R., (**2007**). Polymeric nanoparticles, nanospheres and nanocapsules, for cutaneous applications, Drug Terget Insights, Libertas Academica, 2, 147 – 157.

Guzman L.A., Labhasetwar V., Song C., Jang Y., Lincoff A.M., Levy R., Topol E.J., (**1996**). Local intraluminal infusion of biodegradable polymeric nanoparticles. A novel approach for prolonged drug delivery after balloon angioplasty, Circulation, 94, 1441 – 1448.

H

Hammarlund-Udenaes M., de Lange E.C.M., Thorne R.G., (**2014**). Drug Delivery to the Brain; Phyysiological Concepts, Methodologies and Approaches, AAPSpress, Springer, 10.

Hans ML., Lowman AL., (**2002**). Biodegradable nanoparticles for drug delivery and targeting, Current Opinion in Solid State and Materials Science, 6(4), 319 – 327.

Hansen M.B., Nielsen S.R., Berg K., (**1989**). Re-examination and further development of a precise and rapid dye method for measuring cell growth/cell kill, Journal of Immunological Methods, 119, 203 – 210.

Harris J., (**1992**). Introduction to Biotechnical and Biomedical Applications of Poly(Ethylene Glycol), in Poly ethylene glycol chemistry: Biotechnical and Biomedical Applications, Topics in Applied Chemistry, 1 – 14.

Harris J., Roos C., Djalali R., Rheingans O., Maskos M., Schmidt M., (**1999**). Application of the negative staining technique to both aqueous and organic solvent solutions of polymer particles, Micron, 30, 289 – 298.

Harush-Frenkel O., Debotton N., Benita S., Altschuler Y., (**2007**). Targeting of nanoparticles to the clathrin-mediated encodytic pathway, Biochemical and Biophysical Research Communications, 353, 26 – 32.

He C., Hu Y., Yin L., Tang C., Yin C., (**2010**). Effects of particle size and surface charge on cellular uptake and biodistribution of polymeric nanoparticles, Biomaterials, 31, 3657 – 3666.

Heidel J.D., Yu Z., Liu J.Y., Rele S.M., Liang Y., Zeidan R.K., Kornbrust D.J., Davis M.E., (**2007**). Administration in non-human primates of escalating intravenous doses of targeted nanoparticles containing ribonucleotide reductase subunit M2 siRNA, Proceedings of the National Academy of Sciences, 104(14), 5715 – 5721.

Heunemann P., Prévost S., Grillo I., Marino C.M., Meyer J., Gradzielski M., (**2011**). Formation and structure of slightly anionically charged nano-emulsions obtained by the phase inversion concentration (PIC) method, Soft Matter, 7, 5697 – 5710.

Hewala I.I., (**1995**). Spectrofluorimetric and derivative absorption spectrophotometric techniques for the determination of loperamide hydrochloride in pharmaceutical formulations, Journal of Pharmaceutical and Biomedical Analysis, 13(6), 761 – 767.

Higuchi W.I., (**1962**). Analysis of data on the medicament release from ointments. Journal of Pharmaceutical Sciences, 51(8), 802 – 804.

(1) **Holze**r P., Opioid receptors in the gastrointestinal tract, (**2009**). Regulatory Peptides, 155, 11 – 17.

(2) Holzer M., Vogel V., Mäntele W., Schwartz D., Haase W., Langer K. (**2009**). Physico-chemical characterisation of PLGA nanoparticles after freeze-drying and storage, European Journal of Pharmaceutics and Biopharmaceutics, 72, 428 – 437.

Hu Y., Ding Y., Ding D., Sun M., Zhang L., Jiang X., (**2007**). Hollow Chitosan / Poly (acrylic acid) Nanospheres as Drug Carriers, Biomacromolecules,8, 1069-1076.

Hu K., Shi Y., Jiang W., Han J., Huang J., Jiang X., (**2011**). Lactoferrin conjugated PEG-PLGA nanoparticles for brain delivery: Preparation, characterization and efficacy in Parkinson's disease, International Journal of Pharmaceuticals, 415, 273-283.

Hu C., Liu Y., (**2011**). Quality control in pharmaceuticals: Residual solvents testing and analysis, Wide spectra of quality control, edited by Akyar I., 183 – 210.

Huang C.H., Chen C.M., Lee Y.D., (**2007**). Synthesis of high loading and encapsulation efficient paclitaxel-loaded poly(n-butyl cyanoacrylate) nanoparticles via miniemulsion, International Journal of Pharmaceutics, 338, 267 – 275.

Huang R., Han L., Li J., Liu S., Shao K., Kuang Y., Hua X., Wang X., Lei H., Jiang H., (**2011**). Chlorotoxin-modified macromolecular contrast agent for MRI tumor diagnosis, Biomaterials, 32, 5177 – 5186.

Hunt A., (**1992**). A simple connection between the melting temperature and the glass temperature in a kinetic theory of the glass transition, Journal of Physics: Condensed Matters, 4, L429 – L431.

I

Illum L., Jones P.D., Baldwin R.W., Davis S.S., (**1984**). Tissue distribution of poly(hexyl-2-cyanoacrylate) nanoparticles coated with monoclonal antibodies in mice bearing human

tumor xenografts, Journal of Pharmacolocy and Experimental Therapeutics, 230, 733 – 736.

Ionov M., Garaiova Z., Waczulikova I., Wróbel D., Pedziwiatr-Werbicka E., Gómez-Ramirez R., de la Mata F.J., Klajnert B., Hianik T., Bryszewska M., (**2012**). siRNA carriers based on carbosilane dendrimers affect zeta potential and size of phospholipid vesicles, Biochima et Biophysica Acta, 1818, 2209 – 2216.

Italia J.L., Yahya M.M., Singh D., and Ravi Kumar M.N.V., (**2009**). Biodegradable nanoparticles improve oral bioavailability of amphoterin B and show reduced nephrotoxicity compared to intravenous Fungizone®, Pharmaceutical Research, 26(6), 1324-1331.

Ishihara T., Takeda M., Sakamoto H., Kimoto A., Kobayashi C., Takasaki N., Yuki K., Tanaka K., Takenaga M., Igarashi R., Maeda T., Tamakawa N, Okamoto Y., Otsuka M., Ishida T., Kiwada H., Mizushima Y., Mizushia T., (**2009**). Accelerated blood clearance phenomenon upon repeated injection of PEG-modified PLA-nanoparticles, Pharmaceutical Research, 26, 2270 – 2279.

Izquierdo P., Esquena J., Tadros Th.F., Dederen C., Garcia-Celma M.J., Azemar N., Solans C., (**2002**). Formation and stability of nano-emulsions prepared using the phase inversion temperature method, Langmuir, 18(1), 26 - 36.

Izquierdo P., Esquena J., Tadros Th.F., Dederen C., Feng J., Garcia-Celma M.J., Azemar N., Solans C., (**2004**). Phase behaviour and nano-emulsion formation by the phase inversión temperatura method, Langmuir, 20, 6594 – 6598.

J

Jain R.A., (**2000**). The manufacturing techniques of various drug loaded biodegradable poly(lactide-co-glycolide) (PLGA) devices, Biomaterials, 21, 2475 – 2490.

Jefferies W.A., Brandon M.R., Hunt S.V., Williams A.F., Gatter K.C., Mason D.Y., (**1984**). Transferrin receptor on endothelium of brain capillaries . Nature, 312, 162 – 163.

Jeong Y., Nab H.S., Seo D.Y., Kim D.G., Lee H.C., Jang M.K., Naa S.K., Roh S.H., Kim S., Naha J.W., (**2008**). Ciprofloxacin-encapsulated poly(dl-lactide-co-glycolide) nanoparticles and its antibacterial activity, International Journal of Pharmaceutics, 352, 317 – 323.

(1) **Jiang** J., Mei Z., Xua J., Sun D., (**2013**). Effect of inorganic electrolytes on the formation and the stability of water-in-oil (W/O) emulsions, Colloids and Surfaces A, 429, 82 – 90.

(2) **Jiang** S., Eltoukhy A.A., Love K.T., Langer RE., Anderson D.G., (**2013**). Lipidoid-coated iron oxide nanoparticles for efficient DNA and siRNA delivery

Jiménez J.L., Clemente M.I., Weber N.D., Sánchez J., Ortega P., de la Mata F.J., Gómez R., García D., López-Fernández L.A., Muñoz-Fernández M.A., (**2010**). Carbosilane dendrimers to transfect human astrocytes with small interfering RNA targeting human immunodeficiency virus, Biodrugs, 24(5), 331 – 343.

Joshi M., Pathak S., Sharma S., Patravale V., (**2008**). Solid microemulsion preconcentrate (NanOsorb) of artemether for effective treatment of malaria, International Journal of Pharmaceutics, 362, 172 – 178.

Jumaa M., Müller B.W., (**1998**). The effect of oil components and homogenization conditions on the physicochemical properties and stability of parenteral fat emulsions, International Journal of Pharmaceutics, 163, 81 – 89.

Jumaa M., Müller B.W., (**2000**). Lipid emulsions as a novel system to reduce the haemolytic activity of lytic agents: mechanism of the protective effect, European Journal of Pharmaceutical Sciences, 9, 285 – 290.

K

Kabal'nov A., Pertzov A., Schukin E., (**1987**). Ostwald ripening in two-component disperse phase systems: Application to emulsion stability, Colloids and Surfaces, 24, 19 – 32.

Kabalnov A. S., (**1998**). Coalescence in Emulsions, Modern Aspects of Emulsion Science, edited by Binks B.P., The Royal Society of Chemistry, Cambridge, 205 – 260.

Kabanov A.V., Gendelman H.E., (**2007**). Nanomedicine in the diagnosis and therapy of neurodegenerative disorders, Progress in Polymer Science, 32, 1054 – 1082.

Kahn A.W., Kotta S., Ansari S.H., Sharma R.K., Ali J., (**2012**). Potentials and challenges in self-nanoemulsifying drug delivery systems, Expert Opinion in Drug Delivery, 9(10), 1305 – 1317.

Kaiser E., Colescott R.L., Bossinger C.D., Cook P.I., (**1970**). Color test for detection of free terminal amino groups in the solid-phase synthesis of peptides, Analytical Biochemistry, 34(2), 595 – 598.

Kan P., Chen Zh. B., Kung R.Y., Lee Ch.J., Chu I.M., (**1999**). Study on the formulation of the o/w emulsion as carriers for lipophilic drugs, Colloids and Surfaces B, 15, 117 – 125.

Karlström G., Carlsson A., Lindman B., (**1990**). Phase diagrams of nonionic polymer-water systems. Experimental and theoretical studies of the effects of surfactants and other cosolutes, Journal of Physical Chemistry, 94, 5005 – 5015.

Karolczak K., Rozalska S., Wieczorek M., Labieniec-Watala M., Watala C., (**2012**). Poly(amido)amine dendrimers generation 4.0 (PAMAM G4) reduce blood hyperglycaemia and restore impaired blood–brain barrier permeability in streptozotocin diabetes in rats, International Journal of Pharmaceutics, 436, 508 – 518.

Katsumoto Y., Ushiki H., Graciaa A., Lachaise J., (**2000**). Evolutionary behavior of miniemulsion phases: I. Hard sphere interaction and bound water on miniemulsion droplets. Journal of Physics Condensed Materials, 12, 249 – 264.

Kaur I.P., Bhandari R., Bhandari S., Kakkar V., (**2008**). A potential of solid lipid nanoparticles in brain targeting, Journal of Controlled Release, 127, 97 – 109.

Kim D., El-Shall H., Dennis D., Morey T., (**2005**). Interaction of PLGA nanoparticles with human blood constituents, Colloids and Surfaces B. Biointerfaces, 40(2), 83 – 91.

Kim Y., Kim J. S., Cho H.S., Rha D.S., Kim J.M., Park J.D., Choi B.S., Lim R., Chang H.Y., Chung Y.H., Kwon I.H., Jeong J., Han B.S., Yu I.J., (**2008**). Twenty-Eight-Day Oral Toxicity, Genotoxicity, and Gender-Related Tissue Distribution of Silver Nanoparticles in Sprague-Dawley Rats, Inhalation Toxicology, 20, 575 – 583.

Kirby B.P., Pabari R., Chen C.N., Al Baharna M., Walsh J., Ramtoola Z., (**2013**). Comparative evaluation of the degree of pegylation of poly(lactic-co-glycolic acid) nanoparticles in enhancing central nervous system delivery of loperamide, Journal of Pharmacy and Pharmacology, 65, 1473 – 1481.

Klang Sh., Benita S., (**1998**). Design and evaluation of submicron emulsions as colloidal drug carriers for intravenous administration, Submicron emulsions in drug targeting and delivery, edited by Simon Benita, Ciutat, 119 – 152.

Klaus A., Tiddy GJT, Solans C., Harrar A., Touraud D., Kunz W., (**2012**). Effect of salts on the phase behavior and the stability of nano-emulsions with rapessed oil and an extended surfactant, Langmuir, 28, 8318 – 8328.

Koh J.Y., Choi D.W., (**1987**). Quantitative determination of glutamate mediated cortical neuronal injury in cell culture by lactate dehydrogenase efflux assay, Journal of Neuroscience Methods, 20, 83 – 90.

Kreuter J., (**1991**). Nanoparticle-based drug delivery systems, Journal of Controlled Release, 16, 169 – 176.

Kreuter J., Alyautdin R.N., Kharkevich D., Ivanov A.A., (**1995**). Passage of peptides through the blood-brain barrier with coloidal polymer particles (nanoparticles), Brain Research, 674, 171 – 174.

Kreuter J., (**1996**). Nanoparticles and microparticles for drug and vaccine delivery, Journal of Anatomy, 189(3), 503 – 505.

Kreuter J., Shamenkov D., Petrov V., Ramge P., Cychutek K., Koch-Brandt C., Alyautdin R., (**2002**). Apolipoprotein-mediated transport of nanoparticle-bound drugs across the Blood-brain barrier, Journal of Drug Targeting, 10(4), 317 – 325.

Kreuter J., Ramge P., Petrov V., Hamm S., Gelperina S.E., Engerlhardt B., Alyautdin R., Briesen H., and Begley D.J., (**2003**). Direct evidence that polysorbate-80-coated poly(butylcyanoacrylate) nanoparticles deliver drugs to the CNS via specific mechanisms requiring prior binding of drug to the nanoparticles, Pharmaceutical Research, 20 (3), 409-416.

Kreuter J., (**2004**). Nanoparticles as drug delivery systems, Encyclopedia of nanoscience and nanotechnology, edited by Singh Nawla H., American Scientific Publishers, 7, 161 – 180.

Kreuter J., Hekmatara T., Dreis S., Vogel T., Gelperina S., Langer K., (**2007**). Covalent attachement of apolipoprotein A-I and apolipoprotein B-100 to albumin nanoparticles enables drug transport into the brain, Journal of Controlled Release, 118, 54 – 58.

Kreuter J., (**2012**). Nanoparticulate systems for brain delivery of drugs, Advanced Drug Delivery Reviews, 64, 213 – 222.

Kreuter J., (**2013**). Mechanism of polymeric nanoparticle-based drug transport across the blood-brain barrier (BBB), Journal of Microencapsulation, 30(1), 49 – 54.

Kreuter J., (**2014**). Drug delivery to the central nervous system by polymeric nanoparticles: What do we know?, Advanced Drug Delivery Reviews, 71, 2 – 14.

Krupesh P., Amit P., Vishal P., Jayant D., Chhaganbhai P., (**2010**). Quantitative determination of galantamine hydrobromide in pharmaceutical dosage form by RP-High performance liquid Chromatography, Journal of Chemical and Pharmaceutical Research, 2(2), 36 – 43.

Kulkarni S.A., Feng S.S., (**2013**). Effects of particle size and surface modification on cellular uptake and biodistribution of polymeric nanoparticles for drug delivery, Pharmaceutical Research, 30, 2512 – 2522.

Kumar M.N.V.R., Sameti M., Mohapatra S.S., Kong X., Lockey R.F., Bakowsky U., Lindenblatt G., Schmidt C. H., Lehr C.-M., (**2004**). Cationic Silica Nanoparticles as Gene Carriers: Synthesis, Characterization and Transfection Efficiency In vitro and In vivo, Jorunal of Nanosciences and Nanotechnology, 4(7), 876 – 881.

Kumari A., Kumar Yadav S., Yadav S.C., (**2010**). Biodegradable polymeric nanoparticles based drug delivery systems, Colloids and Surfaces B, 75(1), 1 – 8.

Kunieda H., Hanno K., Yamaguchi S., Shinoda K., (**1985**). The three-phase behavior of a brine(ionic surfactant/nonionic surfactant/oil system: Evaluation of the hydrophile-lipophile balance (HLB) of ionic surfactant, Journal of Colloid and Interface Science, 107(1), 129 – 137.

Kunieda H., Yano N., Solans C., (**1989**). The stability of gel—emulsions in a water/nonionic surfactant/oil system, Colloids and Surfaces, 36(3), 313 – 322.

Kupzig S., Lee S.S., Banting G., (**2010**). Membrane Trafficking, in Techniques in Confocal Microscopy, 1st edition, edited by: Conn P., Academic Press.

L

Labarre D., Vauthier C., Chauvierre C., Petri B., Müller R., Chehimi M.M., (**2005**). Interactions of blood proteins with poly(isobutylcyanoacrylate) nanoparticles decorated with a polysaccharide brush, Biomaterials, 26, 5075 – 5084.

Labhasetwar V., Song C., Levy R.J., (**1997**). Nanoparticle drug delivery for restenosis, Advanced Drug Delivery Reviews, 24, 63 – 85.

Lanctôt K.L., Herrmann N., Yau K.K., Khan L.R., Liu B.A., LouLou B.M., Einarson T.R., (**2003**). Efficacy and safety of cholinesterase inhibitors in Alzheimer's disease: a meta-analysis, CMAJ, 169(6), 557 – 564.

Landfester K., Tiarks F., Hentze H.P., Antonietti M., (**2000**). Polyaddition in miniemulsions: A new route to polymer dispersions, Macromolecular Chemistry and Physics, 201, 1 – 5.

Landfester K., (**2006**). Synthesis of colloidal particles in miniemulsions, Annual Review of Material Research, 36, 231 – 279.

Landry F.B., Bazile D.V., Spenlehauer G., Veillard M., Kreuter, J., (**1996**). Degradation of poly-(DL-lactic acid) nanoparticles coated with albumin in model digestive fluids (USP XXII), Biomaterials, 17, 715 – 723.

Laquintana V., Denora N., Musacchio T., Lasorsa M., Latrofa A., Trapani G., (**2009**). Peripheral Benzodiazepine Receptor ligand–PLGA polymer conjugates potentially useful as delivery systems of apoptotic agents, Journal of Controlled Release, 137, 185 – 195.

Laurell C.B., (**1966**). Quantitative estimation of proteins by electrophoresis in agarose gel containing antibodies. Anals of Biochemistry, 15, 45 – 52.

Laurier Research Instrumentation, (**2007**). Cary Eclipse Fluorescence Spectrophotometer: User guidelines and standard operating procedure.

Lee H.J., Engelhardt B., Lesley J., Bickel U., Pardridge W.M., (**2000**). Targeting Rat Anti-Mouse Transferrin Receptor Monoclonal Antibodies through Blood-Brain Barrier in Mouse, Journal of Pharmacology and Experimental Therapeutics, 292(3), 1048 – 1052.

Lee H., Jeong J.H., Park T.G., (**2002**). PEG grafted polylysine with fusogenic peptide for gene delivery: high transfection efficiency with low cytotoxicity, Journal of Controlled Release, 79(1-3), 283 – 291.

Lee S.J., Jeong J.R., Shin S.C., Kim J.C., Chang Y.H., Chang Y.M., Kim J.D.D., (**2004**). Nanoparticles of magnetic ferric oxides encapsulated with poly(D,L lactide-co-glycolide) and their applications to magnetic resonance imaging contrast agent, Journal of Magnetism and Magnetic Materials, 272 – 276(3), 2432 – 2433.

Lemarchand C., Couvreur P., Vauthier C., Costantini D., Gref R., (**2003**). Study of the emulsion stabilization by graft copolymers using the optical analyzer Turbiscan, International Journal of Pharmaceutics, 254, 77 – 82.

Lewandowsky M., (**1900**) Zur lehre von der cerebrospinalflüssigkeit (On the cerebrospinal fluid), X Z Kin Med, 40, 480 – 494.

Lewinski N., Colvin V., Drezek R., (**2007**). Cytotoxicity of Nanoparticles, Small, 4(1), 26 – 49.

Li J., Zhe B., Shao Y., Liu X., Yang X., Yu Q., (**2009**). Construction of anticoagulant poly (lactic acid) films via surface covalent graft of heparin-carrying microcapsules. Colloids and Surfaces B, 70, 15 – 19.

Li Y., He H., Jia X., Lu W.-L., Lou J., Wei Y., (**2012**). A dual-targeting nanocarrier based on poly(amidoamine) dendrimers conjugated with transferrin and tamoxifen for treating brain gliomas, Biomaterials, 33, 3899 – 3908.

Li X., Takashima M., Yuba E., Harada A., Kono K., (**2014**). PEGylated PAMAM dendromer-doxorubicin conjúgate-hybridized gold nanorod for combined photothermal-chemotherapy, Biomaterials, 35, 6576 – 6584.

Lifshitz I., Slyozov V., (**1961**). The kinetics of precipitation from supersatured solid solutions, Journal of Physics and Chemistry of Solids, 19, 35 – 50.

Lila A.S.A., Nawata K., Shimizu T., Ishida T., Kiwada H., (**2013**). Use of polyglycerol (PG), instead of polyethylene glycol (PEG), prevents induction of the accelerated blood clearance phenomenon against lng-circulating liposomes upon repeated administration, International Journal of Pharmaceutics, 456, 235 – 242.

Lilienfeld S., (**2006**). Galantamine — a Novel Cholinergic Drug with a Unique Dual Mode of Action for the Treatment of Patients with Alzheimer's Disease, CNS Drug Reviews, 8(2), 159 – 176.

Liu X., Kaminski M.D., Chen H., Torno M., Taylor LT., Rosengart A.J., (**2007**). Synthesis and characterization of highly-magnetic biodegradable poly(D,L-lactide-co-glycolide) nanospheres, Journal of Controlled Release, 119, 52 – 58.

Liu Y., Feng S., (**2012**). Surfactant chain length effects on nanoparticles biodegradable polymers for targeted drug delivery, Biomolecular Engineering, 58(11), 3289 – 3297.

Llinàs M., (**2010**). Doctoral Thesis: "Estudi d'emulsions altament concentrades com a sistemes d'alliberació controlada de principis actius".

Loo S.C.J., Ooi C.P., Wee S.H.E., Boey Y.C.F., (**2005**). Effect of isothermal annealing on the hydrolytic degradation rate of poly(lactide-co-glycolide) (PLGA), Biomaterials, 26, 2827 – 2833.

López S., Bastida J., Viladomat F., Codina C., (**2002**). Acetylcholinesterase inhibitory activity of some Amaryllidaceae alkaloids and Narcissus extracts, Life Sciences, 71, 2521 – 2529.

López-Montilla J.C., Herrera-Morales P.E., Pandey S., Shah D.O., (**2002**). Spontaneous emulsification: mechanisms, physicochemical aspects, modeling, and applications, Journal of Dispersions Science and Technology, 23(1-3), 219 – 268.

Löser Messtechnik, (**2014**). Webpage : http://www.loeser-osmometer.de/home-eng.html.

Lu Z., Li J., (**2009**). Correlation between average melting temperature and glass transition temperature in metallic glasses, Applied Physics Letter, 94, 061913 – 061914.

Lu C.-T., Zhao Y.-Z, Wong H. L., Cai J., Peng L., Tian X.-Q., (**2014**). Current approaches to enhance CNS delivery of drugs across the brain barriers, International Journal of Nanomedicince, 9, 2241 – 2257.

Lublin F.D., Whitaker J.N., Eidelman B.H., Miller A.E., Arnason B.G.W., Burks J.S., (**1996**). Management of patients receiving interferon beta-lb for multiple sclerosis: Report of a consensus conference, Neurology, 46, 12 – 18.

Lynch I., Dawson K.A., (**2008**). Protein - nanoparticle interactions, NanoToday, 3(1-2), 40 – 47.

M

Maestro A., Solè I., González C., Solans C., Gutiérrez J.M., (**2008**). Influence of the phase behavior on the properties of ionic nanoemulsions prepared by the phase inversion composition method, Journal of Colloid and Interface Science, 327(2), 433 – 439.

Maláková J., Nobilis M., Svoboda Z., Lísa M., Holcapek M., Kvetina J., Klimes J., Palicka V., (**2007**). High-performance liquid chromatographic method with UV photodiode-array, fluorescence and mass spectrometric detection for simultaneous determination of galantamine and its phase I metabolites in biological samples, Jorunal of Chromatography B, 853, 265 – 274.

Malmsten M., (**2002**). Emulsions, Surfactants and Polymers in Drug Delivery. Drug and the pharmaceutical science, edited by Malmsten M., Marcel Dekker, New York, 122, 161 – 200.

Malvern Instruments Ltd., (**2014**). Webpage: http://www.malvern.com/en/?gclid=Cj0KEQjwyMafBRCU7OCRyc2vitsBEiQAKV4H9EHf0V U7VmZ239j23Xw8SmWWbDZEPqPD02_VpYKZTxsaAtv48P8HAQ.

Mancini G., Carbonara A.O., Heremans J.F., (**1965**). Immunochemical quantitation of antigens by single radial immunodiffusion. Immunochemistry, 2, 235 – 254.

Mangialasche F., Solomon A., Winblad B., Mecocci P., Kivipelto M., (**2010**). Alzheimer's disease: clinical trials and drug development, Lancet Neurology, 9(7), 702 – 716.

Manich G., Cabezón I., Valle J., Duran-Vilaregut J., Camins A., Pallàs M., Pelegrí C., Vilaplana J., (**2013**). Study of the transcytosis of an anti-transferrin receptor antibody with a Fab' cargo across the blood–brain barrier in mice, European Journal of Pharmaceutical Sciences, 49, 556 – 564.

Mansouri S., Lavigne P., Corsi K., Benderdour M., Beaumont E., Fernandes J.C., (**2004**). Chitosan-DNA nanoparticles as non-viral vectors in gene therapy: strategies to improve transfection efficacy, European Journal of Pharmaceutics and Biopharmaceutics, 57, 1 – 8.

Mansouri S., Cuie Y., Winnik F., Shi Q., Lavinge P., Benderdour M., Beaumont E., Fernandes J.C., (**2006**). Characterization of folate-chitosan-DNA nanoparticles for gene therapy, Biomaterials, 27, 2060 – 2065.

Mason T.G., Wilking J.N., Meleson K., Chang C.B., Graves S.M., (**2006**). Nanoemulsions: formation, structures, and physical properties. Journal of Physics: Condensed Matter, 18, R635.

McClements D.J., (**2011**). Edible nanoemulsions: Fabrication, properties, and functional performance, Soft Matter, 7, 2297 – 2316.

McClements D.J., (**2012**). Nanoemulsions versus microemulsions: terminology, differences and similarities, Soft Matter, 8, 1719 – 1729.

Mei Z., Zhu J., Sun D., (**2011**). O/W nano-emulsions with tunable PIT induced by inorganic salts, Colloids and surface A, 375 (1 – 3), 102 – 108.

Mercadante S., (**2010**). Management of cancer pain, Internal Emergency Medicine, 5(1), S31 – S35.

Meziani A., Zrabda A., Touraud M., Clausse M., Krunz W., (**1997**). Can aldehides participate in the nanostructuration of liquids containing charged micelles? Journal of Molecular Liquids, 73-74, 107 – 118.

Meziani A., Touraud D., Zrabda A., Clausse M., Krunz W., (**2000**). Co-surfactant properties of ketones, Journal of Molecular Liquids, 84, 301 – 311.

Michaelis K., Hoffmann M.M., Dreis S., Herbert E., Alyautdin R.N., Michaelis M., Kreuter J., Langer K., (**2006**). Covalent linkage of apolipoprotein E to albumin nanoparticles strongly enhances drug transport into the brain, Journal of Pharmacology and experimental Therapeutics, 317(3), 1246 – 1253.

Minchin R., (**2008**). Nanomedicine: Sizing up targets with nanoparticles, Nature Nanotechnology, 3, 12 – 13.

Miñana-Pérez M., Gutron C., Zundel C., Andérez J.M., Salager J., (**1999**). Miniemulsion formation by transitional inversion, Journal of dispersion Science and Technology, 20, 893 – 905.

Mo Y., Lim LY., (**2004**). Mechanistic study of the uptake of wheat germ agglutinin-conjugated PLGA nanoparticles by A549 cells, Journal of Pharmaceutical Sciences, 93(1), 20-28.

Modi S., Anderson B.D., (**2013**). Determination of drug release kinetics from nanoparticles: overcoming pitfalls of the dynamic dialysis method, Molecular Therapeutics, 10, 3076 – 3089.

Moghimi S.M., Szebeni J., (**2003**). Stealth liposomes and long circulating nanoparticles: critical issues in pharmacokinetics, opsonization and protein-binding properties, Progress in Lipid Research, 42, 463 – 478.

Moghimi S.M., Andersen A.J., Ahmadvand D., Wibroe P.P., Andresen T.L., Hunter A.C., (**2011**). Material properties in complement activation, Advanced Drug Delivery Reviews, 63, 1000 – 1007.

Moolten F.L., (**1986**). Tumor Chemosensitivity Conferred by Inserted Herpes Thymidine Kinase Genes: Paradigm for a Prospective Cancer Control Strategy, Cancer Research, 42, 5276 – 5281.

Morales D., Gutiéreez J.M., García-Celma M.J., Solans C., (**2003**). A study of the relation between bicontinuous microemulsions and oil/water nano-emulsion formation, Langmuir, 19, 7196 – 7200.

Morales D., Solans C., Gutiérrez J.M., Garcia-Celma M.J., Olsson U., (**2006**). Oil/Water droplet formation by temperatura change in the water / C16E6 / mireal oil system, Langmuir, 22, 3014 – 3020.

Moreira de Morais J., Henrique dos Santos O.D., Delicato T., da Rocha-Filho P.A., (**2005**). Characterization and evaluation of electrolyte influence on Canola oil / wáter nano-emulsions, Journal of Dispersion Sciences and Technology, 27, 1009 – 1014.

Morral-Ruiz G., (**2011**). Doctoral thesis: Estudi de la formació de nanopartícules polimèriques obtingudes a partir de nano-emulsions de fase externa aquosa i assossiació d'antiinflammatoris no esteroïdals.

Morral-Ruiz G., Solans C., García M.L., García-Celma M.J., (**2012**). Formation of PEGylated polyurethane and lysine-coated polyuria nanoparticles obtained from O/W nano-emulions, Langmuir, 28(15), 6256 – 6264.

Morris L.S., Schulz R.M., (**1992**). Patient compliance – A review, Journal of Clinical Pharmacy and Therapeutics, 17, 283 – 295.

Mufamadi M., Choonara Y., Kumar P., Modi G., Naidoo D., van Vuuren D., Ndesendo V., du Toita L., Iyuke S.E., Pillay V., (**2013**). Ligand-functionalized nanoliposomes for targeted delivery of galanthamine, 448, 267 – 281.

Müller RH., Maaflen S., Weyhers H., Specht L., Lucks J., (**1996**). Cytotoxicity of magnetite-loaded polylactide, polylactide/glycolide particles and solid lipid nanoparticles, International Journal of Pharmaceutics, 138, 85 – 94.

Mun S., Decker E.A., McClements J., (**2005**). Influence of droplet characteristics on the formation of oil-in-water emulsions stabilized by surfactant-chitosan layers, Langmuir, 21, 6228 – 6234.

Mundargi R., Babu V., Rangaswamy V., Patel P., Aminabhavi T., (**2008**). Nano/micro technologies for delivering macromolecular therapeutics using poly(d,l-lactide-co-glycolide) and its derivatives, Journal of Controlled Release, 125, 193 – 209.

Mura S., Couvreur P., (**2012**). Nanotheranostics for personalized medicine, Advanced Drug Delivery Reviews, 64, 1394 – 1416.

Musyanovych A., Schimtz-Wienke J., Mailänder V., Walther P., Landfester K., (**2008**). Preparation of biodegradable polymer nanoparticles by miniemulsion technique and their cell interactions, Macromolecular Bioscience, 8, 127 – 139.

N

Nakajima H., Tomomasa S., Okabe M., (**1993**). Preparation of nano-emulsions, Recueil des resumes, In: Premier congress mondial de l'emulsion, Paris, 1, 63.

Nakajima H., (**1997**). Microemulsions in cosmetics, edited by C. Solans and H. Kunieda, Industrial applications of microemulsions, vol. 66, Marcel Dekker, New York, 175 – 179.

Nambam J.S., Philip J., (**2012**). Competitive adsoption of polymer and surfactant at a liquid droplet interface and its effect on flocculation of emulsion, Journal of Colloid and Interface Science, 366, 88 – 95.

National Nanotechnology Initiative, (**2014**). Information available at the web: http://www.nano.gov/nanotech-101/what/definition. Consulted on: 1/08/2014.

NCBI, (**2014**).

Neha B., Ganesh B., Preeti K., (**2013**). Drug delivery to the brain using polymeric nanoparticles: a review, International Journal of Pharmaceutical and Life Sciences, 2(3), 107 – 132.

Némati F., Dubernet C., Colin de Verdière A., Poupon M.F., Puisieux L.F., Couvreur P., (**1994**). Some parameters influencing cytotoxicity of the free doxorubicin and doxorubicin-loaded nanoparticles in sensitive and multidrug resistant leukemic murine cells: incubation number of nanoparticles per cell, International Journal of Pharmacology, 102, 55 – 62.

Nicolaos G., Crauste-Manciet S., Farinotti R., Brossard D., (**2003**). Improvement of cefpodoxime proxetil oral absorption in rats by an oil-in-water submicron emulsion, International Journal of Pharmaceutics, 263, 165 – 171.

Nicolas J., Mura S., Brambilla D., Mackiewicz N., Couvreur P., (**2013**). Design, functionalization strategies and biomedical applications of targeted

biodegradable/biocompatible polymer-based nanocarriers for drug delivery, Chemical Society Reviews, 42, 1147 – 1235.

Nizri G., Magdassi S., (**2005**). Solubilization of hydrophobic molecules in nanoparticles formed by polymer–surfactant interactions, Journal of Colloidal and Interfacial Sciences, 291(1), 169 – 174.

Nkansah M.K., Thakral D., Shapiro E.M., (**2011**). Magnetic poly(lactide-co-glycolide) and cellulose particles for MRI-based cell tracking, Magnetic Resonance in Medicine, 65, 1776 – 1785.

Nobs L., Buchegger F., Gurny R., Allémann E., (**2004**). Poly(lactic acid) nanoparticles labeled with biologically active Neutravidin[TM] for active targeting, European Journal of Pharmaceutics and Biopharmaceutics, 58, 483 – 490.

Norde W., Giacomelli C.E., (**2000**). BSA structural changes during homomolecular exchange between the adsorbed and the dissolved states, Journal of Biotechnology, 79, 259 – 268.

O

Obiols-Rabasa M., (**2008**). Doctoral Thesis: Preparation and colloidal properties of latex dispersions stabilized using hydrophobically modified inulin polymeric surfactants.

O'Brien R.W., White L.R., (**1978**). Electrophoretic mobility of spherical colloidal particle, Journal of Chemical Society, Faraday Trans, 2, 1607 – 1626.

Ojha N., Prabhakar B., (**2013**). Advances in Solubility Enhancement Techniques, International Journal of Pharmaceutical Sciences Reviews and Research, 21(2), 351 – 358.

Okassa L.N., Marchais H., Douziech-Eyrolles L., Hervé K., Cohen-Jonathan S., Munnier E., Souc-e M., Linassier C., Dubois P., Chourpa I., (**2007**). Optimization of iron oxide nanoparticles encapsulation within poly(d,l-lactide-co-glycolide) sub-micron particles, European Journal of Pharmaceutics and Biopharmaceutics, 67, 31 – 38.

Olivier J.C., Vauthier C., Taverna M., Ferrier D., Couvreur P., (**1995**). Preparation and characterization of biodegradable poly(isobutylcyano acrylate) nanoparticles with the surface modified by the adsorption of proteins, Colloids and Surfaces B, 4, 349 – 356.

Olivier J.C., Fenart L., Chauvet R., Patriat C., Cecchelli R., Couet W., (**1999**). Indirect evidence that drug brain targeting using polysorbate 80-coated polybutylcyanoacrylate nanoparticles is related to toxicity, Pharmacological Research, 16, 1836 – 1842.

Oshima H., Makino K., (**1996**). Electrophoretic mobility of a particle covered with a partially ion-penetrable polyelectrolyte layer, Colloids and Surfaces A, 109, 71 – 75.

Oslakovic C., Cedervall T., Linse S., Dahlbäck B., (**2012**). Polystyrene nanoparticles affecting blood coagulation, Nanomedicine, 8, 981 – 986.

Owens III, D.E., Peppas N.A., (**2006**). Opsonization, biodistribution, and pharmacokinetics of polymeric nanoparticles, International Journal of Pharmaceutics, 307, 93 – 102.

P

Pal R., (**1998**). A novel method to correlate emulsion viscosity data, Colloids and Surfaces A, 137(1-5), 275 – 286.

Panyam J., Zhou W.-Z., Pradha S., Sahoo S. K., Labhasetwar V., (**2002**). Rapid endo-lysosomal escape of poly(DL-lactide-co-glycolide) nanoparticles: implications for drug and gene delivery, FASEB Journal, 16, 1217 – 1226.

Panyam J., Sahoo SK., Prabha S., Prabha S., Bargar T. and Labhasetwar V., (**2003**). Fluorescence and electron microscopy probes for cellular and tissue uptake of PLGA nanoparticles, Internal Journal of Pharmaceutics, 262, 1-11.

Panyam J., Labhasetwar V., (**2012**). Biodegradable nanoparticles for drug and gene delivery to cells and tissue, Advanced Drug Delivery Reviews, 64, 61 – 71.

Pardridge W.M., (**2002**). Blood-brain barrier drug targeting enables neuroprotection in brain ischemia following delayed intravenous administration of neurotrophins, Advances in Experimental Medicine and Biology, 513, 397 – 430.

Pardridge W.M., (**2008**). Re-Engineering Biopharmaceuticals for Delivery to Brain with Molecular Trojan Horses, Bioconjugate Chemistry, 19(7), 1327 – 1338.

Parveen S., Sahoo S.K., (**2011**). Long circulating chitosan/PEG blended PLGA nanoparticle for tumor drug delivery, European Journal of Pharmacology, 670(2-3), 372 – 383.

Pascolo L., Bortot B., Benseny-Cases N., Gianoncelli A., Tosi G., Ruozi B., Rizzardi C., De Martino E., Vandelli M.A., Severini G.M., (**2014**). Detection of PLGA-based nanoparticles at a single-cell level by synchrotron radiation FTIR spectromicroscopy and correlation with X-ray fluorescence microscopy, International Journal of Nanomedicine, 9, 2791 – 2801.

Patel T., Zhou J., Piepmeier J.M., Saltzman W.M., (**2012**). Polymeric nanoparticles for drug delivery to the central nervous system, Advanced Drug Delivery Reviews, 64, 701 – 705.

Patil S., Sandberg A., Heckert E., Self W., Seal S., (**2007**). Protein adsorption and cellular uptake of cerium oxide nanoparticles as a function of zeta potential, Biomaterials, 28, 4600 – 4607.

Paulme C., (**2012**). Doctoral Thesis: "Design, characterization and applications of polyester nanoparticles obtained by enzymatic polymerization in nano-emulsions prepared by low-energy methods".

Pecora R., (**2000**). Dynamic light scattering measurement of nanometer particles in liquids, Journal of Nanoparticle Research, 2, 123 – 131.

Pham C.T.N., Mitchell L.M., Huang J.L., Lubniewski C.M., Schall O.S., Killgore J.K., Pan D., Wickline S.A., Lanza G.M., Hourcade D.E., (**2011**). Variable Antibody-dependent Activation of Complement by Functionalized Phospholipid Nanoparticle Surfaces, The Journal of Biological Chemistry, 286, 123 – 130.

Pillai O., Panchagnula R., (**2001**). Polymers in drug delivery, Current Opinion in Chemical Biology, 5, 447 – 451.

Pinto Reis C., Neufeld R. J., Ribeiro A. J., Veiga F., (**2006**). Nanoencapsulation I. Methods for preparation of drug-loaded polymeric nanoparticles. Nanomedicine: Nanotechnology, Biology and Medicine, 2(1), 8 – 21.

Pisani M.J., Wheate N.J., Keene F.R., Aldrich-Wright J.R., Collins J.G., (**2009**). Anionic PAMAM dendrimers as drug delivery vehicles for transition metal-based anticancer drugs, Journal of Inorganic Chemistry, 103, 373 – 380.

Pistolis G., Malliaris A., Tsiourvas D., Paleos C.M., (**1999**). Poly(propyleneimine) Dendrimers as pH-Sensitive Controlled-Release Systems, Chemistra A – European Journal, 5(5), 1440 – 1444.

Polizzi M.A., Stasko N.A., Schoenfisch M.H., (**2007**). Water-Soluble Nitric Oxide-Releasing Gold Nanoparticles, Langmuir, 23, 4938 – 4943.

Posadas I., López-Hernández B., Clemente M.I., Jiménez J.L., Ortega P., de la Mata F.J., Gómez R., Muñoz-Fernández M.A., Ceña V., (**2008**). Highly Efficient Transfection of Rat Cortical Neurons Using Carbosilane Dendrimers Unveils a Neuroprotective Role for HIF-1α in Early Chemical Hypoxia-Mediated Neurotoxicity, Pharmaceutical Research, 26(5), 1181 – 1191.

Pretsch E., Bühlmann P., Affolter C., Herrera A., Martínez R., (**2003**). Determinación structural de compuestos orgánicos, edited by Masson, S.A.

Pubchem, (**2014**).

Putnam D., Gentry C.A., Pack D.W., Langer R., (**2001**). Polymer-based gene delivery with low cytotoxicity by a unique balance of side-chain termini, PNAS, 98(3), 1200 – 1205.

Q

Qaddoumi M.G., Gukasyan H.J., Davda J., Labhasetwar V., Kim K.J., Lee V.H.L., (**2003**). Clathrin and caveolin-1 expression in primary pigmented rabbit conjunctival epithelial cells: Role in PLGA nanoparticle endocytosis, Molecular Vision, 9, 559 – 568.

Quintanar-Guerrero D., Allémann E., Doelker E., Fessi H., (**1997**). A mechanistic study of the formation of polymer nanoparticles by the emulsification-diffusion technique, Colloid and Polymer Science, 275, 640 – 647.

R

Rang M.J., Miller C.A., (**1999**). Spontaneous emulsification of oils containing hydrocarbon, nonionic surfactant, and oleyl alcohol, Journal of Colloid and Interface Science, 209, 179 – 192.

Rahman M.A., Harwansh R., Mirza M.A., Hussain S., Hussain A., (**2011**). Oral lipid based drug delivery systems (LBDDS): formulation, characterization and application: a review, Current Drug Delivery Reviews, 8(4), 330 – 345.

Ramon A.L., Bertrand J.R., de Martimprey H., Bernard G., Ponchel G., Malvy C., Vauthier C:, (**2013**). siRNA associated with immunonanoparticles directed against cd99 antigen improves gene expression inhibitionin vivoin Ewing's sarcoma, Journal of Molecular Recognition, 26(7), 318 – 329.

Rao J., McClements D.J., (**2011**). Food-grade microemulsions, nanoemulsions and emulsions: Fabrication from sucrose monopalmitate & lemon oil, Food Hydrocolloids, 25(6), 1413 – 1423.

Ravi Kumar M.N.V., Bakowsky U., Lehr C.M., (**2004**). Preparation and characterization of cationic PLGA nanospheres as DNA carriers, Biomaterials, 25, 1771 – 1777.

Ray P., De A., Min J.J., Tsien R.Y., Gambhir S.S., (**2004**). Imaging Tri-Fusion multimodality reporter gene expression in living subjects, Cancer Research, 64, 1323 – 1330.

Rebolj K., Pahovnik D., Zagar E., (**2012**). Characterization of a protein conjúgate using an asymmetrical-flow flied-flow fractionation and a size-exclusion chromatography with multi-detection system, Analytical Chemistry, 84, 7374 – 7383.

Resomer   RG   752   H, (http://www.resomer.com/product/biodegradable-polymers/Documents/evonik-specification-resomer-rg-752-h.pdf). Last time consulted: October, **2014**).

Ribeiro S., Rijpkema S.G., Durrani Z., Florence A.T., (**2007**). PLGA-dendron nanoparticles enhance immunogenicity but not lethal antibody production of a DNA vaccine against anthrax in mice, International Journal of Pharmaceutics, 331, 228 – 232.

Riches A.C., Sharp J.G.,Thomas D.B., Smith S.V., (**1973**). Blood volume determination in the mouse, The Journal of Physiology, 228, 279 – 284.

Rowe R.C., Sheskey P.J., Owen S.C., (**2006**). Handbook of pharmaceutical excipients, fifth Edition. Edited by: Pharmaceutical press, London, Chicago.

Rolland A., Bourel D., Genetet B., le Verge R., (**1987**). Monoclonal antibodies covalently coupled to polymethacrylic nanoparticles: in vitro specific targeting to human T lymphocytes, International Journal of Pharmaceutics, 39, 173 – 180.

Rosen M.J., (**2004**). Surfactants and interfacial phenomena, Third Edition, John Wiley & Sons Inc., New York.

Ryman-Rasmussen J.P., Riviere J.E., Monteriro-Riviere N.A., (**2007**). Variables influencing interactions of untargeted quantum dot nanoparticles with skin cells and identification of biochemical modulators, Nanoletters, 7, 1344 – 1348.

S

Sadurní N., Solans C., Azemar N., García-Celma M.J., (**2005**). Studies on the formation of O/W nano-emulsions, by low-energy emulsification methods, suitable for pharmaceutical applications, European Journal of Pharmaceutical Science, 26(5), 438 – 445.

Sadurní N., (**2006**). Doctoral thesis: Estudi de la formació de nano-emulsions de fase externa aquosa i solubilització de fàrmacs lipòfils.

Sagitani H., (**1981**). Making homogeneous and fine droplet OW emulsions using nonionic surfactants, Journal of the American Oil Chemists'Society, 58, 738 – 743.

Sahana D.K., Mittal G., Bhardwaj V., Kumar M.N., (**2008**). PLGA nanoparticles for oral delivery of hydrophobic drugs: influence of organic solvent on nanoparticle formation and release behavior in vitro and in vivo using estradiol as a model drug, Journal of Pharmaceutical Sciences, 97(4), 1530 – 1542.

Sahu A., Lambris J.D., (**2001**). Structure and biology of complement protein C3, a connecting link between innate and acquired immunity, Immunological Reviews, 180, 35 – 48.

Sakthivel T., Florence A.T., (**2003**). Adsorption of amphipathic dendrons on polystyrene nanoparticles, International Journal of Pharmaceutics, 254, 23 – 26.

Salas G., Casado C., Teran F.J., Miranda R., Serna C.J., Puerto Morales M., (**2012**). Controlled synthesis of uniform magnetic nanocrystals with high-quality properties fro biomedical applications, Journal of Materials Chemistry, 22, 21065 – 21075.

Salvador-Morales C., Zhang L., Langer R., Farokhzad O.C., (**2009**). Immunocompatibility properties of lipid–polymer hybrid nanoparticles with heterogeneous surface functional groups, Biomaterials, 30, 2231 – 2240.

Santacruz Biotechnology, (**2014**).

Sapsford K.E., Tyner K.M., Dair B.J., Deschamps J.R., Medintz I.L., (**2011**). Analyzing nanomaterial bioconjugates: a review of current and emerging purification and characterization techniques, Analytical chemistry, 83, 4453 – 4488.

Schalbart P., Kawajia M., Fumoto K., (**2010**). Formation of tetradecane nanoemulsion by low-energy emulsification methods, International Journal of Refrigeration, 33(8), 1612 – 1624.

Schärtl W., (**2006**). Light scattering from polymer solutions and nanoparticle dispersions, Springer laboratory, ed. Pasch H., p. 22. ISBN: 978-3-540-71951-9

Shannon H.A., Lutz E.A., (**2002**). Comparison of the peripheral and central effects of the opioid agonists loperamide and morphine in the formalin test in rats, Neuropharmacology, 42(2), 253 – 261.

Shi Sh., Chen H., Cui Y., Tang X., (**2009**). Formulation, stability and degradation kinetics of intravenous cinnarizine lipid emulsion, International Journal of Pharmaceutics, 373(1-2), 147 – 155.

Shimoda A., Sawada S., Kano A., Maruyama A., Moquin A., Winnik F.M., Akiyoshi K., (**2012**). Dual crosslinked hydrogel nanoparticles by nanogel bottom-up method for sustained-release delivery, Colloids and Surfaces B, 99(1), 38 – 44.

Shinoda K., Saito H., (**1968**). The effect of temperature on the phase equilibria and the types of dispersions of the ternary system composed of water, cyclohexane, and nonionic surfactant, Journal of Colloidal and Interface Sciences, 26, 70 – 74.

Shinoda K., Saito H., (**1969**). The stability of O/W type emulsions as functions of temperature and the HLB of emulsifiers: The emulsification by PIT-method, Journal of Colloid and Interface Science, 30, 258 – 263.

Shinoda K., Kunieda H., (**1973**). Conditions to produce so-called microemulsions: Factors to increase the mutual solubility of oil and water by solubilizer, Journal of Colloid and Interface Science, 42(2), 381 – 387.

Sigma-Aldrich. Last time consulted: July (**2014**).

Silva H.D., Cerqueira M.A., Vicente A.A., (**2012**). Nanoemulsions for food applications: development and characterization, Food and Bioprocess Technology, 5(3), 854 – 867.

Sing A.J.F., Graacia A., Lachaise J., Brochette P., Salager J.L., (**1999**). Interactions and coalescence of nanodroplets in translucent O/W emulsions, Colloids and Surfaces A: Physichochemical and Engineering aspects,152(1-2), 31 – 39.

Singh A., Dilnawaz F., Mewar S., Sharma U., Jagannathan N.R., Sahoo S.K., (**2011**). Composite polymeric magnetic nanoparticles for co-delivery of hydrophobic and hydrophilic anticancer drugs and MRI imaging for cancer therapy, Applied Materials and Interfaces, 3, 842 – 856.

Singh R.P., Ramarao P., (**2013**). Accumulated polymer degradation productes as effector molecules in cytotoxicity of polymeric nanoparticles, Toxicological Sciences, 136(1), 131 – 143.

Solans C., Esquena J., Forgiarini A., Usón N., Morales D., Izquierdo P., Azemar N., García-Celma M.J., (**2003**). Nano-emulsions: Formation, properties and applications. In Mittal K.L., Shah, Dinash O. eds. Adsorption and aggregation of surfactants in solution, Marcel Dekker, New York, v 109, 525 – 554.

Solans C., Izquierdo P., Nolla J., Azemar N., García-Celma M.J., (**2005**). Nano-emulsions. Current Opinion in Colloid and Interface Sciences, 10, 102 – 110.

Solans C., Solè I., (**2012**). Nano-emulsions: Formation by low-energy methods, Current Opinion in Colloid and Interface Science, 17, 246 – 254.

Solè I., Maestro A., González C., Solans C., Gutiérrez J.M., (**2006**). Optimization of nano-emulsion preparation by low-energy methods in an ionic surfactant system, Langmuir, 22, 8326 – 8332.

Solè I., Solans C., Maestro A., González C., Gutiérrez J.M., (**2012**). Study of nano-emulsion formation by dilution of microemulsions, Journal of Colloid and Interface Science, 376, 133 – 139.

Sonneville-Aubrun O., Simonnet J.-T., l'Alloret F., (**2004**). Nanoemulsions: a new vehicle for skincare products, Advances in Colloid and Interface Science, 108 – 109, 145 – 149.

Sonneville-Aubrun O., Babayan D., Bordeaux D., Lindner P., Rata G., Cabane B., (**2009**). Phase transition pathways for the production of 100 nm oil-in-water emulsions, Physical Chemistry Chemical Physics, 11, 101 – 110.

Soppimath K.S., Aminabhavi T.M., Kulkarni A.R., Rudzinski W.E., (**2001**). Biodegradable polymeric nanoparticles as drug delivery devices, Journal of Controlled Release, 70(1-2), 1 – 20.

Spectrum®Laboratoires, INC, (**2014**). Webpage: www.spectrumlabs.com

Spernath L., Magdassi S., (**2007**). A new method for preparation of poly-lauryl acrylate nanoparticles from nanoemulsions obtained by the phase inversion temperature process, Polymers for Advanced Technologies, 18, 705 – 711.

Spernath L., Regev O., Levi-Kalisman Y., Magdassi S., (**2009**). Phase transitions in O/W lauryl acrylate emulsions during phase inversion, studied by light microscopy and cryo-TEM, Colloids and Surfaces A, 331(1), 19 – 25.

Stewart K.M., Horton K.L., Kelley S.O., (**2008**). Cell-penetrating peptides as delivery vehicles for biology and medicine, Organic and Biomolecular Chemistry, 6 , 2242 – 2255.

Stolnik S., Garnett M.C., Illum L., Bousta M., Vert M., Davis S.S., (**1995**). The colloidal properties of surfactant-free biodegradable nanospheres from poly(b-malic acid-co-benzyl malate)s and poly(lactic acid-co-glycolide), Colloids and Surfaces A, 97, 235 – 245.

Strickley R.G., (**2006**). Solubilizing excipients in pharmaceutical formulations, Encyclopedia of Pharmaceutical Technology, edited by Swarbrick J., 1, 3334 – 3366.

Suh G.H., YeonJung H., Lee C.U., Oh B.H., Bae J.N., Jung H.Y., Ju Y.S., Yeon B.K., Park J., Hong I., Choi S., Lee J.H., (**2004**). A Prospective, Double-Blind, Community-Controlled Comparison of Three Doses of Galantamine in the Treatment of Mild to Moderate Alzheimer's Disease in a Korean Population, Clinical Therapeutics, 26(10), 1608 – 1618.

Sun Y., Zheng Y., Ran H., Zhou Y., Shen H., Chen Y., Chen H., Krupka T.M., Li A., Li P., Wang Z., Wang Z., (**2012**). Superparamagnetic PLGA-iron oxide microcapsules for dual-modality US/MR imaging and high intensity focused US breast cancer ablation, Biomaterials, 33, 5854 – 5864.

Svenson S., Dendrimers as versatile platform in drug delivery applications, (**2009**). European Journal of Pharmaceutics and Biopharmaceutics, 71, 445 – 462.

Swinyard E.A., (**1990**). Analgesics and antipyretics, in Remington's Pharmaceutical Sciences, Chapter 59, edited by Gennaro A.R. and Remington J.P., Mack Editions, 18th edition.

Sznitzowska M., Janicki S., Dabrowska E., Zurowska-Pryczkowska K., (**2001**). Submicron emulsions as drug carrier. Studies on destabilization of various drugs, European Journal of Pharmaceutical Science, 12(3), 175 – 179.

T

Tadros Th.F., (**1982**). The effect of polymers on dispersion properties, Academic Press.

Tadros Th.F., Vincent B., (**1983**). Encyclopedia of emulsion technology (edited by Becher P.), Marce Decker, 1, 1 – 56.

Tadros Th.F., Izquierdo P., Esquena J., Solans C., (**2004**). Formation and stability of nano-emulsions, Advances in Colloid and Interface Science, 108 – 109, 303 – 318.

Tadros Th.F., (**2005**). Applied surfactants, Principles and applications, Wiley VCH, p. 402.

Tadros Th.F., (**2009**). Emulsions Science and Technology: A general Introduction, Emulsions Science and Technology, edited by Tadros Th.F., Wokingham, 1 – 55.

Taisne L., Walstra P., Cabane B., (**1996**). Transfer of oil between emulsion droplets, Journal of Colloid and Interface Science, 184 378 – 390.

Tamilvanan S., (**2004**). Oil-in-water lipid emulsions: implications for parenteral and ocular delivering systems, Progress in Lipid Research, 43, 489 – 533.

Tamilvanan S., Schmidt S., Müller R., Benita S., (**2005**). In vitro adsorption of plasma proteins onto the surface (charges) modified-submicron emulsions for intravenous administration, European Journal of Pharmaceutics and Biopharmaceutics, 59, 1 – 7.

Tantra R., Schulze P., Quincey P., (**2010**). Effect of nanoparticle concentration on zeta-potential measurement results and reproductibility, Particuology, 8, 279 – 285.

Taylor P., (**1994**). Ostwald ripening in O/W nano-emulsions formed by dilution of O/W microemulsions, Trends in Colloid and Interface Science VIII, Progress in Colloid and Polymer Science, edited by Ottewill R., Rennie A., 97, 199 – 203.

Taylor P., (**1998**). Ostwald ripening in emulions, Advances in Colloid and Interface Science, 75, 107 – 163.

Teixera Z., Dreiss C.A., Lawrence M., Heenan R.K., Mahcado D., Justo G.Z., Guterres S.S., Durán N., (**2012**). Retinyl palmitate polymeric nanocapsules as carriers of bioactives, Journal of Colloid and Interface Science, 382, 36 – 47.

Thielbeer J., Donaldson K., Bradley M., (**2011**). Zeta Potential Mediated Reaction Monitoring on Nano and Microparticles, Bioconjugate Chemistry, 22, 144 – 150.

Timbrell J.A., (**1998**). Biomarkers in toxicology, Toxicology, 129, 1 – 12.

Tosi G., Costantino L., Rivasi F., Ruozi B., Leo E., Vergoni A.V., Tacchi R., Bertolini A., Vandelli M.A., Forni F., (**2007**). Targeting the central nervous system: In vivo experiments with peptide-derivatized nanoparticles loaded with Loperamide and Rhodamine-123, Journal of Controlled Release, 122, 1 – 9.

Tosi G., Vergoni A.V., Ruozi B., Bondioli L., Badiali L., Rivasi F., Costantino L., Forni F., and Vandelli M.A., (**2010**). Sialic acid and glycopeptides conjugated PLGA nanoparticles for

central nervous system targeting: *In vivo* pharmacological evidence and biodistribution. Journal of Controlled Release, 145, 49-57.

Tosi G., Fano R.A:, Bondioli L., Badiali L., Benassi R., Rivasi F., Ruozi B., Forni F., Vandelli A., (**2011**). Investigation on mechanisms of glycopeptide nanoparticles for drug delivery across the blood-brain barrier, Nanomedicine, 6(3), 423 – 436.

Tosi G., Bortot B., Ruozi B., Dolcetta D., Vandelli M.A., Forni F., (**2013**). Severini G.M., Potential use of polymeric nanoparticles for drug delivery across the blood-brain barrier, Current Medicinal Chemistry, 20, 2212 – 2225.

Toti U.S., Guru B.R., Grill A.E., Panyam J., (**2010**). Interfacial activity assisted surface functionalization: A novel approach to incorporate maleimide functional groups and cRGD peptide on polymeric nanoparticles for targeted drug delivery, Molecular Pharmacology, 7(4), 1108 – 1117.

TOXNET (http://toxnet.nlm.nih.gov/cgi-bin/sis/search/a?dbs+hsdb:@term+@DOCNO+4359). Last time consulted: February **2014**.

Trapani A., Sitterberg J., Bakowsky U., Kissel T., (**2009**). The potential of glycol chitosan nanoparticles as carrier for low water soluble drugs, International Journal of Pharmaceutics, 375, 97 – 106.

Trimaille T., Pichot C., Elaïssari A., Fessi H., Briançon S., Delair T., (**2003**). Poly(D,L-lactic acid) nanoparticle preparation and colloidal characterization, Colloid and Polymer Science, 281(12), 1184 – 1190.

Trotta M., Debernardi F., Caputo O., (**2003**). Preparation of solid lipid nanoparticles by a solvent emulsification – diffusion technique, International Journal of Pharmaceutics, 257(1-2), 153 – 160.

U

Ueda M., Kreuter J., (**1997**). Optimization of the preparation of loperamide-loaded poly(L-lactide) nanoparticles by high pressure emulsification-solvent evaporation, Journal of Microencapsulation, 14(5), 593 – 605.

Ugelstad J., El-Aasser M.S., Vanderhoff J.W., (**1973**). Emulsion polymerization: initation of polymerization in monomer droplets, Journal of Polymer Science: Polymer letters, 11(8), 503 – 513.

Ujwala R.B., Redasani V.K., Sachin N.K., (**2013**). Preparation and in-vitro evaluation of loperamide hydrochloride spherical crystals by emulsion solvent diffusion technique, International Journal of Pharmacy and Pharmaceutical Sciences, 5(2), 409 – 413.

Ulbrich K., Hekmatara T., Herbert E., Kreuter J., (**2009**). Transferrin- and transferring-receptor-antibody-modified nanoparticles enable drug delivery across the blood-brain barrier (BBB), European Journal of Pharmaceutics and Biopharmaceutics, 71, 251 – 256.

Usón N., (**2003**). Doctoral thesis: Estudi de la formació de nano-emulsions de tipus aigua en oli, Universitat de Barcelona.

Usón N., García-Celma M.J., Solans C., (**2004**). Formation of water-in-oil (W/O) nanoemulsions in a water/mixed non-ionic surfactant/oil system prepared by a lowenergy emulsification method, Colloids and Surface A,250, 415 – 421.

USP Pharmacopoeia, (**2009**). On-line resource accessible at: http://www.usp.org/.

V

Vauthier C., Dubernet C., Fattal E., Pinto-Alphandary H., Couvreur P., (**2003**). Poly(alkylcyanoacrylates) as biodegradable materials for biomedical applications, Advanced Drug Delivery Reviews, 55, 519 – 548.

Vauthier C., Cabane B., Labarre D., (**2008**). How to concentrate nanoparticles and avoid aggregation?, European Journal of Pharmaceutics and Biopharmaceutics, 69(2), 466 – 475.

(1) **Vauthier** C., Bouchemal K., (**2009**). Methods for the preparation and manufacture of polymeric nanoparticles, Pharmaceutical Research, 26(5), 1025 – 1058.

(2) **Vauthier** C., Linder P., Cabane B., (**2009**). Configuration of bovine serum albumin adsorbed on polymer particles with grafted dextran corona, Colloids and Surfaces B: Biointerfaces, 69, 207 – 215.

Vauthier C., Persson B., Linder P., Cabane B., (**2011**). Protein adsorption and complement activation for di-block copolymer nanoparticles, Biomaterials, 32, 1646 – 1656.

Vergoni A.V., Tosi G., Tacchi R., Vandelli M.A., Bertolini A., Costantino L., (**2009**). Nanoparticles as drug delivery agents specific for CNS: in vivo biodistribution, Nanomedicine, 5, 369 – 377.

Verma A., Stellacci F., (**2009**). Effect of Surface Properties on Nanoparticle–Cell Interactions, Small, 6(1), 12 – 21.

Verwey E.J.W., Overweek J.Th.G., (**1948**). Theory of the stability of lyophobic colloids, Amsterdam: Elsevier.

Vilasau J., (**2010**). Doctoral Thesis: "Influencia del comportamiento fásico de sistemas agua / tensioactivo y del proceso de emulsificación en las propiedades de emulsions de parafina".

Villaroya M., García A.G., Marco-Contelles J., López M.G., (**2007**). An uptade on the pharmacology of galantamine, Expert Opinion on Investigation of Drugs, 16(12), 1987 – 1998.

Vittaz M., Bazile D., Spenlehauer G., Verrecchia T., Veillard M., Puisieux F., Labarre D., (**1996**). Effect of PEO surface density on long-circulating PLA-PEO nanoparticles which are very low complement activators, Biomaterials, 17, 1575 – 1581.

(1) **Voigt** N., Henrich-Noacl P., Kockentiedt S., Hintz W., Tomas J., Sabel B.A., (**2014**). Toxicity of polymeric nanoparticles in vivo and in vitro, Journal of Nanoparticle Research, 16, 2379 – 2392.

(2) **Voigt** N., Henrich-Noack P., Kockentiedt S., Hintz W., Tomas J., Sabel B.A., (**2014**). Surfactants, not size or zeta-potential influence blood-brain bariier passage of polymeric nanoparticles, European Journal of Pharmaceutics and Biopharmaceutics, 87, 19 – 29.

Vonarbourg A., Passirani C., Saulnier P., Benoit J.P., (**2006**). Parameters influencing the stealthiness of colloidal drug delivery systems, Biomaterials, 27, 4356 – 4373.

Vrignaud S., Benoit J.-P., Saulnier P., (**2011**). Strategies for the nanoencapsulation of hydrophilic molecules in polymer-based nanoparticles, Biomaterials, 32, 8593 – 8604.

Vroman L., **Adams** A.L., (**1986**). Why plasma proteins interact at interfaces, in Horbett T.A., Brash J.L., (Eds.), Proteins at Interfaces: physicochemical and biochemical studies, in: ACS Symp, vol 343. ACS, Washington DC, 154 – 164.

Vyas T.K., Shahiwala A., Amiji M.M., (**2008**). Improved oral bioavailability and brain transport of Saquinavir upon administration in novel nanoemulsions formulations, International Journal of Pharmaceutics, 347(1-2), 93 – 101.

W

Wagner C., (**1961**). Theorie der Alterung von Niederschlägen durch Umlesen (Ostwald-Reifung), Zeitschrift für elektrochemie, Berichte der Bunsengesellschaft für physikalische Chemies, 65, 581 – 591.

Walstra P., (**1983**). Formation of emulsions, Encyclopedia of emulsion technology (vol 1), edited by Becher P., Marcel Dekker, New York.

Walstra P., (**1993**). Principles of emulsion formation. Chemical Engineering Sciences, 48, 333 – 349.

Walstra P., (**1996**). Emulsion stability. Encyclopedia of emulsion technology, edited by Becher P., Marcel Dekker, New York, 1 – 62.

Wang Y., Gao S., Ye W., Yoon H., Yang Y., (**2006**). Co-delivery of drugs and DNA from cationic core–shell nanoparticles self-assembled from a biodegradable copolymer, Nature Materials, 5, 791 – 796.

 (1) **Wang** L., Li X., Zhang G., Dong J., Eastoe J., (**2007**). Oil-in-water nanoemulsions for pesticide formulations, Journal of Colloid and Inerface Science, 314, 230 – 235.

(2) **Wang** S.J., Fan X.D., Liu X., Kong J., Liu Y.Y., Wang X., (**2007**). Dendritic carbosilane-based macrophotoinitiator: synthesis, characterization, and photoinitiating behavior, Polymer International, 56(6), 764 – 772.

Wang L., Mutch K.J., Eastoe J., Heenan R.K., Donh J., (**2008**). Nanoemulsions prepared by a two-step low-energy process, Langmuir, 24, 6092 – 6099.

Wang L., Tabor R., Eastoe J., Li X., Heenan R.K., Dong J., (**2009**). Formation and stability of nanoemulsions with mixed ionic-noionic surfactants, Physical Chemistry Chemical Physics, 11, 9772 – 9778.

Wang J., Liu W., Tu Q., Wang J., Song N., Zhang Y., Nie N., Wang J., (**2011**). Folate-Decorated Hybrid Polymeric Nanoparticles for Chemically and Physically Combined Paclitaxel Loading and Targeted Delivery, Biomacromolecules, 12, 228-234.

Wattiaux R., Laurent N., Wattiaux-De Coninck S., Jadot M., (**2000**). Endosomes, lysosomes: their implication in gene transfer, Advanced Drug Delivery Reviews, 41, 201 – 208.

Weber N., Ortega P., Clemente M.I., Shcharbin D., Bryszewska M., de la Mata F.J., Gómez R., Muñoz-Fernández M.A., (**2008**). Characterization of carbosilane dendrimers as effective carriers of siRNA to HIV-infected lymphocytes, Journal of Controlled Release, 123(1), 55 – 64.

Weiner B.B., (**2010**). What is particle size?, in Brookhaver Instruments White Paper.

Weissenböck A., Wirth M., Gabor F., (**2004**). WGA-grafted PLGA-nanospheres: preparation and association with Caco-2 single cells, Journal of Controlled Release, 99, 383-392.

Whitby C.P., Lim L.H., Eskandar N.G., Simovic S., Prestidge C.A., (**2012**). Poly(lactic-co-glycolic acid) as a particulate emulsifier, Journal of Colloids and Interfacial Sciences, 375, 142 – 147.

Winsor P.A., (**1948**). Hydrotropy, solubilisation, and related emulsification processes, Trans. Faraday Soc, 44, 376 – 382.

(1) **Wohlfart** S., Khalansky A.S., Gelperina S., Begley D., Kreuter J., (**2011**). Kinetics of transport of doxorubicin bound to nanoparticles across the blood-brain barrier, Journal of Control Release, 54, 103 – 107.

(2) **Wohlfart** S., Khalansky A.S., Bernreuther C., Michaelis M., Cinatl J., Glatzel M., Kreuter J., (**2011**). Treatment of glioblastoma with poly(isohexyl cyanoacrylate) nanoparticles, International Journal of Pharmaceutics, 415, 244 – 251.

Wohlfart S., Gelperina S., Kreuter J., (**2012**). Transport of drugs across the blood-brain barrier by nanoparticles, Journal of Controlled Release, 161, 264 – 283.

World Health Organization (WHO), (**2011**). Report by the WHO Secretariat on the global burden of mental disorders.

Wretlind A.J., (**1964**). The pharmacological basis for the use of fat emulsions in intravenous nutrition, Acta chirurgica scandinava, Suplementum, 325, 31 – 41.

Wu XS., (**1995**). Synthesis and properties of biodegradable lactic/glycolic acid polymers. In: Wise et al., editors. Encyclopedia Handbook of Biomaterials and Bioengineering. New York: Marcel Dekker, 1151 – 1200.

Wuelfing P.W., Kosuda K., Templeton A.C., Harman A., Mowery M.D., Reed R.A., (**2006**). Polysorbate 80 UV/vis spectral and chromatographic characteristics –defining boundary conditions for use of the surfactant in dissolution analysis, Journal of Pharmaceutical and Biomedical Analysis, 41, 774 – 782.

Y

Yang H., (**2010**). Nanoparticle-Mediated Brain-Specific Drug Delivery, Imaging, and Diagnosis, Pharmaceutical Research, 27, 1759 – 1771.

Yang Y., Leser M.E., Sher A.A., McClements D.J., (**2013**). Formation and stability of emulsions using a natural small molecule surfactant: Quillaja saponin (Q-Naturale®), Food Hydrocolloids, 30, 589 – 596.

Yin Y., Chen D., Qiao M., Wei X., Hu H., (**2007**). Lectin-conjugated PLGA nanoparticles loaded with thymopentin: Ex vivo bioadhesion and in vivo biodistribution, Journal of Controlled Release, 123, 27 – 38.

Yin Win K., Feng S.-S., (**2005**). Effects of particle size and surface coating on cellular uptake of polymeric nanoparticles for oral delivery of anticancer drugs, Biomaterials, 26, 2713-2722.

Z

Zensi A., Begley D., Pontikis C., Legros C., Mihoreanu L., Wagner S., Büchel C., von Briesen H., Kreuter J., (**2009**). Albumin nanoparticles targeted Apo E enter the CNS by transcytosis and are delivered to neurons, Journal of Controlled Release, 137, 78 – 86.

Zhang Y., Pardridge W. M., (**2005**). Delivery of β-Galactosidase to Mouse Brain via the Blood-Brain Barrier Transferrin Receptor, Journal of Pharmacology and Experimental Therapeutics, 313(3), 1075 – 1081.

Zhang W., Gao J., Zhu Q., Zhang M., Ding X., Wang X., Hou X., Fan W., Ding B., Wu X., Wang X., Gao S., (**2010**). Penetration and distribution of PLGA nanoparticles in the human skin treated with microneedles, International Journal of Pharmaceutics, 402, 205 – 212.

Zhou J., Moya S., Ma L., Gao C., Shen J., (**2009**). Polyelectrolyte Coated PLGA Nanoparticles: Templation and Release Behavior, Macromolecular Biosciences, 9, 326 – 335.

Zhou J., Liu J., Shi T., Xia Y., Luo Y., Liang D., (**2013**). Phase separation of siRNA–polycation complex and its effect on transfection efficiency, Soft Matter, 9, 2262 – 2268.

Ziani K., Fang Y., McClements D.J., (**2012**). Fabrication and stability of coloidal delivery systems for flavor oils: Effect of composition and storage conditions, Food Research International, 2012, 46, 209 – 216.

Zimmermann M., Grösgen S., Westwell M.S., Greenfield S.A., (**2008**). Selective enhancement of the activity of C-terminally truncated, but not intact, acethylcholinesterase, Journal of Neurochemistry, 104, 221 – 232.

Zlokovic BV., (**2008**). The blood-brain barrier in health and chronic neurodegenerative disorders, Neuron, 57, 178 – 201.

Zolnik B.Z., González-Fernaández A., Sadrieh N., Dobrovolskaia M.A., (**2010**). Minireview: Nanoparticles and the Immune System, Endocrinology, 151, 458 – 465.

Zweers M.L.T., Engbers G.H.M., Grijpma D.W., Feijen J., (**2004**). In vitro degradation of nanoparticles prepared from polymers based on dl-lactide, glycolide and poly(ethylene oxide), Journal of Controlled Release, 100, 347 – 356.

Chapter 9

GLOSSARY

9.1 Abbreviations

8D3	Rat anti-mouse transferring receptor monoclonal antibody
% MPE	Maximal possible effect
ΔA	Interfacial area increase
$\gamma \Delta A$	Positive free energy
Ab	Antibody
ABC	Accelerated blood clearance
ACh	Acetylcholine
AChE	Acetylcholinesterase
ACN	Acetonitrile
ACTI	Acetylcholine iodide
AD	Alzheimer's disease
AF555	Alexa fluor 555
AFM	Atomic force microscopy
ALS	Amyotrophic lateral sclerosis
anti-TfR	Anti transferring receptor monoclonal antibody
APTT	Activated partial thromboplastin time
APTES	3-aminopropyltrimethoxysilane
Apo	Apolipoprotein
ApoE	Apolipoprotein E
ASO	Antisense oligonucleotide
AU	Arbitrary units
BBB	Blood brain barrier
BCA	Bicinchonic acid kit
BS	Backscattered light
BSA	Bovine serum albumin
C6	Coumarin-6
CH_2	Methylen chemical group
CH_3	Methyl chemical group
CMC	Critic micellar concentration
CNS	Central nervous system
CO	Ester or acid chemical group
COC	Ether chemical group
Da	Daltons (g/mol)
DEPC	diethylpyrocarbonate
DIC	Differential interference contrast

DLS	Dynamic light scattering
DLVO	Derjaguin – Landau – Verwey – Overbeek theory
DMEM	Dulbecco's Modified Eagle's Medium
DMSO	Dimethyl sulfoxide
DSC	Differential scanning calorimetry
DTNB	5,5'-dithiobis[2-nitrobenzoic acid]
E_A	Atractive energy
EE	Encapsulation efficiency
EDC	1-ethyl-3-(3-dimethylaminopropil)carbodiimide
EDTA	Ethylenediaminetetraacetic acid
EMSA	Electrophoretic mobility shift assay
E_R	Repulsive enrgy
Et_3N	Triethylamine
FBS	Fetal bovine serum
FDA	U.S. Food and Drug Administration
FITC	Fluorescein isothiocyanate
FITC-NP	FITC-functionalized nanoparticles
FTIR	Fourier transformed intrarred spectroscopy
Fv	Concentration factor
ΔG	Free energy of formation
GAL	Galanthamine hydrobromide
GPC	Gel permeation chromatography
GRAS	Generally accepted as safe
G2SN	Second generation cationic carbosilane dendron
G2SN-NPs	G2SN functionalized-NPs
G3SN	Third generation cationic carbosilane dendron
G3SN-NPs	G3SN functionalized-NPs
HCl	Hydrochloric acid
HLB	Hydrophilic-lipophilic balance
HPLC	High performance liquid chromatography
H_3PO_4	Ortophosphoric acid
HS	Human serum
HSA	Human serum albumin
ICH	International Conference for Harmonization
IONPs	Iron oxide nanoparticles
IR	Infrarred

i.v.	Intravenous
LDH	Lactate dehydrogenase
LDL	Low-density lipoprotein
LDL-r	Low-density lipoprotein receptor
LOP	Loperamide hydrochloride
LSW	Lifshitz – Slezov – Wagner theory
μE	Microemulsion
MHE	Mark-Houwink equation
MND	Motor neuron disease
MNPs	Magnetic nanoparticles
MPE	Maximal possible effect
MRI	Magnetic resonance imaging
MTT	3(4,5-dimethylthiazol-2-yl)2,5diphenyltetrazolium bromide
MW	Molecular weight
MWCO	Molecular weight cut-off
NaCl	Sodium chloride
$NaH_2PO_4 \cdot H_2O$	Sodium phosphate monobasic
$Na_2HPO_4 \cdot 2H_2O$	Disodium phosphate dibasic
NaOH	Sodium hydroxide
NE	Nano-emulsion
NF	Not functionalized
NL	Non-loaded
N_{HLB}	HLB number
NHS	*N*-hydroxisuccinimide
NP	Nanoparticle
NP@MNPs	MNPs-loaded nanoparticles
NPd	Nanoparticle dispersion
NP-WY	Nanoparticles dispersed in water, with an 'Y' percentage of oil in the O/S mixture of the template NE
NP-XEY	Nanoparticles dispersed in PBS, at a 'X' molar concentration, with an 'Y' percentage of oil in the O/S mixture of the template NE
N/P	Positive to negative ratio
NTA	Nanoparticle tracking analysis
O/S	Oil/surfactant
O/W	Oil-in-water
PBCA	Poly(butyl cyanoacrylate)

PBS	Phosphate buffered saline
PCS	Plasma coagulation system
PD	Parkinson's disease
PDI	Polydispersity index
PEG	Poly(ethylene glycol)
PET	Positron emission tomography
PGA	Poly(glycolic acid)
Pgp	P-glycoprotein
PIC	Phase inversion composition
PIT	Phase inversion temperature
PLA	Poly(lactic acid)
PLGA	Poly-(lactic-co-glycolic) acid
PT	Prothrombin time
PTA	Phosphotungstic acid
PTFE	Polytetrafluoroethylene
PVA	Polyvinyl alcohol
R_g	Gyration radius
R_H	Hydrodynamic radius
RBC	Red blood cells
RES	Reticuloencothelial system
ΔS	Entropy increase
SCF	Supercritical fluid technology
SDS-PAGE	Sodium Dodecyl Sulfate Polyacrylamide Gel Electrophoresis
SEC	Size exclusion chromatography
SEM	Scanning electron microscopy
siRNA	Small interference ribonucleic acid
SLS	Static light scattering
SN	Supernatant
TBE	Tris/Borate/EDTA buffer
TEM	Transmission electron microscopy
TEMED	Tetramethylethylenediamine
TfR	Transferrin receptor
T_g	Glass transition temperature
T_{HLB}	HLB temperature
TGA	Termogravimetric assay
THF	Tetrahydrofurane

TOXNET	Toxicology Data Network
UV	Ultraviolet
VBS^{2+}	Veronal-buffered saline
WHO	World health organization
W/O	Water-in-oil
z_i	Ion valence

9.2 Roman letters

A	Hamaker constant
C_α	Solubility of the dispersed in the continuous phase
C_i	Ion concentration
D	Diffusion coefficient
E	Total energy
F	Faraday's constant
g	Gravity force
g	Grams
H	Hydrophilic groups
K	Debye-Hückel parameter
L	Lipophilic groups
N	Positively charged groups
O	Oil phase
P	Negatively charged groups
r	Radius
R	Gas constant
R	Geometric radius
S	Surfactant
t	Time
T	Transmitted light
Tº	Temperature
V_M	Molar volume of he dispersed phase
W	Water phase
x	Distance between two droplets
z	Number of BSA molecules per NP

364

9.3 Greek letters

γ	Interfacial tension between two phases
ε	Absolute permittivity
ε_0	Vacuum permittivity
ε_p	Solvent permeability
ε_r	Relative permitivity
η	Viscosity
$[\eta]$	Intrinsic viscosity
μ	Electrophoretic mobility
ρ	Density
ζ	Zeta potential
ω_{CO}	Coalescence rate
ω_{CR}	Migration velocity
ω_{OR}	Ostwald ripening rate

Chapter 10

APPENDIX

10.1.   Experimental procedures

10.1.1. Intravenous administration of polymeric nanoparticles and study of the central analgesia by means of Hot Plate test in male CD-1 mice

UNIVERSITAT DE BARCELONA

MEMÒRIA DESCRIPTIVA DEL PROCEDIMENT

PROCEDIMENT DE RECERCA

Documentació requerida en compliment de la normativa vigent: llei 5/1995 de protecció dels animals utilitzats per a experimentació i per a altres finalitats científiques i decret 214/1997 pel qual es regula la utilització d'animals per a experimentació i per a altres finalitats científiques. Aquesta documentació pot estar subjecte a inspecció per part de l'administració en qualsevol moment

1. Dades de l'/la investigador/a responsable del procediment:

Nom i Cognoms	NIF:
Cristina Fornaguera Puigvert	45829745Z

Telèfon	Fax	e-mail
934006100 ext 2302		cristina.fornaguera@iqac.csic.es

1.2. Dades del Centre (nom del centre al que pertany l'/la investigador/a)

Consell Superior d'Investigacions Científiques (IQAC-CSIC)

Unitat /Secció/....	Departament/ Institut /....
Institut de Química Avançada de Catalunya (IQAC-CSIC)	Departament de Nanotecnologia Química i Biomolecular (NQB)

Carrer/plaça	núm.	Codi postal	Ciutat/ Provincia
C/ Jordi Girona	18-26	08034	Barcelona

1.3. Persona/es que realitzaran el procediment (DEGUDAMENT ACREDITAT)

Nom i Cognoms	NIF	e-mail	Acreditació(I/E)
Cristina Fornaguera Puigvert	45829745Z	crisitina.fornaguera@iqac.csic.es	Investigador
David Pérez Cáceres	43543736K	davidperez@ccit.ub.edu	Investigador

369

UNIVERSITAT DE BARCELONA

			Investigador
			Investigador

*I= Investigador E=Experimentador

2.- INSTAL·LACIONS: Indiqueu el lloc on es mantindran els animals durant el procediment::

Unitat d'Experimentació Animal de Farmàcia

3.- TÍTOL DEL PROCEDIMENT (S'entén per procediment la utilització d'un animal amb finalitats experimentals, científiques o educatives. No confongueu projecte amb procediment. Un projecte de recerca pot tenir diferents procediments. Indicar l'espècie del model en el títol).

Administració intravenosa de nanopartícules polimèriques i estudi de l'analgèsia central mitjançant Hot-plate test amb ratolins mascles CD1

3.1.- En cas de tractar-se d'una pròrroga o renovació/ampliació, indicar el número d'ordre assignat per la Generalitat:

4.- SEGUEIX ALGUNA LÍNIA DIRECTRIU OFICIAL?

☐Sí, especificar quina i, si és possible, adjuntar-ne una fotocòpia o document PDF:

X No, però s'adjunten referències de publicacions científiques amb un disseny similar (a ser possible accessibles per via Web o en el seu defecte fotocòpies)

Schröder, Sabel; Nanoparticles, a drug carrier system to pass the blood-brain barrier, permit central analgesic effects of i.v. dalargin injections, Brain Research, 1996, 710, 121 - 124.

Enllaç: http://www.sciencedirect.com/science/article/pii/000689939501375X

Camarasa, Pubill, Escubedo; Association of caffeine to MDMA does not

UNIVERSITAT DE BARCELONA

increase antinociception but potentiates adverse effects of this recreational drug , Brain Research, 2006, 1111, 72 - 82.

Enllaç:
http://www.sciencedirect.com/science/article/pii/S0006899306019937#

☐ No, no existeixen publicacions amb un disseny similar

5.- OBJETIUS

(descriure els principals objectius que es pretenen assolir, explicant els antecedents, avantatges i beneficis que es deriven, utilitzant un vocabulari no excessivament tècnic. Indicar si el procediment està vinculat a un projecte de recerca, especificar quin)

ANTECEDENTS

En els últims anys, diversos estudis han intentat dissenyar vehicles que creuin la barrera hemato-encefàlica (BBB) pel tractament de malalties neurològiques utilitzant vies menys agressives que la intracraneal. Un dels vehicles més estudiats han estat les nanopartícules polimèriques amb diferents vectoritzacions específiques cap als receptors de la BBB.

L'estudi del pas de la BBB es pot fer mitjançant l'efecte analgèsic provocat per la loperamida; un fàrmac que només té efecte analgèsic a nivell central però que per si sol no és capaç de travessar la BBB.

Actualment, s'està portant a terme el disseny de nanopartícules polimèriques amb materials biocompatibles i biodegradables, que s'espera que travessin la BBB.

Prèviament, s'han caracteritzat les nanopartícules preparades. S'ha trobat que compleixen els requeriments de mida (< 200nm) necessaris per utilitzar en la via intravenosa.

Estudis de citotoxicitat en diferents línies cel·lulars (HeLa, HEK i U87) i estudis d'hemòlisi (en sang porcina i humana) han demostrat que la toxicitat és gairebé nul·la (<5% en totes les línies estudiades) en les dosis a administrar.

HIPÒTESI

Les nanopartícules polimèriques funcionalitzades amb un anticòs monoclonal són capaces de travessar la BBB.

OBJECTIUS

Comprovar que les nanopartícules polimèriques funcionalitzades són capaces de travessar la BBB i provocar un efecte analgèsic central als ratolins, no observat quan el fàrmac s'administra sense les nanopartícules.

AVANTATGES/BENEFICIS

Mitjançant aquest procediment, es podria comprovar si les nanopartícules són capaces de travessar la BBB. L'obtenció de nanopartícules capaces de travessar la BBB representaria un gran avanç pel tractament de malalties neurals, dins les quals hi ha incloses les malalties neurodegeneratives, que

UNIVERSITAT DE BARCELONA

actualment afecten a gran part de la població.

PROJECTE DE RECERCA

Aquest treball està inclòs dins del següent projecte de recerca:

Nano3B: Novel nanocarriers as delivery systems across the Blood-Brain barrier

Projecte Intramural del CIBER de Bioingenieria, Biomaterials i Nanomedicina (CIBER-BBN)

6.- DEFINICIÓ DEL MODEL ANIMAL SELECCIONAT I DEL NOMBRE D'ANIMALS A UTILITZAR

6.1. Definició:

Espècie:	Mus musculus
Soca:	CD1
Sexe:	Mascle
Edat o pes:	30 - 35 grams

6.2. Nombre d'animals:

Nombre d'animals a utilitzar en cada procediment	80
Nombre de vegades que està previst realitzar el procediment cada any	1
Duració del procediment*	1

*(Temps que passa, expressat en dies, des de que comença el procediment, no el projecte, fins que finalitza)

7. DECLARACIÓ SOBRE MÈTODES ALTERNATIUS

Per mètodes alternatius s'entenen aquells que no impliquen la utilització d'animals, permeten reduir el nombre d'animals a utilitzar o comporten un menor grau de patiment de l'animal.

Indiqueu els motius pels quals no es planteja aplicar un mètode alternatiu al procediment proposat :

☐ El mètode proposat és un mètode alternatiu.

☐ No existeix cap mètode alternatiu al procediment proposat.

UNIVERSITAT DE BARCELONA

X Existeixen mètodes alternatius, però no estan validats

☐ Altres motius: (Especifiqueu-los detalladament:)

> Tot i que es podria considerar l'ús de models in vitro de BBB, aquests no estan validats i no es poden extrapolar els resultats de creuament de BBB obtinguts a models in vivo.

8. METODOLOGIA I DISSENY

8.1. Descripció del tipus d'estudi, tècniques o procediments quirúrgics previstos, especificant, els tractaments, els grups experimentals i el nombre d'animals que seran emprats en cadascun d'ells.

> **TIPUS D'ESTUDI**
>
> Estudi de l'analgèsia central mitjançant el hot plate test, en ratolins CD1 provocada per l'administració intravenosa de nanopartícules que contenen loperamida i una funcionalització específica per travessar la BBB.
>
> **TÈCNIQUES**
>
> Hot-plate test (test de placa calenta).
>
> La realització del hot plate test es realitzarà de forma controlada. Per evitar que els animals es cremin, com a màxim es deixaran sobre la placa calenta un temps de 25 segons. Si passat aquest temps no mostren cap dels senyals esperats (saltar o tocar-se el morro amb les potes davanteres), es treuran immediatament de la placa.
>
> Aquest procediment sempre es realitzarà sota la supervisió d'una persona.
>
> Durant la resta del procés, no es preveu que l'animal pateixi.
>
> **TRACTAMENT**
>
> Pesada dels animals per saber les dosis exactes.
>
> Prova del temps de reacció basal (mesurat quan l'animal salta o es toca el morro amb les potes del davant) sobre la placa calenta.
>
> Administració intravenosa per la vena de la cua de les diferents mostres. Les mostres s'han ajustat per, en una dosi d'uns 150 microlitres, aconseguir una concentració de loperamida de 3mg/kg.

UNIVERSITAT DE BARCELONA

Passats 15 minuts, es fa la mesura del temps de reacció sobre la placa calenta.

Just acabat el procediment, els animals seran sacrificats mitjançant el mètode de dislocació cervical.

DURADA DEL PROCEDIMENT

1 dia

GRUPS EXPERIMENTALS

1) Grup control negatiu (n = 10). Administració de sèrum.

2) Grup control positiu (n = 10). Administració de morfina.

3) Grup control del tensioactiu (n = 10). Administració d'una solució tamponada amb el tensioactiu utilitzat per formular les nanopartícules.

4) Grup de solució aquosa de loperamida (n = 10). Administració d'una solució tamponada de loperamida amb el tensiactiu.

5) Grup de nanopartícules buides no funcionalitzades (n = 10). Administració d'una dispersió de nanopartícules.

6) Grup de nanopartícules buides funcionalitzades (n = 10). Administració d'una dispersió de nanopartícules funcionalitzades.

7) Grup de nanopartícules amb loperamida no funcionalitzades (n = 10). Administració d'una dispersió de nanopartícules que contenen el fàrmac.

8) Grup de nanopartícules amb loperamida funcionalitzades (n = 10). Administració d'una dispersió de nanopartícules que contenen el fàrmac i estan funcionalitzades.

8.2. Anestèsia:

X No, en cap moment

☐Sí, en aquest cas indicar quin tipus:

☐Ketamina + Xilacina   Via: Dosi:

☐Pentobarbital   Via: Dosi:

☐Uretà   Via: Dosi:

UNIVERSITAT DE BARCELONA

☐ Tiopental   Via: Dosi:

☐ MS-222   Via: Dosi:

☐ Isoflurà   Via: Dosi inducció:

                                        Dosi manteniment:

☐ Altres*:   Via: Dosi:

*Indicar el nom del principi actiu, no el comercial

8.3. Administració de productes / material biològic (cels.)

☐ No, en cap moment

X Sí, en aquest cas indicar el següent:

Producte (nom del principi actiu, no el comercial)	Loperamida hidroclorur o morfina
Via	Intravenosa
Volum	150 microlitres
Dosi	3mg/kg
Concentració	0.7mg/mL
Pauta d'administració	1 vegada solsament de loperamida o morfina depenent del grup

8.4. Privació de menjar i/o beguda

X No, en cap moment

☐ Sí, en aquest cas indicar: ☐ Menjar   ☐ Beguda

Justificar adequadament:

375

UNIVERSITAT DE BARCELONA

En quin moment del procediment:

Hora d'inici

Durada (h)

8.5. Extracció de sang

X No, en cap moment

☐Sí, en aquest cas indicar:

Lloc d'extracció en l'animal	
Volum de cada extracció	
Pauta d'extraccions	

8.6. Risc de zoonosi

X No, en cap moment

☐Sí: En el cas de treballar amb agents biològics, indicar el grup o nivell de risc (I o II, RD 664/1997) i les mesures de seguretat a seguir tant pels investigadors com pel personal de les Unitats d'Experimentació Animal. Cal remarcar que no es poden utilitzar agents de grup III o IV.

8.7. Utilització d'isòtops radioactius

X No, en cap moment

☐Sí: En el cas d'utilitzar isòtops radioactius indicar el tipus d'isòtop, instal·lació a on es farà el procediment i les mesures de seguretat a seguir tant pels investigadors com pel personal de les Unitats d'Experimentació Animal:

8.8.- Administració de dietes especials

X No.

☐Sí.

UNIVERSITAT DE BARCELONA

Breu descripció:

8.9. Utilització de substàncies químiques citotòxiques o citoestàtiques

X No, en cap moment

☐ Sí: En el cas d'utilitzar-les indicar les mesures de seguretat a seguir tant pels

investigadors com pel personal de les Unitats d'Experimentació Animal:

9. SUPERVISIÓ DELS ANIMALS

9.1. Descriure en quines fases del procediment es preveu que l'animal pot experimentar patiment, dolor o angoixa; quin protocol de supervisió s'utilitzarà (indicant paràmetres i valoració numèrica) i quines mesures correctores està previst aplicar.

Nota: Les situacions d'animal comatós o amb automutilacions o una pèrdua de pes >20% també han de ser considerades criteri de punt final independentment de la puntuació total assolida en el protocol de supervisió dels animals.

NO PROCEDEIX

9.2. Analgèsia

X No, en cap moment

☐ Sí, en aquest cas indicar el següent:

Producte (nom del principi actiu, no el comercial)	
Via	
Volum	
Dosi	
Concentració	
Pauta d'administració	

UNIVERSITAT DE BARCELONA

9.3. Criteris de punt final

Indiqueu, si és el cas, quins seran el motius i/o criteris d'aplicació d'eutanàsia abans de finalitzar el procediment si l'estat del animal així ho requereix.

No procedeix.

9.4. Tipus d'eutanàsia en cas de procedir al sacrifici de l'animal per aplicació dels criteris de punt final

☐ Asfixia per atmosfera de CO_2

X Dislocació cervical

☐ Sobredosi d'anestèsia

☐ Altres (especificar i justificar):

10. DESTINACIÓ DELS ANIMALS

10.1. Està previst:

☐ Mantenir els animals vius amb la finalitat de (explicar els motius):

X Sacrificar els animals

10.2. Protocol d'eutanàsia:

☐ Asfixia per atmosfera de CO2
X Dislocació cervical
☐ Sobredosi d'anestèsia (indicar producte, via i dosi)
    Producte:

    Via:

    Dosi:

☐ Decapitació
☐ La realització del procediment implica la mort de l'animal
☐ Altres (especificar i justificar):

UNIVERSITAT DE BARCELONA

La persona sotasignat, en qualitat d'investigador responsable d'aquest procediment, informa:

Que coneix i complirà la legislació i altres normes reguladores de la utilització d'animals per a docència i recerca.

Que és conscient que aquest procediment proposat no pot ser iniciat fins que es compleixin tots aquests requisits:

1) El CEEA informi favorablement el procediment proposat.

2) S'hagi tramès al DMAH la memòria del procediment, l'informe del CEEA i el full de notificació prèvia de procediments.

3) El DMAH hagi concedit, si és el cas, autorització expressa per aquells supòsits que així ho requereixen.

4) En el cas de ser aprovat el procediment, es compromet a tramitar anualment el full de procediments realitzats, així com aquella documentació que a efectes estadístics pugui requerir el DMAH.

5) Sol·licitar un nou informe al Comitè Ètic i una nova autorització al DMAH, si s'escau, prèviament a la introducció de qualsevol canvi rellevant en el protocol i informació que aquí es presenta.

Signatura :

Nom i cognoms : Cristina Fornaguera Puigvert   Lloc i data : Barcelona, 7 de juliol de 2014

10.2. Additional figures/tables

10.2.1. PLGA glass transition temperature in presence of serum
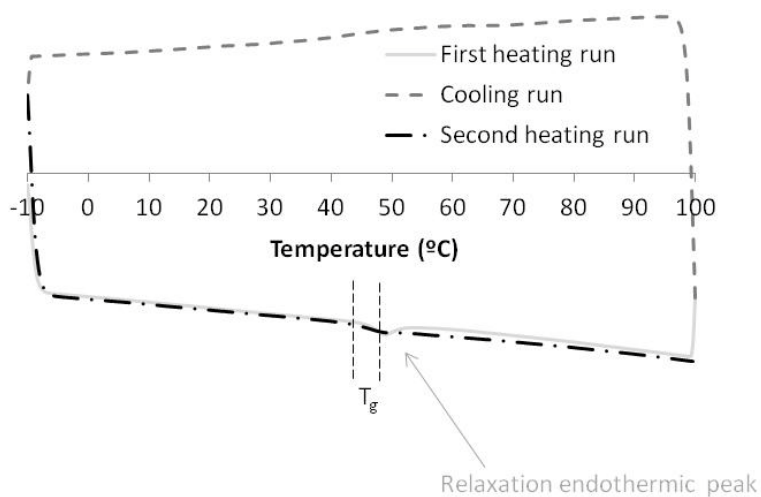
Figure Ap.1: DSC profile of PLGA polymer in presence of 10wt% of FBS: first heating, cooling and second heating runs, from -10ºC to 100ºC in steps of 10ºC/min.

10.2.2. Mobility as a function of the water phase percentage
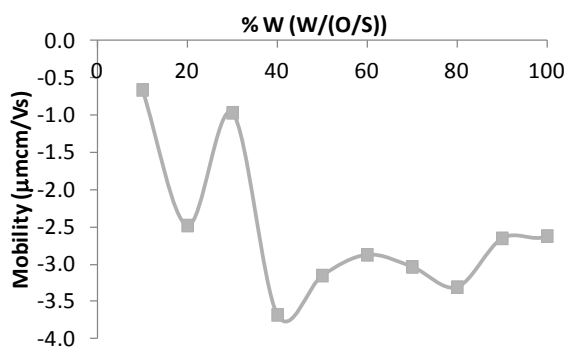
Figure Ap.2: Mobility measurements for a sample with an O/S ratio of 70/30 as a function of aqueous phase content (0.16M), with 4wt % of PLGA in the oil phase.

10.2.3.   Micrographs of optical microscopy
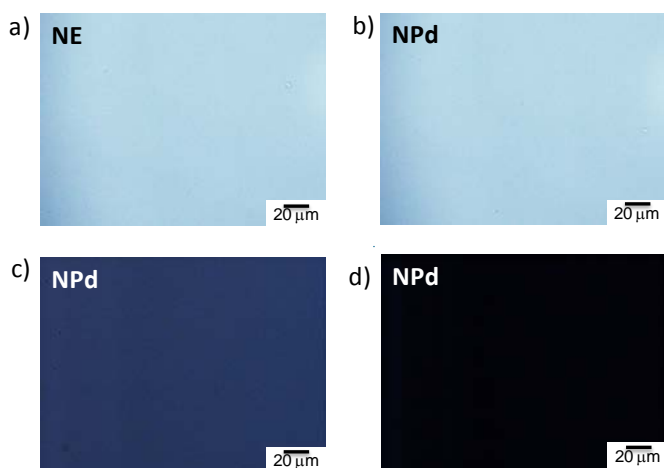
Figure Ap.3: Micrographs from optic microscope of a: a) c) and d) Nano-emulsion with 90wt % of electrolyte solution (0.16M) and 70/30 O/S ratio and b) Nanoparticle dispersion from the *a)* nano-emulsion. a) and b) images were taken under the white light, while b) was taken by differential interfacial contrast and d) using polarizers.

10.2.4.   Polydispersity indexes (PDI)

Table Ap.1: Polydispersity indexes (PDI) of the measured nano-emulsions with 90wt % of water content, as a function of the O/S ratio and electrolyte concentration in the aqueous phase.

O/S	Electrolyte concentration (M)			
	0M	0.03M	0.08M	0.16M
20/80	--	--	--	0.44
30/70	--	--	--	0.40
40/60	0.29	0.32	0.44	0.45
45/50	0.28	--	--	--
50/50	0.21	0.21	0.32	0.45
55/45	0.25	--	--	--
60/40	0.43	0.37	0.39	0.35
70/30	--	0.46	0.30	0.24
80/20	--	0.42	0.31	0.24
85/15	--	--	--	0.27
87.5/12.5	--	--	--	0.25
90/10	--	0.20	0.47	--

Table Ap.2: Polydispersity indexes (PDI) of the measured nano-emulsions with 90wt % of water content (0.16M), as a function of the O/S ratio and PLGA concentration in the oil phase.

O/S	PLGA concentration (%)	
	4 wt%	20wt%
20/80	0.44	--
30/70	0.40	--
40/60	0.45	--
45/55	--	0.31
50/50	0.45	0.49
55/45	--	0.31
60/40	0.35	0.21
70/30	0.24	0.34
80/20	0.24	--
85/15	0.27	--
87.5/12.5	0.25	--

Table Ap.3: Polydispersity indexes (PDI) of the measured nano-emulsions with 90wt % of water content (0.16M), as a function of the O/S ratio and PLGA concentration in the oil phase.

Time (hours)	Temperature	
	25ºC	37ºC
0	0.11	0.50
1	0.19	0.37
2	0.29	0.43
3	0.17	0.41
4	0.32	0.34
5	0.23	0.32
6	0.19	0.30
7	0.18	0.33
8	0.24	0.35

10.2.5. Theoretical calculations of nm^3 as a function of time
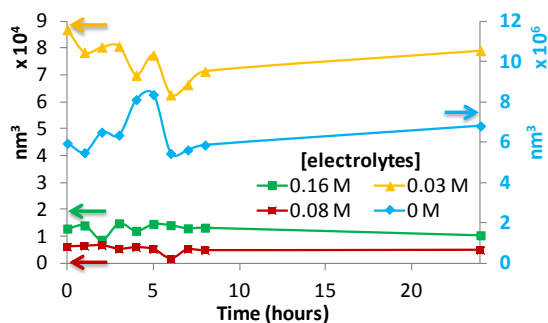
Figure Ap.4: Cube of the hydrodynamic radii of nano-emulsions with 90wt % of aqueous content as a function of the electrolyte concentration and time.

10.2.6. Enhanced optical microscopy with spectral analyses
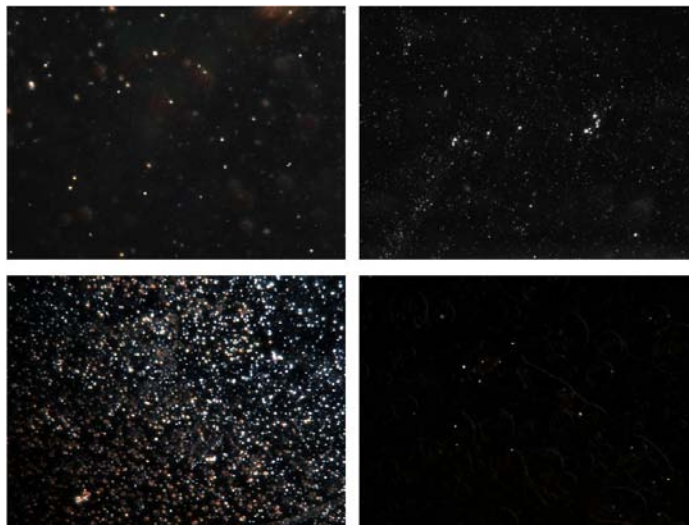
Figure Ap.5: Example micrographs of the C6-loaded nanoparticles, at 100x of magnification, with different coverage of nanoparticles.
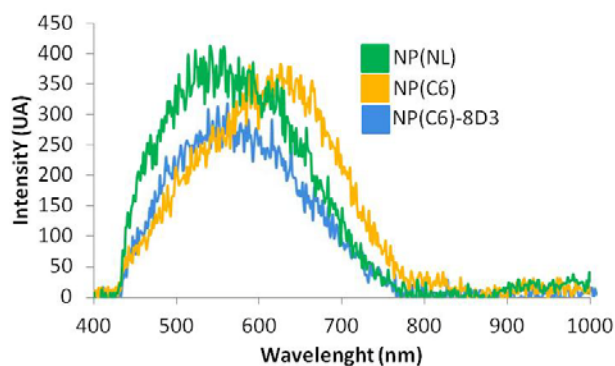
Figure Ap.6: Spectral profiles of nanoparticles, C6-loaded nanoparticles and c6-loaded 8D3-functionalized nanoparticles.
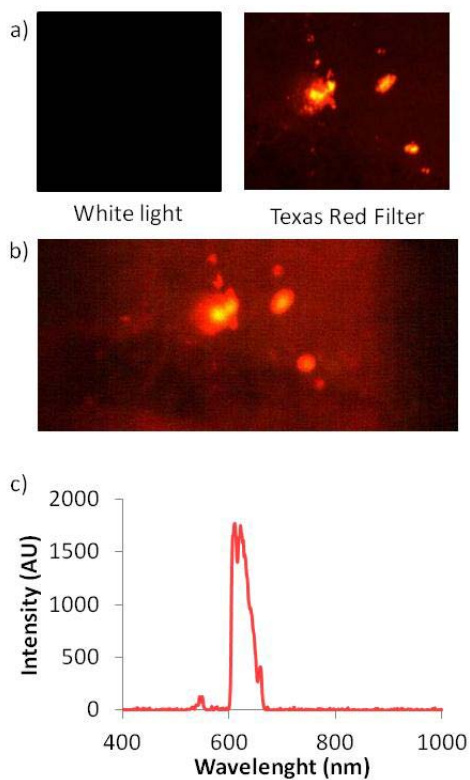
Figure Ap.7: Study of the secondary antibody against the primary anti-TfR antibody, marked with the fluorocrom AF555, by means of enhanced optical microscopy. a) Optical image visualized under different filters; b) Spectral image under white light and c) Spectral profiles.

10.2.7. TGA thermograms from nanoparticle dendronization experiments
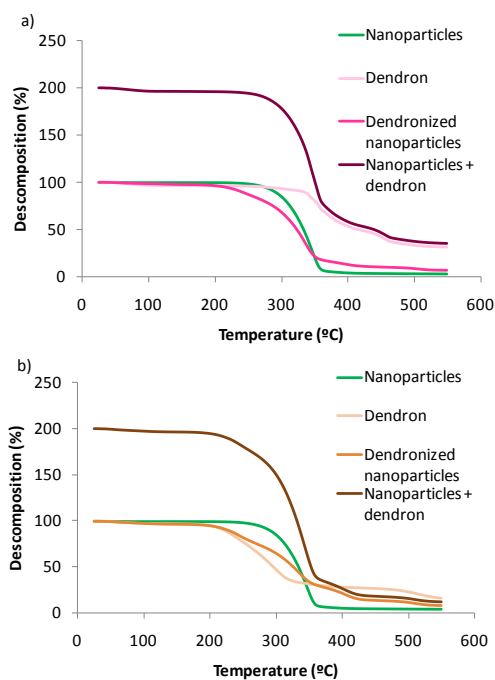
Figure Ap.8: TGA spectra from nanoparticles, dendrons, their physical mixture and dendronized nanoparticles with a) G2SN Dendron and b) G3SN dendron.

10.2.8. Absorption spectra by means of SEC studies

a)   b)
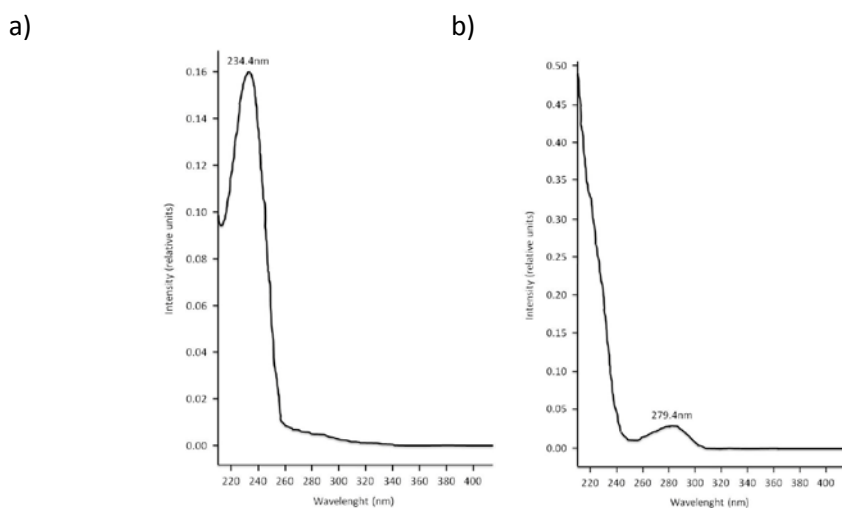
Figure Ap.9: Absorption spectrum for a) PLGA nanoparticles and b) 8D3 antibody.
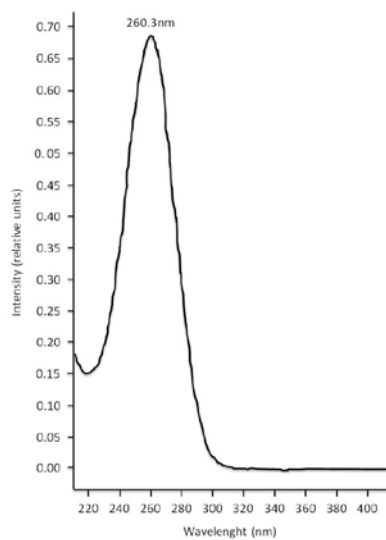
Figure Ap.10: Absorption spectrum for 8D3 functionalized PLGA nanoparticles.
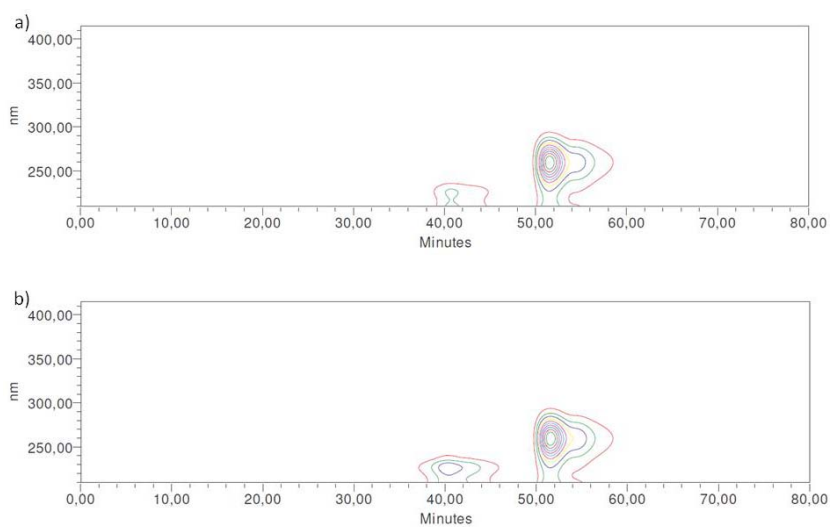
Figure Ap.11: Contour plots of the NP/8D3 complexes with a NP/8D3 ratio of: a) 25/1 and b) 12.5/1.
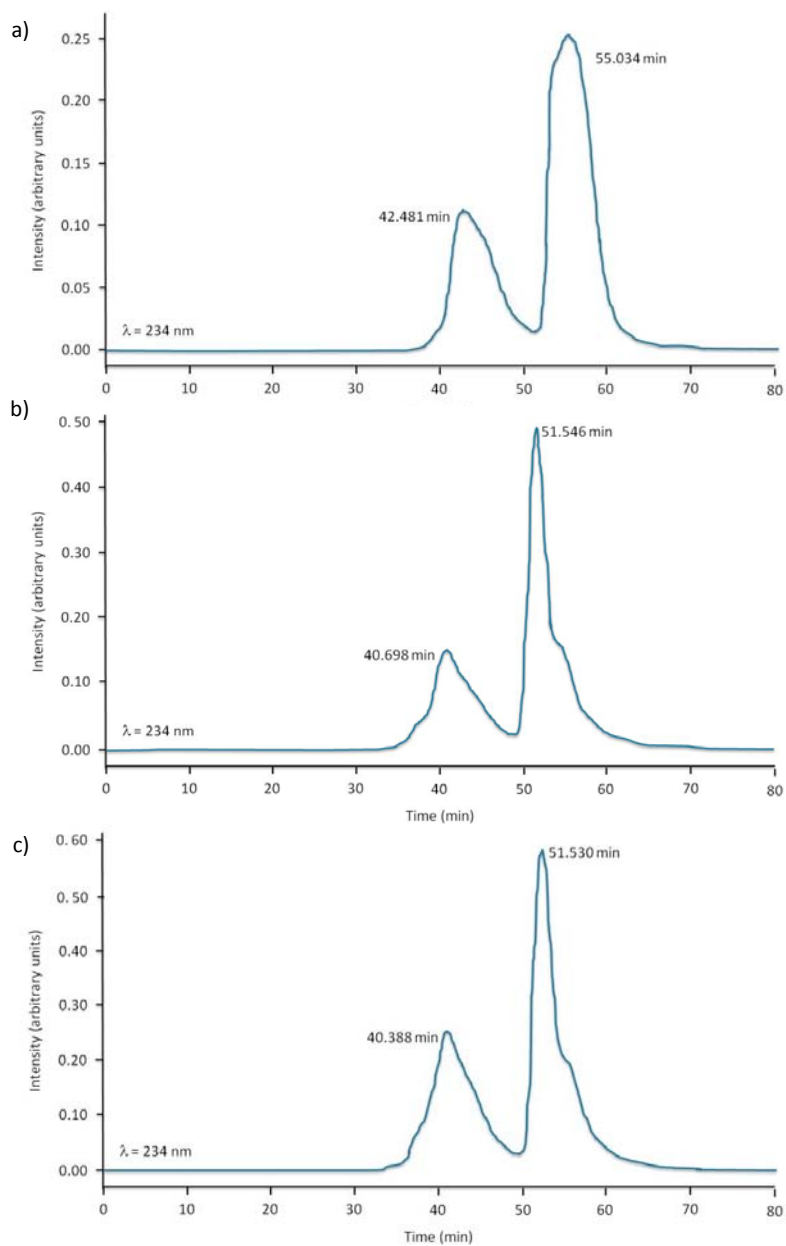
Figure Ap.12: SEC chromatogram of the 8D3-functionalized nanoparticles at 234 nm; with a NP/8D3 ratio of: a) 50/1; b) 25/1; and c) 12.5/1.
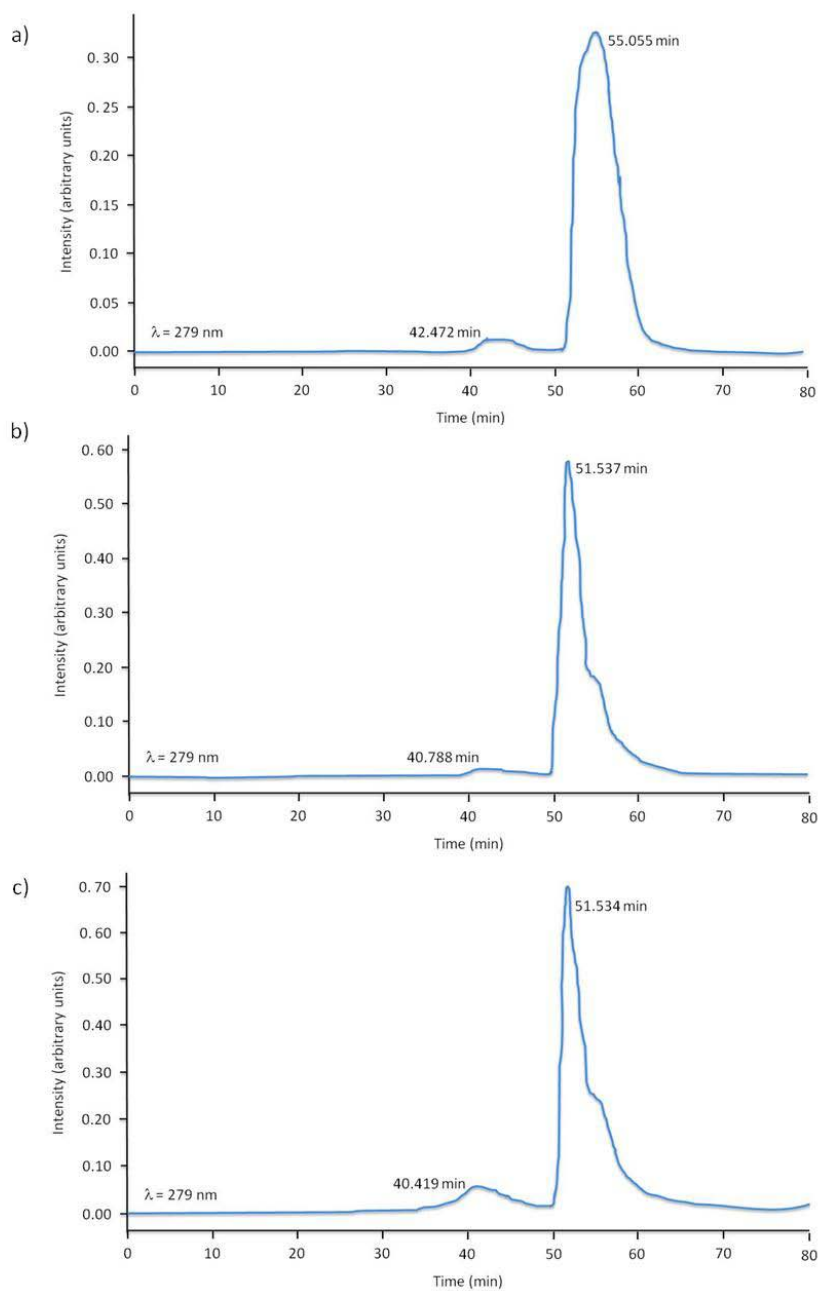
Figure Ap.13: SEC chromatogram of the 8D3-functionalized nanoparticles at 279 nm; with a NP/8D3 ratio of: a) 50/1; b) 25/1; and c) 12.5/1.
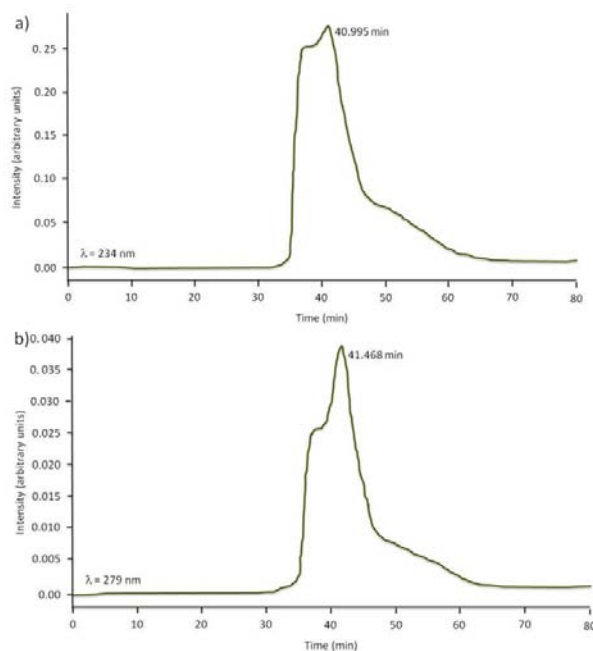
Figure Ap.14: SEC chromatogram of the physical mixture of C6-loaded nanoparticles and 8D3 antibody with a NP/8D3 ratio of 12.5/1 at: a) 234 nm and b) 279 nm.
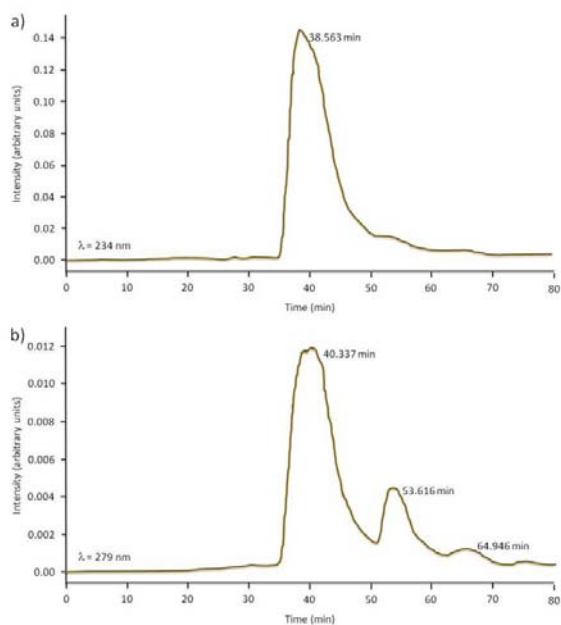
Figure Ap.15: SEC chromatogram of the physical mixture of FITC-NP and 8D3 antibody with a NP/8D3 ratio of 12.5/1 at: a) 234 nm and b) 279 nm.
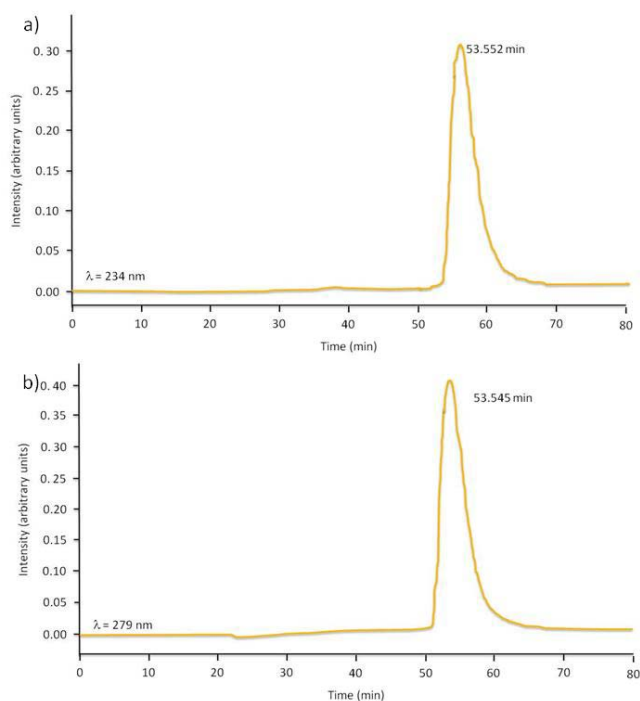
Figure Ap.16: SEC chromatogram of the 8D3-functionalized FITC-NP with a NP/8D3 ratio of 12.5/1 at: a) 234 nm and b) 279 nm.

10.2.9. Protein adsorption onto NP surface by SDS-PAGE electrophoresis
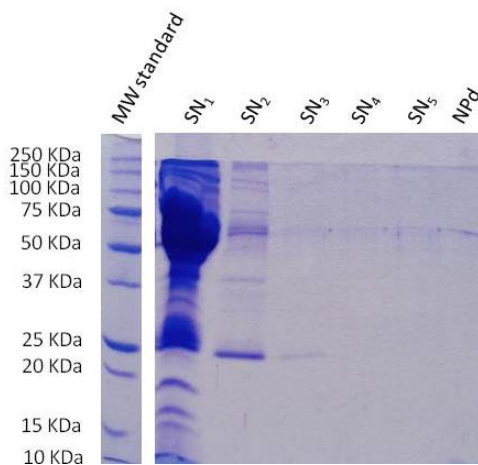
Figure Ap.17: SDS-PAGE electrophoresis showing the proteins contained in 100μg of serum, incubated with NPs. SN = supernatant fraction.

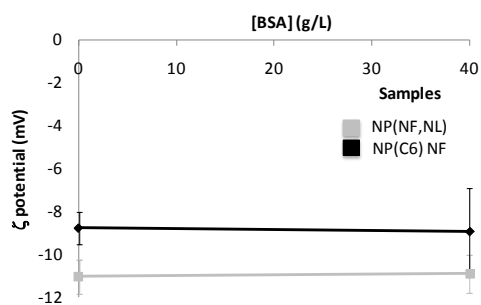### 10.2.10. Adsorption BSA isothermes on nanoparticle surface

Figure Ap.18: Adsorption isotherms of the non-functionalized nanoparticles non-loaded and loaded with Coumarin 6.
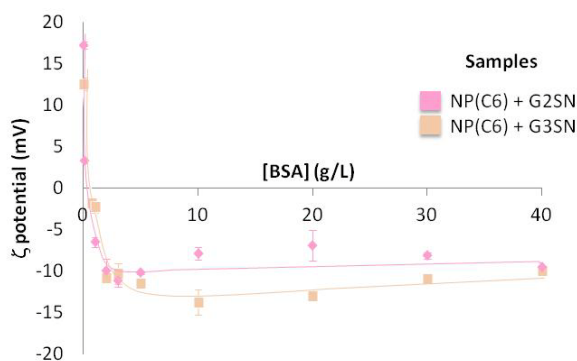
Figure Ap.19: Adsorption isotherms of the C6-loaded nanoparticles functionalized with the second and third generation dendrons.
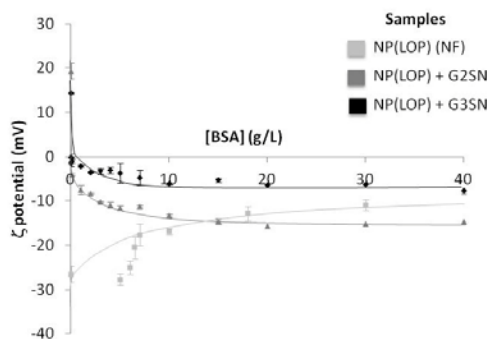

Figure Ap.20: Adsorption isotherms of the loperamide-loaded nanoparticles non-functionalized and functionalized with the second and third generation dendrons.
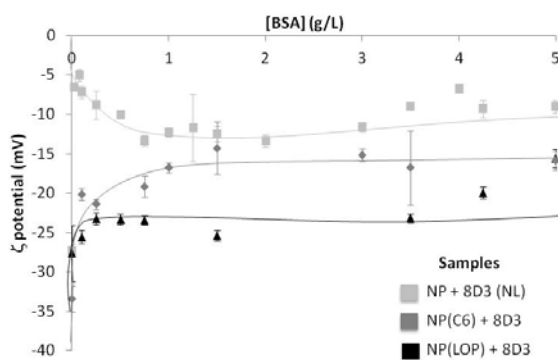
Figure Ap.21: Adsorption isotherms of the 8D3-functionalized nanoparticles non-loaded and loaded with Coumarin 6 and loperamide.

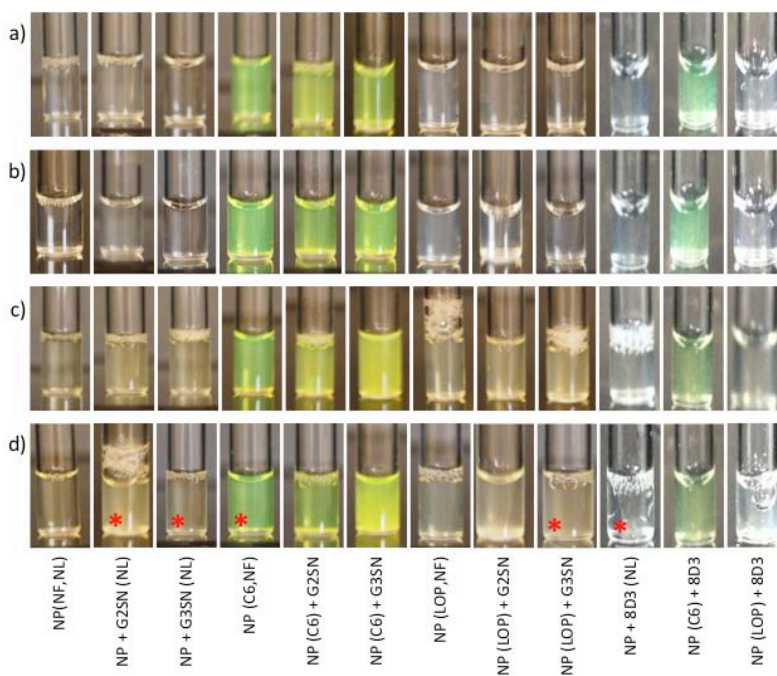## 10.2.11. Studies of the complement activation

Figure Ap.22: Visual appearance of the studied nanoparticles dispersed in VBS^{2+} buffer. a) t= 0h, 0% FBS; b) t= 1h, 0% FBS; c) t= 0h, 25wt% FBS; and d) t= 1h, 25wt% FBS. Red stars indicate samples with increased turbidity as compared with t=0h.
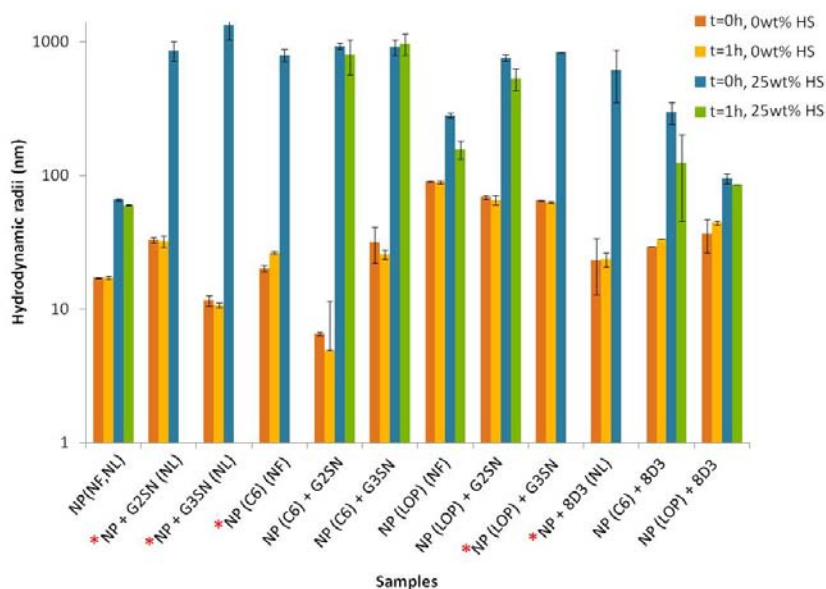
Figure Ap.23: Hydrodynamic radii (nm) of the studied nanoparticles dispersed in VBS^{2+} buffer containing 0 or 25wt% of serum, in the moment of sample preparation (0h) and after 1 hour of incubation. Red stars indicate sedimentated samples with FBS, where measurements after FBS incubation could not be performed.
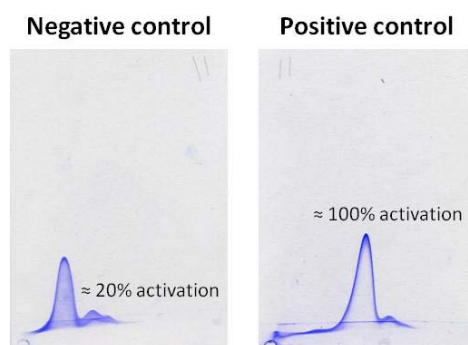

Figure Ap.24: Profile of the 2D-immunoelectrophoresis corresponding to the complement activation for the negative (buffer used in this study) and positive (water) controls.
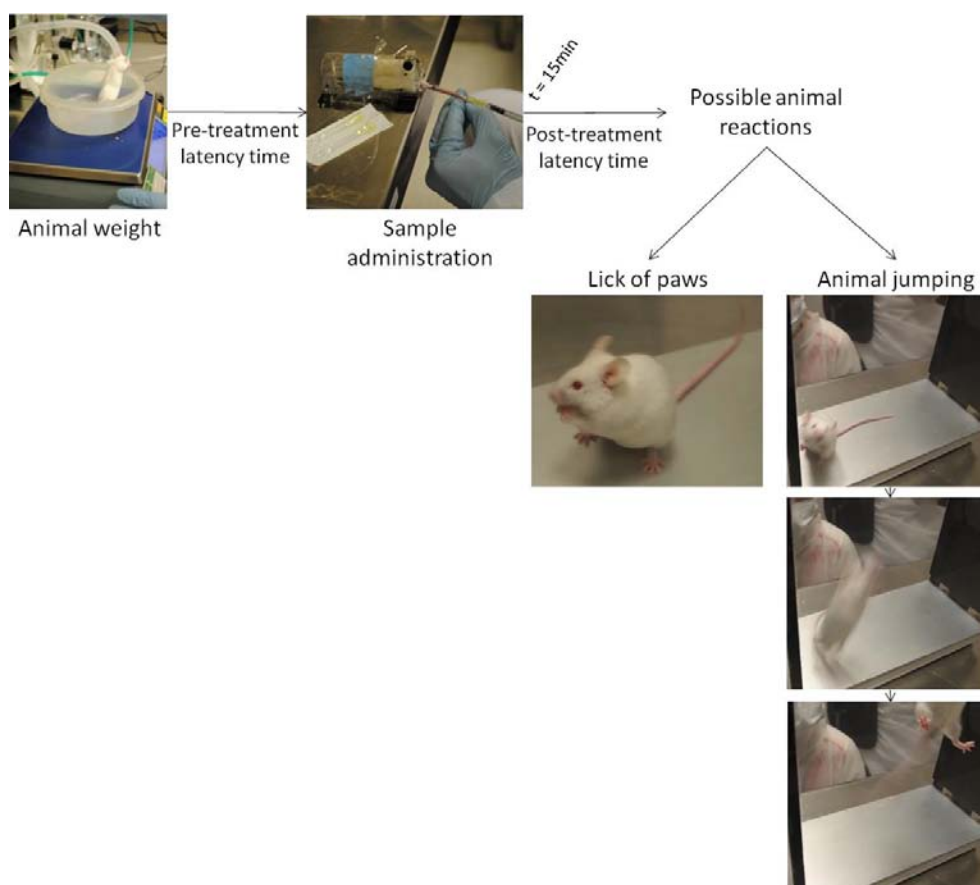
10.2.12. *In vivo* hot plate test

Figure Ap.25: Schematic representation of the whole procedure of animal manipulation to perform the hot plate test.

Table Ap.4: Data and results of the Paired – Sample T Test performed for each group to compare the means between the pre (Time$_{t=0}$) and post (Time$_{t=15}$) – latency times. A level of significance of p = 0.05 was selected and significant differences (Sig. diff.) were studied for each group.

| Sample	Animal number (n)	Time$_{t=0}$ (s)	Time$_{t=15}$ (s)	*p* value	Sig. diff.?
Electrolyte buffer (0.16M)	9	8.22 ± 2.81	6.67 ± 2.64	0.349	No
Aqueous morphine	10	5.70 ± 2.26	14.80 ± 7.10	0.005	Yes
NPs (NL,NF)	9	5.00 ± 3.00	7.44 ± 3.09	0.086	No
NPs (NL, 8D3)	9	4.44 ± 2.24	8.33 ± 6.56	0.048	Yes
NPs (LOP,NF)	9	6.67 ± 2.50	11.55 ± 6.26	0.066	No
NPs (LOP, 8D3)	9	5.44 ± 2.35	15.22 ± 5.06	0.000	Yes
Aqueous Tween 80 + LOP	9	4.78 ± 1.09	20.78 ± 5.40	0.000	Yes
Aqueous Tween 80	8	5.38 ± 1.76	11.13 ± 2.32	0.041	Yes
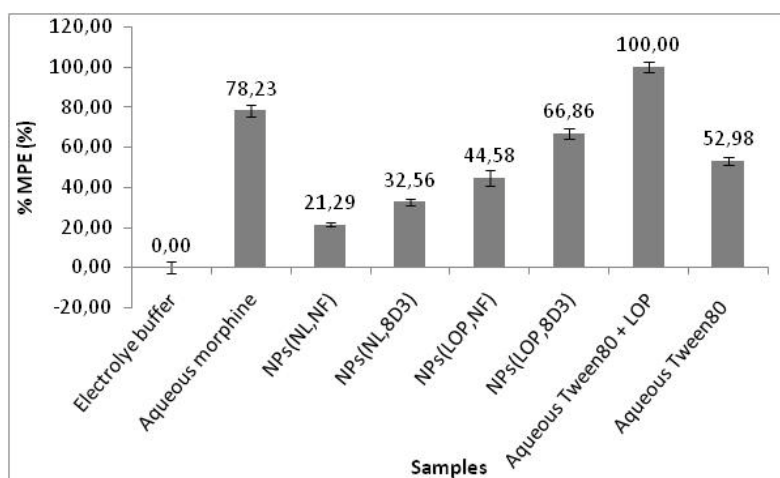
Figure Ap.26: Normalized % MPE (between 0 – 100) of different groups, performed with the pre and post treatment latency times for each group. Labels indicate the mean % MPE.

10.3. Theoretical calculations

10.3.1. Nanoparticle size from nano-emulsion droplet size

The nanoparticle radius can be theoretically assessed by mathematical calculation from the nano-emulsion droplet radius. Since in this thesis all the nano-emulsion droplet sizes were measured with the DLS, the starting values correspond to the hydrodynamic radii.

Surfactants are not considered in these calculations to belong to the droplets / nanoparticles, since they are located at the interface.

Knowing that droplets are composed of oil and polymer, the total volume of the oil phase (corresponding to the sum of droplets' volumes) can be calculated.

$$V_{oilphase} = V(oil + PLGA) \qquad \text{(Ap.1)}$$

The volume of one single droplet, assuming that all droplets have the same size, can be calculated from the hydrodynamic radius, as follows:

$$V_{1droplet} = \frac{4}{3}\pi \cdot r^3 \qquad \text{(Ap.2)}$$

The number of droplets corresponds to the fraction between the total oil volume and the volume of each droplet (Ap.3).

$$N = \frac{V_{oilphase}}{V_{1droplet}} \qquad \text{(Ap.3)}$$

Considering that each droplet will be the template for the formation of a single nanoparticle, the number of nanoparticles is the same than the number of droplets. However, the total volume of nanoparticles, since the solvent is evaporated, corresponds only to the volume of polymer added.

Then, knowing the total number of nanoparticles and the total nanoparticle volume, the volume of each nanoparticle can be calculated as follows:

$$V_{1NP} = \frac{V_{polymer}}{N} \qquad \text{(Ap.4)}$$

Finally, the nanoparticle hydrodynamic radius can be calculated (Ap.5).

$$V_{1droplet} = \frac{4}{3}\pi \cdot r^3$$

$$r = \sqrt[3]{\frac{3}{4\pi} \cdot V_{1droplet}}$$

(Ap.5)

10.3.2. Nanoparticle specific surface area

The nanoparticle surface area is necessary to ensure the same total nanoparticle surface area to compare the experiments of nanoparticle interaction with blood components, which depend more on the nanoparticle surface than on the number of nanoparticles or their size, for example.

These calculations were done according to the article of Vittaz et al. (Vittaz, 1996), following the Equation Ap.6:

$$S = n \cdot 4 \cdot \pi \cdot r^2 = 3 \cdot \frac{V}{r} = 3 \cdot \frac{m}{r \cdot \rho}$$

(Ap.6)

where n is the number of nanoparticles (calculated as explained in Vittaz, 1996), r is the radius of the nanoparticles, V is the total volume of the nanoparticles, m the total weight mass of the polymer and ρ the density of it.

10.3.3. Number of BSA molecules per nanoparticle

In the Results shown in Section 4.6.3.2. (Protein adsorption onto nanoparticle surface), the value of BSA molecules adsorbed onto a single nanoparticle is given. To reach to this value, theoretical calculation from *Vauthier et al.,* (Vauthier, 2009 (2)) were followed. The number of BSA / NP (z) is calculated as indicated in the Equation Ap.7:

$$z = \frac{n_{Ads}}{N_p}$$

(Ap.7)

where n_{Ads} is the number of BSA molecules for a volume unit and N_p is the number of nanoparticles for a volume unit. The calculation of n_{Ads} and N_p is done with equations Ap.8 and Ap.9 respectively:

$$n_{Ads} = \frac{C_{Ads} \cdot N_A}{m} \qquad \text{(Ap.8)}$$

$$N_p = \frac{\Phi}{V_p} \qquad \text{(Ap.9)}$$

where C_{Ads} is the concentration of BSA, N_A is the Avogadro's number, m is the molecular weight of BSA (68000 g/mol), ϕ is the total volume of the nanoparticles per volume unit and V_p is the volume for a single nanoparticle (found by geometric analysis).

10.4. Statistical analyses

10.4.1. Hot plate test: Paired – Sample T Test

Paired Samples Statistics

		Mean	N	Std. Deviation	Std. Error Mean
Pair 1	Time_pre_ttm	4,7778	9	1,09291	,36430
	Time_post_ttm	20,7778	9	5,40319	1,80106

Paired Samples Correlations

		N	Correlation	Sig.
Pair 1	Time_pre_ttm & Time_post_ttm	9	-,136	,726

Paired Samples Test

		Paired Differences							
					95% Confidence Interval of the Difference				Sig. (2-tailed)
		Mean	Std. Deviation	Std. Error Mean	Lower	Upper	t	df	
Pair 1	Time_pre_ttm - Time_post_ttm	-16,00000	5,65685	1,88562	-20,34824	-11,65176	-8,485	8	,000

Figure Ap.27: Example of the tables obtained with the SPSS software for the calculation of the Paired Samples T Test, for the sample containing Tween 80 and loperamide.

399